

Dissertation zur Erlangung des Doktorgrades  
der Fakultät für Chemie und Pharmazie  
der Ludwig-Maximilians-Universität München

---

**Photocontrol of Glutamate-Receptors, Toward an Orthogonal Receptor-Ligand Pair  
and Toward the Total Synthesis of Herquiline A and B**

---

Philipp Sebastian Stawski

aus  
Würzburg

2012

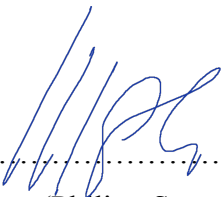
## **Erklärung**

Diese Dissertation wurde im Sinne von § 7 der Promotionsordnung vom 28. November 2011 von Herrn Professor Dr. Dirk Trauner betreut.

## **Eidesstattliche Versicherung**

Diese Dissertation wurde eigenständig und ohne unerlaubte Hilfe erarbeitet.

München, den 7. November 2012



.....  
(Philipp Stawski)

Dissertation eingereicht am	7. November 2012
1. Gutachter:	Prof. Dr. D. Trauner
2. Gutachter:	Prof. Dr. T. Carell
Mündliche Prüfung am	12. Dezember 2012



To Valeria. Only your endless support and love has made this possible.

*“Humans need fantasy to be human. To be the place where the falling angel meets the rising ape.”*  
— Terry Pratchett —

**Part I: Chemical Biology**

	<b>Page</b>
<b>I.1 Photocontrol of Glutamate Receptors</b>	<b>13</b>
1) The Glutamatergic Synapse	13
2) Pharmacology of Ionotropic Glutamate Receptors:	
A Structural Perspective	16
3) Photocontrol of Receptors – The PCL and PTL Concepts	39
4) A Photochromic Agonist of AMPA Receptors	44
5) The Subtype-Selectivity of ATAs	51
6) Triazole-Substituted AMPA Derivatives	52
7) Activity of ATAs in the Blind Retina	55
8) Toward a Universal Photoswitch for AMPA and Kainate Receptors	60
a) A Kainate-Derived Photoswitch	60
b) 3-D-substituted Glutamate Analogues	64
9) Pharmacology of Metabotropic Glutamate Receptors:	
A Structural Perspective	69
10) A Photoswitched Tethered Ligand of mGluRs	79
a) Diastereoselective Synthesis of a PTL for mGluR2	80
b) Optical Control of a Metabotropic Glutamate Receptor	84
 <b>I.2 Toward an Orthogonal Receptor-Ligand Pair based on iGluRs</b>	 <b>106</b>
1) Orthogonal Receptors: State of the Art	107
2) Receptor Design	112
3) Rational Mutation Approach	113
a) GluK2 E738D L439C (“FliGluR”)	115
b) “Bump-Hole” Approach	121
4) Yeast Assay for Glutamate Receptor Activity (“YAGA”)	124
5) Conclusion and Outlook	129

**Part II: Toward the Total Synthesis of Herquiline A & B**

	<b>Page</b>
1) The Herquiline Alkaloids	131
2) Retrosynthesis	134
3) L-Glutamate and L-Pyroglutamate in Total Synthesis	137
4) Toward the Total Synthesis of Herquiline A and B	140
5) Résumé	150
6) Outlook	151

**Part III: Experimental**

	154
--	-----

## III.1 Chemistry

	155
--	-----

1) General Experimental Details and Instrumentation	156
2) A Photochromic Agonist of AMPA Receptors – Synthetic Procedures	157
3) Triazole-Substituted AMPA Derivatives – Synthetic Procedures	181
4) A Kainate-Derived Photoswitch – Synthetic Procedures	185
5) 3-D-substituted Glutamate Analogues – Synthetic Procedures	189
6) A Photoswitched Tethered Ligand of mGluRs – Synthetic Procedures	201
7) Toward an Orthogonal Receptor Ligand Pair – Synthetic Procedures	213
8) Toward the Total Synthesis of Herquiline A & B	217

## III.2 Biology

	236
--	-----

1) General Experimental Details and Instrumentation	237
2) A Photochromic Agonist of AMPA Receptors – Supporting Information	239
3) Mutagenesis and Cloning	241

**Part IV: Spectra**

	243
--	-----

**Part V: Literature and Comments**

	310
--	-----

**Part VI: Acknowledgements**

	330
--	-----

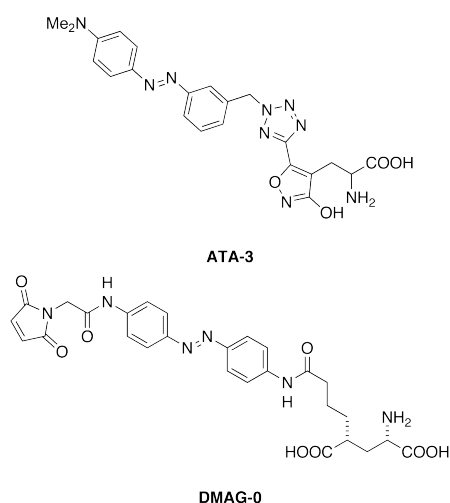
## Part I: Chemical Biology

### I.1 Photocontrol of Glutamate Receptors

Optochemical genetics uses small photo-switchable molecules to control the activity of native or genetically modified receptors. To this end, our group has adapted the concepts of photochromic ligands (PCLs) and photoswitched-tethered ligands (PTLs) to the ionotropic glutamate receptors (iGluRs). For guidance in the design of such molecules, we have compiled comprehensive lists of crystal structures featuring receptor-bound ligands. Among other molecules, we now present a new PCL named ATA-3,

which only acts on AMPA receptors, typically considered the workhorses of mammalian glutamatergic synapses. We show, that ATA-3 is capable of stimulating neurons and bipolar cells in “blind” retinæ. As such, it has become a promising lead-structure in our attempts of using small photoswitchable molecules for the restoration of vision.

Furthermore we report our progress toward a universal photoswitch for AMPA and kainate receptors and the first light-controlled metabotropic glutamate receptor (LimGluR), which uses the PTL DMAG-0 as photoswitchable unit. To this end, we have developed a scalable and reliable route for the synthesis of the PTL. Together with our collaborators at UC Berkeley, we report the performance of the DMAG-0•mGluR2 conjugate both *in vitro* and *in vivo*, and compare it to other methods for the control of G-protein coupled receptors.



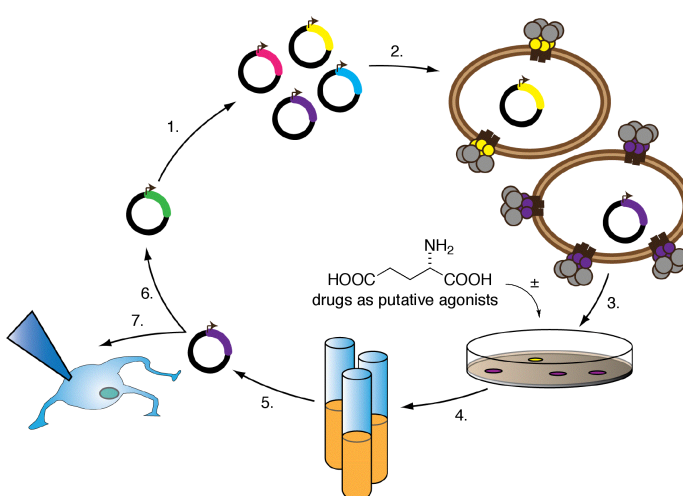
## I.2 Toward an Orthogonal Receptor-Ligand Pair

In the mammalian brain, the majority of excitatory neurotransmission is mediated by ionotropic glutamate receptors (iGluRs) and their dysfunction is related to many neurologic diseases. Therefore, a detailed understanding of their structure and their mode of action is very important for neuroscience. Introduction of artificial proteins to probe native neural systems however often interferes with the natural “landscape” of receptors.

In this project we therefore aim at creating a receptor for the orthogonal activation of glutamatergic synapses, which does not respond to the endogenous ligand, L-glutamate. In order to render the receptor unresponsive to glutamate, but sensitive toward an artificial ligand, we employ the so-called “bump-hole” approach. Hence, we created a “hole” in the receptor’s ligand-binding domain (LBD) by exchanging an amino acid for a sterically less demanding one. At the same time, we synthesized ligands that bear bulky groups, *i.e.* “bumps”, to fill the gap generated by the mutation. So far we have focused our attention on two types of mutation: a) E738D in GluK2 introduced by Fleck *et al.* and b) mutations of L671 in GluA2. The first has already yielded a receptor that is unresponsive to glutamate, but when used in conjunction with the C439C mutation can be activated to a certain extent by light, using the photochromic-tethered ligand MAG-0.

The second set of mutations (L671) has created modified AMPA receptors, which show a marked increase in affinity toward kainate-type agonists. One of them (L671G) efficiently functions as a “MAG”-receptor, *i.e.* it has a higher affinity for the kainate-type ligand MAG-0 than for L-glutamate. Therefore it is a promising lead for the design of an orthogonal receptor-ligand pair.

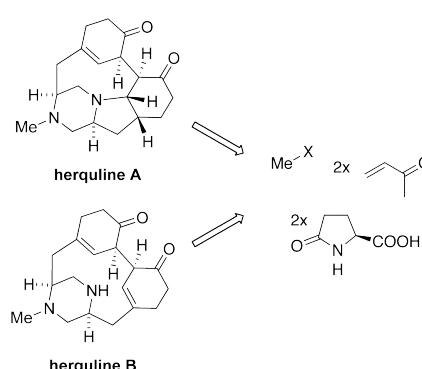
In a complementary approach, we have designed a yeast assay for glutamate receptor activity (“YAGA”), which allows for the screening of both ligands and modified receptors. We plan to use this system, which is based on the conditional rescue of a yeast strain lacking both low- and high-affinity



potassium transporters (SGY1528), for a directed evolution of ionotropic glutamate receptors toward a designer receptor-ligand pair. Thus we seek to provide an orthogonal toolset for the dissection of neural networks.

## Part II: Toward the Total Synthesis of Herquiline A & B

The piperazine alkaloids herquiline A & B were isolated in 1979 by Omura and coworkers from the penicilium strain *penecilium herquei* (Fg-372). Even though their biosynthesis is believed to involve two molecules of L-tyrosine, we decided to address their synthesis using a different approach. Our retrosynthetic analysis shows, that both herquelines can be synthesized



from two molecules of pyroglutamic acid, two molecules of methyl vinyl ketone (MVK) and an additional C<sub>1</sub>-source. The key-step of the synthesis is the transition-metal-mediated intramolecular coupling of two  $\alpha$ -iodo enones.

We here describe our synthetic progress toward these highly unusual natural products and the surprises and pitfalls that lie in the formation of the 12-membered ring present in herquiline A and B.

## **Part I: Chemical Biology**



## Common Abbreviations

Å	Angstrom ( $10^{-10}$ m)
Ac	Acetyl
Bn	Benzyl
Boc	<i>tert</i> -Butyloxycarbonyl
Bu	Butyl
Bz	Benzoyl
CDI	Carbonyldiimidazole
CH <sub>2</sub> Cl <sub>2</sub>	Dichloromethane
COD	1,5-Cyclooctadiene
conc.	concentrated
DEAD	Diethyl azodicarboxylate
DMAP	4-Dimethylaminopyridine
DME	Dimethoxy ethane
DMF	<i>N,N</i> -dimethylformamide
DMSO	Dimethyl sulfoxide
dppe	1,2-Bis(diphenylphosphino)ethane
dppf	1,1'-Bis(diphenylphosphino)ferrocene
dr	diastereomeric ratio
EDCI	1-Ethyl-3-(3-dimethylaminopropyl)carbodiimide
EI	Electron ionization/electron impact (HRMS)
ESI	Electrospray ionisation (HRMS)
Et	Ethyl
Et <sub>2</sub> O	Diethyl ether
EtOAc	Ethyl acetate
EtOH	Ethanol
FA	Formic acid
g	Gram(s)
h	Hour (s)
HBTU	<i>O</i> -(Benzotriazol-1-yl)- <i>N,N,N',N'</i> -tetramethyluronium hexafluorophosphate
HMDS	Bis(trimethylsilyl)amine
HRMS	High resolution mass spectrometry
<i>i</i> -Pr	Iso-propyl
IR	Infrared
LiAlH <sub>4</sub>	Lithium aluminium hydride
M	Molar (concentration)
Me	Methyl
MeOH	Methanol
min	Minute (s)
mp	Melting point
MVK	Methyl vinyl ketone
N	Normal (concentration)
n	Normal (isomers)
NMR	Nuclear magnetic resonance
o	Ortho
p	Para
PE	Petrol ether ( <i>iso</i> -hexanes)
Ph	Phenyl

Pin	Pinacol
PPh <sub>3</sub>	Triphenylphosphine
ppm	Parts per million (NMR)
Pr	Propyl
Py	Pyridine
PYBOP	benzotriazol-1-yl-oxytripyrrolidinophosphonium hexafluorophosphate
R <sub>f</sub>	Retention factor (TLC)
R <sub>t</sub>	Retention time (HPLC)
RT	Room temperature
t	Tertiary (isomer)
TFA	Trifluoroacetic acid
THF	Tetrahydrofuran
TLC	Thin layer chromatography
TMS	Trimethylsilyl
UV	Ultra-violet
δ	Chemical shift (NMR)

## I.1 Photocontrol of Glutamate Receptors

### 1) The Glutamatergic Synapse

The human brain contains approximately 86 billion neurons, which form an estimate of 150 trillion contacts with one another.<sup>[1]</sup> These specific interactions called synapses, are crucial for both the transmission and the processing of information which is passed on at these sites either electrically or chemically. Electrical synapses, *i.e.* “gap junctions”, had long been overlooked. Recently however, there was a resurgence in interest in these relatively small (1-4 nm) synapses, which rather seem to be a cooperative than an alternative way of transmission of information to the exchange of chemicals.<sup>[2]</sup> The latter happens at chemical synapses, where so-called neurotransmitters are exchanged. The most prevalent excitatory neurotransmitter in the mammalian central nervous system (CNS) is L-glutamate, which is released from the presynaptic neuron into the synaptic cleft and received by specialized receptors at the postsynaptic neuron (Fig. 1). To ensure repetitive action of the synapse, specialized cells, *i.e.* glia cells, surround the neurons. Despite their name (greek γλία = glue) these cells not only hold the neurons together, but they rather actively cooperate with them.<sup>[3]</sup>

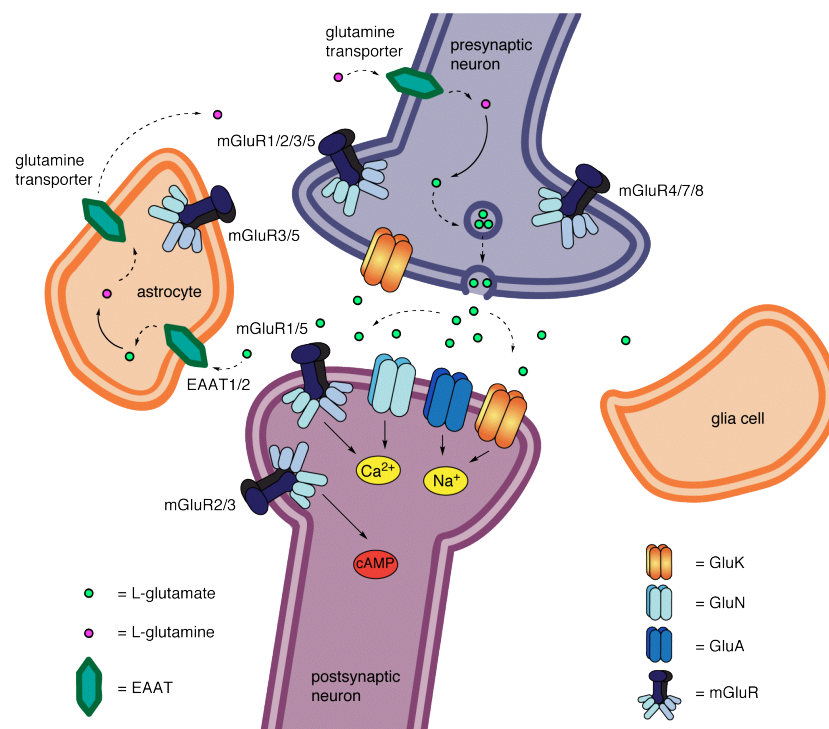


**Figure 1.** Schematic view of a glutamatergic synapse. Movements are indicated in dashed, transformations or regulatory influences are indicated as solid arrows (adapted from different sources).

Astrocytes for example, the most abundant glia cell type in the mammalian CNS, are responsible for clearing the excess of neurotransmitter from the synaptic cleft *via* excitatory amino acid transporters (EAATs). L-glutamate is then transformed into L-glutamine and fed back to the neurons where it can be recycled (Fig. 1).<sup>[4]</sup>

The glutamate-sensitive receptors of neurons can be divided into two groups: metabotropic and ionotropic glutamate receptors (mGluRs and iGluRs). While the latter are ligand-gated ion channels, mGluRs are G-protein coupled receptors. Thus, the response to L-glutamate differs vastly depending on which class of glutamate receptor is being activated. iGluRs are cation-channels and therefore are responsible for the transmission of information by depolarizing the neuron upon action of glutamate. There are three types of ionotropic glutamate receptors: NMDA (GluN1, GluN2A, GluN2B, GluN2C, GluN2D, GluN3A, GluN3B), AMPA (GluA1-4) and kainate (GluK1-5) receptors. While GluAs and GluKs are selective for  $\text{Na}^+$  and  $\text{K}^+$ , NMDA receptors are permeable to  $\text{Ca}^{2+}$ , too, and thus represent an additional way of communication *via* this second messenger (Fig. 1). mGluRs, which are categorized into group I, group II and group III, on the other hand are G-protein coupled receptors and therefore do not contribute to the depolarization of a neuron directly. By coupling of the G-protein subunits ( $\alpha$ ,  $\beta\gamma$ ) to different pathways, they can instead regulate and influence a variety of cellular processes. Their widespread expression – not only in neurons (Fig. 1) – makes metabotropic glutamate receptors an interesting target for both research and medical applications.<sup>[5]</sup>

It is obvious, that such research has always been tightly linked to the development of new techniques. From the silver-staining experiments of Ramon y Cajal in 1888 to the development of patch-clamp electrophysiology by Neher and Sakmann in 1976, new technology has always provided us with an even more detailed understanding of the cellular processes associated with memory, learning and processing of information. It is therefore with no surprise, that biotechnology has claimed its part of neuronal research, since it can provide solutions for both localized (*i.e.* neuron-centered) and network-associated problems. Without a doubt, by harnessing the spatiotemporal control of light, the use of photosensitive proteins like channelrhodopsin and halorhodopsin has revolutionized the way scientists can control the behavior and state of neurons. This new field termed optogenetics,<sup>[6]</sup> however poses an immediate problem to both the application in humans and the research of native neuronal processes, as it uses proteins from other species to control the activity of cells, rather than by exploiting their native machinery.

Our group therefore uses an alternative approach toward the photocontrol of neuronal signaling: the direct control of the receptors, like mGluRs and iGluRs, which are responsible for neurotransmission and processing of information in chemical synapses. To this end, we use small photoswitchable molecules that change their pharmacological properties (*e.g.* affinity, efficacy) upon irradiation with light of different wavelengths. We call this concept “optochemical genetics” since it employs small chemical substances to carry out optogenetic tasks.<sup>[7]</sup>

The design of such molecules requires a detailed understanding of both the structure and the pharmacology of the target-receptors. Accordingly, we like to base our design of new molecules on crystal structures, as they provide additional information beyond simple structure-activity relationships obtained from electrophysiological recordings. This approach has served us well in the past and we therefore decided to compile comprehensive lists of the x-ray structures of iGluRs and mGluRs available and to link them to the known receptor pharmacology. With the information gained, we were able to synthesize new selective molecules for the control of both the ionotropic and the metabotropic glutamate receptors.

The results of our literature survey regarding crystal structures of ionotropic glutamate receptors are summarized in the following chapter and have been published in 2010.<sup>[8]</sup>

*Note:* The formatting of schemes and figures and the citations of the original manuscript has been adjusted to fit the format of this thesis.

## 2) Pharmacology of Ionotropic Glutamate Receptors: A Structural Perspective

*Philipp Stawski, Harald Janovjak and Dirk Trauner*

*(This work was published in Bioorg. & Med. Chem. 2010, 18, 7759–7772)*

### 1. Introduction

Ionotropic glutamate receptors (iGluRs) mediate the fast response to the most prominent excitatory neurotransmitter of the mammalian nervous system. They are tetrameric, ligand-gated, cation-selective ion channels that are found throughout the animal kingdom and have homologs in plants and presumed ancestors in prokaryotes.<sup>[5]</sup> Many human neurological disorders, such as epilepsy and certain forms of mental retardation, as well as stroke, can be linked to iGluRs. As such, their pharmacology, molecular physiology and expression have been studied in great detail.<sup>[9]</sup> Due to a wealth of recent data stemming from structural biology, they now belong to the best-understood types of receptors.<sup>[10]</sup> Important topics of pharmacology, such as agonism vs. antagonism, allosteric modulation, or receptor desensitization can be beautifully illustrated using iGluRs. These crystallographic studies began with cleverly engineered soluble constructs representing the clamshell-like extracellular ligand-binding domain (LBD) of iGluRs<sup>[11]</sup> and recently culminated in a full-fledged structure of GluA2 – one of the most formidable achievements in structural biology to date.<sup>[12]</sup>

The purpose of this article is to provide an overview of the various small-molecule ligands, *i.e.* agonists, antagonists and modulators, that target iGluRs and that have been structurally characterized together with their binding sites. We will not attempt to comprehensively review the pharmacology of iGluRs (a truly monumental task) but rather discuss recent crystallographic results that allow for the interpretation of the available structure-activity relationships and the design of new and improved molecules. Computational investigations, which provide a complimentary approach, are beyond the scope of this review.<sup>[13]</sup> The same is true for the extensive pharmacology and emerging structural biology of metabotropic glutamate receptors (mGluRs), which mediate the slow response to glutamate. Since our review is “ligand-centric”, we will only briefly touch on the wealth of biophysical and biochemical data that have been accumulated to explain important receptor

functions, such as activation, desensitization and trafficking, and we refer the reader to excellent accounts on these topics.<sup>[5, 9]</sup>

Table 1, which is at the heart of this review, lists the names and functional roles of the ligands and their corresponding accession numbers in the Protein Data Bank (pdb)<sup>[14]</sup> in the order of their receptor subtypes. References with further details on the origin, pharmacology, and medical use of the ligands are also provided. The corresponding chemical structures can be found in Figures 4-13. For good measure, we also list the known *apo* structures of receptor LBDs and the structures of amino-terminal domains (*vide infra*). Occasionally, we will discuss popular agonists and antagonists for iGluRs that have not (yet) been crystallized with their receptors. Their binding mode can be often inferred from the existing structural data.

**Table 1.** X-Ray structures of iGluR-LBDs and their ligands. A, ant and mod denote agonists, antagonists and modulators, resp. Structures marked with \* are not published.

Type	PDB code	Ligand(s)	Functional	Mutant(s)	Citation
GluR0	1IIW		apo		[15]
GluR0	1II5	glutamic acid (1)	a		[15]
GluR0	1IIT	L-serine	a		[15]
GluR0	2PYY	glutamic acid (1)	a		[16]
GluA2	1FTO		apo		[17]
GluA2	1MXV	Zn <sup>2+</sup>	apo		[18]
GluA2	1MXW	Zn <sup>2+</sup>	apo		[18]
GluA2	1MXX	Zn <sup>2+</sup>	apo		[18]
GluA2	1MXY	Zn <sup>2+</sup>	apo		[18]
GluA2	1MXZ	Zn <sup>2+</sup>	apo		[18]
GluA2	1MY0	Zn <sup>2+</sup>	apo		[18]
GluA2	1MY1	Zn <sup>2+</sup>	apo		[18]
GluA2	1FTJ	glutamic acid (1)	a		[17]
GluA2	1FTK	kainic acid (17)	a		[17]
GluA2	1FW0	kainic acid (17)	a		[17]
GluA2	1LB8	AMPA (10)	a	L483Y, flop	[19]
GluA2	1LBB	kainic acid (17)	a	N754D	[19]
GluA2	1M5B	2-Me-TetAMPA (8)	a		[20]
GluA2	1M5C	Br-HIBO (13)	a	flop	[20]
GluA2	1M5D	Br-HIBO (13)	a	flop	[20]
GluA2	1M5E	ACPA (10)	a	flop	[20]
GluA2	1M5F	ACPA (10)	a	flop	[20]
GluA2	1MM6	quisqualate (14)	a		[21]
GluA2	1MM7	quisqualate (14), Zn <sup>2+</sup>	a		[21]
GluA2	1MQD	(S)-des-Me-AMPA (5), Li <sub>2</sub> SO <sub>4</sub>	a		[22]
GluA2	1MQG	iodo-willardiine (15e)	a		[23]
GluA2	1MQH	bromo-willardiine (15d)	a		[23]
GluA2	1MQI	fluoro-willardiine (15b)	a		[23]
GluA2	1MQJ	willardiine (15a)	a		[23]
GluA2	1MS7	(S)-des-Me-AMPA (5), Zn(OAc) <sub>2</sub>	a		[22]
GluA2	1MXU	bromo-willardiine (15d)	a		[18]

Type	PDB code	Ligand(s)	Functional	Mutant(s)	Citation
GluA2	1MY2	AMPA	a		[23]
GluA2	1MY3	bromo-willardiine ( <b>15d</b> )	a		[23]
GluA2	1MY4	iodo-willardiine ( <b>15e</b> )	a		[23]
GluA2	1N0T	ATPO ( <b>35</b> )	a		[24]
GluA2	1NNK	ATPA ( <b>6</b> )	a		[25]
GluA2	1NNP	ATPA ( <b>6</b> )	a		[25]
GluA2	1P1N	kainic acid ( <b>17</b> )	a	L138T	[26]
GluA2	1P1O	quisqualate ( <b>14</b> )	a	L138T	[26]
GluA2	1P1Q	AMPA ( <b>4</b> )	A	L138T	[26]
GluA2	1P1U	AMPA ( <b>4</b> )	a	L138T	[26]
GluA2	1P1W	AMPA ( <b>4</b> )	a	L94Y, L138T	[26]
GluA2	1SYH	CPW399 ( <b>16</b> )	a		[27]
GluA2	1SYI	CPW399 ( <b>16</b> )	a	Y702F	[27]
GluA2	1WVJ	4-AHCP ( <b>11</b> )	a		[28]
GluA2	1XHY	kainic acid ( <b>17</b> )	a	Y702F, flop	[27]
GluA2	2AIX	thio-ATPA ( <b>7</b> )	a		*
GluA2	2AL4	quisqualate ( <b>14</b> )	a		[29]
GluA2	2ANJ	kainic acid ( <b>17</b> )	a	Y61W	[30]
GluA2	2GFE	glutamic acid ( <b>1</b> )	a	A476E S673D	[31]
GluA2	2I3V	glutamic acid ( <b>1</b> )	a	G725C	[32]
GluA2	2I3W	glutamic acid ( <b>1</b> )	a	G729C	[32]
GluA2	2P2A	BnTetAMPA ( <b>9</b> )	a		[33]
GluA2	2UXA	glutamic acid ( <b>1</b> )	a	flip	[34]
GluA2	3B6Q	glutamic acid ( <b>1</b> )	a	T686A	[35]
GluA2	3B6T	quisqualate ( <b>14</b> )	a	T686A	[35]
GluA2	3B6W	glutamic acid ( <b>1</b> )	a	T686S	[35]
GluA2	3BFT	TDPA ( <b>12</b> )	a		[36]
GluA2	3BFU	TDPA ( <b>12</b> )	a		[36]
GluA2	3DP6	glutamic acid ( <b>1</b> )	a		[37]
GluA2	3LSL	glutamic acid ( <b>1</b> ), piracetam ( <b>74</b> )	a		[38]
GluA2	2CMO	glutamic acid ( <b>1</b> ), NS-1209 ( <b>47</b> )	a, ant		[39]
GluA2	3KGC	glutamic acid ( <b>1</b> ), Z-200775 ( <b>44</b> ), LY-404187 ( <b>71</b> )	a, ant, mod		[12]
GluA2	1LBC	glutamic acid ( <b>1</b> ), cyclothiazide ( <b>61</b> )	a, mod	N775S	[19]
GluA2	2AL5	fluoro-willardiine ( <b>15b</b> ), aniracetam ( <b>75</b> )	a, mod		[29]
GluA2	2XHD	glutamic acid ( <b>1</b> ), <b>73</b>	a, mod		[40]
GluA2	3BBR	glutamic acid ( <b>1</b> ), <b>70</b>	a, mod		[41]
GluA2	3H6T	glutamic acid ( <b>1</b> ), cyclothiazide ( <b>61</b> )	a, mod		[42]
GluA2	3H6U	glutamic acid ( <b>1</b> ), NS-1493 ( <b>67</b> )	a, mod		[42]
GluA2	3H6V	glutamic acid ( <b>1</b> ), NS-5206 ( <b>68</b> )	a, mod		[42]
GluA2	3H6W	glutamic acid ( <b>1</b> ), NS-5217 ( <b>69</b> )	a, mod		[42]
GluA2	3IJO	glutamic acid ( <b>1</b> ), althiazide ( <b>65</b> )	a, mod		[43]
GluA2	3IJX	glutamic acid ( <b>1</b> ), IDRA-21 ( <b>64</b> )	a, mod		[43]
GluA2	3IK6	glutamic acid ( <b>1</b> ), chlorothiazide ( <b>66</b> )	a, mod		[43]
GluA2	3IL1	glutamic acid ( <b>1</b> ), IDRA-21 ( <b>64</b> )	a, mod		[43]
GluA2	3ILT	glutamic acid ( <b>1</b> ), trichlormethiazide ( <b>63</b> )	a, mod		[43]
GluA2	3ILU	glutamic acid ( <b>1</b> ), hydroflumethiazide ( <b>62</b> )	a, mod		[43]
GluA2	3LSF	glutamic acid ( <b>1</b> ), piracetam ( <b>74</b> )	a, mod		[38]
GluA2	1LB9	DNQX ( <b>40</b> )	ant	L483Y	[19]
GluA2	3B7D	CNQX ( <b>41</b> )	ant		[44]
GluA2	3H03	UBP277 ( <b>36a</b> )	ant		[37]
GluA2	3H06	UBP282 ( <b>36b</b> )	ant		[37]



Type	PDB code	Ligand(s)	Functional	Mutant(s)	Citation
GluA2	3KG2	ZK-200775 ( <b>44</b> )	ant	N241E, N385D, N392Q, K410A, E413A, M414A, E416A, C589A	[12]
GluA2	3BK1	FQX ( <b>46</b> )	ant, photoproduct		[45]
GluA3	3DLN	glutamic acid ( <b>1</b> )	a		[46]
GluA3	3DP4	AMPA ( <b>4</b> )	a		[46]
GluA3	3M3K	glutamic acid ( <b>1</b> )	a	flop	[47]
GluA3	3M3L	glutamic acid ( <b>1</b> ), PEPA ( <b>72</b> )	a, mod		[47]
GluA4	3EN3	kainic acid ( <b>17</b> )	a		[48]
GluA4	3FAS	glutamic acid ( <b>1</b> )	a	flip	[49]
GluA4	3FAT	AMPA ( <b>4</b> )	a	flip	[49]
GluA4	3KEI	glutamic acid ( <b>1</b> )	a	L651V	[50]
GluA4	3KFM	kainic acid ( <b>17</b> )	a	L651V	[50]
GluK1	3C31	Li <sup>+</sup>	apo		[51]
GluK1	3C32	Na <sup>+</sup>	apo		[51]
GluK1	3C33	K <sup>+</sup>	apo		[51]
GluK1	3C34	Rb <sup>+</sup>	apo		[51]
GluK1	3C35	Cs <sup>+</sup>	apo		[51]
GluK1	3C36	NH <sub>4</sub> <sup>+</sup>	apo		[51]
GluK1	1TXF	glutamic acid ( <b>1</b> )	a		[52]
GluK1	1YCJ	glutamic acid ( <b>1</b> )	a		[53]
GluK1	2F36	glutamic acid ( <b>1</b> )	a		[52]
GluK1	2PBW	domoic acid ( <b>18</b> )	a		[54]
GluK1	2WKY	4-AHCP ( <b>11</b> )	a		[55]
GluK1	2ZNS	glutamic acid ( <b>1</b> )	a		*
GluK1	2ZNT	dysiherbaine A ( <b>26a</b> )	a		*
GluK1	2ZNU	dysiherbaine A ( <b>26a</b> )	a		*
GluK1	3FUZ	glutamic acid ( <b>1</b> )	a		*
GluK1	3FV1	dysiherbaine A ( <b>26a</b> )	a		*
GluK1	3FV2	neodysiherbaine A ( <b>26b</b> )	a		*
GluK1	3FVG	MSVIII-19 ( <b>26c</b> )	a		*
GluK1	3FVK	8-deoxy-neodysiherbaine A ( <b>26d</b> )	a		*
GluK1	3FVN	9-deoxy-neodysiherbaine A ( <b>26e</b> )	a		*
GluK1	3FVO	8-epi-neodysiherbaine A ( <b>26f</b> )	a		*
GluK1	3GBA	dysiherbaine A ( <b>26a</b> )	a		[56]
GluK1	3GBB	MSVIII-19 ( <b>26c</b> )	a		[56]
GluK1	1VSO	ATPO ( <b>35</b> )	ant		[54]
GluK1	2F34	UBP-310 ( <b>36d</b> )	ant		[52]
GluK1	2F35	UBP-302 ( <b>36c</b> )	ant		[52]
GluK1	2OJT	UBP-310 ( <b>36d</b> )	ant		[57]
GluK1	2QS1	UBP-315 ( <b>36e</b> )	ant		[56]
GluK1	2QS2	UBP-318 ( <b>36g</b> )	ant		*
GluK1	2QS3	UBP-316 ( <b>36f</b> )	ant		*
GluK1	2QS4	LY-466195 ( <b>37</b> )	ant		*
GluK2	1S7Y	glutamic acid ( <b>1</b> )	a		[52]
GluK2	1S9T	quisqualate ( <b>14</b> )	a		[52]
GluK2	1SD3	(2 <i>S</i> ,4 <i>R</i> )-4-methyl glutamic acid ( <b>21</b> )	a		[52]
GluK2	1TT1	kainic acid ( <b>17</b> )	a		[52]

Type	PDB code	Ligand(s)	Functional	Mutant(s)	Citation
GluK2	1YAE	domoic acid ( <b>18</b> )	a		[58]
GluK2	2I0B	glutamic acid ( <b>1</b> )	a	K494E, I749L, Q753K, E757Q	[59]
GluK2	2I0C	glutamic acid ( <b>1</b> )	a	S775E, Y490C, L752C (crosslinked)	[59]
GluK2	3G3F	glutamic acid ( <b>1</b> )	a		[60]
GluK2	3G3G	glutamic acid ( <b>1</b> )	a	K665R	[60]
GluK2	3G3H	glutamic acid ( <b>1</b> )	a	K665R, I749L, Q753K	[60]
GluK2	3G3I	glutamic acid ( <b>1</b> )	a	I442H, K494E, I749L, Q753K	[60]
GluK2	3G3J	glutamic acid ( <b>1</b> )	a	I442H, K494E, K665R, I749L, Q753K	[60]
GluK2	3G3K	glutamic acid ( <b>1</b> )	a	I442H, K494E, K665R, I749L, Q753K, E757Q	[60]
GluD2	2V3T		apo		[61]
GluD2	2V3U	D-serine ( <b>3</b> )	a		[61]
GluN1	1PB7	glycine ( <b>2</b> )	a		[62]
GluN1	1PB8	D-serine ( <b>3</b> )	a		[62]
GluN1	1PB9	D-cycloserine ( <b>27</b> )	a		[62]
GluN1	1Y1M	cycloleucine ( <b>31</b> )	a		[63]
GluN1	1Y1Z	ACBC ( <b>30</b> )	a		[63]
GluN1	1Y20	ACPC ( <b>29</b> )	a		[63]
GluN1	1PBQ	5,7-dichlorokynurenic acid ( <b>54</b> )	ant		[62]
GluN1/GluN2A	2A5T	glycine ( <b>2</b> ), glutamic acid ( <b>1</b> )	a, a		[64]
GluN2A	2A5S	glutamic acid ( <b>1</b> )	a		[64]
GluA2 ATD	3H5V				[65]
GluA2 ATD	3H5W				[65]
GluK2 ATD	3H6G				[66]
GluK2 ATD	3H6H				[66]
GluA2 ATD	3HSY				*

## 2. An overview of iGluRs

Historically, iGluRs have been grouped according to their distinct responses to certain small molecule agonists, namely AMPA ( $\alpha$ -amino-3-hydroxyl-5-methyl-4-isoxazolepropionic acid), kainate, and NMDA (*N*-methyl-D-aspartate).<sup>[5, 9]</sup> This classification had been upheld in light of more recent sequence data although the pharmacologically defined boundary between AMPA and kainate receptors has blurred over time and now they are often grouped into the so-called “non-NMDA receptor” superfamily. According to a modern nomenclature,<sup>[67]</sup> the

iGluRs comprise AMPA-type receptors (GluA1–GluA4), kainate receptors (GluK1–GluK5) and NMDA receptors (GluN1, GluN2A–GluN2D, GluN3A–GluN3B) (Fig. 2). Two orphan members of the iGluR gene family, GluD1 and GluD2, are also known, but their physiological role remains somewhat mysterious. In addition to this, a prokaryotic, potassium-selective glutamate receptor (GluR0) has been cloned and structurally characterized.<sup>[68]</sup>

AMPA receptors are the workhorses of fast synaptic transmission and are widely expressed throughout the mammalian central nervous system. Potentiation of synaptic responses is achieved through insertion of an increasing number of AMPA receptors at the post-synaptic membrane or the modulation of single channel conductance.<sup>[69]</sup> By contrast, kainate receptors assume more of a modulatory role and are active both on the postsynaptic and presynaptic side. They are also involved in generating synaptic plasticity but have a narrower distribution.<sup>[70]</sup> NMDA receptors primarily function as coincidence detectors and are critical for learning and memory. They are inactive at resting membrane potentials due to a voltage-dependent block of the channel pore by magnesium ions. Activation of AMPA receptors and membrane depolarization releases this inhibition. Unlike most AMPA and kainate receptors, NMDA receptors are permeable to calcium ions which triggers various intracellular signaling cascades.<sup>[71]</sup> Alternative splicing and RNA editing, whose most notable effects are on trafficking and  $\text{Ca}^{2+}$  permeability, complicate the genetic and functional analysis of iGluRs.<sup>[72]</sup>

Ionotropic glutamate receptors function as a complex of four individual subunits. Whereas the NMDA-receptors are obligate heterotetramers, the AMPA and kainate receptors can exist as homo- and heterotetramers within one subfamily. For example, the major kainate receptor in the human brain consists of GluK2 and GluK5.<sup>[73]</sup> NMDA receptors are composed of subunits that bind to glycine or D-serine (NR1 and NR3) and subunits that are activated by glutamate (NR2). NR1 and NR2A are the most abundant forms in the fully developed human brain.<sup>[74]</sup>

Each individual subunit of an iGluR features an extracellular amino-terminal domain (ATD), which is involved in subfamily-specific tetramerization, an extracellular LBD that interacts with the neurotransmitter, a transmembrane domain (TMD) that forms the cation-selective pore and a cytoplasmatic carboxy-terminal domain (CTD) involved in receptor localization and modulation. The ATD and LBD of iGluRs have often been compared to clamshells (or Venus fly-traps). Starting from the N-terminus, the polypeptide first forms the ATD followed by a part of both lobes of the LBD clamshell, then dips into the membrane as

transmembrane helix 1, the pore loop, and transmembrane helix 2, then rises again to the extracellular side to complete the remainder of the LBD clamshell, and finally crosses the membrane once more as transmembrane helix 1 to end up as a CTD of varying length. Structurally, the LBD clamshell can be easily dissected in an “upper lobe” (relative to the cell membrane), which is also known as D1, and a “lower lobe”, known as D2.

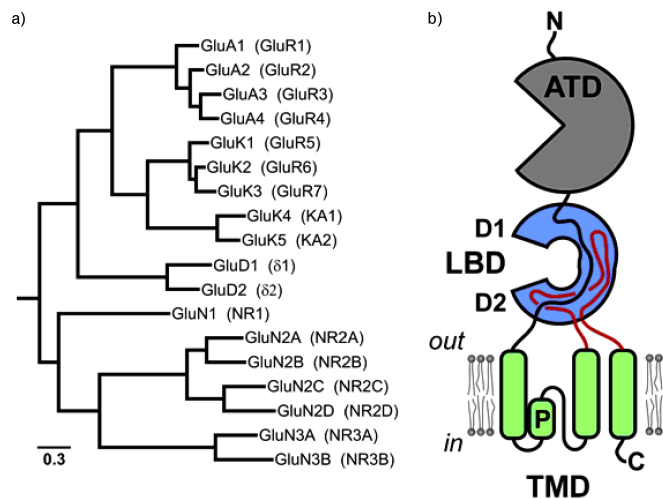


**Figure 2.** a) Maximum likelihood phylogeny of human iGluRs where the branch lengths are proportional to the amount of inferred evolutionary change. Sequences were aligned with Muscle<sup>[75]</sup> and phylogeny was calculated using FastTree.<sup>[76]</sup> b) Domain structure of eukaryotic iGluRs. ADT = amino-terminal domain, LBD = ligand-binding domain, D1 = upper lobe of the LBD, D2 = lower lobe of the LBD, TMD = transmembrane domain, P = pore helix.

### 3. The three-dimensional structure of iGluRs and the LBD clamshell

Very recently, the whole crystal structure of a functional tetrameric AMPA receptor complete with its ATD, LBD and TMD was disclosed (pdb 3KG2, Fig. 3).<sup>[12]</sup> This structure reveals that homotetrameric iGluRs are approximately  $C_4$ -symmetric in their TMDs and  $C_2$ -symmetric with respect to extracellular domains. The first two helices and re-entrant loop of the TMD closely resemble those of potassium channels. Due to this “symmetry mismatch” (or, rather, reduction in symmetry), the four sequence-identical chains of iGluRs fall into two conformational subtypes, which is reflected in two types of LBD clamshells. Although the fold of these clamshells is very similar overall, they are oriented at different angles with respect to the  $C_2$ -axis of symmetry and it is the ipsilateral clamshells that form a dimer exclusively *via* contacts in the D1 lobes. Upon activation, the clamshells close and the separation of their D2 lobes increases. This movement is mechanically linked to the second transmembrane helix and opens a gate in the TMD. It also creates mechanical tension within

the LBD multimer, which is alleviated by subsequent separation of the D1 lobes, a process that results in receptor desensitization and channel inactivation.<sup>[32]</sup>

The crystallization and functional analysis of individual LBD clamshells has been greatly aided by soluble constructs (so called S1-S2 constructs) that capture most of their essential structural features and have allowed for the development of the above gating model. Coordinates of these constructs are available for two prokaryotic glutamate receptors, the AMPA receptors GluA2, GluA3, and GluA4, the kainate receptors GluK1 and GluK2, the NMDA receptor subunits GluN1, GluN3 (glycine sites), and GluN2A (glutamate site), as well as the orphan receptor GluD2. These have been crystallized as monomers or dimers and with a variety of agonists, antagonists and – in the case of AMPA receptors - several modulators that are known to influence receptor desensitization. A handful of *apo* structures are also available (Table 1).

Since the human vocabulary concerning clamshells is somewhat limited compared with our ability to describe our own anatomy, we occasionally find it useful to speak of the LBD in terms of a human head and mouth. A “nose”-like loop can be found in all crystal structures of iGluR LBDs and we orient the clamshell in Figs. 3 and 5 such that the nose protrudes to the left. We prefer this orientation for the comparative analysis of the X-ray structures since the “mouth” (or cleft) of the LBD points towards the spectator and provides a perspective of glutamate and its congeners that corresponds to Fig. 4 (*vide infra*). The cleft of the clamshell is lined by “lips”, which can be fully closed or partially open to accommodate portions of a ligand.

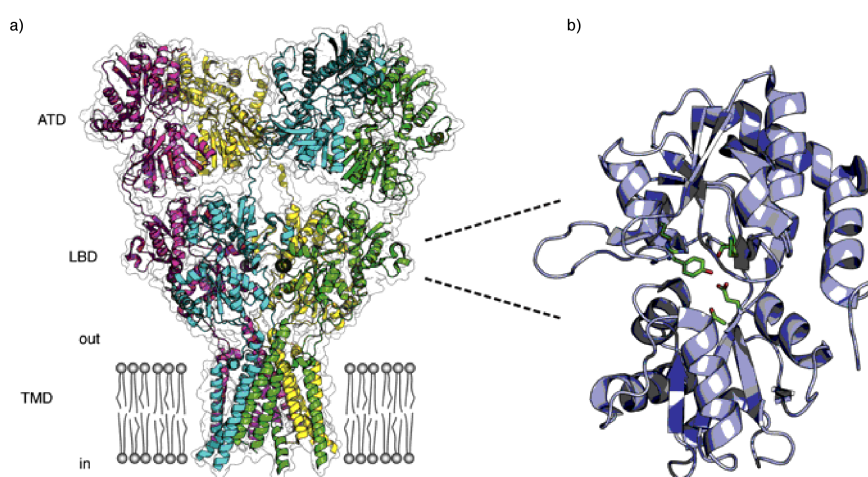


**Figure 3.** a) Overall structure of iGluRs exemplified by GluA2 (pdb 3KG2). b) Close-up of a clamshell with important residues highlighted (GluA2 S1S2 from pdb 1FTM)

#### 4. The binding mode of endogenous ligands: Glutamate, glycine and D-serine

The binding-mode and conformation of glutamate is highly conserved in AMPA, kainate and NMDA receptors (Fig. 4). The most conspicuous interaction is a salt-bridge between a positively charged arginine side-chain protruding from the roof of D1 and the negatively charged C1-carboxylate of glutamate (**A** in Fig. 4c). This interaction is found in all functional eukaryotic iGluRs and mutation of the Arg residue leads to complete loss of channel function.<sup>[77]</sup> The protonated alpha-amino group of the ligand primarily interacts with a conserved glutamate residue at the C-terminal end of an antiparallel beta sheet on the D2 lobe (**D** in Fig. 4c). Conservative mutants wherein this residue is replaced with an aspartate have much lower affinity for the neurotransmitter.<sup>[78], [79], [80]</sup> Together, these highly conserved residues form what we call the “amino acid clamp”, which brings the two lobes of the clamshell together upon binding of the ligand (Fig. 4b). In addition to these primary interactions, there is an aromatic residue on D1 that forms the ceiling of the binding site and is in hydrophobic contact with the beta-methylene (*C*-3) of glutamate and its derivatives (**B** in Fig. 4c). This residue is a tyrosine in all structurally characterized AMPA/kainate receptors, a phenylalanine in GluN1 and a histidine in GluN2A. A hydrogen bond involving the ligand’s ammonium group and the backbone carbonyl of a proline residue provides additional affinity to the D1 lobe (**C** in Fig. 4c).

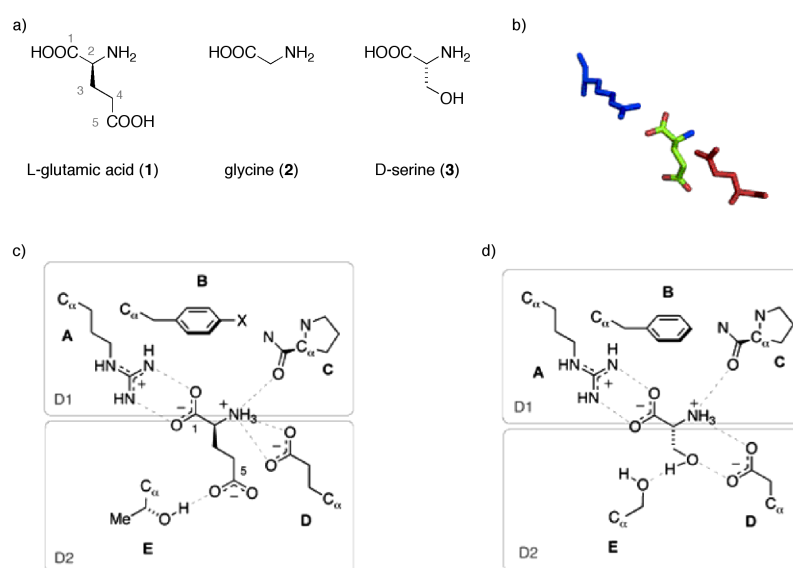


**Figure 4.** a) Endogenous ligands for AMPA, kainate and NMDA receptors. b) The amino acid-clamp. c) Schematic diagram of the major interactions of glutamate with residues on D1 and D2. d) Schematic diagram of the glycine and D-serine binding site.

On the other side, the C-5-carboxylate of the glutamate ligand mostly interacts with a threonine residue that sits at the C-terminal end of the so-called “helix F” in the D2 lobe. In all structurally characterized iGluRs (with the exception of GluR0), this helix features a Ser-Thr or Ala-Thr motif at its tip (**E** in Fig. 4c). Interestingly, the helix dipole is oriented with its positive end toward the negatively charged carboxylate of glutamate or corresponding bioisosteric groups in agonists.

Glycine and D-serine bind to the GluN1 and GluN3 LBDs in a very similar manner (Fig. 4d). The canonical amino acid-clamp is present, save that the glutamate in position **D** is replaced by an aspartate (*cf.* pdb 1PB7). The aromatic lid is a phenylalanine side chain and the proline backbone-carbonyl interacts with the ammonium group as usual. The helix dipole of helix F now points toward the alpha amino carboxylate. Overall, this creates a more compressed binding pocket, in accordance with the smaller ligands it accommodates. The hydroxymethyl side chain of D-serine, which has been recently identified as an endogenous ligand released by glial cells,<sup>[81]</sup> interacts with the serine side chain that is part of the Ser-Thr motif on top of this helix (*cf.* pdb 1PB8).

## 5. Binding modes of agonists and antagonists

A large number of agonists and antagonists bound to iGluR LBDs have been crystallized and several trends can be deduced from these data. Generally, agonists bind deeply within the cleft of the clamshell and allow the clamshell to close to a large degree. The degree of clamshell-closure more or less correlates with the efficacy of the agonists (Fig. 5).<sup>[11]</sup> Accordingly, partial agonists, such as substituted willardiines (for AMPA receptors) or domoic acid (for kainate receptor), close the clamshell to a lesser degree than full agonists. This is a somewhat simplified picture since the ligand-induced response and coupling to the TMD is complex, the clamshells function as dimers of dimers, and heteromultimeric iGluRs must be taken into account. It should be noted that in partially closed LBDs there are several “exit tunnels” that allow substituents to protrude between the lips.

By contrast, competitive antagonists strongly bind to interaction sites **A-C** on D1 and to a lesser extent to residues on D2. In most cases, they literally pry the clamshell open (Fig. 5b).<sup>[11]</sup> This “foot in the door” mechanism explains how relatively minor changes can turn an agonist into an antagonist and provides a general paradigm for antagonists in clamshell-containing receptors.

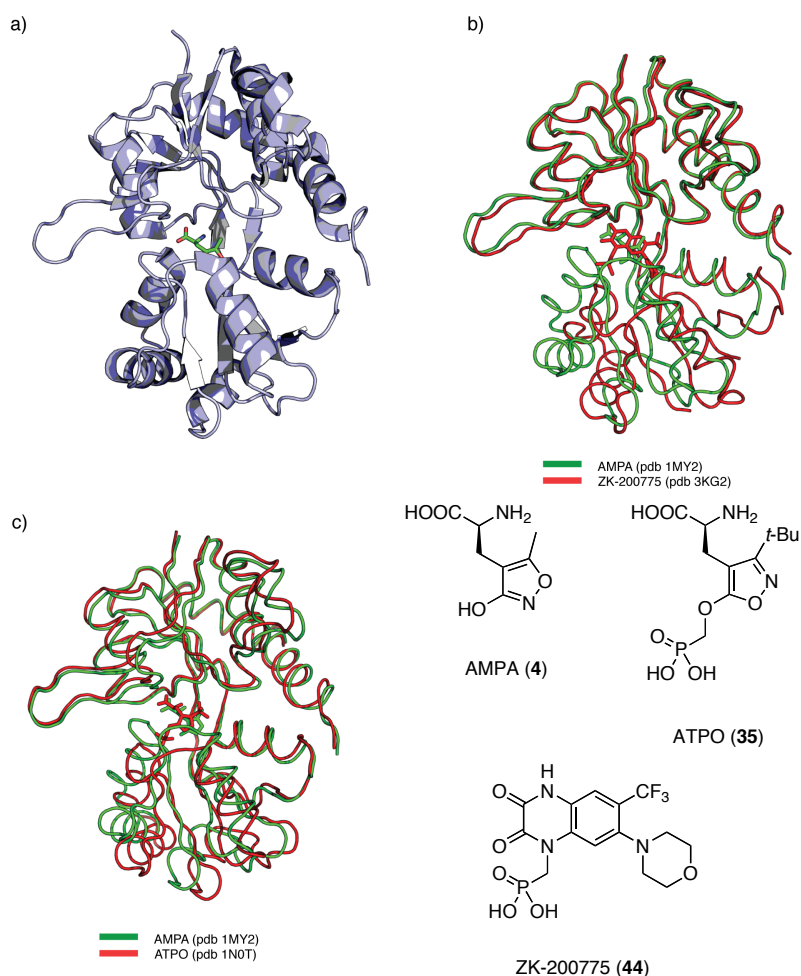


**Figure 5.** a) Binding mode of a typical agonist, AMPA, to GluA2 (pdb 1MY2) . b) The foot-in-the-door mechanism of antagonism. Structure of the GluA2 LBD bound to AMPA (pdb 1MY2), a selective agonist, overlaid with the LBD bound to ZK-200775 (44), a selective antagonist (pdb 3KG2). c) Structure of the GluA2 LBD bound to glutamate (pdb 1MY2) overlaid with the GluA2 LBD occupied by the AMPA-derived antagonist ATPO (pdb 1N0T).

## 6. Agonists for AMPA/kainate receptors

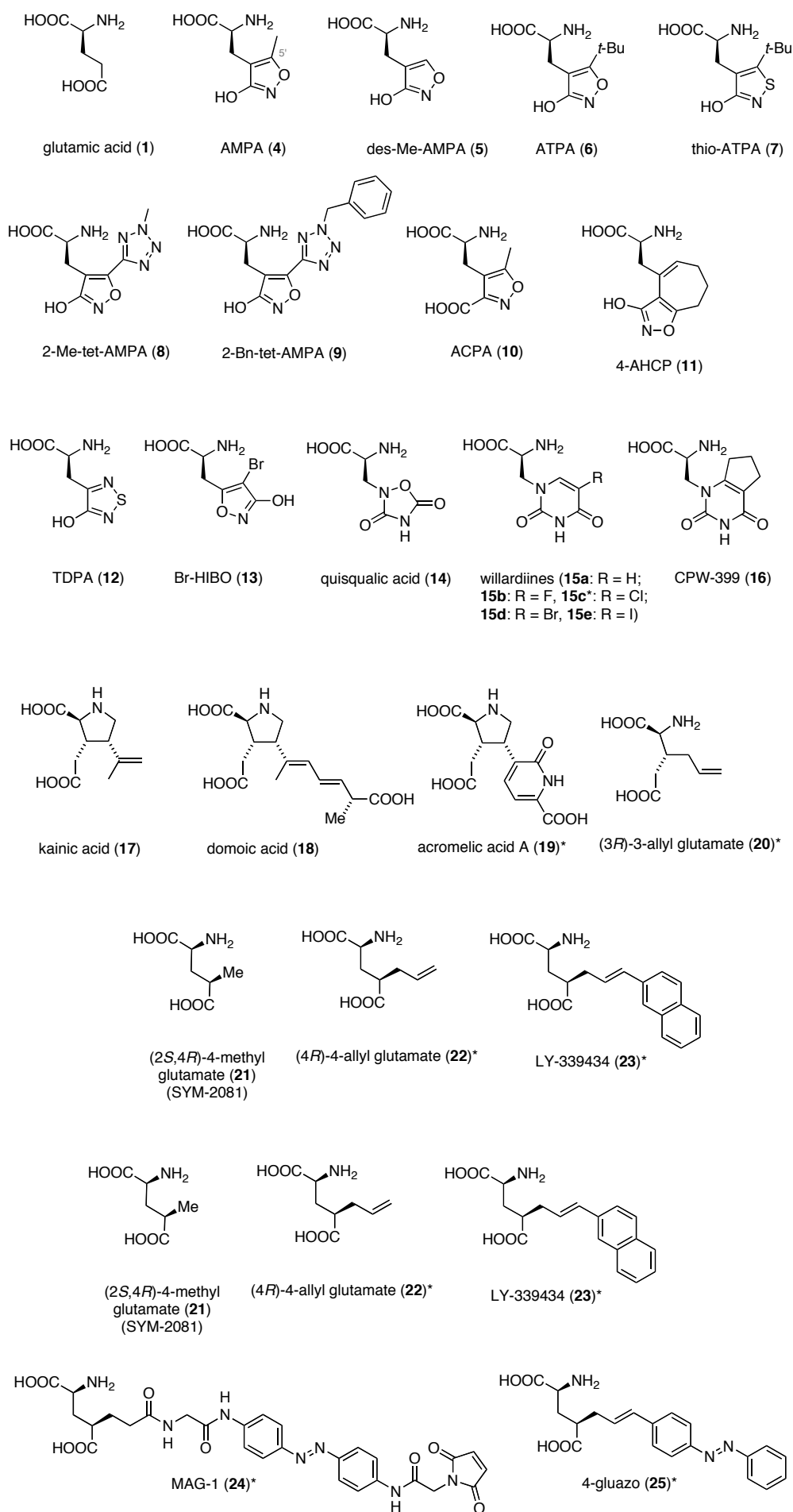
Structurally, agonists and partial agonists of AMPA and kainate receptors are more or less directly derived from glutamate. They invariably feature the alpha-amino acid moiety of the neurotransmitter and bind to the amino acid-clamp in the canonical fashion (cf. Fig. 4b,c). Their other end interacts with helix F and other residues of D2, sometimes mediated by water molecules. There is considerable structural variety with respect to this part of the molecules and there are several positions where the parent glutamate backbone can be substituted without losing agonist activity. The configuration at these positions is crucial and can be easily explained by the available X-ray structures.

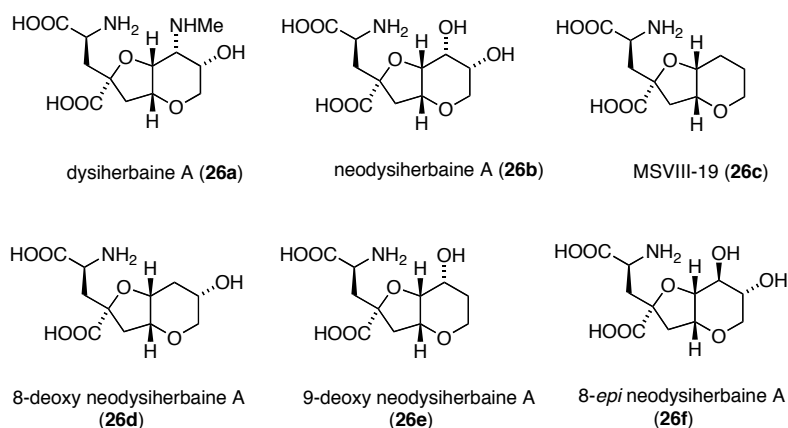


Figure 6 provides an overview of agonists for AMPA-kainate receptors, which can be classified as follows:

a) Glutamate derivatives wherein C-4 and C-5 have been replaced by flat, conformationally rigid heterocycles (Fig. 6; **2-16**). All of these compounds bind with their alpha-amino moiety in the usual fashion and interact with helix F on D2 with their heterocyclic moieties (**E** in Fig. 4). These are in most cases negatively charged and function as bioisosters of the C-5-carboxylate. The classical agonist AMPA (**4**) and its derivatives (**5-10**), as well as 4-ACP (**11**), TDBA (**12**), bromo-HIBO (**13**), and the natural products quisqualic acid (**14**) and willardiine (**15a**) belong to this class. A series of substituted willardiines has been prepared with increasingly bulky halogen substituents (**15b-e**). These progressively lose potency as the substituents prevent closure of the clamshell to an increasing degree.<sup>[23]</sup>

Many derivatives of AMPA have been synthesized and the structure-activity relationships of this class of agonists are well defined. The isoxazole ring can be substituted with a variety of residues at position 5', which can even result in selectivity within receptor families. For instance, the bulky *tert*-butyl substituent on the heterocycle in ATPA (**7**) provides very high selectivity for GluK1.<sup>[82]</sup> Bn-Tet-AMPA, which has a slimmer and more elongated substituent, was found to be selective for GluA2-4.<sup>[33]</sup> The benzyl substituent of the latter substituent protrudes into a region of the clamshell that is not occupied by other agonists (*cf.* pdb 2P2A). ACPA (**10**) and 4-AHCP (**11**) are expanded and enlarged versions of AMPA that still function as agonists.





**Figure 6.** Chemical structures of AMPA/kainate receptor agonists. Compounds marked with an asterisk have not yet been crystallized with their receptors.

b) L-Glutamate derivatives wherein C-3 has been substituted and is D-configured (Fig. 6; **17-20**). Compounds of this type often feature a secondary amine as part of a pyrrolidine ring and resemble the natural excitotoxin kainic acid (**17**), which is in itself a conformationally rigidified version of glutamate. Interestingly, the selectivity of kainic acid itself for kainate receptors is rather poor. Indeed, X-ray structures exist for kainic acid bound to GluA2 and GluK2 (pdb 2ANJ and 1TT1). The natural products domoic acid (**18**) and acromelic acid (**19**) are kainic acid derivatives with elongated and heterocyclic side chains, respectively. Only **18** has been cocrystallized with the GluK1 and GluK2 LBDs but it is unlikely that acromelic acid A (**19**) and its many natural and synthetic variants<sup>[83]</sup> will yield surprises. Interestingly, the long unsaturated side chain of the partial agonist **18** protrudes out of the closed clamshell of GluK2 and is partially solvent exposed (pdb 1YAE). Simple glutamate derivatives alkylated in position 3, such as **20**, have been barely explored structurally although the pharmacological profile of **20** looks promising.<sup>[84]</sup> Similarly, *N*-substituted derivatives of L-glutamate, such as *N*-methyl-L-glutamate, have not been systematically evaluated to date,<sup>[85]</sup> although the crystal structures suggest that some substituents could be tolerated.

c) Compounds wherein C-4 of glutamate has been substituted and is L-configured (Fig. 6, **21-26**). These glutamate derivatives, such as 4-methyl glutamate (**21**) or LY-339434 (**23**), are often selective for kainate receptors.<sup>[84]</sup> Their substituents at C-4 point towards the cleft of the clamshell and can be quite large. They have guided the development of several azobenzene derivatives (*e.g.* L-MAG1 **24**, and 4-GluAzo, **25**), which have been used to convert iGluRs into photoreceptors.<sup>[86]</sup> The extremely potent seizurogenic natural product dysiherbaine A (**26a**) and its natural and semisynthetic derivatives (**26b-f**) also belong to this class, demonstrating that the glutamate scaffold can tolerate a quaternary center at the C-4

position. The relatively complex heterobicyclic ring system of the dysiherbaines is deeply buried in the LBD of GluK1 (*e.g.* pdb 3FV1) and its exact composition determines selectivity for GluK1 *vs.* GluK2.<sup>[10c]</sup>

Fig. 7 shows the conformation of bound glutamate and several agonists in a Newman projection along (C-2)-(C-3). It is apparent that this conformation is highly conserved and the (C-1)-(C-2)-(C-3)-(C-4) dihedral angle is always close to 180° with all agonists and in all receptors. By contrast the (C-2)-(C-3)-(C-4)-(C-5) dihedral angle varies to a larger degree and is *ca.* 60° for glutamate and *ca.* 90° for kainate, respectively, in GluA2 (pdb 1FTJ, 2ANJ).

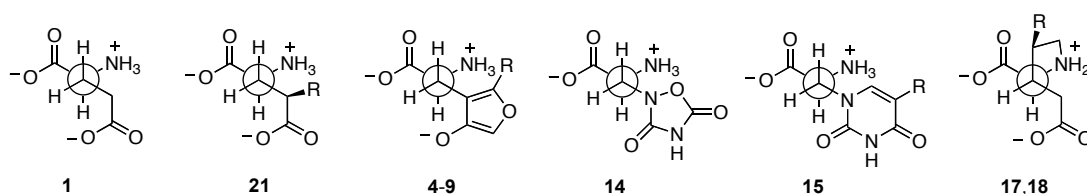


**Figure 7.** Conformation of selected agonists in the binding site.

Despite the large number of agonist-bound X-ray structures, it is difficult to come up with selectivity rules for AMPA *vs.* kainate receptors, in accordance with their diminishing pharmacological discrimination. Looking at the structure of selective agonists bound to their receptor LBD, it seems that kainate receptors can “chew a bigger chunk”. However, when the structures of GluA2 and GluK1 bound to the same ligand are overlaid, there seems to be little difference with respect to the peptide backbone (glutamate: pdb 1FTJ and pdb 3FUZ, kainate: pdb 1FW0 and pdb 1TT1). Therefore, selectivity has to be assessed on a case-to-case basis and the exact arrangement of non-conserved residues lining the clamshell cleft has to be taken into account. For instance, specific residues have been identified that confer selectivity *e.g.* for ATPA to GluK1<sup>[82b]</sup> and for Bn-tet-AMPA (**9**) to GluA2-4.<sup>[33]</sup>

## 7. Agonists for NMDA receptors

Selective agonists of NMDA receptors are usually simple amino acids or amino acid derivatives. Of course, one needs to distinguish between compounds that primarily target the glycine sites (GluN1 or GluN3) and those that bind preferentially to the glutamate sites (GluN2), with their various subtypes. Whereas a wide range of agonists for glycine sites have been crystallized together with their receptor LBDs (**3**, **27**, **29-31**, Fig. 8), there are only two structures of the glutamate site (GluN2A), both with glutamate itself (pdb 2A5T, 2A5S). None of the well-established synthetic agonists shown in Fig. 9 have been crystallized with their

receptors. In particular, there is no structure to date featuring NMDA (**32**), which would be useful in explaining the high selectivity of the eponymous ligand.

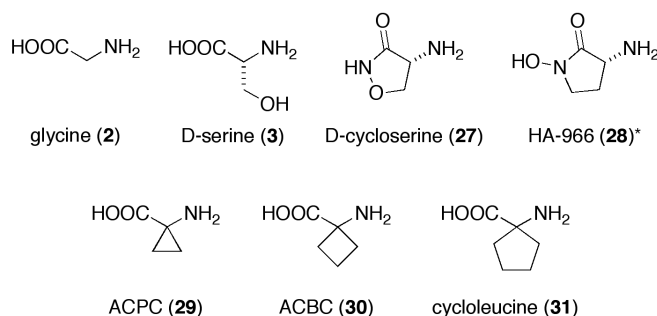


**Figure 8.** Agonists targeting the glycine site of NMDA receptors (GluN1 and GluN3). Compounds marked with an asterisk have not yet been crystallized with their receptors.

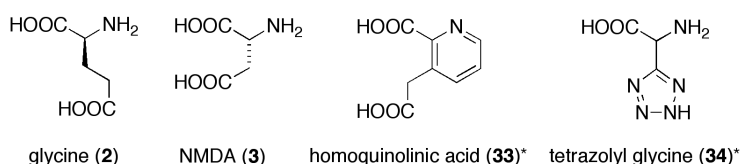


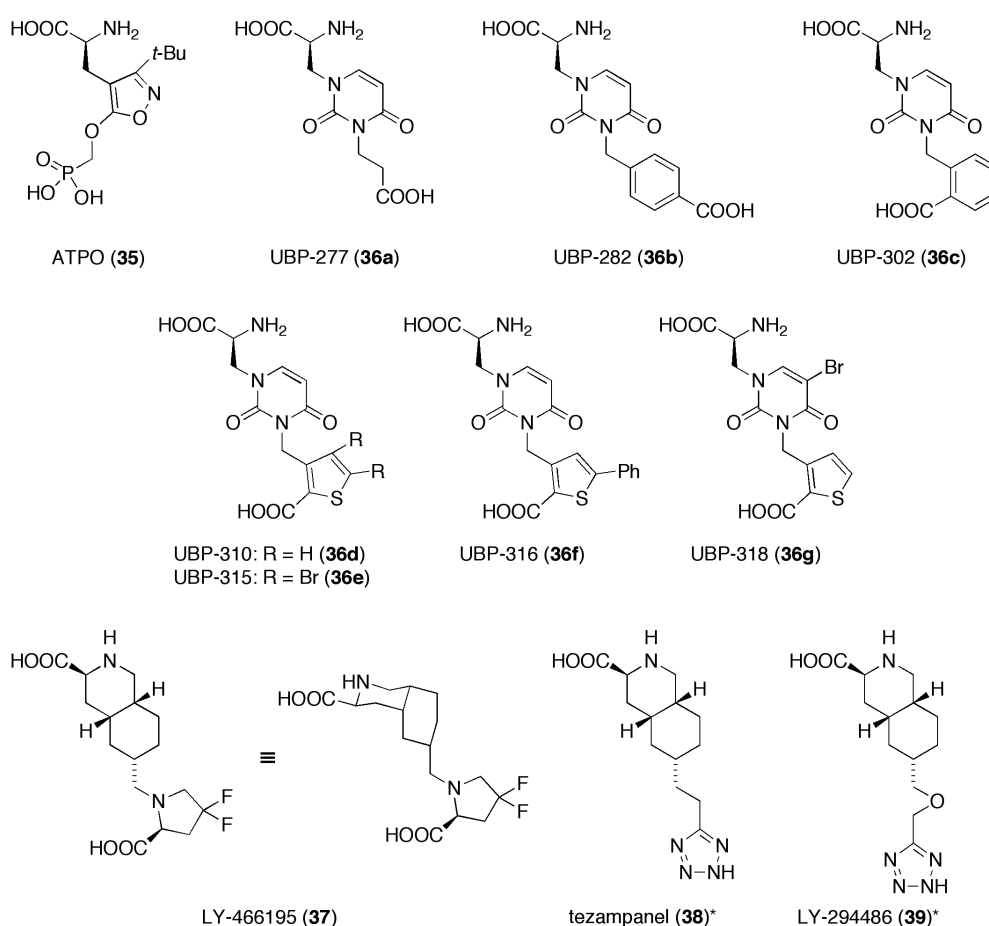
**Figure 9.** Agonists targeting the glutamate site of NMDA receptors (GluN2). Compounds marked with an asterisk have not yet been crystallized with their receptors.

## 8. Antagonists for AMPA/Kainate receptors

Antagonists of AMPA and kainate receptors show a much wider structural variety than agonists and can belong to one of two major structural classes (Fig. 10):

a) Expanded versions of agonists (Fig. 10; **35–39**). These bear the canonical alpha-amino acid motif of agonists but have their negatively charged other end moved further away. As elongated molecules, they still interact with the amino acid-clamp and the top of helix F thus prying the clamshell open. The phosphonate ATPO (**35**), derived from ATPA, and the willardiine derivatives **36a–g** are typical representatives of this category. A number of kainate receptor-selective *cis*-decahydroisoquinolines, such as LY-466195 (**37**), tezampanel (**38**) or LY-294486 (**39**), also belong to this group. They are, in a sense, ring-expanded and homologated versions of kainic acid. LY-466195 (**37**) has been crystallized together with GluK1 and shows the typical amino acid-clamp binding and interaction with helix F in the largely open clamshell (pdb 2QS4).

b) Quinoxalines (Fig. 10; **40-46**). These are classical antagonists of AMPA receptors, represented by DNQX (**40**) and its congeners CNQX (**41**), NBQX (**42**), YM-90K (**43**) and ZK-200775 (**44**). Quinoxaline antagonists interact with the canonical D1-arginine but do not appear to make much contact with the conserved D2-glutamate residue. The “aromatic lid” on the S1 lobe of the receptor (usually a tyrosine) stacks tightly against the flat and conformationally rigid aromatic core of these antagonists (*e.g.* pdb 1LB9). With the exception of the high affinity antagonist ZK-200775 (**44**), which contains an additional phosphonate moiety, the quinoxalines do not appear to interact strongly with the top of helix F or any other residue in D2 but they do form hydrogen bonds to the backbone carbonyl of the highly conserved proline residue on D1. A special case is the quinoxaline FQX (**46**), which is one of the photoproducts of the azide ANQX (**45**). ANQX was developed as a photoaffinity-label and used to study AMPA-receptor trafficking.<sup>[87], [88]</sup>



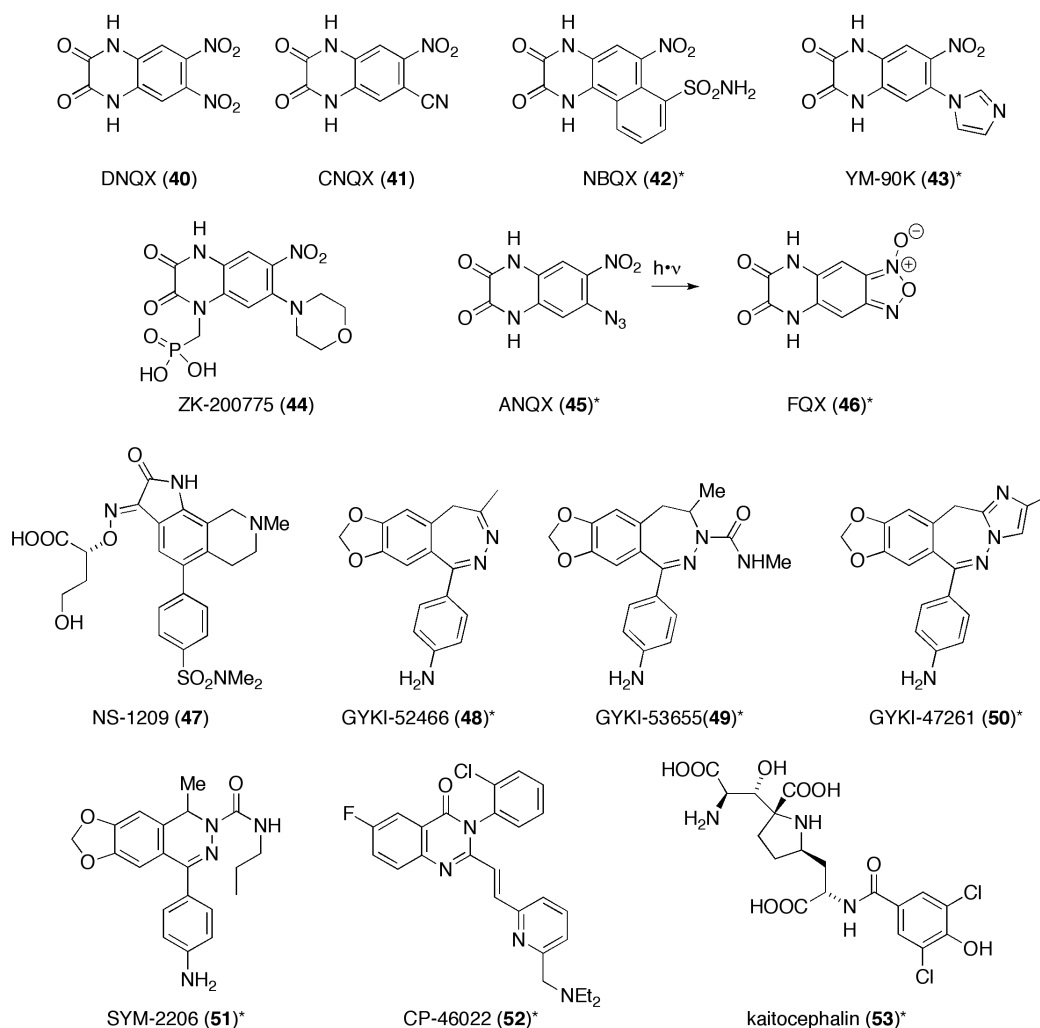


**Figure 10.** Chemical structures of AMPA/kainate receptor antagonists. Compounds marked with an asterisk have not yet been crystallized with their receptors.

In addition to this, there is one structural outlier, NS-1209 (47), which has been crystallized together with glutamate in a GluA2 clamshell dimer (pdb 2CMO). The carboxylate and the oxime ether nitrogen of this clinically interesting antagonist interact with the D1 arginine, whereas the central aromatic ring stacks tightly against the lid-tyrosine.

To date, there are no crystal structures available for 2,3-benzodiazepines, such as GYKI-52466 (48), GYKI-53655 (49), or GYKI-47261 (50), which are highly selective antagonists of AMPA/kainate receptors. These compounds, as well their congeners SYM-2206 (51) and CP-46022 (52), are non-competitive antagonists and presumably bind to an allosteric site on the receptor. Unfortunately, there is also currently no structure featuring the natural product kaitocephalin (53), which has been characterized as an AMPA receptor antagonist but is also a potent inhibitor of NMDA receptors.<sup>[89], [90]</sup> As a twofold D-amino acid and an L-amino acid with a quaternary stereocenter and a benzoyl residue it would be very interesting to see how (or if) this compound binds to the clamshell.

## 9. Antagonists for NMDA receptors

A large number of antagonists targeting NMDA receptors have been developed in academia and industry but only one of these has been crystallized together with its receptor: 1,3-Dichlorokynurenic acid (**55**) binds to the GluN1 clamshell and interacts with the conserved arginine and the proline carbonyl, but makes few polar contacts otherwise (Fig. 11; pdb 1PBQ). It stacks against the aromatic lid (a phenylalanine) and appears to be stabilized by the helix-dipole of helix F. The compound is a halogenated derivative of the tryptophan metabolite kynurenic acid (**54**), which was initially isolated from the urine of dogs by Justus von Liebig.<sup>[91]</sup> There are no structures featuring the very potent antagonist L-689560 (**56**) or the quinoxaline derivative CGP-78608 (**57**). It should be noted that quinoxalines more commonly associated with AMPA receptors, such as CNQX (**41**), also target the glycine site of NMDA receptors.<sup>[92]</sup>

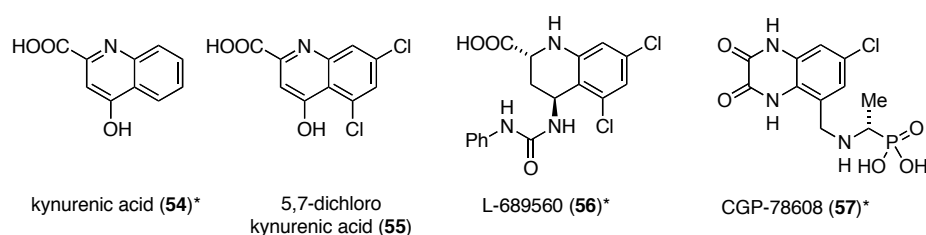


**Figure 11.** Antagonists targeting the glycine site of NMDA receptors (GluN1 and GluN3). Compounds marked with an asterisk have not yet been crystallized with their receptors.

Unfortunately, no structures are available for antagonists bound to the glutamate binding-site of NMDA receptors, in particular the widely used antagonist AP-5 (**58**) and its congeners **59** and **60** (Fig. 12). The NMDA-receptor selectivity of these aminophosphonates is presently difficult to understand.

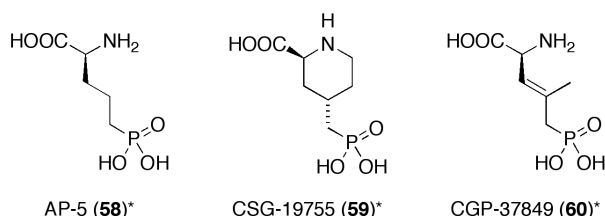


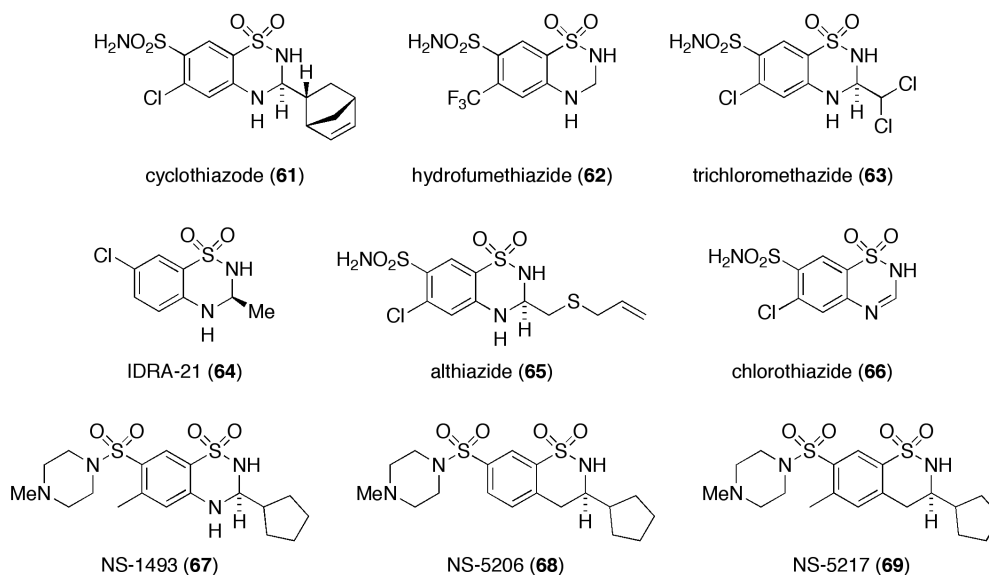
**Figure 12.** Antagonists targeting the glutamate site of NMDA receptors (GluN2). None of these have been crystallized with their receptors.



## 10. Modulators and channel blockers of iGluRs

Like most ion channels, iGluRs desensitize following prolonged activation. This event takes place relatively rapidly (within milliseconds) in AMPA/kainate receptors but requires more time (tens to hundreds of milliseconds) in NMDA receptors.<sup>[5]</sup> Due to its important role in physiology, desensitization has been studied in great detail and many modulators have been developed.<sup>[32]</sup> There are several crystal structures of GluA2 receptor LBDs that have helped define the mechanism of desensitization (Fig. 13). Modulators generally bind to the LBD interface between the D1 lobes, thus inhibiting or slowing down their separation in the course of desensitization.

Modulators display a wide structural variety but certain chemotypes can be identified (Fig. 13): a) Benzothiadiazine derivatives, such as cyclothiazide (**61**), and its congeners **62-69**; b) linear sulfonamides, *e.g.* the *C*<sub>2</sub>-symmetrical *bis*-sulfonamide **70**, LY-404187 (**71**) and PEPA (**72**); and c) pyrrolidones and acyl pyrroles, *e.g.* piracetam (**74**), aniracetam (**75**) or CX-614 (**76**). The structure of cyclothiazide (**61**) bound between the D1-lobes of two clamshells is shown in Fig. 14.



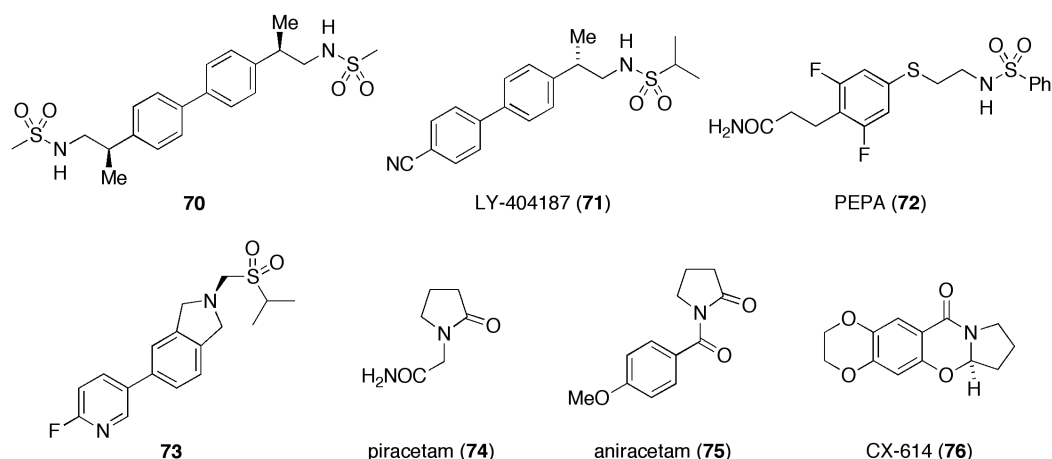


**Figure 13.** Modulators of AMPA receptors.

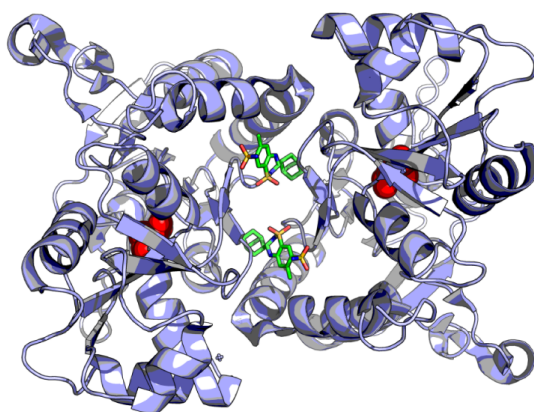


**Figure 14.** Structure of cyclothiazide (**61**) bound to an LBD dimer (pdb 3H6T). The clamshell dimer is seen from the intracellular side and bound glutamate is displayed as red spheres.

With only one structure of an iGluR featuring a TMD available (pdb 3KG2), it comes as no surprise that the binding-sites of NMDA-receptor blockers, such as MK-801 (**77**), phencyclidine (**78**), ketamine (**79**) or the recently discovered natural product lophocladine A (**80**)<sup>[93]</sup>, have not yet been structurally characterized (Fig. 15).

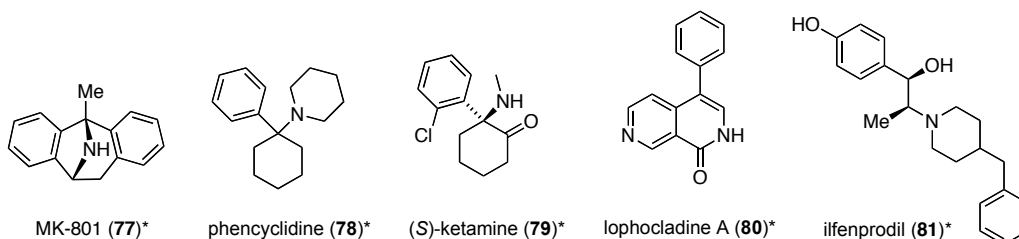


**Figure 15.** Compounds that block the TMD of the NMDA receptors or target the ATD of iGluRs. None of these have been crystallized with the TMD or ATD.

However, since blockers of fourfold-symmetrical potassium channels are amenable to structural studies,<sup>[94]</sup> it seems possible that we will soon understand how these important blockers operate. Related structural studies could also explain the voltage-dependent block of NMDA receptors by  $Mg^{2+}$  and of non-NMDA receptors by spermine. Finally, several structures of the ATD of iGluRs have been published (Table 1) but, to date, none of these feature a functionally important ligand, such as  $Zn^{2+}$ , a polyamine, or the developmental drug ifenprodil (**81**) which interacts with GluN3 and functions as an NMDA receptor antagonist.<sup>[95]</sup>

## 9. Conclusion

Almost 150 structures of agonists, antagonist and modulators bound to LBDs of iGluRs, as well as several *apo* structures, are now available and many more can be expected in future years (Table 1). Hopefully, crystal structures of GluA1 and GluK3-5 or a full-fledged NMDA receptor will soon emerge in this rapidly moving field. Structural studies of the C-terminal domain of iGluRs could help answer questions regarding receptor localization and modulation. On the ligand side, we are still missing coordinates for several important and interesting agonists and antagonists (*e.g.* NMDA, AP-5, kaitocephalin, 4-GluAzo, GYKI-52466). Nevertheless, we are beginning to understand which molecular features determine subtype-selectivity as far as this is possible using detailed but static crystal structures. After all, one should bear in mind that affinities, let alone efficacies, cannot be reliably calculated with our current techniques, even when multiple crystal structures are available for calibration and comparison. However, the existing crystal structures provide guidance where to substitute known ligands (*e.g.* glutamate itself, AMPA, or kainate) to achieve the desired effect. They certainly offer a rationale for the development of new and possibly more selective agonists and antagonists, exploiting spaces in the clamshell and its cleft that have not been occupied by existing types and interactions with non-conserved amino acid residues that have not been addressed. The design of ligands with new functional properties, *e.g.* responsiveness to light, will also benefit from continued structural studies. Finally, this wealth of structural information could allow for the design of orthogonal receptors that cease to respond to the natural agonists but can be activated by unnatural, orthogonal ligands.

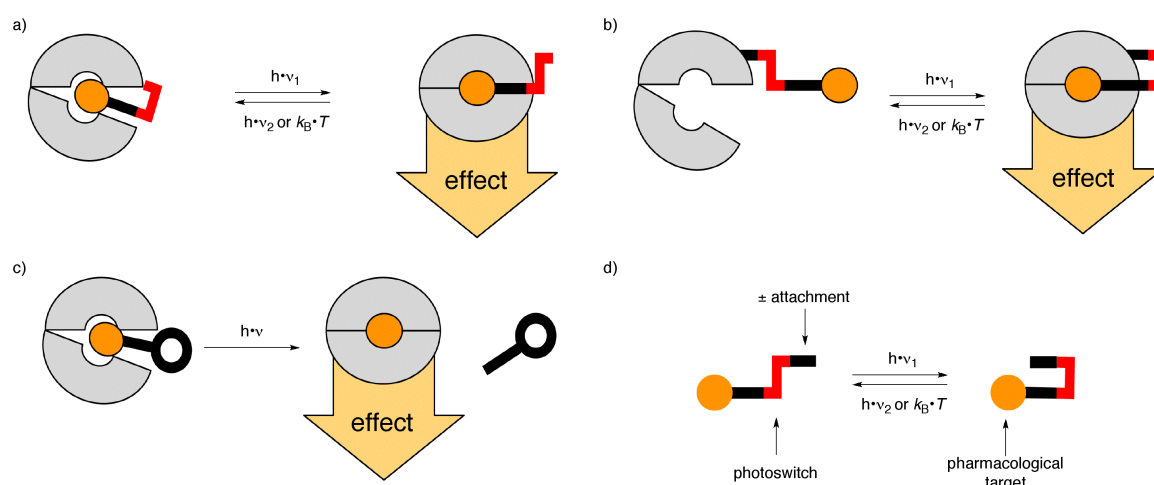
## **10. Acknowledgements**

We thank the Center for Integrated Protein Studies, Munich (CIPSM) and the Munich School of Neuroscience (MSN) for financial support. P.S. is grateful to the Fond der Chemischen Industrie for a Kekulé Scholarship. We also thank Dr. Martin Sumser and Dr. Eddie Myers for helpful comments.

### 3) Photocontrol of Glutamate Receptors – The PCL and PTL Concepts

Given the wealth of structural information presented in the previous chapter, one can easily be misled to believe, that the design of more selective drugs acting on iGluRs has become an easy task. Admittedly, both ligand- and structure-based approaches have been facilitated by the plethora of x-ray structures and pharmacologically described ligands, but at the same time it has become evident, that the interactions of iGluR and ligand are highly sensitive toward manipulation. As such, even with modern, computer-based approaches like docking, attempts to synthesize new ligands still can fail. Unfortunately, such results are rarely published,<sup>[96]</sup> even though they nicely highlight the limitation of the aforementioned methods.

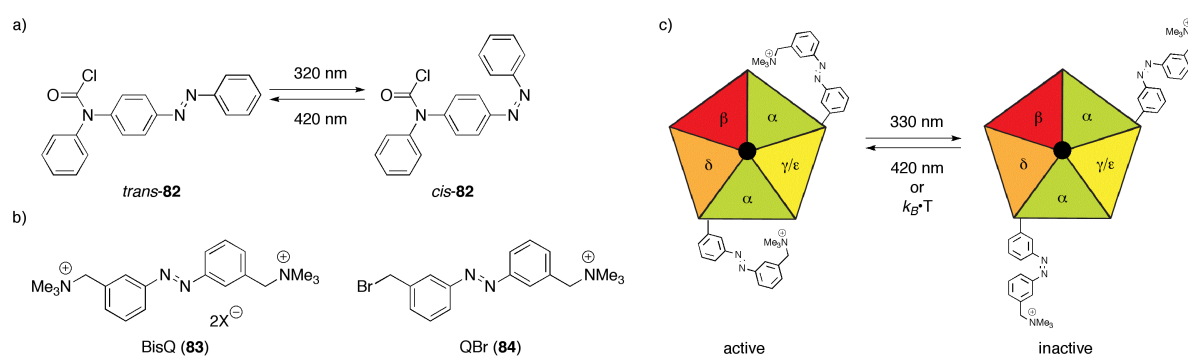
It is our believe, that in addition to ligand- and structure-based approaches, a detailed understanding of molecular function, based on atoms themselves, is a prerequisite for success in chemical biology in general and in the research of ionotropic glutamate receptors in particular. Therefore, chemical and biological education go side-by-side in our group, which has a longstanding interest to provide neuroscience with new chemical tools for the dissection of neuronal networks. With great success we have developed both photochromic and photoswitched tethered ligands (PCLs and PTLs), which have been used in a variety of applications.<sup>[86b, 97]</sup> The concept of these two photosensitization strategies, as well as the general make-up of a photoswitch are illustrated in Scheme 1.



**Scheme 1.** Three different photosensitization strategies: a) the photochromic ligand (PCL), b) the photoswitchable tethered ligand (PTL) and c) the caged ligand (CL) approach. d) The general make-up of a PCL/PTL.

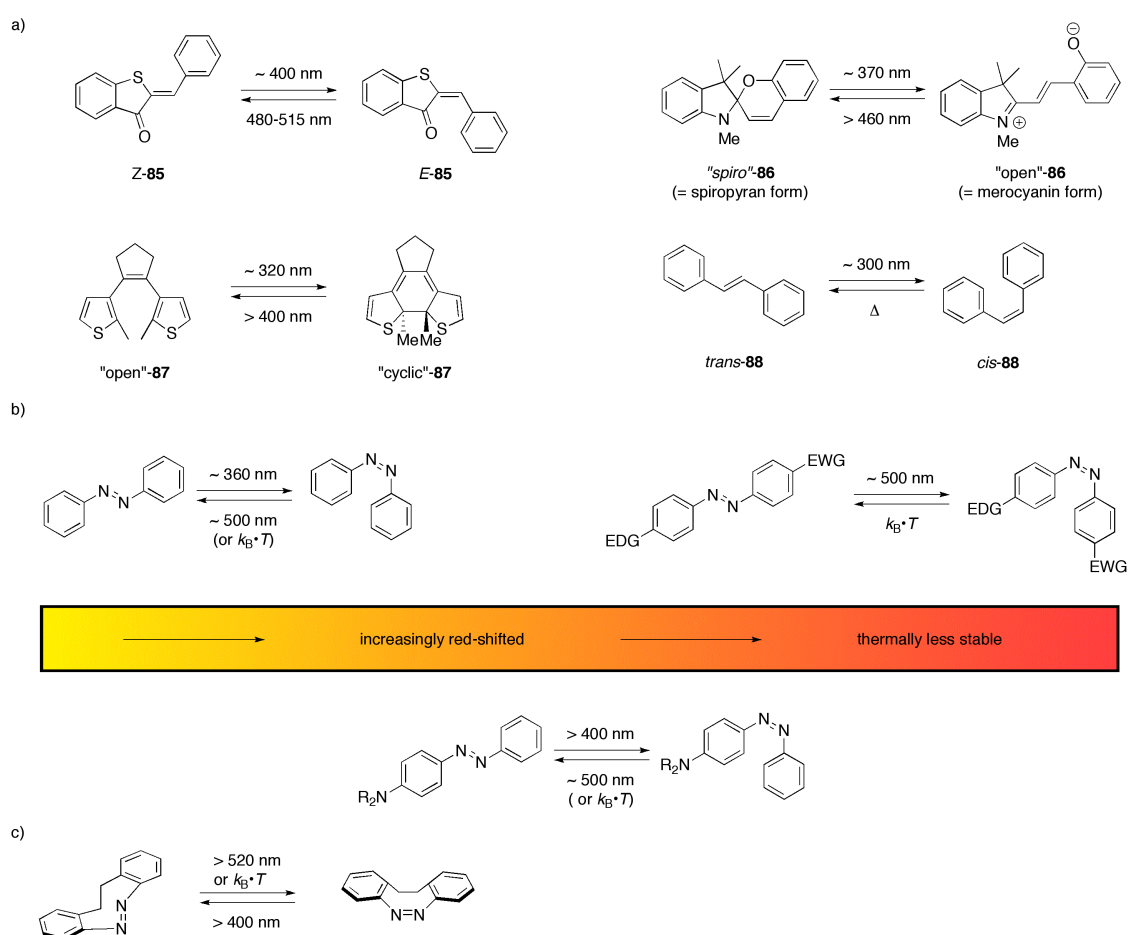
The design of PCLs and PTLs is simple: a pharmacologically active molecule is fused to a suitable photoswitch, which allows the resulting conjugate to change its affinity and/or efficacy to the biological target upon irradiation with light. In PTLs, the photoswitch is connected to an additional group, which allows covalent linking of the photoswitchable ligand to the target protein (Scheme 1a,b,d). To this end, suitable attachment-sites either have to be present in the receptor or have to be introduced by genetic manipulation. In contrast to the classical method of photosensitization by caged molecules (Scheme 1c),<sup>[98]</sup> the PCL/PTL concept offers the advantage of reversibility, *i.e.* PCLs and PTLs essentially act as “reversibly caged” molecules. Unlike other strategies to induce biological effects with light (photosensitive proteins,<sup>[6a, 99]</sup> crosslinking of protein structures with photoswitches,<sup>[100]</sup> or incorporation of unnatural, photoswitchable amino acids)<sup>[101]</sup> this method only requires a minimum of manipulation of both target protein and cell. For PCLs, selectivity can be achieved just by variation of the pharmacologically active group and for PTLs either innate attachment-sites present in the native receptor, or single-point mutations can be used to provide suitable sites for bioconjugation.<sup>[102]</sup>

A seminal work by Erlanger in 1968 introduced azobenzenes as the photoswitchable unit of choice for photochromic ligands.<sup>[103]</sup> They fused diphenylcarbamyl chloride, a potent inactivator of chymotrypsin, to the diazobenzene unit in order to yield carbamyl chloride **82** that light-dependently inactivates chymotrypsin (Scheme 2a). Later, they synthesized the first PCL and the first PTL of nicotinic acetylcholine receptors (nAChRs) called BisQ (**83**) and QBr (**84**).<sup>[104]</sup> These quaternary ammonium ions (Scheme 2b) act by binding to the acetylcholine binding-site of nAChRs, a class of pentameric ligand-gated ion channels. The PTL-version, QBr (**84**), was covalently attached to a native cysteine residue close to the active site after reduction of the extracellular cysteins.



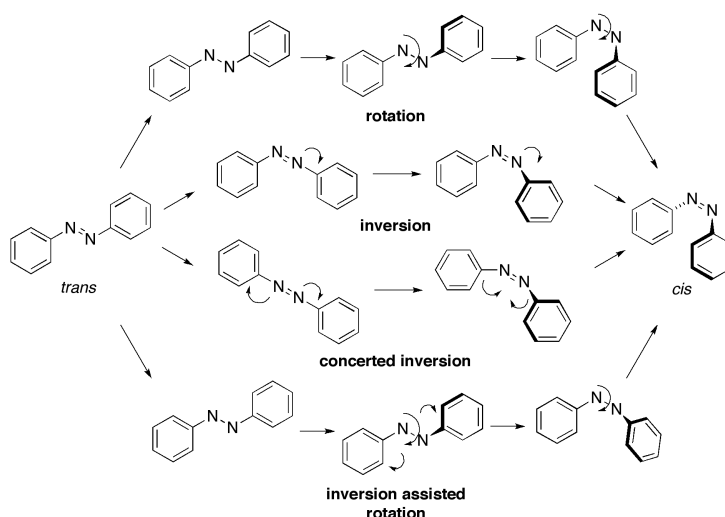
**Scheme 2.** a) Switching of PADPCC (**82**), a light-dependent inactivator of chymotrypsin. b) BisQ (**83**) and QBr (**84**) the first PCL and PTL of nAChRs. c) Schematic mode of action of **84** on nAChRs.

Since Erlanger's groundbreaking work, diazobenzenes have proven themselves as suitable photoswitchable units for biological application, even though they are not the only small molecules capable of this task. Hemithioindogols (**85**), spiropyrans (**86**), 1,2-dithienylethenes (**87**) and stilbenes (**88**) are some alternatives to azobenzenes and in some aspects like switching-speed, absorption coefficients, or toxicity problems they can even outperform them (Scheme 3a).<sup>[105]</sup> Yet we and others have generally found diazobenzenes to be a good choice for PCLs and PTLs,<sup>[106]</sup> since they are easily substituted, stable under a variety of chemical transformations (*e.g.* Pd-catalyzed couplings, acids, bases, oxidations and reductions), exert a strong mechanical force upon photoisomerization and show high quantum yields (up to 0.6 for the *cis-trans* isomerization).<sup>[107]</sup> In general, there are four types of azobenzenes: regular (*i.e.* scarcely substituted), amino-, pseudo-stilbene- (*i.e.* push-pull substituted) and cyclic azobenzenes (Scheme 3b-c).<sup>[108]</sup>



**Scheme 3.** a) Assorted photoswitchable molecules. b) Spectral and photophysical properties of increasingly red-shifted azobenzenes. c) Cyclic, *i.e.* thermally *cis*-stable azobenzenes.

The photophysical properties of these chromophores are highly dependent on their substitution pattern. While for regular (and for tetra-*ortho* substituted) azobenzenes the *trans* and the *cis* state are reasonably stable and even can be separated,<sup>[109]</sup> for aminoazobenzenes and the pseudo-stilbene (push-pull) type, the *cis* state becomes thermally less stable and the absorption spectra are substantially redshifted.<sup>[108]</sup> For biological applications this is of course highly desired, since it allows for the use of visible light instead of UV to promote the isomerization, which however comes at the cost of having to rely on thermal relaxation from the *cis* to the *trans* form. This is due to their interesting mode of photoisomerization. In general, *trans*-azobenzenes adopt a planar structure with  $C_{2h}$  symmetry, while *cis*-azobenzenes prefer a non-planar conformation with  $C_2$  symmetry (Scheme 4).<sup>[110]</sup> There are four possible modes of interconversion between the *trans*- and *cis*-state (Scheme 4). It is generally accepted however, that the *trans* to *cis* isomerization proceeds *via* an inversion from the  $S_1$  state. For the *cis* to *trans* interconversion studies seem to suggest a rotational pathway for the photoisomerization and inversion for thermal relaxation.<sup>[108]</sup> The UV absorption spectra of *trans* azobenzenes consist of a strong band resulting from the  $\pi$ - $\pi^*$  transition (320 nm for unsubstituted molecules) and a less strong absorbing (since symmetry-forbidden)  $n$ - $\pi^*$  band. For *cis*-azobenzenes the absorption of the  $n$ - $\pi^*$  band is significantly stronger while the  $\pi$ - $\pi^*$  loses intensity. The  $n$ - $\pi^*$  transition excites azobenzenes to their  $S_1$ , the  $\pi$ - $\pi^*$  to their  $S_2$  states.<sup>[109, 111]</sup>



**Scheme 4.** Four different interconversion pathways from *trans*- to *cis*-azobenzenes.

In addition to the obvious conformational changes accompanying the isomerization, the dipole moment increases from nearly 0 Debye for *trans*- to ca. 3 Debye for *cis*-azobenzenes. Moreover, the carbon tail-to-tail distance changes by about 3.5 Å.<sup>[112]</sup> These properties make



diazobenzenes very useful molecular machines for optochemical tools,<sup>[106]</sup> especially for PCLs and PTLs.

It is because of the high variability of azobenzenes that our group decided to use them for the design of more selective ligands and to expand the scope of the PCL/PTL-concept to the other members of the iGluR family: the NMDA and AMPA receptors. Given the unique role of GluAs (*cf.* Chapter 1), they are one of the most interesting targets for optochemical genetics.<sup>[7]</sup> Our efforts toward an AMPA-selective photochromic ligand and their results are described in the following chapter and have been published in 2012.<sup>[113]</sup>

*Note:* The numbering, the outline of figures and schemes, and the citations of the original paper have been adjusted to fit the format of this thesis.

#### 4) A Photochromic Agonist of AMPA Receptors

*Philipp Stawski, Martin Sumser and Dirk Trauner*

(This work was published in *Angew. Chem. Int. Ed.* **2012**, *51*, 5748-5751 and *Angew. Chem.* **2012**, *124*, 5847-5850.)

Optochemical genetics uses small photoswitchable molecules to control neuronal activity. These can be attached covalently or non-covalently to their target proteins which can be ligand or voltage-gated ion channels as well as G-protein coupled receptors. The integration of the resulting hybrid photoreceptors into excitable cells allows for the control of neural networks with the temporal and spatial precision that only light provides.<sup>[7]</sup>

Among different targets for optochemical genetics, ionotropic glutamate receptors (iGluRs) stand out due to their central role in synaptic transmission. These ion channels are gated by glutamate (**1**) and fall into three major classes, each of which is marked by a distinct pharmacology (Fig. 16b).<sup>[9]</sup> The so-called AMPA receptors (GluAs), named after the selective agonist 2-amino-3-(5-methyl-3-hydroxyisoxazol-4-yl)propanoic acid (**4**), can be considered the workhorses of glutamatergic synapses. They are responsible for the major part of the excitatory neurotransmission in the mammalian central nervous system and are mostly positioned at the center of the postsynaptic density. Kainate receptors (GluKs), named after kainic acid (**17**), in contrast are located primarily on the periphery of the synaptic cleft and play more of a supporting and modulatory role. NMDA-receptors, named after their selective response to the agonist *N*-methyl-D-aspartate (**32**), are both voltage and ligand sensitive ion channels and function as coincidence detectors of postsynaptic depolarization and synaptic glutamate release.<sup>[5]</sup>

Our group has a longstanding interest in converting iGluRs into photoreceptors for optochemical applications. So far, our efforts have been focused on kainate receptors due to the well-defined architecture of their clamshell-like ligand-binding domain (LBD) and their readily interpretable pharmacology (Fig. 16a). Our efforts have yielded LiGluR, a light-gated ionotropic glutamate receptor, wherein a derivative of glutamate was covalently tethered to the surface of the LBD through a photoswitchable linker (PTL).<sup>[86a]</sup> Shortly thereafter we introduced a photochromic ligand (PCL) for kainate receptors that functions as a “reversibly caged glutamate”.<sup>[86b]</sup> This molecule, termed 4-GluAzo (**25**), is an azobenzene derivative of glutamate that changes its affinity and efficacy to GluK1 and GluK2 upon photoisomerization.

As such, it can be used to reversibly control neuronal activity with different wavelengths of light (Fig. 16c and d).

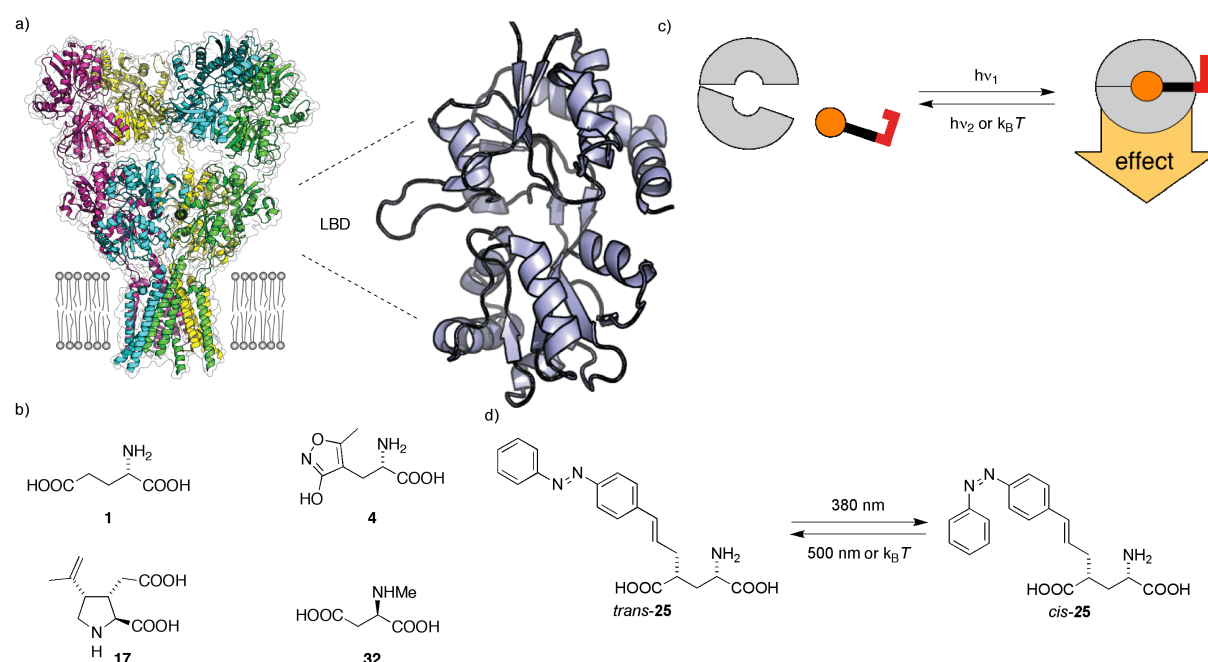


**Figure 16.** a) General structure of a glutamate receptor (derived from pdb 3KG2) with a close-up of the LBD. b) The four principal ligands of iGluRs. c) Schematic mode of action of a photochromic ligand. d) 4-GluAzo (**25**), a PCL acting on kainate receptors.

The rational design of suitable photoswitches for AMPA, kainate and NMDA receptors has been greatly facilitated by the availability of numerous X-ray crystal structures<sup>[8]</sup> The clamshell-like ligand-binding domains of these receptors have been crystallized in conjunction with a variety of agonists, such as AMPA and domoic acid, antagonists such as DNQX, as well as modulators such as cyclothiazide. Very recently, the crystal structure of a full tetrameric GluA2 receptor assembly has been disclosed<sup>[12]</sup> This seminal structure provided insights into the overall architecture and symmetry of AMPA receptors in particular and ionotropic glutamate receptors in general.

Although the clamshell-like LBDs of AMPA and kainate receptors share a similar overall architecture there are subtle differences that apparently prevent 4-(*R*)-substituted glutamate derivatives such as 4-GluAzo (**25**) to act as agonists. One of the reasons for this may be that the LBD of AMPA receptors is closed more tightly around the ligand in their activated form. Thus side chains attached to a glutamate molecule cannot be as easily accommodated as in the case of GluKs. Therefore, glutamate derivatives with a photoswitchable side chain like 4-GluAzo (**25**) were eventually deemed unsuitable for the light-dependent stimulation of AMPA receptors. In spite of extensive structural and functional data and considerable efforts,

our attempts to develop photochromic agonists for AMPA receptors had so far been unsuccessful. Accordingly we decided to radically change our molecular design resulting in a new class of molecules we named ATAs (Azobenzene-Tetrazolyl-AMPAs, **89a-d**, Fig. 17). These compounds are photochromic derivatives of AMPA itself, which selectively target GluA receptors expressed in HEK cells and neurons. One of them (**89c**) effectively triggers neuronal firing in the dark and quickly inactivates when irradiated with blue-green light. As such, it could be a useful tool for the study of neural circuitry controlled by AMPA receptors and a potential therapeutic tool for the restoration of vision with artificial photoswitches in the retina.

The design of **89a-d** is based on a recently published X-ray structure of the GluA2 LBD in conjunction with the potent and highly selective agonist BnTetAMPA (**9**), developed by the Clausen group.<sup>[114]</sup> This molecule is a derivative of AMPA, wherein the methyl substituent on the isoxazole ring is replaced with a tetrazole that is benzylated in the *N*-2-position. As seen in the crystal structure, the benzyl substituent occupies a cleft in the receptor that is different from the “exit tunnel” that we previously exploited in the kainate receptors (Fig. 17).

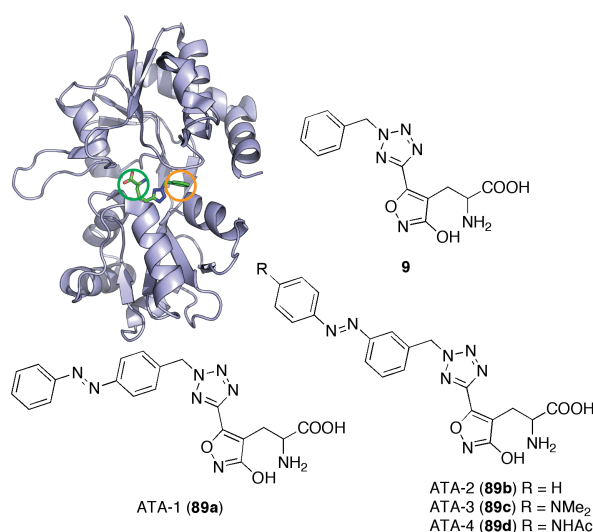
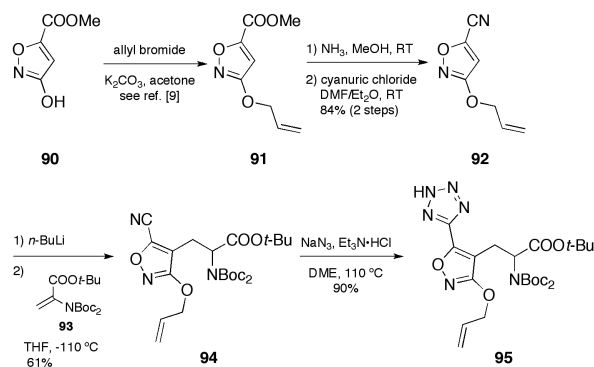


**Figure 17.** The structure of BnTetAMPA (**9**) and its complex with the GluA2 LBD and the structures of ATA-1 (**89a**) and ATA-2-4 (**89b-d**) shown in their respective *trans*-form. The green circle indicates the previous, whereas the orange circle shows the approximate location of the newly identified “exit tunnel”.

This structure suggested to us that extending the benzene to an azobenzene would allow the molecule to reach the solvent exposed surface while still permitting the ligand binding domain (LBD) to close sufficiently for receptor activation. It could also be deduced from this

structure that this elongation would require a *meta*-substitution with respect to the first benzene ring of the azobenzene unit.

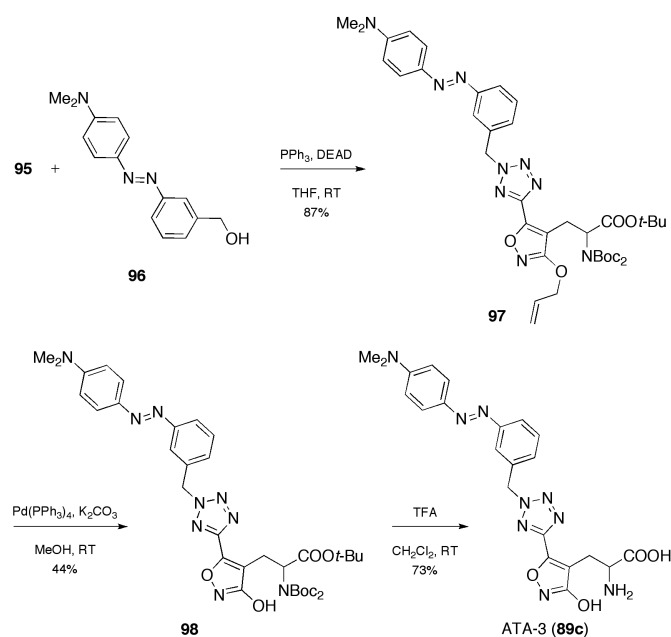
To test our hypothesis that ATAs would function as photochromic agonists we synthesized several versions **89a-d** (Fig. 17). These molecules have different substitution patterns and photophysical properties due to the presence or absence of substituents in the 4'-position of the azobenzene. The dimethylamino substituent in ATA-3 (**89c**), for instance, shifts the action spectrum of the azobenzene toward the red ( $\lambda_{\text{max}} = 456 \text{ nm}$ ), which allows for the use of longer wavelengths that are better tolerated by cells during prolonged exposure. The representative synthesis of ATA-3 (**89c**) was modeled after the published route to BnTetAMPA (**9**)<sup>[114]</sup> (Schemes 5 and 6). It commenced with the known hydroxyl isoxazole **90**,<sup>[115]</sup> which was protected as the allyl ether to ensure facile removal of the protective group at a later stage of the synthesis.<sup>[116]</sup> The resulting methyl ester **91** was then converted to the corresponding nitrile **92** in a two-step procedure.<sup>[117]</sup> Lithiation of the latter followed by conjugate addition of the obtained organolithium compound to dehydroalanine **93** yielded racemic AMPA derivative **94**. This step required careful optimization but could be carried out reliably and on large scale at very low temperatures. A 1,3-dipolar cycloaddition of nitrile **94** with *in-situ* generated hydrazoic acid then furnished tetrazole **95**, which served as a key intermediate in the synthesis of all ATAs (**89a-d**).



**Scheme 5.** Synthesis of the racemic key intermediate **95**.

Mitsunobu-coupling of tetrazole **95** with diethyl azodicarboxylate (DEAD) gave the *N*-2-alkylated tetrazole **97** as the major isomer (Scheme 6). The undesired, *N*-1-alkylated regio-isomer could be separated by HPLC after removal of the allyl group using  $\text{Pd}(\text{PPh}_3)_4$  in methanol/ $\text{K}_2\text{CO}_3$ ,<sup>[118]</sup> which yielded hydroxy isoxazole **98**. Subsequent global deprotection using trifluoroacetic acid (TFA) gave ATA-3 (**89c**) after purification. The synthesis of

analogs **89b** and **89d** as well as the *para*-substituted control compound **89a** was carried out analogously.<sup>[119]</sup>



**Scheme 6.** Synthesis of the PCL ATA-3 (**89c**).

As anticipated, ATA-3 (**89c**) and ATA-4 (**89d**) showed significant red-shifted absorption spectra compared to ATA-1 (**89a**) and ATA-2 (**89b**).<sup>[119]</sup> For all molecules except **89c** switching from *trans* to *cis* and *vice versa* could be observed in the UV when irradiated with the appropriate wavelengths.<sup>[119]</sup> ATA-3 (**89c**) could not be actively switched from its *cis*- to its *trans*-state in physiological buffer solution because of the complete overlap of the  $\pi$ - $\pi^*$  and  $n$ - $\pi^*$  absorption bands. Thermal relaxation however was later found to be sufficiently fast under these conditions (*vide infra*).

With **89a-d** in hand we assessed their biological activity in mouse cortical slices and HEK293T cells using whole-cell patch-clamp electrophysiology (Fig. 18 and 19). While ATA-1 (**89a**) was found to be completely inactive in both cell types compounds **89b-d** proved to be effective *trans*-agonists of GluA2 transiently expressed in HEK293T cells. This confirmed that the *meta*-substitution at the azobenzene moiety is a necessary structural requirement.

Since ATA-3 (**89c**) showed the highest activity and best kinetics we decided to focus our further investigations on this PCL. Its action spectrum at GluA2 recorded in HEK293T cells is shown in Figure 18. As designed, **89c** elicited the strongest inward current in its dark-adapted *trans*-state. Irradiation with varying wavelengths of light then produced photostationary states that gave less or no current at all (Fig. 18a).

In addition, the kinetics of ATA-3 (**89c**) currents in the dark and at different wavelengths of light were determined (Fig. 18b). We found that the fastest abrogation of current was achieved by switching from darkness to 480 nm light ( $\tau_{\text{off}} = 47.2 \pm 7.7$  ms).<sup>[119]</sup> By contrast when **89c** was tested against GluK2 no response (neither agonistic nor antagonistic) was observed.<sup>[119]</sup> This demonstrates the selectivity of the ATA chemotype for AMPA over kainate receptors.

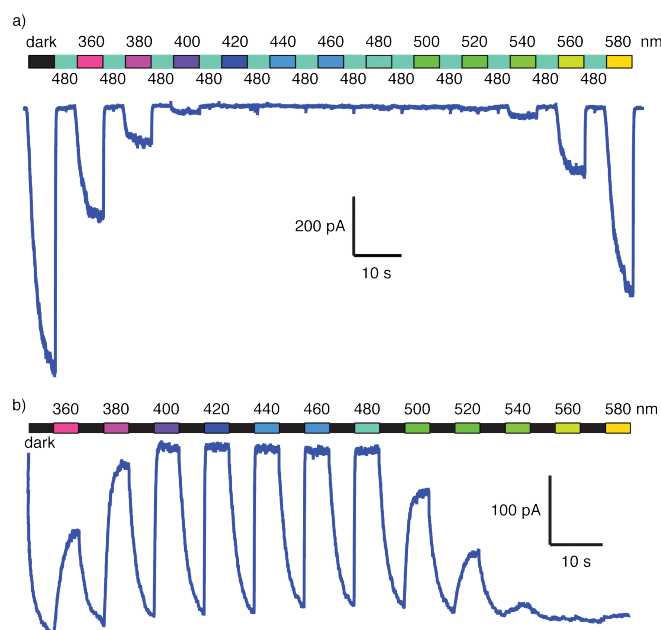


**Figure 18.** a) Action spectrum of ATA-3 (**89c**) acting on GluA2 expressed in HEK cells. b) Action spectrum recorded with intermittent darkness from a different GluA2 expressing cell ( $c = 50 \mu\text{M}$ ).

As a final characterization step, we determined the efficacy of ATA-3 (**89c**) at GluA2. The compound acts as a partial agonist with an  $\text{EC}_{50}$  of  $24 \mu\text{M}$  in the dark and is virtually inactive at 480 nm illumination.<sup>[119]</sup> One should bear in mind that enantiopure material will likely show considerably higher activity as has been observed for other AMPA-derivatives.<sup>[82a, 120]</sup>

We then evaluated the ability of **89c** to control action potentials (APs) in excitable cells. APs were recorded from layer 2/3 neurons in mouse cortical slices. When ATA-3 (**89c**) was applied at  $50 \mu\text{M}$  concentration trains of APs could be generated reliably upon switching from 480 nm light to darkness (Fig. 19). Due to the moderate intensity of the light used ( $20.3 \text{ mW/mm}^2$ ) recordings could be performed over prolonged periods of time without any apparent photodamage.

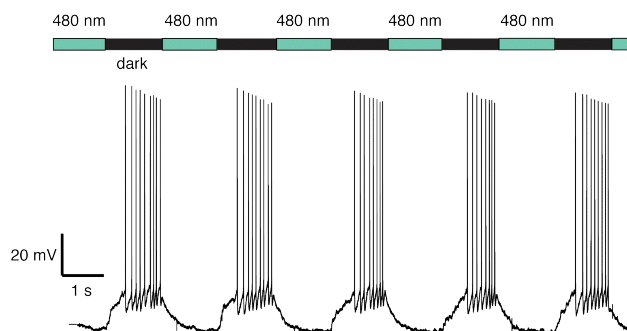


**Figure 19.** Reversible generation of action potentials by **89c** in mouse cortical neurons (clamped at -65 mV).

The activity of ATA-3 (**89c**) in neural networks was further probed using known glutamate receptor pharmacology. GYKI-52466,<sup>[121]</sup> an AMPA-selective antagonist, blocked the effect of the PTL as did the AMPA/kainate antagonist CNQX. Additional experiments with the selective NMDA antagonist AP-5<sup>[122]</sup> failed to prevent AP firing.<sup>[119]</sup> This demonstrates that **89c** can discriminate between all three subtypes of iGluRs and selectively acts on AMPA receptors.

In summary, we have developed a photochromic agonist of AMPA receptors that stimulates neurons in the dark but can be rapidly turned off when irradiated with blue-green light at moderate intensities. ATA-3 (**89c**) uses a novel “exit tunnel” that should allow for the design of new, highly AMPA-selective ligands. Given the prominence of AMPA receptors in synaptic transmission, this molecule could be used as an effective tool to optically control neuronal activity in a wide variety of networks. Its response to light matches the logic of OFF-bipolar cells, and by extension OFF retinal ganglion cells, which increase firing in the darkness and show decreased activity when light reaches their receptive field. As such, ATA-3 (**89c**) could be a useful component of our ongoing efforts to restore vision with small photochromic molecules.



## 5) The Subtype-Selectivity of ATAs

As mentioned before, the PCL 4-GluAzo (**25**) had been found to be a potent GluK1/GluK2 agonist.<sup>[86b]</sup> It was found later however, that it is also a GluA2 antagonist.<sup>[123]</sup> To rule out similar cross-activities of the ATA PCLs, the subtype-selectivity of ATA-3 (**89c**) was further investigated. In the experiments discussed earlier, the selectivity of **89c** was shown in cortical slice preparations using the AMPA-selective, noncompetitive antagonist GYKI-52466.<sup>[121]</sup> Accordingly, we were pleased to find, that ATA-3 (**89c**) did not show any activity at GluK2 receptors expressed in HEK293T cells either (Fig. 20a).

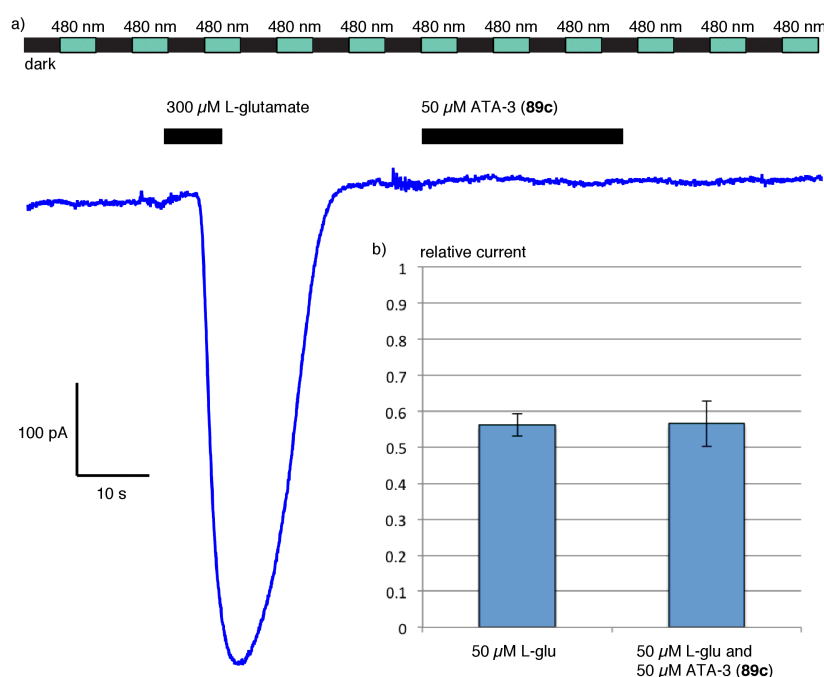


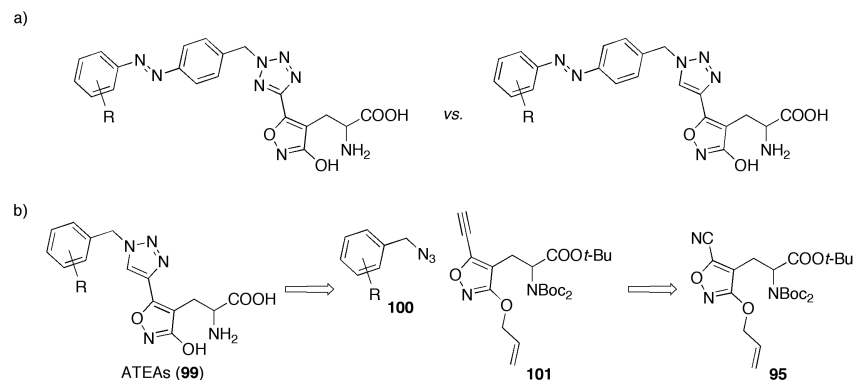
**Figure 20.** a) Voltage-clamp recording of a HEK293T cell expressing GluK2. b) Comparison of L-glutamate (L-Glu) induced currents at GluK2 with or without co-administration of ATA-3 (**89c**).

With the agonism of ATA-3 (**89c**) at GluK2 ruled out, we assessed the possibility of its antagonism at the named receptor. To our relief, glutamate-induced currents at GluK2 were the same in the presence and in the absence of **89c** under varying illumination (Fig. 20b), thus indicating no competitive antagonistic effects.

These results once more proved the high variability of the PCL approach. Given a valid binding mode, selection of a subtype-specific pharmacophore can be used to target PCLs efficiently to selected receptor subtypes without the imminent danger of cross-activity.

## 6) Triazole-Substituted AMPA Derivatives

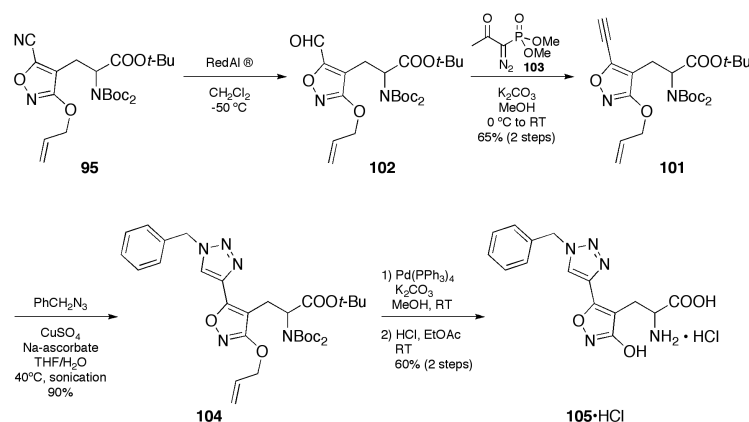
Encouraged by the results of the azobenzene substituted tetrazolyl AMPAs (ATAs), we asked ourselves, whether the synthesis of AMPA-selective PCLs based on BnTetAMPA could be further simplified. Due to the low selectivity of the alkylation of the H-tetrazoles during the synthesis of the ATAs, we explored options to carry out this reaction by more regioselective means. A literature survey however showed, that there are only a few methods for the selective formation of 2,5-substituted tetrazoles. All the procedures found were either not compatible with our synthetic strategy, did not work in our hands,<sup>[124]</sup> or were selective for the wrong, *i.e.* the 1,5-regiochemistry.<sup>[125]</sup> We therefore turned away from the tetrazole motif and planned to assemble the PCLs *via* a copper-mediated 1,3-dipolar Huisgen cycloaddition between an alkyne and an azide (*i.e.* “click-chemistry”),<sup>[126]</sup> effectively replacing the tetrazole with a triazole (Scheme 7). As these kind of reactions are known to proceed with high regioselectivity and under mild conditions,<sup>[127]</sup> we were positive, that we could assemble the Azobenzene Tetrazolyl AMPAs (ATeAs, **99**) from benzyl azides **100** and the alkyne **101**. The latter could be synthesized from a common precursor to all ATAs, nitrile **95** (Scheme 7b).



**Scheme 7.** a) Comparison of ATAs and ATeAs. b) Retrosynthetic analysis of ATeAs (**99**).

Starting from AMPA-derivative **95**, a variety of reduction methods to convert the heterocyclic nitrile into the corresponding aldehyde (DIBAL-H, Red-Al®, LiAlH<sub>4</sub>, LiAlH(Ot-Bu)<sub>3</sub>, Raney-Ni) were screened.<sup>[128]</sup> Most notably, DIBAL-H, which is otherwise known to carry out the selective reduction of nitriles to aldehydes,<sup>[129]</sup> led to complete decomposition of the starting material. It was only with RedAl®, that the transformation could be carried out reliably. We assumed, that the difference in the reactivity is due to the softer nature of the hydride donor, while still preserving enough reactivity to carry out the desired transformation. After reduction and purification, the resulting aldehyde was efficiently converted into an

alkyne using the Ohira-Bestman reagent **103**<sup>[130]</sup> yielding alkyne **101** in acceptable yields over two steps from nitrile **95** (Scheme 8).



**Scheme 8.** Synthesis of the ATeA prototype **105**.

With alkyne **101** in hand, the triazole formation by click-reaction was carried out in high yields using benzyl azide and copper(I) generated *in situ* from copper(II) sulfate and sodium ascorbate (Scheme 8).<sup>[131]</sup> The subsequent deprotection was carried out analogously to the synthesis of ATA-3 (**89c**). Using Pd(PPh<sub>3</sub>)<sub>4</sub> and hydrochloric acid in ethyl acetate alkyne **104** was deprotected to give the archetype of triazolyl-substituted AMPAs, **105**, in 60% over two steps (Scheme 8).

Unfortunately, when **105** was applied to mouse cortical neurons (puff-application; data not shown), no activity could be observed. Despite the high similarity to BnTetAMPA (**9**), substitution of the *N*-1-nitrogen with a CH-group had rendered triazole **105** inactive in ionotropic glutamate receptors. This can be rationalized by investigating the binding-mode of BnTetAMPA (**9**) in GluA2 (Figure 21).<sup>[33]</sup>

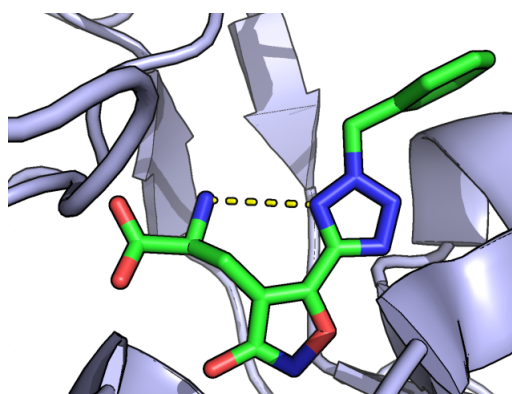


**Figure 21.** BnTetAMPA (**9**) bound to GluA2 (pdb accession code 2P2A).

As indicated in Figure 21, an intramolecular hydrogen bond between the  $\text{NH}_2$ -group and *N*-1 stabilizes and locks BnTetAMPA (**9**) in a conformation, that allows the benzyl substituent to occupy the entrance to the new “exit tunnel”. As this is not possible for molecules of the ATeA-type, the triazolyl substituted AMPA derivatives were eventually deemed unsuitable as AMPA PCLs.

## 7) Activity of ATAs in the Blind Retina

Since we had shown that ATAs are effective agonists of GluA2 and can be used to control the activity of neurons, it was time to explore its utility beyond the mere proof-of-concept. A problem, which all photoswitchable molecules used in optochemical genetics have to face when moving from single, isolated cells to functional networks, is the absorption of light by the surrounding tissue. Even though solutions to this problem such as light delivery by optical fibers,<sup>[132]</sup> stimulation by radio frequencies,<sup>[133]</sup> or two-photon excitation do exist,<sup>[134]</sup> we have not yet been able to shift the absorption spectra of our azobenzenes to harness the low absorption of biological tissue between 700 nm and 1400 nm, often referred to as “optical window” (Fig. 22a).<sup>[135]</sup> There is one part of the mammalian body however, that not only permits the access of light, but is built most efficiently to perceive it: the eye (Fig. 22b). Light enters through the cornea and the pupil, is focused by the lens, passes the vitreous humor and finally reaches the retina.<sup>[136]</sup>

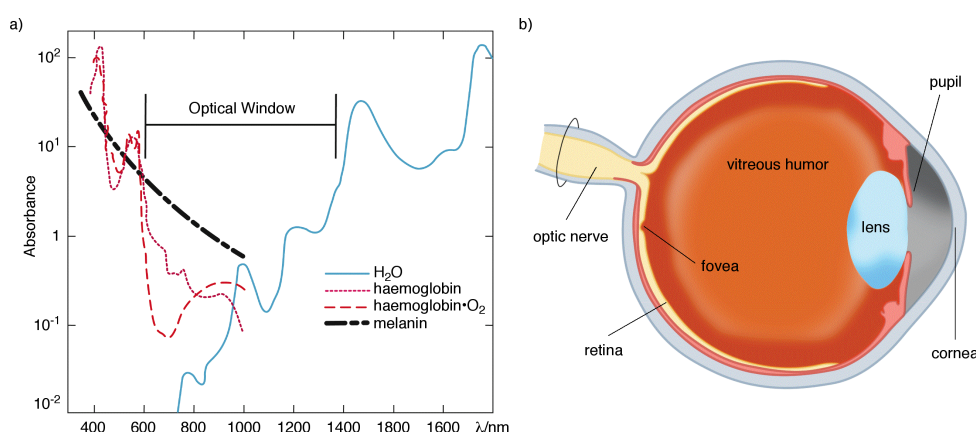
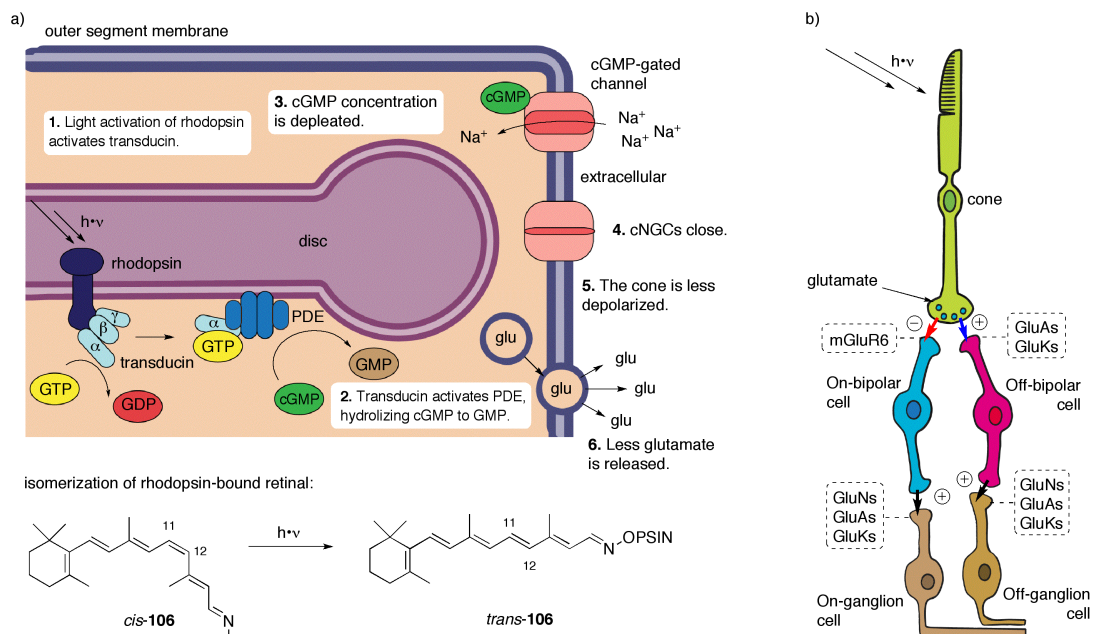


**Figure 22.** a) The absorption coefficients of different tissue constituents according to Hamblin<sup>[135]</sup>. b) General makeup of the mammalian eye (adapted from Purves<sup>[136]</sup>).

Evolutionary, the retina is part of the central nervous system, but its structure is significantly less complex than other tissues of the CNS, like *e.g.* the brain. There are only five types of neurons present in the retina, which are stacked in different layers: specialized photoreceptors (*i.e.* rods and cones), horizontal, bipolar, amacrine and ganglion cells. The latter connect the signals received by the photoreceptors and passed on to the bipolar cells to the optical nerve. Interestingly, the cellular makeup of the retina is such that the light first passes through the ganglion, amacrine, bipolar and horizontal cells, before reaching the rods and cones. In order to maintain vision for a long time, the retina is surrounded by the retinal

pigment epithelium, a thin layer that plays a critical role in both support and preservation of the photoreceptors.

Rods and cones harbor light sensitive pigments in membranous discs, which are the reason of their photosensitivity. Unlike other neurons in the CNS, photoreceptors do not fire action potential, but rather gradually change their membrane potential, thus modulating their neurotransmitter release. The molecular source of phototransduction is rhodopsin (Scheme 9a), a G-protein coupled receptor, which binds 11-*cis*-retinal as its pigment. Upon excitation by a photon, it is isomerized to 11-*trans* retinal and the accompanying structural changes result in an exchange of GDP for GTP at its bound G-protein, transducin. Its  $G_\alpha$  subunit couples to phosphodiesterase 6 (PDE), which in turn catalyzes the hydrolysis of cGMP to GMP thus depleting its intracellular concentration. Since cyclic nucleotides serve as ligands for so-called cyclic-nucleotide-gated channels (cNGCs), activation of rhodopsin ultimately results in less glutamate release by the photoreceptor cell due to the hyperpolarization caused by closure of cGMP-gated channels (Scheme 9a).

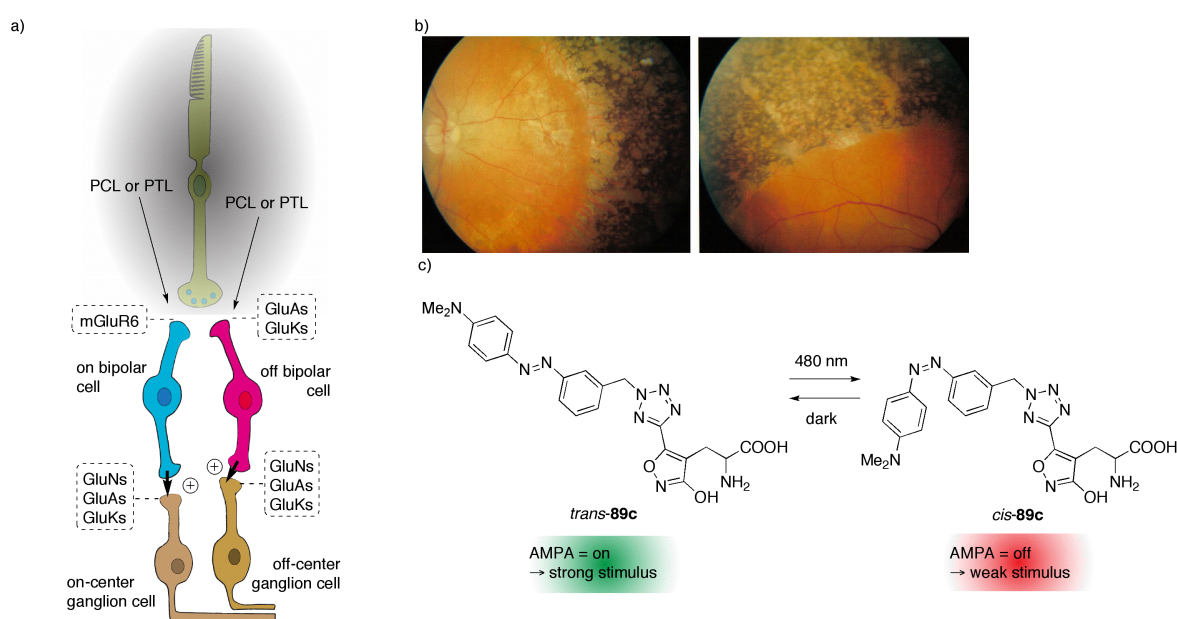


**Scheme 9.** a) The vision cascade. From the isomerization of 11-*cis* retinal (**106**) to glutamate release from the photoreceptor cells (adapted from [136]). b) The role of different glutamate receptors during the transmission of information *via off*- and *on*-bipolar cells.

Following their release, the neurotransmitters are sensed by glutamate receptors located at the postsynaptic termini of bipolar cells (Scheme 9b). There are two types of bipolar cells connecting to the photoreceptors: On- and Off-bipolar cells. While the On-cells become more activated upon perception of light (by an inverted coupling of mGluR6 to

cNGCs *via*  $G_{i/o}$ ), Off-bipolar cells become more quiescent (due to less glutamate released by the photoreceptor). Both bipolar cell types stimulate ganglion cells in the end and due to their opposing polarity, they play an important role in the computational circuitry of the retina.<sup>[136]</sup>

Since the sole reason for the eye's photosensitivity are the rods and cones, loss of the latter inevitably results in blindness, because there is no input signal generated for the bipolar cells (Scheme 10a). In fact, degeneration of the photoreceptor cells due to a diverse group of hereditary disorders – commonly referred to as retinitis pigmentosa (RP) – is affecting as much as up to 1 out of 7000 people worldwide.<sup>[137]</sup> A main reason for the degeneration of rods and cones is a nonfunctional retinal pigment epithelium (Scheme 10b).



**Scheme 10.** a) Consequences of loss of photoreceptors and possible starting points for artificial stimulation of the remaining bipolar cells. b) Typical view of an RP-diseased retina.<sup>[138]</sup> c) The logic of the AMPA-selective PCL ATA-3 (**89c**) matches the one found in off-bipolar cells.

In our group there is an effort to use small photoswitchable molecules to restore input to the cut-off bipolar (or other) cells in the retina and thus to treat blindness as caused by RP. In a rodent model, collaborators were able to show, that the PTL approach (LiGluR) can be used to restore visual responses.<sup>[139]</sup> Obviously, for an application in humans PCLs seem to be better suited, since they don't require genetic manipulation. Instead, they require a high degree of pharmacological selectivity in order to only target certain receptors, which are expressed in the retina.

mGluR6 is one of the most evident targets for the PCL approach since it is exclusively expressed in on-bipolar cells. Recent studies have however shown, that bipolar cells in RP-

diseased retinæ lose their mGluR6 and iGluR-mediated responses both in humans and in rodent models. Ganglion and amacrine cells, interneurons that provide inhibitory input to ganglion cells upon excitation from bipolar cells, however retain their glutamate-sensitivity.<sup>[140]</sup> We were therefore excited to investigate the effect of the AMPA-selective PTL ATA-3 (**89c**) in the blind retina, since its logic matches the one of off-bipolar cells (*i.e.* activation in the dark and inactivation when irradiated with 480 nm light; *vide supra*) and for that reason off-ganglion cells, too (Scheme 10c).

Triple knock-out mice retinæ (cng-/-, rho-/-, opn4-/-) were treated with ATA-3 (**89c**) at 25  $\mu$ M and their responses to darkness and blue light were recorded from ganglion cells using a multielectrode array (MEA) setup. We were pleased to find, that the recordings of the individual 64 channels – when in contact with a ganglion cell – showed a marked increase in spiking rate upon switching from 480 nm light to darkness (Fig. 23).

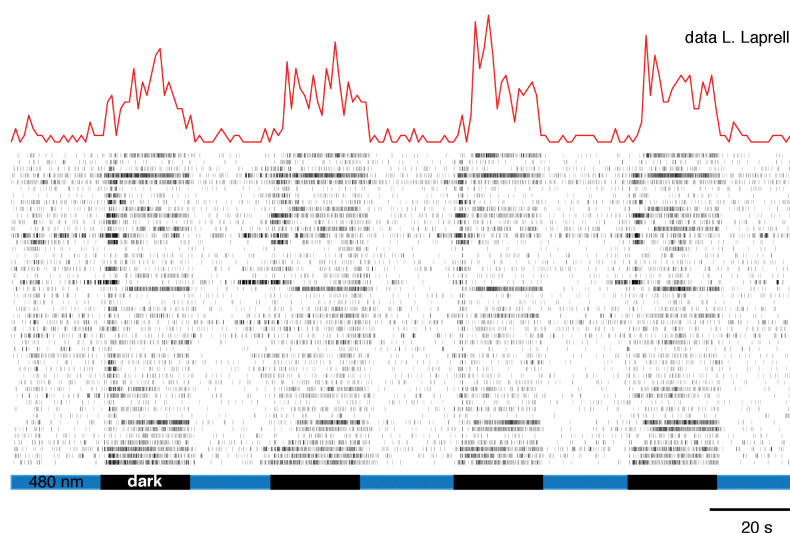


**Figure 23.** Exemplary data of a cng-/-, rho-/-, opn4-/- retina treated with 25  $\mu$ M ATA-3 (**89c**) in the dark and under 480 nm illumination. The top traces represent the mean over all channels.

The statistics indicate that the activation of ATA-3 (**89c**) results in a five-fold increase of spiking rate and that the effect is indeed connected to the AMPA-selective PCL. Control experiments in retinæ without ATA-3 (**89c**) showed no increase in the spike-rate when switching from blue light to darkness (Fig. 24).



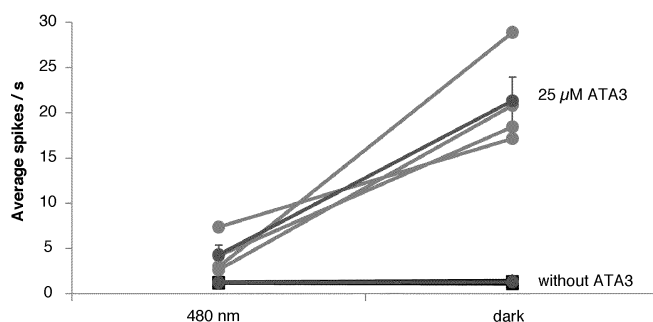
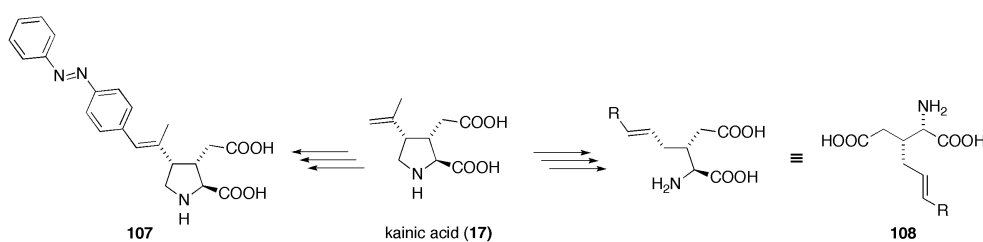


**Figure 24.** Spiking rate in the presence and in the absence of 25  $\mu$ M ATA-3 (**89c**) under 480 nm illumination and in the dark.

Moreover, we were pleased to find that ATA-3 (**89c**) is able to elicit both on- and off-responses in triple knockout retinæ, thus suggesting the presence of an intact visual circuitry. A detailed analysis and pharmacological investigation of **89c**'s mode of action will follow in due course.<sup>[141]</sup> Especially we are interested by which cells of the knock-out retina ATA-3 (**89c**) elicits its effect. This will determine its potential as a lead structure in the restoration of vision using small molecules. Ideally, we would like to target the Off-bipolar cells to further investigate their role in the vision process. However, as studies have shown that a direct stimulation of retinal ganglion cells (RGCs) with epiretinal electrode implants is a viable strategy for the restoration of vision,<sup>[142]</sup> we will investigate the response of RGCs to ATA-3, too. Owing to these promising first results, it can be expected that ATA-3 (**89c**) will prove to be a new and highly potent tool for the research of retinal neuronal networks. Investigations of its potential as a therapeutic lead for chemical approaches to restoring vision (CARV) are currently underway.<sup>[141]</sup>

## 8) Toward a Universal Photoswitch for AMPA and Kainate Receptors

In our attempt to synthesize a photochromic agonist of AMPA receptors, we surveyed the known GluA receptor pharmacology and found that – besides glutamate – kainic acid (**17**) could be used as a scaffold, from which to build a PCL that acts on both AMPA and kainate receptors (Scheme 11, left). Moreover, upon close inspection of the binding mode of **17** in GluA2 and GluK2, we concluded, that 3-D-substituted glutamate derivatives like **108**, should follow the same logic (Scheme 11, right). Given the wealth of information on 4-substituted glutamic acid analogues,<sup>[83b, 84, 143]</sup> we were surprised to find that their 3-alkylated congeners are severely underexplored and that there is no report on their subtype-selectivity.<sup>[144]</sup> We therefore decided to follow these two approaches in order to come up with a “universal” photoswitch for both AMPA and kainate receptors.



**Scheme 11.** A kainate-derived, universal PCL **107** and 3-D-substituted glutamate analogues **108**.

### a) A Kainate-Derived Photoswitch

Kainic acid (**17**) is a marine alkaloid isolated from the Japanese seaweed “kainin-sou” (*diginea simplex*).<sup>[145]</sup> Along with domoic acid (**18**) and the acromelic acids (**19**) it resembles a conformationally restricted version of L-glutamate (Fig. 25).

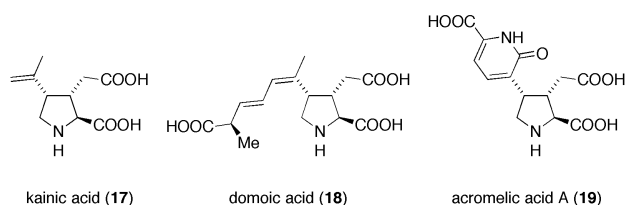
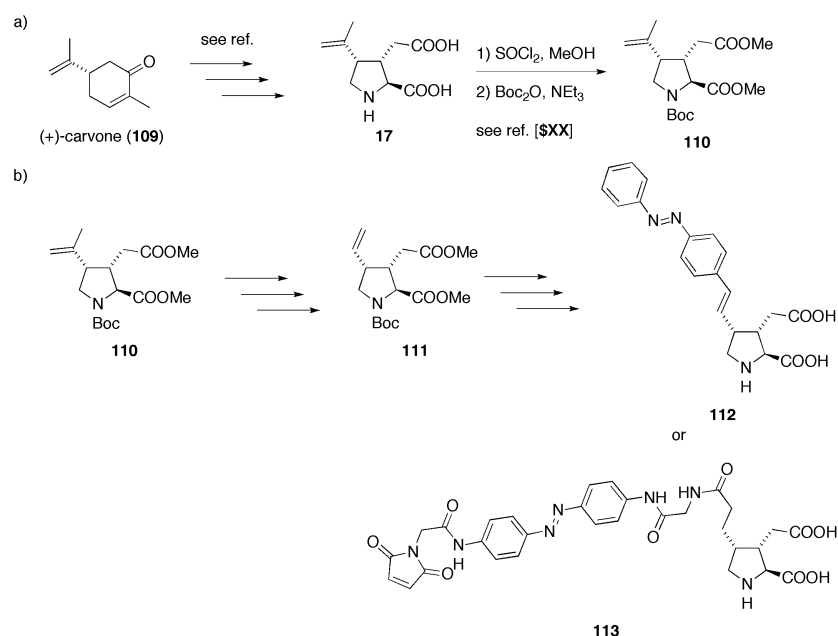


**Figure 25.** Kainic acid (**17**), domoic acid (**18**) and acromelic acid A (**19**).

Due to their interesting pharmacological properties, many synthetic analogues of kainic acid have been prepared<sup>[83a, 146]</sup> For these, natural kainic acid has commonly been used as starting material and the shortage in supply of **17** from natural sources has therefore prompted many

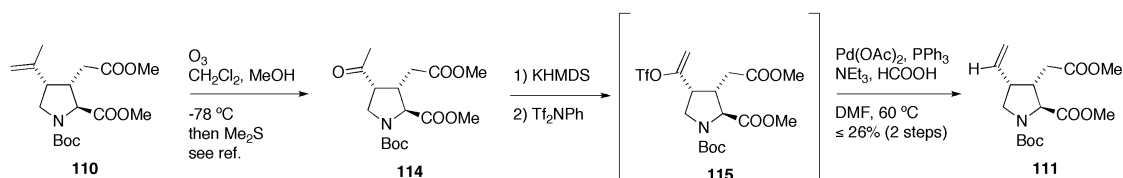
chemists to develop synthetic strategies toward this alkaloid.<sup>[147]</sup> Moreover, the challenging construction of the three contiguous stereocenters has led to several methodology-oriented syntheses, too. Among them are such “classics” as Oppolzers 1982 approach, in which an Alder ene-reaction is used to form the pyrrolidine ring.<sup>[148]</sup>

In order to access synthetically useful quantities of **17** however, we decided to rely on a more recent route, which was published by Fukuyama and coworkers in 2011.<sup>[149]</sup> Starting from (+)-carvone (**109**), we obtained kainic acid on a gram-scale in just 13 steps and protected it according to known literature procedures (Scheme 12a).<sup>[83a]</sup> We then planned to degrade the isopropenyl group to a vinyl group in order to use it as a functional handle in our studies (Scheme 12b).



**Scheme 12.** a) Total synthesis of kainic acid (**17**) from (+)-carvone (**109**) and its protection to diester **110**. b) Envisioned synthesis of *nor*-kainic acid derivative **111** and a derived PCL and PTL.

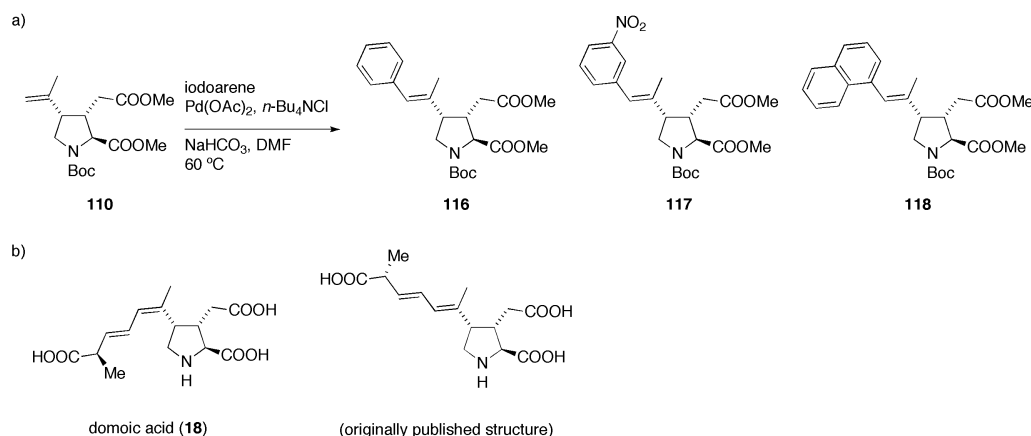
After ozonolysis of **110** and reductive workup, we obtained the known ketone **114** in excellent yields (Scheme 13).<sup>[83a]</sup> Unfortunately, all our attempts to transform **110** into an alkene using reduction-elimination,<sup>[150]</sup> or Bamford-Stevens/Shapiro protocols<sup>[151]</sup> failed. We therefore screened conditions for the coupling of enol-triflate **115** to a hydride source.<sup>[152]</sup> None of the conditions however yielded *nor*-kainic acid **111** in synthetically useful yields (Scheme 13) even though we tested various methods for the formation of **115** from ketone **114** using different bases (LiHKMS/KHMDS) and triflate sources (Tf<sub>2</sub>O, PhNTf<sub>2</sub>, Comins-reagent).<sup>[153]</sup> We therefore decided to abandon this route in favor of a different approach toward substituted kainoids.



**Scheme 13.** Degradation of kainic acid (**17**) to protected *nor*-kainic acid **111**

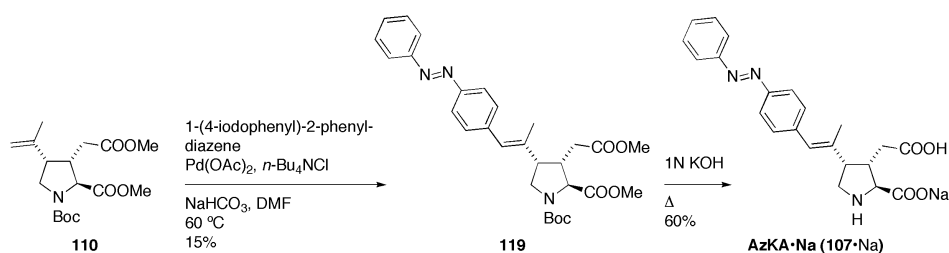
We were pleased to find, that a number of direct modifications of the isopropenyl group in kainic acid have been reported.<sup>[83a, 146a, 146d]</sup> Among these, a certain set of Jeffery modified Heck conditions (*n*-Bu<sub>4</sub>NCl, NaHCO<sub>3</sub>, DMF)<sup>[154]</sup> immediately caught our attention (Scheme 14a)<sup>[146a]</sup> and we decided to use this methodology to synthesize a kainate-based PCL.

Aryl-substituted kainic acids like the *m*-nitrophenyl analogue **117** are known to elicit activity at kainate receptors even though they do not follow the substitution pattern of domoic acid (**18**), but rather its initially proposed structure (Scheme 14b).<sup>[146e]</sup>



**Scheme 14.** a) Palladium-catalyzed synthesis of the aryl-substituted kainic acid analogues **116**, **117** and **118**. b) Structure of domoic acid (**18**) and its originally published structure.

Using the Heck conditions described earlier,<sup>[146a]</sup> we coupled protected kainic acid analogue **110** to 1-(3-iodophenyl)-2-phenyl diazene<sup>[155]</sup> and obtained azobenzene **119** as a single diastereomer, yet in low yields. Subsequent deprotection by saponification in 1 M aqueous KOH, finally yielded the kainate-based PCL AzKA (**107**) as its sodium salt in 60% after reversed phase purification (Scheme 15). A structural analysis of **107** using NMR (NOESY) proved the *cis*-relationship of the azobenzene moiety and the former isopropenyl methyl group.



**Scheme 15.** Synthesis of diazobenzene-substituted kainic acid analogue AzKa (**107**).

With diazo-kainic acid **107** synthesized, we evaluated its activity in mouse cortical neurons and HEK293-T cells by patch-clamp electrophysiology. We found that AzKa (**107**) acts as a relatively potent agonist of kainate receptors in HEK293T-cells (Fig. 26), but shows only weak photoswitching ( $3.8 \pm 0.3\%$ ,  $n = 3$ ). Conversely, there was hardly any effect in the slice preparation. While other PCLs (4-GluAzo, ATA-3) seem to suppress receptor desensitization, we reasoned that **107** might not do the same.

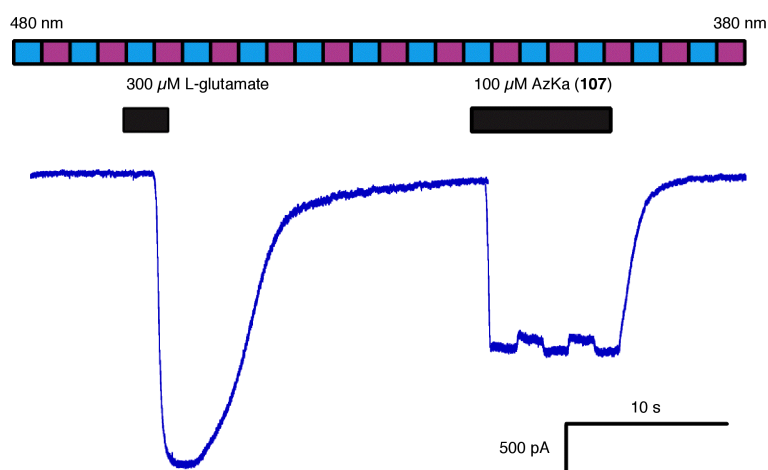
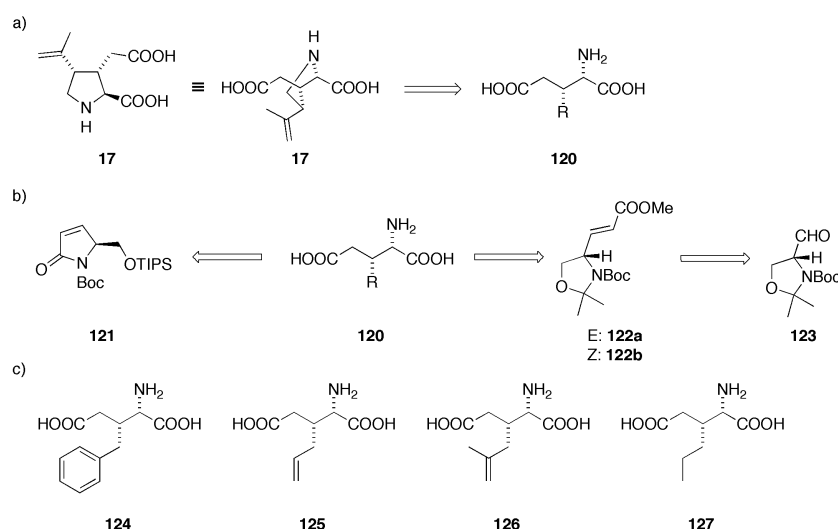


**Figure 26.** Voltage-clamp recording of AzKa (**107**) acting on GluK2 at 100 μM.

To investigate this hypothesis, we tested the effect of AzKA (**107**) in cortical neurons in the presence of ConA (TTX-treated to prevent AP-firing) to find an enhanced activity of the kainate-based PCL. Additionally we found, that **107** is more efficacious in hippocampal NA1 neurons. To fully understand these phenomena, we will investigate the effect of sterically more demanding (*meta*-substituted) and redshifted versions of AzKA (**107**).

## b) 3-D-Substituted Glutamate Analogues

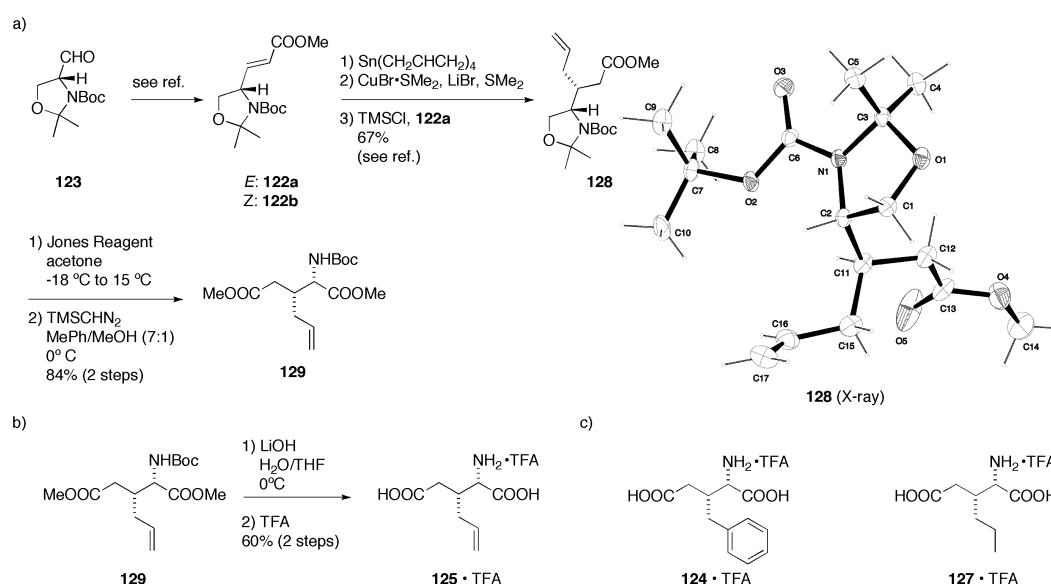
In addition to our experiments with the kainic acid-derived photoswitch **107**, we were positive that the underexplored class of 3-D-substituted glutamic acid analogues (**120**), which essentially can be regarded as *seco*-kainic acids (Scheme 16a), would be a useful platform from which to build a universal PCL/PTL for both kainate and AMPA receptors. Retrosynthetically, 3-alkylated glutamic acids can be accessed either by 1,4-addition of nucleophiles to a pyroglutamate-derived enone **121**, or by Michael addition to  $\alpha,\beta$ -unsaturated esters **122** derived from Garner's aldehyde (**123**; Scheme 16b). Both routes are literature-known,<sup>[144, 156]</sup> yet while the first requires several red-ox manipulations and suffers from low yields and diastereoselectivity, the second is high yielding and reasonably selective in terms of stereochemistry at the 3 position. In fact, a couple of 3-D-substituted glutamate analogues (**124-127**) have been prepared using this general approach (Scheme 16c).<sup>[144, 156]</sup> Their mode of action and especially their receptor subtype selectivity however were unfortunately never elucidated.



**Scheme 16.** a) 3-D-substituted glutamic acids **120** are *seco*-kainoids. b) Two retrosynthetic routes to 3-alkylated glutamate analogues. c) Four literature-known 3-D-substituted glutamates (**124-127**).

Modeling our synthesis according to known protocols,<sup>[144, 156]</sup> we started our synthesis of 3-D-substituted glutamic acid analogues from D-serine, which was converted into Garner's aldehyde (**123**).<sup>[157]</sup> After a Horner-Wadsworth-Emmons (HWE) olefination of aldehyde **123** with trimethyl phosphonoacetate,<sup>[144b]</sup> the  $\alpha,\beta$ -unsaturated ester **122** was obtained as a mixture of *E/Z*-isomers. Remarkably, the ratio of *E* vs. *Z* of approximately 3:1, was quite high for a stabilized HWE reagent, but fortunately the two diastereomers could be

separated by column chromatography and only the major *E*-isomers was used in the following Michael addition. For this, we prepared allyllithium from tetraallyl tin and transmetallated it to the cuprate using copper(I)bromide dimethylsulfide complex.<sup>[158]</sup> After a smooth 1,4-addition of the obtained Gilman cuprate to enone **122a** in the presence of trimethylsilyl chloride and dimethyl sulfide (Scheme 17a), we obtained hemi-aminal **128** (unlike previous reports) as a single diastereomer. This seems to suggest, that the Michael addition is more selective for the *trans*-isomer **122a**, since in the synthesis by Wermuth and coworkers, a mixture of **122a** and **122b** was used.<sup>[144b]</sup> Fortunately, we could prove the relative stereochemistry of the Michael adduct **128** to be *L* by X-ray crystallography (Scheme 17a, inset). With the structure of oxazolidine **128** confirmed, careful cleavage of the hemi-aminal with an excess of Jones reagent,<sup>[159]</sup> followed by oxidation of the primary alcohol and protection of the resulting carboxylic acid using trimethylsilyl diazomethane,<sup>[160]</sup> gave diester **129** in high yields over two steps (Scheme 17a). Standard deprotection manipulations finally yielded (3*R*)-allyl glutamic acid (**125**) as the TFA salt (Scheme 17b). Its analogues, **127** and **124** were prepared by hydrogenation of **125** and by the literature known addition of benzylmagnesium bromide to enone **122b**, followed by the same oxidation-deprotection sequence.<sup>[144b]</sup>



**Scheme 17.** a) Synthesis of protected (3*R*)-allyl glutamate **129** via oxazolidin **128** and X-ray structure of **128**. b) Exemplary deprotection of **129** to glutamate analogue **125**. c) Two additional, literature known 3-D-alkylated glutamic acids **124** and **127**.

Since the subtype-selectivity of the 3-D-alkylated glutamates **124**, **125** and **126** was still unknown, we decided to evaluate their properties in the most prevalent kainate and AMPA receptors – GluK2 and GluA2 – expressed in HEK293T cells. To our surprise, all three molecules proved to be highly kainate-selective ligands with no detectable activity in GluA2 even up to 1 mM (Figure 27). This might be rationalized by the fact, that kainic acid (**17**) only shows weak partial agonism at AMPA receptors, too.<sup>[26]</sup> Experiments regarding the subtype selectivity in mouse cortical slice preparations using selective iGluR antagonists (data not shown) were unfortunately inconclusive and we therefore decided to only probe their pharmacological profile in iGluRs expressed in HEK293T cells.

The relative activity of the three ligands, which had not been investigated at defined iGluR populations before,<sup>[156]</sup> can be ranked in the order benzyl > allyl > propyl with benzylated glutamate **124** acting as a full and the others acting as partial agonists of GluK2 (Fig. 27). While there was no obvious structure-activity relationship (SAR) between the aromatic- and the alkene-substituted glutamate analogue, it is noteworthy, that the sp<sup>2</sup>-hybridization at carbon C2 of the sidechain seems to be a prerequisite for high receptor activity as shown previously by Hashimoto and coworkers, too.<sup>[156]</sup>

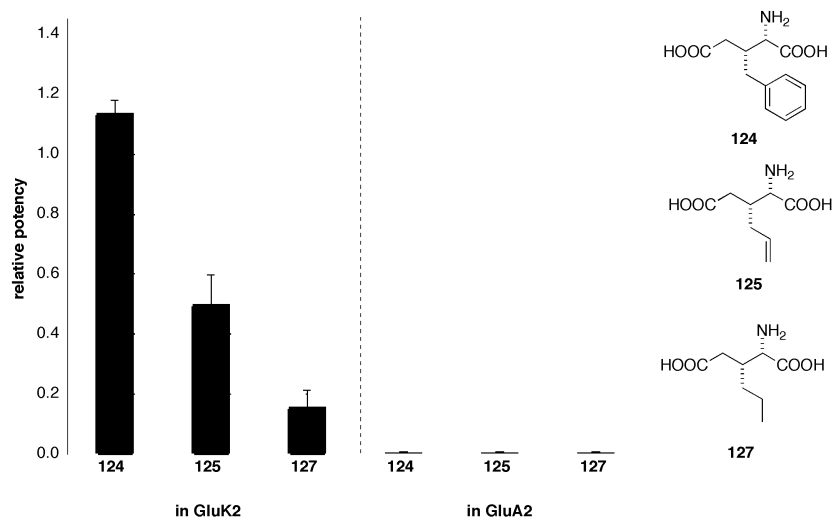
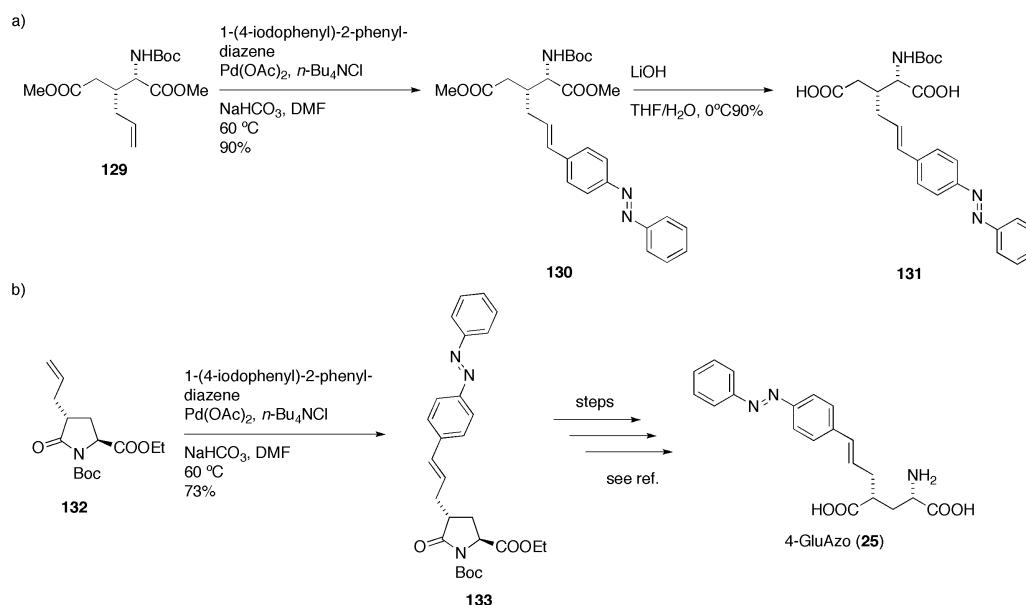


**Figure 27.** Potency of glutamate analogues **124**, **125** and **127** (1 mM) relative to saturating glutamate (500  $\mu$ M) at GluK2 and GluA2 (data  $\pm$  SEM; n = 5).

Since to us substitution of allylated glutamic acid **124** by metathesis or Heck reaction seemed easiest, we decided to use this scaffold to build a kainate/AMPA PCL. Employing the same set of Jeffery-modified Heck conditions as for the kainate-based PCL **107**,<sup>[146a]</sup> we reacted ester **129** and 1-(4-iodophenyl)-2-phenyldiazene to yield diazobenzene **130** in 90% as a single diastereomer (Scheme 18a). Encouraged by these results, we tried the same protocol

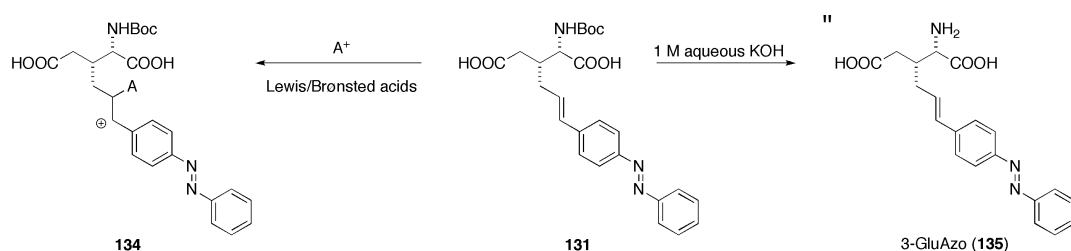


for the synthesis of a precursor to 4-GluAzo (**25**) and indeed obtained **133** in significantly higher yields than the protocol used previously (Scheme 19b).<sup>[86b]</sup>



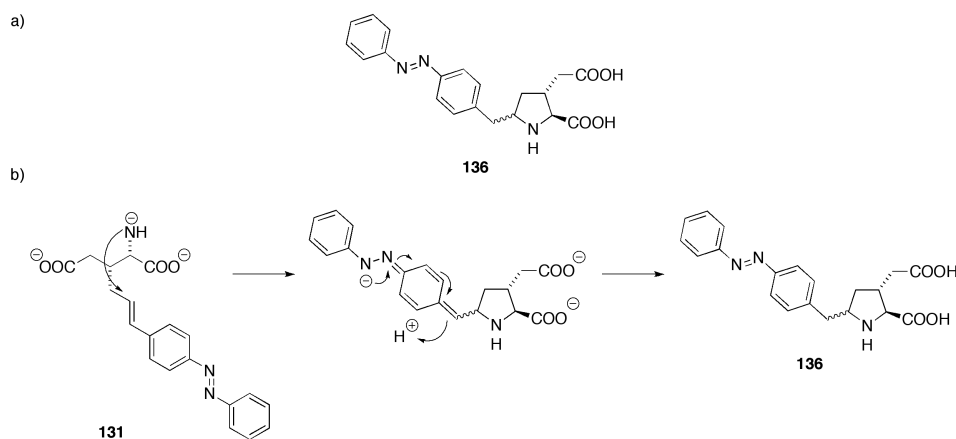
**Scheme 18.** a) Synthesis of protected 3-GluAzo (**130**) and its saponification. b) Efficient synthesis of (4*R*)-substituted pyroglutamate **133**, a key-intermediate in the synthesis of 4-GluAzo (**25**).

Saponification of the ester with lithium hydroxide in THF/water yielded the corresponding diacid **131**, which was subjected to a number of methods for the deprotection of Boc-groups. Unfortunately, Brønsted- and Lewis-acidic conditions (TFA/CH<sub>2</sub>Cl<sub>2</sub>, HCl/EtOAc, HCl/1,4-dioxane, FA/CH<sub>2</sub>Cl<sub>2</sub>, TMSOTf/CH<sub>2</sub>Cl<sub>2</sub>, TMSI/CH<sub>2</sub>Cl<sub>2</sub>, NaI/acetone) lead to decomposition – presumably due to protonation/alkylation of the sensitive styrene double bond (Scheme 17, left). Attempts to deprotect diacid **131** under pyrolytic conditions (140 °C, 10<sup>-3</sup> mBar) yielded the corresponding pyroglutamate. Basic conditions (1 M aqueous KOH) on the other hand yielded a product, which showed a high-resolution mass in accordance with the desired structure of 3-GluAzo (Scheme 19).



**Scheme 19.** Reaction pathway leading to decomposition of diacid **131** under Lewis/Brønsted acidic conditions and the attempted deprotection using aqueous KOH.

However, the NMR spectra indicated the absence of the two vinylic protons. Despite the low amounts of material obtained, a detailed analysis of the obtained 2D-spectra seems to suggest a rearrangement to pyrrolidine **136** – an unambiguous assignment was however not possible. Possibly, the formation of pyrrolidine **136** might proceed *via* a nucleophilic attack of the  $\alpha$ -nitrogen to the vinyl group, forming a stabilized benzylic anion, which is reprotonated to yield **136** (Scheme 20b).



**Scheme 20.** a) Putative structure of **136** with. b) Proposed mechanism leading to its formation starting from diacid **131**.

While we could not deprotect **131** to yield 3-GluAzo (**135**), we instead assessed the activity of its rearranged product **136** in mouse layer 2/3 neurons. Unfortunately, **136** did not show any notable effects, which is reasonable given that it deviates strongly from the substitution pattern of known iGluR agonists.

## 9) Pharmacology of Metabotropic Glutamate Receptors: A Structural Perspective

Metabotropic glutamate receptors (mGluRs) belong to family C (mGluR/pheromone) of G-protein coupled receptors (GPCRs), the largest group of genes in the human genome. They are expressed in- and outside the central nervous system and are associated with a broad spectrum of physiological processes (for the special role of mGluR6 in ON-bipolar cells see Chapter 5). Compared to *e.g.* ion channels however, the action of mGluRs is subtler, as they provide means for the modulation of cellular processes using second-messengers. Accordingly, mGluRs have become the target of therapeutic research for the treatment of Alzheimer's and Parkinson's disease, anxiety and schizophrenia.<sup>[161]</sup> Even though the structural information available from crystal structures of mGluR ligand binding domains is not as rich, as for example for iGluRs (*cf.* Table 1), the structure-activity relationships obtained from extensive screening efforts have yielded numerous compounds for the selective modulation of mGluR activity. A full mGluR structure has regrettably not been published yet. Nevertheless, the X-ray data present provides invaluable information and explanation for agonism or antagonism of compounds and the design of new ligands of mGluRs (Table 2).

**Table 2.** X-Ray structures of mGluR-LBDs. Entries marked with an \* have not been published yet.

Type	PDB code	Ligand(s)	Functional	Mutant(s)	Citation
mGluR1	1ISR	L-glutamate (1), Gd <sup>3+</sup>	a	-	[162]
mGluR1	3KS9	LY341495 (146)	ant	-	*
mGluR1	1ISS	MCG	ant	-	[162]
mGluR1	1EWK	L-glutamate (1)	a	(dimer)	[163]
mGluR1	1EWT	APO	-	-	[163]
mGluR1	1EWV	APO	-	-	[163]
mGluR3	2E4U	L-glutamate (1)	a	-	[164]
mGluR3	2E4V	DCG-IV	a	-	[164]
mGluR3	2E4W	(1 <i>S</i> ,4 <i>S</i> )-ACPD	a	-	[164]
mGluR3	2E4X	(1 <i>S</i> ,4 <i>R</i> )-ACPD (145)	a	-	[164]
mGluR3	2E4Y	(2 <i>R</i> ,4 <i>R</i> )-APDC (172)	-	-	[164]
mGluR3	3SM9	LY341495 (146)	ant	-	*
mGluR5	3LMK	L-glutamate (1)	a	-	*
mGluR7	2E4Z	MES	-	-	[164]
mGluR7	3MQ4	LY341495 (146)	ant	-	*

The neuromodulatory role of mGluRs and the underlying mechanisms that ultimately lead to the modulation of synaptic transmission will be in the focus of this chapter.

### a) Structure and Function of mGluRs

As a member of class C GPCRs, metabotropic glutamate receptors belong to the superfamily of seven transmembrane receptors (7TM). As such, they are integral membrane proteins and feature the canonical seven transmembrane helices (TM1-7). Unlike family A members, mGluRs have a large extracellular *N*-terminal domain, which forms the binding site of endogenous ligands. Due to its structure, this part of mGluRs is often referred to as the venus flytrap domain (VFD), which is comparable to the clamshell of iGluRs. Like the latter, the VFD performs a  $\sim 31^\circ$  movement upon binding of glutamate. This conformational change is then relayed to the intracellular parts of the receptor by the cysteine-rich domains (CRDs). There are nine important cysteines in the CRD, eight of which are linked by disulfide bonds. The ninth C is connected to the venus flytrap domain and has been shown to be crucial for intracellular signaling.<sup>[165]</sup> The transmembrane helices (TM1-7) have been found to be the site of mGluR modulation by kinases, as well as positive and negative modulators (PAMs and NAMs; Fig. 28a).<sup>[5]</sup> The intracellular loops formed by TM1-7 are responsible for binding of the respective G-proteins. The second intracellular loop in particular has been found to confer G-protein coupling specificity (*vide supra*).<sup>[5]</sup> Last but not least, the *C*-terminus of mGluRs has been shown to interact with multiple proteins and thus regulate mGluR signaling.<sup>[5]</sup>

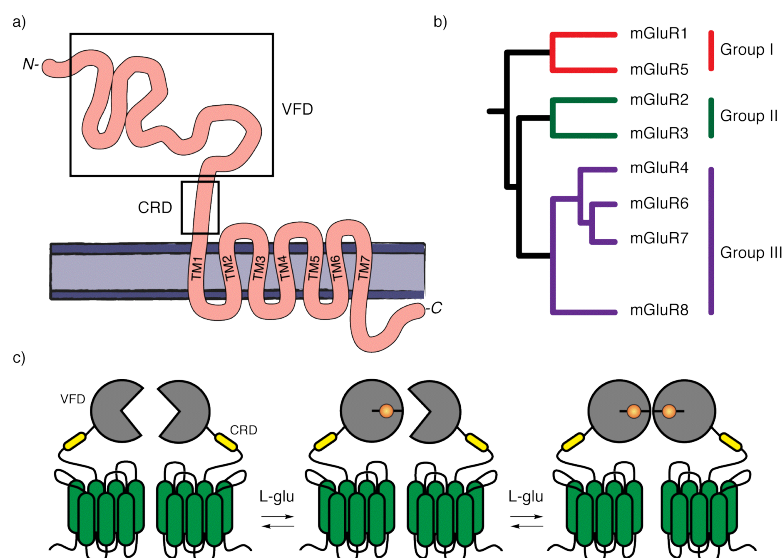


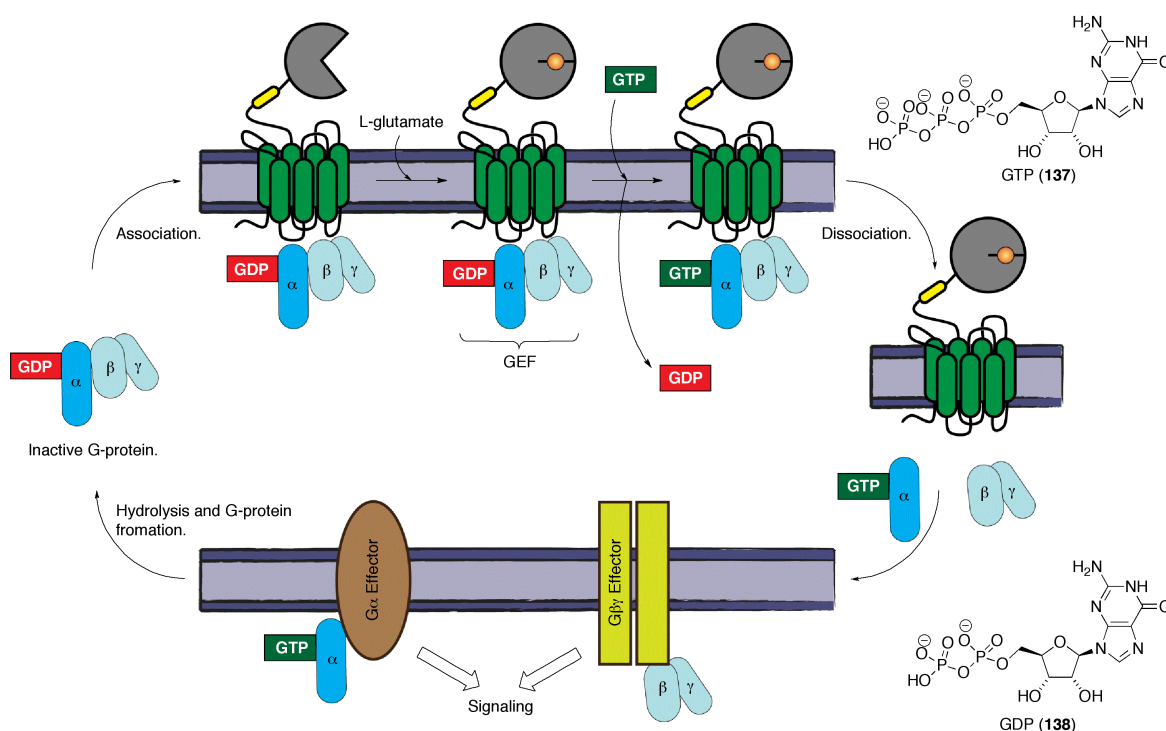
**Figure 28.** a) Schematic structure of an mGluR including the venus-flytrap (VFD), the cysteine-rich (CRD) and the seven transmembrane domains (TM1-7). b) Phylogenetic tree of the eight mGluRs. c) Mode of action of a functional mGluR dimer.

The metabotropic glutamate receptors have been organized in Group I (mGluR 1 and 5), Group II (mGluR2 and 3) and Group III (mGluR4, 6, 7 and 8) according to similarities in their amino acid sequence, signaling properties and pharmacology (Fig. 28b).

Functional metabotropic glutamate receptors are constitutive dimers, which are held together by both covalent and non-covalent bonds in the VFD, hydrophobic interactions of the TMs and possibly interactions of the C-termini (Fig. 28c).<sup>[166]</sup> Like in iGluRs, the predisposition of the ligand binding domains to dimerize is retained in the crystallization constructs, thus providing direct evidence for the functional importance of this association. Due to this, open-open, open-closed and closed-closed crystal structures have been obtained both in the presence and the absence of L-glutamate (**1**). This indicates an interesting functional explanation for the basal activity of mGluRs and suggests a mere stabilization effect of **1** in this equilibrium of states.<sup>[5]</sup> Most interestingly, it has been found that already one molecule of L-glutamate is enough to result in activation of some mGluRs (*vide infra*).<sup>[167]</sup>

### b) Receptor Activation and Intracellular Response

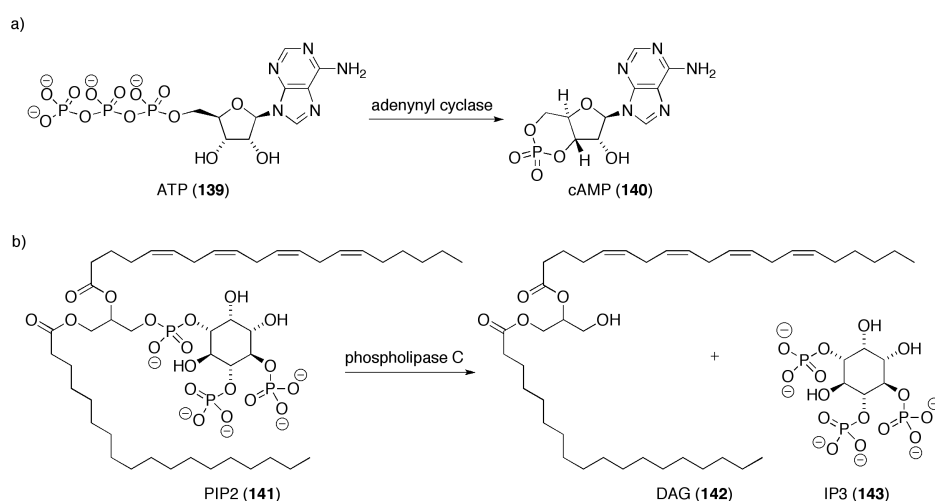
Much like in iGluRs, binding of glutamate to the VFD of metabotropic glutamate receptors causes a convergence of the two lobes, which form the ligand-binding domain (LBD, Scheme 21).



**Scheme 21.** mGluR activation-cycle and the chemical structures of GDP (**138**) and GTP (**137**).

This conformational change is then relayed to the intracellular loops of the receptor *via* the CRD. There, a G-protein complex consisting of a  $G_\alpha$ , a  $G_\beta$  and a  $G_\gamma$  subunit is bound. In the receptor's inactive state, the  $G_\alpha$  binds to guanosine diphosphate (GDP, **138**). Upon the action of glutamate, the G-protein's  $G_\alpha$  serves as a GDP exchange factor (GEF), promoting an exchange of GDP for guanosine triphosphate (GTP, **137**) and concomitant dissociation of the active  $G_\alpha$  from the  $G_{\beta,\gamma}$  subunits. The individual subunits can then activate other effector molecules (*vide supra*) and thus trigger different cellular responses. Ultimately, the  $G_\alpha$  is hydrolyzed and a new (inactive) G-protein complex is formed, which again binds to the mGluR (Scheme 21).<sup>[168]</sup>

There are in general two  $G_\alpha$  proteins by which the activity of mGluRs is coupled to intracellular processes:  $G_{\alpha i/o}$ , which inhibits adenynyl cyclases and thus the production of cyclic adenosine monophosphate (cAMP, **140**), and  $G_{\alpha q}$  promoting the cleavage of phosphatidylinositol-4,5-biphospahte (PIP2, **141**) into the second messengers diacyl glycerol (DAG, **142**) and inositol-1,4,5-triphosphate (IP3, **143**) by phospholipase C (Scheme 22).



**Scheme 22.** Production of cAMP (**140**) from adenosine triphosphate (ATP, **139**) by action of an adenynyl clidcase. b) Cleavage of PIP2 (**141**) into DAG (**142**) and IP3 (**143**) by PLC. The DAG shown bears the most common acyl residues of diacyl glycerols, stearic acid and arachidonic acid.<sup>[169]</sup>

For Group I mGluRs, the  $G_{\alpha q}$  pathway is predominant. Therefore, their activation results in activation of PLC and by means of IP3 (**143**) ultimately in the release of  $Ca^{2+}$  from internal storages. Together with the DAG (**142**) resulting from cleavage of PIP2 (**141**), this activates protein kinase C (PKC). Most interestingly it was found that mGluR1 can modulate the function of L-type calcium channels in cerebellar neurons by an unknown  $G_\alpha$  mechanism. At the same time it can be activated by  $Ca^{2+}$  directly, and it has been shown that mGluR5 can inhibit  $K^+$  channels and thus increase neuronal excitability.<sup>[3, 5]</sup>

Group II and Group III mGluRs couple to  $G_{\alpha i/o}$ , thus inhibiting adenyl cyclase. Conversely, Group II metabotropic glutamate receptors may potentiate cAMP formation by modulation of other  $G_s$ -coupled receptors *via* their respective  $G_{\beta\gamma}$  subunits.<sup>[3]</sup> Interestingly, this second signaling pathway seems to be the predominant mode of action of type II and III mGluRs, as the inhibition of cAMP production seems to be less pronounced. mGluR7 for example can inhibit P/Q-type  $Ca^{2+}$  channels through its  $G_{\beta\gamma}$  subunit after displacement of the latter by  $Ca^{2+}$ -loaded calmoduline. Additionally, both Group II and III mGluRs can activate G-protein coupled inward rectifying potassium channels (GIRKs) by action of their  $G_{\beta\gamma}$  proteins. Thus mGluRs can indirectly hyperpolarize neurons.<sup>[3]</sup>

By a combination of all of these signaling pathways, metabotropic glutamate receptor can modulate neuronal excitability by controlling both  $Ca^{2+}$  and  $K^+$  conductances. Moreover, they are involved in long-term depression and potentiation (LTD and LTP) by modulation of the fast acting iGluRs and they can induce slow excitatory synaptic responses *via*  $Na^+/Ca^{2+}$  exchangers and TRPC channels. Since a full account of this matter cannot be given in this short summary, the reader may be referred to some excellent books for a more detailed discussion.<sup>[3, 5]</sup>

### c) Structural Determinants of Receptor Activation

As stated earlier, the general mechanism of mGluR activation by L-glutamate (**1**) can be compared to the one found in iGluR, as the degree of VFT closure can be correlated to the receptor activity and thus to the ligand's function (Fig. 29).

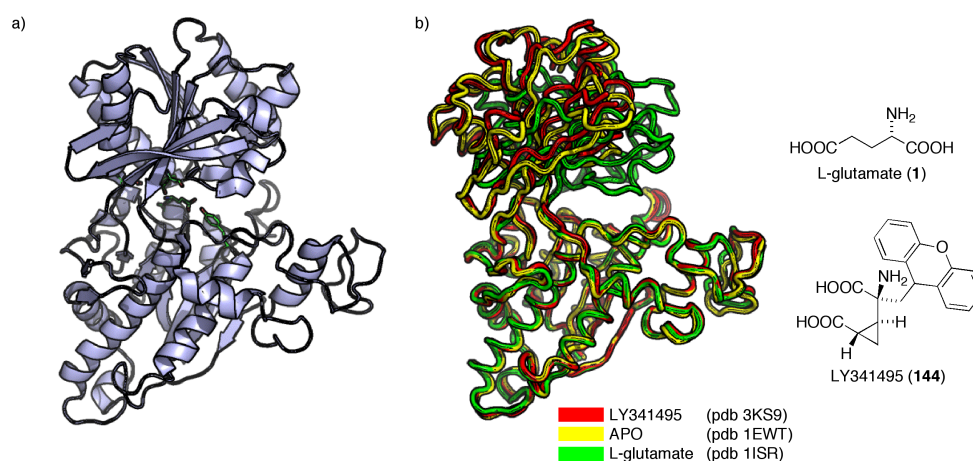


**Figure 29.** a) X-ray structure of L-glutamate (**1**) in mGluR1 (pdb code 1ISR) with the principal binding residues shown as sticks. b) Comparison of mGluR1 VFD-closure from an alignment of antagonist-bound (red), apo (yellow), and agonist-bound structures (green).

Like for the clamshell of iGluRs, orthosteric agonists stabilize the venus flytrap in a closed conformation and orthosteric antagonists pry it open by exerting steric bulk (*cf.* Fig. 29b). Unlike in iGluRs however, occupancy of a single mGluR monomer is enough to promote partial receptor activation.<sup>[167]</sup> The mode of action of both positive and negative modulators cannot be explained as easily. Nevertheless, it is important to note that some positive modulators bind at the TMs and can act as agonists when the VFD is deleted, thus suggesting a conformational effect, which is impaired in the presence of the extracellular domains.<sup>[170]</sup>

The orthosteric ligand-binding site is very well conserved between the mGluRs. The conserved residues interact with the  $\alpha$ -carboxy and the  $\alpha$ -amino group of L-glutamate (Fig. 30a). Residues interacting with the sidechain of **1** are however less preserved. Thus they provide an explanation for the observed subtype selectivity of different ligands. Moreover, the receptor-bound conformation of L-glutamate (**1**) differs greatly from the one found in crystal structures of ionotropic glutamate receptors. While the latter prefer the so-called “folded conformation”, mGluRs bind glutamate in another low energy state, the “extended conformation” (Fig. 30b).<sup>[163]</sup>

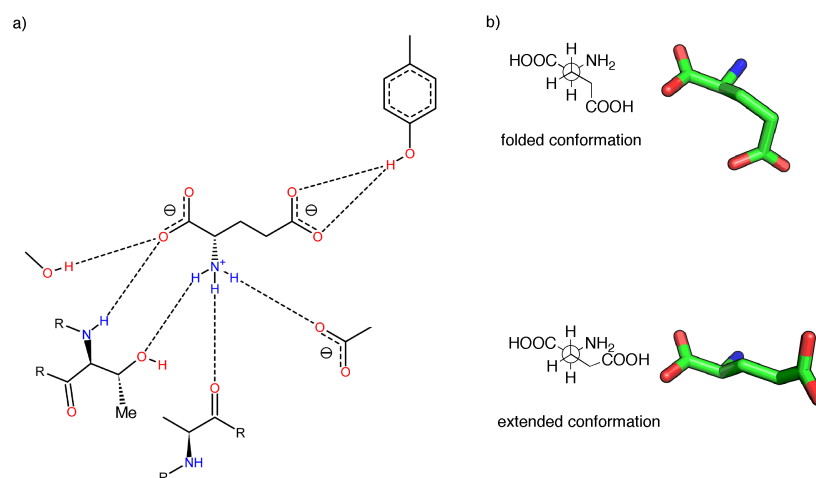


**Figure 30.** a) Illustration of the hydrogen bonds formed by the five principal binding residues in mGluR1 as generated by PoseView.<sup>[171]</sup> b) Comparison of the binding-modes of L-glutamate (**1**) in iGluRs preferring the folded (top) and mGluRs preferring the extended conformation (lower).

This notion is important, as the lowest energy conformations of 4-alkylated glutamate analogues differ depending on the configuration at C-4. While for 4-L-configured molecules the folded arrangement is favored, a 4-D-substitution results in the extended form dominating, thus avoiding a steric clash of the sidechain's primary CH<sub>2</sub> and the  $\alpha$ -NH<sub>2</sub> group. This offers an interesting stereochemical switch, by which agonists or antagonists derived from L-glutamic acid can be targeted at either iGluRs or mGluRs (*cf.* chapter 6).



#### d) Structures of Orthosteric Agonists, Antagonists, positive and negative Modulators and Allosteric Agonist

In general, orthosteric agonists of metabotropic glutamate receptors are L-glutamate analogues, which may be conformationally constrained. Antagonists are  $\alpha$ -amino acids that bear bulky groups, which prevent a closure of the VFD. For all agonists crystallized, the aforementioned extended conformation is observed. This section will provide an overview of orthosteric agonists, antagonists and modulators of Group I-III metabotropic glutamate receptors. It however does not aim at being comprehensive, but rather to illustrate the structural wealth of mGluR ligands. For more detailed analysis of mGluR pharmacology the reader may be referred to excellent reviews.<sup>[161, 172]</sup>

Besides of the principal ligand – L-glutamic acid (**1**) – (1*S*,3*R*)-ACPD (**145**) does not discriminate between the different metabotropic glutamate receptors, too. Most interestingly, the conformational restriction in **145** allows the molecule to adopt a conformation perfectly matching the one found in the crystal structures of mGluRs containing L-glutamate. The (3*S*)-isomer of **145** has been crystallized, too, and the comparison of the respective structures has yielded valuable information on the binding determinants of subtype-selective mGluR agonists (Fig. 31a).<sup>[173]</sup> Despite not being selective (activity in Group II & III),<sup>[172]</sup> LY341495 (**146**) can be regarded as the prototypical mGluR antagonist, beautifully illustrating the “foot in the door” mechanism. In **146** the  $\alpha$ -xanthene methyl moiety prevents an approach of the two VFD lobes, almost like a car-jack jammed in between the LBD hemispheres. Thus, VFD-closure and subsequently receptor activation are prevented.<sup>[174]</sup> It should be noted however, that the reason for the antagonism of **146** at mGluRs is not the alkylation of the  $\alpha$ -carbon, but rather the steric bulk of the substituent, as molecules substituted with smaller alkyl chains (*e.g.* methyl) at *C*-1 can be highly selective Group III agonists (*vide infra*).

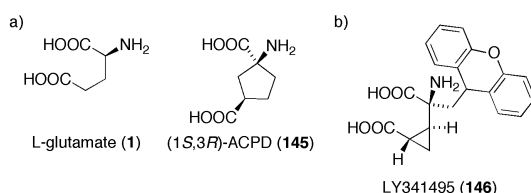


**Figure 31.** a) Nonselective mGluR agonists. b) The non-discriminating antagonist LY341495 (**146**).

The first selective mGluR agonist reported was L-quisqualic acid (**14**), a known and potent iGluR agonist. In general, both orthosteric agonists and antagonist show the  $\alpha$ -amino acid motif and a hydrogen-bond acceptor is located in an appropriate distance to mimic the  $\omega$ -

carboxy group of (*S*)-glutamic acid (**1**) in the extended conformation (Fig. 32a,b). However, there are such intriguing structures such as the agonist *trans*-azetidine-2,4-dicarboxylic acid (*t*-ADA, **149**) and the cubane-containing antagonist (*S*)-ACUDA (**152**).<sup>[175]</sup> Functionally, orthosteric antagonists act by preventing VFD-closure by exerting steric bulk.

The correlation between the structures of positive and negative allosteric modulators (PAMs and NAMs) and their function is unfortunately less obvious – if at all present. A common motif of these molecules however is the presence of large hydrophobic (aromatic) moieties, which are presumably interact with the TMs of metabotropic glutamate receptors.<sup>[5]</sup> Despite the lack of a general structure activity concept, a detailed analysis of individual PAMs and NAMs has yielded valuable information on the mechanism of receptor activation (Fig. 32c,d).<sup>[5]</sup>

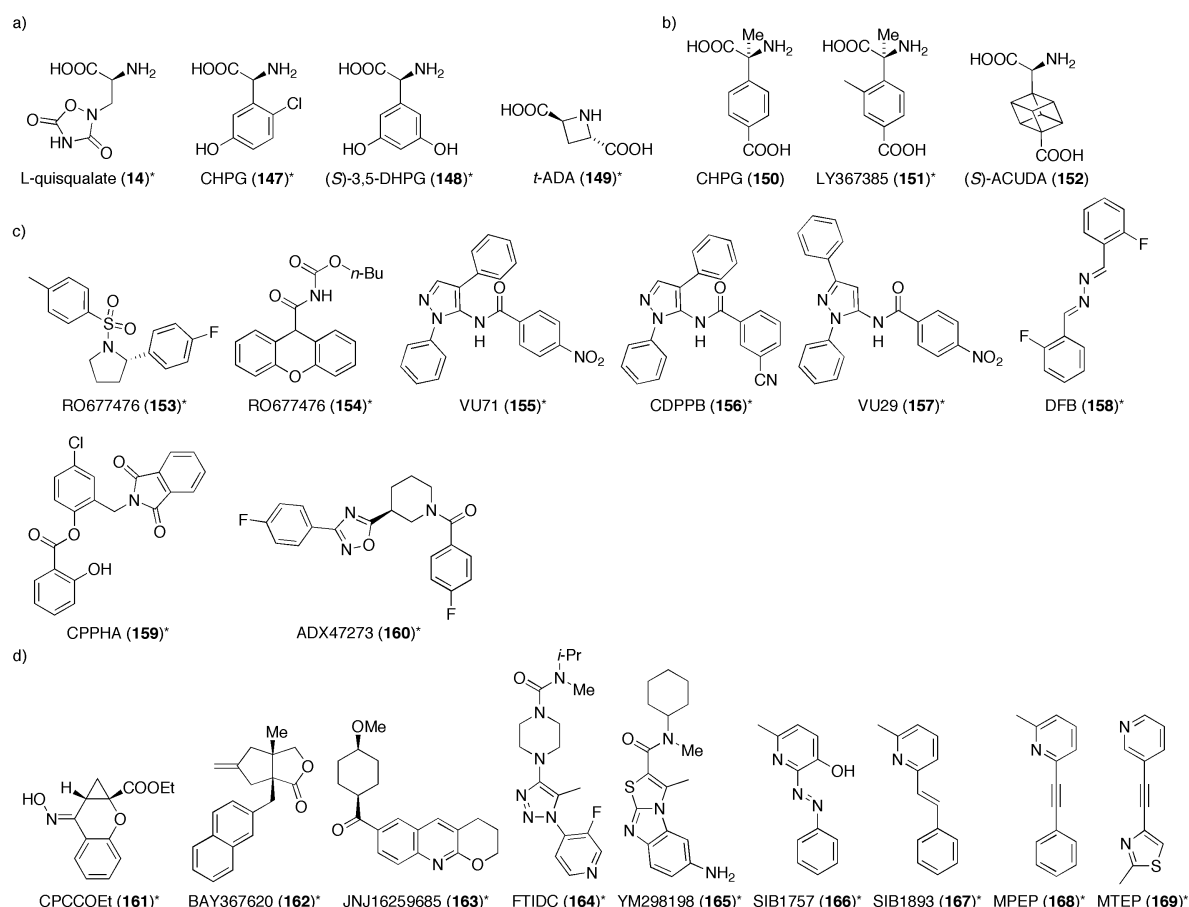


**Figure 32.** Group I-preferring a) agonists, b) antagonists, c) positive modulators and d) negative modulators. Molecules marked with an \* have not yet been crystallized with a receptor.

Among the negative allosteric modulators, there are such interesting structures as the chromene-derivative CPCCOEt (**161**) and the azobenzene SIB1757 (**166**). Unfortunately, there is no information whether **166** is photochromic (*i.e.* photoswitchable).<sup>[176]</sup>

Agonists with a preference for Group II mGluRs are conformationally highly restricted. LY354740 (**170**) and LY379268 (**171**) feature a (oxa) bicyclo[3.1.0]hexane motif and in L-CCG-I (**173**) C-3 and C-4 have been bridged by a cyclopropane (Fig. 33a).<sup>[177]</sup> Both PAM LY487379 (**174**) and the biphenyl-containing BINA (**175**) are highly selective for mGluR2, yet again there does not seem to be an obvious structure-activity relationship (Fig. 33b).<sup>[178]</sup>

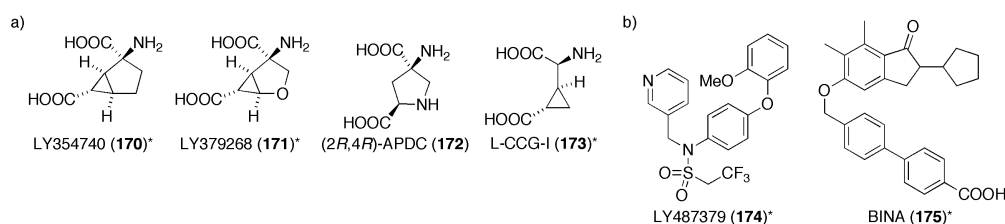


**Figure 33.** Group II-prefering a) agonists and b) positive modulators. Molecules marked with an \* have not been crystallized yet.

Group III-prefering agonists (Fig. 34a) include L-AP4 (**176**) and its cyclic and phosphate analogues Z-cyclopentyl-AP4 (**177**) and MAP4 (**178**).<sup>[179]</sup> Most interestingly L-AP5, a homolog of **176**, which bears an additional CH<sub>2</sub> group, is a selective NMDA antagonist.<sup>[9]</sup> Then again, the elongated AMPA-derivative, (*S*)-homo-AMPA (**181**),<sup>[180]</sup> is a selective mGluR6 agonist, indicating an intriguing connection to iGluR pharmacology.<sup>[9]</sup>

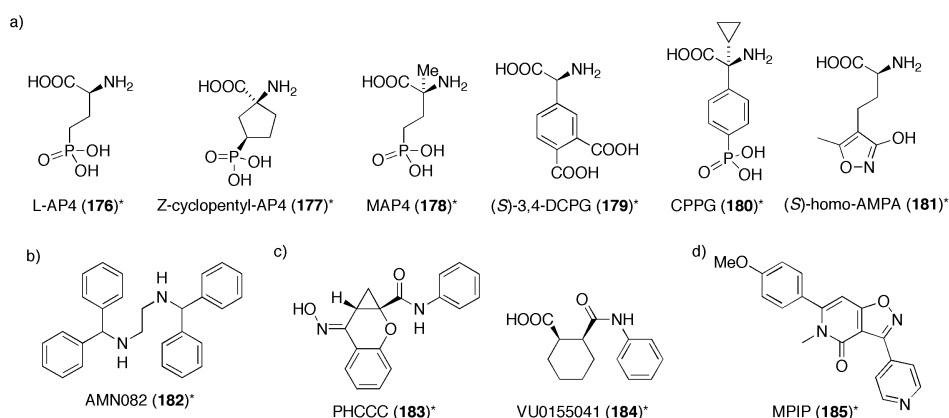


**Figure 34.** Group III-prefering a) agonists, b) allosteric agonists, c) positive modulators and d) negative modulators. Molecules marked with an \* have not yet been crystallized with a receptor.

Most interestingly, there is an allosteric agonist, the *N,N'*-dibenzhydryl-1,2-diamine AMN082 (**182**, Fig. 34b), which selectively activates mGluR7. Despite the lack of information on its allosteric binding site, it has been shown to induce mGluR7-dependant stress-hormone release.<sup>[181]</sup> Unfortunately, none of these Group III-prefering molecules including the PAMs

and NAMs (Fig. 34c,d) have been crystallized with their respective targets. Therefore, a structure-based analysis of their mode of action remains complicated.

#### **e) Résumé**

In summary, the information that can be gained from X-ray structures of metabotropic glutamate receptor VFDs is rather limited when compared to the 150 structures of iGluR ligand-binding domains. At the same time however, the amount of information available from structure-activity relationship screenings is enormous and surely reflects the importance of mGluRs for both academic and pharmacological research. As metabotropic glutamate receptors play an important modulatory role in synaptic transmission, it is no wonder that enormous effort have been taken to find both positive and negative modulators, which can be used in the treatment of various neuronal disorders. Given the explanatory power of crystal structures, it is to be expected that the structural collections will be expanded and they will for sure – at some point – include full-fledged mGluRs, as other 7TM receptors such as rhodopsin and GABA<sub>B</sub> receptors have already been crystallized, too.<sup>[182]</sup>

## 10) A Photoswitched Tethered Ligand of mGluRs

Given the success of our group controlling both endogenous and genetically modified iGluRs both *in vitro* and *in vivo*, we were highly interested in exploring the option of applying the PCL/PTL concept to metabotropic glutamate receptors, too. As targets, the group II mGluRs mGluR2 and mGluR3 were selected because of their importance in memory formation and for being major drug targets for neuropsychiatric disorders. By comparing the binding mode of L-glutamate (**1**) in mGluRs (*cf.* Chapter 5) and by homology modeling of mGluR2 and mGluR3 (*vide infra*) we anticipated, that we could not use the same molecules as previously in GluK2 (*i.e.* MAG-0, MAG-1), as they had the “wrong” configuration at C-4 (Figure 35a,b). Initial experiments had confirmed our hypothesis that – unlike for iGluRs – we would need D-configured molecules like **187** (Figure 35c) in order to photosensitize mGluRs using the PTL concept.<sup>[183]</sup> To us, this stereochemical switch (*i.e.* L to D) was a stroke of luck, since we could use many of the strategies that had been used to synthesize LMAGs, too.<sup>[86a]</sup>

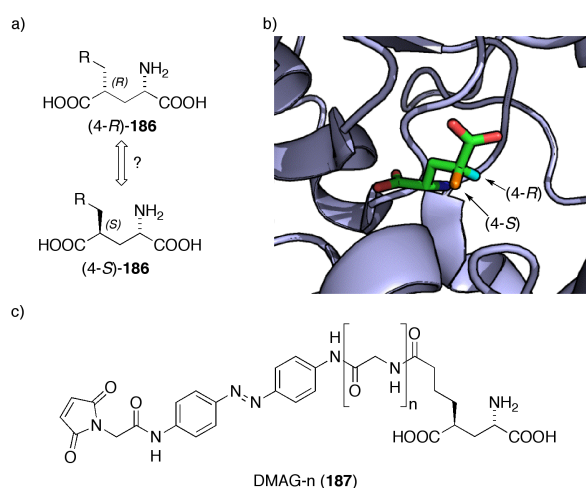
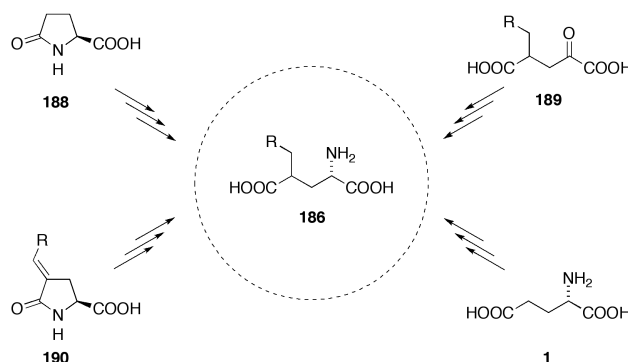


**Figure 35.** a) L- or D-configured glutamic acid analogues. b) mGluR3 (pdb 2E4U) as a model receptor of L- or D-substituted glutamate analogues. c) The prototype of DMAG-n **187** ( $n = 0, 1, 2$ ).

With the biological and the synthetic target identified, we were now faced with the challenge of synthesizing DMAGs (**187**) in both a diastereoselective and high-yielding way, since we would need multiple 100 mg for biological testing *in vitro* and *in vivo*. The following chapter therefore reports our considerations to the synthesis of these 4-D-substituted glutamate derivatives.

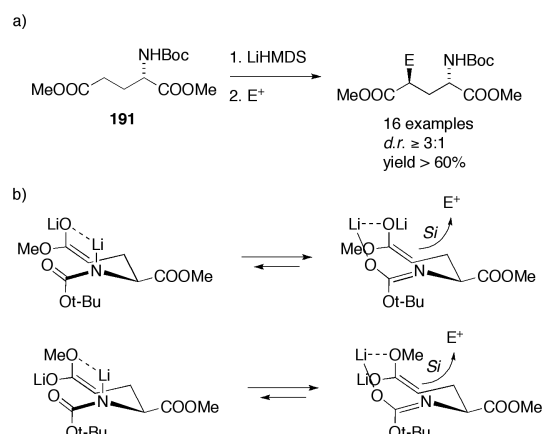
### a) Diastereoselective Synthesis of a PTL for mGluR2

Owing to the high interest in 4-alkylated glutamic acids as selective ligands for ionotropic glutamate receptors and EAAT inhibitors,<sup>[184]</sup> the most commonly used strategy for their synthesis is the alkylation of pyroglutamic acid (**188**). Alternatives include enzyme mediated transamination to ketone **189**,<sup>[184-185]</sup> hydrogenation of aldol-condensation products like **190** using Adam's catalyst,<sup>[186]</sup> or direct alkylation of glutamic acid **1**.<sup>[187]</sup> Many of them however either suffer from low yields or diastereoselectivity, or could not be applied to our envisioned synthesis since they are not compatible with the chemical functionalities of the target molecule (Scheme 23).



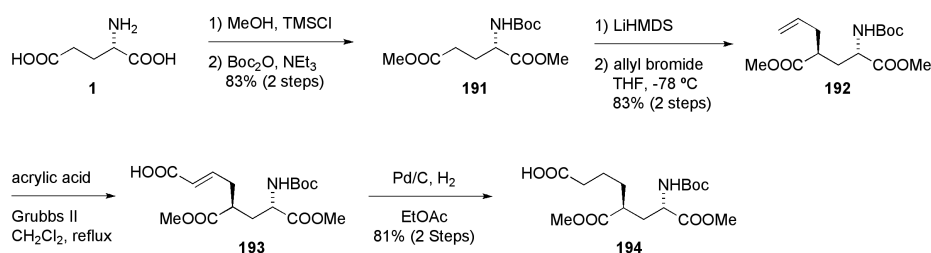
**Scheme 23.** Synthesis of 4-substituted glutamic acid analogues from different precursors.

We were therefore pleased to find, that protocols for the direct alkylation of *N*-Boc glutamic acid dimethyl ester (**191**) reported by Hanessian and coworkers promised high stereoselectivity and high yields for a variety of electrophiles (Scheme 24a).<sup>[188]</sup> Moreover, the only observed diastereomers were all *D*-configured, as was required for our synthesis of a PCL for mGluR2. This high selectivity can be rationalized by the transition state shown in Scheme 24b. It involves an intramolecular coordination of the dianion generated from *N*-Boc glutamic acid dimethyl ester (**191**) by a lithium cation and alkylation from the thermodynamically most favored conformations. In both cases, electrophiles only seem to attack from the *Si*-face (Scheme 24b).<sup>[188]</sup>



**Scheme 24.** a) Direct alkylation of N-Boc glutamic acid dimethyl ester (**191**) proceeds *via* a dianion. b) Transition state of the alkylation. The attack of the electrophile exclusively happens from the *Si*-face of the ester enolate.

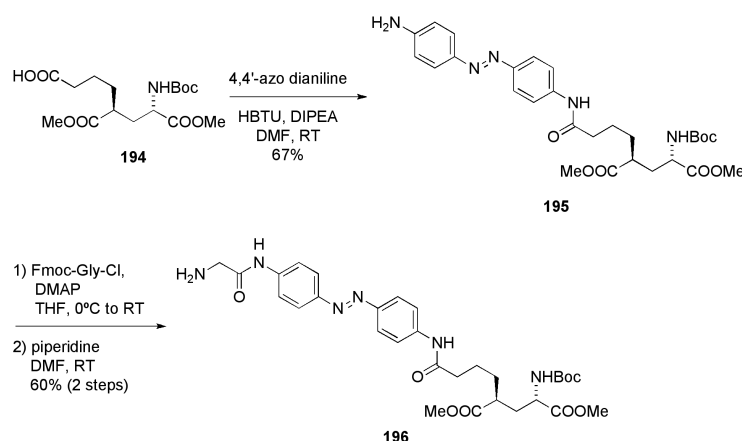
The representative synthesis of DMAG-0 (**187**,  $n = 0$ ) started from L-glutamic acid (**1**), which was protected by standard protocols.<sup>[189]</sup> Using the methodology developed by Hanessian and coworkers,<sup>[188]</sup> diester **191** was alkylated in the 4-position using lithium hexamethyldisilazide and an excess of allyl bromide to yield D-allylated glutamate **192** as a single diastereomer in good yields. Subsequent extension of the alkene chain using a metathesis reaction with acrylic acid gave enoate **193**, which then had to be selectively reduced. Unfortunately, we could not use the metathesis catalyst Grubbs II as the hydrogenation catalyst as described in some protocols.<sup>[190]</sup> Hence, resorting to palladium on charcoal under an H<sub>2</sub>-atmosphere, we obtained acid **194** in very good yields on a gram scale over two steps, which served as a key intermediate in our synthesis of PTLs for mGluR2 (Scheme 25).



**Scheme 25.** Diastereoselective synthesis of key-intermediate **194** from L-glutamic acid (**1**).

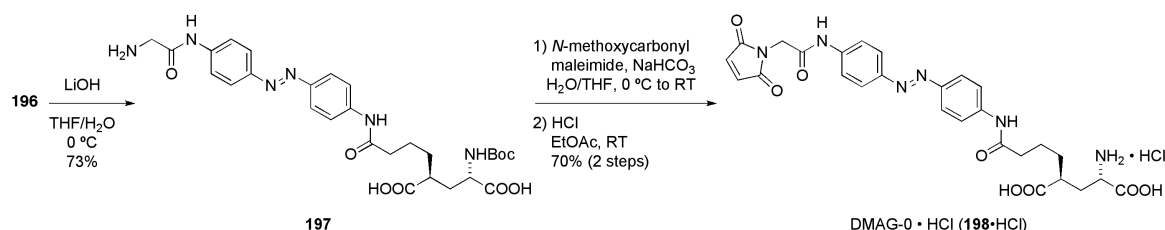
With **194** in hand, the following steps were modeled after the initial LMAG-synthesis.<sup>[86a]</sup> However, the known procedures could be improved to provide a higher-yielding access to PTLs for metabotropic glutamate receptors.

Starting from acid **194**, we introduced the photoswitchable unit, 4,4'-azo dianiline, by an amide coupling. Interestingly, HBTU proved superior to other coupling agents like CDI, EDCI, PYBOP or Ghosez's reagent.<sup>[191]</sup> Another amide formation using Fmoc glycine, which was activated as the acid chloride using oxalyl chloride and catalytic amounts of DMF, gave the corresponding fluorenyl carbamate-protected bisamide, which was deprotected using piperidine in DMF to yield the primary amine **196** (Scheme 26). Other, gentler activation methods (HBTU, CDI, EDCI, PYBOB) did not yield any coupling product, probably due to the low nucleophilicity of the anilinic amino function.



**Scheme 26.** Representative synthesis of DMAG-0 precursor **196**: Coupling to the photoswitch 4,4'-azo dianiline and installation of the terminal glycine moiety.

Dimethyl ester **196** was subsequently saponified using lithium hydroxide in water/THF to yield diacid **197** in good yields. For the installation of the maleimide functionality, we used a slightly modified protocol than the one used in the synthesis of L-configured MAGs.<sup>[86a]</sup> Additionally, we found, that in order to obtain high yields the *N*-methoxycarbonyl maleimide reagent had to be purified just before use by column chromatography. Finally, treatment of the obtained cabamate with HCl-saturated ethyl acetate gave DMAG-0 (**198**) in very good yields over two steps as its HCl-salt (Scheme 27).



**Scheme 27.** Representative synthesis of DMAG-0: Saponification, maleimide formation and global deprotection yields DMAG-0 (**198**) as its HCl-salt after deprotection.



Using this scalable and efficient route, we obtained tether-models DTM-0 (**199**) and DTM-1 (**200**), which lack the photoswitch and bear no or one glycine unit respectively. Additionally, we synthesized DMAG-1 (**198**), which has an additional glycine spacer and which had previously been synthesized using a different route (Fig. 36).<sup>[86a]</sup>

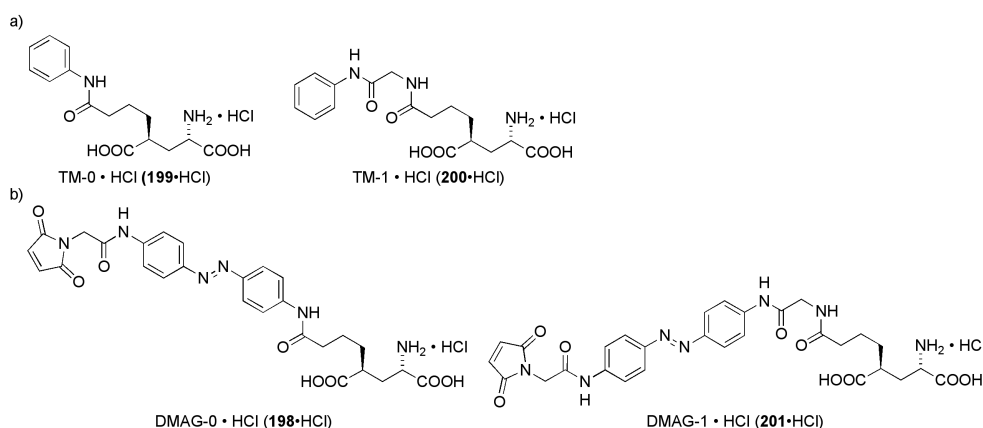


**Figure 36.** a) Tether-models DTM-0 (**199**) and DTM-1 (**200**). b) PTLs DMAG-0 (**198**) and DMAG-1 (**201**) obtained as their HCl-salts using a novel, diastereoselective and scalable route.

With both the tether-models and the 4-D-substituted PTLs synthesized, we sent the molecules to our collaboration partners in the Group of Ehud Isacoff, UC Berkeley, for biological evaluation. The results of their findings are summarized in the following section and have been submitted for publication.

*Note:* The numbering, the outline of figures and schemes, and the citations of the original manuscript have been adjusted to fit the format of this thesis.

## **b) Optical Control of a Metabotropic Glutamate Receptor**

Joshua Levitz, Carlos Pantoja, Benjamin Gaub, Harald Janovjak, Brian Kane, Philipp Stawski, Dirk Trauner and Ehud Y. Isacoff

(This work was submitted for publication in **2012**)

### **Summary**

We have developed an approach to elucidate the function of GPCRs by chemically re-engineering them to be sensitive to light. The class C glutamate-gated GPCRs, mGluR2, mGluR3 and mGluR6, which couple to Gi/o, were derivatized with photoswitchable ligands to generate light-agonized and light-antagonized receptors. The light agonized “LimGluR2” and “LimGluR3” respond to glutamate and to light in the same way, desensitize modestly and slowly and recover completely. The photoswitches are bistable, enabling activation by a brief light pulse to be sustained in the dark before being switched off by longer wavelength light pulse. Light-driven deactivation is fast and supports multiple reproducible rounds of on/off switching. Optical activation of LimGluR2 gates two of the primary functions of mGluR2: suppression of neuronal firing and inhibition of neurotransmitter release. Photo-antagonism relieves inhibitory tone during spontaneous activity. These light-gated mGluRs pave the way for determining the function of mGluRs and their heterodimeric combinations in synaptic plasticity, memory and disease.

### **Introduction**

The ability to turn protein function on and off with light provides the opportunity to reversibly manipulate signaling in living cells with a high spatiotemporal precision that is not achievable using traditional pharmacological or genetic approaches. Light-gated ion channels and pumps can be used to elicit strong depolarizing and hyperpolarizing photocurrents<sup>[97d, 192]</sup> Complementary to direct optical control of neuronal firing are efforts to remote control modulatory signaling proteins. Of special interest are G-protein coupled receptors (GPCRs), the largest family of membrane signaling proteins. These receptors respond to a wide-array of stimuli and contain a signature seven transmembrane domain that couples to heterotrimeric G-proteins, including the G<sub>q</sub>, G<sub>s</sub>, G<sub>i</sub>, and G<sub>i/o</sub>.<sup>[193]</sup> These pathways exert different effects, but primarily play roles in controlling second messenger levels and regulating other signaling proteins, including ion channels and kinases. Due to their ubiquity and importance in many diseases, GPCRs are the most explored drug targets in all of biology. Despite this, the specific

biochemical, physiological, and behavioral roles of many GPCRs are not well understood and make this field ripe for the application of new tools for high-precision probing.

Engineered GPCRs that respond to non-native ligands—the so-called RASSLs and DREADDs—have been used to orthogonally activate G protein pathways *in vitro*<sup>[150a]</sup> and *in vivo*.<sup>[194]</sup> Because these receptors lack the spatiotemporal precision of optical manipulation, interest has remained in the development of light-activated GPCRs. Until the present, the effort has centered on the naturally light-sensitive rhodopsin<sup>[195]</sup> and melanopsin<sup>[196]</sup> and chimeras that combine the transmembrane portions of rhodopsin with the cytoplasmic loops of adrenergic or serotonergic receptors to couple to other G-proteins<sup>[6b, 197]</sup> The rat rhodopsin RO4 has been used to couple via  $G_{i/o}$  to G-protein activated inward rectifier (GIRK) channels in HEK293 cells and cultured hippocampal neurons, and thereby to control excitability as well as rhythmic activity in chick spinal cord<sup>[195a]</sup> and mouse cerebellum.<sup>[198]</sup> Chimeras between bovine rhodopsin and either the human  $\alpha_1$  or  $\beta_2$  adrenergic receptor have been shown to light-activate  $G_q$  and  $G_s$ .<sup>[197a]</sup> These “optoXRs” have been used *in vivo* to modulate activity in the nucleus accumbens and thereby control reward-related behavior in mice.<sup>[6b]</sup> Most recently, a chimera between RO4 and the C-terminus of the 5-HT1A receptor was shown to mimic serotonergic signaling in the dorsal raphe nuclei.<sup>[197b]</sup>

A major advantage of vertebrate opsin-based GPCRs is their use of the naturally bioavailable retinal as the chromophore. However, there are two potential disadvantages. First, unlike the microbial opsins, in which retinal is permanently bound, the isomerized *trans*-retinal dissociates from rhodopsin and must be replaced by fresh *cis*-retinal.<sup>[199]</sup> In photoreceptor cells fresh *cis*-retinal is delivered efficiently from the retinal pigment epithelium and under physiological conditions only a very small fraction of rhodopsins are photo-bleached at any one time, thus assuring a large population of unbleached rhodopsin.<sup>[200]</sup> However, in the rest of the nervous system the concentration of *cis*-retinal is lower and the replenishment of bleached retinal may be slower. Moreover, the deactivation of rhodopsin is slow in the absence of the photoreceptor cell-specific enzymatic pathway.

We report here an alternative approach to engineering light gating into GPCRs in which we use photoswitchable tethered ligands (PTLs). The attraction of this approach is that it provides optical control over the native receptor, so that in addition to providing heterologous control of G protein signaling, it provides the unique possibility for investigating the normal function of that receptor. The PTL approach has been used to light-block  $K^+$  channels and light-activate ionotropic glutamate receptors,<sup>[86a, 97j, 201]</sup> providing for fast bidirectional photoswitching, bistability, and modularity.<sup>[202]</sup>

We targeted the metabotropic glutamate receptors (mGluRs), class C GPCRs that, like ionotropic glutamate receptors, are allosterically regulated by glutamate binding to a large extracellular clamshell ligand binding domain (LBD).<sup>[161]</sup> The LBDs form back-to-back homo- or hetero-dimers whose glutamate-induced rearrangement is propagated via a cysteine-rich domain to a 7- transmembrane domain whose cytoplasmic loops interact with G proteins.<sup>[163, 173, 203]</sup> Other GPCRs of this class include T1R taste receptors, vomeronasal pheromone receptors, GABAB receptors, and the calcium receptor.<sup>[203]</sup> The mGluRs are divided into three groups based on sequence homology.<sup>[161]</sup> We focused initially on the group II mGluRs, mGluR2 and 3, which couple to the  $G_{i/o}$  pathway to inhibit adenylyl cyclase,<sup>[204]</sup> and which also activate GIRK channels, thereby reducing excitability, and inhibit voltage-gated calcium channels, thereby inhibiting neurotransmitter release.<sup>[205]</sup> Presynaptic group II mGluRs also play roles in long term depression and potentiation of synaptic transmission in multiple brain regions including the hippocampus,<sup>[206]</sup> nucleus accumbens,<sup>[207]</sup> striatum,<sup>[208]</sup> and amygdala.<sup>[209]</sup> Genetic knock-out and pharmacological studies have implicated mGluR2 and 3 in spatial memory,<sup>[210]</sup> motor coordination,<sup>[211]</sup> and other aspects of cognition.<sup>[212]</sup> Because of these important physiological roles, group II mGluRs are major drug targets for neuropsychiatric disorders including anxiety, depression, and schizophrenia.<sup>[213]</sup> We extended our engineering to the Group III mGluR, mGluR6. Members of this family also couple to the  $G_{i/o}$  pathway and have been implicated in similar cellular functions. But they display different expression profiles, subcellular targeting and regulation *via* PDZ ligands, kinases, and  $Ca^{2+}$ /calmodulin.

We used a combination of structural analysis and novel test compounds to develop PTLs with appropriate stereochemistry, length and molecular composition and a powerful but simple and fast battery of Monte-Carlo simulations to predict appropriate cysteine attachment sites on the LBD. The approach was successful and we report examples of both photo-agonism and photo-antagonism. The photo-agonism of mGluR2 in neurons evokes rapid optical activation and deactivation, as well as bistable photo-control, can be used to control excitability and pre-synaptic inhibition in cultured neurons, and also works in intact brain slices. *In vivo*, mGluR2 photo-agonism can be used to reversibly and repeatedly modulate escape behavior in larval zebra fish. Furthermore, we demonstrate that this approach may be generalized by engineering agonistic photocontrol of the group II mGluR, mGluR3, and antagonistic photocontrol of the group III mGluR, mGluR6. The introduction of photosensitivity into native GPCRs provides the means for probing their biological functions at a level of precision not previously available. Optical control of mGluRs, one of the largest families of GPCRs that

respond to a single neurotransmitter, and one of the brain's major neurotransmitters at that, paves the way for determining the function of each receptor type and the many heteromeric combinations that they make in the multiple neuron types and brain regions where they are expressed.<sup>[214]</sup>

### **Experimental Procedures Chemical Synthesis**

The chemical synthesis of DMAG-0, DMAG-1 and D-tether models was carried out as described in the Supplementary Information. The synthesis of L-tether model has been described previously.<sup>[86a]</sup> Homology modeling and Monte-Carlo simulations to select MAG attachment sites are described in Supplemental Information.

### **Molecular Biology and Gene Expression in Cultured Cells**

Mutations were introduced into plasmids using the QuickChange mutagenesis kit (Agilent) and transfection was performed using Lipofectamine 2000 (Invitrogen) and the calcium phosphate method for HEK 293 cells and neurons, respectively. See Supplementary Information for details.

### **Cultured Cell Electrophysiology**

HEK 293, HEK 293T, and Dissociated Neuron whole cell patch clamp electrophysiology coupled with wavelength-specific illumination was performed using standard techniques. See Supplementary Information for details.

### **Hippocampal Slice Gene Expression and Electrophysiology**

Hippocampi were obtained from postnatal Sprague-Dawley rats (postnatal days 6 and 7) and 400  $\mu$ m slices were prepared, cultured, and electrophysiology was performed as previously described (Janovjak et al., 2010), with minor variations. See Supplementary Information for details.

### **Zebrafish Transgenesis**

Expression of mGluR2-L300C was targeted to neurons using the UAS/GAL4 system. See Supplementary Information for details.

### **Zebrafish Behavioral Assay**

Swim and escape responses were elicited using an 8 Ohm mini-speaker (Radioshack) and images were captured using a behavioral camera (IDS, USB 2 uEye).<sup>[119]</sup>

## Statistics and Data Analysis

Data was analyzed using Clampfit (Axon Instruments) and Origin (OriginLab) software. Statistical analysis was performed using Microsoft Excel. All values reported are mean  $\pm$  s.e.m.

## Results

### Tether Model Pharmacology and Synthesis of Photoswitches

To design photocontrol of mGluR2, we first inspected the available crystal structures of mGluR clamshells in their open and closed forms, which show that glutamate is bound in a highly conserved conformation. Using a homology model of mGluR2 based on the closed, glutamate-bound structure of mGluR3 (PDB ID: 2E4U) we asked if there is an access channel by which a PTL could reach a thiol- reactive end to the lip of the LBD for cysteine attachment while its glutamate end is bound in the ligand binding site. The model reveals such an access channel (Fig. S1A) that may provide a route to the 4' carbon of glutamate, which was the site of attachment for the linker in previously described MAG PTLs. It was also apparent that substituents attached to the 4'-position of glutamate with D-stereochemistry will point to the solvent-exposed side of the clamshell (Fig. S1B, C) and thus, this configuration seemed best suited for tether attachment. This observation is consistent with pharmacological studies indicating that 4' substituted glutamate analogues with D stereochemistry produce more potent activation of mGluR2.<sup>[215]</sup> To further test what types of molecules may be used to control mGluR2, we tested, as a free ligand, L-Tether-1 (previously referred to as "tether model").<sup>[86a]</sup> This compound contains one ring of the azobenzene, a linker and the glutamate moiety and thus mimics half of MAG (Fig. 37A). Wild type rat mGluR2 and GIRK1 were co-expressed in HEK293 cells. Whole-cell voltage clamp recordings showed large inward currents in response to glutamate but no response to 1-3 mM L-Tether-1 and no effect of L-Tether-1 on the glutamate response, indicating lack of both agonism and antagonism. We next examined compounds with 4' D-stereochemistry and either one or two glycine linkers connecting the glutamate group and the benzene ring (D-Tether-0 and D-Tether-1; Fig. S1A). 1 mM D-Tether-0 activated mGluR2 currents to  $26 \pm 5\%$  ( $n=6$ ; Fig. S1D) of the size of currents activated by saturating (1 mM) glutamate. 1 mM D-Tether-1 showed no activation but reduced the currents evoked by 1 mM glutamate by  $55 \pm 1\%$  ( $n=4$ ; Fig. S1E). These tether models confirmed our stereochemical predictions and provided the impetus for synthesizing DMAG-0 and DMAG-1 (Fig. 37B).

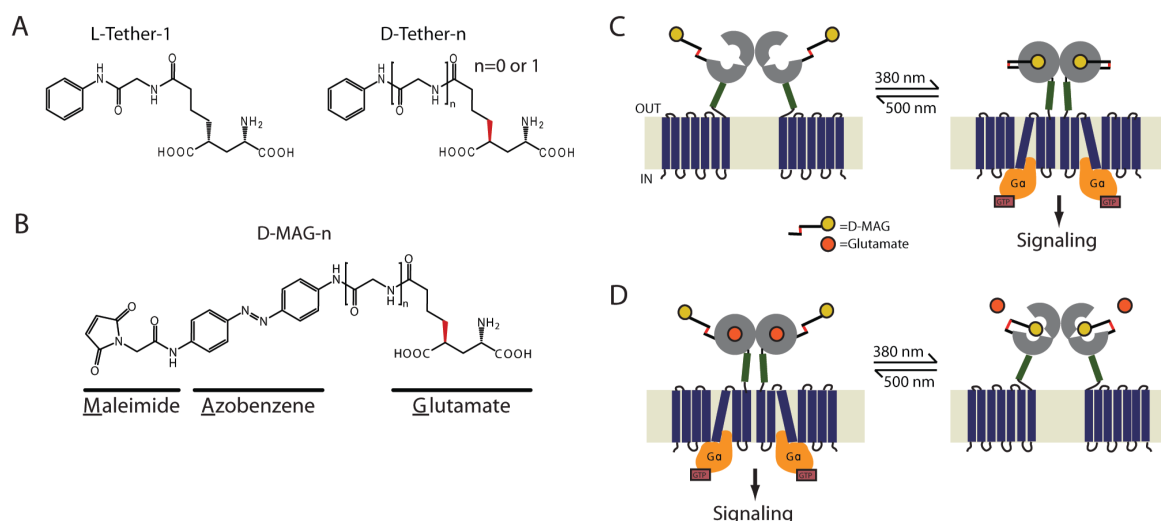


**Figure 37.** Design of photoswitches for light-control of mGluR2. (A) Chemical structure of tether models including previously described L-Tether-1 and new 4' D versions with two different linker lengths (D-Tether-0 and D-Tether-1) (B) Structure of DMAG molecules. 380 nm light maximally isomerizes to the cis state, whereas 500 nm light isomerizes to the trans state. Spontaneous thermal relaxation from cis to trans occurs over tens of minutes at room temperature. (C) Schematic of light-induced agonism. mGluRs contain a ligand-binding clamshell domain (LBD; grey) that is coupled to a 7-transmembrane domain (TMD; green) by a cysteine rich domain (CRD, dark blue). Agonist binding to the LBD initiates clamshell closure, which rearranges a dimer interface with a partner LBD of a second subunit and transmits a conformational change via the TMD to the cytoplasmic domain, thereby activating G-proteins. Under 380 nm illumination DMAG enters the cis state and reorients the glutamate moiety into the ligand binding site to drive clamshell closure and activate G protein and downstream signaling. (D) Schematic of 380 nm-induced antagonism. Glutamate (dark orange circles) is shown in the bound, activated state of mGluR2. Upon photoisomerization the glutamate end of MAG enters the binding site and prevents clamshell closure, thus deactivating the receptor.

### Monte Carlo Simulations of DMAG-0 Reach

In order to rationally design light-gated versions of mGluR2, we used Monte Carlo simulations to identify geometrically appropriate cysteine-attachment points for the conjugation of DMAG-0. First we built a homology model of mGluR2 in the open, glutamate-bound state using the mGluR1 open, glutamate-bound crystal structure (PDB ID 1EWK) as a template. We then generated molecular models of DMAG-0 with geometries of cis- and trans-azobenzene based on earlier experimentally determined coordinates that were validated computationally.<sup>[216]</sup> After manually positioning the glutamate-group of DMAG-0 in the binding pocket, the Monte-Carlo multiple minimum (MCMM) algorithm<sup>[217]</sup> was used to search the space accessible to DMAG-0 with single-bond rotations as degrees of freedom. Twenty thousand orientations/structures were generated by MCMM and for each the distance from the cysteine-reactive maleimide (Mal) group of MAG to every residue on the surface of

the LBD was measured automatically. Simulations were performed for both *cis*- and *trans*-conformations of DMAG-0 (Figure 38A shows a superposition of 20 conformations of DMAG-0 bound to the LBD of mGluR2 from the *cis* simulation.) The conformational search identified eight clusters of 3-8 residues that were significantly populated by the Mal-group of DMAG-0 (Figure 38B). Notably, the region between residues 299 and 305 contained multiple residues with high frequencies, as well as substantially higher scores for *cis* than for *trans*, indicating that such sites may allow for selective activation of mGluR2 in the *cis* state.

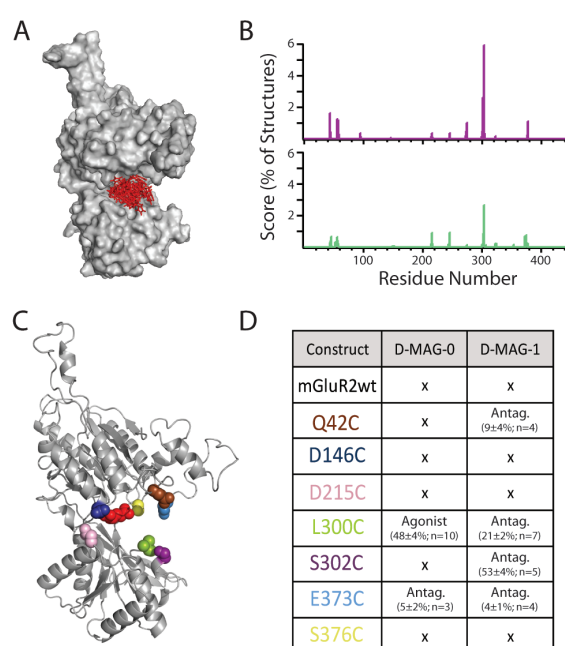


**Figure 38.** Monte Carlo simulations and cysteine-scanning of mGluR2 ligand-binding domain. (A) *cis*-DMAG-0 (red stick depiction) with glutamate end bound in LBD (gray surface depiction) is shown in 20 superposed conformations calculated by Monte Carlo simulation using homology model of the mGluR2 LBD in the open, glutamate-bound conformation. (B) Results of DMAG-0 simulations for *cis* and *trans* conformations. Lines indicate the frequency with which the maleimide end of MAG approaches within 6 Å of the Ca of a particular residue in the *cis* state (purple) and *trans* state (green). (C) Open homology model of mGluR2 LBD showing native side chains of 7 residues individually substituted to cysteine. (D) Results of photoswitching of DMAG-0 and DMAG-1 attached at each of the seven positions. “x” indicates no photoresponse. Agonistic and antagonistic effects are quantified (mean + s.e.m.) relative to response to 1 mM glutamate. Data from >2 different coverslips for all conditions tested.

The Monte Carlo simulations reveal amino acids whose C $\alpha$  positions are near the maleimide. We selected a subset of seven residues with orientations favorable (not pointing into the core of the protein) for the maleimide end of MAG to conjugate and for its glutamate end to enter the ligand-binding site without steric clashes. Seven candidate sites were identified: Q42,



D146, E373 and S376 in the upper lobe of the LBD, L300 and S302 on the lower lobe, and D215 at the hinge (Fig. 38C). Each site was individually substituted with cysteine and co-expressed with GIRK1 in HEK293 cells.

### **Photo-Antagonism by DMAG-1: LimGluR2-block**

We focused initially on two MAG attachment sites, L300C and S302C, because of their high scores in the Monte Carlo simulations and their large photo-effects in initial experiments (Fig. 38B, D). Cells expressing either variant were labeled with either DMAG-0 or DMAG-1 (50-100  $\mu$ M) for 30-60 minutes, patch-clamped in the whole cell configuration and alternately challenged with 380 nm light to isomerize the photoswitch to *cis* and 500 nm light to isomerize to *trans*. This was done in the absence of glutamate to determine if there was photo-agonism or in the presence of glutamate to determine if there was photo-antagonism.

Following labeling at S302C and L300C with DMAG-1 we found that illumination at 380 and 500 nm had no effect on the current (Fig. 3A, S2A). However, in the presence of L-glutamate, 380 nm light induced a marked decrease in the current that was reversed by illumination at 500 nm (Fig. 3A, S2A). Repeated switching between 380 and 500 nm light toggled the glutamate-induced current between high and low levels. The percentage photo-antagonism was  $21 \pm 2\%$  ( $n = 7$ ) for DMAG-1 at L300C and  $53 \pm 4\%$  ( $n = 5$ ) at S302C in 1 mM glutamate. At concentrations greater than 1mM, photoantagonism was decreased (Fig. S2B), indicating a competitive mechanism. Due to the large potency of the 302C substitution in combination with DMAG-1 in photo-antagonism of mGluR2, we term this tool “LimGluR2-block”. Of the seven attachment sites that were selected for study, four (including L300C and S302C) showed photo-antagonism with DMAG-1 (Figure 2C, D). These results are consistent with the antagonism of the D- Tether-1 compound, observed above.

### **Photo-Agonism by DMAG-0: LimGluR2**

We next turned to the version of MAG that was based on the agonist D-Tether-0, namely DMAG-0. Of the seven sites that we examined, only two had a photo-response to DMAG-0: L300C showed robust photo-agonism (Fig. 39B) and S373C had weak photo-antagonism (Fig. 39D). We focused on the L300C/DMAG-0 combination because of the utility of photo-activation, and refer to it henceforth as “LimGluR2”. Voltage ramps confirmed that the light-activation of LimGluR2 at 380 nm was due to the opening of the same inward-rectifying potassium conductance as was activated by glutamate (Fig. S3A). The photo-activation of LimGluR2 by 380 nm light yielded currents about half as large as those evoked by saturating

glutamate ( $48 \pm 4\%$  compared to 1 mM glutamate,  $n = 10$ ; Fig. 39C). Illumination at 500 nm terminated the activation of the GIRK1 channels as rapidly as they were activated by 380 nm light (Fig. 39B, C).

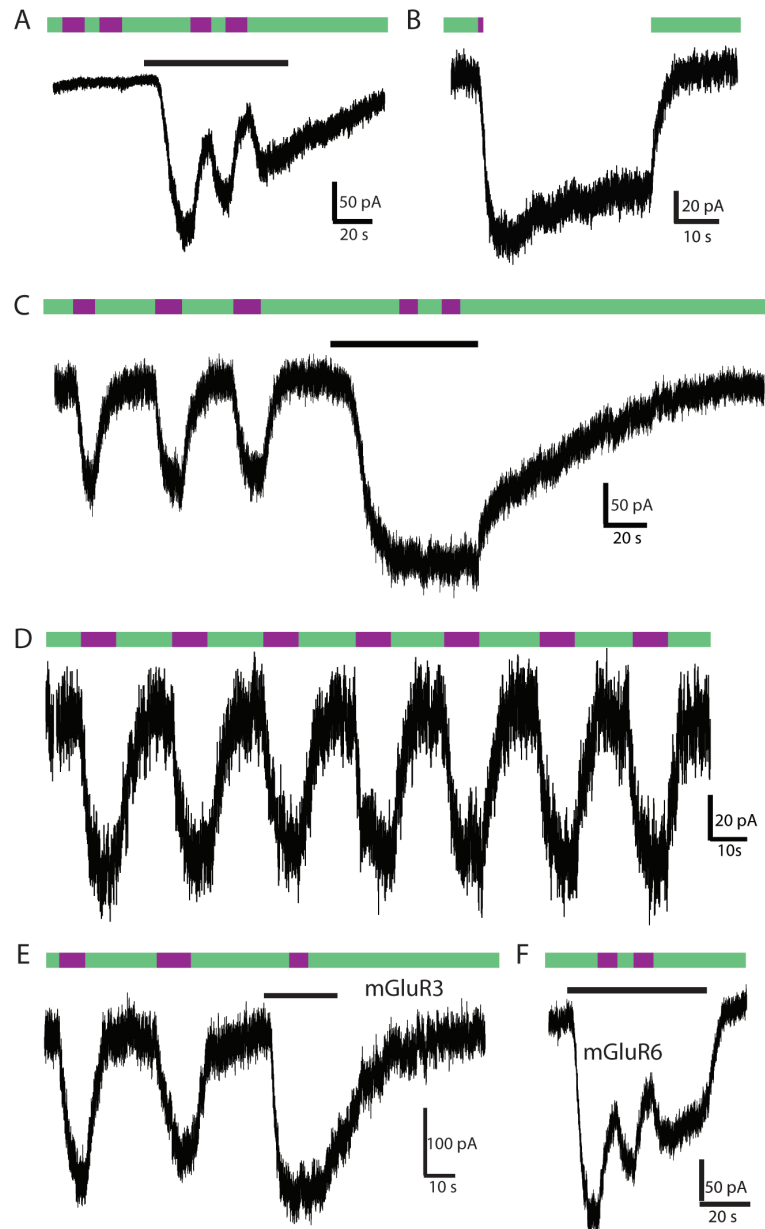


**Figure 39.** Photo-antagonism of mGluR2 and mGluR6 and photo-agonism of mGluR2 and mGluR3. (A-F) Effects of photoswitching DMAG0 and DMAG1 on the activation of GIRK1 current in HEK293 cells. (A) When DMAG-1 is attached to S302C (“LimGluR2-block”) light has no effect in the absence of glutamate, but 380 nm light evokes photo-antagonism in the presence of glutamate. Black bars indicate application of 1 mM L-glutamate. Green bars indicate illumination with 500 nm light and purple bars indicate 380 nm light. (B, C) When DMAG-0 is attached to L300C 380 nm light evokes GIRK1 current on its own. GIRK1 current trace shows sustained response in the dark following a brief illumination at 380 nm (B). The current remains activated until deactivation is initiated by 500 nm light. No photo- antagonism is seen in the presence of glutamate, indicating that DMAG-0 is not a partial

agonist of mGluR2- L300C (C). (D) GIRK1 current evoked by repetitive rounds of photo-activation and photo- deactivation of mGluR2-L300C-DMAG-0 ("LimGluR2") by pulses of 380 nm and 500 nm light, respectively. (E) When DMAG-0 is attached to mGluR3-Q306C ("LimGluR3") robust 380 nm-induced antagonism is seen. Similar to LimGluR2, no photo-antagonism was seen in the presence of glutamate. (F) When DMAG-0 is attached to mGluR6-K306C ("LimGluR6-block") robust 380 nm-induced photoantagonism is seen, indicating that the PTL approach can be extended to group III mGluRs.

An advantageous property of azobenzene photoswitches is their bistability, which makes it possible to produce persistent occupancy in the dark of the activating *cis* state following a photo-isomerizing light pulse.<sup>[97d, 218]</sup> Indeed, we found that a brief (1 s) activating light pulse at 380 nm, which was long-enough for the azobenzene to reach the photostationary state, evoked a period of GIRK activation that persisted for tens of seconds in the dark, and which could be rapidly turned off by illumination with 500 nm light (Fig. 39B). During this bout of protracted activation in the dark the current declined by ~10-20%, a decline that was similar to what was seen under continuous illumination of LimGluR2 at 380 nm, as well as in response to extended application of glutamate.

Notably, no antagonism of the glutamate response was induced by illumination at 380 nm (Fig. 4C, S3C). This suggests that the lack of full activation by DMAG-0 attached to L300C is not due to partial agonism by *cis*-DMAG-0, but to incomplete occupancy of the *cis* state at 380 nm<sup>[218]</sup> and, possibly, to incomplete labeling of the engineered cysteine. Application of glutamate following initiation of illumination at 380 nm increased the inward current above the level induced by light alone (Fig. S3B). This result further indicates that MAG does not lock the LBD in a partially activated conformation, but rather functions as a full agonist in a fraction of subunits.

Repeated bouts of photoswitching of LimGluR2 yielded multiple rounds of photo-activation of GIRK1 channels without decline of the response (Fig. 39D). The reproducibility of the optical activation of LimGluR2 is consistent with the lack of GRK-dependent desensitization of mGluR2.<sup>[219]</sup> Having observed that LimGluR2 can be rapidly turned on and off with light and repeatedly activated in a reproducible manner, we asked how it compares with the earlier light-gated GPCRs which are made either of rhodopsin or of rhodopsin chimeras. To address this, we tested the critical light-gated component of all of the prior GPCRs: rhodopsin. Rat rhodopsin, RO4, which also couples to GIRK1 channels,<sup>[195a]</sup> was expressed in HEK293 cells and the cells were incubated for prolonged times (40 minutes) in 1  $\mu$ M 11-*cis* retinal in the dark. Illumination of cells co-expressing RO4 and GIRK1 with 490 nm light activated large inward GIRK currents (Fig. S4A) that were similar in amplitude and

rise time to those evoked by optical activation of LimGluR2 (Fig. S4B). However, the GIRK1 deactivation kinetics of RO4 upon light off were much slower than the deactivation kinetics during light-driven deactivation of LimGluR2 (Fig. S4A-C). Due to the slow deactivation kinetics of RO4, repeated optical stimulation was limited to intervals of 90 s (Fig. S4D). Even at this long interval (6-times longer than the one which produced reproducible photo-activation of LimGluR2) the RO4-mediated responses declined significantly from pulse to pulse (Fig. S4D,F). In contrast, LimGluR2 photo- responses were stable in amplitude (Fig. 39D, S4E,F).

### **Generalization of Photocontrol to mGluR3 and mGluR6**

To test if the PTL approach could be generalized to optically control other mGluRs, we tested cysteine substitutions in, mGluR3, a second group II mGluR member, and mGluR6, a member of group III mGluRs, at residues that are homologous to L300 and S302 of mGluR2 (Fig S5A). Optical control of mGluR3 is attractive because of the lack of agonists and antagonists that differentiate between mGluR2 and 3, while mGluR6 is an important target for photocontrol because of its central role in synaptic transmission from photoreceptors to ON bipolar cells in the retina. Figure S5B, C and D summarizes the results of the mutational screens of mGluR2, mGluR3 and mGluR6. Interestingly, photoswitching of DMAG-0 or DMAG-1 anchored at sites of mGluR3 and mGluR6 that are homologous to mGluR2's L300 and S302 yielded similar effects in mGluR3 and different effects in mGluR6, where only photo- antagonism was observed, providing a readout of the degree of geometric similarity near the LBD binding pocket.

Conjugation of mGluR3 Q306C (the homolog of mGluR2-L300C) with DMAG-0 produced strong photo-agonism ("LimGluR3") under 380 nm light in HEK293T cells co-transfected with GIRK1 (Fig. 39E). The photocurrents were  $74 \pm 12$  % ( $n = 6$  cells) the amplitude of 1 mM glutamate evoked currents, indicating that LimGluR3 is even more robust than LimGluR2. Conjugation of mGluR6-K306C (the homolog of mGluR2-L300C) with DMAG-0 produced a robust photo-antagonism under 380 nm light (Fig. 39F). The percentage photo-antagonism was  $40 \pm 3$  % ( $n = 5$  cells) for DMAG-0 at mGluR6-K306C in 1 mM glutamate. We term this tool "LimGluR6-block".

The ability of optical stimulation of LimGluR2 and 3 to evoke large GIRK1 currents, that persist in the dark, but which can be rapidly deactivated by light and which, moreover, can be sculpted by alternating light pulses into trains of reproducible effector activation and deactivation represent important advantages over previous light-gated GPCRs based on

rhodopsin with loops from ligand-gated GPCRs, since, outside of photoreceptor cells, rhodopsin deactivates slowly and does not recover completely. An additional advantage is that, functionally, LimGluR2 is a native receptor (altered only by a cysteine mutation and conjugation with DMAG-0, which does not alter sensitivity to standard mGluR pharmacological agonists and antagonists; Fig. S3D,E,F) and so could make it possible to optically stimulate native mGluR2 targets with light. We next tested this possibility in neurons.

### Optical Control of Excitability in Hippocampal Neurons

We examined the ability of LimGluR2 to optically activate the native downstream targets of mGluR2 in cultured hippocampal neurons. These include GIRK channels in the cell body<sup>[220]</sup> and voltage-gated calcium channels in the presynaptic nerve terminal.<sup>[221]</sup> Indeed, we found that the cysteine-substituted mGluR2-L300C, tagged with eGFP at the C- terminus, is distributed throughout the soma and many fine processes of the neuron (Fig. 40B).

We first tested the expectation that activation by LimGluR2 of cell body GIRK channels would decrease excitability (Fig. 40A). In high extracellular potassium (60 mM) and under voltage clamp, illumination with 380 nm light evoked large inward currents that were deactivated by 500 nm light (Fig. S6A). Interestingly, even though photoswitching was done at the same light intensity in the two cell types ( $0.4 \text{ mW/mm}^2$  at 380 nm), the photo-activation rate was ~5-fold faster in neurons than in the HEK293 cells (respectively, the single exponential fits were:  $\tau = 1.03 \pm 0.06 \text{ s}$ ,  $n = 5$ , versus  $5.69 \pm 0.69$ ,  $n = 8$ ; unpaired, 1-tailed t-test,  $p = 0.004$ ). This is consistent with previous observations of faster activation of GIRK channels by native GiPCRs in cultured neurons compared to heterologously expressed receptors in HEK293 cells that are co-transfected with GIRK.<sup>[222]</sup> The observation suggests that LimGluR2 assembles into the native G-protein signaling machinery of neurons.

To test the ability of LimGluR2 to modulate neuronal excitability via GIRK channel activation, we performed current clamp experiments. Neurons expressing LimGluR2 were labeled with DMAG-0 and given 2 s depolarizing current injections, in 10 pA increments, under current clamp. This was done during alternating illumination with 380 nm and 500 nm light. Photo-activation of LimGluR2 at 380 nm greatly decreased the number of action potentials fired evoked by each level of depolarization (Fig. 40C,D). This optical inhibition was highly reversible and repeatable (Fig. 40C and G; Fig S6B). The photo-currents were big enough to evoke a reversible 5-15 mV hyperpolarization at the resting potential (Fig. 40E) and, in accordance with the bistability of the system, the hyperpolarization and silencing

persisted for tens of seconds in the dark after activation of LimGluR2 by a brief 380 nm light pulse (Fig. 40E,F).

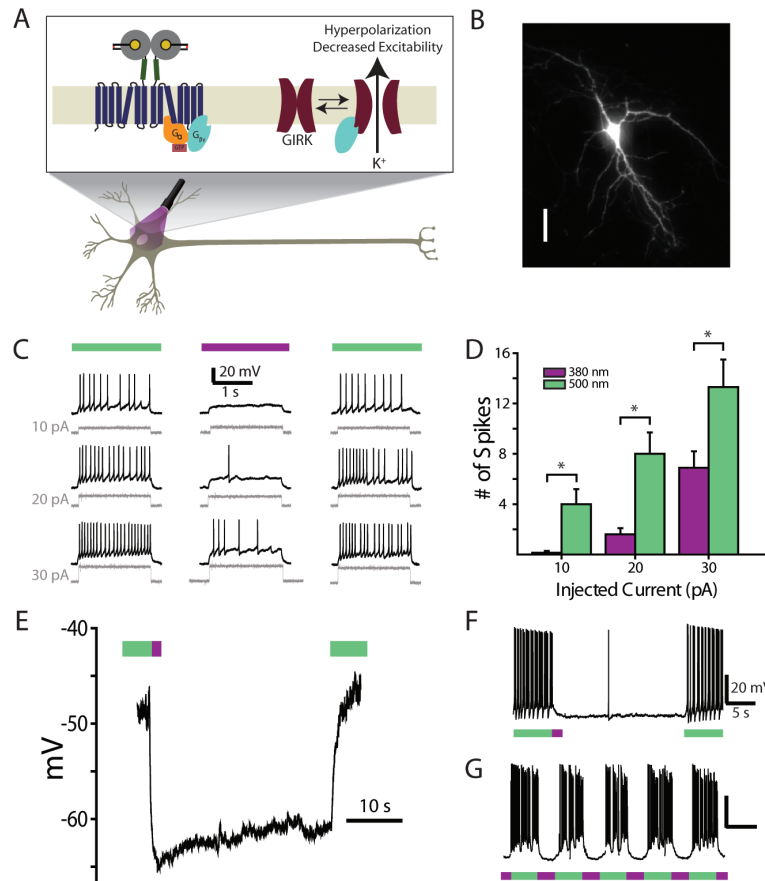


**Figure 40.** LimGluR2 hyperpolarizes and reduces excitability in cultured hippocampal neurons. (A) Schematic showing LimGluR2 mediated control of excitability via GIRK channels. Note: Light is applied to entire field of view. (B) LimGluR2-eGFP is widely distributed in cultured hippocampal neuron. Scale = 50  $\mu$ m. (C) Representative cell shows trains of spikes elicited by depolarizing current steps (gray traces) when LimGluR2 is off (500 nm illumination, green bar) are reversibly suppressed by activation of LimGluR2 (380 nm illumination, violet bar). (D) Summary of current step experiments shown in (C) for 8 cells. Bars indicate number of spikes in response to 2 s current injections under 380 nm (violet bar) or 500 nm (green bar) light. Star indicates statistical significance (paired, 1-tailed t-test,  $p = 0.009$ ,  $0.004$ , and  $0.009$ , respectively, for currents of 10, 20, and 30 pA). (E, F) Representative cells show bistability of LimGluR2. (E) Hyperpolarization from resting-potential in representative cell in the response to brief (1 s) LimGluR2 activation by 380 nm light (violet bar) persists for tens of seconds in the dark before LimGluR2 deactivation by 500 nm light (green bar). (F) The persistent activation in the dark effectively suppresses spikes. LimGluR2 activation induced an average hyperpolarization of  $8 \pm 4$  mV ( $n=15$ ) from resting potentials ranging from -40 to -60 mV. (G) Representative trace shows repeatable spike silencing by photocontrol of LimGluR2.

We next tested if photo-antagonism by “LimGluR2-block” could alter spike-firing patterns. In regions with high transfection efficiency (>1 transfected neuron per field of view) optical antagonism of mGluR2 with 380 nm light resulted in an increased firing frequency that was reversed by 500 nm light (Fig. S6C,D). This experiment demonstrates that LimGluR2-block is a robust enough tool to alter neuronal signaling properties despite incomplete antagonism. This result indicates that under basal signaling conditions there is sufficient inhibitory tone produced by glutamate binding to mGluR2 to suppress spike firing.

### **Optical Control of Synaptic Transmission and Short Term Plasticity in Hippocampal Autapses**

Group II metabotropic glutamate receptors are known to traffic to presynaptic terminals and play inhibitory roles in synaptic transmission and plasticity.<sup>[161]</sup> We asked whether LimGluR2 would provide for optical control of neurotransmitter release (Fig. 41A). We expressed mGluR2-L300C in low-density hippocampal cultures in which there are so few neurons that each neuron forms synapses onto itself (autapses). Cells were patch-clamped in the whole cell mode and we recorded postsynaptic currents elicited by brief depolarization steps, which elicited single action potentials. Excitatory post-synaptic currents (EPSCs) were detected in some cells (Fig. 5B) and inhibitory post-synaptic currents (IPSCs) were detected in others (Fig. 41C). EPSCs and IPSCs were identified based on the kinetics of decay with EPSCs approximately ten times faster than IPSCs (~5 ms vs. 50 ms), as has been described previously.<sup>[223]</sup> Activation of LimGluR2 by illumination at 380 nm rapidly and reversibly inhibited both the EPSCs ( $41 \pm 5\%$ ,  $n = 8$ ) and IPSCs ( $36 \pm 3\%$ ,  $n = 4$ ) (Fig. 41B and C). Furthermore, LimGluR2 could be used to optically inhibit EPSC amplitude repeatedly (Fig. S6D).

In contrast to the potent inhibition by LimGluR2, there was no optical inhibition in either cells transfected with GFP instead of LimGluR2 or cells transfected with LimGluR2 but not labeled with DMAG-0 (Fig. 5D). Moreover, there was no change in baseline PSC amplitude in labeled and transfected (LimGluR2) cells compared to GFP-transfected or unlabeled cells ( $223 \pm 64$  pA ;  $n = 12$  vs.  $262 \pm 68$  pA;  $n=5$  vs.  $232 \pm 91$  pA;  $n = 5$ ), indicating that expression of LimGluR2 does not produce a long-term homeostatic change in synaptic strength. In addition, the optical inhibition of transmission by LimGluR2 produced no change in PSC decay time (Fig. S7A), time to peak (Fig. S7B) or jitter (S.E.M of time to peak), leaving the post-synaptic currents unchanged in shape (Fig. S7C).

To test if the LimGluR2-mediated optical inhibition of transmission proceeds through a

pre-synaptic mechanism, we performed paired pulse experiments. The optical inhibition of transmission by illumination with 380 nm light was associated with a substantial increase in the relative size of the EPSC evoked by the second pulse (Fig. 41E).

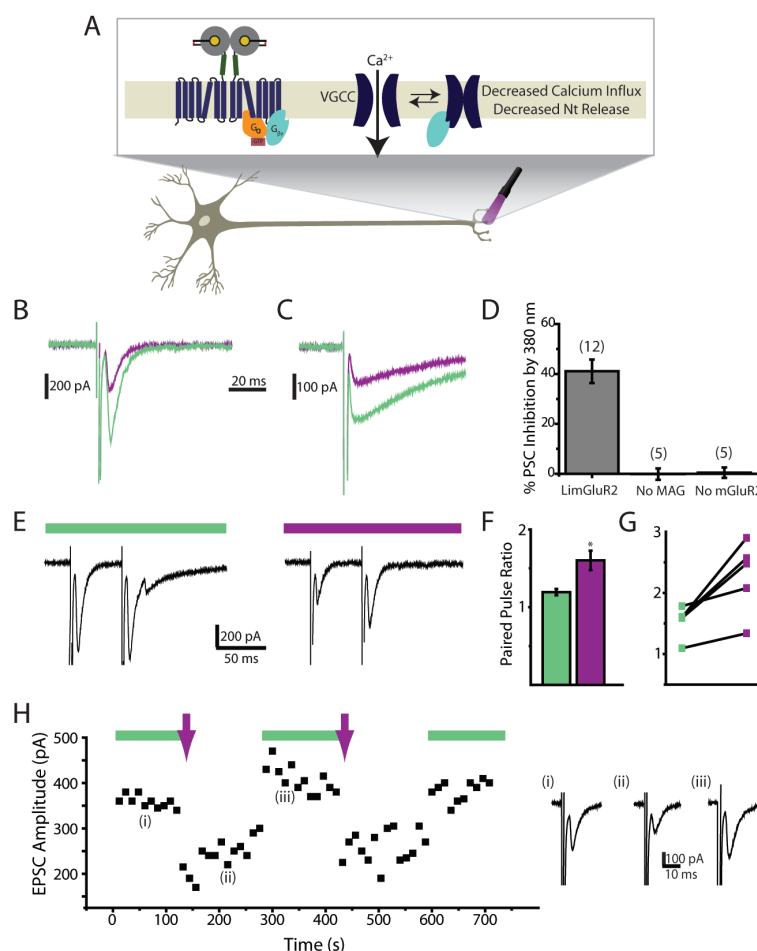


**Figure 41.** Optical activation of LimGluR2 reversibly decreases excitatory and inhibitory post-synaptic currents and increases paired pulse facilitation at hippocampal autapses. (A) Schematic shows optical control of neurotransmitter release via LimGluR2 triggered G-protein suppression of opening of a presynaptic voltage-gated calcium channel (VGCC). (B, C) Representative autaptic excitatory (B) and inhibitory (C) post synaptic currents elicited by short (2 ms) depolarizing steps are decreased in amplitude by LimGluR2 activation by 380 nm light (violet traces) compared to deactivation by 500 nm light (green traces). (D) Pooled inhibition of EPSCs and IPSCs by optical activation of LimGluR2 compared to controls in which mGluR2 (L300C) was expressed but not labeled with DMAG-0 and where mGluR2 was not expressed. Values in parentheses denote number of cells tested. (E) Representative single sweeps of paired pulse recordings (50 ms inter-stimulus interval) of EPSCs under 500 nm light (green bar) followed by 380 nm light (violet bar). (F) Summary of paired pulse ratio (PPR) values for representative cell. 380 nm light (violet bar) significantly increased the PPR compared to 500 nm light (green bar) (n=10 sweeps/condition; paired, 1-tailed t-test,  $p = 0.008$ ). (G) Plot of average PPRs measured for 5 autaptic cells under 500 nm light (green symbols) and 380 nm



light (violet symbols). (H) Representative EPSC amplitudes from a cell showing repeatable, bistable optical inhibition of an excitatory autapse. Illumination at 500 nm to deactivate LimGluR2 is followed by brief (1 s) illumination at 380 nm (violet arrows) followed by a period of darkness until illumination at 500 nm to deactivate LimGluR2 was resumed. Inserts (i), (ii), and (iii) show EPSCs from indicated times.

This increase in paired pulse ratio was significant (Fig. 41F and G; paired, 1-tailed t test,  $p = 0.01$ ). This indicates that activation of LimGluR2 inhibits postsynaptic currents by decreasing release probability and, thereby, increasing facilitation. This is exactly the mechanism by which native mGluR2 acts presynaptically via inhibition of N and P/Q type voltage-gated calcium channels, as has been observed for native group II mGluRs at the calyx of Held<sup>[221b]</sup> and for heterologously expressed receptors and channels in HEK293 cells.<sup>[224]</sup> Notably, the paired pulse ratio in LimGluR2 positive cells was the same as that in GFP-transfected cells (respectively  $1.5 \pm 0.1$ ,  $n = 5$  vs.  $1.4 \pm 0.3$ ,  $n = 4$ ), indicating that expression and labeling of LimGluR2 does not alter the basal release.

Finally, we tested the ability of LimGluR2 to produce multiple rounds of inhibition of transmission and recovery and for the inhibition to outlast the activating light pulse due to the bistable nature of the photoswitch. Illumination at 380 nm reversibly and reproducibly inhibited EPSC amplitude (Fig. 41H and S7E). Brief photo-activation produced sustained inhibition of synaptic transmission that persisted in the dark for minutes, but which could be rapidly reversed by illumination at 500 nm. These experiments show that LimGluR2 provides a powerful means for the optical control of presynaptic inhibition of neurotransmitter release.

#### Optical Control of Neuronal Excitability in Hippocampal Slices

To examine applicability in intact tissue, we tested LimGluR2 in cultured hippocampal slices. Slices prepared from P6-P8 rats were transfected with LimGluR2 (mGluR2-L300C) and td-Tomato (as a transfection marker) by Biolistic gene transfer. Expression was seen in scattered cells located throughout the hippocampus. Slices were incubated with DMAG-0 and whole cell patch-clamp recordings were performed on cells two or three layers below the surface of the slice. At resting potential (between -45 mV and -65 mV) LimGluR2 activation by illumination at 390 nm induced a small (3-8 mV), reversible hyperpolarization (Fig. 42A). In response to depolarizing current injections, illumination at 390 nm reproducibly decreased action potential firing rate (Fig. 42B, C), as was seen in the dissociated cultured neurons (Fig. 40C, D). Illumination with 500 nm light restored firing frequency to levels seen before LimGluR2 activation. In addition, LimGluR2 activation was able to decrease spontaneous spike firing (Fig. 42D) in a bistable, rapidly reversible and reproducible manner, with similar

efficacy to the photo- control of dissociated cultured neurons. Importantly, LimGluR2 expression and DMAG-0 labeling did not adversely affect neurons, leaving the average resting membrane potential unaltered (Fig. S8A).

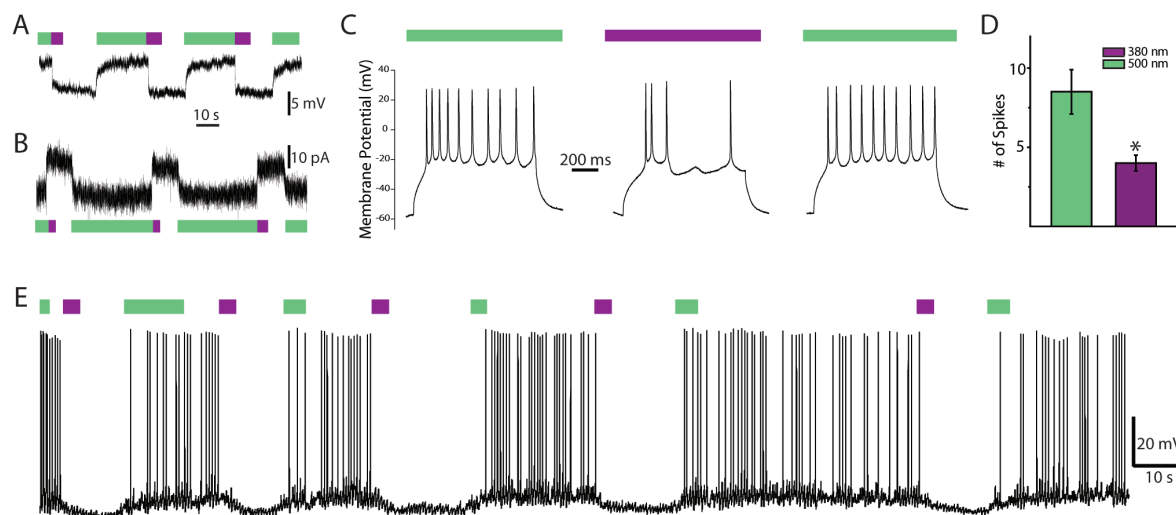


**Figure 42.** LimGluR2-mediated control of neuronal excitability in hippocampal slice. (A) Hyperpolarization is triggered by illumination at 390 nm (violet bar) and reversed by illumination at 500 nm (green bar) in a representative cell. (B) Representative cell recorded in whole-cell patch in cultured hippocampal slice shows spike firing in response to 1s, 200 pA depolarizing current injections during 500 nm (green bars) or 380 nm (violet bar) illumination. LimGluR2 activation reversibly decreases the number of spikes. (C) Summary of optical control of spike firing in response to current steps in LimGluR2-positive neurons (n = 6 cells). Star indicates statistical significance (paired, 1-tailed t-test,  $p = 0.024$ ). (D) Representative trace showing reversible, bistable silencing of spontaneous activity by LimGluR2.

Also, no photo-effects were observed with DMAG-0 but in absence of mGluR2-300C (S8B,D) or with mGluR2-300C but in absence of DMAG-0 (S8C), indicating that orthogonality is maintained in slices. These results indicate that expression, labeling, and optical activation of LimGluR2 are attainable in intact tissue, providing a powerful means to probe the role of G-protein signaling in general, and mGluRs in particular, in the native preparation. We next turned to in vivo experiments to determine if global LimGluR2 activation in neurons could alter behavior.

### Optical Control of Zebrafish Behavior

We evaluated if LimGluR2 activation affected the zebrafish escape response. The escape response in zebrafish is a well-characterized behavior in teleost fish that is similar to the mammalian startle.<sup>[225]</sup> The mammalian acoustic startle response is mediated by eighth

cranial nerve inputs to circuits in the lower brainstem that process auditory inputs to provide a behavioral output thought to involve activity of giant reticulospinal neurons of the caudal pontine reticular nucleus. The homologous circuit in teleost fish also receives inputs from the eighth cranial nerve, converging onto three pair of giant reticulospinal neurons. Mauthner cells are the largest of these reticulospinal neurons involved in startle and seem to play a predominant role. Excitatory afferent inputs initiated by startle stimuli converge directly onto the Mauthner cells, but also provide feed-forward electrical inputs to glycinergic interneurons that inhibit Mauthner firing bilaterally. Experiments with graded stimuli, similar to the sound/vibration stimulus protocol described in the present study, have revealed that at lower stimulus intensities the feed-forward inhibition dominates and that at higher stimulus intensity excitatory inputs overcome the inhibition to induce firing of Mauthner cells and escape behavior.<sup>[226]</sup>

We generated transgenic zebrafish (*Danio Rerio*) in which LimGluR2(L300C) expression is driven by repeats of the GAL4 Upstream Activating Sequence (UAS). We crossed UAS:LimGluR2 zebrafish to HuC:GAL4;UAS:Kaede fish to generate HuC:Gal4;UAS:Kaede;UAS:LimGluR2 zebrafish. The HuC promoter drives pan-neuronal expression of Gal4 and consequently of LimGluR2. The UAS:Kaede transgene is used as a fluorescent marker for HuC:Gal4 transgene presence. LimGluR2-expressing zebrafish 5 days post-fertilization (dpf) that were exposed to DMAG-0 for 45 minutes and recovered for 1 hour in the dark were healthy, responsive to touch and indistinguishable from untreated zebrafish or from fish treated with DMAG-0 that did not contain the UAS:LimGluR2 transgene.

Fish at 5 dpf were individually mounted in a glass-well petri dish with the head embedded in agar and subjected to sound/vibration stimuli (900 Hz, 120 ms) ranging from low energy to high energy (0.1 mVpp- 10 mVpp, 0.5 mVpp increments), administered by a mini-speaker inserted between the dish and a glass slide set on a microscope stage. At lower energy levels the sound/vibration stimulus induced forward swims, while higher energy levels elicited escape responses with the typical C-bend.<sup>[227]</sup> LimGluR2 was photo-controlled by patterned illumination applied caudal to the eyes. To activate LimGluR2 we illuminated the fish with 380 nm light for 400 ms and to deactivate it we applied 510 nm light for 1s. When fish were subjected to sub-threshold sound/vibration stimuli that did not induce forward swims or escape responses in the dark, activation of LimGluR2 increased the probability of an escape response (Fig. 43C,D). This effect was reversed by 510 nm light and could be toggled back and forth multiple times by repeatedly turning activating and deactivating LimGluR2 (Fig. 43C). The behavior of fish expressing LimGluR2 but not labeled with DMAG-0 was not

altered by light (Fig. 43D). This result establishes that LimGluR2 can be used to study G protein signaling in intact neural circuits *in vivo*.

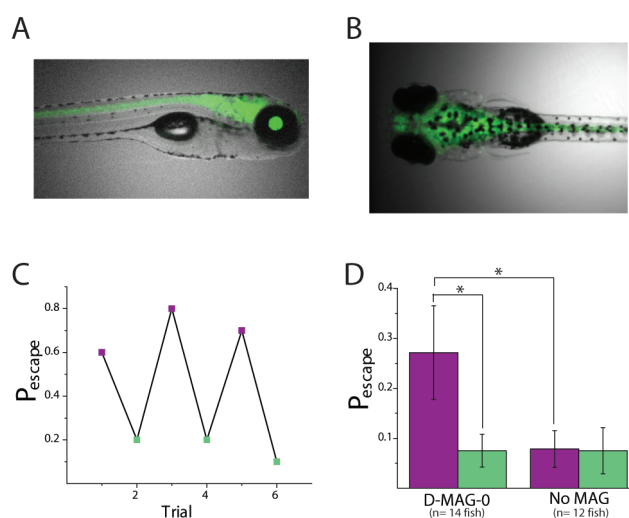


**Figure 43.** Photo-agonism of LimGluR2 increases escape response probability in zebrafish. (A, B) UAS- GFP imaging shows pan-neuronal expression in HUC-GAL4 driver line. (C) Representative fish showing reversible modulation of escape response probability. Each data point represents the escape probability during a period of ten trials. Violet and Green points represent trials after illumination at 510 and 380 nm, respectively. (D) Summary of LimGluR2-mediation of escape response. Green bars indicate illumination with 510 nm light and purple bars indicate 380 nm light. Stars indicate statistical significance ( $p = 0.007$  for comparison of 510 nm vs. 380 nm illumination for MAG-labeled fish with 1-tailed paired T-Test and  $p=0.03$  for comparison of MAG-labeled and unlabeled fish with 1 tailed unpaired T-Test).

## Discussion

We present the rational design and synthesis of new tethered glutamate photoswitches (DMAGs) and their protein attachment sites in the native vertebrate glutamate GPCRs, the mGluRs, which endows these receptors with the ability to be gated by light. The approach works to produce photo-agonism in mGluR2 and mGluR3 or photo-antagonism of mGluR2 and mGluR6. The design was based on the X-ray structures of mGluR LBDs and on experiments with synthetic ligands that model a portion of the MAG photoswitch (the “tether models”), which indicated that, unlike the requirement for L-stereochemistry at the 4'-position of MAG in the light gating the iGluR6 channel,<sup>[86a]</sup> mGluR2 requires D-stereochemistry at the 4'-position. This led us to synthesize a new pair of MAGs: DMAG-0 and DMAG-1. To determine the amino acid side chains within reach of DMAG, we used a simple and novel Monte Carlo simulation in which the glutamate end of MAG resided in the binding pocket and its maleimide end was free to move in the *cis* and *trans* states of the azobenzene,

providing a guide for where to place cysteine attachment sites for the MAG. Of seven attachment sites that were selected for study, four showed photo-responses with DMAG-1 and two showed photo-responses with DMAG-0, considerably accelerating the engineering process. The attraction of this approach is that only two Monte Carlo simulations are needed (one for *cis* and one for *trans*) to predict all of the appropriate attachment sites for a particular PTL-receptor pair – something only requiring a few days of computation on a single processor.

We show that, despite their limited homology (66% identity between mGluR2 and mGluR3 and 44% identity between mGluR2 and mGluR6), photo-control can be generalized within the mGluR family from mGluR2 to the other Group II member mGluR3 and the Group III member mGluR6, with the same D stereoisomer linkage to the glutamate of MAG being required. Differences in photo-switching with a particular MAG at homologous sites of these three mGluRs provides reveals differences between their LBDs.

The photo-agonism with DMAG-0 at position L300C of mGluR2, LimGluR2, which we developed first, became the principle chemical-optogenetic tool employed in this study, but LimGluR3 has even stronger photo-agonism. In comparison with rhodopsin, which is the basis of most of the prior light-gated GPCRs that could be used for heterologous control, and which returns to its resting state after a light pulse in a light-independent and slow manner, LimGluR2 can be actively toggled both on and off, yielding faster kinetics. Moreover, LimGluR2 permits repetitive stimulation at high rates without decline, whereas rhodopsin declines substantially in potency even at much lower repetition rates. In addition, rhodopsin requires constant illumination to be activated, which increases the chance of tissue damage and can act as a confounding variable for behavioral studies, while LimGluR2 is bistable, eliminating the need for constant illumination. Most importantly, optical control of native GPCRs provides a unique opportunity to examine their biological roles. A powerful complement to photo-agonism for such an effort is the photo-antagonism that we demonstrate for mGluR2 and mGluR6.

Two of the mechanisms by which mGluR2 regulates neuronal activity are shown to be accessible to optical control using LimGluR2 in hippocampal neurons. First, LimGluR2 photo-activation of somato-dendritic GIRK channels suppresses excitability. This suppression can be turned on and off repeatedly and reproducibly for many illumination cycles and can be maintained for extended periods in the dark until it is rapidly toggled off by illumination at the longer wavelength. Alternatively, LimGluR2-block photo-antagonism induced an increase in firing frequency indicating that basal activity of mGluR2 plays a role in regulating network

activity. Second, optical activation of presynaptic LimGluR2 provides a robust means of inhibiting neurotransmitter release. Here the bistability and repeatability of LimGluR2 signaling make it possible to flexibly control synaptic transmission over a wide range of time scales. Moreover, given the importance of group II and III mGluRs in long term plasticity, photo-agonism and photo-antagonism should make it possible to determine the precise spatial (*i.e.* pre- vs. post-synaptic; synaptic vs. peri-synaptic) and temporal properties of signaling by individual receptors to mediate lasting changes in synaptic strength. When coupled with genetic targeting, LimGluRs will allow for the dissection of the functions of mGluRs in specific cell-types, including both neurons and glia, and in different brain regions to define their roles in circuit function and behavior. Currently, such experiments are not possible because in many systems the same mGluRs are expressed in multiple cell types, and may not be distinguished pharmacologically.

We demonstrate the utility of LimGluR2 for photo-manipulation of vertebrate behavior via the reversible modulation of the escape response, a widely-studied behavior that is intriguingly similar in architecture and pharmacological regulation<sup>[227-228]</sup> to the mammalian startle response.<sup>[229]</sup> LimGluR2 was activated in an area that covers the hindbrain circuits that control the escape response and the spinal cord. Activation of LimGluR2 decreased the threshold of the escape response. Conceivably, mGluR2 activation decreases synaptic transmission through pre-synaptic mechanisms that affect inhibitory neurons disproportionately when compared to the effect in excitatory neurons. This effect could be due to cell-specific differences in receptor expression or coupling of LimGluR2 to downstream effectors. Interestingly, group II mGluRs are widely expressed in the brain of teleost fish,<sup>[230]</sup> raising the possibility that the behavioral effects that we observed are naturally regulated by these receptors. Future experiments can use a combination of genetic targeting with cell-type specific GAL4 enhancer-trap lines, finely targeted illumination and both photo-agonism and antagonism to address this possibility.

Importantly, LimGluR2 transgenic expression and labeling with DMAG-0 was found to be non-toxic and to not affect behavior in the absence of receptor activation. The bistability afforded by our optical switch allowed us to toggle receptor activity in intact animals using brief pulses of light, where behavior was then assessed over an extended time in the dark, avoiding both photo-toxicity and a potential behavioral confound of light.

While there are major similarities between GPCRs, which couple to the same pathways, such as the  $G_{i/o}$  or  $G_q$  pathways, downstream, non-canonical effectors and regulators are known to be specific to individual receptors. For instance, within the mGluR family different

receptors, which couple to the same G-protein pathway, nevertheless couple to different effectors in a cell-dependent manner<sup>[16, 161, 224]</sup> and this specificity can be complicated by diverse forms of hetero-dimerization with other family members that respond to the same transmitter, but also with GPCRs from other families which respond to distinct ligands.<sup>[214, 231]</sup> Furthermore, regulation in the form of subcellular localization, post-translational modification, and desensitization can be widely different among GPCRs in the same family.<sup>[193, 232]</sup> Thus, LimGluRs provide a novel, high precision way to probe the role of specific mGluR signaling in different cell types. Since LimGluR2 maintains close to native ligand sensitivity, knock-in mice with a single point mutation to introduce a cysteine anchor at position 300 should allow for high resolution, specific orthogonal photo-agonism or photo-antagonism while maintaining the receptor's native function. Given the lack of specificity of pharmacological agonists within the group II mGluRs, this would provide a new way to specifically probe the receptor's function in anxiety, depression, and schizophrenia, for which they are major drug targets.<sup>[213]</sup>

## Acknowledgments

We thank Andrew P. Mariani for 11-*cis* retinal, J.P. Pin for the mGluR plasmids, and E. Reuveny for the GIRK1 plasmid; K. Durkin, K. Dubay, A. Reiner, T. Berger, and G. Sandoz for helpful discussion; S. Berlin, A. Guyon, and S. Szobota for help with slice cultures and Z. Fu, for technical assistance; K.

McDaniel, J. Maxfield, J. Saint-Hillaire, and D. Weinman for fish care; Philipp Gut (UCSF) for plasmids; Baier Lab (UCSF) for fish lines; E. Carroll for discussion and help with set up; and the College of Chemistry, UC Berkeley, for computing resources funded by NSF CHE-0233882 and CHE-0840505. Support for the work was provided by the Nanomedicine Development Center for the Optical Control of Biological Function, PN2EY018241 (D.T. & E.Y.I.), the Human Frontier Science Program, RGP0013/2010 (E.Y.I.), the Deutsche Forschungsgemeinschaft (SFB 879, D.T.), the Fond der Chemischen Industrie (Kekulé fellowship to P.S.), a postdoctoral fellowship of the European Molecular Biology Organization (H.J.), and a predoctoral fellowship from the Fulbright Foundation (B.G.).

## I.2 Toward an Orthogonal Receptor-Ligand Pair based on iGluRs

Nature has endowed animals and plants with highly sophisticated means to both sense chemicals in their environment and to use them for transmission of information for their own purposes. From pheromones in yeast to neurotransmitters in humans, specialized receptors bind these chemicals and relay the information *via* intracellular processes. There are two general mechanisms for the transduction of signals through the plasma membrane: *via* stimulus-gated channels (*i.e.* the ionotropic pathway) or stimulus-actuated proteins (*i.e.* the metabotropic pathway). In both cases, the cell responds to an extracellular signaling molecule and creates a response that can be anything from a change in membrane potential (if for example a channel is activated), release of second messengers, changes in transcription, changes in growth, apoptosis, etc. It is therefore with no surprise, that this enormous complexity has both fascinated and challenged scientists to unravel the different pathways associated with biological signaling. Among methods such as knock-out, development of selective drugs to silence or activate certain biological circuits or introduction of exogenous proteins, building entirely new signaling pathways has become one of the most powerful approaches. Such attempts can include both the manipulation of messenger molecules (by chemical) as well as their receptors and the associated ways of signaling (by biological means) and have therefore become a prime example of chemical biology.

The investigation of glutamate receptors (both ionotropic and metabotropic) has for long been governed by the search for more selective agonists, antagonists or modulators and has therefore been a domain of pharmacology. With the option of photocontrol of mGluRs and iGluRs, our group has introduced a completely new way of dissecting the glutamatergic circuitry.<sup>[97h]</sup> Thus, the PCL/PTL concept shifts the research of glutamate receptors into the realm of photochemical genetics. Even though our approach has been highly successful,<sup>[97d, 97h, 97i]</sup> harnessing the spatiotemporal control of light is not enough to prevent a problem, which reminds of the observer effect in physics. By introduction of our photochromic molecules or the genetically modified receptors for the covalent attachment of PTLs, the response of glutamatergic networks to their native neurotransmitter, *i.e.* L-glutamate, is inevitably changed. Since LiGluR will hetero-tetramerize with its natural congener GluK2, introduction of the PTL-conjugate into a neuron will change the synaptic landscape of glutamate receptors. Even though soluble, photochromic ligands (PCLs) lack the problem of introducing genetically modified receptors, they will for sure create an unwanted response by residual activity outside of the area of interest, thus perturbing the natural glutamatergic circuitry.



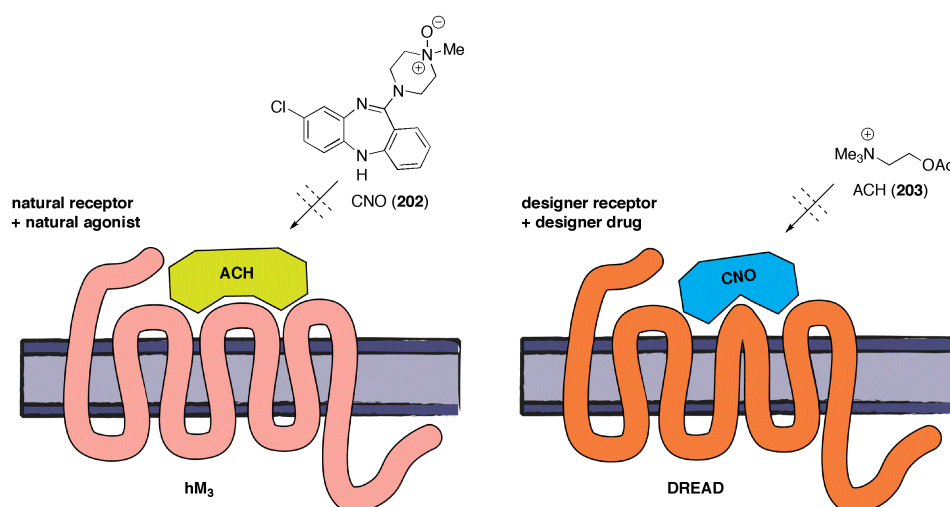
Faced with this dilemma, we decided to investigate ways of creating an iGluR-based orthogonal receptor-ligand system, which does not interfere with the native synaptic landscape. This would both include orthogonality in tetramerization (*i.e.* no tetramer formation between native and artificial receptors) as well as in ligand specificity (*i.e.* no activation by L-glutamate (**1**) and in turn no activation of natural iGluRs by the artificial ligand). Such reengineering of native receptors into an orthogonal receptor is admittedly no entirely new concept (*vide supra*). There are, however, only a few rather recent cases that have yielded fully orthogonal receptor-ligand systems. The most relevant publications, which have inspired this work, will be showcased in the following section.

### 1) Orthogonal Receptors: State of the Art

The gene family of G-protein coupled receptors (GPCRs) is by far the biggest target for pharmaceutical discovery.<sup>[233]</sup> They activate a variety of G-protein pathways ( $G_i$ ,  $G_s$ ,  $G_q$ ) and regulate many biological responses.<sup>[168]</sup> It is due to this importance, that GPCRs have become the target of reengineering to induce and modulate signal-transduction both *in vivo* and *in vitro*. Even though there is some confusion about the name of such artificial receptors, designer receptors exclusively activated by designer drugs (DREADs)<sup>[234]</sup> and receptors activated solely by synthetic ligands (RASSLs)<sup>[235]</sup> are (more or less) orthogonal receptor-ligand pairs developed by the clever combination of chemical and biological approaches.

Since the development of a  $\beta$ -adrenergic receptor by Strader and coworkers, which ceases to respond to its natural ligand and instead can be activated by artificial molecules due to a single-point mutation,<sup>[236]</sup> RASSLs and DREADs have been evolved on the basis of human  $\kappa$ -opioid, 5HT<sub>4</sub>, melanocortin 4, M<sub>3</sub> and M<sub>4</sub> muscarinic,  $\alpha$ 2-adrenergic and rat muscarinic M3 receptors. Initially, existing drugs, which had been developed by the pharmaceutical industry for different purposes, were used to activate these artificial receptors. Accordingly, these systems suffered from immense background due to the nonselective binding of their chemical actuators unless their “natural targets” had been knocked out.<sup>[150a]</sup> Armbruster and coworkers found an elegant solution to this problem by means of combining a pharmacologically inert chemical, clozapine-*N*-oxide (CNO, **202**), with directed evolution of the parent receptor to only allow binding of **202** instead of its endogenous ligand (Scheme 28).<sup>[234]</sup> Due to the high similarity of all GPCRs as members of the seven transmembrane receptors (7TMRs), this general concept should be applicable to almost all members of the family and existing RASSLs/DREADs can indeed be coupled to different G-proteins by

substitution of intracellular domains, making this work a milestone in the development of orthogonal G-protein coupled receptors.<sup>[237]</sup>



**Scheme 28.** General concept of modern RASSLs/DREADs based on the human muscarinic acetylcholine receptor M3 (hM<sub>3</sub>), its native ligand acetylcholine (ACH, **203**) and the pharmacologically inert ligand CNO (**202**) acting on a DREAD.

A different approach toward the orthogonal control of mammalian signal transduction pathways is the introduction of xenoreceptors or channels, which can interface to or influence the endogenous signaling cascades. An example for a receptor interfacing to the G-protein pathway is the drosophila allatostatin receptor (AR). Allatostatins are neuropeptide hormones, which inhibit the generation of the juvenile hormone and reduce food intake in drosophila and other insects or crustaceans.<sup>[238]</sup> In mammals, there is no natural target for the allatostatins and hence their receptor, a GPCR, has been used to inactivate neurons in rats, ferrets and monkeys. Its mode of action involves the activation of G-protein coupled inward rectifying potassium channels (GIRKs) by the  $\beta\gamma$ -subunit of AR's associated G-protein. Due to this hyperpolarization, the allatostatin/AR/GIRK system effectively reduces neuronal excitability and can be used to dissect neuronal networks.<sup>[239]</sup>

A more direct way of controlling the excitability of cells using ion channels was yet again discovered in *C. elegans*. Glutamate-gated chloride channels (GluCl) from these nematodes were found to be sensitive to avermectins, anthelmintic and insecticidal macrolides isolated from fermentation broths of the actinomycete *S. avermitis* (Fig. 44).<sup>[240]</sup> Owing to the high affinity of these GluCl to the semisynthetic macrolide ivermectin (a 9:1 mixture of **204** and **205**), they can be used to effectively silence neurons due to their Cl<sup>-</sup>-conductance induced by low nanomolar concentrations (5 nM) of **204** and **205**.<sup>[241]</sup>

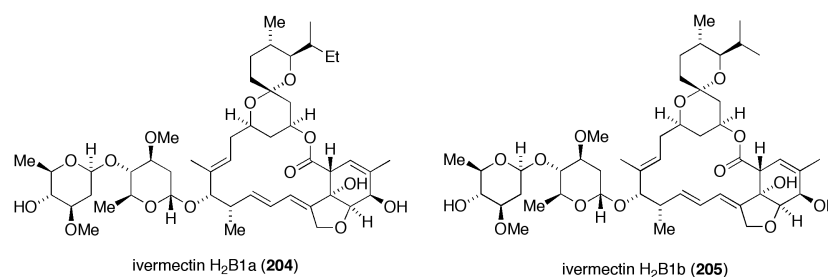
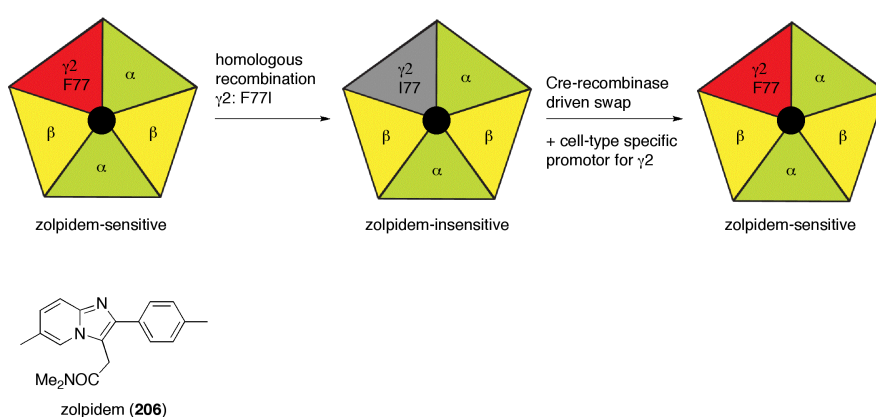


**Figure 44.** Ivermectin macrolides H<sub>2</sub>B1a (**204**) and H<sub>2</sub>B1b (**205**).

Even though this system seems to be fully orthogonal, ivermectin is known to have different effects on GABA, P2X<sub>2</sub> and neuronal AChRs.<sup>[242]</sup> Therefore, side-effects can not be excluded in long-time experiments, even though the most probable, *i.e.* GABA-potential, was not found by Lester and coworkers (at 5 nM ivermectin).<sup>[241]</sup>

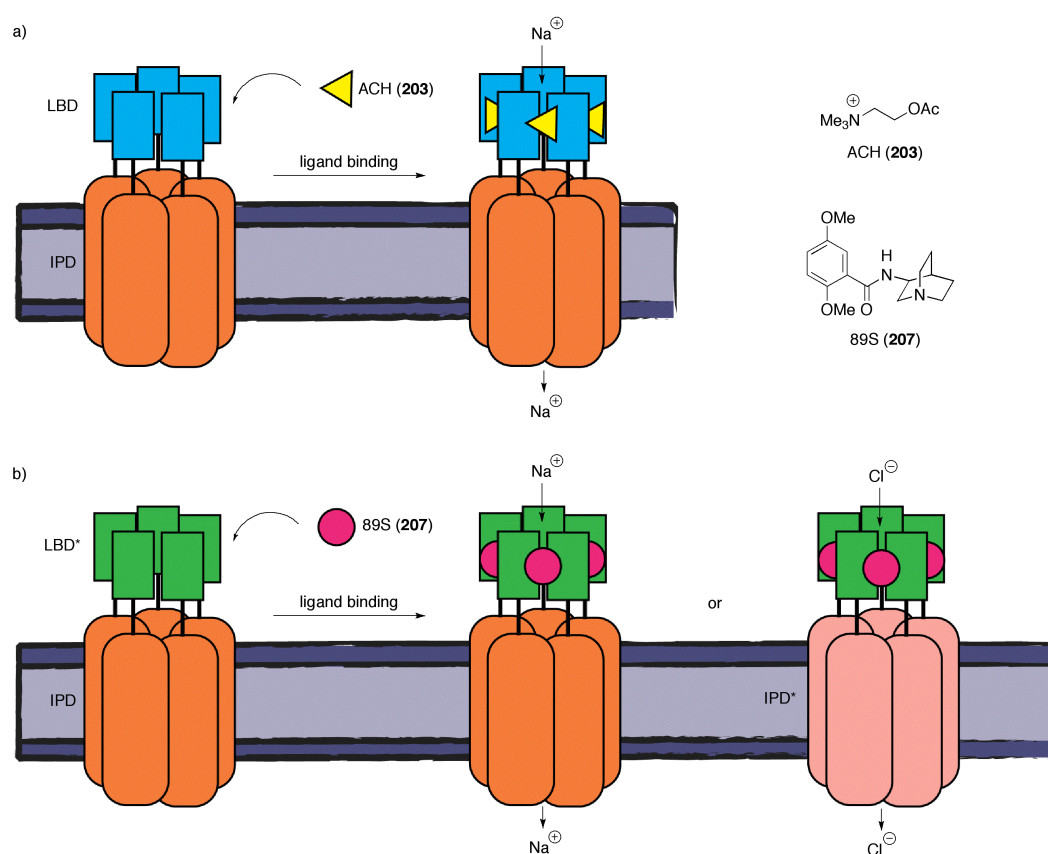
Wulff *et al.* have reported a different approach for orthogonal control of neuronal excitability by ion channels, which uses engineered  $\gamma$ -amino butyric acid receptors (GABA<sub>A</sub>Rs).<sup>[243]</sup> In the latter, the  $\gamma$ 2-subunit confers sensitivity to the artificial drug zolpidem (**206**), which is a competitive agonist to GABA. If however, phenylalanine F77 of  $\gamma$ 2 is mutated to isoleucine (F77I), the resulting GABA<sub>A</sub>Rs which incorporate  $\gamma$ 2-F77I become unresponsive to **206**. In a tour de force of biological methods, the authors created transgenic mice, in which the natural, zolpidem-sensitive subunit had been replaced by an insensitive version. They then used Cre-recombinase-catalyzed site-specific recombination to restore sensitivity to zolpidem (**206**) in purkinje cells and thus silence them (Scheme 29).



**Scheme 29.** Schematic of engineered GABA<sub>A</sub> receptors for the modulation of specific neuronal cell types by the zolpidem-sensitive subunit  $\gamma$ 2.

Most remarkably, the authors demonstrate that hyperpolarization of named neurons results in immediate motor-deficits of the animals expressing the  $\gamma 2$ -F77 subunit.<sup>[243]</sup>

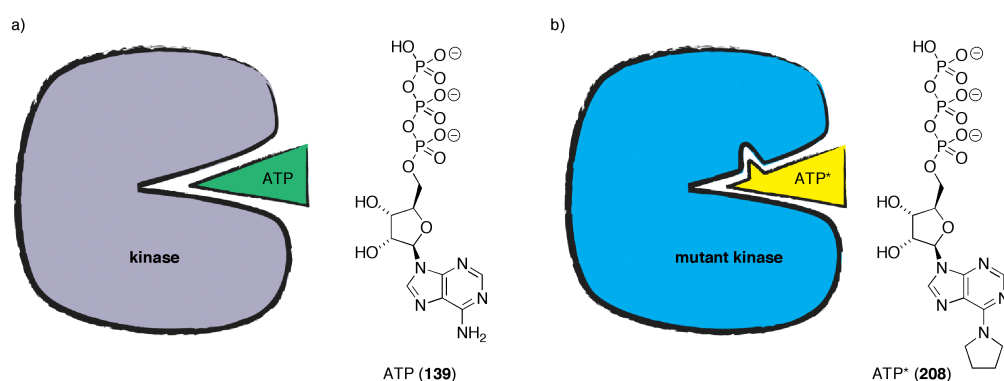
Surprisingly, it was only very recently that an orthogonal neuron-activating receptor-ligand system was reported. In a seminal work, Sternson and coworkers designed ligand-binding domains (LBDs) of nicotinic acetylcholine receptors (nAChRs) that are activated by an artificial, otherwise pharmacologically inactive quinuclidine-derived ligand 89S (**207**). Highlighting the high variability of their approach, the authors showed that the 89S-sensitive LBD could be fused to ion pore domains (IPD) of GABA<sub>A</sub>, glycine and 5HT<sub>3</sub> receptors, thereby creating both depolarizing cation channels (5HT<sub>3</sub>) and hyperpolarizing anion channels (GABA<sub>A</sub>, glycine receptor). This was possible, because the  $\alpha 7$ -LBD behaves like an isolated component, which can be fused to IPDs of other pentameric ligand-gated channels to change characteristics such as ion selectivity or conductance (Scheme 30).<sup>[244]</sup>



**Scheme 30.** a) Mode of action of an endogenous, acetylcholine-gated nAChR. b) Schematic design of orthogonal de- and hyperpolarizing ion channels based on a common ligand-binding domain (LBD\*), which binds the quinuclidine-derived molecule 89S (**207**), and two different ion pore domains (IPD and IPD\*).

This work highlights the power of combining extensive biological screening (for suitable mutations) and prudent chemical synthesis (by understanding the molecular mechanism underlying the binding of quinuclidine-agonists).

In a way, Sternson's methodology is related to a technique introduced by Shokat, commonly known as "bump-hole approach". It refers to altering an enzyme's ligand/cofactor specificity by chemically introducing steric bulk on the ligand ("bump"), which can only be accommodated by a modified protein. This is achieved by reducing the size of residues flanking the binding-site by a point mutation ("hole"). Shokat and coworkers used this technique to map the target specificity of tyrosine kinases, which otherwise would have been difficult to do, owing to redundancy of phosphorylating enzymes. They created a mutant kinase (I338G), which had a low affinity for adenosine triphosphate (ATP, **139**), but can bind the non-natural analogue **208** (Scheme 31).<sup>[245]</sup>



**Scheme 31.** Schematic of the "bump-hole approach" of rous sarcoma tyrosine kinase (v-Src). a) A wild-type kinase and natural ATP (**139**). b) Mutant kinase with a "hole" and ATP analogue ATP\* (**208**) with a sterically demanding pyrrolidine ring, *i.e.* the "bump".

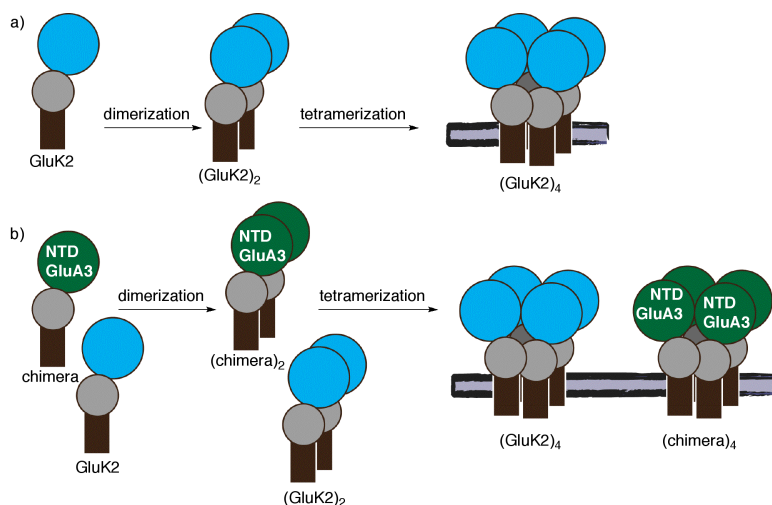
The authors show, that this approach not only can be used to create kinases sensitive to ATP-analogues, but also can be engineered to be sensitive toward inhibitors, that do not block the wild-type enzyme. Using this methodology, kinases inducing pre-mitotic cell cycle arrest could be identified in yeast.<sup>[246]</sup>

Inspired by this work, we decided to first base our design of an orthogonal, ionotropic receptor (iXR) on a rational selection of both parent iGluRs and mutations. Our progress toward such an iXR is outlined in the next section.

## 2) Receptor Design

Judging from the available literature on the design of orthogonal receptor-ligand pairs, we were now faced with a set of three separate problems: 1. Find a drug that is pharmacologically inactive but activates a mutant iGluR, 2. Design an iGluR mutant, which does not respond to glutamate (or which has a significantly decrease affinity for its natural ligand), but does bind the designer ligand, and 3. Prevent cross-tetramerization of mutant and wild-type receptors.

Thankfully, the latter problem can be addressed by exploiting the underling mechanisms of glutamate-receptor tetramerization. In general, it is accepted that iGluRs form so called “dimer of dimers”, *i.e.* GluR-monomers first form dimers of their own kind and then dimerize with another dimer of the same or another GluR-type to form the functional receptor (Scheme 32a).<sup>[247]</sup> Stern-Bach and coworkers were able to show that such dimerization, or tetramerization events respectively, are initiated by interaction of the *N*-terminal domains (NTDs) and then further strengthened by interactions of the ligand-binding (LBDs) and transmembrane domains (TMDs). By creating chimeras with different NTDs they were able to explore the different requirements for functional tetramerization and (as a side-effect) create iGluRs that exclusively assemble with their own kind (Scheme 32b).<sup>[248]</sup>



**Scheme 32.** a) Tetramerization of iGluRs according to the dimer of dimer model. b) Chimeras resulting from fusing GluA3 NTDs to GluK2 LBD and TMD, which only co-assemble with themselves.

Using this technique, we were sure to suppress hetero-tetramerization of our envisioned constructs and we gratefully received a chimeric construct of a GluA3 NTD fused to the GluK2 LBD and TMD from Y. Stern-Bach to be used as a template. For the initial screen of suitable mutations within the ligand-binding domain however, we decided to use unaltered GluK2 constructs and to introduce the found mutations into the NTD3-R6 receptor later on.



### 3) Rational Mutation Approach

The ligand-binding domain of iGluRs forms highly specialized hydrogen bonds involving both amino acid residues and hydrate water molecules to stabilize L-glutamate in its preferred “bent” conformation. Said interactions are crucial for the efficient binding, LBD-closure, inter-domain stabilization and thus receptor activation.<sup>[5]</sup> It is therefore not surprising, that only a handful of mutations involving the principal binding residues are known, which do not completely abolish iGluR-response or expression.<sup>[78]</sup> It has been suggested that this is part of a quality check mechanism for functional iGluR subunits.<sup>[79-80]</sup> E738D for example seems to be tolerated in GluK2, the  $EC_{50}$  for glutamate however is significantly shifted from 191  $\mu\text{M}$  to 52 mM.<sup>[79]</sup> This can in part be attributed to a massive disruption of the H-bonding network that both binds L-glutamate and stabilizes the S1-S2 domains in a closed conformation (Fig. 45).

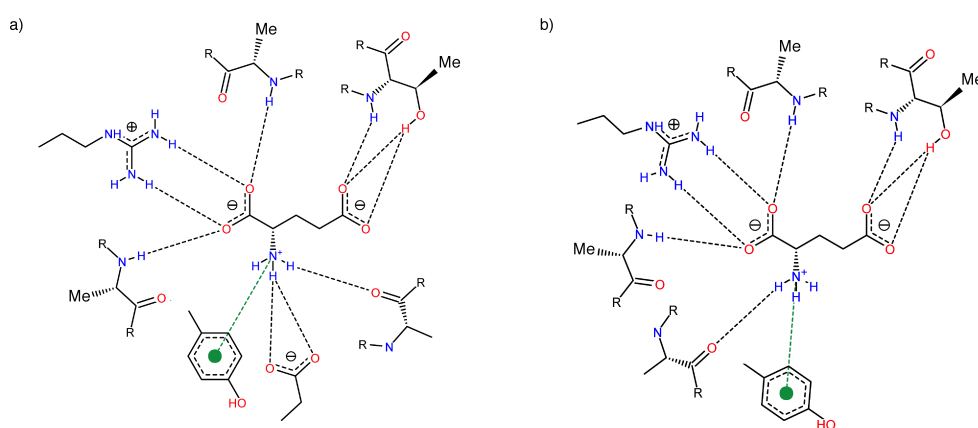


**Figure 45.** Hydrogen-bonds (omitting the water molecules) in the GluK2 LBD (pdb code 1S7Y) generated by PoseView.<sup>[249]</sup> a) Wild-type LBD. b) E738D mutation.

Despite these massive changes in the LBD, Fleck and coworkers have shown that GluK2 E738D is still a functional receptor, which does traffic normally to the cell's surface.<sup>[79]</sup> Together with the marked loss of affinity for glutamate, we selected this mutation as a perfect candidate for a “bump-hole” approach, since already two of our three requirements (*vide supra*) toward an orthogonal ionotropic receptor were met by the E738D variant of GluK2. We felt, that the third criterion, *i.e.* a ligand capable of activating the mutant channel with enhanced efficacy could be developed once enough structure-activity relationship (SAR) data had been collected.

Judging from the literature, we concluded that the iGluR LBD had indeed been evolved to bind amino-acid like molecules and therefore looked out for further, non-invasive mutations, which would not involve the principle binding residues (other than E738D) and

therefore most likely would result in fully functional and trafficked receptors. A highly conserved, nonpolar residue flanking the ligand-binding cavity in kainate-, NMDA- and AMPA-type glutamate receptors caught our eye (Fig. 46).

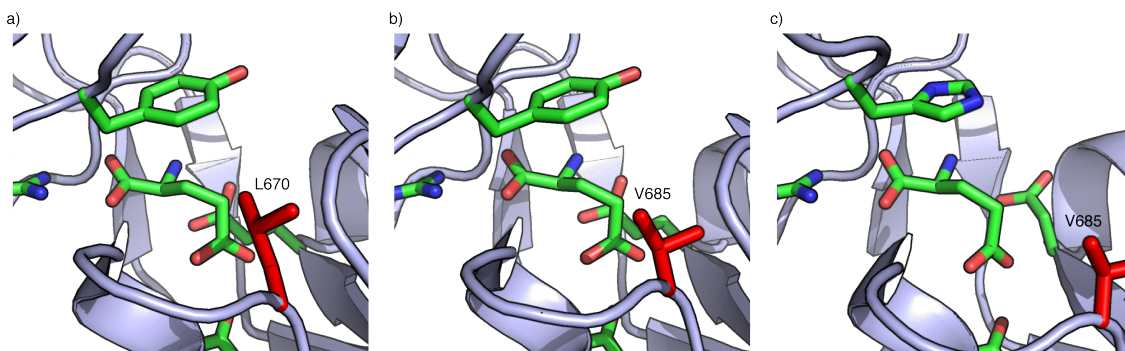


**Figure 46.** X-Ray structures of L-glutamate in the LBDs of a) GluA2 (pdb code 1FTJ), b) GluK2 (pdb code 1S7Y) and GluN2a (pdb code 2A5S) with the principal binding residues shown as sticks and the putative site of mutation highlighted in red.

In all glutamate-binding domains of iGluRs, a leucine or valine residue occupies this functional position (alignment not shown; positions L671, V685 and V685 in GluA2, GluK2 and GluN2a respectively). Functional analysis of V685A, V685L and V685F GluN2A mutants by Bräuner-Osborne and coworkers revealed that not only are named mutations tolerated, they also distinctly shift the  $EC_{50}$  of glutamate – for both the sterically more (V685L, V685F) and less demanding (V685A) variants.<sup>[250]</sup> The related mutation of leucine 671 to threonine (L671T) was reported by Armstrong, Mayer and Gouaux in the AMPA receptor GluA2. Most notably, not only did this modification shift the efficacy of glutamate by a factor of almost 9 (from 21  $\mu$ M to 177  $\mu$ M), it also inverted the relative potencies of kainate and AMPA, making kainic acid (**17**) a partial agonist with 24% efficacy compared to glutamate (up from 2%) and an  $EC_{50}$  of 65  $\mu$ M (down from 174  $\mu$ M).<sup>[26]</sup> Encouraged by these findings, we planned to use mutations of residues L671 and V685 respectively to create a “hole” in the LBD which could then be occupied by for example sterically demanding 4-substituted glutamic acid or kainic acid derivatives bearing additional substituents on the isopropylene moiety.



### a) GluK2 E738D L439C (“FliGluR”)

The first mutation we assessed as a candidate for an orthogonal receptor based on GluK2 was E738D, which had been reported by Fleck and coworkers.<sup>[79]</sup> With this mutant we were sure to tackle the problem of reduced affinity for L-glutamate while still having reasonable surface expression. Since we were interested on how E738D influences the receptor properties, we decided to introduce named modification in one of our LiGluR constructs bearing a C-terminal GFP-tag and a WPRE element for enhanced expression.<sup>[86a, 251]</sup> The exchange of glutamate 738 for an aspartate was realized using single point mutagenesis and we termed the new construct (*i.e.* GluK2•GFP E738D L439C + WPRE) “FliGluR” acknowledging the work of Fleck *et al.* First we expressed the corresponding plasmid in HEK293T cells and determined the EC<sub>50</sub> of L-glutamate with the desensitization of the receptors blocked by concanavaline A (ConA).<sup>[252]</sup> In accordance with the literature we observed a left-shifted half-maximal concentration of 11 mM, as ConA is known to render agonists more potent (Fig. 47).<sup>[252]</sup> Even though their affinity toward the receptor had been shifted to the high micromolar range (data not shown), we could estimate the EC<sub>50</sub> values of the known GluK2 agonists quisqualate (**14**) and kainic acid (**17**) to still be lower than the one of L-glutamate (**1**).<sup>[253]</sup>

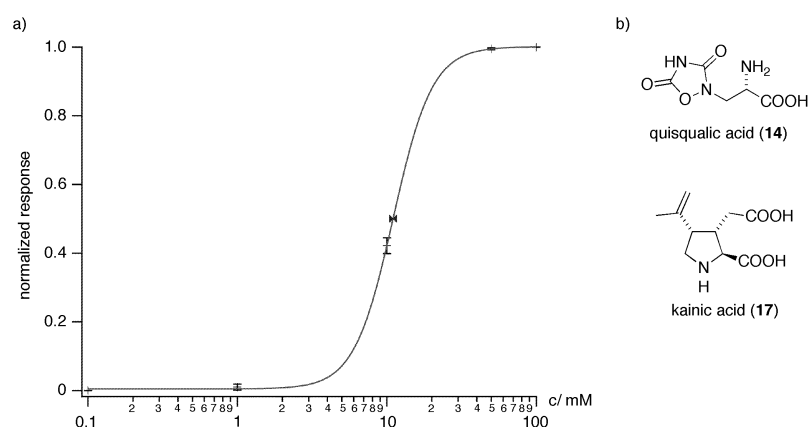
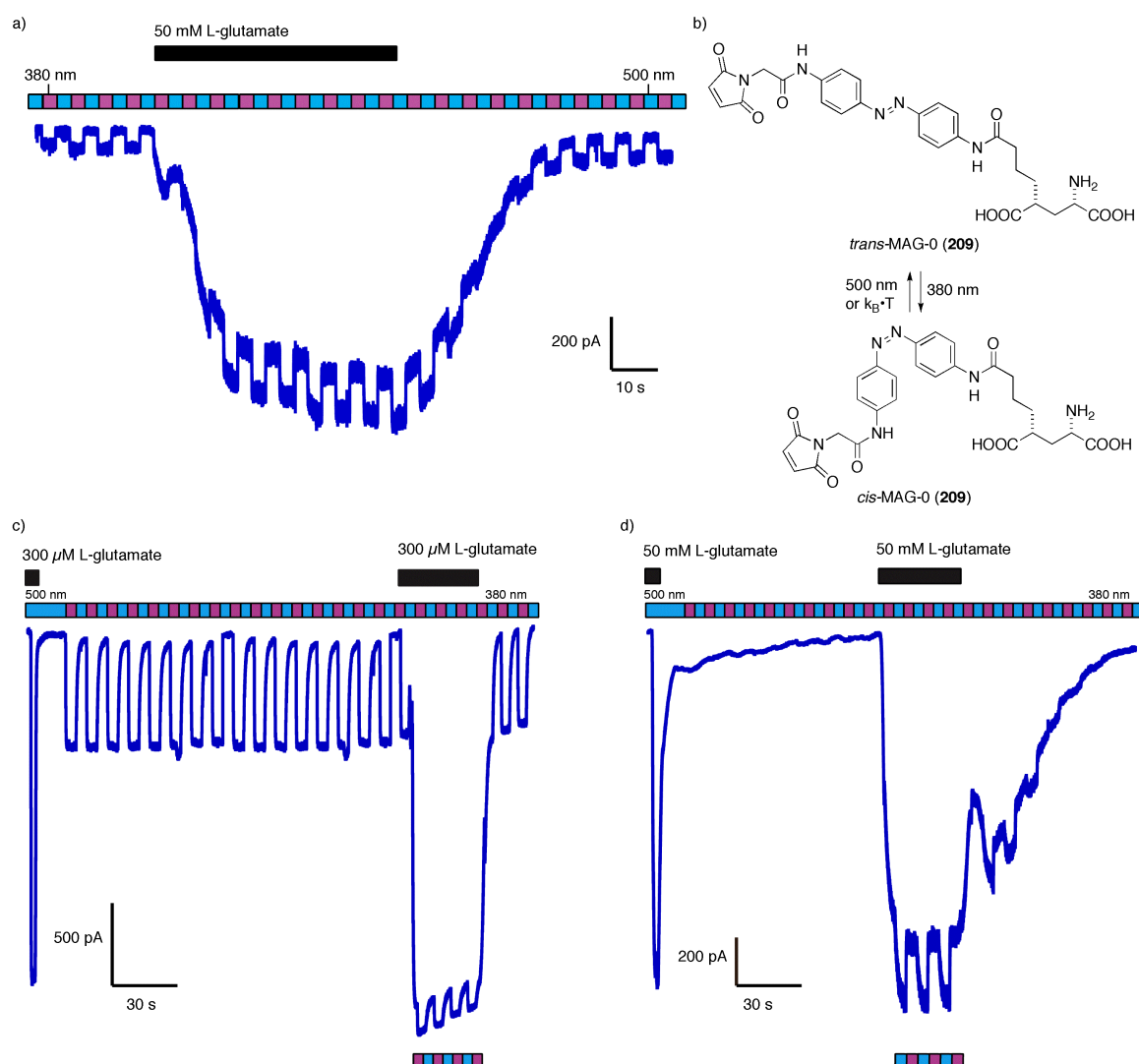


**Figure 47.** a) Dose-response curve of L-glutamate (**1**) in ConA-treated HEK293T cells expressing FliGluR ( $n = 9$ ; mean  $\pm$  SEM) relative to saturating glutamate (50 mM). b) Two full agonists of FliGluR (ConA-treated): quisqualic acid (**14**) and kainic (**17**).

Amazed by these results, we asked whether FliGluR could already be used as a orthogonal photoswitchable receptor, since it did not show any activation by the maximal L-glutamate concentrations observed in synapses of  $>1$  mM.<sup>[254]</sup> Hence, we expressed FliGluR in HEK293T cells and labeled the construct with MAG-0 (**209**) or MAG-1 (**24**) according to

established procedures.<sup>[86a]</sup> The results of our photoswitching experiments are summarized in Scheme 33.



**Scheme 33.** a) Photoswitching of FliGluR with MAG-1 (**24**) with partial co-administration of 50 mM L-glutamate. b) Structure and schematic light-induced isomerization of MAG-0 (**209**). c) Photoswitching of LiGluR with MAG-0 and partial co-administration of 300 μM L-glutamate. d) Photoswitching of FliGluR with partial co-administration of 50 mM L-glutamate.

We were pleased to find, that the FliGluR-MAG-1 conjugate did indeed show photocurrents upon switching from 500 nm to 380 nm of light (Scheme 33a), albeit only with low efficiency ( $10.5 \pm 0.5\%$  photocurrent;  $n = 4$ ). We therefore decided to compare the performance of LiGluR to its mutant with the strongest PTL MAG-0 (**209**; Scheme 33b,c) attached.<sup>[97g]</sup>

In our hands, the LiGluR-MAG-0 system performed well with  $29 \pm 3\%$  photo-switching ( $n = 5$ ). Most interestingly, we observed an excess-current of  $9.4 \pm 0.9\%$  ( $n = 4$ ) when changing from 500 nm to 380 nm of light while co-administering 300 μM L-glutamate

(Scheme 33c). For FliGluR however, there was hardly any photocurrent ( $1.8 \pm 0.2\%$ ,  $n = 3$ ) and upon co-administration of 50 mM glutamate, MAG-0 (**209**) acted as a photoswitchable antagonist ( $18.5 \pm 0.4\%$  reduction of current,  $n = 3$ ). Moreover, FliGluR showed a significantly slower response both to glutamate and to switching with light (Scheme 33d). This seems to indicate, that by mutation of E738 to aspartate, both MAG-0 (**209**) and MAG-1 (**24**) had been rendered weaker agonists than L-glutamate (**1**).

Since it had been shown that labeling of LiGluR proceeds with higher efficiency when pre-irradiating the MAG-containing solution with 380 nm of light,<sup>[255]</sup> we tried to attach MAG-0 to FliGluR using the highest concentration soluble in water and irradiated it for 30 s. Aiming at an affinity-based labeling process, we were disappointed to find that there was no increase in photocurrent (data not shown). Yet, when perfusing with 50 mM L-glutamate and switching from 500 nm to 380 nm of light, we observed an excess-current like in LiGluR for some cells, thus indicating indeed a labeling-dependent effect. Moreover, we realized that there seemed to be a cooperative effect of L-glutamate (**1**) and MAG-0 (**209**) for some concentrations, as the change in current did vary relative to the concentration of **1** (see wash out in Scheme 33d). Eventually however, our results were inconclusive since we could not further improve the rate of labeling due to the limited solubility of the PTL in water. We therefore decided to abandon the option of controlling our GluK2 E738D construct with light and rather focus on exploring its pharmacological profile.

Accordingly, we screened for lead structures for a selective activation of FliGluR in order to create an orthogonal receptor-ligand system capable of sustained stimulation by administration of a drug. To this end, we assembled a small library of commercially available compounds. Since iGluRs have evolved from simpler congeners binding not only to L-glutamate (**1**), but a variety of different amino acids,<sup>[68]</sup> we first selected molecules resembling amino acids and derivatives thereof for our screening (Fig. 48a). In addition, we decided to synthesize a few molecules, which could fill the space opened up by mutation of glutamate 738 to aspartate (Fig. 48b). Accordingly we selected 2-(aminomethyl)pentanedioic acid (**228**) as a carbon-, and hydrazine-derivatives **229** and **230** as nitrogen-extended versions of L-glutamate (**1**) and kainic acid (**17**) respectively.

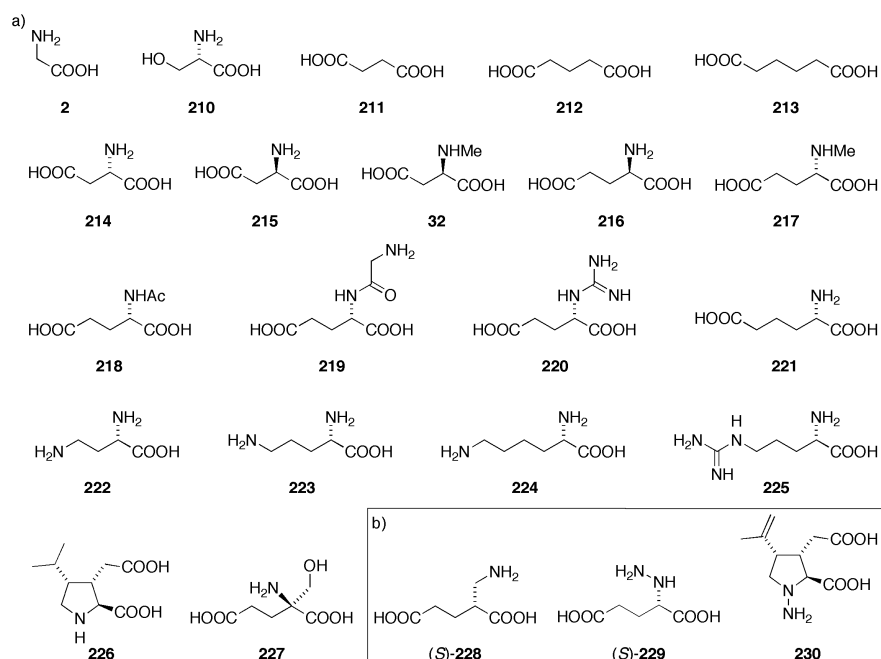
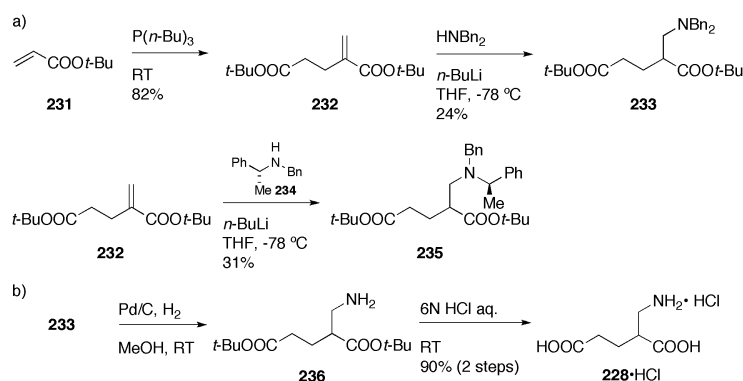


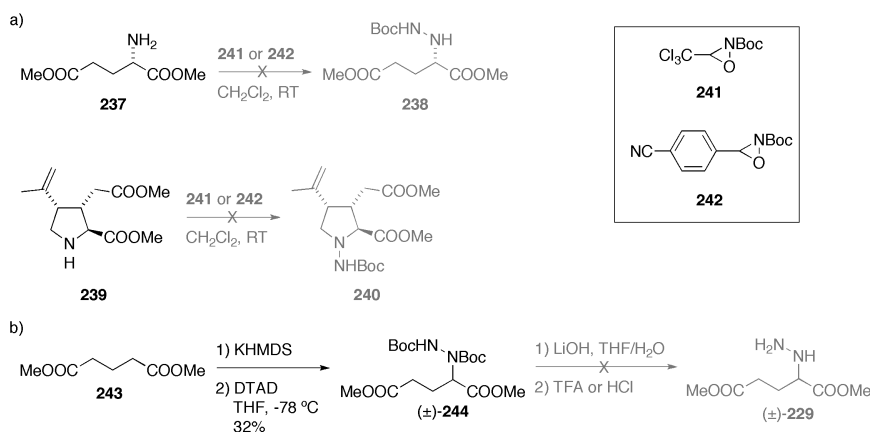
**Figure 48.** a) Commercially available ligands to be screened for activity in FliGluR. b) Envisioned ligands to be synthesized for the bump-hole approach with GluK2 E738D.

The synthesis of racemic  $\beta$ -amino acid **228** was carried out in a simple four-step sequence. Dimerization of *tert.*-butyl acrylate (**231**) by Baylis-Hillman reaction furnished 2-methylene pentanedioate **232** according to known protocols (Scheme 34).<sup>[256]</sup> For the succeeding hetero Michael addition of dibenzylamine we screened a variety of conditions including catalytic amounts of  $\text{CeCl}_3 \cdot \text{NaI}$  on silica, otherwise known to carry out the desired transformation in good yields.<sup>[257]</sup> After some experimentation however, we found that deprotonation with *n*-butyllithium<sup>[258]</sup> and concomitant addition of the resulting lithium amide to Michael-System **232** yielded the protected  $\beta$ -amino acid **233** in good yields. For a resolution of the enantiomers, we also tried an addition of (*R*)-*N*-benzyl- $\alpha$ -methylbenzylamine (**234**) as a chiral auxiliary group after deprotonation to the lithium amide. For a first evaluation of the properties of **228** however, we decided to use racemic material and therefore did not separate the diastereomers. As the final step of the synthesis, deprotection by hydrogenolysis and acid-mediated cleavage of the *tert.*-butyl esters gave racemic  $\beta$ -amino acid **228** as a colorless, hygroscopic solid in good yields over two steps (Scheme 34).



**Scheme 34.** a) Synthesis of the protected  $\beta$ -amino acids **223** and **235**. b) Deprotection of **233**.

The synthesis of the hydrazine derivatives **229** and **230** proved to be considerably more challenging. Since especially for the kainic acid derivative **230** a modified total synthesis was hardly practical, we were pleased to find an approach reported by Collet and coworkers using the electron-poor oxaziridines **241** and **242** as electrophilic amination reagents (Scheme 35a).<sup>[259]</sup> Unfortunately, we could not obtain the Boc-protected hydrazines in reproducible yields using the oxaziridines as an electrophilic nitrogen source. A racemic approach toward **229** from dimethyl glutarate, which was deprotonated using KHMDS and addition of the resulting potassium enolate to di-*tert*-butyl azodicarboxylate (DTAD), finally yielded the protected  $\alpha$ -hydrazino acid ( $\pm$ )-**244** in 32% (Scheme 35b).



**Scheme 35.** a) Attempted electrophilic amination of glutamic and kainic acid derivatives **237** and **239**. b) Attempted synthesis of racemic hydrazine derivative ( $\pm$ )-**229**.

Deprotection of ( $\pm$ )-**244** using lithium hydroxide followed by TFA or HCl did not yield the expected *N*-aminated amino acid ( $\pm$ )-**229**. We screened other methods of deprotection, but could not identify the problem. Although we found spectroscopic hints (HRSM, NMR) that we had indeed synthesized hydrazino acid ( $\pm$ )-**229**, we could not obtain it in pure form.

Despite this, we were now ready to screen the small set of ligands shown in Figure 48 for. To this end, we expressed the FliGluR construct in HEK293T cells and analyzed its response to the various compounds (1 mM) relative to saturating L-glutamate (50 mM) by whole cell patch-clamp electrophysiology. Disappointingly, we did not find any significant activation of the receptor by any of the molecules screened (data not shown). Therefore, we decided to further analyze the properties of this mutated GluK2 LBD.

In collaboration with Gisbert Schneider (ETH Zürich) we studied the behavior of both the wild type (wt) and mutated ligand-binding domains using molecular dynamics (MD). To this end, we correlated the stability of both LBDs to their pocket size (Fig. 49).

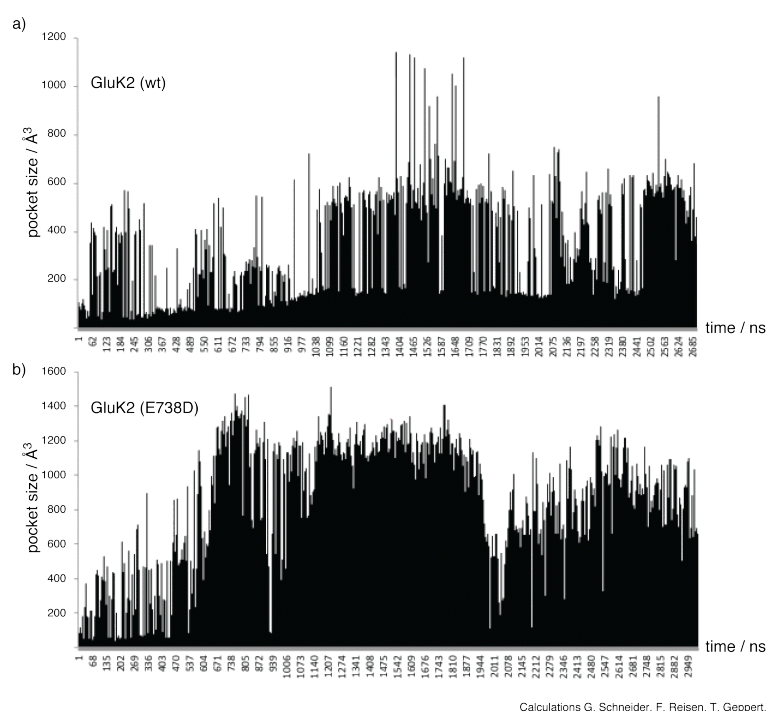


**Figure 49.** a) Molecular dynamics simulation of the GluK2 LB (pdb code 1S7Y). b) Molecular dynamics simulation of the FliGluR LBD (derived from pdb code 1S7Y).

We found that the mutated LBD in fact has a high probability of residing in open, *i.e.* high-volume conformations, whereas the wild type seems to stay in its closed state for a longer period of time. Taking into account previous reports by Kurnikova *et al.*,<sup>[260]</sup> which seem to indicate a disruption of ligand recognition and orientation by E738D, we concluded that in order to come forth with an orthogonal receptor-ligand pair for the FliGluR construct, we might either have to resort to *in silico* docking methods, or a high-throughput screen of bigger libraries (*vide infra*). Accordingly we decided to shift the focus away from E738D in favor of mutations of the nonpolar residues L671 and V685 in GluA2 and GluK2 respectively.

### b) “Bump-Hole” Approach

Since we did not obtain any SAR information from the experiments with FliGluR and our small ligand set, we next evaluated the potential of GluA2 L671 and GluK2 V685 mutants to be used as potential iGluR-based orthogonal receptors. To directly address the most drastic alterations of the wild-type receptors, *i.e.* leucine or valine to glycine or serine, resulting in the biggest “holes”, we introduced named changes in GluA2 and GluK2 using single point mutagenesis.<sup>[119]</sup> Plasmids coding for GluA2 L671G, L671S and GluK2 V685G respectively were expressed in HEK293T cells and their response to L-glutamate (**1**) was determined by whole cell patch-clamp electrophysiology. While for the GluK2 mutants we did not observe any currents – probably due to incorrect folding of the protein – the affinity toward **1** had indeed been decreased substantially in the modified AMPA-type receptors (Fig. 50).

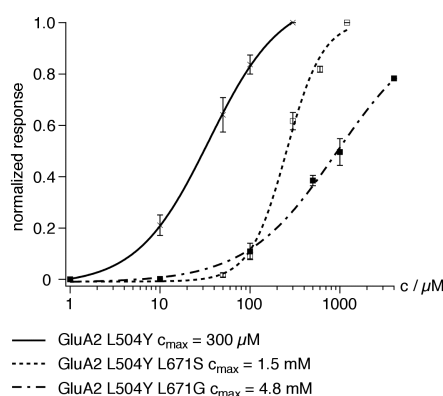


**Figure 50.** Dose-response curves of L-glutamate (**1**) in GluA2 L671S (red), GluA2 L671G (green;  $n = 5$ ; data  $\pm$  SEM) and “wt” GluA2 L504Y receptors (blue;  $n = 8$ ; data  $\pm$  SEM) relative to saturating glutamate (see graphs). In all three cases, the desensitization was blocked by the L504Y mutation.

In comparison to their “natural” congener ( $\text{EC}_{50} = 35 \mu\text{M}$ ), GluA2 L671S and L671G mutants had  $\text{EC}_{50}$  values of 255  $\mu\text{M}$  and 914  $\mu\text{M}$  respectively. To address whether mutations of leucine 671 to either glycine or serine had also influenced the ligand-specificity in comparison to the parent AMPA receptor, we determined the efficacy of kainic acid (**17**) in GluA2 L671G. As expected, we found a substantially increased activity of **17** in case of the L671G mutant ( $61 \pm 5\%$  efficacy). For this alterations of the GluA2 LBD, our data even exceeds the trend reported by Gouaux *et al.* for the related L671T mutation,<sup>[26]</sup> thus indicating a strong shift toward preference of kainic acid (Fig. 51).

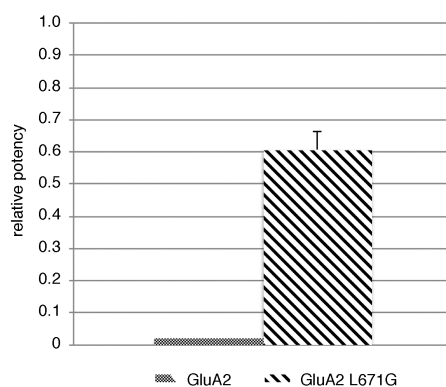


**Figure 51.** Relative potency of kainic acid (2 mM) in wild-type GluA2 (solid) and GluA2 L671G (dashed;  $n = 5$ , data  $\pm$  SEM) to L-glutamate (1 mM and 4 mM). The desensitization of receptors was blocked by the L504Y mutation.

With this data in hand, we concluded that mutation of the nonpolar residues L671 had indeed created strong candidates for a bump-hole approach toward an orthogonal receptor-ligand pair. Moreover, we were interested whether the receptors might now accept different substrates as their wild-type counterparts. As our group had previously tried to design a photoswitchable tethered receptor-ligand system based on GluA2, we screened the GluA2 L671G mutation for activation by MAG-type molecules. While lacking proper tether-models, we directly used MAG-0 (**209**) as a potential agonist. We were pleased to find, that unlike for the wild-type, the exchange of a leucine for glycine had indeed rendered **209** an agonist of AMPA-type receptors bearing the L671G mutation (Fig. 52).

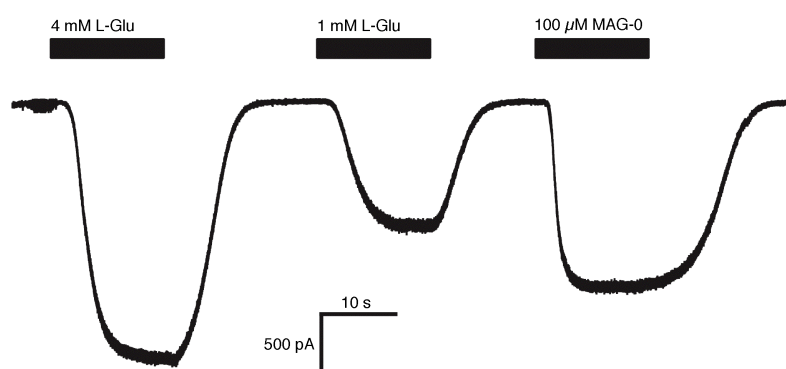


**Figure 52.** Exemplary voltage-clamp recording of GluA2 L504Y L671G (holding potential -70 mV).



Much to our delight, MAG-0 (**209**) showed  $74 \pm 5\%$  ( $n = 3$ ) depolarization at  $100 \mu\text{M}$ . At the same concentration, L-glutamate (**1**) only showed  $14 \pm 3\%$  ( $n = 5$ ) current. Not only is this the first time we have found a molecule, which is more efficacious than the native ligand L-glutamate (**1**), but at the same time, the L671G mutation offered the opportunity to design a PTL-receptor system based on GluA2, since it had apparently created an exit tunnel for 4-L-alkylated glutamate analogues like **209** (Fig. 53).

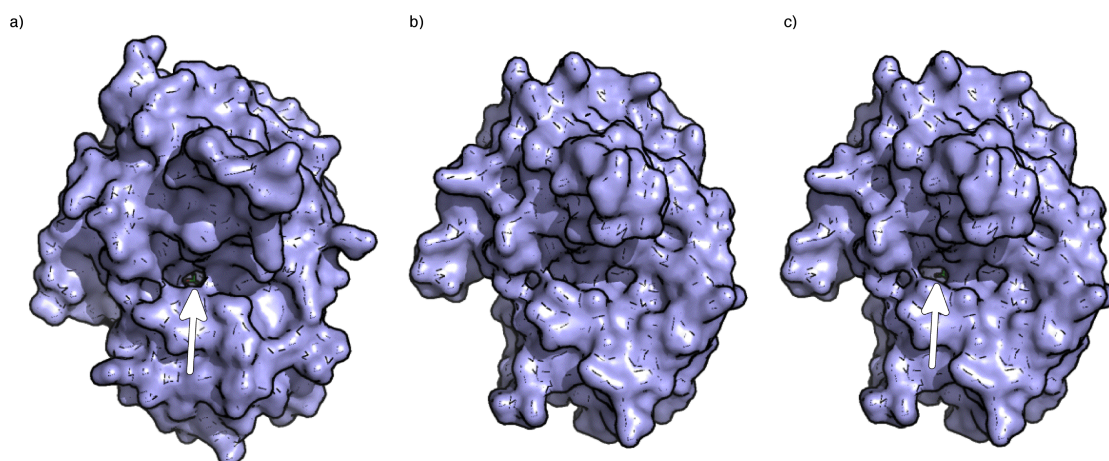
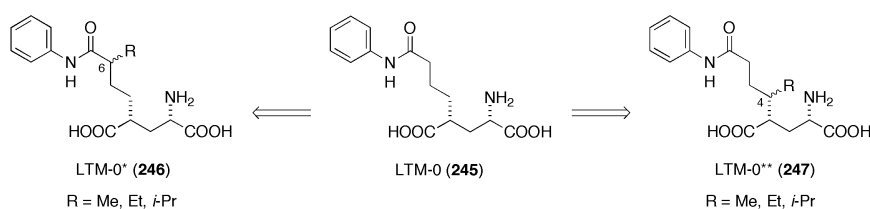


**Figure 53.** Comparison of the GluK2 and GluA2 LBDs. a) GluK2 wt (pdb code 1S7Y). b) GluA2 wt (pdb code 1FTJ). c) GluA2 L671G (based on pdb code 1FTJ). The presence and position of the exit tunnel is indicated by a red arrow.

To test our hypothesis that GluA2 L671G might be used in conjugation with MAG-0, we introduced the homologous cysteine mutation as used in LiGluR (L439C) in our receptor. Changing leucine 422 into a cysteine however, did not yield a viable construct, since we could not observe any glutamate-induced currents in HEK293T cells transfected with GluA2 L422C L504Y L671G. Possibly, the third mutation prevents proper folding of the iGluR monomers. In future experiments, we will therefore independently address different mutations for the covalent attachment of a photoswitch using the maleimide-Michael approach and combine them with our kainate-type AMPA receptor GluA2 L671G.

With respect to our goal of creating an orthogonal receptor-ligand pair using named receptor, we will synthesize molecules derived from LTM-0 (**245**), which can fill the hole generated by the L671G mutation more efficiently than MAG-0 (**209**), or its tether-model **245**. Initial docking experiments suggest that derivatives like **246**, **247** bearing an additional alkyl substituent in the 4- or in the 6-position should be very promising (Scheme 36).



**Scheme 36.** Envisioned orthogonal ligands derived from tether-model LTM-0 (**245**).

Since the two substitutions of L671 presented above had resulted in a substantially altered ligand-specificity and decreased affinity toward the native neurotransmitter L-glutamate (**1**), it was time to screen for more possible bioorthogonal ligands. Judging from our experience with small libraries (*vide supra*) and comparing our advances to the ones of Armbruster, Conklin and Sternson,<sup>[150a, 234, 244]</sup> we however concluded, that for the development of an iXR we would need efficient means for both the screening of compounds and mutations. This, we felt, could not be realized by manual patch-clamp electrophysiology. Accordingly, we decided to develop means to help us identify suitable receptor-ligand combinations. Ideally, such methods would be amenable to high-throughput, *i.e.* automated processing and might allow for both unguided mutation of receptors by random mutagenesis and improvement of rationally designed mutants by *e.g.* directed evolution at the same time. The following chapter summarizes our progress toward such a screening system.

#### 4) Yeast Assay for Glutamate Receptor Activity (YAGA)

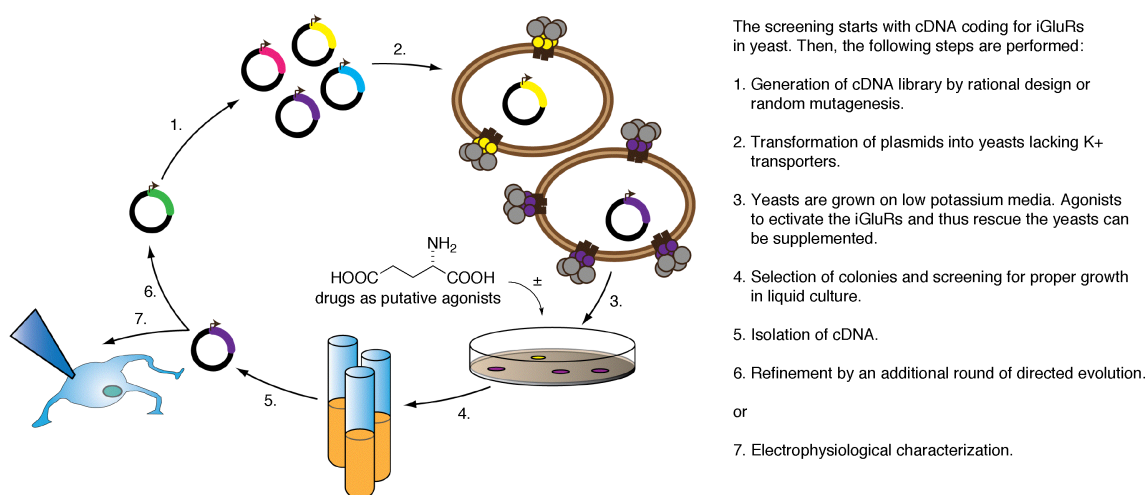
Challenged with the problem of rationally selecting potential ligands for our mutated iGluRs, we felt that in the absence of sufficient structure-activity relationship data, high-throughput screening might be better suited to come forth with lead structures, which could then be used to optimize receptor-ligand interactions. Unfortunately, we did not find any literature precedence describing such a method in ionotropic glutamate receptors. Even though we experimented with fluorescence-based assays similar to those used by Sternson and coworkers,<sup>[244]</sup> this did not yield reliable data.

We therefore felt that a yeast-based system similar to the one used to improve RASSLS/DREADS,<sup>[237]</sup> would be ideal for our purposes. Moreover, directed evolution might be used to improve any found iXR-ligand combinations. Unfortunately, unlike for the human muscarinic M3 receptor, there is no biochemical method of coupling iGluR-activity to yeast growth *via* the pheromonic signaling pathway.<sup>[261]</sup> We therefore devised a strategy to relay the information of LBD-closure to a signal enhancing growth in *S. cerevisiae*.

In collaboration with Harald Janovjak (IST Austria, Wien) we designed a yeast screen, which employs a method developed by Reuveny *et al.* for the investigation of G $\beta\gamma$ -dependent

activation of inward rectifying potassium channels (IRKs).<sup>[262]</sup> Using a yeast strain (SGY1528) lacking both low and high affinity potassium transporters ( $\Delta trk1$ ,  $\Delta trk2$ ),<sup>[263]</sup> they screened for mutant IRKs not requiring interaction with a  $G_{\beta\gamma}$  unit. Such channels allow  $K^+$  ions to pass the cell membrane and thus alleviate the potassium-starved yeasts' growth deficit. We envisioned using the same approach, but intended to replace the inward rectifying  $K^+$  channels by ionotropic glutamate receptors to supply the  $K^+$ -deficient yeast with potassium ions. Unlike IRKs however, modern iGluRs hardly discriminate between monovalent ions, since they lack the typical TXVGYG filter sequence found in  $K^+$  channels.<sup>[264]</sup> The selectivity of sodium over potassium in GluA2 for example is  $P_{Na}/P_K = 0.67$ ,<sup>[68]</sup> where P is the permeability for the respective ions. In GluR0 and other bacterial glutamate receptors, an enhanced discrimination between sodium and potassium ions is observed ( $P_{Na}/P_K = 0.01$  for GluR0).<sup>[68]</sup> Together with similarities to  $K^+$  channels in the pore topology,<sup>[265]</sup> this supports the idea that there might be an evolutionary link between iGluRs and potassium channels. Recently, an ionotropic glutamate receptor bearing both the TXVGYG-motif and the domain architecture of modern iGluRs, thus resembling a “missing link” between the two channels, has been described.<sup>[266]</sup>

Our yeast assay for glutamate receptor activity (YAGA) can be divided into seven individual steps (Scheme 37) starting from cDNA for the expression of selected iGluRs in yeasts: (1.) A library of mutant iGluRs is generated either by rational design (*vide supra*) or using error-prone PCR.<sup>[267]</sup>



**Scheme 37.** Conceptual scheme showing the rescue of  $K^+$ -starved yeast by functional expression of ionotropic glutamate receptors and the application to the directed evolution of an iXR.

(2.) Yeasts lacking potassium transporters (SGY1528)<sup>[263]</sup> are transfected with the DNA library. (3.) The auxotrophic yeasts are grown on K<sup>+</sup>-poor media to select for those functionally expressing the mutant iGluRs. The medium can be supplemented with selected drugs to be screened as putative agonists of the iXRs. (4.) Colonies, which are rescued by the action of functional receptors are picked and screened for proper growth properties in liquid culture. (5.) The cDNA of the best candidates is isolated and can be subjected to (6.) another round of directed evolution or (7.) may be functionally characterized using electrophysiology.

To set up a library of iGluRs for expression in yeasts, we selected GluA2 and GluK2 as the parent receptors and cloned them into a vector under the control of a pMet promoter, so we could later suppress the protein expression by supplementing L-methionine to the growth medium.<sup>[268]</sup> We decided to use the modern ionotropic glutamate receptors GluA2 and GluK2 (*r. norvegicus*) as a template and chose the respective R-variants at their Q/R editing site, thus preventing the potentially toxic influx of calcium ions into the yeast by rendering the pore impermeable to Ca<sup>2+</sup> ions.<sup>[269]</sup> While by using GluR0 we would have had the benefit of K<sup>+</sup>-selectivity too,<sup>[68]</sup> we reasoned that the pharmacological characterization of GluA2 and GluK2 is far more developed and should help us to select potential agonists for the iXRs. In order to ensure prolonged activation of the receptors by the action of either glutamate or any other drug supplemented to the yeast, we blocked the desensitization of the receptors with the L504Y mutation in GluA2 and with K531G and D776K respectively in GluK2.<sup>[78, 270]</sup> Thus, we would not have to rely on the metabolic stability of cyclothiazide or concanavaline A.<sup>[252]</sup> Additionally, we designed plasmids bearing both vertebrate and yeast Kozak consensus sequences in order to study the influence of different expression levels of the iGluRs.<sup>[271]</sup> The necessary alterations of the ionotropic glutamate receptors (Q/R site, non-desensitizing mutations, Kozak sequence) were carried out using standard techniques,<sup>[119]</sup> to yield a set of cDNAs, which is summarized in Table 3.

**Table 3.** Summary of the generated pMet cDNA library coding for iGluRs.

Name	Parent iGluR	Q/R	Kozak	Non-desensitizing mutation
A1.1	GluA2	R	TAGACCATG	L504Y
A2.1	GluA2	R	AAAAAAATG	L504Y
K1.1	GluK2	R	TAGACCATG	K531G
K2.1	GluK2	R	AAAAAAATG	K531G
K1.2	GluK2	R	TAGACCATG	D776K
K2.2	GluK2	R	AAAAAAATG	D776K

With the first collection of plasmids for the expression of iGluRs in yeast in hand, we turned to our collaboration partners in the group of Katja Strässer (LMU Munich) to evaluate the ability of the different constructs to rescue the SGY1528 strain (gracious gift from Eitan Reuveny) on low  $K^+$  media. The yeasts were transfected with the respective constructs and grown with varying amounts of L-glutamate (**1**) and  $K^+$  (Fig. 54).

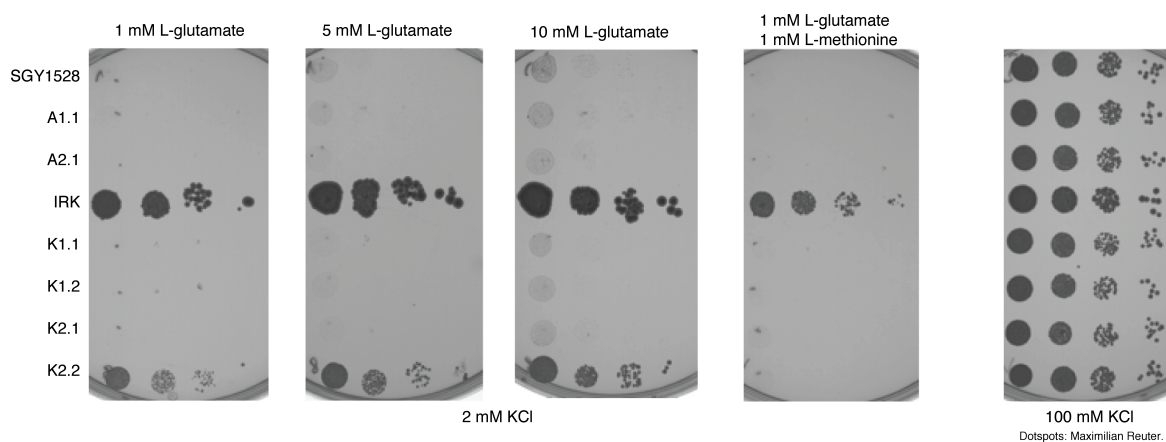


**Figure 54.** Dotspot assay of yeasts (SGY1528) expressing iGluRs. The colonies were grown under different conditions as indicated (IRK = inward rectifying potassium channel not requiring activation by a  $G_{\beta\gamma}$  dimer).<sup>[262]</sup>

We found that the strain used (SGY1528) did indeed show the expected behavior of inhibited growth on low  $K^+$  media and could either be rescued by supplementing KCl (100 mM), or expression of the mutant IRK developed by Reuveny and coworkers.<sup>[262]</sup> Much to our delight, one of our constructs, K2.2 (*i.e.* GluK2<sub>R</sub> D776K), did also show the same ability, however with slightly diminished potency. As can be seen in Figure 54, the yeasts were able to grow in the presence of 1 mM, 5 mM and 10 mM glutamate (concentrations at or well beyond the saturation-limit), while without the supplement there was no growth (not shown).<sup>[119]</sup> Most importantly, this effect was mitigated in the presence of 1 mM L-methionine, indicating a correlation of protein expression to the enhanced growth rate. The persistent growth of IRK-expressing yeast can be attributed to residual protein concentrations, as reported in the original paper by Reuveny *et al.*<sup>[262]</sup> Unfortunately the effect of K2.2-expression was not as profound as the one for the potassium channel, this however may be attributed to their relative sizes. Glutamate receptor monomers with their *ca.* 900 amino acids are considerably more complex than IRKs, which generally have a size of about 550 amino acids.

Despite this difference, we decided to analyze the growth properties of yeasts expressing the kainate receptor K2.2 in liquid media. By doing this, we sought to investigate the effect of other kainate-type agonists (*e.g.* kainic acid) or antagonists (*e.g.* CNQX) more

easily than by using plate-cultured yeasts. Accordingly, we grew K2.2-transfected yeasts (SGY1528) in liquid culture and measured their time-dependent growth in 96-well plates. A summary of these statistics is shown in Figure 55.

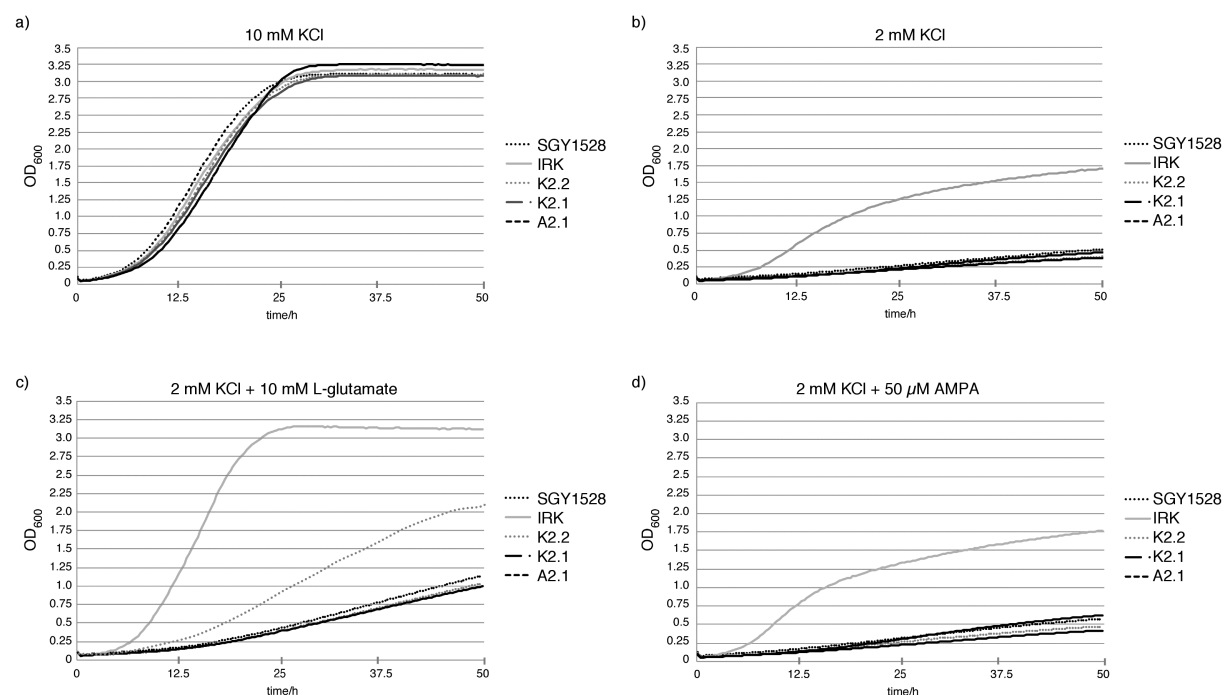


**Figure 55.** Liquid culture of SGY1528 yeasts expressing the different iGluR constructs (additives and concentrations as indicated).

As expected, all yeasts grow well at 100 mM KCl (Fig. 55a) and only the IRK-construct rescues the growth-deficient strain (SGY1528) at a KCl concentration of 2 mM (Fig. 55b). While 1 mM of L-glutamate (**1**) is commonly considered to be saturating at modern iGluRs, we reasoned that due to the yeast cell wall, there might be a concentration gradient of glutamate and we would have to increase its concentration. Accordingly, we used 10 mM L-glutamate (**1**) and were please to find, that the also kainate receptor K2.2 promotes an enhanced growth as compared to the other constructs (Fig. 55c). Moreover, we verified that this is indeed a pharmacologically significant effect, since AMPA (albeit at a lower concentration) is not able to activate the kainate-type receptor construct (Fig. 55d). Given the relative permeability of iGluRs for potassium over sodium (approx. 3:2), it is reasonable to expect a diminished growth when compared to the inward-rectifying potassium channel (IRK). We will therefore explore options to enhance the K<sup>+</sup>-selectivity of our iGluR constructs by *e.g.* expressing GluR0 or the artificial, potassium-selective glutamate receptor HyLighter.<sup>[68, 97d]</sup> Nonetheless, the growth obtained from K2.2 in the presence of 10 mM L-glutamate (**1**) is already enough to be used as a screening platform for mutations toward an

orthogonal receptor-ligand pair and we will report our progress toward such an iXR in due course.

## 5. Conclusions and Outlook

In summary we have developed several approaches toward an orthogonal receptor-ligand system based on ionotropic glutamate receptors. Our attempts to rationally design mutations that can alter iGluR-specificity have so far yielded receptors, which show a highly reduced affinity toward L-glutamate. At the same time, we have shown that some of our modified iGluRs can be controlled using the photoswitched tethered ligand (PTL) approach. Additionally, we have created modified AMPA receptors, which show a marked increase in affinity toward kainate-type ligands. One of them efficiently functions as a “MAG”-receptor, *i.e.* it has a higher affinity for MAG-0 (**209**) than for its endogenous ligand L-glutamate (**1**). We hope to use these constructs to design a PTL-receptor system of GluAs, which would be highly interesting for the neurobiological community, as AMPARs are responsible for the major part of the excitatory neurotransmission at glutamatergic synapses. Therefore, a light-gated, tethered AMPA receptor (“LiGluA”) would be a great addition to our portfolio of optogenetic tools.

In a complementary approach toward an orthogonal receptor-ligand pair, we have designed a yeast assay for glutamate receptor activity (“YAGA”), which allows for the screening of both ligands and modified receptors. We plan to use this system, which is based on the conditional rescue of a yeast strain lacking both low- and high-affinity potassium transporters (SGY1528), for a directed evolution of ionotropic glutamate receptors toward a designer receptor-ligand pair. Thus we seek to provide an orthogonal toolset for the dissection of neural networks.

**Part II: Toward the Total Synthesis of Herquline A & B**



## II. Toward the Total Synthesis of Herquiline A & B

*Philipp Stawski, Giulio Volpin and Dirk Trauner*

While arguably the most glorious field of organic chemistry, total synthesis is at the same time the most controversial. Starting with Wöhler's synthesis of urea,<sup>[272]</sup> the era of total synthesis has yielded such epochal achievements as Woodward and Eschenmoser's 1973 synthesis of cobyrinic acid and the synthesis of prostaglandins F<sub>2α</sub> and E<sub>2</sub> by Corey in 1969.<sup>[273]</sup> While those and related endeavors have surely both promoted the development of synthetic strategies and our understanding of natural product chemistry, it is questionable, whether the current direction toward more and more complex targets, such as maitotoxin,<sup>[274]</sup> will have the same effect, or whether this will finally mark total synthesis as a science conducted in an ivory tower. Regardless of such arguments however, we believe that total synthesis is mainly – and has ever been – a highly successful method of training organic chemist in a variety of techniques, which would otherwise be difficult to combine. Accordingly, we regard the total synthesis of natural products as a field, in which students can both explore and push the boundaries of chemical synthesis and, more importantly, of their own knowledge and skills. The following chapters describe our attempts toward the synthesis of such two small, yet challenging natural products, herquiline A and B.

*Note: This work was conducted partially in collaboration with Giulio Volpin (planning and supervision of G.V.'s master thesis by P.S.).<sup>[275]</sup>*

### 1) The Herquiline Alkaloids

The herquiline alkaloids A and B were isolated in 1979 and 1996 by Omura and coworkers from the penicillium strain FG-3772, a soil isolate.<sup>[276]</sup> It was immediately clear, that herquiline A (**248**) and B (**249**) did not match any structure previously extracted from this fungus (Fig. 56). However, it was not before a crystal structure of **248** was obtained by Matsumoto and coworkers,<sup>[277]</sup> that the molecular architecture of both alkaloids could be determined unambiguously. Herquiline A and B (**248**, **249**) bear a piperazine ring and in herquiline B (**249**) there are also two cyclohexenones present. In addition to that, there is a pyrrolidine ring incorporated in **248**, making it a pentacyclic system. Unfortunately, the 2-dimensional drawings of both herquiline A and B do not adequately represent their strained

nature. As can be seen from the X-ray structure of **248**, all the rings appear to be distorted and the piperazine ring resides in a boat conformation (Fig. 56).

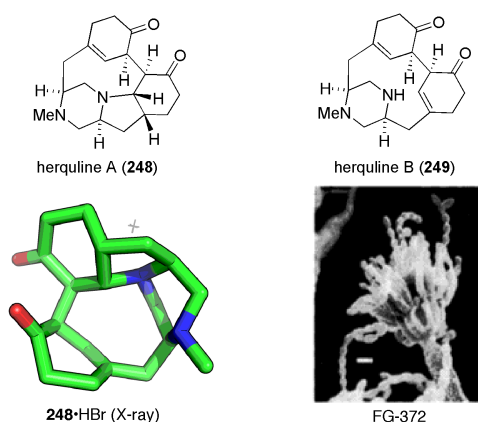
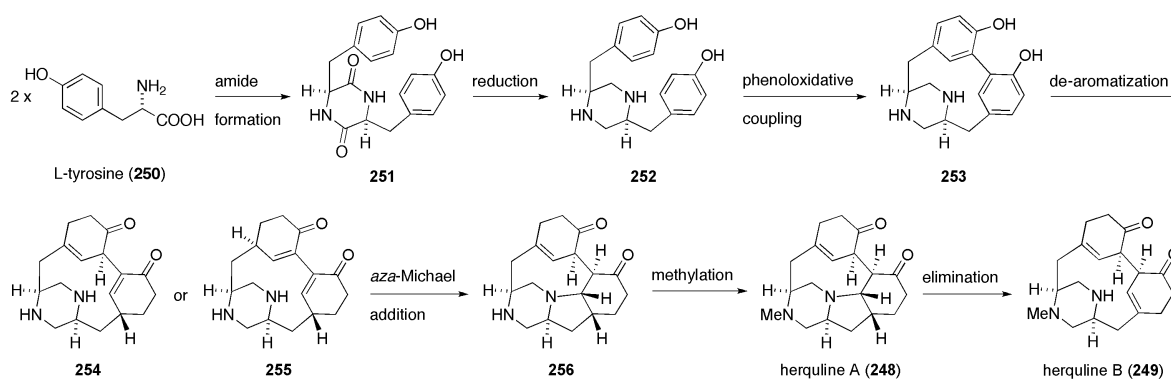


**Figure 56.** The chemical structures of herquiline A and B (**248** and **249** respectively), the X-ray structure of **248**·HBr and a scanning electron micrograph of the penicillium strain FG-372.<sup>[277]</sup>

Since the chemical synthesis of these structural features promised to be challenging, we selected the herquelines as a target of our total synthesis program.

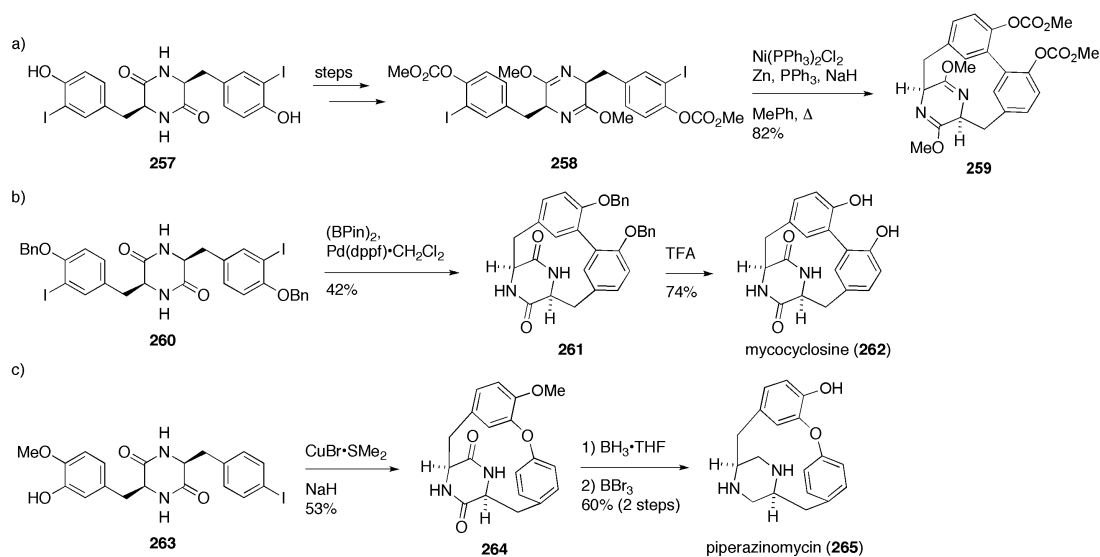
Biosynthetically, it is believed that both **248** and **249** stem from two molecules of L-tyrosine (**250**), which undergo cyclization to form a diketopiperazine (Scheme 38). Omura and coworkers have presented evidence for this, since supplementing **250** to the fermentation broth increased the amount of herquiline alkaloids isolated. Unfortunately, they did not conduct a labeling study to unambiguously prove the incorporation of the aromatic amino acid in herquiline A and B. Despite this, Omura's biosynthetic proposal seems reasonable, as it links the herquiline alkaloids to the known class of dityrosine alkaloids. This class of natural products is known to undergo phenoloxidative couplings, yielding either C-O- or C-C-coupled products such as piperazinomycin or mycrocyclosin (*vide infra*).<sup>[278]</sup>



**Scheme 38.** Omura's proposed biosynthesis of herquiline A and B (**248**, **249**).

It is unclear, at which stage of the biosynthesis the diketopiperazine is reduced to the piperazine. However, it can be assumed, that following coupling and dearomatization, the proposed *aza*-Michael addition of the piperazine nitrogen in **254** will proceed more easily, if the reduction happens earlier in the synthesis (Scheme 28). It is important to note, that the hypothetical  $C_2$ -symmetric intermediate **255** might serve as a substrate for the aforementioned hetero-Michael addition, too. This would however require an additional double-bond migration after formation of the pyrrolidine ring. To complete the biosynthetic proposal, methylation of the secondary amine **256** would yield herquiline A (**248**). This might then serve as a precursor to herquiline B (**249**) via an E2 elimination, yielding the triple-substituted double bond rather than reforming the Michael-system (Scheme 38).

So far, there has been only one report on the attempted total synthesis of the herquiline alkaloids by Norioishi and coworkers.<sup>[279]</sup> The authors constructed the 12-membered ring of herquiline B (**249**) by an efficient intramolecular coupling of an iodotyrosine-derived diketopiperazine **257**, which was protected as the *bis*-imido ether **258** (Scheme 39a).<sup>[279]</sup>



**Scheme 39.** a) Reported progress toward the herquiline alkaloids by Norioishi *et al.* b) Key-step in the total synthesis of mycocyclusine (**262**). c) Key-step in the synthesis of piperazinomycin (**265**).

Most notably, only carbonate **258** could be coupled to give the cyclic product, while both the free phenol and the diketopiperazine could not. Despite this, there has been no further report on the progress of their total synthesis so far. The recently published total synthesis of the related natural product mycocyclusine (**262**) by Hutton and coworkers,<sup>[280]</sup> which used an elegant borylation-Suzuki-Miyaura coupling sequence, does not report any similar constraints (Scheme 39b). Boger *et al.* state, that during their synthesis of piperazinomycin (**265**), they could only promote the ring-closure – using a modified Ullman-coupling – when the

piperazine moiety was still at the keto-piperazine stage (Scheme 39c).<sup>[281]</sup> This seems to indicate a strong dependency of this type of reactions on the conformation of the piperazine ring. The present reports suggest an increased preference of boat-like structures with an axial position of substituents, when there is still an  $sp^2$ -center present in the piperazine ring (*i.e.* diketopiperazine or bis-imido ether stage).<sup>[282]</sup> Any synthetic plan involving formation of a piperazine-bridging macrocycle, therefore has to account for these conformational requirements.

## 2) Retrosynthesis

Structurally, the herquelines (**248**, **249**) belong to the class of piperazine alkaloids. Arguably, their structural attraction is due to their tetracyclic and pentacyclic cores, which make up a compact arrangement of four contiguous and two isolated stereocenters. Both molecules share the bi(cyclohexenedione) motif. Given the pK<sub>A</sub> of ketones, the  $\alpha$ -stereocenters adjacent to those carbonyl groups can be considered to be under thermodynamic control, as they would otherwise epimerize under the isolation conditions. The other two stereocenters in the piperazine ring bear a configuration, which is in agreement with the proposed biosynthetic origin from L-tyrosine.<sup>[277]</sup> In herquiline A (**248**), the octahydro-1H-indole, or dodecahydro-pyrazino[1,2-*a*]indole moieties (Fig. 57) are challenging, since they form a highly strained, cage-like structure (*cf.* X-ray, Fig. 56). It is important to note (*vide infra*), that to accommodate these conformational constraints, the piperazine ring reside in the thermodynamically unfavorable boat-conformation.

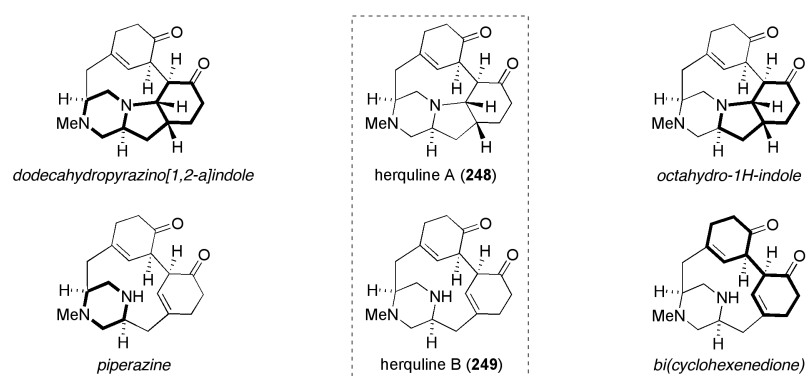
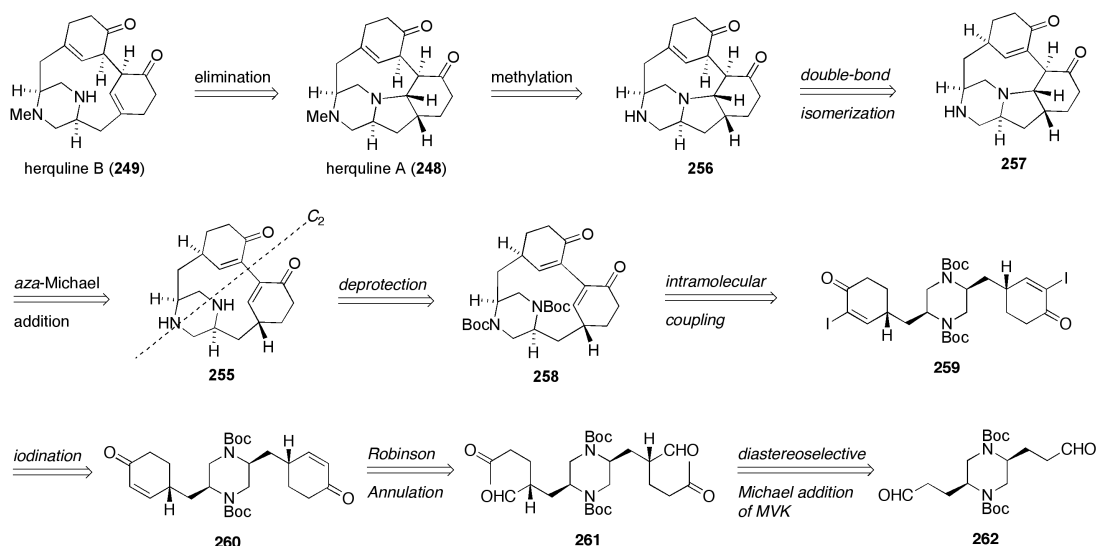


**Figure 57.** The structural features of the herquiline alkaloids (the respective motifs are shown in bold).

Taking into account the strained nature of herquiline A and B, we decided not to access the herquelines *via* the octahydro-1H-indole, or dodecahydro-pyrazino[1,2-*a*]indole motifs. We rather decided to approach **248** and **249** as a bi(cyclohexenedione)-bridged piperazine. This would allow us to access the two natural products *via* the formation of a 12-membered ring,

rather than having to synthesize the [6.5.6] system first and then the nine-membered ring, as we were convinced, that such a reaction would suffer from the increase ring-strain of this smaller carbocycle.<sup>[283]</sup>

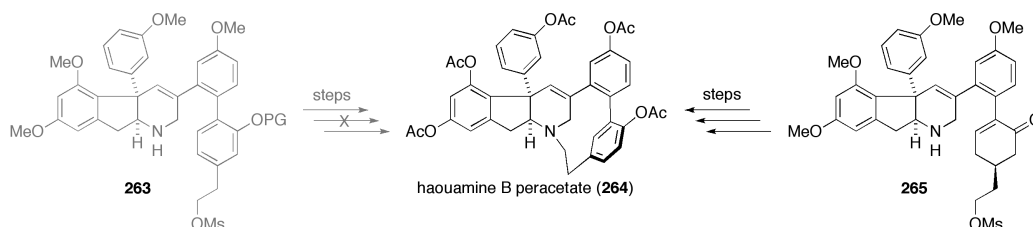
Our retrosynthetic analysis is based on the insight, that the  $C_2$ -symmetric diketone **255** might be a valid biosynthetic precursor to both herquiline alkaloids (*cf.* Scheme 38). Assuming, that herquiline B (**249**) is formed from herquiline A (**248**) in an E2-type elimination, the latter can be synthesized by methylation of the secondary amine **256** (Scheme 40). We suggest, that a double-bond isomerization of the conjugated double-bond of the resulting  $\alpha,\beta$ -unsaturated enone **257** can be achieved under acidic or basic conditions, since the unconjugated double-bond is of the same order of substitution (triple-substituted) and corresponds to the constitution as found in the natural product.



**Scheme 40.** Retrosynthesis part I: from the herquiline alkaloids to the  $C_2$ -symmetric precursors **255** and **258**. (MVK = methylvinyl ketone).

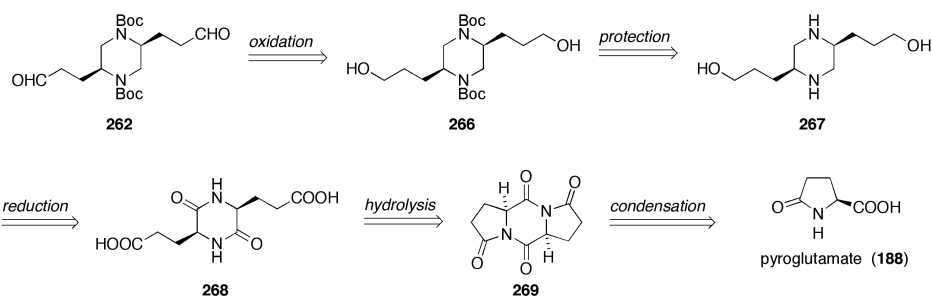
The herquiline A core-structure is formed by an *aza*-Michael addition of either of the two nitrogen atoms in the  $C_2$ -symmetric dienone **255**. To avoid any addition preceding this step, we envision masking the piperazine with Boc groups. As a key step of the synthesis, we envision a novel and challenging intramolecular reductive coupling of the bis( $\alpha$ -iodo ketone) **259**, since this is an established method for the synthesis of bi(cyclohexenediones) intermolecularly.<sup>[284]</sup> For an intramolecular process however, we reasoned that introducing the more flexible cyclohexenones should compensate for the aforementioned conformational requirements of strategies involving macrocyclizations to a bridged piperazine. This general approach, which has recently been successfully been applied by Baran *et al.* in the total synthesis of the macrocyclophane haouamine A,<sup>[285]</sup> and by our group in the total synthesis of

the assigned structure of haouamine B,<sup>[286]</sup> is based on the fact, that there are only three  $sp^2$  centers in a cyclohexenone as compared to six in a benzene ring. It is for this reason, that the alkylative ring-closure to **264** only worked on the cyclohexenone- and not on the biaryl-stage (Scheme 41).



**Scheme 41.** Synthesis of the assigned structure of haouamine B peracetate (**264**) from a cyclohexenone precursor *via* alkylation.

For our proposed retrosynthesis, iodoenone **259** can be accessed from dialdehyde **262**, after a diastereoselective addition of methylvinyl ketone (MVK), followed by a double-Robinson annulation and iodination of the resulting dienone **260**. We found, that dialdehyde **262** can be traced back to the corresponding diol **266** and thus to the diamino diol **267** after selective protection of the piperazine nitrogens using a carbamate protecting group (Scheme 42).



**Scheme 42.** Retrosynthesis part II: reduction-oxidation and condensation-hydrolysis sequences connecting the  $C_2$ -symmetric dialdehyde **262** to (S)-pyroglutamic acid (**188**).

As the reduction of diketopiperazines is an obvious, and for that reason well documented approach for the synthesis of piperazines, **267** can be traced back to lactam **268** by reduction using *e.g.* lithium aluminium hydride. Much to our delight we found, that **268** is a literature-known compound, which can be synthesized from (S)-pyroglutamic acid (**188**) in just two steps.<sup>[287]</sup>

We were, of course, fascinated by the idea, that we could link both herquiline alkaloids to (S)-pyroglutamate (**188**), as this would be a nice connection to the chemical biology work

discussed in previous chapters. Before reporting our progress toward herquiline A and B however, we will briefly summarize the use of L-pyroglutamic acid (**188**) and L-glutamate (**1**) in the total synthesis of natural products.

### 3) L-Glutamate and L-Pyroglutamate in Total Synthesis

The 21 proteinogenic L-amino acids are ideal substrates for ex-chiral pool approaches, as they do not only provide a stereocenter, but many different functionalities, which can be exploited in the total synthesis of natural products. Among those readily available amino acids, this chapter will focus on the use of (*S*)-glutamate (**1**) and (*S*)-pyroglutamic acid (**188**) in total synthesis. (Bio)synthetically, **188** is obtained from L-glutamic acid (**1**) by condensation. The biosynthesis of **1** itself is highly interesting, as it connects to the Krebs-cycle and hence to energy production of the cell. (*S*)-glutamate (**1**) is synthesized by transamination to  $\alpha$ -ketoglutarate, which is a key-intermediate of glycolysis. As such, **1** can be considered as one of the main biosynthetic storages of nitrogen. Moreover, the biochemical role of L-glutamate (**1**) is not only limited to serving as a precursor for the synthesis of other amino acids, the synthesis of peptides and the use as neurotransmitter, it is also the cofactor of monooxygenases in its deaminated form (*i.e.*  $\alpha$ -ketoglutarate) and thus plays a major role in the oxidative processing of other metabolites.<sup>[288]</sup>

The use of (*S*)-glutamic acid (**1**) and L-pyro-glutamate (**188**) in total synthesis is widespread. In addition to serving as a starting material for the preparation of chiral auxiliaries,<sup>[289]</sup> there are more than 28 syntheses of or toward natural products incorporating those two forms of glutamate in their carbon skeleton (*i.e.* no simple glutamic amides).<sup>[290]</sup> A selection of those, which retain the amino-function, are depicted in Figure 58. The structures feature a variety of different natural product classes, among them rather small molecules like acivicin (**283**) synthesized by Silverman and coworkers,<sup>[290d]</sup> and such enormous hexapeptide alkaloids like the dimeric chloptosin (**274**) prepared by the Ley group.<sup>[290k]</sup> For a detailed discussion of their synthesis the reader may be referred to the original manuscripts.<sup>[290b-d, 290g, 290k, 290m, 290o, 290q-v, 290x, 290aa]</sup> Despite this diversity, all molecules shown in Figure 58 retain the  $\alpha$ -amino stereocenter present in **1** or **188**, even though the respective syntheses have been realized using quite different chemical synthons (*vide infra*).

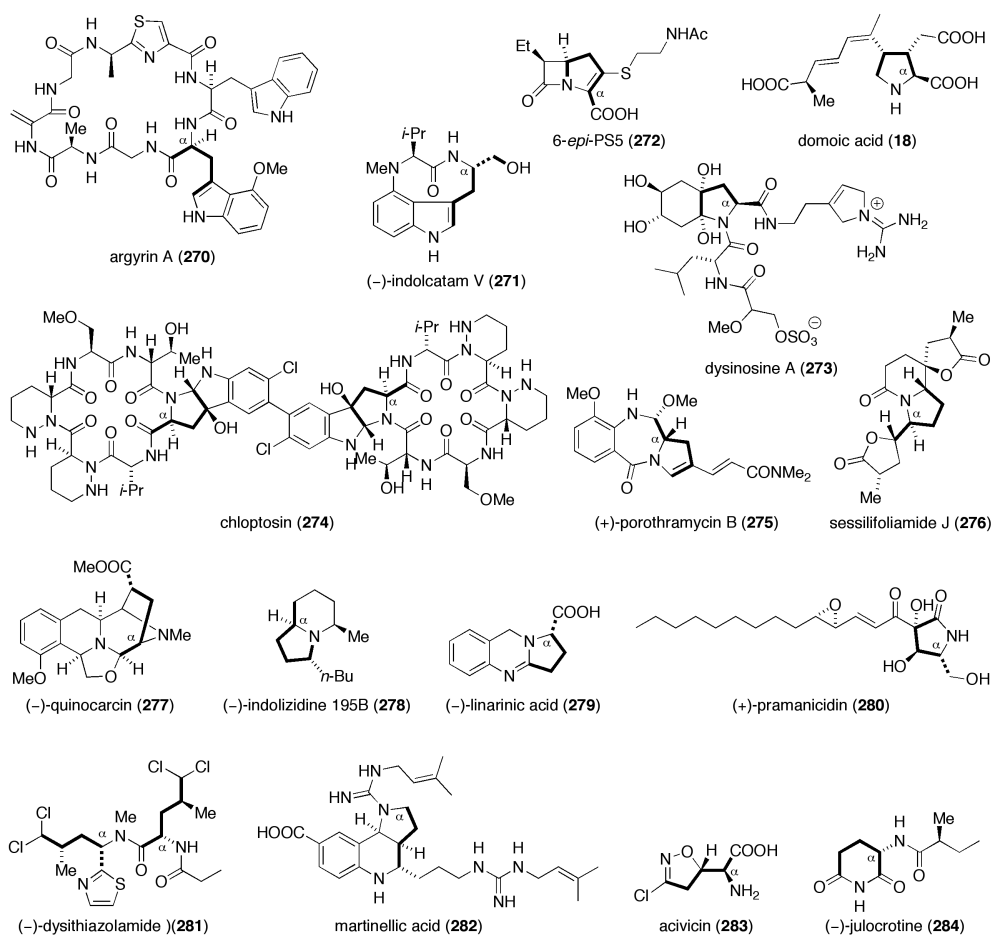


**Figure 58.** Natural products synthesized from either L-pyroglutamate (**1**) or L-glutamic acid (**188**) where the amino group has been converted to another function. The carbons corresponding to the precursor are shown in bold. The  $\alpha$ -amino carbon has been marked with an  $\alpha$ .

At the same time, there are several syntheses incorporating the glutamate carbon skeleton, but not the amino-function. Thus, L-glutamate does not only serve as a chiral building block for alkaloids such as indolactam V (**272**), porothramycin B (**275**) or martinellie acid (**282**), but also for polyketide and terpenoid natural products such as 13,4-*threo* desicomacin (**286**) and eldanolide (**288**) (Fig. 59).<sup>[290l, 290p, 290q, 290s, 290t]</sup> To this end, the  $\alpha$ -amino group has been converted into another functionality in those molecules. In most of them, like *e.g.* the indolizidine alkaloid (+)-swainsonine (**289**) or the spiroketal (+)-calyculin A (**285**), it has been transformed into an oxygen-bearing stereocenter using diazotization or similar substitution strategies resulting in a deamination (*vide infra*).<sup>[290j, 290ab]</sup> In other molecules like reblastin (**287**), isoaltholacton (**290**) and (+)-quebrachamine (**291**),<sup>[290a, 290w, 290y]</sup> the glutamic descent is hardly recognizable any more. Especially in **291** since the  $\alpha$ -stereocenter has been lost completely after serving as a template for the diastereoselective alkylation in the  $\omega$ -position. This is a very powerful approach, since depending on whether



the alkylation is performed on L-glutamic acid (**1**) or (*S*)-pyroglutamate (**188**), different diastereoselectivities can be obtained (*cf.* chapter I.7).

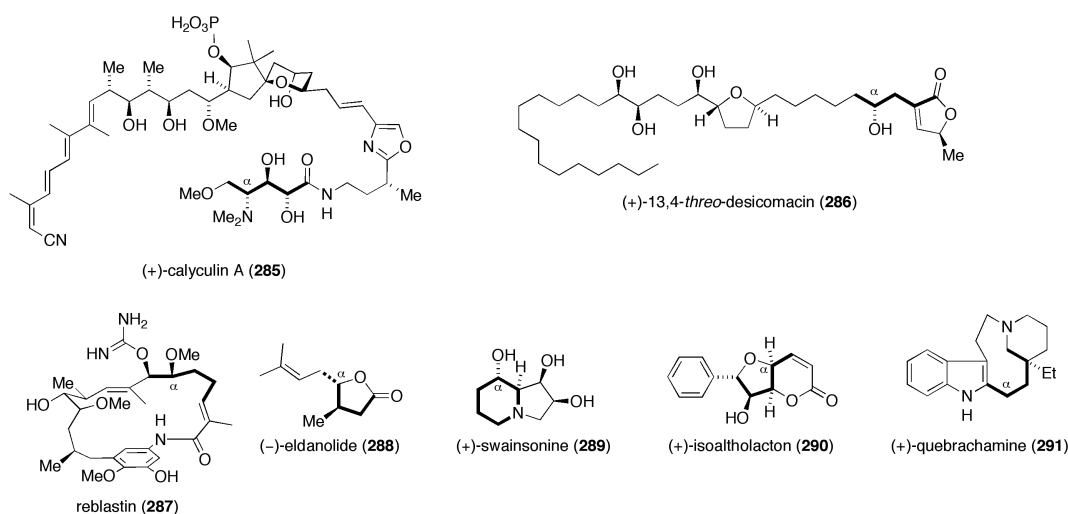
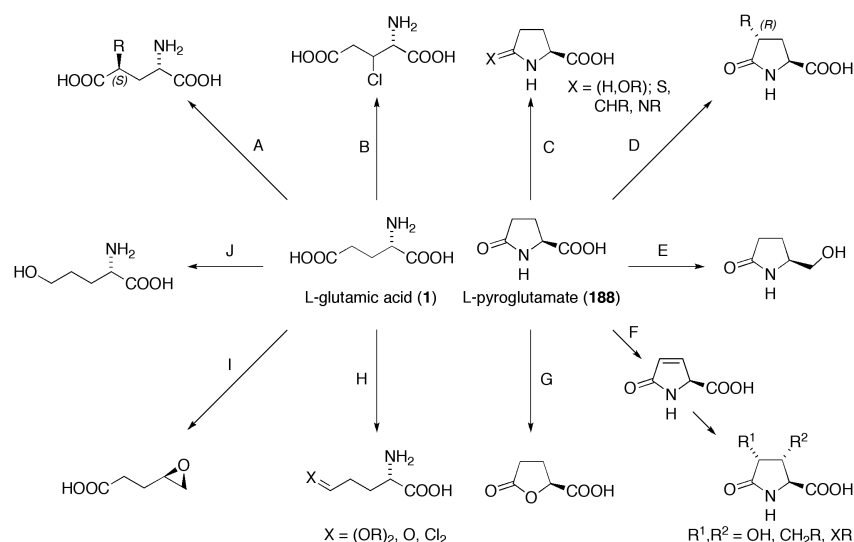


**Figure 59.** Natural products synthesized from either L-pyroglutamate (**1**) or L-glutamic acid (**188**) where the amino group has been converted to another function. The carbons corresponding to **1** are shown in bold. The  $\alpha$ -amino carbon has been marked with an  $\alpha$ .

While a detailed analysis of the methods used to synthesize the molecules shown in Figures 58 and 59 would go beyond the scope of this work, we will rather focus on the key transformations performed on both L-glutamic (**1**) and L-pyroglutamic acid (**188**). As mentioned earlier, diastereoselective alkylation of C-4 is one of the most commonly used reactions in glutamate chemistry (Scheme 43 A, D).<sup>*e.g.* [84, 188]</sup> Selective manipulation of either carboxyl groups (Scheme 43 C, E, H, J) are non the less important and provide a variety of functional handles, which can be further elaborated.<sup>*e.g.* [290b, 290h, 290k, 290o, 291]</sup> Among the most interesting transformations of glutamates however are reactions introducing substituents in the 3-position. This can be realized either by selective chlorination and displacement of the halogen (Scheme 43 B),<sup>*e.g.* [290d]</sup> or by dehydrogenation to the enone and subsequent Michael addition of nucleophiles.<sup>*e.g.* [292]</sup> Reactions of such  $\alpha,\beta$ -unsaturated systems with 1,3-dipoles or dienes, yield 3,4-syn-disubstituted glutamate analogues.<sup>*e.g.* [293]</sup> Such glutamic enones can also be subjected to dihydroxylations, giving 3,4-dihydroxy pyrrolidones (Scheme 43 F).<sup>*e.g.* [294]</sup> Another key-transformation involves exchange of the  $\alpha$ -stereocenter nitrogen for an oxygen. This can be realized either by lactonization after diazotization and intramolecular substitution under double inversion, or by formation of a terminal epoxide (Scheme 43 G, I).<sup>*e.g.* [290a, 290l]</sup>

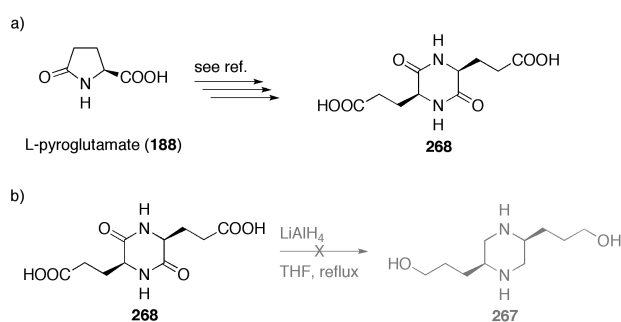


**Scheme 43.** Typical synthetic transformations of L-glutamic (**1**) or L-pyrroglutamic acid (**188**). Only key-modifications are shown, protecting group and other modifications have been omitted for clarity.

In summary, L-glutamate (**1**) and L-pyrroglutamate (**188**) can be regarded as versatile building blocks for the total synthesis of many different natural product classes. They allow for a variety of chemical transformations and the introduction of both carbon- and heteroatom-substituted stereocenters at any of the three central carbon atoms.

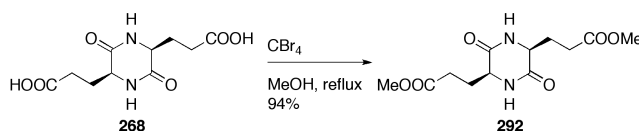
#### 4) Toward the Total Synthesis of Herquiline A and B

Owing to its high versatility, we were positive that (*S*)-pyrroglutamic acid (**188**) would prove as a good starting material for our envisioned synthesis of herquiline A and B (**248**, **249**). It commenced with the transformation of **188** into the glutamic diketopiperazine **268** using a procedure reported by Parrish and Mathias (Scheme 44a).<sup>[287]</sup> Unfortunately, initial studies had shown, that a direct reduction of **268** to the amino alcohol **267** using  $LiAlH_4$  or  $BH_3 \cdot THF$  was not possible.<sup>[275]</sup> The main reason for this was the low solubility of diketopiperazine **268** in organic solvents except for DMF or DMSO (Scheme 44b).



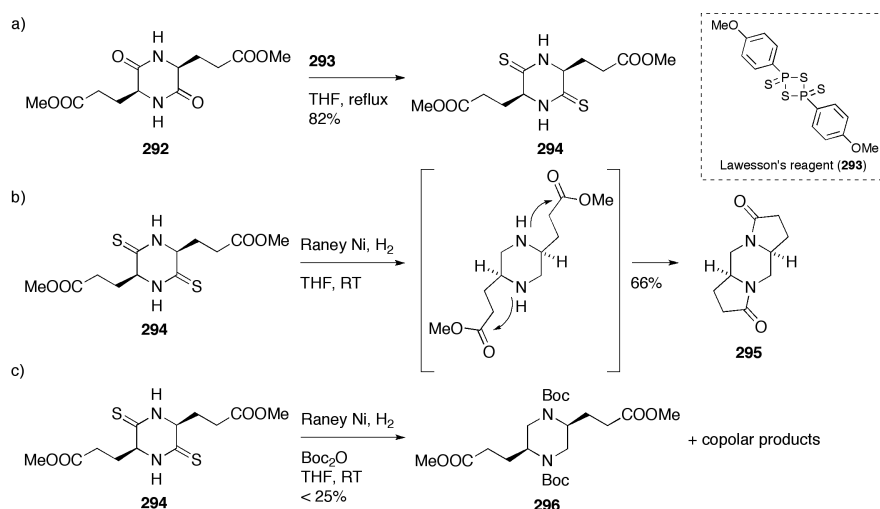
**Scheme 44.** a) Formation of glutamic diketopiperazine **268** from (*S*)-pyrroglutamic acid (**188**). b) Attempted direct reduction of **268** to aminoalcohol **267**.

We therefore decided to investigate a stepwise protocol for reduction of glutamic diketopiperazine **268**. To this end, we first formed the dimethyl ester **292** in order to improve the solubility. After intensive experimentation,<sup>[275]</sup> we found that the esterification worked best under conditions using CBr<sub>4</sub> as a catalyst (Scheme 45).<sup>[295]</sup>



**Scheme 45.** a) Esterification of diacid **268** using CBr<sub>4</sub> as catalyst.

Since diketopiperazines are known for their low solubility, we decided to first reduce the lactam carboxyl groups while leaving the esters untouched. To this end, we converted **292** into dithioketopiperazine **294** in good yields using Lawesson's reagent (**293**, Scheme 46a). However, desulfurization using Raney-Nickel<sup>[296]</sup> did not yield the desired piperazine dimethyl ester, but the piperazine bislactam **295**, which resulted from an intramolecular attack of the intermediary formed secondary amine (Scheme 46b).

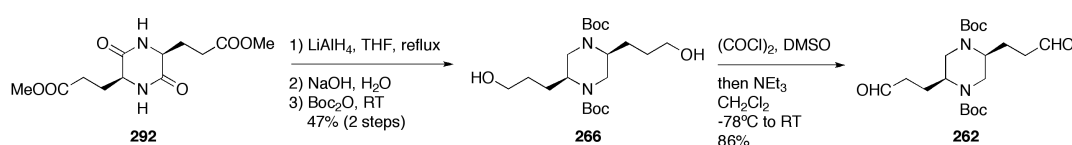


**Scheme 46.** a) Thionylation of diketopiperazine **292** using Lawesson's reagent. b) Dethionylation attempt leading to bislactam **295**. c) Dethionylation and *in situ* protection yields the Boc-protected piperazine **296**.

Attempts to protect the free piperazine with Boc-anhydride *in situ* did unfortunately not yield the clean carbamate **296**. Instead, we isolated a mixture of products, which contained **296** as indicated by HRMS and NMR along with a chromatographically and spectroscopically very similar molecule – probably a diastereomer of **296** resulting from epimerization during the

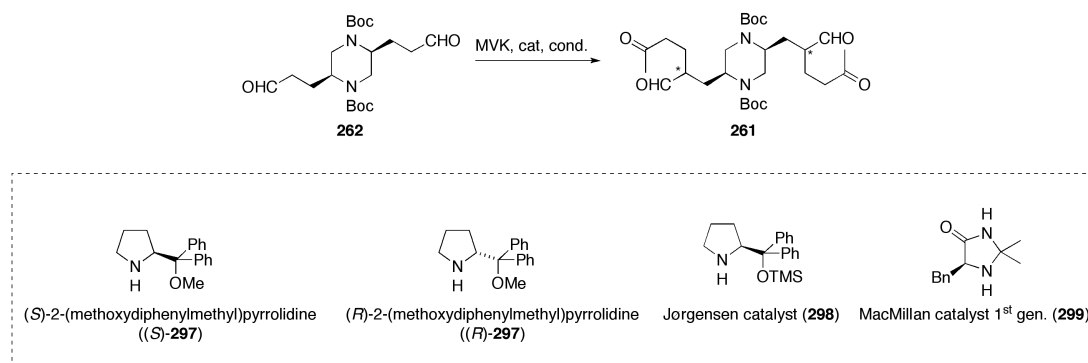
desulfurization (Scheme 46c). Due to these problems, we decided to not follow up on this route

Since our two-step approach toward the reduction of the diketopiperazine was unsuccessful, we again focused on a one-pot reduction. Based on our initial studies,<sup>[275]</sup> we first reduced ester **292**, which showed an improved solubility in THF as compared to diacid **268**. After considerable optimization of the reaction conditions, we obtained diol **266** in acceptable yield upon reduction using lithium aluminium hydride and chemoselective protection of the piperazine as di(*tert*.-butyl) carbamate. Oxidation-state adjustment under Swern conditions then yielded the piperazine dialdehyde **262** in 86% (Scheme 47).<sup>[297]</sup>



**Scheme 47.** Reduction of glutamic diketopiperazine dimethyl ester **292** and oxidation of the primary alcohol under Swern-conditions to dialdehyde **262**.

With **262** in hands, we now had to form keto-aldehyde **261** in a diastereoselective manner, as this should set the stereocenter at the cyclohexenone (Table 4). To this end, we screened a variety of reagents and organocatalysts known to promote an addition of MVK  $\alpha$  to primary aldehydes. Trimethylsilyl diethylamide gave ketoaldehyde **261** in good yields and – as expected – without any apparent stereoinduction (Table 4, entry 1).<sup>[298]</sup> Screening several organocatalysts, we found that both enantiomers of 2-(methoxydiphenylmethyl) pyrrolidine (**297**) did yield the desired product in acceptable yields (Table 4, entries 2 and 3). While with (*S*)-**297** we obtained an encouraging 1 : 2.7 mixture of diastereomers, its enantiomer, (*R*)-**297**, did only give a low 1.7 : 1 ratio (mismatched case). Unfortunately, the *meso*-compound could not be differentiated from the *C*<sub>2</sub>-symmetric products and the absolute configuration of the different isomers could not be assigned. However, by comparison to products obtained by others,<sup>[299]</sup> it is reasonable to assume that (*R*)-**297** does in fact yield the configuration matching the one of herquiline A and B. In contrast to the 2-(methoxydihphenylmethyl) pyrrolidines, neither Jørgensen's nor MacMillan's 1<sup>st</sup> gen. catalyst (**298**, **299**) did yield the product in detectable yields (Table 4, entries 4 and 5).

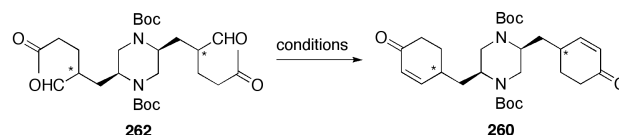
**Table 4.** Reaction conditions for the organocatalytic addition of MVK to dialdehyde **262**.

Entry	Catalyst/Reagent	Conditions	Yield	d.r.
1	TMSNEt <sub>2</sub>	MeCN, reflux <sup>[298]</sup>	74%	1 : 2 : 1
2	( <i>S</i> )- <b>297</b>	ethyl-3,4-dihydroxybenzoate, MVK (neat), 4 °C <sup>[299a, 300]</sup>	51%	"1 : 2.7"
3	( <i>R</i> )- <b>297</b>	ethyl-3,4-dihydroxybenzoate, MVK (neat), 4 °C <sup>[299a, 300]</sup>	44%	"1.7 : 1"
4	<b>298</b>	MVK (neat), RT <sup>[301]</sup>	-	-
5	<b>299</b>	TFA, MVK (neat), RT <sup>[301]</sup>	-	-

With the keto-aldehyde **261** synthesized as both stochastic and enriched diastereomeric mixtures, we turned our attention to the upcoming Robinson annulation, which should form the two six-membered rings of the natural products and retain the stereocenter introduced in the previous step. A literature survey on the condensation of  $\alpha$ -branched aldehydes to 2-cyclohexenones substituted solely in the 4-position was unfortunately not very encouraging. There are only a handful of methods, which are compatible to Boc-protecting groups and which have been used for the stereoselective synthesis of enones with a stereocenter at C-4. While we tested the reagent systems introduced by Baran/Chakraborti and Nicolaou/Srihari alongside other methods (Table 5). Most notably, the recently published use of (*S*)-1-(pyrrolidin-2-ylmethyl)pyrrolidine•TFA as an organocatalysts for the Robinson annulation of keto-aldehydes to 4-substituted cyclohexenones, did not retain the stereoinformation in **261** (Table 5, entry 13). Much to our surprise, only the reagent-system of tetra-*n*-butyl ammonium hydroxide together with potassium hydroxide in THF/Et<sub>2</sub>O as introduced by Nicolaou and Srihari, did promote the desired transformation in acceptable yields (Table 5, entries 5-9). We found, that there was a strong connection between the concentration of the reaction and the yields obtained. This seems to suggest that there is a substantial amount of inter- instead of intra-molecular condensation when using too high

concentrations. High dilution did eliminate the problem, yet – due to the low reagent concentrations – the reaction times increased to up to three days (Table 5, entry 7).

**Table 5.** Reaction conditions for the Robinson annulation of **261** to enone **260**.



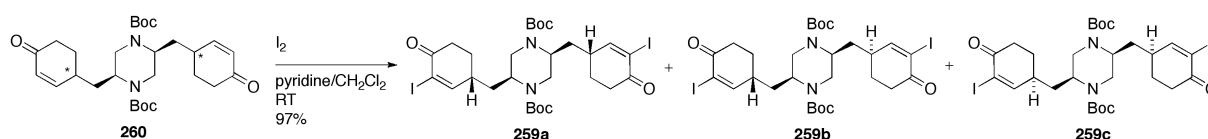
Entry	Conditions	Comment	d.r.
1	LiOH, MeOH, RT <sup>[302]</sup>	decomp.	-
2	LiOH, <i>i</i> -PrOH, RT <sup>[299a]</sup>	decomp.	-
3	LiOH, CF <sub>3</sub> CH <sub>2</sub> OH, RT	decomp.	-
4	LiOH, (CF <sub>3</sub> ) <sub>2</sub> CHOH, RT	traces	n.d.
5	( <i>n</i> -Bu) <sub>4</sub> NOH, KOH, THF/Et <sub>2</sub> O, Δ, c = 63 mM <sup>[299b, 303]</sup>	traces	-
6	( <i>n</i> -Bu) <sub>4</sub> NOH, KOH, THF/Et <sub>2</sub> O, Δ, c = 10 mM	48%	1 : 2 : 1
7	( <i>n</i> -Bu) <sub>4</sub> NOH, KOH, THF/Et <sub>2</sub> O, Δ, c = 3 mM, 3 d	57%	1 : 2 : 1
8	cf. entry 6, but d.r. (s.m.) = "1.7 : 1"		1 : 2 : 1
9	cf. entry 6, but d.r. (s.m.) = "1 : 3.1"		1 : 2 : 1
10	pTsOH <sup>[304]</sup>	n.r.	-
11	Na <sub>2</sub> SO <sub>4</sub> , THF, RT	traces	n.d.
12	MgSO <sub>4</sub> , THF, RT <sup>[301]</sup>	decomp.	-
13	( <i>S</i> )-1-(pyrrolidin-2-ylmethyl)pyrrolidine•TFA, RT	45%	1 : 2 : 1

decomp. = decomposition, n.d. = not determined, n.r. = no reaction, s.m. = starting material

While we finally obtained enone **261** in reproducible yields, we found that there was a substantial loss of diastereomeric purity under the conditions used. Regardless of the diastereomeric excess of the keto-aldehydes **262**, we always obtained a 1:2:1 mixture of the three possible diastereomeric enones. While they could be discriminated by NMR, we could not separate the *meso* and the two *C*<sub>2</sub>-symmetric compounds at this stage. Despite varying reaction parameters such as concentration, time and temperature, all our attempts to retain the diastereomeric excess introduced in the previous step failed. It is to assume, that our substrate for the Robinson annulation, **261**, is exceptionally prone to deprotonation α to the aldehyde. While a more in-depth screening of reaction parameters might yield conditions, which preserve the stereoinformation at *C*-4, none of the conditions screened resulted in a diastereospecific formation of **260**.

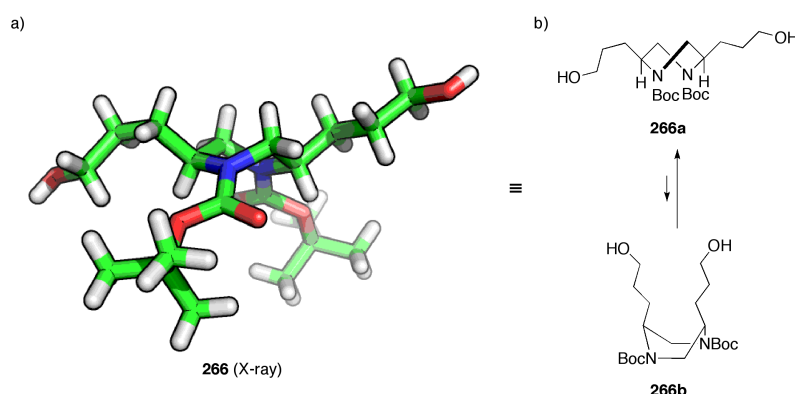
Accordingly, we decided to continue our work with the stochastic mixture to then later separate the individual isomers, so we could determine their potential use as coupling substrates in the upcoming key-step individually.

The mixture of diastereomeric enones was subsequently iodinated using  $I_2$  in pyridine/ $CH_2Cl_2$ ,<sup>[299a]</sup> to yield the  $\alpha$ -iodo enones **259a-c**, which could be separated by HPLC (Scheme 48). Unfortunately, the absolute configuration of neither of the two  $C_2$ -symmetric iodides **259a** and **259c** could be assigned.



**Scheme 48.** Formation of the three diastereomeric  $\alpha$ -iodo enones **259a-c**.

With our key-intermediates **259a-c** synthesized, we were now ready to explore reaction conditions for the envisioned intramolecular reductive cyclization. However, as we had decided to reduce the diketopiperazine early in the synthesis, we were lacking factors inducing a conformational bias toward a boat-like structure. Moreover, an obtained crystal structure of the parent diol **266**<sup>[275]</sup> seems to suggest a preferred equatorial position of the substituents. Most interestingly, the central heterocycle does not reside in a chair or in a boat, but in a twist-boat conformation (Scheme 29a). While this is usually considered a high-energy conformation, effects of the crystal lattice, which most notably deviates from the  $C_2$ -symmetry, might help stabilize it.



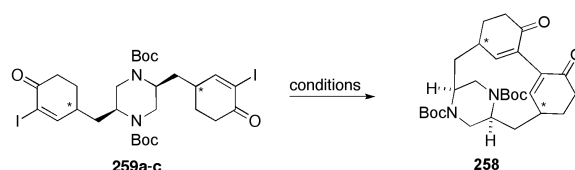
**Scheme 49.** a) X-ray structure of diol **266**. b) Conformational analysis of the **266**.

Assuming that the solid-state structure captures the true conformation of diol **266** in solution – and by that analogy of the  $\alpha$ -iodo enones **259a-c**, too – twist-boat **266a** would have to

equilibrate to the boat conformer **266b** for an efficient coupling as envisioned in our total synthesis. After all, this corresponds to the conformation of the piperazine ring as found in herquiline A and B (**248**, **249**). While this might be considered a potential pitfall in our synthetic strategy, we were still positive that the key-step coupling could be carried out at the piperazine oxidation stage, since we had considerably increased the conformational freedom of our coupling substrate due to the 4-substituted cyclohexenones (*vide supra*).

Accordingly, we went forth to evaluate several conditions, which seemed promising for the desired intramolecular reductive macrocyclization. To rule out any influence of the C-4 stereocenters at the enones, we tried the different methods on each isomer separately. While there was no obvious difference in their reactivity by TLC and LC-MS, products could not always be isolated for each isomer, since both isolation and purification proved challenging. The conditions, to which the  $\alpha$ -iodo enones **259a-c** were subjected, are summarized in Table 6.

**Table 6.** Reaction conditions screened for the intramolecular coupling of **259a-c**.



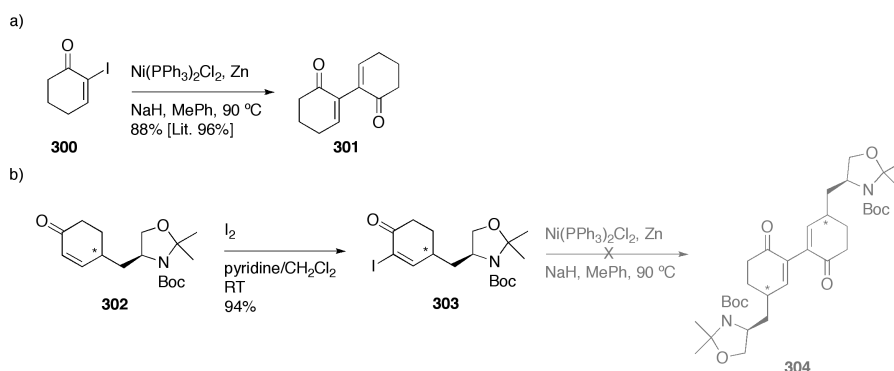
Entry	Conditions	Comments
1	Ni(PPh <sub>3</sub> ) <sub>2</sub> Cl <sub>2</sub> , Zn, PPh <sub>3</sub> , NaH, MePh, 90 °C <sup>[284a]</sup>	decomp.
2	Ni(PPh <sub>3</sub> ) <sub>2</sub> Cl <sub>2</sub> , Zn, PPh <sub>3</sub> , NaH, THF, 90 °C	decomp.
3	Ni(PPh <sub>3</sub> ) <sub>2</sub> Cl <sub>2</sub> , Zn, PPh <sub>3</sub> , THF, RT	dehalogenation
4	Ni(PPh <sub>3</sub> ) <sub>2</sub> Cl <sub>2</sub> , Zn, PPh <sub>3</sub> , DMF, 55 °C	<b>306</b> (5%)
5	Ni(COD) <sub>2</sub> , THF, -78 °C to RT <sup>[305]</sup>	complex mixture
6	Ni(COD) <sub>2</sub> , THF, -78 °C to reflux	complex mixture
6	Ni(COD) <sub>2</sub> , PPh <sub>3</sub> , DMF, RT to 120 °C	complex mixture
7	Ni(PPh <sub>3</sub> ) <sub>4</sub> , DMF, 0 °C to RT	complex mixture
8	Ni(PPh <sub>3</sub> ) <sub>4</sub> , DMF, 0 °C to 90 °C	complex mixture
9	Ni(COD) <sub>2</sub> , dppp, DMF, RT to 130 °C	complex mixture
10	Ni(COD) <sub>2</sub> , P( <i>n</i> -Bu) <sub>3</sub> , DMF, RT to 40 °C	complex mixture
11	Ni(COD) <sub>2</sub> , P( <i>n</i> -Bu) <sub>3</sub> , THF; -78 °C to RT; c = 4 mM	<b>305</b> , <b>306</b> (5%)
12	like entry 10; addition of <b>259a-c</b> by syringe pump (2 h)	<b>305</b> (16%), <b>306</b>
14	In, LiCl, Pd/C <sup>[284b]</sup>	complex mixture



<b>15</b>	Cu, DMF, 130 °C	decomp.
<b>16</b>	Cu (activated), RT to 130 °C	decomp.
<b>17</b>	Cu, neat, 140 °C sealed tube	decomp.
<b>18</b>	CuTC, NMP, RT to 130 °C <sup>[306]</sup>	decomp.
<b>19</b>	Me <sub>6</sub> Sn <sub>2</sub> (1.1 eq), Pd(PPh <sub>3</sub> ) <sub>4</sub> , THF, 50 °C <sup>[307]</sup>	dehalogenation
<b>20</b>	<i>n</i> -Bu <sub>6</sub> Sn <sub>2</sub> , Pd(PPh <sub>3</sub> ) <sub>4</sub> , THF; 50 °C	dehalogenation; complex mixture
<b>21</b>	Me <sub>6</sub> Sn <sub>2</sub> , Pd(PPh <sub>3</sub> ) <sub>4</sub> , THF; workup; PEPPSI- <i>i</i> Pr	decomp.
<b>22</b>	(BPin) <sub>2</sub> , Pd(dppf)Cl <sub>2</sub> , KOAc, DMSO, 80 °C <sup>[308]</sup>	decomp.
<b>23</b>	<b>309</b> , CuCl, DMF, 70 °C <sup>[309]</sup>	<b>306</b> (24%).

reagents and conditions as indicated; decomp = decomposition

Unfortunately, we were not able to isolate the desired product **258** in any of the reactions. When using simpler substrates like **300** however, we obtained the  $\alpha,\alpha'$ -coupled product **301** in yields very close to those published (Scheme 50a).<sup>[284a]</sup> To assess, whether this is due to conformational problems during the formation of the 12-membered ring, we prepared a model  $\alpha$ -iodo enone **303**, which resembles a monomeric version of piperzines **259a-c** and which was readily available from enone **302** prepared for an alternative approach toward the herquelines previously.<sup>[275]</sup> Much to our surprise, the model did not yield any bis(cyclohexenone) product **304** when subjected to Ni(PPh<sub>3</sub>)<sub>4</sub>/Zn/NaH, but decomposed under the reaction conditions (Scheme 50b).



**Scheme 50.** a) Coupling of the simple  $\alpha$ -iodo enone **300** in good yields. b) Attempted coupling of model enone **303** derived from L-glutamic acid (**1**).

Assuming that the hemi-aminal is stable under these coupling conditions, we reasoned that there might be a general problem with the reaction intermediates and some of the functionalities in both model system and piperazine dione (*vide infra*), as it has been suggested that Ni-mediated biaryl-couplings might proceed *via* radical intermediates.<sup>[310]</sup>

Even though the other nickel-based methods mainly lead to proto-dehalogenation (Table 6, entry 3), we were amazed by the side-products we obtained using high dilution conditions and  $\text{Ni}(\text{COD})_2/\text{PBU}_3$  in stoichiometric amounts (Table 6, entries 11 and 12). In addition to the iodinated and deiodinated dimers **305** and **307**, we found the 24-membered macrocycle **306** and even the 36-membered trimer **308** – the latter could however only be characterized by HRMS since it was a minor constituent of the reaction mixture (Fig. 60).

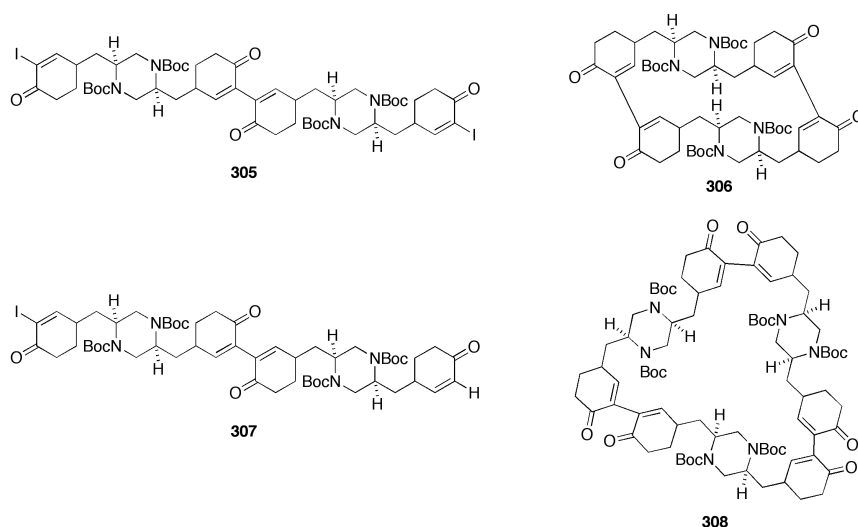
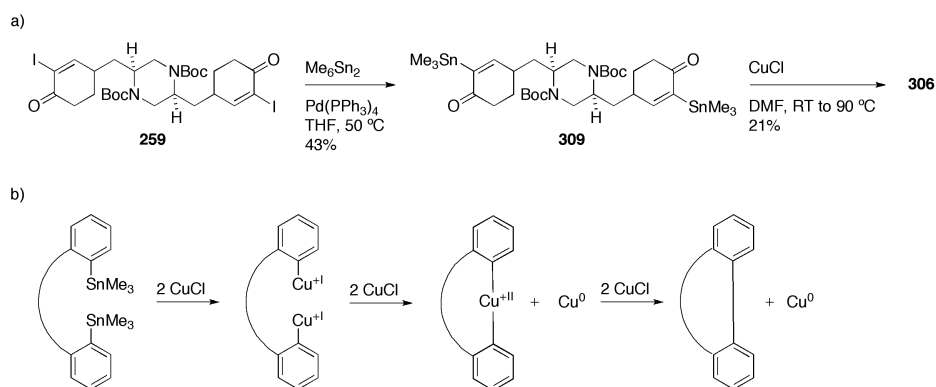


**Figure 60.** Dimers **304–307** and trimer **308** isolated from the coupling reactions.

This seemed to suggest that there is in fact a reaction pathway available leading to  $\alpha,\alpha'$ -coupled dienones. Yet, increasing the dilution factor by employing pseudo-high-dilution conditions (addition of iodides **259a–c** by a syringe pump) did not produce any detectable amounts of the desired product **258**, nor did it increase the amount of dimers isolated. It instead seemed to enhance the rate of proto-dehalogenation. Because of these problems and since it has been speculated, that nickel-based biaryl couplings might proceed *via* radical intermediates,<sup>[310]</sup> we wanted to explore alternative metals to promote the coupling.

Accordingly, we evaluated a number of conditions used in both the coupling of  $\alpha$ -iodo enones and aryl iodides. Most notably, a method, which was developed by Lee *et al.* and which had been shown to promote a reductive C–C bond formation of the simple iodoenone **300** (*cf.* Scheme 50a) using a two metal reagent system of indium and palladium,<sup>[284b]</sup> did yet again not yield any product but a complex mixture (Table 6, entry 14). Unfortunately so did classical Ullman-type conditions (Table 6, entries 15–17) and copper(I)-thiophene-2-carboxylate (CuTC, Table 6, entry 18), probably due to the harsh reaction conditions required according to the literature.

Since all our approaches toward the macrocycle **258** using one-step procedures had been unsuccessful, we decided to explore the option of two-step protocols. However, neither a borylation-Suzuki-Miaura coupling sequence nor Stille-Kelly conditions, where the active vinyl-metal species is formed *in situ*, did provide us with any product.<sup>[307-308]</sup> In the latter case however, we could identify both the mono- and the distannylated dienone as products of the reaction. To exploit this finding, we synthesized distannane **309** on purpose (Scheme 51a) and explored its potential oxidative dimerization using copper(I) or (II) salts. This relatively underdeveloped method is believed to proceed *via* a transmetallation to a dicopper species, which then first disproportionates to give a copper(II) intermediate. Reductive elimination furnishes the C-C bond in the end (Scheme 51b).<sup>[311]</sup> Yet again, the attempted intramolecular coupling of distannane **309** using copper(I) chloride did not yield the desired twelve-membered carbocycle **258** but again the 24-membered C<sub>2</sub>-symmetric dimer **306** (Table 6, entry 23).

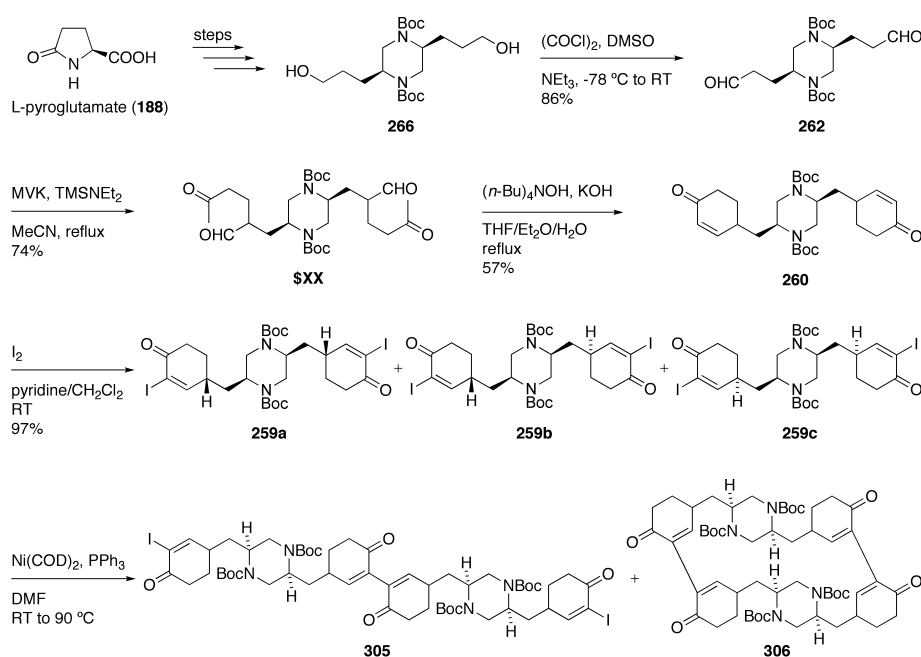


**Scheme 51.** a) Attempted two-step cyclization *via* the distannane **309**. b) Proposed mechanism for the  $\text{Cu(I)}$ -mediated C-C bond formation from distannanes.

Having screened a variety of different coupling conditions without success, we felt that we had to reconsider our initial ideas on the reactivity and the conformational arrangement of  $\alpha$ -iodo enones **259a-c**. The fact that we observed inter- instead of intramolecular coupling even at high dilution suggests, that there is no general incompatibility of the reagents and the starting material. We reasoned that there rather might be a conformational problem, such as that a 13-membered, metal-bridged intermediate cannot be formed or is less reactive than other possible reaction pathways. In further studies we will seek to overcome this problem by enforcing more reactive conformations (*vide supra*).

## 5) Résumé

In summary we have developed a scalable route to advanced piperazine precursors for the total synthesis of herquiline A and B (**248**, **249**), two tyrosine-derived alkaloids isolated from a broth of *penicillium herquei*. Our synthesis starts from the readily available starting material L-pyroglutamic acid (**188**), which serves as a chiral precursor and sets the two stereocenters at the piperazine core. Further key-transformations involve formation of the piperazine ring by reduction of a diketopiperazine and an organocatalytic addition of MVK to aldehyde **262**. The following installation of the two cyclohexenones in **260** by a double Robinson annulation can – in principle – be developed into a diastereoselective process (Scheme 52).



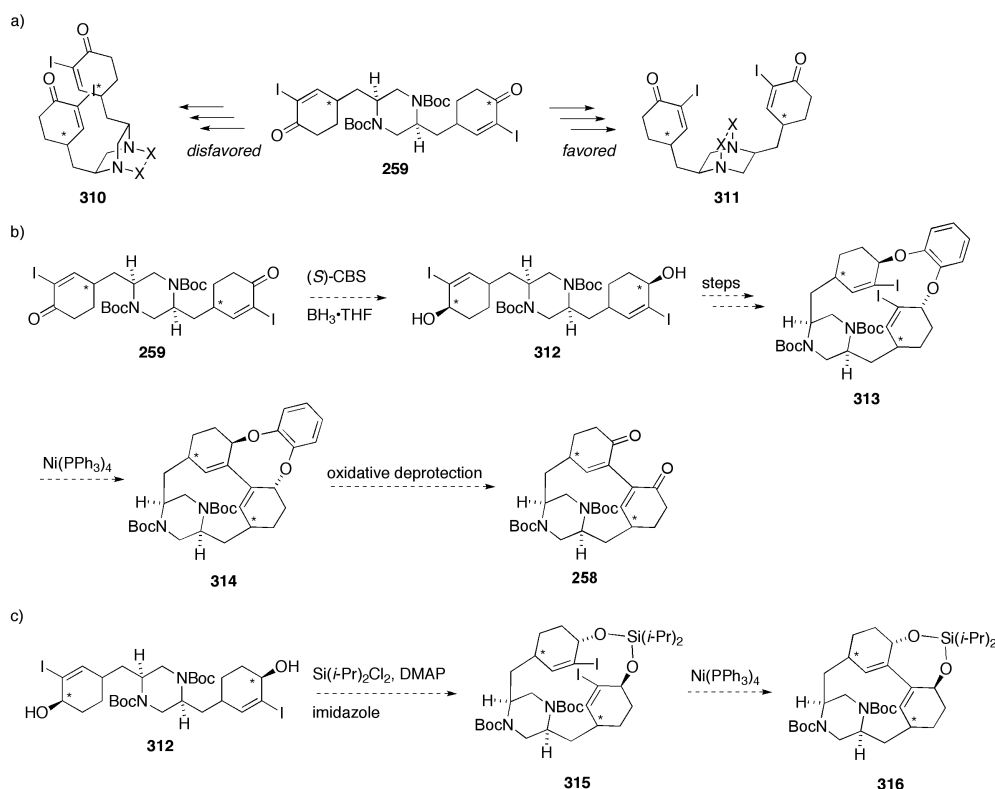
**Scheme 52.** Summary of the accomplished goals toward the herquiline alkaloids.

While we obtained the coupling precursors **259a-c** from dienones **260** in very good yield, we have yet to assign the absolute configuration of the obtained  $\text{C}_2$ -symmetric  $\alpha$ -iodo diastereomers. So far our attempts to intramolecularly couple the vinyl iodides have not yielded any twelve-membered macrocycles. Instead we have isolated the linear and cyclic dimers **305** and **306**. This seems to suggest that there is in fact a reaction pathway leading to  $\alpha, \alpha'$ -coupled dienones, which might be redirected toward the desired products. Our current results however indicate that there is a conformational problem preventing the intramolecular coupling. Future strategies will therefore have to assess this issue by locking the cyclization precursors in an orientation, which facilitates ring closure (*vide infra*).

## 6) Outlook

The results of our present coupling strategy seem to suggest that there is a conformational problem preventing the formation of the twelve-membered ring in the key intermediate **258** of our synthesis. As shifting the conformer-equilibrium toward the boat-geometry by heating did not succeed, we will instead investigate chemical options to lock the piperazine in a conformation that allows the two iodoenones to interact.

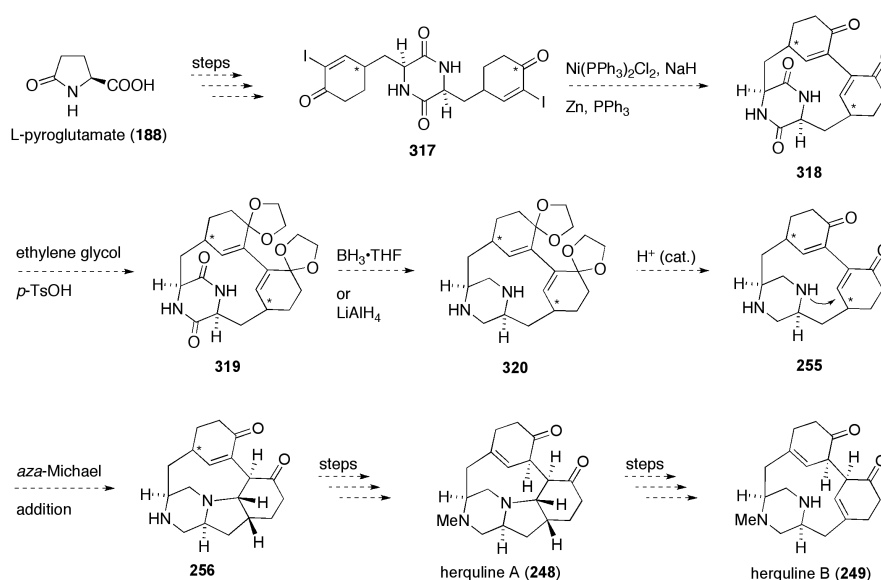
To us, there seem to be two general solutions to this problem: 1. tethering of the piperazine ring and 2. tethering of the  $\alpha$ -iodo enones. For the first option, a literature survey suggest that when forming DABCO-like structures by linking the piperazine nitrogens, the all-equatorial arrangement **311**, which allows the piperazine substituents to minimize their steric repulsion, is generally preferred over the axial arrangement **310** (Scheme 53a).<sup>[312]</sup> Accordingly, our future efforts will focus on strategies that involve tethering *via* the cyclohexenone moieties (Scheme 53b,c).



**Scheme 53.** a) Tethering strategy involving formation of DABCO-like structures. b) Envisioned reduction-tethering sequence *via* the catechol linked di(vinyl iodide) **313**. c) An alternative, silicon-based tethering strategy *via* the dialkoxysilane **315**.

We therefore seek to diastereoselectively reduce the  $\alpha$ -iodoenones to the corresponding allylic alcohols **312** using the Corey-Backshi-Shibata catalyst.<sup>[313]</sup> The hydroxy groups can then serve as handles for possible catechol- or silicon-based tethering methods forming 18- or 17-membered macrocycles respectively (Scheme 53b,c). The key-transformation would then involve a macrocyclic ring-closure to the [6.6.7.12] and [6.6.8.12] pentacyclic ring systems **314** or **316**. While these reactions might suffer from transannular ring strain, especially the silicon-based method should benefit from the Thorpe-Ingold effect induced by bulky substituents on the silicon. Using standard transformations, both coupling products can then be converted into the  $\alpha, \alpha'$ -coupled dienone **258**, which can then be processed further along the routes of the original proposal.

Alternative strategies to the herquiline alkaloids might involve a combination of the results obtained in this study and the methods used to synthesize other (diketo)piperazine alkaloids like mycocyclosin (**262**) or piperazinomycin (**265**).<sup>[280-281]</sup> Hutton and coworkers have shown that bis(iodoaryl)diketopiperazines can be coupled efficiently using the conditions developed by Lin *et al.*<sup>[280]</sup> Accordingly, our revised strategy will involve transformation of L-pyroglutamic acid (**188**) to the diketopiperazine  $\alpha$ -iodo dienone **317**, which can then be coupled intramolecularly. Following this key-step, the enone carbonyls will be protected to yield ketal **319**. After reduction of the diketopiperazine to the piperazine using *e.g.*  $\text{LiAlH}_4$ ,<sup>[314]</sup> acetal deprotection and concomitant *aza*-Michael addition will form the dodecahydro-pyrazino[1,2-*a*]indole moiety present in herquiline A (Scheme 54).



**Scheme 54.** An alternative synthetic strategy toward the herquiline alkaloids, which combines the results of this study and preceding approaches toward (diketo)piperazine alkaloids.

The remaining steps of the synthesis will then involve methylation of **256** and double bond-isomerization as proposed in the original retrosynthetic analysis. Finally, herquline A (**248**) can be obtained, which we will use to probe its biosynthetic relationship to herquline B (**249**).

### **III. Experimental**



### **III. 1 Chemistry**

### 1) General Experimental Details and Instrumentation

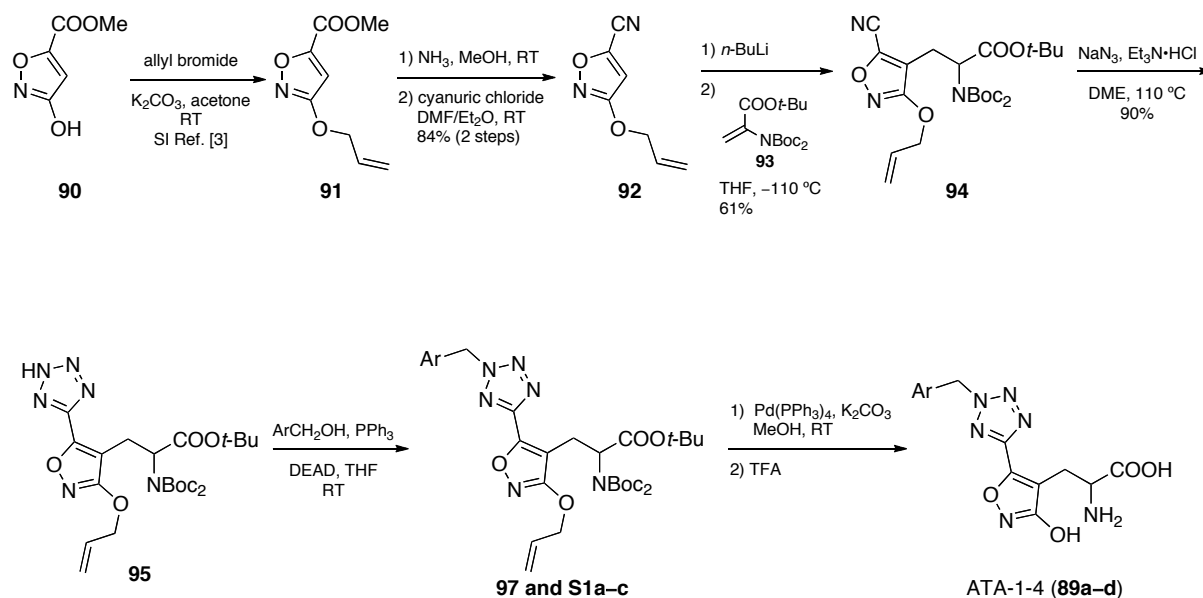
Unless stated otherwise, all reactions were carried out under an Argon atmosphere in oven-dried glassware. Solvents for extraction and flash column chromatography were purchased in technical grade and distilled under reduced pressure prior to use. Flash column chromatography was performed using Merck silica gel ( $\text{SiO}_2$ ; 40-63  $\mu\text{m}$ , 60 Å) or Waters C18 (C18; 55-105  $\mu\text{m}$ , 125 Å) as the stationary phase with forced flow as reported in <sup>[315]</sup>. Reactions and chromatography fractions were monitored with Merck silica gel 60 F254 or Machery-Nagel RP-18W/UV glass plates and visualized using a 254 nm UV lamp and/or by treatment with a suitable stain (potassium permanganate, ceric ammonium molybdate, ninhydrine, and anisaldehyde) followed by heating. Tetrahydrofuran (THF) and diethyl ether ( $\text{Et}_2\text{O}$ ) were distilled from sodium benzophenone. *n*-Butyllithium (*n*-BuLi) was titrated using iodine prior to use. All other solvents, as well as starting materials and reagents were obtained from commercial sources and used without further purification or were prepared according to the procedures cited.

Unless otherwise specified, proton ( $^1\text{H}$ ) and carbon ( $^{13}\text{C}$ ) spectra were recorded at 300 K in the solvents indicated. The Varian Mercury spectrometers used were operated at 300 MHz, 400 MHz and 600 MHz for proton nuclei and 75 MHz, 100 MHz and 150 MHz for carbon nuclei. For  $^1\text{H}$  NMR spectra signals arising from residual non-deuterated solvent were used as the internal standard and the solvent shifts reported by Fulmer *et al.*<sup>[316]</sup> were used as reference.  $^1\text{H}$  NMR data are denoted as follows: chemical shift ( $\delta$ ) (multiplicity, coupling constant(s)  $J$  (Hz), relative integral (,assignment)) where multiplicity is defined as: s = singlet; d = doublet; t = triplet; q = quartet; m = multiplet;  $m_c$  = centrosymmetric multiplet; br = broad; a = apparent or combinations thereof. For regio-isomeric mixtures fractions of protons are reported for integrals to illustrate the ratio of isomers. The assignment of atoms is based on suitable 2D-spectra (HSQC, HMBC, COSY, NOESY). The atom numbers do not follow IUPAC-conform rules, but are rather based on practical considerations.

Melting points (mp) were determined with a Stanford Research Systems MPA120 apparatus and are uncorrected. UV-spectra (UV) were obtained using a Varian Cary 50 Scan UV/Vis spectrometer and Helma SUPRASIL precision cuvettes (10 mm light path). Infrared spectra ( $\tilde{\nu}$ ) were recorded on a Perkin-Elmer BXII-FTIR spectrometer equipped with an ATR unit. Samples were analyzed as neat materials. A Varian MAT CH7A mass spectrometer was used to obtain low- and high-resolution electron impact (EI) mass spectra. Low- and high-resolution electrospray (ESI) mass spectra were obtained on a Varian MAT 711 MS instrument operating in either positive or negative ionization modes.

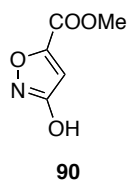
## 2) A Photochromic Agonist of AMPA Receptors – Synthetic Procedures

Overview:



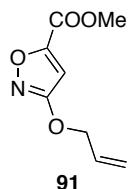
**Supporting Scheme 1.** Generalized scheme for the synthesis of ATA-type molecules.

### Methyl 3-hydroxyisoxazole-5-carboxylate (**90**)

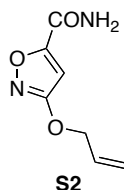


Isoxazole **90** was synthesized according to known procedures.<sup>[115]</sup> The analytical data matched those reported previously.

### Methyl 3-(allyloxy)isoxazole-5-carboxylate (**91**)



Allyl ether **91** was synthesized according to known procedures.<sup>[116]</sup> The analytical data matched those reported previously.

**3-(allyloxy)isoxazole-5-carboxamide (S2)**

To ester **91** (9.60 g, 52.4 mmol) was added aqueous ammonia (85 mL, 25% in H<sub>2</sub>O) at 0 °C and the mixture was allowed to warm to room temperature while stirring over the course of 13 h. The precipitate was collected and dried to yield 8.70 g (98%) of pure amide **S2** as a colorless solid.

$R_f = 0.27$  (CH<sub>2</sub>Cl<sub>2</sub>/MeOH/AcOH/H<sub>2</sub>O = 90:10:2:2).

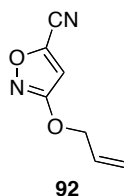
mp (MeOH/H<sub>2</sub>O) = 147-148 °C.

IR (ATR):  $\tilde{\nu}$  = 3364 (m), 3177 (m), 3149 (m), 1687 (s), 1676 (s), 1631 (s), 1615 (s), 1496 (s), 1453 (s), 1345 (s), 1240 (s), 1104 (s), 970 (s), 932 (s) cm<sup>-1</sup>.

<sup>1</sup>H NMR (acetone-*d*<sub>6</sub>, 400 MHz)  $\delta$  6.62 (s, 1H), 6.07 (ddt,  $J = 17.2$  Hz,  $J = 10.5$  Hz,  $J = 5.8$  Hz, 1H), 5.44 (adq,  $J = 17.2$  Hz,  $J = 1.5$  Hz, 1H), 5.29 (adq,  $J = 10.5$  Hz,  $J = 1.2$  Hz, 1H), 4.78 (ddd,  $J = 5.8$  Hz,  $J = 1.5$  Hz,  $J = 1.2$  Hz, 2H) ppm.

<sup>13</sup>C NMR (acetone-*d*<sub>6</sub>, 100 MHz)  $\delta$  172.5, 165.4, 157.8, 133.2, 119.1, 98.3, 71.4 ppm.

HRMS (ESI) Calc. for C <sub>7</sub> H <sub>9</sub> N <sub>2</sub> O <sub>3</sub> <sup>+</sup> :	169.0608 [M+H] <sup>+</sup>
Found:	169.0601 [M+H] <sup>+</sup> .

**3-(allyloxy)isoxazole-5-carbonitrile (92)**

To a solution of amide **S2** (8.50 g, 50.5 mmol) in DMF (100 mL) was added cyanuric chloride (9.32 g, 50.5 mmol) in Et<sub>2</sub>O/DMF (1:2, 60 mL) at 0 °C over 20 min. The resulting mixture was allowed to warm to room temperature over the course of 3 h. A colorless precipitate

formed and the solution turned yellow. Et<sub>2</sub>O (250 mL) was added to the reaction mixture and the organic phase was washed successively with saturated aqueous NaHCO<sub>3</sub> (2 × 150 mL), 10% aqueous NaCl (1 × 200 mL) and brine (1 × 200 mL). The organic phase was dried over Na<sub>2</sub>SO<sub>4</sub>, filtered and concentrated. Normal phase flash column chromatography (SiO<sub>2</sub>; *n*-pentane/Et<sub>2</sub>O = 16:1) yielded 7.12 g (94%) of nitrile **92** as a colorless, volatile liquid.

$R_f = 0.4$  (*n*-Pentane/Et<sub>2</sub>O = 16:1).

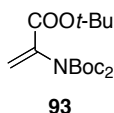
IR (ATR):  $\tilde{\nu} = 3144$  (w), 2248 (w), 1599 (s), 1502 (s), 1418 (m), 1350 (m), 1245 (w), 1140 (w), 1034 (w), 989 (w), 928 (w), 811 (w) cm<sup>-1</sup>.

<sup>1</sup>H NMR (CD<sub>2</sub>Cl<sub>2</sub>, 400 MHz)  $\delta$  6.62 (s, 1H), 6.06 (ddt,  $J = 17.2$  Hz,  $J = 10.5$  Hz,  $J = 5.8$  Hz, 1H), 5.45 (m<sub>c</sub>, 1H), 5.35 (m<sub>c</sub>, 1H), 4.80 (ddd,  $J = 5.7$  Hz,  $J = 1.5$  Hz,  $J = 1.2$  Hz, 2H) ppm.

<sup>13</sup>C NMR (CD<sub>2</sub>Cl<sub>2</sub>, 100 MHz)  $\delta$  171.3, 143.3, 131.7, 119.8, 108.7, 105.9, 72.0 ppm.

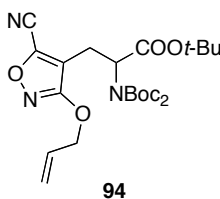
HRMS (EI)	Calc. for C <sub>7</sub> H <sub>7</sub> N <sub>2</sub> O <sub>2</sub> <sup>+</sup> :	151.0508 [M+H] <sup>+</sup>
	Found:	151.0494 [M+H] <sup>+</sup> .

### ***tert*-butyl 2-(bis(*tert*-butoxycarbonyl)amino)acrylate (**93**)**



Dehydroalanine **93** was synthesized according to known procedures.<sup>[114]</sup> The spectroscopic data matched those reported previously.

### ***tert*-butyl 3-(3-(allyloxy)-5-cyanoisoxazol-4-yl)-2-(bis(*tert*-butoxycarbonyl)amino)propanoate (**94**)**



To a solution of nitrile **92** (500 mg, 3.33 mmol) in THF (17 mL) was added dropwise precooled (-110 °C) *n*-BuLi (1.4 mL, 3.50 mmol; 2.5 M in hexanes) in THF (2.5 mL) over 10 min at -110 °C with a double tipped needle and the obtained deep red solution was stirred for

30 min. A precooled ( $-110\text{ }^{\circ}\text{C}$ ) solution of *tert*-butyl 2-(bis(*tert*-butoxycarbonyl)amino)acrylate (**93**; 1.14 g, 3.33 mmol) in THF (4.5 mL) was added dropwise to the reaction and stirring was continued for 2 h. The mixture was quenched by addition of precooled HCl in MeOH (4.0 mL, 0.06 M) at  $-108\text{ }^{\circ}\text{C}$ . To the obtained pale yellow solution was added saturated aqueous  $\text{NH}_4\text{Cl}$  (20 mL) and the mixture was allowed to warm to room temperature. The biphasic mixture was extracted with EtOAc (4 x 15 mL), dried over  $\text{MgSO}_4$ , filtered and concentrated. Purification by normal phase flash column chromatography ( $\text{SiO}_2$ ; PE/EtOAc = 17:1) gave 1.03 g (61%) of propanoate **94** as a colorless solid.

$R_f = 0.4$  (PE/EtOAc = 10:1).

mp (PE/EtOAc) =  $73\text{ }^{\circ}\text{C}$ .

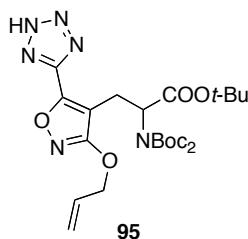
IR (ATR):  $\tilde{\nu} = 2980$  (w), 2938 (w), 1728 (s), 1697 (s), 1551 (s), 1382 (m), 1367 (s), 1356 (s), 1143 (s), 1122 (s), 978 (s)  $\text{cm}^{-1}$ .

$^1\text{H}$  NMR ( $\text{CDCl}_3$ , 400 MHz)  $\delta$  6.16-5.98 (m, 1H), 5.42 (add,  $J = 17.2\text{ Hz}$ ,  $J = 1.4\text{ Hz}$ , 1H), 5.32 (add,  $J = 10.5\text{ Hz}$ ,  $J = 1.2\text{ Hz}$ , 1H), 4.99 (dd,  $J = 9.8\text{ Hz}$ ,  $J = 5.0\text{ Hz}$ , 1H), 4.79 (adt,  $J = 5.8\text{ Hz}$ ,  $J = 1.3\text{ Hz}$ , 2H), 3.29-3.14 (m, 2H), 1.45 (s, 27 H) ppm.

$^{13}\text{C}$  NMR ( $\text{CDCl}_3$ , 75 MHz)  $\delta$  169.9, 168.1, 152.3, 141.1, 131.4, 119.8, 117.2, 108.3, 83.6, 82.4, 71.8, 57.2, 28.1, 28.0, 22.1 ppm.

HRMS (ESI) Calc. for  $\text{C}_{24}\text{H}_{35}\text{N}_3\text{NaO}_8^+$ : 516.2322  $[\text{M}+\text{Na}]^+$   
Found: 516.2317  $[\text{M}+\text{Na}]^+$ .

***tert*-butyl 3-(3-(allyloxy)-5-(2*H*-tetrazol-5-yl)isoxazol-4-yl)-2-(bis(*tert*-butoxycarbonyl)amino)propanoate (**95**)**



To a solution of nitrile **94** (1.00 g, 2.03 mmol) in DME (20 mL) was added sodium azide (145 mg, 2.23 mmol) and  $\text{NEt}_3 \cdot \text{HCl}$  (307 mg, 2.23 mmol). The resulting suspension was stirred for 68 h at 110 °C in a sealed tube (external bath temperature). The mixture was cooled to room temperature and the solvent removed under reduced pressure. Normal phase flash column chromatography ( $\text{SiO}_2$ ;  $\text{CH}_2\text{Cl}_2/\text{MeOH}/\text{AcOH}/\text{H}_2\text{O} = 90:10:0.6:0.6$ ) yielded 984 mg (90%) of tetrazole **95** as a colorless solid.

$R_f = 0.2$  ( $\text{CH}_2\text{Cl}_2/\text{MeOH}/\text{AcOH}/\text{H}_2\text{O} = 90:10:0.6:0.6$ ).

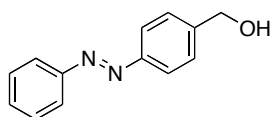
mp ( $\text{CH}_2\text{Cl}_2/\text{MeOH}/\text{AcOH}/\text{H}_2\text{O}$ ) = 199 °C (decomp.).

IR (ATR):  $\tilde{\nu} = 2980$  (m), 2936 (m), 1777 (m), 1736 (s), 1701 (s), 1506 (m), 1367 (s), 1236 (s), 1137 (s), 1098 (s)  $\text{cm}^{-1}$ .

$^1\text{H}$  NMR ( $\text{CDCl}_3$ , 600 MHz)  $\delta$  6.09 (ddt,  $J = 17.2$  Hz,  $J = 10.6$  Hz,  $J = 5.7$  Hz, 1H), 5.46 (dd,  $J = 17.3$  Hz,  $J = 1.40$  Hz, 1H), 5.33 (dd,  $J = 10.5$  Hz,  $J = 1.3$  Hz, 1H), 5.17 (dd,  $J = 7.6$  Hz,  $J = 5.9$  Hz, 1H), 4.85 (mc, 2H), 3.43 (dd,  $J = 15.0$  Hz,  $J = 5.7$  Hz, 1H), 3.32 (dd,  $J = 15.0$  Hz,  $J = 7.9$  Hz, 1H), 1.49 (s, 9H), 1.43 (s, 18H) ppm.

$^{13}\text{C}$  NMR ( $\text{CDCl}_3$ , 150 MHz)  $\delta$  170.7, 170.0, 152.5, 131.8, 119.2, 108.2, 84.2, 83.3, 71.3, 57.8, 28.1 (2x), 23.0 ppm (2 C obscured).

HRMS (ESI) Calc. for  $\text{C}_{24}\text{H}_{36}\text{N}_6\text{NaO}_8^+$ : 559.2492  $[\text{M}+\text{Na}]^+$   
 Found: 559.2488  $[\text{M}+\text{Na}]^+$ .

**(4-(phenyldiazenyl)phenyl)methanol (S2)****S2**

To a solution of 4-aminobenzyl alcohol (2.50 g, 20.3 mmol) in glacial acetic acid (100 mL) was added nitrosobenzene (2.39 g, 22.3 mmol) and the mixture was stirred overnight at room temperature. The solvent was removed under reduced pressure, the residue taken up in EtOAc (100 mL), washed with a saturated aqueous solution of saturated aqueous NaHCO<sub>3</sub> (2 x 20 mL) and brine (1 x 20 mL). The organic phase was dried over MgSO<sub>4</sub>, filtered and concentrated. Normal phase flash column chromatography (SiO<sub>2</sub>; PE/EtOAc = 4:1 to 3:1) yielded 3.65 g (85%) of alcohol **S2** as an orange solid.

R<sub>f</sub> = 0.4 (PE/EtOAc = 2:1).

mp (PE/EtOAc) = 134 °C.

UV (DMSO): λ<sub>max</sub> = 330 nm.

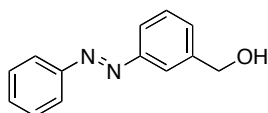
IR (ATR):  $\tilde{\nu}$  = 3293 (br m), 1582 (w), 1442 (m), 1348 (m), 1302 (m), 1150 (m), 1024 (s), 1008 (s), 850 (s), 830 (s), 762 (s) cm<sup>-1</sup>.

<sup>1</sup>H NMR (acetone-*d*<sub>6</sub>, 400 MHz) δ 7.95-8.89 (m, 4H), 7.62-7.51 (m, 5H), 4.76 (d, *J* = 5.8 Hz, 2H), 4.39 (t, *J* = 5.8 Hz, 1OH) ppm.

<sup>13</sup>C NMR (acetone-*d*<sub>6</sub>, 100 MHz) δ 153.5, 152.5, 147.1, 132.0, 130.1, 128.0, 123.5 (2x), 64.2 ppm.

HRMS (ESI) Calc. for C <sub>13</sub> H <sub>13</sub> N <sub>2</sub> O <sup>+</sup> :	213.1028 [M+H] <sup>+</sup>
Found:	213.1022 [M+H] <sup>+</sup> .



**(3-(phenyldiazenyl)phenyl)methanol (S3)****S3**

To a solution of 3-aminobenzyl alcohol (2.50 g, 20.3 mmol) in glacial AcOH (100 mL) was added nitrosobenzene (2.39 g, 22.3 mmol) and the mixture was stirred overnight at room temperature. The solvent was removed under reduced pressure, the residue taken up in EtOAc (100 mL) and washed with a saturated aqueous solution of NaHCO<sub>3</sub> (2 x 20 mL) and brine (1 x 20 mL). The organic phase was dried over MgSO<sub>4</sub>, filtered and concentrated. Normal phase flash column chromatography (SiO<sub>2</sub>; PE/EtOAc = 4:1 to 3:1) yielded 3.53 g (82%) of alcohol **S3** as a red solid.

$R_f = 0.5$  (PE/EtOAc = 2:1).

mp (PE/EtOAc) = 37 °C.

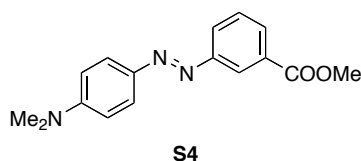
UV (DMSO):  $\lambda_{\max} = 325$  nm.

IR (ATR):  $\tilde{\nu} = 3191$  (br m), 1586 (w), 1472 (m), 1448 (m), 1360 (m), 1243 (m), 1148 (m), 1124 (m), 1019 (s), 918 (m), 799 (s), 770 (s) cm<sup>-1</sup>.

<sup>1</sup>H NMR (CD<sub>3</sub>CN, 400 MHz)  $\delta$  7.96-7.86 (m, 3H), 7.84-7.77 (m, 1H), 7.64-7.47 (m, 5H), 4.70 (d,  $J = 4.9$  Hz, 2H), 3.36 (t,  $J = 5.9$  Hz, 1OH) ppm.

<sup>13</sup>C NMR (CD<sub>3</sub>CN, 100 MHz)  $\delta$  115.6, 115.5, 144.7, 132.3, 130.4, 130.3, 130.2, 123.6, 122.6, 121.2, 64.3 ppm.

HRMS (ESI) Calc. for C <sub>13</sub> H <sub>13</sub> N <sub>2</sub> O <sup>+</sup> :	213.1028 [M+H] <sup>+</sup>
Found:	213.1022 [M+H] <sup>+</sup> .

**methyl 3-((4-(dimethylamino)phenyl)diazenyl)benzoate (S4)**

To a solution of methyl 3-aminobenzoate (1.00 g, 6.62 mmol) in 4 N HCl (50 mL) was added sodium nitrite (0.456 g, 6.62 mmol) at 0 °C and the mixture was stirred for 30 min *N,N*-dimethylaniline (0.84 mL, 6.62 mmol) was added and stirring was continued for 1 h. The deep red solution was added to ice-cold saturated aqueous NaHCO<sub>3</sub> (300 mL). After the CO<sub>2</sub> evolution had ceased, the biphasic mixture was extracted with EtOAc (3 x 150 mL). The combined organic extracts were dried over MgSO<sub>4</sub>, filtered and concentrated to yield the crude product as a red solid which was recrystallized from PE/EtOAc to afford 1.53 g (82%) of azobenzene **S4** as a red solid.

$R_f = 0.4$  (PE/EtOAc = 4:1).

m.p. (PE/EtOAc) = 93-95 °C.

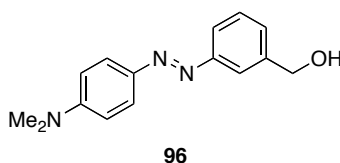
UV (DMSO):  $\lambda_{\max} = 433$  nm.

IR (ATR):  $\tilde{\nu} = 2947$  (w), 2908 (w), 1720 (s), 1602 (s), 1521 (m), 1398 (m), 1368 (s), 1291 (s), 1276 (s), 1141 (s), 1069 (s), 812 (s), 753 (s) cm<sup>-1</sup>.

<sup>1</sup>H NMR (acetone-*d*<sub>6</sub>, 400 MHz)  $\delta$  8.55-8.54 (m, 1H), 8.07-8.03 (m, 2H), 7.88 (d,  $J = 9.3$  Hz, 2H), 7.65 (td,  $J = 7.8$  Hz,  $J = 0.5$  Hz, 1H), 6.85 (d,  $J = 9.3$  Hz, 2H), 3.94 (s, 3H), 3.11 (s, 6H) ppm.

<sup>13</sup>C NMR (acetone-*d*<sub>6</sub>, 100 MHz)  $\delta$  167.0, 154.1 (2x), 144.1, 132.2, 130.7, 130.3, 127.4, 126.0, 123.3, 112.4, 52.6, 40.4 ppm.

HRMS (ESI) Calc. for C <sub>16</sub> H <sub>18</sub> N <sub>3</sub> O <sub>2</sub> <sup>+</sup> :	284.1399 [M+H] <sup>+</sup>
Found:	284.1394 [M+H] <sup>+</sup> .

**3-((4-(dimethylamino)phenyl)diazenyl)phenyl)methanol (96)**

To a solution of ester **S4** (500 mg, 1.76 mmol) in THF (20 mL) was added LiAlH<sub>4</sub> (3.18 mL, 3.18 mmol; 1.0 M in THF) at 0 °C and the mixture was stirred for 30 min at room temperature. The reaction was poured on ice-cold saturated aqueous NH<sub>4</sub>Cl. The mixture was extracted with EtOAc (3 x 50 mL) and the combined organic extracts were dried over MgSO<sub>4</sub>, filtered and concentrated. Normal phase flash column chromatography (SiO<sub>2</sub>, PE/EtOAc = 3:1) yielded 435 mg (97%) of alcohol **14** as golden plates.

R<sub>f</sub> = 0.4 (PE/EtOAc = 2:1).

mp (PE/EtOAc) = 118-120 °C.

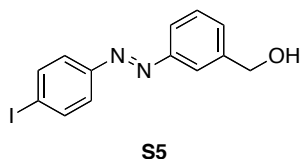
UV (DMSO): λ<sub>max</sub> = 421 nm.

IR (ATR):  $\tilde{\nu}$  = 3401 (br, w), 2961 (w), 2904 (w), 1594 (m), 1520 (m), 1372 (m), 1258 (s), 1060 (s), 1020 (s), 820 (s), 795 (s) cm<sup>-1</sup>.

<sup>1</sup>H NMR (acetone-*d*<sub>6</sub>, 400 MHz)  $\delta$  7.89-7.81 (m, 3H), 7.73-7.69 (m, 1H), 7.47 (at, *J* = 7.6 Hz, 1H), 7.44-7.40 (m, 1H), 6.90-6.81 (m, 2H), 4.74 (d, *J* = 5.9 Hz, 2H), 4.35 (t, *J* = 5.9 Hz, 1OH), 3.10 (s, 6H) ppm.

<sup>13</sup>C NMR (acetone-*d*<sub>6</sub>, 100 MHz)  $\delta$  154.0, 153.7, 144.6, 144.2, 129.6, 128.4, 125.6, 121.7, 120.6, 112.4, 64.4, 40.3 ppm.

HRMS (ESI) Calc. for C <sub>15</sub> H <sub>18</sub> N <sub>3</sub> O <sup>+</sup> :	256.1450 [M+H] <sup>+</sup>
Found:	256.1449 [M+H] <sup>+</sup> .

**(3-((4-iodophenyl)diazenyl)phenyl)methanol (S5)**

To a solution of 1-iodo-4-nitrosobenzene<sup>[317]</sup> (500 mg, 2.15 mmol) in glacial AcOH (40 mL) was added (3-aminophenyl)methanol (264 mg, 2.15 mmol) and the mixture was stirred at room temperature overnight. The solvent was removed under reduced pressure and the residue partitioned between EtOAc (200 mL) and saturated aqueous NaHCO<sub>3</sub> solution (100 mL). The organic phase was washed with brine (100 mL), dried over MgSO<sub>4</sub>, filtered and concentrated. Normal phase flash column chromatography (SiO<sub>2</sub>; PE/EtOAc = 5:1 to 2:1) yielded 620 mg (85%) of azobenzene **S5** as an orange solid.

$R_f = 0.5$  (PE/EtOAc = 2:1).

mp (PE/EtOAc) = 115 °C.

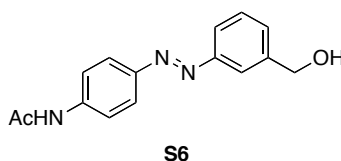
UV (DMSO):  $\lambda_{\max} = 341$  nm.

IR (ATR):  $\tilde{\nu} = 3330$  (br s), 2923 (w), 2868 (w), 1575 (m), 1564 (m), 1392 (m), 1044 (s), 1022 (s), 998 (s), 827 (s) cm<sup>-1</sup>.

<sup>1</sup>H NMR (acetone-*d*<sub>6</sub>, 400 MHz)  $\delta$  8.02-7.92 (m, 3H), 7.87-7.78 (m, 1H), 7.74-7.69 (m, 2H), 7.61-7.50 (m, 2H), 4.7 (d,  $J = 5.7$  Hz, 2H), 4.40 (t,  $J = 5.8$  Hz, 1OH) ppm.

<sup>13</sup>C NMR (acetone-*d*<sub>6</sub>, 100 MHz)  $\delta$  153.4, 152.9, 145.1, 139.5, 130.5, 130.0, 125.3, 122.5, 121.3, 98.1, 64.2 ppm.

HRMS (ESI) Calc. for C <sub>13</sub> H <sub>12</sub> IN <sub>2</sub> O <sup>+</sup> :	338.9994 [M+H] <sup>+</sup>
Found:	338.9992 [M+H] <sup>+</sup> .

***N*-(4-((3-(hydroxymethyl)phenyl)diazenyl)phenyl)acetamide (S6)**

To a solution of azobenzene **S5** (250 mg, 0.739 mmol) in DMF (12 mL) was added acetamide (87.3 mg, 1.48 mmol), *N,N*-dimethylethylenediamine (24  $\mu$ L, 0.222  $\mu$ mol) and potassium phosphate (314 mg, 1.48 mmol). The mixture was degassed and CuI (14.1 mg, 73.9  $\mu$ mol) was added. The mixture was stirred at 80°C for 5 h. The reaction was allowed to cool to room temperature and then poured on saturated aqueous NaHCO<sub>3</sub> (30 mL). The mixture was extracted with EtOAc (4 x 50 mL) and the combined organic extracts were dried over MgSO<sub>4</sub>, filtered and concentrated. Normal phase flash column chromatography (CH<sub>2</sub>Cl<sub>2</sub>/MeOH = 95:5 to 93:7) yielded 133 mg (67%) of acetamide **S6** as an orange solid.

$R_f$  = 0.33 (CH<sub>2</sub>Cl<sub>2</sub>/MeOH = 93:7).

mp (PE/EtOAc) = 175-176 °C.

UV (DMSO):  $\lambda_{\text{max}}$  = 361 nm.

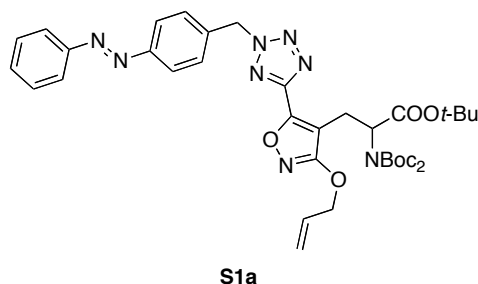
IR (ATR):  $\tilde{\nu}$  = 3304 (br m), 3264 (br m), 3200 (br m), 1681 (s), 1668 (s), 1592 (s), 1544 (s), 1502 (s), 1405 (s), 1304 (s), 1151 (s), 1012 (s) cm<sup>-1</sup>.

<sup>1</sup>H NMR (acetone-*d*<sub>6</sub>, 400 MHz)  $\delta$  9.45 (br s, 1H), 7.96-7.83 (m, 5H), 7.80-7.74 (m, 1H), 7.55-7.44 (m, 2H), 4.76 (d,  $J$  = 5.8 Hz, 2H), 4.36 (t,  $J$  = 5.8 Hz, 1OH), 2.14 (s, 3H) ppm.

<sup>13</sup>C NMR (acetone-*d*<sub>6</sub>, 100 MHz)  $\delta$  169.2, 153.6, 149.1, 144.9, 143.4, 129.8, 129.6, 124.5, 122.1, 121.0, 120.0, 64.2, 24.4 ppm.

HRMS (ESI) Calc. for C <sub>15</sub> H <sub>16</sub> N <sub>3</sub> O <sub>2</sub> <sup>+</sup> :	270.1243 [M+H] <sup>+</sup>
Found:	270.1239 [M+H] <sup>+</sup> .

***tert*-butyl 3-(3-(allyloxy)-5-(2-(4-(phenyldiazenyl)benzyl)-2*H*-tetrazol-5-yl)isoxazol-4-yl)-2-(bis(*tert*-butoxycarbonyl)amino)propanoate (S1a)**



To a solution of DEAD (167  $\mu$ L, 363  $\mu$ mol; 40% in toluene) and tetrazole **95** (150 mg, 280  $\mu$ mol) in THF (10 mL) was added  $\text{PPh}_3$  (95.3 mg, 363  $\mu$ mol) and the mixture was stirred for 5 min at room temperature. Then a solution of alcohol **S2** (77.1 mg, 363  $\mu$ mol) in THF (10 mL) was added and the reaction was stirred overnight at room temperature. EtOAc (30 mL) and saturated aqueous  $\text{NH}_4\text{Cl}$  solution (25 mL) were added. The biphasic mixture was extracted with EtOAc (3 x 50 mL). The combined extracts were dried over  $\text{MgSO}_4$ , filtered and concentrated. Normal phase flash column chromatography ( $\text{SiO}_2$ ; PE/EtOAc = 6:1 to 5:1) yielded 156 mg (76%) of *N*-1 and *N*-2 alkylated tetrazoles **S1a** (1:2.5 ratio by NMR) as an orange resin.

$R_f$  = 0.3 (PE/EtOAc = 4:1).

UV (DMSO):  $\lambda_{\text{max}}$  = 322 nm.

IR (ATR):  $\tilde{\nu}$  = 2979 (m), 2932 (m), 1790 (w), 1734 (s), 1699 (s), 1536 (m), 1502 (m), 1366 (s), 1286 (s), 1231 (s), 1141 (s), 1119 (s)  $\text{cm}^{-1}$ .

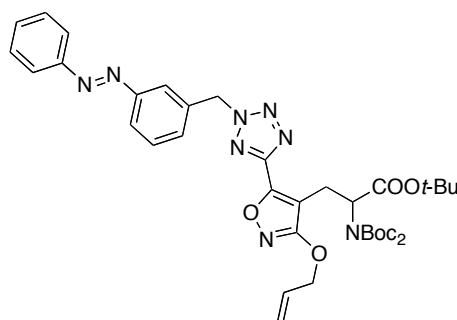
$^1\text{H}$  NMR ( $\text{CDCl}_3$ , 400 MHz; 1:2.5 mixture of regio-isomers)  $\delta$  7.93-7.87 (m, 3.3 H), 7.58-7.48 (m, 4.2H), 7.30-7.17 (m, 0.9H), 6.85-6.81 (m, 0.6H), 6.09-6.03 (m, 1.0H), 5.95-5.90 (m, 1.63H), 5.78-5.76 (m, 0.4H), 5.44-5.39 (m, 1.0H), 5.31-5.28 (m, 1.0H), 5.25-5.16 (m, 1.0H), 4.82 (add,  $J$  = 5.7 Hz,  $J$  = 1.3 Hz, 1.93H), 3.50-3.38 (m, 2.1H), 1.46 (s, 9.1H), 1.37-1.34 (m, 18.0H) ppm.

$^{13}\text{C}$  NMR ( $\text{CDCl}_3$ , 100 MHz; 1:2.5 mixture of regio-isomers)  $\delta$  171.4, 171.1, 168.9, 168.6, 156.6, 155.5, 153.0, 152.8, 152.6, 152.5, 152.1, 144.5, 136.0, 135.2, 132.2, 131.7, 131.7, 131.5, 131.5, 129.5, 129.3, 129.3, 129.1, 129.0, 127.9, 123.6, 123.6, 123.1, 123.1, 121.2,

120.6, 119.4, 119.0, 111.4, 108.0, 83.0, 82.8, 81.9, 81.8, 71.5, 71.1, 58.0, 57.8, 56.86, 56.6, 52.3, 28.1, 28.0 (2x), 22.2, 21.9 ppm.

HRMS (ESI) Calc. for  $C_{37}H_{46}N_8NaO_8^+$ : 753.3336  $[M+Na]^+$   
 Found: 753.3331  $[M+Na]^+$ .

***tert*-butyl 3-(3-(allyloxy)-5-(2-(3-(phenyldiazenyl)benzyl)-2*H*-tetrazol-5-yl)isoxazol-4-yl)-2-(bis(*tert*-bu-toxycarbonyl)amino)propanoate (S1b)**



**S1b**

To a solution of DEAD (113  $\mu$ L, 287  $\mu$ mol; 40% in toluene) and tetrazole **95** (140 mg, 261  $\mu$ mol) in THF (5 mL) was added  $PPh_3$  (75 mg, 287  $\mu$ mol) and the mixture was stirred for 5 min at room temperature before a solution of alcohol **S3** (60.9 mg, 287  $\mu$ mol) in THF (2 mL) was added and the reaction was stirred overnight at room temperature. EtOAc (20 mL) and saturated aqueous  $NH_4Cl$  solution (20 mL) were added. The biphasic mixture was extracted with EtOAc (3 x 50 mL), the combined extracts were dried over  $MgSO_4$ , filtered and concentrated. Normal phase flash column chromatography ( $SiO_2$ ; PE/EtOAc = 6:1) yielded 167 mg (88%) of *N*-1 and *N*-2 alkylated tetrazoles **S1b** (5.7:1 ratio by NMR) as an orange resin.

$R_f$  = 0.3 (PE/EtOAc = 4:1).

UV (DMSO):  $\lambda_{max}$  = 324 nm.

IR (ATR):  $\tilde{\nu}$  = 2980 (w), 2935 (w), 1791 (w), 1734 (s), 1700 (s), 1537 (m), 1503 (m), 1366 (s), 1282 (m), 1231 (s), 1141 (s), 1119 (s)  $cm^{-1}$ .

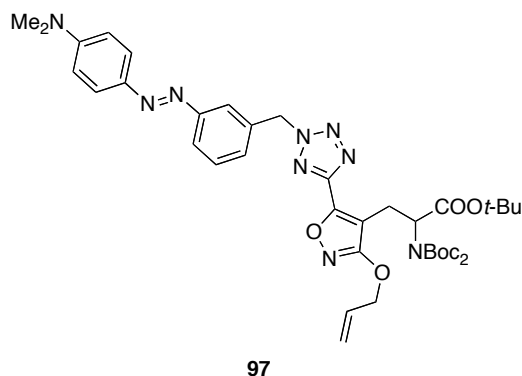
$^1H$  NMR ( $CDCl_3$ , 400 MHz; 1:2.5 mixture of regio-isomers)  $\delta$  8.01-7.84 (m, 3.2H), 7.60-7.42 (m, 4.2H), 7.32-6.72 (m, 1.2H), 6.14-6.00 (m, 0.94H), 5.99-5.91 (m, 1.7H), 5.75-5.66 (m,

0.3H), 5.44-5.38 (m, 1.0H), 5.35-5.27 (m, 1.2H), 5.25-5.16 (m, 1.0H), 4.81 (add,  $J = 5.8$  Hz,  $J = 1.3$  Hz, 2.0H), 3.61-3.32 (m, 2.1H), 1.48-1.44 (m, 9.1H), 1.39-1.31 (m, 18.0H) ppm.

$^{13}\text{C}$  NMR ( $\text{CDCl}_3$ , 100 MHz; 1:2.5 mixture of regio-isomers)  $\delta$  171.4, 171.1, 168.9, 168.6, 156.5, 155.5, 153.1, 152.5, 152.1, 152.1, 144.5, 134.6, 133.9, 132.2, 131.7, 131.6, 131.5, 130.9, 130.5, 130.1, 130.0, 129.3, 129.2, 128.9, 127.8, 127.4, 124.0, 123.3, 123.1, 122.9, 122.8, 120.5, 119.4, 119.0, 111.4, 108.0, 83.0, 82.9, 82.8, 81.9, 81.8, 71.5, 71.1, 58.1, 57.8, 57.0, 52.4, 28.1, 28.0, 22.2, 21.9 ppm.

HRMS (ESI) Calc. for  $\text{C}_{37}\text{H}_{46}\text{N}_8\text{NaO}_8^+$ : 753.3336  $[\text{M}+\text{Na}]^+$   
Found: 753.3332  $[\text{M}+\text{Na}]^+$ .

***tert*-butyl 3-(3-(allyloxy)-5-(2-(3-((4-(dimethylamino)phenyl)diazenyl)benzyl)-2*H*-tetrazol-5-yl)isoxa-zol-4-yl)-2-(bis(*tert*-butoxycarbonyl)amino)propanoate (**97**)**



To a solution of DEAD (222  $\mu\text{L}$ , 485  $\mu\text{mol}$ ; 40% in toluene) and tetrazole **95** (200 mg, 373  $\mu\text{mol}$ ) in THF (10 mL) was added  $\text{PPh}_3$  (127 mg, 485  $\mu\text{mol}$ ) and the mixture was stirred for 5 min at room temperature. Alcohol **96** (124 mg, 485  $\mu\text{mol}$ ) was added to the mixture and the reaction was stirred overnight at room temperature. EtOAc (20 mL) and saturated aqueous  $\text{NH}_4\text{Cl}$  solution (20 mL) were added. The biphasic mixture was extracted with EtOAc (3 x 50 mL), the combined extracts were dried over  $\text{MgSO}_4$ , filtered and concentrated. Normal phase flash column chromatography ( $\text{SiO}_2$ ; PE/EtOAc = 4:1) yielded 250 mg (87%) of *N*-1 and *N*-2 alkylated tetrazoles **97** (2:3 ratio by NMR) as a red solid.

$R_f = 0.6$  (PE/EtOAc = 2:1).

mp (PE/EtOAc) = 57  $^\circ\text{C}$ .



UV (DMSO):  $\lambda_{\text{max}} = 429 \text{ nm}$ .

IR (ATR):  $\tilde{\nu} = 2979 \text{ (w)}, 2934 \text{ (w)}, 1791 \text{ (w)}, 1733 \text{ (s)}, 1699 \text{ (s)}, 1600 \text{ (s)}, 1557 \text{ (s)}, 1519 \text{ (s)}, 1505 \text{ (s)}, 1365 \text{ (s)}, 1283 \text{ (s)}, 1230 \text{ (s)}, 1135 \text{ (s)}, 1119 \text{ (s)} \text{ cm}^{-1}$ .

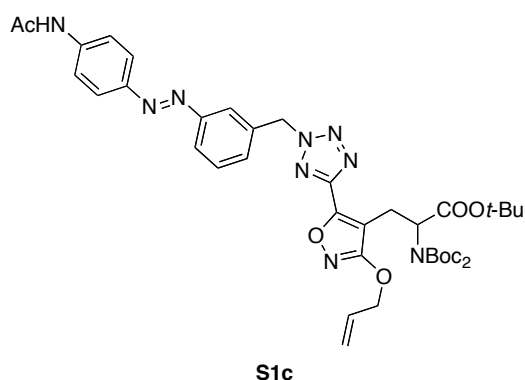
$^1\text{H}$  NMR ( $\text{CDCl}_3$ , 600 MHz; 2:3 mixture of regio-isomers)  $\delta$  7.93-7.76 (m, 3.9 H), 7.50-7.31 (m, 2.0H), 6.76 (d,  $J = 9.0 \text{ Hz}$ , 2.0H), 5.94 (s, 0.9H), 5.93-5.87 (m, 1.2H), 5.45-5.39 (m, 1.0H), 5.33-5.27 (m, 1.0H), 5.26-5.17 (m, 1.0H), 4.86-4.79 (m, 2.0H), 3.61-3.35 (m, 2.1H), 3.10 (s, 6.0H), 1.46-1.45 (m, 9.0H), 1.36 (s, 7.3H), 1.33 (s, 10.6H) ppm.

$^{13}\text{C}$  NMR ( $\text{CDCl}_3$ , 150 MHz; 2:3 mixture of regio-isomers)  $\delta$  171.3, 171.1, 168.9, 168.6, 156.5, 155.6, 152.6, 152.1, 152.0, 144.5, 134.4, 133.6, 132.2, 131.8, 129.9, 129.8, 129.2, 128.8, 125.5, 125.4, 123.4, 122.6, 122.2, 122.2, 119.4, 118.9, 111.7, 111.3, 107.9, 83.0, 82.8, 81.9, 81.7, 71.5, 71.1, 58.1, 57.9, 57.2, 52.6, 40.5, 28.1, 28.0, 28.0, 22.2, 22.0 ppm.

HRMS (ESI) Calc. for  $\text{C}_{39}\text{H}_{52}\text{N}_9\text{O}_8^+$ : 774.3939  $[\text{M}+\text{H}]^+$

Found: 774.3938  $[\text{M}+\text{H}]^+$ .

***tert*-butyl 3-(5-(2-(3-((4-acetamidophenyl)diazenyl)benzyl)-2*H*-tetrazol-5-yl)-3-(allyloxy)isoxazol-4-yl)-2-(bis (*tert*-butoxycarbonyl)amino)propanoate (S1c)**



To a solution of DEAD (167  $\mu\text{L}$ , 364  $\mu\text{mol}$ ; 40% in toluene) and tetrazole **95** (150 mg, 280  $\mu\text{mol}$ ) in THF (10 mL) was added  $\text{PPh}_3$  (88.1 mg, 336  $\mu\text{mol}$ ) and the mixture was stirred for 5 min at room temperature before alcohol **S6** (90.5 mg, 336  $\mu\text{mol}$ ) was added and the reaction was stirred overnight at room temperature. EtOAc (20 mL) and saturated aqueous  $\text{NH}_4\text{Cl}$  solution (20 mL) were added. The biphasic mixture was extracted with EtOAc (3 x 50 mL), the combined extracts were dried over  $\text{MgSO}_4$ , filtered and concentrated. Normal phase flash

column chromatography (SiO<sub>2</sub>; CH<sub>2</sub>Cl<sub>2</sub>/MeOH = 97:3) yielded 168 mg (76%) of *N*-1 and *N*-2 alkylated tetrazoles **S1c** (8:9 ratio by NMR) as an orange solid.

$R_f = 0.4$  (CH<sub>2</sub>Cl<sub>2</sub>/MeOH = 95:5).

m.p. (CH<sub>2</sub>Cl<sub>2</sub>/MeOH) = 45 °C.

UV (DMSO):  $\lambda_{\max} = 365$  nm.

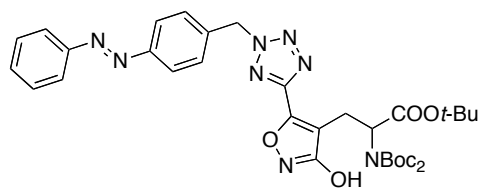
IR (ATR):  $\tilde{\nu} = 3253$  (w), 3189 (w), 2980 (w), 1732 (s), 1697 (s), 1594 (m), 1538 (s), 1503 (s), 1437 (s), 1366 (s), 1229 (s), 1142 (s), 1118 (s) cm<sup>-1</sup>.

<sup>1</sup>H NMR (CDCl<sub>3</sub>, 600 MHz; 9:8 mixture of regio-isomers and rotamers)  $\delta$  7.89-7.83 (m, 4.1H), 7.73-7.65 (m, 2.1H), 7.59-7.42 (br m, 3.5H), 6.11-6.03 (m, 1.0H), 6.00-5.94 (m, 1.0H), 5.94-5.89 (m, 1.1H), 5.42 (add,  $J = 17.3$  Hz,  $J = 7.0$  Hz,  $J = 1.3$  Hz, 0.9H), 5.30 (add,  $J = 15.5$  Hz,  $J = 10.5$  Hz,  $J = 1.2$  Hz, 1.1H), 5.24-5.17 (m, 0.9H), 4.87-4.80 (m, 2.2H), 3.56-3.38 (m, 1.9H), 2.22 (s, 3.0H), 1.46-1.44 (m, 8.9H), 1.38-1.30 (m, 18.1H) ppm.

<sup>13</sup>C NMR (CDCl<sub>3</sub>, 150 MHz; 9:8 mixture of regio-isomers and rotamers)  $\delta$  171.4, 171.1, 168.9, 168.6, 156.5, 155.5, 153.1, 153.1, 152.6, 152.1, 152.1, 148.9, 148.9, 144.5, 134.6, 133.8, 132.2, 131.7, 130.7, 130.2, 130.1, 123.0, 124.4, 124.3, 123.9, 123.2, 122.8, 122.8, 119.8, 119.7, 119.4, 119.0, 111.4, 108.0, 83.0, 82.9, 82.0, 81.8, 81.8, 71.5, 71.1, 58.1, 57.9, 57.0, 52.4, 28.1, 28.0, 28.0, 25.0, 22.2, 22.0 ppm.

HRMS (ESI) Calc. for C <sub>39</sub> H <sub>49</sub> KN <sub>9</sub> O <sub>9</sub> <sup>+</sup> :	826.3285 [M+K] <sup>+</sup>
Found:	826.3284 [M+K] <sup>+</sup> .

***tert*-butyl 2-(bis(*tert*-butoxycarbonyl)amino)-3-(3-hydroxy-5-(2-(4-(phenyldiazenyl)benzyl)-2*H*-tetra-zol-5-yl)isoxazol-4-yl)propanoate (**S7a**)**

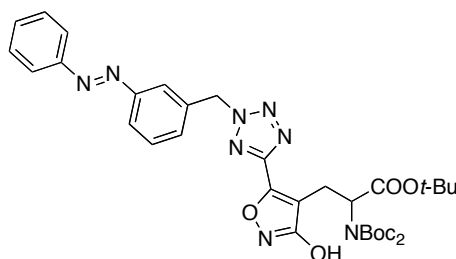


**S7a**

To a solution of protected isoxazole **S1a** (140 mg, 192  $\mu\text{mol}$ ) in MeOH (10 mL) was added  $\text{Pd}(\text{PPh}_3)_4$  (22.2 mg, 19.2  $\mu\text{mol}$ ) and the mixture was stirred for 5 min.  $\text{K}_2\text{CO}_3$  (53.1 mg, 384  $\mu\text{mol}$ ) was added and stirring was continued for 2 h. The mixture was diluted with EtOAc (60 mL) and washed with saturated aqueous  $\text{NH}_4\text{Cl}$  (15 mL) and brine (15 mL). The organic phase was dried over  $\text{MgSO}_4$ , filtered and concentrated. Normal phase flash column chromatography ( $\text{SiO}_2$ ;  $\text{CH}_2\text{Cl}_2/\text{MeOH} = 97:3$  to  $95:5$ ) yielded the free hydroxy isoxazole **S7a** as an orange wax, which was used directly in the next step.

$R_f = 0.3$  ( $\text{CH}_2\text{Cl}_2/\text{MeOH} = 95:5$ ).

***tert*-butyl 2-(bis(*tert*-butoxycarbonyl)amino)-3-(3-hydroxy-5-(2-(3-(phenyldiazenyl)benzyl)-2*H*-tetra-zol-5-yl)isoxazol-4-yl)propanoate (**S7b**)**

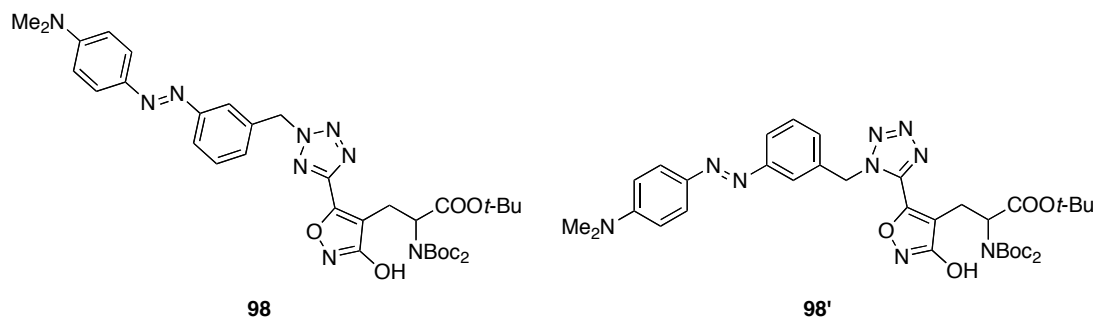


**S7b**

To a solution of protected isoxazole **S1b** (160 mg, 219  $\mu\text{mol}$ ) in MeOH (10 mL) was added  $\text{Pd}(\text{PPh}_3)_4$  (25.3 mg, 21.9  $\mu\text{mol}$ ) and the mixture was stirred for 5 min.  $\text{K}_2\text{CO}_3$  (60.5 mg, 438  $\mu\text{mol}$ ) was added and stirring was continued for 2 h. The mixture was diluted with EtOAc (60 mL) and washed with saturated aqueous  $\text{NH}_4\text{Cl}$  and brine (15 mL each). The organic phase was dried over  $\text{MgSO}_4$ , filtered and concentrated. Normal phase flash column chromatography ( $\text{SiO}_2$ ;  $\text{CH}_2\text{Cl}_2/\text{MeOH} = 95:5$  to  $94:6$ ) yielded the free hydroxy isoxazole **S7b** as an orange wax, which was used directly in the next step.

$R_f = 0.2$  ( $\text{CH}_2\text{Cl}_2/\text{MeOH} = 95:5$ ).

*tert*-butyl 2-(bis(*tert*-butoxycarbonyl)amino)-3-(5-(2-(3-((4-(dimethylamino)phenyl)diazenyl)benzyl)-2*H*-tetrazol-5-yl)-3-hydroxyisoxazol-4-yl)propanoate (**98**) and *tert*-butyl 2-(bis(*tert*-butoxycarbonyl)amino)-3-(5-(1-(3-((4-(dimethylamino)phenyl)diazenyl)benzyl)-1*H*-tetrazol-5-yl)-3-hydroxyisoxazol-4-yl)propanoate (**98'**)



To a solution of isoxazole **97** (200 mg, 258  $\mu$ mol) in MeOH (10 mL) was added Pd(PPh<sub>3</sub>)<sub>4</sub> (14.9 mg, 12.9  $\mu$ mol). After stirring for 5 min, K<sub>2</sub>CO<sub>3</sub> (71.4 mg, 517  $\mu$ mol) was added and stirring was continued for 2 h at room temperature. The mixture was diluted with EtOAc (50 mL) and the organic phase was washed with saturated aqueous NH<sub>4</sub>Cl solution and brine (20 mL each). The organic phase was dried over MgSO<sub>4</sub>, filtered and concentrated. The crude product was first passed over a short plug of silica (eluting with CH<sub>2</sub>Cl<sub>2</sub>/MeOH = 9:1) and – after evaporation of the solvent – was purified by reversed phase HPLC (Varian Dynamax 250x21.4 mm Microsorb 60-8 C18 column equipped with a Dynamax HPLC guard column operating on a Varian PrepStar HPLC system; H<sub>2</sub>O/MeCN/0.1% formic acid; 15 mL/min; gradient program: t = 0 min, 80% MeCN; t = 90 min, 85% MeCN) to yield 84 mg (44%) of *N*-2-alkylated tetrazole **98** (*R*<sub>t</sub> = 24.8 min) and 46 mg (24%) of its *N*-1-alkylated isomer **98'** (*R*<sub>t</sub> = 22.6 min) as red solids.

**98:**

*R*<sub>f</sub> = 0.5 (CH<sub>2</sub>Cl<sub>2</sub>/MeOH = 9:1).

mp (H<sub>2</sub>O/MeCN) = 95 °C.

UV (DMSO):  $\lambda_{\text{max}}$  = 429 nm.

IR (ATR):  $\tilde{\nu}$  = 2979 (w), 2932 (w), 1790 (w), 1733 (s), 1699 (s), 1600 (s), 1520 (s), 1365 (s), 1232 (s), 1150 (s), 1122 (s) cm<sup>-1</sup>.

$^1\text{H}$  NMR ( $\text{CDCl}_3$ , 600 MHz)  $\delta$  7.90 (t,  $J = 1.7$  Hz, 1H), 7.87 (m<sub>c</sub>, 2H), 7.83 (m<sub>c</sub>, 1H), 6.75 (d,  $J = 9.2$  Hz, 2H), 5.91 (m<sub>c</sub>, 2H), 5.17 (dd,  $J = 8.3$  Hz,  $J = 5.6$  Hz, 1H), 3.55 (dd,  $J = 14.7$  Hz,  $J = 5.5$  Hz, 1H), 3.43 (dd,  $J = 14.7$  Hz,  $J = 8.3$  Hz, 1H), 3.09 (s, 6H), 1.45 (s, 9H), 1.36 (s, 18H) ppm.

$^{13}\text{C}$  NMR ( $\text{CDCl}_3$ , 150 MHz)  $\delta$  170.6, 170.2, 156.3, 155.4, 153.7, 152.8, 152.1, 143.6, 133.6, 129.9, 129.2, 125.4, 123.4, 122.2, 111.6, 108.2, 83.2, 82.5, 58.2, 57.2, 40.4, 28.1, 28.0, 22.4 ppm.

HRMS (ESI) Calc. for  $\text{C}_{36}\text{H}_{48}\text{N}_9\text{O}_8^+$ : 734.3626  $[\text{M}+\text{H}]^+$   
 Found: 734.3628  $[\text{M}+\text{H}]^+$ .

The *N*-2 alkylation was evident due to the following HMBC correlations:

HMBC	H	C
	5.91	122.2
	5.91	129.2
	5.91	133.6

**98'**:

$R_f = 0.5$  ( $\text{CH}_2\text{Cl}_2/\text{MeOH} = 9:1$ ).

mp ( $\text{H}_2\text{O}/\text{MeCN}$ ) = 98-103 °C.

UV (DMSO):  $\lambda_{\text{max}} = 428$  nm.

IR (ATR):  $\tilde{\nu} = 2978$  (w), 2933 (w), 1732 (m), 1698 (m), 1600 (s), 1520 (m), 1365 (s), 1231 (s), 1135 (s)  $\text{cm}^{-1}$ .

$^1\text{H}$  NMR ( $\text{CDCl}_3$ , 600 MHz)  $\delta$  7.87-7.82 (m, 3H), 7.77 (dd,  $J = 7.9$  Hz,  $J = 1.1$  Hz, 1H), 7.42 (t,  $J = 7.8$  Hz, 1H), 7.34 (d,  $J = 7.7$  Hz, 1H), 6.72 (d,  $J = 9.2$  Hz, 2H), 5.95 (s, 2H), 5.12 (dd,  $J = 6.7$  Hz,  $J = 5.8$  Hz, 1H), 3.55 (dd,  $J = 14.8$  Hz,  $J = 6.8$  Hz, 1H), 3.32 (dd,  $J = 14.8$  Hz,  $J = 5.7$  Hz, 1H), 3.08 (s, 6H), 1.45 (s, 9H), 1.40 (s, 18H) ppm.

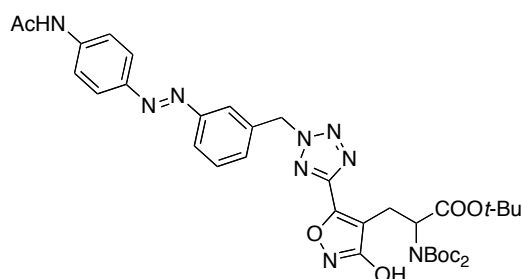
$^{13}\text{C}$  NMR ( $\text{CDCl}_3$ , 150 MHz)  $\delta$  171.7, 170.6, 153.7, 152.8, 152.6, 152.2, 144.3, 143.6, 134.2, 129.8, 128.9, 125.4, 122.8, 122.3, 111.6, 111.3, 83.7, 83.6, 58.5, 52.7, 40.4, 28.0, 28.0, 23.3 ppm.

HRMS (ESI) Calc. for  $C_{36}H_{48}N_9O_8^+$ : 734.3626  $[M+H]^+$   
Found: 734.3625  $[M+H]^+$ .

The *N*-1 alkylation was evident due to the following HMBC correlations:

HMBC	H	C
	5.95	122.3
	5.95	128.9
	5.95	134.2
	5.95	144.3

***tert*-butyl 3-(5-(2-(3-((4-acetamidophenyl)diazenyl)benzyl)-2*H*-tetrazol-5-yl)-3-hydroxyisoxazol-4-yl)-2-(bis(*tert*-butoxycarbonyl)amino)propanoate (S7c)**

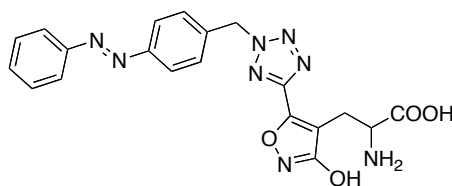


**S7c**

To a solution of protected isoxazole **S1c** (132 mg, 168  $\mu$ mol) in MeOH (10 mL) was added  $Pd(PPh_3)_4$  (9.68 mg, 8.38  $\mu$ mol) and the mixture was stirred for 5 min.  $K_2CO_3$  (43.3 mg, 335 mmol) was added and stirring was continued for 1 h. EtOAc (40 mL) was added and the organic phase was washed with a saturated aqueous  $NH_4Cl$  solution and brine (15 mL each). The organic phase was dried over  $MgSO_4$ , filtered and concentrated. Normal phase flash column chromatography ( $SiO_2$ ,  $CH_2Cl_2/MeOH = 93:7$ ) yielded the free hydroxy isoxazole **S7c** as a red wax, which was used directly in the next step.

$R_f = 0.4$  ( $CH_2Cl_2/MeOH = 9:1$ ).

**2-amino-3-(3-hydroxy-5-(2-(4-(phenyldiazenyl)benzyl)-2H-tetrazol-5-yl)isoxazol-4-yl)propanoic acid (ATA-1, 89a)**



ATA-1 (**89a**)

To a solution of hydroxyl isoxazole **S7a** in  $\text{CH}_2\text{Cl}_2$  (15 mL) was added TFA (15 mL) at 0 °C and the mixture was stirred for 2 h. The solvent was removed under reduced pressure and the residue purified using reversed phase flash column chromatography (C18;  $\text{H}_2\text{O}/\text{MeCN}/\text{FA} = 100:0:0.1\%$  to  $6:4:0.1\%$ ) to yield 39 mg (49%, 2 steps) of ATA-1 (**89a**) as a mixture of regio-isomers as a yellow solid. The *N*1- and *N*2-alkylated isomers (2:7 by NMR) could not be separated.

$R_f = 0.5$  ( $\text{H}_2\text{O}/\text{MeCN}/\text{FA} = 1:1:0.1\%$ ).

mp ( $\text{H}_2\text{O}/\text{MeCN}$ ) > 170 °C (decomp.).

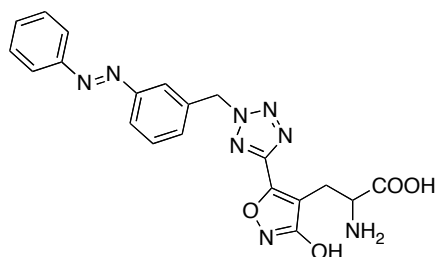
UV (HEPES-ringer):  $\lambda_{\text{max}} = 320$  nm.

IR (ATR):  $\tilde{\nu} = 3156$  (w), 2960 (w), 1607 (br m), 1486 (s), 1308 (s), 1201 (m), 1119 (w), 1062 (w)  $\text{cm}^{-1}$ .

$^1\text{H}$  NMR ( $\text{DMSO}-d_6$ , 600 MHz)  $\delta$  7.93-7.85 (m, 4.1H), 7.68-7.54 (m, 4.7H), 7.47 (d,  $J = 8.7$  Hz, 0.4H), 6.19 (m, 1.6H), 6.03-5.97 (m, 0.5H), 3.78-3.70 (m, 1.0), 3.34-3.23 (m, 1.2H), 3.16-3.03 (0.8H) ppm.

$^{13}\text{C}$  NMR ( $\text{DMSO}-d_6$ , 150 MHz)  $\delta$  171.7, 171.2, 156.0, 153.2, 151.9, 151.9, 151.7, 150.1, 145.0, 137.6, 136.8, 131.8, 131.8, 129.7, 129.5, 129.5, 128.9, 123.0, 123.0, 122.6, 122.6, 107.8, 55.9, 52.5, 51.5, 24.2 ppm.

HRMS (ESI) Calc. for $\text{C}_{20}\text{H}_{17}\text{N}_8\text{O}_4^-$ :	433.1378 $[\text{M}-\text{H}]^-$
Found:	433.1377 $[\text{M}-\text{H}]^-$

**2-amino-3-(3-hydroxy-5-(2-(3-(phenyldiazenyl)benzyl)-2H-tetrazol-5-yl)isoxazol-4-yl)propanoic acid (ATA-2, 89b)**ATA-2 (**89b**)

To a solution of hydroxyl isoxazole **S7b** in CH<sub>2</sub>Cl<sub>2</sub> (15 mL) was added TFA (15 mL) at 0 °C and the mixture was stirred for 2 h. The solvent was removed under reduced pressure and the residue purified using reversed phase flash column chromatography (C18; H<sub>2</sub>O/MeCN/FA = 100:0:0.1% to 6:4:0.1%) to yield 44 mg (47%, 2 steps) of ATA-2 (**89b**) as a mixture of regio-isomers as a yellow solid. The *N*1- and *N*2-alkylated isomers (1:3 by NMR) could not be separated.

R<sub>f</sub> = 0.5 (H<sub>2</sub>O/MeCN/FA = 1:1:0.1%).

mp (H<sub>2</sub>O/MeCN) > 209 °C (decomp.).

UV (HEPES-ringer): λ<sub>max</sub> = 320 nm.

IR (ATR):  $\tilde{\nu}$  = 3189 (w), 1609 (br m), 1485 (s), 1401 (m), 1318 (s), 1262 (m), 1244 (m), 1060 (m) cm<sup>-1</sup>.

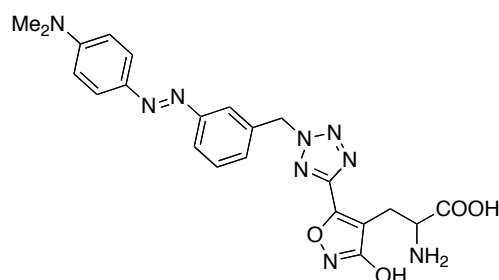
<sup>1</sup>H NMR (DMSO-*d*<sub>6</sub>, 600 MHz) δ 11.05-8.90 (br s, 1.8H), 8.01-7.83 (m, 3.3H), 7.70-7.56 (m, 4.2H), 7.39-6.72 (m, 0.5H), 6.22 (mc, 1.3H), 6.05 (s, 0.5H), 3.80-3.72 (m, 1.0H), 3.36-3.24 (m, 1.1H), 3.19-3.06 (m, 1.0H) ppm.

<sup>13</sup>C NMR (DMSO-*d*<sub>6</sub>, 150 MHz) δ 171.7, 171.2, 171.0, 156.0, 153.2, 152.1, 152.0, 151.8, 151.8, 150.2, 145.0, 135.9, 135.1, 131.8, 131.5, 130.8, 130.2, 130.1, 129.5, 129.5, 128.7, 123.2, 122.6, 122.3, 121.9, 119.7, 111.0, 107.8, 55.9, 52.5, 52.2, 51.5, 39.5, 24.4, 24.2 ppm.

HRMS (ESI) Calc. for C <sub>20</sub> H <sub>17</sub> N <sub>8</sub> O <sub>4</sub> <sup>-</sup> :	433.1378 [M-H] <sup>-</sup>
Found:	433.1379 [M-H] <sup>-</sup> .



**2-amino-3-(5-(2-(3-((4-(dimethylamino)phenyl)diazenyl)benzyl)-2H-tetrazol-5-yl)-3-hydroxyisoxazol-4-yl)propanoic acid (ATA-3, 89c)**



ATA-3 (**89c**)

To a solution of hydroxy-isoxazole **98** (65 mg, 88.6  $\mu$ mol) in  $\text{CH}_2\text{Cl}_2$  (25 mL) was added TFA (25 mL) at 0  $^\circ\text{C}$  and the mixture was stirred for 1 h at that temperature and then for additional 2 h at room temperature. The solvent was removed and the residue purified using reversed phase flash column chromatography (C18;  $\text{H}_2\text{O}/\text{MeCN}/\text{FA} = 9:1:0.1\%$  to  $6:4:0.1\%$ ) to yield 31 mg (73%) of ATA-3 (**89c**) as an orange solid.

$R_f = 0.5$  ( $\text{H}_2\text{O}/\text{MeCN}/\text{FA} = 6:4:0.1\%$ ).

mp ( $\text{H}_2\text{O}/\text{MeCN}$ ) > 188  $^\circ\text{C}$  (decomp.).

UV (HEPES-ringer):  $\lambda_{\text{max}} = 456$  nm.

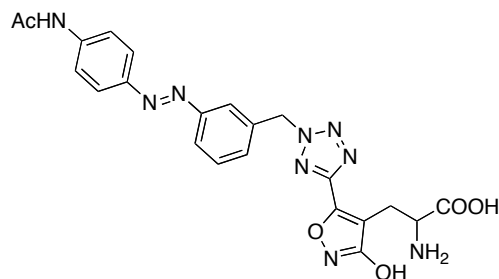
IR (ATR):  $\tilde{\nu} = 3055$  (w), 1634 (m), 1610 (s), 1521 (m), 1480 (s), 1362 (s), 1336 (s), 1320 (s), 1170 (s), 1161 (s), 1134 (s), 1122 (s), 810 (s)  $\text{cm}^{-1}$ .

$^1\text{H}$  NMR ( $\text{DMSO}-d_6$ , 600 MHz)  $\delta$  11.87-8.00 (br s, 3H), 7.85 (m, 1H), 7.81-7.76 (m, 3H), 7.56 (at,  $J = 7.8$  Hz, 1H), 7.47 (d,  $J = 7.7$  Hz, 1H), 6.83 (d,  $J = 9.2$  Hz, 2H), 6.17 (m, 2H), 3.73 (dd,  $J = 7.0$  Hz,  $J = 3.7$  Hz, 1H), 3.31 (dd,  $J = 15.9$  Hz,  $J = 3.6$  Hz, 1H), 3.10 (dd,  $J = 16.0$  Hz,  $J = 7.0$  Hz, 1H), 3.06 (s, 6H) ppm.

$^{13}\text{C}$  NMR ( $\text{DMSO}-d_6$ , 150 MHz)  $\delta$  171.8, 171.2, 156.0, 153.2, 152.7, 152.7, 142.5, 134.8, 129.9, 129.4, 124.9, 122.4, 121.6, 111.6, 107.9, 56.1, 52.5, 39.8, 24.2 ppm.

HRMS (ESI) Calc. for $\text{C}_{22}\text{H}_{24}\text{N}_9\text{O}_4^+$ :	478.1946 $[\text{M}+\text{H}]^+$
Found:	478.1947 $[\text{M}+\text{H}]^+$ .

**3-(5-(2-(3-((4-acetamidophenyl)diazenyl)benzyl)-2H-tetrazol-5-yl)-3-hydroxyisoxazol-4-yl)-2-aminopropanoic acid (ATA-4, 89d)**



ATA-4 (**89d**)

To a solution of hydroxy-isoxazole **S7c** in  $\text{CH}_2\text{Cl}_2$  (20 mL) was added TFA (20 mL) at 0 °C and the mixture was stirred for 1 h at that temperature and then for additional 2 h. at room temperature. The solvent was removed and the residue purified using reversed phase flash column chromatography (C18;  $\text{H}_2\text{O}/\text{MeCN}/\text{FA} = 9:1:0.1\%$  to  $1:1:0.1\%$ ) to yield 56 mg (68%, 2 steps) of ATA-4 (**89d**) as an orange solid. The *N*-1- and *N*-2-alkylated isomers could not be separated. By trituration with  $\text{H}_2\text{O}/\text{MeCN}$ , the ratio could be enhanced to up to 2:9.

$R_f = 0.5$  ( $\text{H}_2\text{O}/\text{MeCN}/\text{FA} = 1:1:1\%$ ).

mp ( $\text{H}_2\text{O}/\text{MeCN}$ ) > 213 °C (decomp.).

UV (HEPES-ringer):  $\lambda_{\text{max}} = 349$  nm.

IR (ATR):  $\tilde{\nu} = 3299$  (w), 3160 (w), 3014 (w), 1668 (s), 1595 (m), 1524 (s), 1487 (s), 1405 (s), 1304 (s), 1262 (s), 1243 (s), 1202 (m), 1152 (m)  $\text{cm}^{-1}$ .

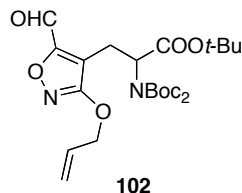
$^1\text{H}$  NMR ( $\text{DMSO}-d_6$ , 600 MHz)  $\delta$  10.52 (s, 1.0H), 8.38 (s, 1.6H), 7.93-7.74 (m, 5.8H), 7.65-7.52 (m, 2.0H), 6.16 (s, 1.7H), 5.99 (s, 0.4H), 3.55-3.46 (m, 1.0H), 3.36-3.31 (m, 1.0H), 2.91-2.76 (m, 0.9H), 2.13-2.06 (m, 3.0H) ppm.

$^{13}\text{C}$  NMR ( $\text{DMSO}-d_6$ , 150 MHz)  $\delta$  175.8, 175.5, 171.3, 170.8, 168.9, 165.3, 157.0, 152.2, 152.2, 151.0, 147.9, 147.3 (2x), 145.7, 142.8, 136.2, 135.2, 130.8, 130.1, 123.8, 122.9, 122.2, 122.0, 121.6, 119.1, 114.7, 111.2, 55.8, 54.6, 51.4, 39.5, 25.5, 24.2. ppm.

HRMS (ESI) Calc. for  $\text{C}_{22}\text{H}_{21}\text{N}_9\text{NaO}_5^+$ : 514.1558  $[\text{M}+\text{Na}]^+$   
 Found: 514.1558  $[\text{M}+\text{Na}]^+$ .

### 3) Triazolyl-Substituted AMPA derivatives – Synthetic Procedures

#### *tert*-butyl 3-(3-(allyloxy)-5-formylisoxazol-4-yl)-2-(bis(*tert*-butoxycarbonyl)amino)propanoate (**102**)



To a solution of nitrile **95** (100 mg, 203  $\mu$ mol) in MePh (5 mL) was drop-wise added RedAl® (125  $\mu$ L, 405  $\mu$ mol; 65% in MePh) at -50 °C and the resulting mixture was stirred for 60 min. The reaction was quenched by addition of 5% aqueous H<sub>2</sub>SO<sub>4</sub> (5 mL) at 0 °C and the biphasic mixture was allowed to warm to RT over 30 min. Brine (15 mL) was added and the mixture extracted with EtOAc (4 x 20 mL). The combined organic extracts were dried over MgSO<sub>4</sub>, filtered and concentrated. The obtained aldehyde **102** was sufficiently pure to be used directly in the next step. An analytical sample was obtained by preparative TLC (SiO<sub>2</sub>; CH<sub>2</sub>Cl<sub>2</sub>/MeOH = 95:5).

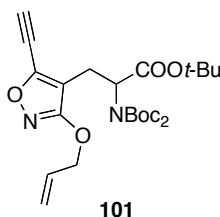
R<sub>f</sub> = 0.2 (PE/EtOAc = 10:1).

IR (ATR):  $\tilde{\nu}$  = 2980 (w), 2927 (w), 1735 (s), 1700 (s), 1510 (s), 1367 (s), 1279 (s), 1253 (m), 1147 (s), 1123 (s) cm<sup>-1</sup>.

<sup>1</sup>H NMR (CDCl<sub>3</sub>, 600 MHz)  $\delta$  9.82 (s, 1H), 6.07 (ddt,  $J$  = 17.2 Hz,  $J$  = 10.5 Hz,  $J$  = 5.7 Hz, 1H), 5.43 (add,  $J$  = 17.3 Hz,  $J$  = 1.5 Hz,  $J$  = 1.5 Hz, 1H), 5.32 (add,  $J$  = 10.5 Hz,  $J$  = 1.2 Hz,  $J$  = 1.2 Hz, 1H), 4.42 (dd,  $J$  = 10.8 Hz,  $J$  = 4.4 Hz, 1H), 4.82 (dt,  $J$  = 5.7 Hz,  $J$  = 1.2, 2H), 3.43 (dd,  $J$  = 14.5 Hz,  $J$  = 10.8 Hz, 1H), 3.30 (dd,  $J$  = 14.6 Hz, 4.4 Hz, 1H), 1.47 (s, 9H), 1.43 (s, 18H) ppm.

<sup>13</sup>C NMR (CDCl<sub>3</sub>, 150 MHz)  $\delta$  179.2, 170.9, 168.5, 161.7, 152.4, 131.8, 119.4, 113.2, 83.4, 82.2, 71.4, 57.5, 28.1 (2x), 21.6 ppm.

HRMS (ESI) Calc. for C<sub>24</sub>H<sub>37</sub>N<sub>2</sub>NaO<sub>9</sub><sup>+</sup>: 519.2313 [M+Na]<sup>+</sup>  
 Found: 519.2312 [M+Na]<sup>+</sup>.

***tert*-butyl 3-(3-(allyloxy)-5-ethynylisoxazol-4-yl)-2-(bis(*tert*-butoxycarbonyl)amino)propanoate (**101**)**

To a suspension of  $K_2CO_3$  and crude aldehyde **102** in MeOH (10 mL) was added the Ohira-Bestmann reagent<sup>[130]</sup> (49.5 mg, 258  $\mu$ mol) at 0 °C and the mixture was allowed to warm to RT over 3 h. Saturated aqueous  $NH_4Cl$  solution (25 mL) was added and most of the MeOH removed on the rotavap. Water (just enough to dissolve all salts) was added and the mixture extracted using EtOAc (4 x 25 mL). The combined organic extracts were dried over  $MgSO_4$ , filtered and concentrated. Normal phase flash-column chromatography ( $SiO_2$ ; PE/EtOAc = 7:1) yielded 50 mg (63%, 2 steps) of alkyne **101** as a colorless oil.

$R_f$  = 0.3 (PE/EtOAc = 7:1).

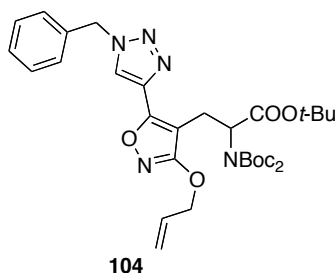
IR (ATR):  $\tilde{\nu}$  = 3247 (w), 2981 (m), 2119 (w), 1736 (s), 1702 (s), 1514 (s), 1368 (s), 1282 (m), 1147 (s)  $cm^{-1}$ .

$^1H$  NMR ( $CDCl_3$ , 400 MHz)  $\delta$  6.06 (ddt,  $J$  = 17.3 Hz,  $J$  = 10.5 Hz,  $J$  = 5.7 Hz, 1H), 5.40 (addd,  $J$  = 17.3 Hz,  $J$  = 1.5 Hz,  $J$  = 1.5 Hz, 1H), 5.29 (addd,  $J$  = 10.5 Hz,  $J$  = 1.3 Hz,  $J$  = 1.3 Hz, 1H), 4.99 (dd,  $J$  = 10.7 Hz,  $J$  = 4.4 Hz, 1H), 4.76 ( $m_c$ , 2H), 3.57 (s, 1H), 3.17 (dd,  $J$  = 14.8 Hz,  $J$  = 10.7 Hz, 1H), 3.09 (dd,  $J$  = 14.8 Hz,  $J$  = 4.4 Hz, 1H), 1.46 (s, 9H), 1.44 (s, 18H) ppm.

$^{13}C$  NMR ( $CDCl_3$ , 100 MHz)  $\delta$  170.2, 168.8, 152.2, 150.9, 132.2, 119.0, 111.1, 87.8, 83.0, 82.0, 71.0, 70.3, 57.8, 28.1 (2x), 22.1 ppm.

HRMS (ESI) Calc. for  $C_{25}H_{36}N_2NaO_8^+$ : 515.2364  $[M+Na]^+$   
 Found: 515.2362  $[M+Na]^+$ .

***tert*-butyl 3-(3-(allyloxy)-5-(1-benzyl-1*H*-1,2,3-triazol-4-yl)isoxazol-4-yl)-2-(bis(*tert*-butoxycarbonyl)amino)propanoate (**104**)**



To a solution of alkyne **101** (5.0 mg, 12.7  $\mu\text{mol}$ ) in THF/water (1 mL, 1:1) was added benzyl azide (2.5 mg, 19.1  $\mu\text{mol}$ ),<sup>[LIT]</sup>  $\text{CuSO}_4 \cdot 5\text{H}_2\text{O}$  (0.6 mg, 2.55  $\mu\text{mol}$ ) and sodium ascorbate (0.6 mg, 3.19  $\mu\text{mol}$ ). After stirring overnight at RT or for 30 min. at 40 °C in a sonicator bath, the reaction was diluted with brine (10 mL) and extracted with EtOAc (5 x 5 mL). The organic extracts were combined, dried over  $\text{MgSO}_4$ , filtered and concentrated. Normal phase flash-column chromatography ( $\text{SiO}_2$ ;  $\text{CH}_2\text{Cl}_2/\text{MeOH} = 97:3$ ) yielded 6.0 mg (90%) of triazole **104** as a colorless oil.

$R_f = 0.3$  ( $\text{CH}_2\text{Cl}_2/\text{MeOH} = 97:3$ ).

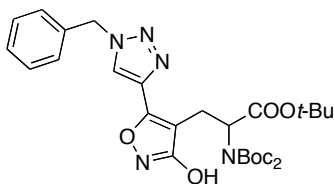
IR (ATR):  $\tilde{\nu} = 2980$  (m), 2934 (w), 2363 (w), 1736 (s), 1701 (s), 1502 (s), 1456 (m), 1367 (s), 1289 (m), 1144 (s)  $\text{cm}^{-1}$ .

$^1\text{H}$  NMR ( $\text{CDCl}_3$ , 600 MHz)  $\delta$  7.82 (s, 1H), 7.43-7.28 (m, 5H), 6.07 ( $m_c$ , 1H), 5.59 (d,  $J = 14.8$  Hz, 1H), 5.55 (d,  $J = 14.8$  Hz, 1H), 5.40 (add,  $J = 17.3$  Hz,  $J = 1.5$  Hz,  $J = 1.5$  Hz), 5.29-5.23 (m, 2H), 4.77 ( $m_c$ , 2H), 3.48 (dd,  $J = 14.7$  Hz,  $J = 4.1$  Hz, 1H), 3.39 (dd,  $J = 14.7$  Hz,  $J = 10.9$  Hz, 1H), 1.47 (s, 9H), 1.36 (s, 18H) ppm.

$^{13}\text{C}$  NMR ( $\text{CDCl}_3$ , 150 MHz)  $\delta$  171.3, 169.1, 159.0, 152.2, 138.3, 134.3, 132.5, 129.4, 129.1, 128.6 (rotamer), 128.3, 127.7 (rotamer), 126.7 (rotamer), 121.9, 118.6, 103.5, 82.6, 81.6, 70.8, 58.4, 54.5, 28.1, 28.0, 21.9 ppm.

HRMS (ESI) Calc. for  $\text{C}_{32}\text{H}_{43}\text{N}_5\text{NaO}_8^+$ : 648.3004  $[\text{M}+\text{Na}]^+$   
 Found: 648.3005  $[\text{M}+\text{Na}]^+$ .

***tert*-butyl 3-(5-(1-benzyl-1*H*-1,2,3-triazol-4-yl)-3-hydroxyisoxazol-4-yl)-2-(bis(*tert*-butoxycarbonyl)amino)propanoate (**S8**)**

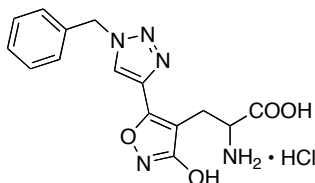


**S8**

To a solution of allyl ether **104** (6.0 mg, 11.4  $\mu\text{mol}$ ) in MeOH (1.5 mL) was added  $\text{Pd}(\text{PPh}_3)_4$  (1.3 mg, 1.14  $\mu\text{mol}$ ) and  $\text{K}_2\text{CO}_3$  (9.5 mg, 68.5  $\mu\text{mol}$ ) at RT and the suspension was stirred for 1 h. Brine (4 mL) was added and the resulting mixture extracted with EtOAc (4 x 3 mL). The combined organic extracts were dried over  $\text{MgSO}_4$ , filtered and concentrated. Normal phase flash column chromatography ( $\text{SiO}_2$ ;  $\text{CH}_2\text{Cl}_2/\text{MeOH} = 95:5$ ) yielded 5.0 mg (90%) of the free hydroxy isoxazole **S8** as a colorless oil, which was used directly in the next step.

$R_f = 0.5$  ( $\text{CH}_2\text{Cl}_2/\text{MeOH} = 9:1$ ).

**2-amino-3-(5-(1-benzyl-1*H*-1,2,3-triazol-4-yl)-3-hydroxyisoxazol-4-yl)propanoic acid hydrochloride (**105**•HCl)**



**105**•HCl

A solution of hydroxyisoxazole **S8** in EtOAc (1 mL) was saturated with HCl (generated from NaCl and conc.  $\text{H}_2\text{SO}_4$ ) and the resulting mixture was stirred for 1 h at RT. The product was triturated with  $\text{Et}_2\text{O}$  and pentane and collected by sedimentation. Thus, 1 mg (30%, 2 steps) of HCl-salt **105**•HCl were obtained as a colorless, hygroscopic solid. Using a modified route, removing the allyl group before the click reaction and then treating the hydroxyisoxazole with HCl-saturated EtOAc as before, the yields could be improved drastically (60%, 2 steps).

$R_f = 0.6$  ( $\text{C}_{18}$ ,  $\text{H}_2\text{O}/\text{MeCN} = 3:2$ ).

m.p. ( $\text{EtOAc}/\text{Et}_2\text{O}$ )  $>180$  (decomp.).

IR (ATR):  $\tilde{\nu}$  = 1734, 1635, 1521, 1497, 1435, 1229, 1179, 1050 (no relative intensities assigned due to strong OH band from hydrate water)  $\text{cm}^{-1}$ .

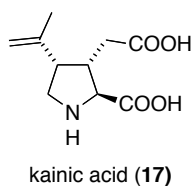
$^1\text{H}$  NMR ( $\text{CDCl}_3$ , 600 MHz)  $\delta$  7.50-7.39 (m, 5H), 5.71 (s, 2H), 3.46 (dd,  $J$  = 9.7 Hz,  $J$  = 4.9 Hz, 1H), 2.88 (dd,  $J$  = 14.3 Hz,  $J$  = 5.0 Hz, 1H), 2.66 (dd,  $J$  = 14.3,  $J$  = 9.7 Hz, 1H) (1 H obscured) ppm.

$^{13}\text{C}$  NMR ( $\text{CDCl}_3$ , 150 MHz)  $\delta$  182.2, 177.4, 156.6, 137.7, 134.6, 129.1, 128.8, 128.1, 106.8, 55.6, 54.0, 27.6 (1 C obscured) ppm.

HRMS (ESI) Calc. for  $\text{C}_{15}\text{H}_{15}\text{N}_5\text{NaO}_4^+$ : 352.1016  $[\text{M}+\text{Na}]^+$   
 Found: 352.1014  $[\text{M}+\text{Na}]^+$ .

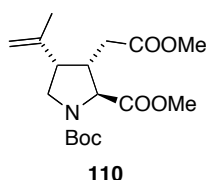
#### 4) A Kainate-Derived Photoswitch – Synthetic Procedures

##### Kainic acid (17)

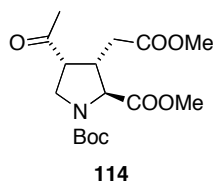


Kainic acid (**17**) was synthesized from (+)-carvone according to known procedures.<sup>[149]</sup> The spectral data matched those reported previously.

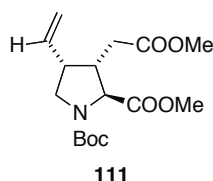
##### (2*S*,3*S*,4*S*)-1-*tert*-butyl 2-methyl 3-(2-methoxy-2-oxoethyl)-4-(prop-1-en-2-yl)pyrrolidine-1,2-dicarboxylate (**110**)



Boc-protected kainic acid dimethyl ester (**110**) was synthesized according to known literature procedures.<sup>[83a, 146c]</sup> The spectral data matched those reported previously.

**(2*S*,3*S*,4*R*)-1-*tert*-butyl 2-methyl 4-acetyl-3-(2-methoxy-2-oxoethyl)pyrrolidine-1,2-dicarboxylate (**114**)**

Ketone **114** was synthesized according to known literature procedures.<sup>[83a]</sup> The spectral data matched those reported previously.

**(2*S*,3*S*,4*R*)-1-*tert*-butyl 2-methyl 3-(2-methoxy-2-oxoethyl)-4-vinylpyrrolidine-1,2-dicarboxylate (**111**)**

To a solution of ketone **114** (20 mg, 58.2  $\mu$ mol) in THF (2 mL) was added KHMDS (128  $\mu$ L, 64.1  $\mu$ mol; 0.5 M in toluene) at -78 °C and the mixture was stirred for 25 min. To this, a precooled solution of PhNTf<sub>2</sub> (25.0 mg, 69.9  $\mu$ mol) in THF (1 mL) was added drop-wise and stirring was continued for 1.5 h. The reaction was quenched by addition of saturated aqueous NH<sub>4</sub>Cl (5 mL) and was allowed to warm to room temperature. The biphasic mixture was extracted with ethyl acetate (3 x 10 mL) and the combined organic extracts were dried over MgSO<sub>4</sub>, filtered and concentrated.

$R_f$  (OTf ether) = 0.4 (CH<sub>2</sub>Cl<sub>2</sub>/EtOAc = 20:1).

To a solution of the crude triflic enol ether in DMF (2 mL) was added PPh<sub>3</sub> (3.06 mg, 11.6  $\mu$ mol) and the mixture was degassed with Ar for 10 min. NEt<sub>3</sub> (24.3  $\mu$ L, 175  $\mu$ mol) and Pd(OAc)<sub>2</sub> (1.31 mg, 5.58  $\mu$ mol) were added. The reaction was stirred for 5 min. at room temperature, formic acid (6.04  $\mu$ L, 160  $\mu$ mol) was added and the mixture stirred at 60 °C for 30 min. (Note: after some minutes, the reaction color changes from yellow to dark red/brownish within a couple seconds.) After cooling to room temperature, the reaction mixture was diluted with saturated aqueous NH<sub>4</sub>Cl (20 mL) and extracted with ethyl acetate (3 x 20 mL). The combined organic extracts were dried over MgSO<sub>4</sub>, filtered and concentrated. Normal phase flash column chromatography (SiO<sub>2</sub>; CH<sub>2</sub>Cl<sub>2</sub>:EtOAc = 22:1) yielded 5.0 mg (26%) of protected *nor*-kainic acid **111** as a colorless oil.

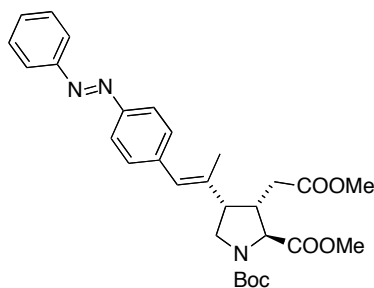


$R_f = 0.3$  ( $\text{CH}_2\text{Cl}_2/\text{EtOAc} = 15:1$ ).

$^1\text{H}$  NMR ( $\text{CDCl}_3$ , 400 MHz; 4:6 ratio of Boc-rotamers)  $\delta$  5.65 (ddd,  $J = 17.1$  Hz,  $J = 10.4$  Hz,  $J = 8.5$  Hz, 1H), 5.19-5.06 (m, 2H), 4.05-3.89 (m, 1H), 3.76-3.72 (m, 3H), 3.71-3.62 (m, 4H), 3.53-3.36 (m, 1H), 3.10-3.00 (m, 1H), 2.78 (m<sub>c</sub>, 1H), 2.55-2.38 (m, 2H), 1.46 (s, 4H), 1.40 (s, 5H) ppm.

$^{13}\text{C}$  NMR ( $\text{CDCl}_3$ , 100 MHz; Boc-rotamers)  $\delta$  172.9, 172.6, 172.2 (2x), 154.5, 153.8, 134.5, 118.3, 80.5, 80.4, 63.4, 63.2, 52.5, 52.3, 50.4, 50.1, 44.3, 43.6, 42.9, 33.5, 33.4, 28.5, 28.4 ppm.

**(2*S*,3*S*,4*S*)-1-*tert*-butyl 2-methyl 3-(2-methoxy-2-oxoethyl)-4-((*E*)-1-(4-((*E*)-phenyldiazenyl)phenyl)prop-1-en-2-yl)pyrrolidine-1,2-dicarboxylate (**119**)**



**119**

To a solution of protected kainic acid **110** (200 mg, 586  $\mu\text{mol}$ ) in degassed DMF (20 mL) was added  $\text{Pd}(\text{OAc})_2$  (26.3 mg, 117  $\mu\text{mol}$ ), tetrabutylammonium chloride (212 mg, 762  $\mu\text{mol}$ ),  $\text{NaHCO}_3$  (98.4 mg, 1.17 mmol) and 1-(4-iodophenyl)-2-phenyl-diazene (235 mg, 762  $\mu\text{mol}$ ) and the mixture was 60 °C overnight. Saturated aqueous  $\text{NH}_4\text{Cl}$  (20 mL) and brine (20 mL) were added and the mixture was extracted with EtOAc (3 x 20 mL). The combined organic extracts were washed with 10% aqueous NaCl solution (3 x 20 mL) and brine (1 x 20 mL), were dried over  $\text{MgSO}_4$ , filtered and concentrated. Normal phase flash column chromatography ( $\text{SiO}_2$ ; PE/EtOAc = 5:1 to 3:1) yielded 46 mg (15%) of azobenzene-substituted kainic acid derivative **119** as an orange thick oil.

$R_f = 0.3$  ( $\text{CH}_2\text{Cl}_2/\text{EtOAc} = 4:1$ ).

IR (ATR):  $\tilde{\nu} = 3321$  (w), 1737 (s), 1694 (s), 1575 (m), 1391 (m), 1202 (w), 1161 (w)  $\text{cm}^{-1}$ .

UV ( $\text{CH}_2\text{Cl}_2$ ):  $\lambda_{\text{max}} = 344$  nm.

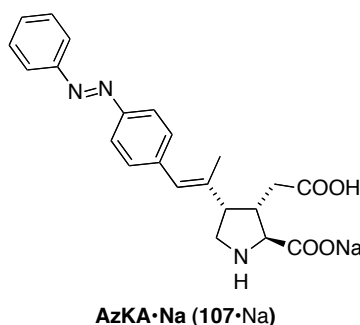
$[\alpha]_D^{24} = -38.0$  ( $c = 0.1$ ,  $\text{CH}_2\text{Cl}_2$ ).

$^1\text{H}$  NMR ( $\text{CDCl}_3$ , 400 MHz; 2:3 mixture of rotamers)  $\delta$  7.94-7.85 (m, 4H), 7.55-7.44 (m, 3H), 7.36-7.32 (m, 2H), 6.30 (s, 1H), 4.20 (d,  $J = 3.8$  Hz, 0.4 H), 4.11 (d,  $J = 4.1$  Hz, 0.5H), 3.87-3.73 (m, 4H), 3.73-3.57 (m, 4H), 3.28-3.16 (m, 1H), 3.04-2.94 (m, 1H), 2.51-2.32 (m, 2H), 1.87 (s, 3H), 1.52-1.40 (m, 9H) ppm.

$^{13}\text{C}$  NMR ( $\text{CDCl}_3$ , 100 MHz; 2:3 mixture of rotamers)  $\delta$  172.8, 172.6, 172.4, 172.3, 154.4, 153.8, 152.8, 151.1, 140.3, 136.5, 136.4, 131.1 (2x) 129.8 (2x), 129.2, 127.4, 127.2, 122.9 (2x), 80.6, 64.3, 64.0, 52.6, 52.4, 52.1 (2x), 48.3, 48.0, 47.8, 47.6, 42.7, 41.7, 33.5 (2x), 28.6, 28.4, 18.0, 17.8 ppm.

HRMS (ESI) Calc. for  $\text{C}_{29}\text{H}_{36}\text{N}_3\text{O}_6^+$ : 522.2595  $[\text{M}+\text{H}]^+$   
Found: 522.2599  $[\text{M}+\text{H}]^+$ .

#### AzKA•Na (107•Na)



Protected kainic acid derivative 119 (25 mg, 47.9  $\mu\text{mol}$ ) was heated under reflux in 1N KOH (30 mL) and MeOH (just enough to dissolve everything) for 18 h. MeOH was distilled off and the mixture was heated under reflux for another 18h. The mixture was acidified to pH = 3 by addition of AcOH, solids were filtered off and washed with water. The filtrate was neutralized by addition of saturated aqueous  $\text{NaHCO}_3$  solution and placed on a RP18 column. Reversed phase flash column chromatography ( $\text{C}_{18}$ ;  $\text{H}_2\text{O}/\text{MeCN} = 100:0$  to 50:50) yielded 12 mg (60%) of the sodium salt AzKA•Na (107•Na) as an orange solid.

$R_f = 0.4$  ( $\text{C}_{18}$ ;  $\text{H}_2\text{O}/\text{MeCN} = 3:2$ ).

IR (ATR):  $\tilde{\nu} = 2927$  (w), 1628 (m), 1576 (s), 1437 (m), 1392 (s), 1223 (m), 1049 (m)  $\text{cm}^{-1}$ .

UV (HEPES-ringer):  $\lambda_{\max}$  = 368 nm.

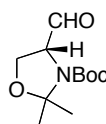
$^1\text{H}$  NMR ( $\text{D}_2\text{O}$ , 400 MHz)  $\delta$  7.52-7.21 (m, 7H), 6.99 (d,  $J$  = 8.2 Hz, 2H), 5.82 (s, 1H), 3.16 (d,  $J$  = 3.4 Hz, 1H), 3.02-2.88 (m, 1H), 2.73-2.53 (m, 3H), 2.06-1.89 (m, 2H), 1.60 (s, 3H) ppm.

$^{13}\text{C}$  NMR ( $\text{D}_2\text{O}$ , 100 MHz)  $\delta$  181.3 (2x), 151.8, 149.6, 141.3, 139.2, 129.7, 129.3, 125.3, 122.2 (2x), 67.0, 50.5, 47.3, 44.1, 37.4, 18.1 ppm.

HRMS (ESI) Calc. for  $\text{C}_{22}\text{H}_{24}\text{N}_3\text{O}_4^+$ : 394.1761  $[\text{M}+\text{H}]^+$   
 Found: 394.1759  $[\text{M}+\text{H}]^+$ .

## 5) 3-D-Substituted Glutamate Analogues – Synthetic Procedures

### (*S*)-Garner's aldehyde (**123**)

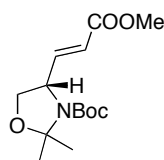


**123**

(*S*)-Garner's aldehyde (**123**) was synthesized according to literature procedures and used directly in the next step.<sup>[157]</sup> The spectral data matched those reported previously.

$R_f$  = 0.6 (PE/EtOAc = 2:1).

### (*S,E*)-*tert*-butyl 4-(3-methoxy-3-oxoprop-1-enyl)-2,2-dimethyloxazolidine-3-carboxylate (**122a**)



*E*: **122a**  
*Z*: **122b**

To a solution of the (*S*)-Garner's aldehyde **123** (3.97 g, 17.3 mmol) in MeCN (80 mL), lithium chloride (0.806 g, 19.0 mmol), DIPEA (3.30 mL, 19.0 mmol) and trimethyl phosphonoacetate (3.47 g, 19.0 mmol) were added at 0 °C. The mixture was stirred for 3 h at 0 °C and then 1 h at RT. Water (160 mL) was added to the reaction mixture and the acetonitrile was removed under reduced pressure. The residue was extracted with ether (4 x 100 mL) and the combined

organic extracts were washed with aqueous HCl (1 M, 100 mL) and brine (100 mL), dried over  $\text{MgSO}_4$  and concentrated. Normal phase flash column chromatography ( $\text{SiO}_2$ ; PE/EtOAc = 14:1 to 10:1) yielded 3.01 g (61%) of enone **122a** and 1.20 g (24%) of its *Z*-isomer **122b** as colorless solids.

$R_f = 0.4$  (PE/EtOAc = 4:1);  $R_f$  (*Z*-isomer) = 0.6 (PE/EtOAc = 4:1).

IR (ATR):  $\tilde{\nu} = 3388$  (w), 2975 (m), 1721 (s), 1697 (s), 1660 (m), 1364 (m), 1167 (m)  $\text{cm}^{-1}$ .

$[\alpha]_D^{18} = +63.6$  ( $c = 0.5$ ,  $\text{CH}_2\text{Cl}_2$ ).

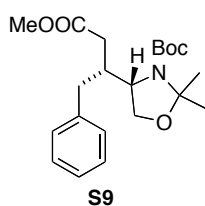
$^1\text{H}$  NMR ( $\text{CDCl}_3$ , 400 MHz, rotamers)  $\delta$  6.85-6.73 (m, 1H), 5.89 (dd,  $J = 1.2$  Hz,  $J = 15.6$  Hz, 1H), 4.61-4.31 (m, 1H), 4.08 (dd,  $J = 9.1$ ,  $J = 6.4$  Hz, 1H), 3.78 (dd,  $J = 9.1$ ,  $J = 2.4$  Hz, 1H), 3.74 (br s, 3H), 1.69-1.32 (m, 15H) ppm.

$^{13}\text{C}$  NMR ( $\text{CDCl}_3$ , 100 MHz, rotamers)  $\delta$  167.5, 153.0, 147.9 (2x), 122.8, 95.3, 81.1, 68.4, 59.2 (2x), 52.2, 28.9, 27.5, 24.7 ppm.

HRMS (ESI) Calc. for  $\text{C}_{14}\text{H}_{27}\text{N}_2\text{O}_5^+$ : 303.1914  $[\text{M}+\text{NH}_4]^+$

Found: 303.1914  $[\text{M}+\text{NH}_4]^+$ .

**(*S*)-tert-butyl 4-((*R*)-4-methoxy-4-oxo-1-phenylbutan-2-yl)-2,2-dimethyloxazolidine-3-carboxylate (**S9**)**



To a suspension of LiBr (541 mg, 6.3 mmol) and  $\text{CuBr} \cdot \text{SMe}_2$  (647.4 mg, 3.1 mmol, 3.0 eq) in THF (10.8 mL) was drop-wise added benzylmagnesium chloride (6.3 mL, 6.3 mmol; 1 M in THF) and the mixture was stirred for 40 min. A pre-cooled solution of oxazolidine **122a** (300 mg, 1.05 mmol) and  $\text{TMSCl}$  (402  $\mu\text{L}$ , 3.14 mmol) in THF (9 mL) was added in portions and the reaction was stirred 2 h at  $-40^\circ\text{C}$ . The reaction was quenched by addition of saturated aqueous  $\text{NH}_4\text{Cl}$  (6 mL) and the biphasic mixture was allowed to warm to RT. More saturated ammonium chloride solution (30 mL) was added and the phases were separated. The

aqueous phase was extracted with EtOAc (4 x 50 mL) and the combined organic phases were washed with brine (50 mL), dried over  $\text{MgSO}_4$ , filtered and concentrated. Purification by normal phase flash column chromatography ( $\text{SiO}_2$ ; PE/EtOAc = 10:1) yielded 344 mg (87%) of ester **S9** as a colorless oil.

$R_f = 0.6$  (PE/EtOAc = 4:1).

IR (ATR):  $\tilde{\nu} = 2976$  (m), 1735 (s), 1693 (s), 1363 (m), 1162 (m)  $\text{cm}^{-1}$ .

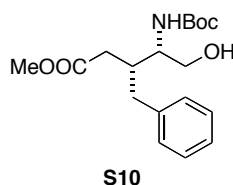
$[\alpha]_D^{18} = +9.6$  (c = 0.25,  $\text{CH}_2\text{Cl}_2$ ).

$^1\text{H}$  NMR ( $\text{CD}_3\text{CN}$  400 MHz, 70 °C)  $\delta$  7.32-7.25 (m, 2H), 7.24-7.15 (dd,  $J = 8.1$ ,  $J = 6.4$  Hz, 3H), 3.97-3.88 (m, 2H), 3.84-3.77 (m, 1H), 3.55 (s, 3H), 2.90-2.78 (m, 1H), 2.68 (dd,  $J = 13.8$ ,  $J = 6.5$  Hz, 1H), 2.51 (dd,  $J = 15.9$ ,  $J = 4.3$  Hz, 2H), 2.24-2.11 (m, 1H), 1.59-1.29 (m, 15H) ppm.

$^{13}\text{C}$  NMR ( $\text{CD}_3\text{CN}$ , 100 MHz, 70 °C)  $\delta$  174.4, 153.8, 141.2, 130.4, 129.5, 127.3, 95.2, 80.9, 64.8, 60.0, 52.0 (2x), 39.92, 39.14, 35.01, 28.95, 27.09, 23.75, 1.32. ppm.

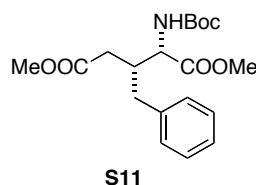
HRMS (ESI) Calc. for  $\text{C}_{21}\text{H}_{32}\text{NO}_5^+$ : 378.2275  $[\text{M}+\text{H}]^+$   
 Found: 378.2274  $[\text{M}+\text{H}]^+$ .

**(3R,4S)-methyl 3-benzyl-4-(tert-butoxycarbonylamino)-5-hydroxypentanoate (S10)**



To a solution of oxazolidine **S9** (343 mg, 0.913 mmol) and *p*TsOH (26.1 mg, 0.137 mmol) in MeOH (10 mL) was added water (8.2  $\mu\text{L}$ , 0.46 mmol) and the reaction was stirred for 3 d at RT. Pyridine (19.2  $\mu\text{L}$ , 0.237 mmol) was added and the reaction mixture was concentrated. The residue was purified using normal phase flash column chromatography ( $\text{SiO}_2$ ;  $\text{CH}_2\text{Cl}_2/\text{MeOH} = 98:2$ ) to yield 277 mg (90%) of alcohol **S10** as a colorless oil which was used directly in the next step without further characterization.

$R_f = 0.3$  ( $\text{CH}_2\text{Cl}_2/\text{MeOH} = 97.5:2.5$ ).

**(2*S*,3*R*)-dimethyl 3-benzyl-2-(*tert*-butoxycarbonylamino)pentanedioate (S11)**

To a biphasic mixture of alcohol **S10** (200 mg, 0.622 mmol) in CH<sub>2</sub>Cl<sub>2</sub> (3 mL) and water (6 mL) was added TEMPO (48 μL, 0.311 mmol) and DAIB (501 mg, 1.56 mmol). The reaction mixture was stirred 3 h at RT, when water (60 mL) was added and the pH was adjusted with KHSO<sub>4</sub> to pH = 2. The phases were separated and the aqueous solution was extracted with EtOAc (6 x 30 mL). The combined organic extracts were dried over Na<sub>2</sub>SO<sub>4</sub>, filtered and concentrated. The residue was dissolved in MeOH (20 mL) and the resulting solution was cooled to 0 °C. TMS-diazomethane (3.9 mL, 8.28 mmol) was added in portions over 3 h. The excess of the reagent was quenched by addition of acetic acid (267 μL, 4.67 mmol) and the crude reaction mixture was concentrated. Purification by normal phase flash column chromatography (SiO<sub>2</sub>; PE/EtOAc = 7:1) yielded 151 mg (68%, 2 steps) of diester **S11** as a colorless oil.

$R_f = 0.3$  (PE/EtOAc = 4:1).

IR (ATR):  $\tilde{\nu} = 3368$  (m), 2952 (m), 1735 (s), 1711 (s), 1365 (m), 1162 (m) cm<sup>-1</sup>.

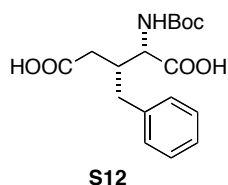
$[\alpha]_D^{18} = +26.8$  (c = 0.5, CH<sub>2</sub>Cl<sub>2</sub>).

<sup>1</sup>H NMR (CDCl<sub>3</sub>, 400 MHz)  $\delta$  7.29-7.23 (m, 2H), 7.21-7.17 (m, 1H), 7.14 (dd,  $J = 8.1$  Hz,  $J = 1.4$  Hz, 2H), 5.11 (d,  $J = 8.3$  Hz, 1H), 4.59 (d,  $J = 8.1$  Hz, 1H), 3.66 (s, 3H), 3.59 (s, 3H), 2.91-2.80 (m, 1H), 2.64 (dd,  $J = 13.8$ ,  $J = 5.7$  Hz, 1H), 2.5-2.33 (m, 2H), 2.30-2.14 (m, 1H), 1.38 (s, 9H) ppm.

<sup>13</sup>C NMR (CDCl<sub>3</sub>, 100 MHz)  $\delta$  172.8, 172.45, 155.8, 138.7, 129.4, 128.6, 126.7, 80.2, 55.8, 52.5, 51.9, 51.8, 39.8, 36.3, 35.1, 28.4 ppm.

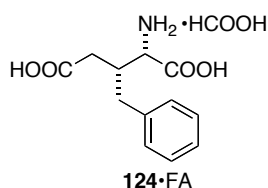
HRMS (ESI) Calc. for C<sub>19</sub>H<sub>27</sub>KNO<sub>6</sub><sup>+</sup>: 404.1470 [M+K]<sup>+</sup>

Found: 404.1475 [M+K]<sup>+</sup>.

**(2*S*,3*R*)-3-benzyl-2-(*tert*-butoxycarbonylamino)pentanedioic acid (**S12**)**

To a solution of diester **S12** (121 mg, 365  $\mu$ mol) in THF/water (6 mL, 1:1) was added LiOH (159 mg, 6.62 mmol) at 0 °C and the reaction mixture was stirred for 90 min at RT. The biphasic mixture was acidified by addition of FA (235  $\mu$ L, 6.62 mmol) and subsequently purified using reverse phase flash column chromatography (C18, H<sub>2</sub>O/MeCN/FA = 100:0:0.1% to 3:2:0.1%) to yield 91 mg (80%) of diacid **S12** as a colorless solid, which was used directly in the next step.

$R_f$  = 0.4 (C18, H<sub>2</sub>O/MeCN/FA = 4:1:0.1%)

**(2*S*,3*R*)-2-amino-3-benzylpentanedioic acid formate salt (**124•FA**)**

Diacid **S12** (90.5 mg, 0.268 mmol) was treated with a saturated solution of HCl in EtOAc (6 mL) and stirred overnight at RT. The product was precipitated by addition of Et<sub>2</sub>O (90 mL) and collected by sedimentation. Due to formation of byproducts, the product was purified by reversed phase flash column chromatography (C18, water/0.1% FA) to yield 10 mg (15%) of formate salt **124•FA** as a colorless solid.

$R_f$  = 0.2 (C18, H<sub>2</sub>O/0.1% FA).

m.p. (H<sub>2</sub>O) > 300 °C (decomp.).

IR (ATR):  $\tilde{\nu}$  = 3511 (m), 2583 (m), 2786 (m), 1601 (s), 1421 (s), 1365 (m), 1162 (m) cm<sup>-1</sup>.

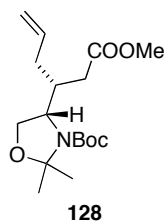
$[\alpha]_D^{18}$  = +14.0 (c = 0.2, H<sub>2</sub>O).

<sup>1</sup>H NMR (D<sub>2</sub>O, 400 MHz)  $\delta$  7.32-7.21 (m, 2H), 7.20-7.11 (m, 3H), 3.25-3.19 (m, 1H), 2.60-2.46 (m, 1H), 2.41-2.29 (m, 2H), 2.15-2.01 (m, 1H), 2.00-1.89 (m, 1H) ppm.

$^{13}\text{C}$  NMR ( $\text{D}_2\text{O}$ , 100 MHz)  $\delta$  181.8, 181.6, 140.5, 129.4, 128.4, 126.0, 57.9, 42.1, 39.0, 35.0 ppm.

HRMS (ESI) Calc. for  $\text{C}_{12}\text{H}_{14}\text{NO}_4^-$ : 236.0928  $[\text{M}-\text{H}]^-$   
Found: 236.0927  $[\text{M}-\text{H}]^-$ .

**(S)-tert-butyl 4-((R)-1-methoxy-1-oxohex-5-en-3-yl)-2,2-dimethyloxazolidine-3-carboxylate (**128**)**

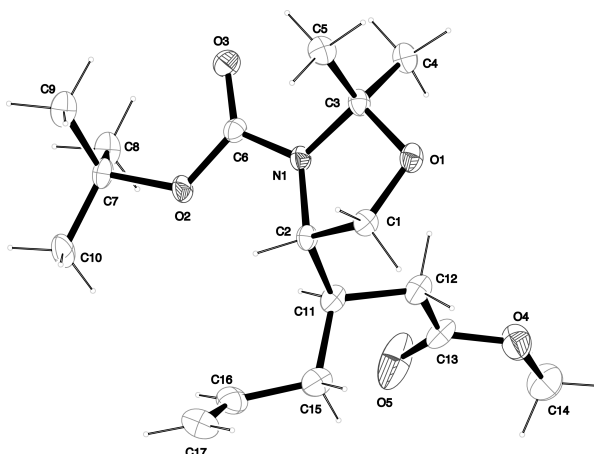


To a solution of tetraallyl tin (593  $\mu\text{L}$ , 2.47 mmol) in  $\text{Et}_2\text{O}$  (5 mL) was added MeLi (5.2 mL, 10.3 mmol; 1.6 M in  $\text{Et}_2\text{O}$ ) at 0  $^\circ\text{C}$  and the mixture was stirred for 20 min. This salt-free allyllithium solution was transferred to a suspension of  $\text{CuBr}\cdot\text{SMe}_2$  (984 mg, 4.80 mmol) and  $\text{SMe}_2$  (8.3 mL, 114 mmol) in  $\text{Et}_2\text{O}$  (15 mL) at -78  $^\circ\text{C}$  and then stirred for 10 min. To the dark mixture was added a solution of oxazolidine **122a** (447 mg, 1.6 mmol) and  $\text{TMSCl}$  (599  $\mu\text{L}$ , 4.70 mmol) in  $\text{Et}_2\text{O}$  (5 mL) in portions. After stirring for 16 h at -78  $^\circ\text{C}$ , the reaction mixture was warmed to -60  $^\circ\text{C}$  and stirred at that temperature for further 3 h before it was quenched by fast addition of saturated aqueous  $\text{NH}_4\text{Cl}$  (30 mL). After warming to RT, more saturated  $\text{NH}_4\text{Cl}$  (20 mL) was added to dissolve all of the precipitate. The mixture was stirred until the lower, aqueous phase turned blue.  $\text{EtOAc}$  (20 mL) was added, the phases were separated and the aqueous phase was extracted with  $\text{EtOAc}$  (4 x 50 mL). The combined organic extracts were washed with aqueous KF (10 mL; 10%), dried over  $\text{MgSO}_4$ , filtered and concentrated. Normal phase flash column chromatography ( $\text{SiO}_2$ ;  $\text{PE}/\text{EtOAc}$  = 10:1) gave 345 mg (67%) of allylated ester **128** as a colorless solid and a single diastereomer, which was proven by X-ray crystallography (P. Mayer). Suitable crystals for X-ray analysis were grown by diffusion of PE into a solution of **128** in  $\text{Et}_2\text{O}$ .



**Supporting Table 1.** Crystallographic data for **128**.

net formula	C <sub>17</sub> H <sub>29</sub> NO <sub>5</sub>
<i>M<sub>r</sub></i> /g mol <sup>-1</sup>	327.416
crystal size/mm	0.50 × 0.15 × 0.11
<i>T</i> /K	173(2)
radiation	MoKα
diffractometer	'Oxford XCalibur'
crystal system	triclinic
space group	<i>P</i> 1
<i>a</i> /Å	5.9071(11)
<i>b</i> /Å	9.248(2)
<i>c</i> /Å	9.547(2)
α/°	102.27(2)
β/°	104.524(19)
γ/°	103.797(19)
<i>V</i> /Å <sup>3</sup>	469.29(17)
<i>Z</i>	1
calc. density/g cm <sup>-3</sup>	1.1585(4)
μ/mm <sup>-1</sup>	0.084
absorption correction	'multi-scan'
transmission factor range	0.77914–1.00000
refls. measured	2925
<i>R</i> <sub>int</sub>	0.0382
mean σ( <i>I</i> )/ <i>I</i>	0.0655
θ range	4.53–25.48
observed refls.	1393
<i>x</i> , <i>y</i> (weighting scheme)	0.0801, 0
hydrogen refinement	constr
Flack parameter	−0.7(19)
refls in refinement	2140
parameters	208
restraints	3
<i>R</i> ( <i>F</i> <sub>obs</sub> )	0.0514
<i>R</i> <sub>w</sub> ( <i>F</i> <sup>2</sup> )	0.1298
<i>S</i>	0.924
shift/error <sub>max</sub>	0.001
max electron density/e Å <sup>-3</sup>	0.293
min electron density/e Å <sup>-3</sup>	−0.174

**Supporting Figure 1.** X-Ray crystal structure of **128**.

$R_f = 0.6$  (PE/EtOAc = 4:1).

m.p. (PE/Et<sub>2</sub>O) = 61-64 °C.

IR (ATR):  $\tilde{\nu} = 3367$  (m), 3075 (w), 2975 (m), 1737 (s), 1689 (s), 1363 (s), 1164 (m) cm<sup>-1</sup>.

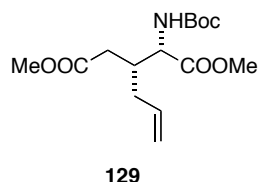
$[\alpha]_D^{18} = +13.2$  (c = 0.5, CH<sub>2</sub>Cl<sub>2</sub>).

<sup>1</sup>H NMR (CDCl<sub>3</sub>, 600 MHz; rotamers)  $\delta$  5.83-5.67 (m, 1H), 5.07-4.98 (m, 2H), 4.12-2.86 (m, 2H), 3.79 (dd,  $J = 9.3$  Hz,  $J = 1.8$  Hz, 1H), 3.64 (s, 3H), 2.71-2.45 (m, 2H), 2.25-2.09 (m, 2H), 1.66-1.52 (m, 3H), 1.48 (s, 9H), 1.44 (s, 3H) ppm.

<sup>13</sup>C NMR (CDCl<sub>3</sub>, 150 MHz; rotamers)  $\delta$  207.0, 173.7, 136.2, 117.0, 94.5, 94.0, 80.29, 63.8, 59.5, 58.6, 51.6, 36.8, 36.4, 34.2, 33.9, 28.6, 28.5, 27.0, 26.3, 24.1, 22.6 ppm.

HRMS (ESI) Calc. for C<sub>17</sub>H<sub>29</sub>KNO<sub>5</sub><sup>+</sup>: 366.1677 [M+K]<sup>+</sup>  
Found: 366.1683 [M+K]<sup>+</sup>.

**(2*S*,3*R*)-dimethyl 3-allyl-2-(*tert*-butoxycarbonylamino)pentanedioate (**129**)**



To a solution of hemi-aminal **128** (500 mg, 1.53 mmol) in acetone (50 mL) was added Jones Reagent (3.43 mL, 9.16 mmol; 2.67 M) at 0 °C and the mixture was allowed to warm to 15 °C over 4 h. Excess of Jones Reagent was quenched by addition of *i*-PrOH and stirring for 15 min at RT. The pH was adjusted to pH = 3-4 by addition of saturated aqueous NaHCO<sub>3</sub>. The mixture was diluted with EtOAc (100 mL) and solids were filtered off over a celite-plug eluting with EtOAc. To the biphasic mixture was added brine (100 mL) and 2N HCl (a few drops to ensure pH = 3-4) and extracted with EtOAc (3 x 50 mL). The combined organic extracts were dried over Na<sub>2</sub>SO<sub>4</sub>, filtered and concentrated. The residue was dried on high-vacuum, dissolved in MePh/MeOH (7:1, 80 mL) and TMSCHN<sub>2</sub> (1.15 mL, 2.29 mmol; 2M in hexanes) was drop-wise added at 0°C. Stirring was continued for 15 min, then the excess of TMSCHN<sub>2</sub> was destroyed by addition of AcOH. The solvent was removed under reduced pressure and the residue was purified using normal phase flash column chromatography

(SiO<sub>2</sub>; PE/EtOAc = 7:1) to yield 406 mg (84%; 2 steps) of dimethyl ester **129** as a colorless oil.

$R_f = 0.4$  (PE/EtOAc = 4:1).

IR (ATR):  $\tilde{\nu} = 3372$  (w), 3077 (w), 2977 (w), 1735 (s), 1711 (s), 1366 (m), 1157 (s) cm<sup>-1</sup>.

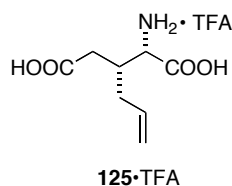
$[\alpha]_D^{18} = +26.8$  (c = 0.5, CH<sub>2</sub>Cl<sub>2</sub>).

<sup>1</sup>H NMR (CDCl<sub>3</sub>, 400 MHz)  $\delta$  5.76-5.61 (m, 1H), 5.20-5.12 (m, 1H), 5.10-5.02 (m, 2H), 4.55-4.47 (m, 1H), 3.73 (s, 3H), 3.66 (s, 3H), 2.62-2.49 (br m, 1H), 2.37 (dd,  $J = 16.7$  Hz,  $J = 7.6$  Hz, 1H), 2.29 (dd,  $J = 16.7$  Hz,  $J = 6.3$  Hz, 1H), 2.14-2.06 (m, 1H), 2.03-1.92 (m, 1H), 1.42 (s, 9H) ppm.

<sup>13</sup>C NMR (CDCl<sub>3</sub>, 100 MHz)  $\delta$  172.9, 172.4, 155.7, 135.2, 118.0, 80.1, 55.8, 52.4, 51.8, 37.6, 35.1, 34.8, 28.4 ppm.

HRMS (ESI) Calc. for C <sub>15</sub> H <sub>24</sub> NO <sub>6</sub> <sup>-</sup> :	314.1609 [M-H] <sup>-</sup>
Found:	314.1607 [M-H] <sup>-</sup> .

### (2*S*,3*R*)-3-allyl-2-aminopentanedioic acid TFA salt (**125**•TFA)



To a solution of diester **129** (150 mg, 0.476 mmol) in THF/water (7 mL, 1:1) was added LiOH (228 mg, 9.51 mmol) and the reaction was stirred for 4 h at 0 °C. The reaction was quenched by addition of formic acid (313  $\mu$ L, 9.51 mmol) and the pH value was adjusted with KHSO<sub>4</sub> to pH = 2. The resulting mixture was diluted with water (5 mL) and the aqueous solution was extracted with EtOAc (6 x 10 mL). The combined organic extracts were dried over Na<sub>2</sub>SO<sub>4</sub>, filtered and concentrated. The residue was cooled to 0 °C, dissolved in TFA/CH<sub>2</sub>Cl<sub>2</sub> (9 mL, 1:1) and stirred for 2 h. Water (10 mL) was added and the crude reaction mixture was concentrated. The resulting syrup was re-dissolved in water (15 mL) and

extracted with EtOAc (1 x 5 mL) and ether (1 x 5 mL). The aqueous layer was lyophilized over night to yield 120 mg (89%) of TFA-salt **125**•TFA as a colorless solid.

$R_f = 0.6$  (C18; H<sub>2</sub>O, 0.1% FA).

IR (ATR):  $\tilde{\nu} = 3372$  (w), 2972 (m), 2551 (w), 1974 (br), 1656 (m), 1418 (m), 1182 (s), 1140 (s) cm<sup>-1</sup>.

m.p. (H<sub>2</sub>O) = 117-122 °C (decomp).

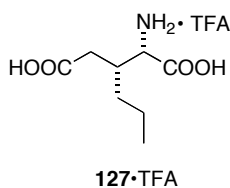
$[\alpha]_D^{18} = +10.0$  (c = 0.2, H<sub>2</sub>O).

<sup>1</sup>H NMR (D<sub>2</sub>O, 400 MHz)  $\delta$  5.67-5.54 (m, 1H), 4.91-4.80 (m, 2H), 3.01 (d,  $J = 4.0$  Hz, 1H), 2.05-1.91 (m, 3H), 1.90-1.71 (m, 2H) ppm.

<sup>13</sup>C NMR (D<sub>2</sub>O, 100 MHz)  $\delta$  182.0, 181.8, 136.9, 116.6, 58.3, 39.6, 39.5, 33.6 ppm.

HRMS (ESI) Calc. for C <sub>15</sub> H <sub>24</sub> NO <sub>6</sub> <sup>-</sup> :	186.0766 [M-H] <sup>-</sup>
Found:	186.0771 [M-H] <sup>-</sup>

**(2S,3R)-2-amino-3-propylpentanedioic acid TFA salt (**127**•TFA)**



To a solution of 3-allyl-glutamic acid TFA salt **125**•TFA (20 mg, 69.9  $\mu$ mol) in MeOH (3 mL) was added Pd/C (7.5 mg, 7.0  $\mu$ mol; 10% on charcoal) and the vessel was purged with N<sub>2</sub> and then charged with H<sub>2</sub>. After stirring for 4.5 h at RT, solids were filtered off over a short celite column (eluting with MeOH) and the solvent was removed under reduced pressure to yield 20 mg (quant.) of glutamate-analogue TFA salt **127**•TFA as a colorless solid.

$R_f = 0.6$  (C18; H<sub>2</sub>O, 0.1% FA).

IR (ATR):  $\tilde{\nu}$  = 3217 (m), 2963 (m), 2545 (w), 1994 (br), 1710 (s), 1581 (s), 1431 (m), 1209 (s)  $\text{cm}^{-1}$ .

m.p. (MeOH) > 117 °C (decomp).

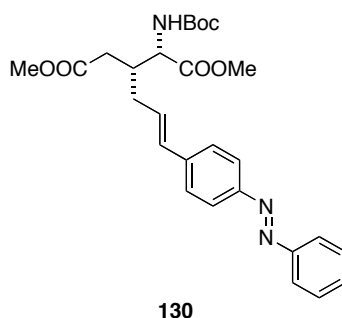
$[\alpha]_D^{18} = +6.0$  (c = 0.1, H<sub>2</sub>O).

<sup>1</sup>H NMR (D<sub>2</sub>O, 400 MHz)  $\delta$  3.85-3.79 (m, 1H), 2.41-2.30 (m, 3H), 1.31-1.13 (m, 4H), 0.80-0.64 (m, 3H) ppm.

<sup>13</sup>C NMR (D<sub>2</sub>O, 100 MHz)  $\delta$  176.6, 172.4, 56.7, 35.2 (2x), 31.7, 19.4, 12.9 ppm.

HRMS (ESI) Calc. for C <sub>8</sub> H <sub>14</sub> NO <sub>4</sub> <sup>-</sup> :	188.0928 [M-H] <sup>-</sup>
Found:	188.0926 [M-H] <sup>-</sup>

**(2*S*,3*R*)-dimethyl 2-(*tert*-butoxycarbonylamino)-3-((*E*)-3-(4-(phenyldiazenyl)phenyl)allyl)pentanedioate (**130**)**



To a solution of diester **129** (150 mg, 476  $\mu\text{mol}$ ) in degassed DMF (20 mL) was added Pd(OAc)<sub>2</sub> (21.4 mg, 95.1  $\mu\text{mol}$ ), NaHCO<sub>3</sub> (79.9 mg, 951  $\mu\text{mol}$ ), tetrabutylammonium chloride (172 mg, 618  $\mu\text{mol}$ ) and 1-(4-iodophenyl)-2-phenyl-diazene (191 mg, 618  $\mu\text{mol}$ ). The suspension was degassed with Ar and then stirred overnight at 60 °C. The reaction was quenched by addition of saturated aqueous NH<sub>4</sub>Cl (20 mL) and the mixture was extracted with EtOAc (3 x 20 mL). The combined organic extracts were washed with 10% aqueous NaCl solution (2 x 30 mL) and brine (1 x 30 mL), dried over MgSO<sub>4</sub>, filtered and concentrated. Normal phase flash column chromatography (SiO<sub>2</sub>; PE/EtOAc = 5:1 to 3:1) yielded 213 mg (90%) of azobenzene **130** as an orange wax.

$R_f$  = 0.4 (PE/EtOAc = 3:1).

IR (ATR):  $\tilde{\nu}$  = 3430 (w), 2960 (w), 1724 (s), 1709 (s), 1507 (m), 1232 (w), 1152 (m)  $\text{cm}^{-1}$ .

UV ( $\text{CH}_2\text{Cl}_2$ ):  $\lambda_{\text{max}}$  = 364 nm.

$[\alpha]_D^{18}$  = +7.0 ( $c$  = 0.1,  $\text{CH}_2\text{Cl}_2$ ).

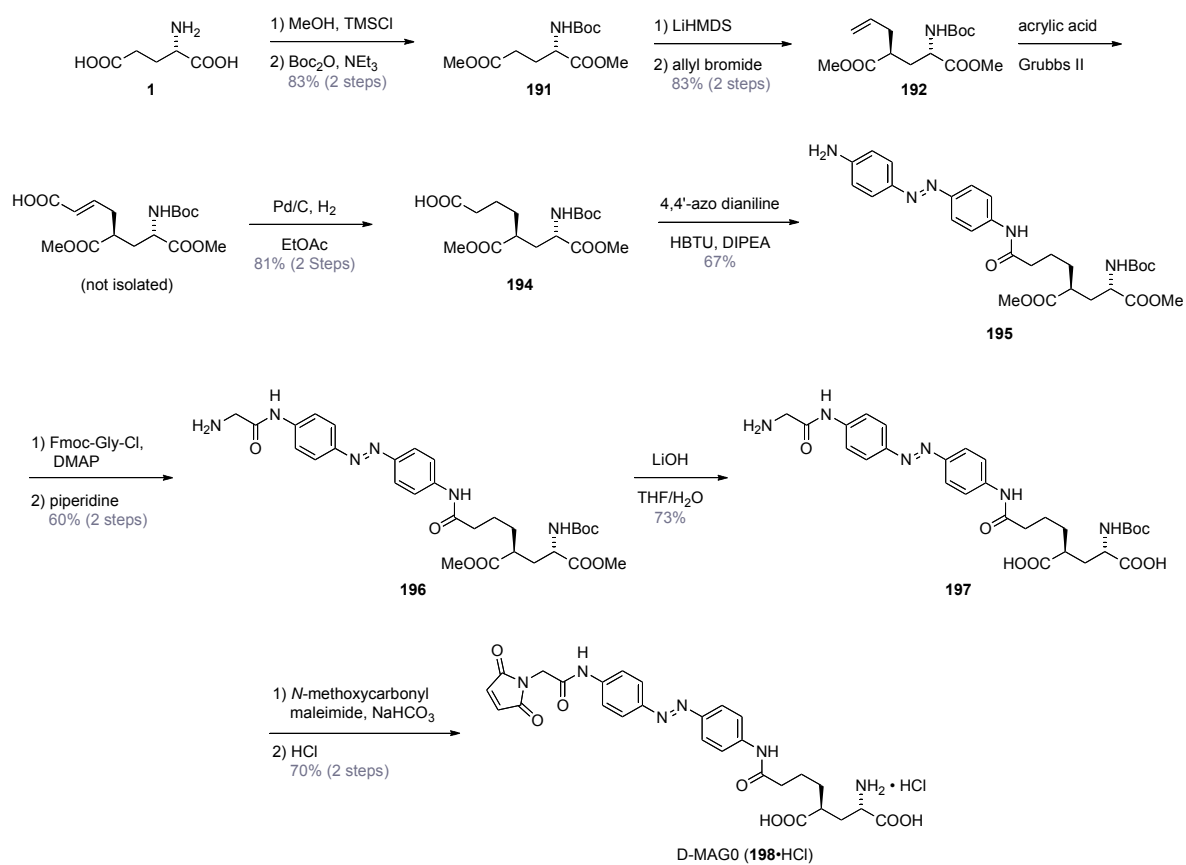
$^1\text{H}$  NMR ( $\text{CDCl}_3$ , 400 MHz)  $\delta$  7.95-7.83 (m, 4H), 7.57-7.41 (m, 5H), 6.47 (d,  $J$  = 15.7 Hz, 1H), 6.28-6.18 (m, 1H), 5.27-5.14 (m, 1H), 4.62-4.50 (m, 1H), 3.73 (s, 3H), 3.64 (s, 3H), 2.81-2.65 (m, 1H), 2.48 (dd,  $J$  = 16.7 Hz,  $J$  = 7.2 Hz, 1H), 2.40-2.27 (m, 2H), 2.25-2.15 (m, 1H), 1.45 (s, 9H) ppm.

$^{13}\text{C}$  NMR ( $\text{D}_2\text{O}$ , 100 MHz)  $\delta$  172.9, 172.4, 155.8, 152.9, 151.9, 139.9, 132.3, 131.0, 129.2, 129.1, 126.9, 123.4, 122.9, 80.3, 56.0, 52.6, 51.9, 38.2, 35.7, 34.2, 28.4 ppm.

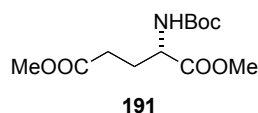
HRMS (ESI) Calc. for  $\text{C}_{27}\text{H}_{33}\text{N}_3\text{NaO}_6^+$ : 518.2262  $[\text{M}+\text{H}]^+$   
 Found: 518.2255  $[\text{M}+\text{H}]^+$ .

## 6) A Photoswitched Tethered Ligand of mGluRs – Synthetic Procedures

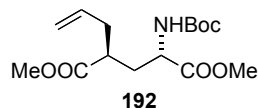
Overview:



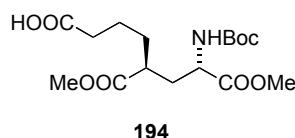
**Supporting Scheme 2.** Stereoselective synthesis of D-MAG0 (**198•HCl**) starting from L-glutamic acid (**1**).

**(*S*)-dimethyl 2-(*tert*-butoxycarbonylamino)pentanedioate (191)**

Boc glutamic acid dimethyl ester **191** was synthesized according to literature procedures.<sup>[189]</sup> The spectral data matched those reported previously.

**(2*S*,4*S*)-dimethyl 2-allyl-4-(*tert*-butoxycarbonylamino)pentanedioate (192)**

Allylated glutamic acid derivative **192** was synthesized according to literature procedures.<sup>[188]</sup> The analytical data matched those reported previously.

**(5*S*,7*S*)-7-(*tert*-butoxycarbonylamino)-8-methoxy-5-(methoxycarbonyl)-8-oxo-octanoic acid (194)**

To a solution of pentanedioate **192** (1.50 g, 4.76 mmol) and freshly distilled acrylic acid (0.46 mL, 6.66 mmol) in degassed CH<sub>2</sub>Cl<sub>2</sub> (25 mL) was added solid Grubbs II catalyst (238 mg, 0.238 mmol) and the mixture was heated under reflux for 4 h. The reaction was allowed to cool to room temperature and was passed over a plug of celite eluting with EtOAc (100 mL). After removal of the solvent under reduced pressure, the tan residue was dissolved in EtOAc (100 mL) and Pd/C (507 mg, 0.476 mmol; 10% Pd on charcoal) was added. The vessel was purged with N<sub>2</sub>, charged with H<sub>2</sub> and the reaction was stirred overnight at room temperature. The mixture was filtered over a plug of celite eluting with EtOAc (100 mL) and the solvent was removed under reduced pressure. Normal phase column chromatography (SiO<sub>2</sub>; CH<sub>2</sub>Cl<sub>2</sub>/EtOAc/AcOH = 4:1:1% to 3:2:1%) yielded 1.40 g (81%, 2 steps) of acid **194** as a tan oil.

$R_f = 0.6$  (CH<sub>2</sub>Cl<sub>2</sub>/EtOAc/AcOH = 3:2:1%).

IR (ATR):  $\tilde{\nu} = 2954$  (w), 1708 (s), 1515 (m), 1436 (m), 1367 (m), 1212 (m), 1157 (s), 1052 (m), 1023 (w) cm<sup>-1</sup>.

$[\alpha]_D^{24} = +8.8$  ( $c = 1.0$ , CH<sub>2</sub>Cl<sub>2</sub>).



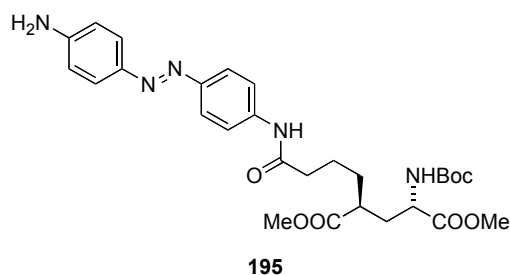
$^1\text{H}$  NMR ( $\text{CDCl}_3$ , 300 MHz)  $\delta$  4.99 (d,  $^3J = 8.6$  Hz, 1H), 4.42-4.25 (m, 1H), 3.72 (s, 3H), 3.68 (s, 3H), 2.60-2.42 (m, 1H), 2.34 (t,  $^3J = 6.7$  Hz, 2H), 2.12-1.86 (m, 2H), 1.76-1.54 (br m, 4H), 1.43 (s, 9H) ppm.

$^{13}\text{C}$  NMR ( $\text{CDCl}_3$ , 75.5 MHz)  $\delta$  178.4, 175.9, 172.9, 155.5, 80.3, 52.6, 52.3, 52.0, 42.0, 34.6, 33.7, 31.7, 28.4, 22.2 ppm.

HRMS (ESI) Calc. for  $\text{C}_{16}\text{H}_{27}\text{NNaO}_8^+$ : 384.1634  $[\text{M}+\text{Na}]^+$

Found: 384.1626  $[\text{M}+\text{Na}]^+$ .

**(2*S*,4*S*)-dimethyl 2-(4-(4-((*E*)-(4-aminophenyl)diazenyl)phenylamino)-4-oxobutyl)-4-(*tert*-butoxycarbonylamino)pentanedioate (**195**)**



To a solution of acid **194** (1.20 g, 3.32 mmol) in DMF (150 mL) was added 4,4'-azo dianiline (1.41 g, 6.64 mmol), DIPEA (2.30 mL, 13.3 mmol) and HBTU (1.39 g, 3.65 mmol) and the mixture was stirred overnight at room temperature. The solvent was removed under reduced pressure and the residue was partitioned between ethyl acetate (500 mL) and a saturated aqueous solution of  $\text{NaHCO}_3$  (200 mL). The organic phase was washed with saturated aqueous  $\text{NaHCO}_3$  (200 mL), water (200 mL) and brine (200 mL), dried over  $\text{MgSO}_4$ , filtered and concentrated. Normal phase flash column chromatography ( $\text{SiO}_2$ ;  $\text{CH}_2\text{Cl}_2/\text{EtOAc} = 4:1$  to 3:2) afforded 1.23 g (67%) of amide **195** as an orange solid.

$R_f = 0.3$  ( $\text{CH}_2\text{Cl}_2/\text{EtOAc}/\text{ACOH} = 7:3:1\%$ ).

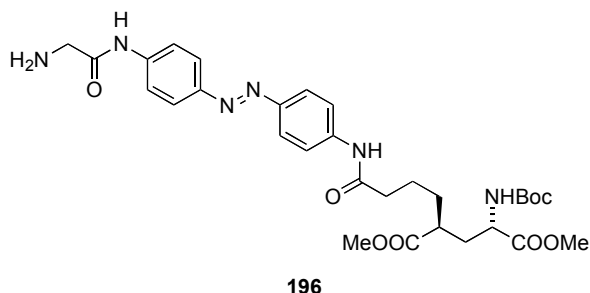
m.p. ( $\text{CH}_2\text{Cl}_2/\text{EtOAc}$ ) = 82.8-88.5  $^\circ\text{C}$ .

$[\alpha]_D^{24} = +32.0$  ( $c$  0.1,  $\text{CH}_2\text{Cl}_2$ ).

UV ( $\text{CH}_2\text{Cl}_2$ ):  $\lambda_{\text{max}} = 384$  nm.

<sup>13</sup>C NMR (CDCl<sub>3</sub>, 100 MHz) δ 176.0, 172.7, 171.2, 155.9, 149.5, 149.3, 145.7, 139.9, 125.1, 123.4, 119.9, 114.8, 80.6, 52.7, 52.1, 52.0, 41.3, 36.7, 35.5, 30.9, 28.5, 23.1 ppm.

**(2*S*,4*S*)-dimethyl 2-(4-(4-((*E*)-(4-(2-aminoacetamido)phenyl)diazenyl)phenylamino)-4-oxobutyl)-4-(*tert*-butoxycarbonylamino)pentanedioate (196)**


$$R_f(\text{FmocGly adduct}) = 0.3 \text{ (CH}_2\text{Cl}_2/\text{MeOH} = 95:5).$$

The residue was dissolved in DMF (200 mL) and piperidine (1.30 mL, 13.2 mmol) was added. The mixture was stirred overnight at room temperature and then concentrated under reduced pressure. The residue was partitioned between saturated aqueous NaHCO<sub>3</sub> (300 mL) and EtOAc (150 mL). The organic phase was washed with saturated aqueous NaHCO<sub>3</sub> solution (2 x 100 mL), water (100 mL) and brine (100 mL), dried over Na<sub>2</sub>SO<sub>4</sub>, filtered and concentrated. The product was purified using normal phase column chromatography (SiO<sub>2</sub>; CH<sub>2</sub>Cl<sub>2</sub>/MeOH/AcOH/H<sub>2</sub>O = 9:1:1%:1% to 4:1:1%:1%). The product containing fractions were washed with saturated aqueous NaHCO<sub>3</sub> (1 x 200 mL), dried over Na<sub>2</sub>SO<sub>4</sub>, filtered and concentrated to yield 803 mg (60%, 2 steps) of the primary amine **196** as a red solid.

$R_f = 0.4$  (CH<sub>2</sub>Cl<sub>2</sub>/MeOH/AcOH/H<sub>2</sub>O = 7:3:1%:1%).

m.p. (CH<sub>2</sub>Cl<sub>2</sub>/MeOH) = 146-156 °C.

$[\alpha]_D^{24} = +30.0$  ( $c$  0.1, CH<sub>2</sub>Cl<sub>2</sub>).

UV (CH<sub>2</sub>Cl<sub>2</sub>):  $\lambda_{\max} = 368$  nm.

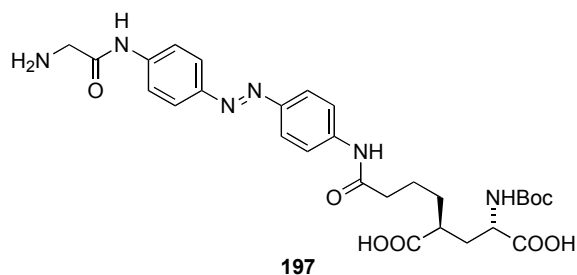
IR (ATR):  $\tilde{\nu} = 3282$  (w), 2920 (m), 2850 (m), 1682 (m), 1591 (m), 1528 (s), 1500 (m), 1434 (m), 1409 (m), 1366 (m), 1299 (m), 1249 (s), 1153 (s) cm<sup>-1</sup>.

<sup>1</sup>H NMR (CDCl<sub>3</sub>, 400 MHz)  $\delta$  9.64 (s, 1H), 8.35-8.20 (m, 1H), 8.00-7.84 (m, 4H), 7.83-7.64 (m, 4H), 5.13 (d,  $J = 8.9$  Hz, 1H), 4.44-4.26 (m, 1H), 3.72 (s, 3H), 3.69 (s, 3H), 3.51 (s, 2H), 2.62-2.47 (m, 1H), 2.46-2.22 (m, 2H), 2.09-1.91 (m, 2H), 1.89-1.62 (m, 6H), 1.46 (s, 9H) ppm.

<sup>13</sup>C NMR (CDCl<sub>3</sub>, 100 MHz)  $\delta$  176.0, 172.7, 171.3, 171.1, 155.9, 149.2, 149.0, 140.0, 129.3, 124.0, 123.9, 119.8, 119.6, 80.6, 52.7, 52.1, 52.0, 45.3, 41.3, 36.7, 35.5, 30.9, 28.5, 23.1 ppm.

HRMS (ESI) Calc. for C <sub>30</sub> H <sub>41</sub> N <sub>6</sub> O <sub>8</sub> <sup>+</sup> :	613.2986 [M+H] <sup>+</sup>
Found:	613.2975 [M+H] <sup>+</sup> .

**(2*S*,4*S*)-2-(4-(4-((*E*)-(4-(2-aminoacetamido)phenyl)diazenyl)phenylamino)-4-oxo butyl)-4-(*tert*-butoxycarbonylamino)pentanedioic acid (**197**)**



To a solution of diester **196** (760 mg, 1.24 mmol) in THF/water (100 mL; 2:1) was added LiOH (743 mg, 31.0 mmol) at 0 °C and the reaction was stirred for 1 h. The mixture was neutralized by addition of formic acid (1.17 mL, 31.0 mmol) and THF was removed under reduced pressure. The residual aqueous solution was added on top of a RP18 column, washed with water/formic acid (100 mL, 0.1% FA) and the crude product was purified by reversed phase flash column chromatography (C18; H<sub>2</sub>O/MeCN/FA = 99.9:0:0.1 to 74.9:25:0.1) to yield 529 mg (73%) of diacid **197** as an orange solid.

$R_f = 0.4$  (C18; H<sub>2</sub>O/MeCN/FA = 65:35:1%).

mp (H<sub>2</sub>O/MeCN) > 180 °C decomp.

$[\alpha]_D^{24} = -14.8$  ( $c$  0.1, MeCN/H<sub>2</sub>O = 9:1).

UV (MeCN):  $\lambda_{\max} = 369$  nm.

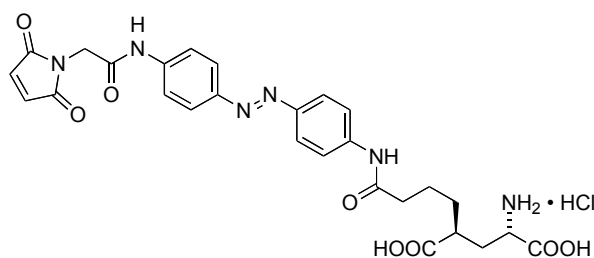
IR (ATR):  $\tilde{\nu} = 2929$  (w), 2362 (m), 2337 (m), 1662 (m), 1592 (m), 1534 (m), 1497 (m), 1301 (m), 1248 (m), 1153 (m) cm<sup>-1</sup>.

<sup>1</sup>H NMR (DMSO-*d*<sub>6</sub>, 400 MHz)  $\delta$  10.3-10.2 (m, 1H), 8.27 (br s, 3H), 7.89-7.84 (m, 2H), 7.82-7.78 (m, 6H), 6.63 (d,  $J = 7.9$  Hz, 1H), 3.91 (dd,  $J = 8.0$  Hz,  $J = 8.1$  Hz, 1H), 3.80 (s, 2H), 2.43-2.30 (m, 3H), 1.86-1.84 (m, 6H), 1.36 (s, 9H) ppm.

<sup>13</sup>C NMR (DMSO-*d*<sub>6</sub>, 100 MHz)  $\delta$  176.4, 174.3, 171.5, 164.2, 155.1, 148.0, 147.5, 142.2, 140.8, 123.5, 123.4, 119.5, 119.3, 77.9, 52.2, 41.7, 36.6, 34.5, 33.5, 30.9, 28.2, 23.0 ppm.

HRMS (ESI) Calc. for $C_{28}H_{37}N_6O_8^+$ :	585.2673 $[M+H]^+$
Found:	585.2665 $[M+H]^+$ .

**(2*S*,4*S*)-2-amino-4-(4-(4-((*E*)-(4-(2-(2,5-dioxo-2,5-dihydro-1*H*-pyrrol-1-yl)acetamido)-phenyl)diazenyl)phenylamino)-4-oxobutyl)pentanedioic acid hydrochloride (D-MAG0, 198•HCl)**



D-MAG0 (**198**•HCl)

To a solution of diacid **197** (50.0 mg, 42.8  $\mu$ mol) in saturated aqueous  $\text{NaHCO}_3$  (7 mL) was added finely ground *N*-methoxycarbonylmaleimide (26.5 mg, 117  $\mu$ mol) under vigorous stirring at 0 °C. The mixture was stirred for 30 min and then diluted with THF (7 mL). The ice bath was removed for 10 min. The solution was re-cooled to 0 °C, acidified to pH 1-2 with aqueous 1.0 M  $\text{H}_2\text{SO}_4$  and extracted with ethyl acetate (2 x 25 mL). The combined organic extracts were dried over  $\text{Na}_2\text{SO}_4$ , filtered and concentrated. Normal phase flash column chromatography ( $\text{SiO}_2$ ;  $\text{CH}_2\text{Cl}_2/\text{MeOH}/\text{AcOH}/\text{H}_2\text{O}$  = 9:1:0.6%:0.6%) yielded the maleimide adduct as an orange solid.

$R_f$ (maleimide diacid) = 0.5 ( $\text{SiO}_2$ ;  $\text{CH}_2\text{Cl}_2/\text{MeOH}/\text{AcOH}/\text{H}_2\text{O}$  = 4:1:1%:1%).

The crude product was directly treated with a saturated solution of HCl in EtOAc (20 mL). After stirring for 2 h at room temperature, the resulting purple suspension was diluted with  $\text{Et}_2\text{O}$  (30 mL) and the solid was collected by sedimentation. The product was re-suspended in  $\text{Et}_2\text{O}$  (20 mL) and sedimented again. Removal of the solvent afforded 40.0 mg (70%, 2 steps) of D-MAG0 (**198**•HCl) as a purple solid.

$R_f$  = 0.3 ( $\text{C}_{18}$ ;  $\text{H}_2\text{O}/\text{MeCN}/\text{FA}$  = 3:2:0.1%).

m.p. ( $\text{Et}_2\text{O}/\text{EtOAc}$ ) > 180 °C (decomp.).

$[\alpha]_D^{24}$  = +81.8 ( $c$  = 0.1, HEPES buffer + 0.1% DMSO).

UV (HEPES ringer, 0.1% DMSO):  $\lambda_{\text{max}} = 362 \text{ nm}$ .

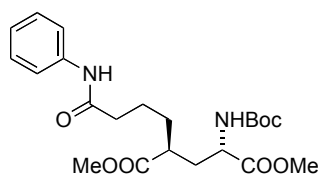
IR (ATR):  $\tilde{\nu} = 2916 \text{ (w)}, 1710 \text{ (s)}, 1592 \text{ (s)}, 1535 \text{ (s)}, 1499 \text{ (m)}, 1428 \text{ (m)}, 1412 \text{ (m)}, 1300 \text{ (m)}, 1250 \text{ (s)}, 1151 \text{ (s)} \text{ cm}^{-1}$ .

$^1\text{H}$  NMR (DMSO- $d_6$ , 600 MHz)  $\delta$  10.8 (s, 1H), 10.4 (s, 1H), 8.42 (br s, 3H), 7.86-7.74 (m, 8H), 7.19 (s, 2H), 4.32 (s, 2H), 3.79 (br s, 1H), 2.64-2.56 (m, 1H), 2.42-2.29 (m, 2H), 2.09-2.01 (m, 1H), 1.84 (ddd,  $J = 6.0 \text{ Hz}, J = 7.8 \text{ Hz}, J = 13.9 \text{ Hz}$ , 1H), 1.66-1.51 (m, 4H) ppm.

$^{13}\text{C}$  NMR (DMSO- $d_6$ , 150 MHz)  $\delta$  175.5, 171.4, 170.7, 170.6, 165.3, 147.8, 147.5, 142.1, 141.1, 135.0, 123.4 (2 C), 119.4, 119.2, 50.3, 40.5, 40.3, 36.2, 31.7, 31.1, 22.2 ppm.

HRMS (ESI) Calc. for  $\text{C}_{27}\text{H}_{29}\text{N}_6\text{O}_8^+$ : 565.2047  $[\text{M}+\text{H}]^+$   
Found: 565.2039  $[\text{M}+\text{H}]^+$ .

**(2S,4S)-dimethyl 2-(*tert*-butoxycarbonylamino)-4-(4-oxo-4-(phenylamino)butyl) pentane-dioate (**S13**)**



**S13**

To a solution of acid **194** (50 mg, 0.138 mmol) in DMF (5 mL) was added HBTU (56 mg, 152  $\mu\text{mol}$ ), DIPEA (48  $\mu\text{L}$ , 277  $\mu\text{mol}$ ) and aniline (16 mg, 166  $\mu\text{mol}$ ) and the solution was stirred overnight at room temperature. EtOAc (20 mL) and saturated aqueous  $\text{NaHCO}_3$  (30 mL) were added and the mixture was extracted with EtOAc (4 x 20 mL). The combined organic extracts were washed with 10% aqueous  $\text{NaCl}$  (2 x 20 mL) and brine (1 x 20 mL). The organic phase was dried over  $\text{MgSO}_4$ , filtered and concentrated. Normal phase flash column chromatography ( $\text{SiO}_2$ ;  $\text{CH}_2\text{Cl}_2/\text{MeOH} = 97:3$ ) yielded 42 mg (97%) of amide **S13** as a colorless oil.

$R_f = 0.3$  ( $\text{CH}_2\text{Cl}_2/\text{MeOH} = 95:5$ ).

$[\alpha]_D^{24} = -16.6$  ( $c = 1.0$ ,  $\text{CH}_2\text{Cl}_2$ ).

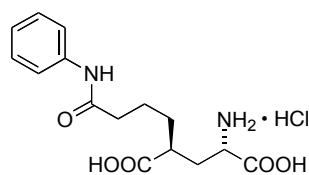
IR (ATR):  $\tilde{\nu}$  = 3318 (w), 2951 (w), 1731 (s), 1715 (s), 1690 (s), 1668 (s), 1599 (s), 1538 (s), 1499 (s), 1441 (s), 1366 (m), 1249 (m), 1159 (s)  $\text{cm}^{-1}$ .

$^1\text{H}$  NMR ( $\text{CDCl}_3$ , 400 MHz)  $\delta$  7.91 (br s, 1H), 7.60-7.46 (m, 2H), 7.30 (t,  $J$  = 7.9 Hz, 2H), 7.08 (t,  $J$  = 7.4 Hz, 1H), 5.08 (d,  $J$  = 8.9 Hz, 1H), 4.42-4.25 (m, 1H), 3.71 (s, 3H), 3.68 (s, 3H), 2.56-2.45 (m, 1H), 2.38-2.29 (m, 2H), 2.03-1.91 (m, 2H), 1.88-1.58 (m, 4H), 1.45 (s, 9H) ppm.

$^{13}\text{C}$  NMR ( $\text{CDCl}_3$ , 100 MHz)  $\delta$  176.0, 172.8, 171.1, 155.8, 136.3, 129.1, 124.2, 120.0, 80.5, 52.6, 52.1, 41.4, 38.8, 36.7, 35.4, 31.1, 28.5, 23.1 ppm.

HRMS (ESI) Calc. for  $\text{C}_{22}\text{H}_{32}\text{N}_2\text{NaO}_7^+$ : 459.2107  $[\text{M}+\text{Na}]^+$   
 Found: 459.2100  $[\text{M}+\text{Na}]^+$ .

**(2*S*,4*S*)-2-amino-4-(4-oxo-4-(phenylamino)butyl)pentanedioic acid hydrochloride (TM-0, 199•HCl)**



TM-0 (199•HCl)

To a solution of diester **S13** (30 mg, 69  $\mu\text{mol}$ ) in THF/ $\text{H}_2\text{O}$  (6 mL, 1:1) was added LiOH (66 mg, 2.7 mmol) at 0  $^\circ\text{C}$  and the mixture was stirred for 1 h. The mixture was neutralized by addition of formic acid (104  $\mu\text{L}$ , 2.7 mmol) and THF was removed under reduced pressure. The crude product was placed on a RP18 column and washed with  $\text{H}_2\text{O}$ /0.1% FA. Reversed phase flash column chromatography ( $\text{C}_{18}$ ;  $\text{H}_2\text{O}$ /MeOH/FA = 9:1:0.1% to 3:2:0.1%) yielded Boc-protected **199** as a colorless solid, which was used directly in the next step.

$R_f$  (diacid) = 0.5 ( $\text{C}_{18}$ ;  $\text{H}_2\text{O}$ /MeOH/FA = 3:2:0.1%).

The obtained diacid was treated with HCl-saturated EtOAc (10 mL) and stirred for 2 h at room temperature. The suspension was treated with  $\text{Et}_2\text{O}$  (50 mL) and the product was collected by sedimentation. The residual solvent was removed under reduced pressure to yield 11 mg (46%, 2 steps) of HCl-salt **199•HCl** as a colorless, hygroscopic solid.

m.p. (Et<sub>2</sub>O/EtOAc) > 200 °C (decomp.).

$[\alpha]_D^{24} = +68.0$  (c 0.1, HEPES ringers).

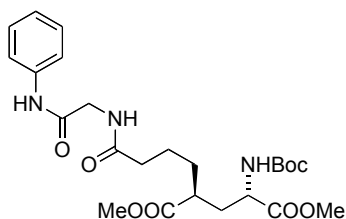
IR (ATR):  $\tilde{\nu} = 2924$  (w), 1701 (m), 1656 (m), 1595 (s), 1539 (s), 1498 (s), 1442 (s), 1311 (w), 1199 (s), 1154 (m) cm<sup>-1</sup>.

<sup>1</sup>H NMR (DMSO-*d*<sub>6</sub>, 600 MHz)  $\delta$  9.97 (s, 1H), 7.59 (dd,  $J = 0.9$  Hz,  $J = 8.5$  Hz, 2H), 7.27 (dd,  $J = 7.5$  Hz,  $J = 8.5$  Hz, 2H), 7.02 (dd,  $J = 4.2$  Hz,  $J = 10.5$  Hz, 1H), 3.73 (m, 1H), 2.64-2.53 (m, 1H), 2.29 (t,  $J = 6.9$  Hz, 2H), 2.04-1.97 (m, 1H), 1.87-1.80 (m, 1H), 1.63-1.46 (m, 4H) ppm.

<sup>13</sup>C NMR (DMSO-*d*<sub>6</sub>, 150 MHz)  $\delta$  175.5, 170.9, 170.6, 139.3, 128.6, 122.9, 119.0, 50.5, 40.5, 36.1, 32.0, 31.1, 22.4 ppm.

HRMS (ESI) Calc. for C<sub>15</sub>H<sub>20</sub>N<sub>2</sub>NaO<sub>5</sub><sup>+</sup>: 331.1270 [M+Na]<sup>+</sup>  
Found: 331.1264 [M+Na]<sup>+</sup>.

**(2*S*,4*S*)-dimethyl 2-(*tert*-butoxycarbonylamino)-4-(4-oxo-4-(2-oxo-2-(phenylamino)ethyl-amino)butyl)pentanedioate (S14)**



**S14**

To a solution of acid **194** (50 mg, 138  $\mu$ mol) in DMF (5 mL) was added HBTU (58 mg, 152  $\mu$ mol), DIPEA (48  $\mu$ L, 277  $\mu$ mol) and 2-amino-*N*-phenylacetamide hydrochloride (28 mg, 152  $\mu$ mol). The solution was stirred overnight at room temperature. Saturated aqueous NaHCO<sub>3</sub> (30 mL) was added and the mixture was extracted with EtOAc (3 x 20 mL). The combined organic extracts were washed with saturated aqueous NH<sub>4</sub>Cl (1 x 30 mL), 10% aqueous NaCl (2 x 20 mL) and brine (1 x 20 mL). The organic phase was dried over MgSO<sub>4</sub>, filtered and concentrated. Normal phase flash column chromatography (SiO<sub>2</sub>; CH<sub>2</sub>Cl<sub>2</sub>/MeOH = 97:3) yielded 68 mg (99%) of amide **S14** as a colorless oil.

$R_f = 0.2$  (CH<sub>2</sub>Cl<sub>2</sub>/MeOH = 95:5).



$[\alpha]_D^{24} = +3.2$  ( $c = 1$ ,  $\text{CH}_2\text{Cl}_2$ ).

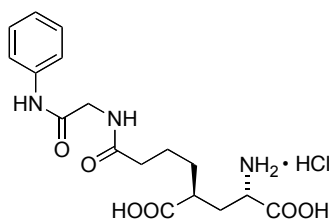
IR (ATR):  $\tilde{\nu} = 3296$  (w), 2952 (w), 1731 (s), 1697 (s), 1652 (s), 1600 (m), 1526 (s), 1499 (s), 1443 (s), 1366 (m), 1249 (m), 1160 (s)  $\text{cm}^{-1}$ .

$^1\text{H}$  NMR ( $\text{DMSO-}d_6$ , 600 MHz)  $\delta$  8.91 (s, 1H), 7.53 (d,  $J = 7.7$  Hz, 2H), 7.30 (t,  $J = 7.9$  Hz, 2H), 7.09 (t,  $J = 7.4$  Hz, 1H), 6.92 (br s, 1H), 5.05 (d,  $J = 8.9$  Hz, 1H), 4.32 ( $m_c$ , 1H), 4.13 ( $m_c$ , 2H), 3.70 (s, 3H), 3.64 (s, 3H), 2.52-2.45 (m, 1H), 2.29 ( $m_c$ , 2H), 2.00-1.90 (m, 2H), 1.77-1.54 (m, 4H), 1.42 (s, 9H) ppm.

$^{13}\text{C}$  NMR ( $\text{DMSO-}d_6$ , 150 MHz)  $\delta$  175.9, 173.8, 172.8, 167.4, 155.7, 137.9, 129.1, 124.5, 120.0, 80.4, 52.6, 52.2, 52.0, 44.7, 41.8, 35.7, 34.9, 31.5, 28.4, 23.1 ppm.

HRMS (ESI) Calc. for  $\text{C}_{24}\text{H}_{35}\text{N}_3\text{NaO}_8^+$ : 516.2322  $[\text{M}+\text{Na}]^+$   
 Found: 516.2312  $[\text{M}+\text{Na}]^+$ .

**(2*S*,4*S*)-2-amino-4-(4-oxo-4-(2-oxo-2-(phenylamino)ethylamino)butyl)pentane-dioic acid hydrochloride (TM-1, 200•HCl)**



TM1 (200•HCl)

To a solution of diester **S14** (40 mg, 81  $\mu\text{mol}$ ) in THF/water (6 mL, 1:1) was added LiOH (78 mg, 3.24 mmol) at 0 °C and the mixture was stirred for 1 h. The solution was neutralized by addition of formic acid (122  $\mu\text{L}$ , 3.24 mmol) and THF was removed under reduced pressure. The crude product was placed on a RP18 column and washed with  $\text{H}_2\text{O}/0.1\%$  formic acid. Reversed phase flash column chromatography ( $\text{C18}$ ;  $\text{H}_2\text{O}/\text{MeOH}/\text{FA} = 9:1:0.1\%$  to 3:2:0.1%) yielded Boc-protected **200** as a colorless solid which was used directly in the next step.

$R_f$ (diacid) = 0.4 ( $\text{C18}$ ;  $\text{H}_2\text{O}/\text{MeOH}/\text{FA} = 7:3:1\%$ ).

The obtained diacid was treated with HCl-saturated EtOAc (10 mL) and stirred for 2 h at RT. The suspension was treated with  $\text{Et}_2\text{O}$  (50 mL) and the product was collected by

sedimentation. Removal of the residual solvent afforded 24 mg (74%, 2 steps) of HCl-salt **200**•HCl as a colorless, hygroscopic solid.

m.p. (Et<sub>2</sub>O/EtOAc) > 210 °C (decomp).

$[\alpha]_D^{24} = +62.4$  (c = 0.1, HEPES buffer).

IR (ATR):  $\tilde{\nu}$  = 2929 (w), 1597 (m), 1542 (s), 1498 (s), 1445 (m), 1411 (m), 1312 (m), 1202 (s) cm<sup>-1</sup>.

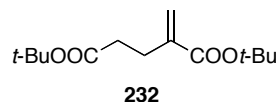
<sup>1</sup>H NMR (DMSO-*d*<sub>6</sub>, 600 MHz)  $\delta$  10.15 (s, 1H), 8.49 (br s, 3H), 8.25 (t, *J* = 5.8 Hz, 1H), 7.60 (d, *J* = 7.7 Hz, 2H), 7.28 (m<sub>c</sub>, 2H), 7.02 (t, *J* = 7.4 Hz, 1H), 3.87 (d, *J* = 5.9 Hz, 2H), 3.78 (t, *J* = 7.1 Hz, 1H), 2.59 (m<sub>c</sub>, 1H), 2.25-2.10 (m<sub>c</sub>, 2H), 1.10-1.99 (m, 1H), 1.88-1.75 (m, 1H), 1.60-1.39 (m, 4H) ppm.

<sup>13</sup>C NMR (DMSO-*d*<sub>6</sub>, 150 MHz)  $\delta$  175.6, 172.4, 170.7, 168.0, 139.0, 128.7, 123.2, 119.1, 50.3, 42.7, 40.3, 35.0, 31.8, 31.1, 22.5 ppm.

HRMS (ESI) Calc. for C <sub>17</sub> H <sub>24</sub> N <sub>3</sub> O <sub>6</sub> <sup>+</sup> :	366.1665 [M+H] <sup>+</sup>
Found:	366.1659 [M+H] <sup>+</sup> .

## 7) Toward an Orthogonal Receptor-Ligand Pair based on iGluRs – Synthetic Procedures

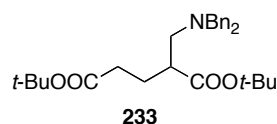
### di-*tert*-butyl 2-methylenepentanedioate (**232**)



Diester **232** was synthesized according to known procedures.<sup>[256]</sup> The spectral data matched those reported previously.

$R_f = 0.6$  (PE/EtAOc = 16:1).

### di-*tert*-butyl 2-((dibenzylamino)methyl)pentanedioate (**233**)



To a solution of dibenzylamine (616 mg, 3.12 mmol) in THF (10 mL) was added *n*-butyl lithium (1.21 mL, 3.02 mmol; 2.5 M in hexanes) at -78 °C and the mixture was stirred for 30 min. To the deep violet solution was added precooled acrylate **232** (500 mg, 1.95 mmol) in THF (5 mL) and stirring was continued for 20 min. Saturated aqueous NH<sub>4</sub>Cl solution (20 mL) was added and the mixture was allowed to warm to RT. The biphasic mixture was extracted with EtOAc (3 x 50 mL) and the combined organic extracts were dried over MgSO<sub>4</sub>, filtered and concentrated. Normal phase flash column chromatography (SiO<sub>2</sub>; PE/EtOAc = 16:1) yielded 210 mg (24%) of protected homoglutamate **233** as a colorless liquid.

$R_f = 0.3$  (PE/EtOAc = 16:1).

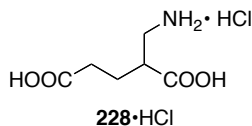
IR (ATR):  $\tilde{\nu} = 2976$  (w), 2931 (w), 2798 (w), 1724 (s), 1494 (w), 1452 (w), 1365 (m), 1248 (m), 1144 (s), 1028 (w), 846 (w) cm<sup>-1</sup>.

<sup>1</sup>H NMR (CDCl<sub>3</sub>, 400 MHz)  $\delta$  7.34-7.27 (m, 8H), 7.25-7.20 (m, 2H), 3.62 (d,  $J = 13.6$  Hz, 2H), 3.46 (d,  $J = 13.6$  Hz, 2H), 2.80 (dd,  $J = 8.7$  Hz,  $J = 12.4$  Hz, 1H), 2.67-2.58 (m, 1H), 2.40 (dd,  $J = 5.9$  Hz,  $J = 12.4$  Hz, 1H), 2.18 (ddd,  $J = 5.0$  Hz,  $J = 6.7$  Hz,  $J = 8.3$  Hz, 2H), 1.85-1.61 (m, 2H), 1.46 (s, 9H), 1.44 (s, 9H) ppm.

214

HRMS (ESI) Calc. for  $C_{29}H_{42}NO_4^+$ : 468.3108  $[M+H]^+$   
 Found: 468.3103  $[M+H]^+$ .

**(*R/S*)-2-(aminomethyl)pentanedioic acid hydrochloride (**228**•HCl)**



*Exemplary procedure:*

To a solution of protected homoglutamate **233** (100 mg, 0.21 mmol) in methanol (5 mL) was added  $Pd(OAc)_2$  (14 mg, 64  $\mu$ mol). The vessel was flushed with  $N_2$  and then charged with  $H_2$  and the mixture was stirred under an  $H_2$  atmosphere overnight.

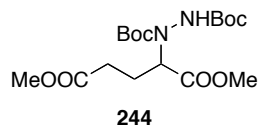
$R_f$  (primary amine) = 0.1 ( $CH_2Cl_2/MeOH/AcOH/H_2O = 9:1:0.1:0.1$ ).

Palladium was filtered off over celite eluting with methanol (80 mL) and the solvent was removed under reduced pressure. To the resulting colorless oil was added 6 M HCl (3 mL) and the mixture was stirred for 2 h at room temperature. The solvent was removed under reduced pressure and the residue co-evaporated with water (3x) and dried to yield 38 mg (90%) of HCl salt **228**•HCl as a colorless, hygroscopic solid.

IR (ATR):  $\tilde{\nu} = 1705$  (s), 1609 (m), 1457 (w), 1402 (w), 1197 (m), 1021 (w)  $cm^{-1}$ .

$^1H$  NMR ( $D_2O$ , 400 MHz)  $\delta$  3.32 (dd,  $J = 9.1$  Hz,  $J = 13.2$  Hz, 1H), 3.21 (dd,  $J = 4.5$  Hz,  $J = 13.2$  Hz, 1H), 2.95-2.85 (m, 1H), 2.56 (td,  $J = 3.1$  Hz,  $J = 7.3$  Hz, 2H), 2.10-1.90 (m, 2H) ppm.

$^{13}C$  NMR ( $D_2O$ , 100 MHz)  $\delta$  177.0, 176.0, 41.6, 39.8, 30.7, 24.1 ppm.

**(*R/S*)-di-*tert*-butyl 1-(1,5-dimethoxy-1,5-dioxopentan-2-yl)hydrazine-1,2-dicarboxylate (244)**

To a solution of dimethyl glutarate (500 mg, 3.12 mmol) in THF (10 mL) was added KHMDS (7.49 mL, 3.75 mmol; 0.5 M in THF) at -78 °C and the mixture was stirred for 20 min. A solution of di-*tert*-butyl azodicarboxylate (934 mg, 4.06 mmol) in THF (5 mL) was slowly added to the reaction mixture and stirring was continued for 1 h. The reaction was quenched by addition of AcOH (1 mL) at -78 °C. Saturated aqueous NH<sub>4</sub>Cl solution (20 mL) was added and the mixture was allowed to warm to RT. The biphasic mixture was extracted with EtOAc (3 x 50 mL). The combined organic extracts were dried over MgSO<sub>4</sub>, filtered and concentrated. Normal phase flash column chromatography (SiO<sub>2</sub>; PE/EtOAc = 5:1 to 4:1) yielded 394 mg (32%) of protected hydrazine **244** as a colorless oil.

$R_f$  = 0.3 (PE/EtOAc = 4:1).

IR (ATR):  $\tilde{\nu}$  = 327 (w), 2978 (w), 1312 (s), 1710 (s), 1478 (w), 1456 (w), 1392 (m), 1366 (m), 1241 (m), 1148 (s) cm<sup>-1</sup>.

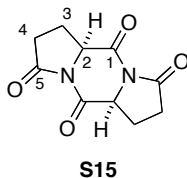
<sup>1</sup>H NMR (CDCl<sub>3</sub>, 400 MHz; mixture of rotamers)  $\delta$  6.50-6.14 (br m, 1H), 4.98-4.67 (br m, 1H), 3.73 (s, 3H), 3.66 (s, 3H), 2.83-2.45 (m, 2H), 2.36-2.19 (m, 1H), 2.09-1.98 (m, 1H), 1.53-1.38 (m, 18H) ppm.

<sup>13</sup>C NMR (CDCl<sub>3</sub>, 100 MHz; mixture of rotamers)  $\delta$  173.8, 172.0, 171.6, 155.9, 155.7, 155.2, 82.7, 82.2, 81.6, 81.1, 61.2, 59.3, 52.6, 51.7, 30.9, 30.5, 28.3 (2x), 28.2, 24.2, 23.9 ppm.

HRMS (ESI) Calc. for C<sub>17</sub>H<sub>30</sub>N<sub>2</sub>NaO<sub>8</sub><sup>+</sup>: 413.1894 [M+Na]<sup>+</sup>  
 Found: 413.1892 [M+Na]<sup>+</sup>.

## 8) Toward the Total Synthesis of Herquiline A & B – Synthetic Procedures

### (5a*S*,10a*S*)-tetrahydrodipyrrolo[1,2-*a*:1',2'-*d*]pyrazine-3,5,8,10(5a*H*,10a*H*)-tetraone (S15)



Tricycle **S15** was synthesized according to literature procedures.<sup>[287]</sup>

m.p. (Ac<sub>2</sub>O/pyridine) > 295 °C (decomp).

$[\alpha]_D^{24} = -96.0$  (c = 1.0, DMSO).

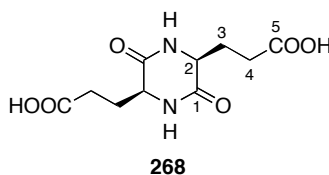
IR (ATR):  $\tilde{\nu} = 1763$  (s), 1696 (m), 1680 (m), 1322 (s), 1296 (s), 1257 (s), 1214 (s), 948 (m) cm<sup>-1</sup>.

<sup>1</sup>H NMR (DMSO-*d*<sub>6</sub>, 400MHz)  $\delta$  4.84 (t, *J* = 8.5 Hz, 2H, *H*-2), 2.58 (ddd, *J* = 17.6 Hz, *J* = 10.9 Hz, *J* = 9.5 Hz, 2H, *H*<sub>a</sub>-4), 2.43 (ddd, *J* = 17.6 Hz, *J* = 9.2 Hz, *J* = 3.1 Hz, 2H, *H*<sub>b</sub>-4), 2.27-2.11 (m, 4H, *H*-3) ppm.

<sup>13</sup>C NMR (DMSO-*d*<sub>6</sub>, 100 MHz)  $\delta$  172.7 (C-5), 165.6 (C-1), 58.4 (C-2), 31.3 (C-4), 18.9 (C-3) ppm.

HRMS (ESI) Calc. for C<sub>10</sub>H<sub>10</sub>N<sub>2</sub>NaO<sub>4</sub><sup>+</sup>: 245.0533 [M+Na]<sup>+</sup>  
Found: 245.0531 [M+Na]<sup>+</sup>.

### 3,3'-((2*S*,5*S*)-3,6-dioxopiperazine-2,5-diyl)dipropionic acid (268)



Glutamic diketopiperazine (**268**) was synthesized according to literature procedures.<sup>[287]</sup>

m.p. (H<sub>2</sub>O) > 263 °C (decomp).

$[\alpha]_D^{24} = -41.9$  ( $c = 1.0$ , DMSO).

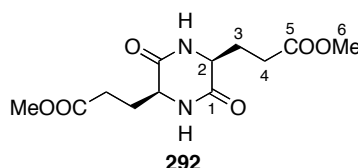
IR (ATR):  $\tilde{\nu} = 3209$  (w), 2360 (w), 1700 (s), 1628 (m), 1422 (m), 1318 (m), 1262 (s), 1220 (m), 1122 (m)  $\text{cm}^{-1}$ .

$^1\text{H}$  NMR (DMSO- $d_6$ , 400MHz)  $\delta$  8.17 (d,  $J = 1.5$  Hz, 2H,  $H\text{-N}$ ), 3.87 (t,  $J = 6.1$  Hz, 2H,  $H\text{-2}$ ), 2.31 ( $m_c$ , 4H,  $H\text{-4}$ ), 2.00-1.80 (m, 4H,  $H\text{-3}$ ) ppm.

$^{13}\text{C}$  NMR (DMSO- $d_6$ , 100 MHz)  $\delta$  173.9 ( $C\text{-5}$ ), 167.9 ( $C\text{-1}$ ), 53.2 ( $C\text{-2}$ ), 29.3 ( $C\text{-4}$ ), 28.2 ( $C\text{-3}$ ) ppm.

HRMS (ESI) Calc. for  $\text{C}_{10}\text{H}_{14}\text{N}_2\text{NaO}_6^+$ : 281.0744  $[\text{M}+\text{Na}]^+$   
Found: 281.0740  $[\text{M}+\text{Na}]^+$ .

**dimethyl 3,3'-((2*S*,5*S*)-3,6-dioxopiperazine-2,5-diyl)dipropionate (**292**)**



To a suspension of glutamic diketopiperazine **268** (12.7 g, 49.2 mmol) in MeOH (900 mL) was added  $\text{CBr}_4$  (4.89 g, 14.8 mmol) and the turbid mixture was heated under reflux for 12 h. The obtained clear solution was allowed to cool to room temperature, concentrated and the precipitate was re-suspended in  $\text{Et}_2\text{O}$  (500 mL). The colorless solid was filtered off, washed with  $\text{Et}_2\text{O}$  (3 x 200 mL) and dried on high vacuum to yield 13.3 g (94%) of diketopiperazine diester **292** as a colorless, fluffy solid.

$R_f = 0.2$  ( $\text{CH}_2\text{Cl}_2/\text{MeOH} = 95:5$ ).

m.p. ( $\text{Et}_2\text{O}/\text{MeOH}$ ) = 183-184  $^\circ\text{C}$ .

$[\alpha]_D^{24} = -42.5$  ( $c = 1.0$ , DMSO).

IR (ATR):  $\tilde{\nu} = 3199$  (w), 1737 (s), 1673 (s), 1437 (m), 1328 (m), 1259 (m), 1200 (s), 1178 (s), 1112 (m), 1001 (m), 808 (m)  $\text{cm}^{-1}$ .

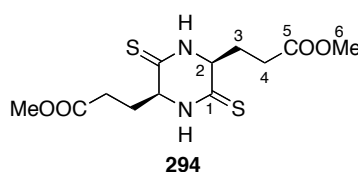


$^1\text{H}$  NMR (DMSO- $d_6$ , 400 MHz)  $\delta$  8.20 (d,  $J$  = 1.0 Hz, 2H,  $H$ -N), 3.88 (td,  $J$  = 5.6 Hz,  $J$  = 1.7 Hz, 2H,  $H$ -2), 3.59 (s, 6H,  $H$ -6), 2.40 (m<sub>c</sub>, 4H,  $H$ -4), 2.04-1.84 (m, 4H,  $H$ -3) ppm.

$^{13}\text{C}$  NMR (DMSO- $d_6$ , 100 MHz)  $\delta$  172.8 (C-5), 167.7 (C-1), 53.2 (C-2), 51.4 (C-6), 29.0 (C-4), 28.0 (C-3) ppm.

HRMS (ESI) Calc. for  $\text{C}_{12}\text{H}_{18}\text{N}_2\text{O}_6\text{Na}^+$ : 309.1057  $[\text{M}+\text{Na}]^+$   
 Found: 309.1053  $[\text{M}+\text{Na}]^+$ .

**dimethyl 3,3'-((2*S*,5*S*)-3,6-dithioxopiperazine-2,5-diyl)dipropionate (**294**)**



To a solution of diketopiperazine **292** (1.00 g, 3.49 mmol) in THF (75 mL) was added Lawesson's reagent (0.849 g, 2.10 mmol) and the mixture was heated under reflux for 3 h. The solvent was removed under reduced pressure and the crude product was purified using normal phase column chromatography ( $\text{SiO}_2$ ; dryload;  $\text{CH}_2\text{Cl}_2/\text{MeOH}$  = 98:2) to yield a yellow solid which was recrystallized from toluene to yield 906 mg (82%) of dithiodiketopiperazine **294** as an off-white solid.

$R_f$  = 0.4 ( $\text{CH}_2\text{Cl}_2/\text{MeOH}$  = 95:5).

m.p. (MePh) = 178 °C (decomp).

$[\alpha]_D^{24} = +4.7$  ( $c$  = 1.0, DMSO).

IR (ATR):  $\tilde{\nu}$  = 3138 (m), 3039 (m), 2947 (m), 1732 (s), 1538 (s), 1433 (m), 1322 (m), 1246 (m), 1175 (s), 1146 (s), 1045 (m)  $\text{cm}^{-1}$ .

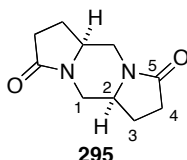
$^1\text{H}$  NMR (DMSO- $d_6$ , 400 MHz)  $\delta$  10.89 (d,  $J$  = 2.6 Hz,  $H$ -N), 4.27-4.21 (m<sub>c</sub>, 2H,  $H$ -2), 3.60 (s, 6H,  $H$ -6), 2.58-2.43 (m, 4+1H,  $H$ -4 and DMSO- $d_6$ ), 2.40-2.30 (m, 2H,  $H_a$ -3), 2.12-2.01 (m, 2H,  $H_b$ -3) ppm.

$^{13}\text{C}$  NMR (DMSO- $d_6$ , 100 MHz)  $\delta$  195.0 (C-1), 172.4 (C-5), 62.2 (C-2), 51.4 (C-6), 30.4 (C-3), 29.5 (C-4) ppm.

HRMS (ESI) Calc. for  $\text{C}_{12}\text{H}_{19}\text{N}_2\text{O}_4\text{NaS}_2^+$ : 319.0781  $[\text{M}+\text{H}]^+$

Found: 319.0783  $[\text{M}+\text{H}]^+$ .

**(5a*S*,10a*S*)-octahydrodipyrrolo[1,2-*a*:1',2'-*d*]pyrazine-3,8-dione (**295**)**



To a slurry of Raney-Ni (0.4 mL) was added methanol (5 mL) and the supernatant was removed. This was repeated two times, more methanol (2 mL) was added and the suspension was transferred to a solution of dithioketopiperazine **294** (20 mg, 62.8  $\mu\text{mol}$ ) in methanol (2 mL). The vessel was purged with  $\text{H}_2$  and the mixture was stirred for 28 h at room temperature. The mixture was filtered over celite and the solvent was removed under reduced pressure. The crude product was purified using normal phase column chromatography ( $\text{SiO}_2$ ;  $\text{CH}_2\text{Cl}_2/\text{MeOH}$  = 95:5 to 9:1) to yield 8 mg (66%) of tricycle **295** as a colorless oil.

$R_f$  = 0.5 ( $\text{CH}_2\text{Cl}_2/\text{MeOH}$  = 9:1).

$[\alpha]_D^{24} = -70.0$  ( $c$  = 0.23,  $\text{CH}_2\text{Cl}_2$ ).

IR (ATR):  $\tilde{\nu}$  = 3398 (br w), 1665 (s), 1416 (m), 1351 (w), 1318 (w), 1278 (w), 1260(w)  $\text{cm}^{-1}$ .

$^1\text{H}$  NMR (DMSO- $d_6$ , 400 MHz)  $\delta$  4.09 (dtd,  $J$  = 4.8 Hz,  $J$  = 7.1 Hz,  $J$  = 10.7 Hz, 2H,  $H$ -2), 3.63 (dd,  $J$  = 4.8 Hz,  $J$  = 12.6 Hz, 2H,  $H_a$ -1), 3.40-3.32 (m, 2H,  $H_b$ -1), 2.52-2.39 (m, 4H,  $H$ -4), 2.34-2.26 (m, 2H,  $H_a$ -3), 1.72 (dtd,  $J$  = 7.1 Hz,  $J$  = 9.5 Hz,  $J$  = 12.8 Hz, 2H,  $H_b$ -3) ppm.

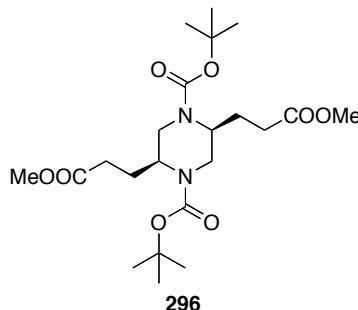
Signals corresponding to a putative diastereomer:  $\delta$  4.26 (dd,  $J$  = 4.2 Hz,  $J$  = 12.9 Hz), 3.54-3.56 (m), 2.26-2.21 (m) ppm.

$^{13}\text{C}$  NMR (DMSO- $d_6$ , 100 MHz)  $\delta$  174.6 (C-5), 52.6 (C-2), 46.6 (C-1), 30.6 (C-4), 24.3 (C-3) ppm.

Signals corresponding to a putative diastereomer:  $\delta$  54.9, 46.0, 30.3, 21.8 ppm.

HRMS (ESI) Calc. for $C_{10}H_{15}N_2O_2^+$ :	195.1128 $[M+H]^+$
Found:	195.1126 $[M+H]^+$ .

**(2*S*,5*S*)-di-*tert*-butyl 2,5-bis(3-methoxy-3-oxopropyl)piperazine-1,4-dicarboxylate (**296**)**



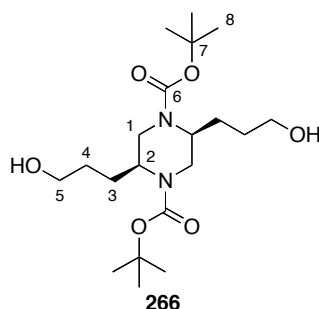
To a solution of Raney-Ni in water (0.1 mL) was added repeatedly THF (2 mL) and, after the solids had settled again, the supernatant was removed. The washed catalyst was suspended in THF (2 mL), thio-amide **294** (50 mg, 157  $\mu$ mol) and  $Boc_2O$  (85.7 mg, 393  $\mu$ mol) were added and the vessel was purged with argon and then charged with  $H_2$ . After stirring for 3 h more Raney-Ni (0.4 mL suspension, washed) was added and stirring was continued for 30 min. The suspension was filtered over celite eluting with EtOAc (20 mL). The solvent was removed under reduced pressure and the crude product purified by normal phase flash column chromatography ( $SiO_2$ ;  $CH_2Cl_2/MeOH = 98:2$  to  $95:5$ ) to yield 18 mg (< 25%) of piperazine **296** and possibly diastereomers as a colorless oil.

$R_f = 0.4$  ( $CH_2Cl_2/MeOH = 95:5$ ).

$^1H$  NMR (DMSO- $d_6$ , 400 MHz; mixture of rotamers)  $\delta$  4.31-3.94 (m, 3H), 3.88 (d,  $J = 13.9$  Hz, 0.5H), 3.73 (d,  $J = 13.8$  Hz, 0.5 H), 3.69-3.64 (m, 6H), 3.11 (dt,  $J = 4.1$  Hz,  $J = 13.8$  Hz, 0.5H), 3.01 (dt,  $J = 4.1$  Hz,  $J = 13.8$  Hz, 0.5 H), 2.52 (dd,  $J = 10.6$  Hz,  $J = 13.9$  Hz, 1H), 2.42-2.18 (m, 4H), 1.89-1.85 (m, 1H), 1.85-1.63 (m, 3H), 1.47-1.39 (m, 18H) ppm.

$^{13}C$  NMR (DMSO- $d_6$ , 100 MHz; mixture of rotamers)  $\delta$  173.7, 173.5, 173.5, 173.4, 155.6, 155.2, 155.2, 155.1, 80.5, 80.4, 80.3, 52.7, 51.8 (2x), 50.5, 50.3, 49.1, 49.0, 41.9, 41.7, 40.4, 40.3, 30.7, 30.6, 30.5, 30.3, 28.5, 27.0, 24.0, 23.9, 23.8, 23.8 ppm.

HRMS (ESI) Calc. for $C_{22}H_{38}N_2NaO_8^+$ :	481.2520 $[M+Na]^+$
Found:	481.2526 $[M+Na]^+$ .

**(2*S*,5*S*)-di-*tert*-butyl 2,5-bis(3-hydroxypropyl)piperazine-1,4-dicarboxylate (**266**)**

To a suspension of  $\text{LiAlH}_4$  (9.54 g, 251 mmol) in THF (350 mL) was added ester **292** (7.20 g, 25.1 mmol) at 0 °C in portions and the resulting mixture was heated under reflux for 22 h. The grey suspension was cooled to 0 °C and diluted with  $\text{Et}_2\text{O}$  (150 mL). To the mixture were carefully added water (10 mL), aqueous NaOH (10 mL; 15%) and again water (30 mL). The white suspension was allowed to warm to RT and stirred for 30 min.  $\text{Na}_2\text{SO}_4$  (10 g) were added and stirring was continued for 20 min. Solids were filtered off and washed with THF (2 x 200 mL). The filtrate was concentrated and the residue dissolved in THF (100 mL) and EtOH (just enough to dissolve all solids). To the clear solution was added  $\text{Boc}_2\text{O}$  (11.5 g, 52.8 mmol) at 0 °C and the solution was allowed to warm to RT over night. The crude reaction mixture was diluted with saturated aqueous  $\text{NaHCO}_3$  (100 mL) and extracted with EtOAc (4 x 100 mL). The combined organic extracts were dried over  $\text{Na}_2\text{SO}_4$ , filtered and concentrated (water bath temperature: 30 °C). Normal phase flash column chromatography ( $\text{SiO}_2$ ;  $\text{CH}_2\text{Cl}_2/\text{MeOH}$  = 98:2 to 95:5) yielded 4.72 g (47%) of diol **266** as a colorless solid.

$R_f$  = 0.3 ( $\text{CH}_2\text{Cl}_2/\text{MeOH}$  = 95:5).

m.p. ( $\text{CH}_2\text{Cl}_2/\text{MeOH}$ ) = 103-104 °C.

$[\alpha]_D^{24} = +84.2$  ( $c$  = 0.5,  $\text{CH}_2\text{Cl}_2$ ).

IR (ATR):  $\tilde{\nu}$  = 3452 (m), 2976 (w), 2942 (w), 2867 (w), 1670 (s), 1419 (s), 1366 (s), 1152 (s), 1052 (s)  $\text{cm}^{-1}$ .

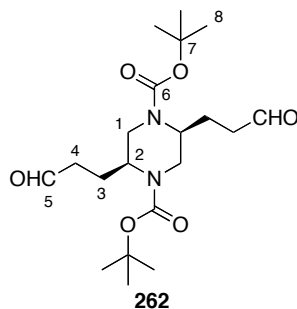
$^1\text{H}$  NMR ( $\text{CDCl}_3$ , 600 MHz)  $\delta$  4.05-3.89 (br s, 4H,  $H_{-2} + H_{a-1}$ ), 3.65-3.54 ( $m_c$ , 4H,  $H_{-5}$ ), 2.58 (dd,  $J$  = 11.6 Hz,  $J$  = 13.7 Hz, 2H,  $H_{b-1}$ ), 1.59-1.48 (m, 6H,  $H_{-3}$  and  $H_{-4}$ ), 1.46-1.34 (m, 20H,  $H_{-8}$  and  $H_{-3}$  or  $H_{-4}$ ) ppm.

$^{13}\text{C}$  NMR ( $\text{CDCl}_3$ , 150 MHz)  $\delta$  155.6 (C-6), 80.2 (C-7), 62.4 (C-5), 53.1 (C-2), 42.1 (br, C-1), 28.6 (C-3 or C-4), 28.5 (C-8 and C-3 or C-4) ppm.

HRMS (ESI) Calc. for  $\text{C}_{20}\text{H}_{38}\text{N}_2\text{NaO}_6^+$ : 425.2622  $[\text{M}+\text{Na}]^+$

Found: 425.2627  $[\text{M}+\text{Na}]^+$ .

**(2*S*,5*S*)-di-*tert*-butyl 2,5-bis(3-oxopropyl)piperazine-1,4-dicarboxylate (**262**)**



To a solution of DMSO (2.91 mL, 41.0 mmol) in  $\text{CH}_2\text{Cl}_2$  (120 mL) was added  $(\text{COCl})_2$  (12.3 mL, 24.6 mmol; 2M in  $\text{CH}_2\text{Cl}_2$ ) at  $-78^\circ\text{C}$  and the solution was stirred for 30 min. A solution of diol **266** (3.30 g, 8.20 mmol) in  $\text{CH}_2\text{Cl}_2$  (30 mL) was added with a cannula and stirring was continued for 1 h.  $\text{NEt}_3$  (11.4 mL, 82.0 mmol) was added drop-wise and the mixture was allowed to warm to room temperature over 12 h. The reaction was poured on 10% aqueous NaCl solution (150 mL) and the resulting biphasic mixture was extracted with  $\text{CH}_2\text{Cl}_2$  (4 x 100 mL). The combined organic extracts were washed successively with 1N HCl (2 x 100 mL), saturated aqueous  $\text{NaHCO}_3$  (2 x 100 mL) and brine (1 x 100 mL). The organic phase was dried over  $\text{Na}_2\text{SO}_4$ , filtered and concentrated. Normal phase flash column chromatography ( $\text{SiO}_2$ ; PE/EtOAc = 2:1 to 3:2) yielded 2.82 g (86%) of aldehyde **262** as a colorless oil.

$R_f = 0.4$  (PE/EtOAc = 1:1).

$[\alpha]_D^{24} = +71.0$  ( $c = 1.0$ ,  $\text{CH}_2\text{Cl}_2$ ).

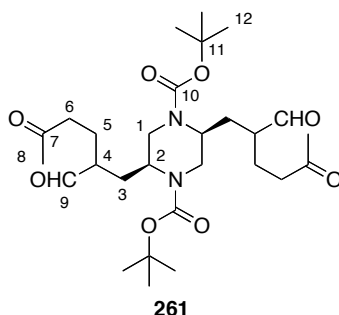
IR (ATR):  $\tilde{\nu} = 2973$  (w), 2932 (w), 1724 (m), 1685 (s), 1403 (s), 1365 (s), 1248 (m), 1154 (s), 1137 (s), 865 (m), 770 (m)  $\text{cm}^{-1}$ .

$^1\text{H}$  NMR ( $\text{CDCl}_3$ , 400 MHz)  $\delta$  9.77 (s, 2H, *H*-5), 4.16-3.89 (br m, 4H, *H*-2 and *H*<sub>a</sub>-1), 2.52 (m<sub>c</sub>, 6H, *H*<sub>b</sub>-1 and *H*-4), 1.82-1.62 (m, 4H, *H*-3), 1.43 (s, 18H, *H*-8) ppm.

$^{13}\text{C}$  NMR ( $\text{CDCl}_3$ , 100 MHz)  $\delta$  201.4 (C-5), 155.7 (C-6), 80.6 (C-7), 52.7 (C-2), 42.0 (br, C-1), 40.4 (C-4), 28.5 (C-8), 24.1 (C-3) ppm.

HRMS (EI) Calc. for  $\text{C}_{20}\text{H}_{34}\text{N}_2\text{O}_6^+$ : 398.2411  $[\text{M}]^+$   
 Found: 398.2410  $[\text{M}]^+$ .

**(2*S*,5*S*)-di-*tert*-butyl 2,5-bis(2-formyl-5-oxohexyl)piperazine-1,4-dicarboxylate (**261**)**



*Procedure A (TMSNEt<sub>2</sub>):*

To a solution of aldehyde **262** (2.8 g, 7.03 mmol) in MeCN (100 mL) was added MVK (1.71 mL, 21.1 mmol) and TMSNEt<sub>2</sub> (663  $\mu\text{L}$ , 3.51 mmol) and the mixture was heated under reflux overnight. The solvent was removed under reduced pressure and the residue purified using normal phase flash column chromatography ( $\text{SiO}_2$ ; PE/EtOAc = 2:3 to 1:2) to yield 2.80 g (74%) of keto-aldehyde **261** (mixture of diastereomers) as a colorless oil. NMR indicated a ratio of 1:1 for the two aldehyde signals at 9.60 and 9.53 ppm (200 MHz).

*Procedure B ((S)-2-(methoxydiphenylmethyl)pyrrolidine):*

To a solution of aldehyde **262** (50.0 mg, 125  $\mu\text{mol}$ ) in MVK (31  $\mu\text{L}$ , 376  $\mu\text{mol}$ ) was added (S)-2-(methoxydiphenylmethyl)pyrrolidine (3.4 mg, 12.5  $\mu\text{mol}$ ) and ethyl 3,4-dihydroxybenzoate (9.1 mg, 50.2  $\mu\text{mol}$ ) at 0  $^\circ\text{C}$  and the resulting mixture was stirred at 4  $^\circ\text{C}$  for 4 d. NMR indicated a ratio of 1:3.1 for the two aldehyde signals at 9.60 and 9.53 ppm (200 MHz). Normal phase flash column chromatography ( $\text{SiO}_2$ ; PE/EtOAc = 2:3 to 1:2) yielded 34 mg (74%) of keto-aldehyde **261** (mixture of diastereomers) as a colorless oil.

*Procedure B ((R)-2-(methoxydiphenylmethyl)pyrrolidine):*

To a solution of aldehyde **262** (25.0 mg, 62.7  $\mu\text{mol}$ ) in MVK (31  $\mu\text{L}$ , 376  $\mu\text{mol}$ ) was added (R)-2-(methoxydiphenylmethyl)pyrrolidine (3.4 mg, 12.5  $\mu\text{mol}$ ) and ethyl 3,4-dihydroxybenzoate (4.6 mg, 25.1  $\mu\text{mol}$ ) at 0  $^\circ\text{C}$  and the resulting mixture was stirred at 4  $^\circ\text{C}$  for 4 d. NMR indicated a ratio of 1.7: 1 for the two aldehyde signals at 9.60 and 9.53 ppm (200 MHz).

Normal phase flash column chromatography (SiO<sub>2</sub>; PE/EtOAc = 2:3 to 1:2) yielded 15 mg (44%) of keto-aldehyde **261** (mixture of diastereomers) as a colorless oil.

*Analytical data for the stochastic mixture (Procedure A):*

$R_f = 0.4$  (PE/EtOAc = 1:2).

$[\alpha]_D^{24} = +42.6$  (c = 1.0, CH<sub>2</sub>Cl<sub>2</sub>).

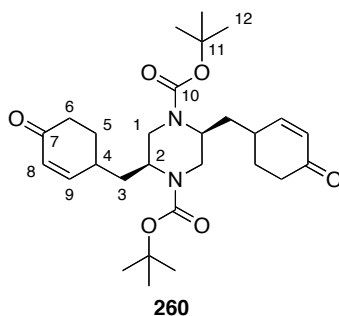
IR (ATR):  $\tilde{\nu} = 2975$  (w), 2931 (w), 1686 (s), 1478 (w), 1413 (m), 1365 (m), 1247 (w), 1153 (m), 1108 (m) cm<sup>-1</sup>.

<sup>1</sup>H NMR (CDCl<sub>3</sub>, 600 MHz, mixture of diastereomers and rotamers)  $\delta$  9.60 (m<sub>c</sub>, 1H, *H*-9), 9.54 (m<sub>c</sub>, 1H, *H*-9\*), 4.24-3.80 (br m, 4H, *H*-2 and *H*<sub>a</sub>-1), 2.83-2.30 (m, 8H, *H*<sub>b</sub>-1 and *H*-4 and *H*-6), 2.13 (m<sub>c</sub>, 6H, *H*-8), 1.97-1.84 (m, 3H, *H*<sub>a</sub>-3 and *H*<sub>a</sub>-5), 1.84-1.73 (m, 3H, *H*<sub>a</sub>\*-3 and *H*<sub>b</sub>-5), 1.48-1.29 (m, 20H, *H*-12 and *H*<sub>b</sub>-3/*H*<sub>b</sub>-3\*) ppm.

<sup>13</sup>C NMR (CDCl<sub>3</sub>, 150 MHz, mixture of diastereomers and rotamers)  $\delta$  207.7 (*C*-7), 203.4 (*C*-9), 155.5 (*C*-10), 80.8 (*C*-11), 51.4 (*C*-2), 48.1 (*C*-4\*), 47.4 (*C*-4), 42.1 (br, *C*-1), 40.6 (*C*-1\*), 40.4 (*C*-6), 31.3 (*C*-3\*), 30.8 (*C*-3\*), 30.7 (*C*-3), 30.2 (2x, *C*-8), 28.5 (*C*-12), 23.1 (*C*-5), 22.8 (*C*-5\*) ppm.

HRMS (EI)	Calc. for C <sub>28</sub> H <sub>46</sub> N <sub>2</sub> O <sub>8</sub> <sup>+</sup> :	538.3254 [M] <sup>+</sup>
	Found:	538.3264 [M] <sup>+</sup> .

**(2*S*,5*S*)-di-*tert*-butyl 2,5-bis((4-oxocyclohex-2-enyl)methyl)piperazine-1,4-dicarboxylate (260)**



To a solution of stochastic keto-aldehyde **261** (500 mg, 0.928 mmol) in THF/Et<sub>2</sub>O (300 mL, 1:2) was added an aqueous solution of KOH (100 mL; 0.1 M) and *n*-Bu<sub>4</sub>NOH (186 μL, 0.186 mmol; 1M in H<sub>2</sub>O) at 0°C and the mixture was heated under reflux for 24 h. The reaction was diluted with saturated aqueous NH<sub>4</sub>Cl solution (20 mL) and extracted with EtOAc (3 x 25 mL). The combined organic extracts were dried over MgSO<sub>4</sub>, filtered and concentrated. Normal phase flash column chromatography (SiO<sub>2</sub>; PE/EtOAc = 2:3) yielded 266 mg (57%) of enone **260** (mixture of diastereomers) as a colorless wax. The (*R,S*) isomer could not be discriminated from its C<sub>2</sub>-symmetrical diastereomers. The ratio of the α-protons of the enone indicated a 1:1 ratio of (*R*)- and (*S*)-configured cyclohexenone moieties.

$R_f = 0.2$  (PE/EtOAc = 2:3).

$[\alpha]_D^{24} = -6.2$  ( $c = 1.0$ , CH<sub>2</sub>Cl<sub>2</sub>).

IR (ATR):  $\tilde{\nu} = 3353$  (w), 2973 (w), 2929 (w), 1737 (w), 1676 (s), 1392 (w), 1665 (m), 1245 (m), 1153 (m), 1033 (w) cm<sup>-1</sup>.

<sup>1</sup>H NMR (CDCl<sub>3</sub>, 600 MHz, mixture of diastereomers and Boc rotamers)  $\delta$  7.01-6.89 (br s, 1H, *H*-9), 6.80 (add,  $J = 2.4$  Hz,  $J = 10.2$  Hz, 1H, *H*-9\*), 5.98 (add,  $J = 2.2$  Hz,  $J = 8.2$  Hz,  $J = 10.2$  Hz, 2H, *H*-8), 4.41-3.86 (br m, 4H, *H*-2 and *H*<sub>a</sub>-1), 2.59-2.44 (m, 6H, *H*<sub>b</sub>-1 and *H*-4 and *H*<sub>a</sub>-3 and *H*<sub>a</sub>-6), 2.40-2.26 (m, 3H, *H*<sub>b</sub>-3 or *H*<sub>b</sub>-6 and *H*<sub>a</sub>-5), 2.16-2.07 (m, 1H, *H*<sub>a</sub>-5\*), 1.79-1.65 (m, 3H, *H*<sub>a</sub>-3 or *H*<sub>a</sub>-6 and *H*<sub>b</sub>-5\*), 1.64-1.57 (m, 1H, *H*<sub>b</sub>-3\* or *H*<sub>b</sub>-6\*), 1.44 (mc, 19H, *H*-12 and *H*<sub>b</sub>-3\* or *H*<sub>b</sub>-6\*), 1.37-1.30 (m, 1H, *H*<sub>b</sub>-3\* or *H*<sub>b</sub>-6\*) ppm.

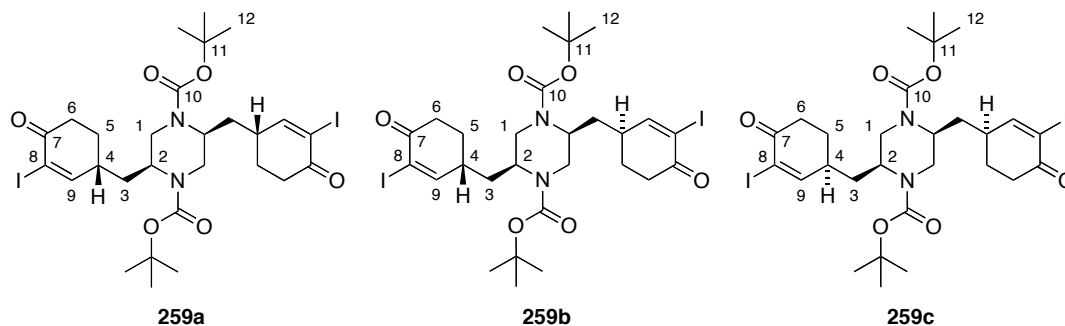
<sup>13</sup>C NMR (CDCl<sub>3</sub>, 150 MHz, mixture of diastereomers and Boc rotamers)  $\delta$  199.4 (*C*-7), 155.7 (*C*-10), 155.6 (*C*-10\*), 154.2 (br, *C*-9), 153.9 (*C*-9\*), 129.6 (*C*-8), 129.3 (*C*-8\*), 80.9 (*C*-



11), 51.3 (*C*-2), 51.2 (*C*-2'), 50.9 (*C*-2\*), 50.8 (*C*-2\*'), 42.0 (br, *C*-1), 36.9 (*C*-3 or *C*-6), 36.8 (*C*-6 or *C*-3), 33.2 (*C*-4), 32.6 (*C*-4\*), 29.2 (*C*-5), 29.0 (*C*-5\*), 28.5 (2x, *C*-12) ppm.

HRMS (EI) Calc. for  $C_{28}H_{42}N_2O_6^+$ : 502.3037  $[M]^+$   
 Found: 502.3032  $[M]^+$ .

**(2*S*,5*S*)-di-*tert*-butyl 2,5-bis(((*R*)-3-iodo-4-oxocyclohex-2-enyl)methyl)piperazine-1,4-dicarboxylate, (2*S*,5*S*)-di-*tert*-butyl 2,5-bis(((*S*)-3-iodo-4-oxocyclohex-2-enyl)methyl)piperazine-1,4-dicarboxylate and (2*S*,5*S*)-di-*tert*-butyl 2-(((*R*)-3-iodo-4-oxocyclohex-2-enyl)methyl)-5-(((*S*)-3-iodo-4-oxocyclohex-2-enyl)methyl)piperazine-1,4-dicarboxylate (**259a**, **259b** and **259c**)**



To a solution of the diastereomeric mixture of enones **260** (1.00 g, 1.99 mmol) in  $CH_2Cl_2$ /pyridine (120 mL, 5:1) was added  $I_2$  (1.10 g, 4.38 mmol) at 0°C. The solution was allowed to warm to RT and stirred for 8 h. The reaction mixture was diluted with  $CH_2Cl_2$  (200 mL) and poured on a saturated aqueous solution of  $NH_4Cl$  and a few drops of saturated  $NaS_2O_3$  solution. The mixture was extracted with  $CH_2Cl_2$  (3 x 40 mL) and the combined organic fractions were washed successively with 1N HCl (2 x 40 mL) and brine (1 x 40 mL). The  $CH_2Cl_2$ -phase was dried over  $MgSO_4$ , filtered and concentrated. Normal phase flash column chromatography ( $SiO_2$ ; PE/EtOAc = 1:1) yielded 1.46 g (97%) of a mixture of the vinyl iodides **259** as a colorless oil. HPLC showed a 1:2:1 ratio of diastereomers. Separation by preparative HPLC (Varian Microsorb60Si8; flow = 80 mL/min; gradient program:  $t = 0$ : PE/EtOAc = 10%;  $t = 25$  min: PE/EtOAc = 90%) yielded 213 mg (14%), 496 mg (33%) and 313 mg (21%) of the individual diastereomeric  $\alpha$ -iodo enones **259a**, **259b** and **259c** as colorless, light- and temperature-sensitive solids. The absolute configuration of the fast and the slow eluting  $C_2$ -symmetric fractions (**259a**, **259c**) could not be assigned.

*Analytical data for the fast eluting diastereomer (259a or 259c):*

$R_f = 0.5$  (PE/EtOAc = 1:1).

$R_t = 15.6$  min.

m.p. (PE/EtOAc) > 119 °C (decomp.).

$[\alpha]_D^{24} = -4.0$  (c = 0.2, CH<sub>2</sub>Cl<sub>2</sub>).

IR (ATR):  $\tilde{\nu} = 2971$  (w), 2923 (w), 1682 (s), 1583 (w), 1414 (m), 1364 (w), 1320 (w), 1249 (w), 1153 (m) cm<sup>-1</sup>.

<sup>1</sup>H NMR (CDCl<sub>3</sub>, 600 MHz)  $\delta$  7.59 (d,  $J = 2.4$  Hz, 2H, *H*-9), 4.36-4.13 (br m, 2H, *H*-2), 4.13-3.87 (br m, 2H, *H*<sub>a</sub>-1), 2.76 (ddd,  $J = 4.4$  Hz,  $J = 5.2$  Hz,  $J = 16.7$  Hz, 2H, *H*-4), 2.68-2.59 (br m, 2H, *H*<sub>b</sub>-1 and *H*<sub>b</sub>-1), 2.57-2.48 (m, 4H, *H*<sub>a</sub>-5), 2.47-2.32 (br m, 2H, *H*<sub>b</sub>-5), 1.83-1.67 (m, 4H, *H*<sub>b</sub>-5 and *H*<sub>a</sub>-3), 1.46 (s, 18H, *H*-12), 1.40-1.31 (m, 2H, *H*<sub>b</sub>-3) ppm.

<sup>13</sup>C NMR (CDCl<sub>3</sub>, 150 MHz)  $\delta$  192.1 (*C*-7), 162.7 (br, *C*-9), 155.7 (*C*-10), 104.1 (*C*-8), 81.1 (*C*-11), 51.1 (*C*-2), 42.2 (br, *C*-1), 37.9 (br, *C*-4), 36.5 (*C*-3), 35.8 (*C*-6), 29.0 (*C*-5), 28.6 (*C*-12) ppm.

HRMS (ESI) Calc. for C <sub>28</sub> H <sub>44</sub> I <sub>2</sub> N <sub>3</sub> O <sub>6</sub> <sup>+</sup> :	772.1314 [M+NH <sub>4</sub> ] <sup>+</sup>
Found:	772.1306 [M+NH <sub>4</sub> ] <sup>+</sup> .

*Analytical data for the (R,S) isomer 259b:*

$R_f = 0.4$  (PE/EtOAc = 1:1).

$R_t = 16.6$  min.

m.p. (PE/EtOAc) > 120 °C (decomp.).

$[\alpha]_D^{24} = -44.0$  (c = 0.2, CH<sub>2</sub>Cl<sub>2</sub>).

IR (ATR):  $\tilde{\nu}$  = 2971 (w), 2923 (w), 1682 (s), 1578 (w), 1414 (w), 1364 (w), 1320 (w), 1272 (w), 1243 (w), 1153 (m)  $\text{cm}^{-1}$ .

$^1\text{H}$  NMR ( $\text{CDCl}_3$ , 600 MHz)  $\delta$  7.74 (br s, 1H,  $H$ -9), 7.59 (d,  $J$  = 2.4 Hz, 1H,  $H$ -9\*), 4.35-4.14 (br m, 2H,  $H$ -2), 4.13-3.89 (br m, 2H,  $H_a$ -1), 2.81-2.72 (m, 2H,  $H_a$ -6), 2.67-2.58 (br m, 2H,  $H$ -4), 2.58-2.45 (m, 4H,  $H_b$ -6 and  $H_b$ -1), 2.38 (br s, 1H,  $H_a$ -5), 2.19-2.12 (m, 1H,  $H_a$ -5\*), 1.86-1.75 (m, 2H,  $H_b$ -5 and  $H_b$ -5\*), 1.74-1.68 (m, 1H,  $H_a$ -3), 1.63-1.55 (m, 2H,  $H_a$ -3\* and  $\text{H}_2\text{O}$ ), 1.52-1.42 (m, 19H,  $H_b$ -3\*), 1.38-1.31 (m, 1H,  $H_b$ -3) ppm.

$^{13}\text{C}$  NMR ( $\text{CDCl}_3$ , 150 MHz)  $\delta$  192.0 ( $C$ -7), 162.8 ( $C$ -9), 162.2 ( $C$ -9\*), 155.7 ( $C$ -10), 155.6 ( $C$ -10\*), 104.2 ( $C$ -8), 104.1 ( $C$ -8\*), 81.3 ( $C$ -11), 81.2 ( $C$ -11\*), 51.1 ( $C$ -2), 50.7 ( $C$ -2\*), 42.0 (br  $C$ -1), 37.8 ( $C$ -2), 37.2 ( $C$ -2\*), 36.5 ( $C$ -3), 36.3 ( $C$ -3\*), 35.9 ( $C$ -6), 35.8 ( $C$ -6\*), 29.3 ( $C$ -5), 29.0 ( $C$ -5\*), 28.6 ( $C$ -12), 28.6 ( $C$ -12\*) ppm.

HRMS (ESI) Calc. for  $\text{C}_{28}\text{H}_{44}\text{I}_2\text{N}_3\text{O}_6^+$ : 772.1314  $[\text{M}+\text{NH}_4]^+$   
 Found: 772.1308  $[\text{M}+\text{NH}_4]^+$ .

*Analytical data for the slow eluting diastereomer (259c or 259a):*

$R_f$  = 0.3 (PE/EtOAc = 1:1).

$R_t$  = 17.9 min.

m.p. (PE/EtOAc) > 112 °C (decomp.).

$[\alpha]_D^{24} = -93.0$  ( $c$  = 0.2,  $\text{CH}_2\text{Cl}_2$ ).

IR (ATR):  $\tilde{\nu}$  = 2970 (w), 2923 (w), 1682 (s), 1582 (w), 1416 (m), 1364 (m), 1322 (w), 1268 (w), 1158 (m)  $\text{cm}^{-1}$ .

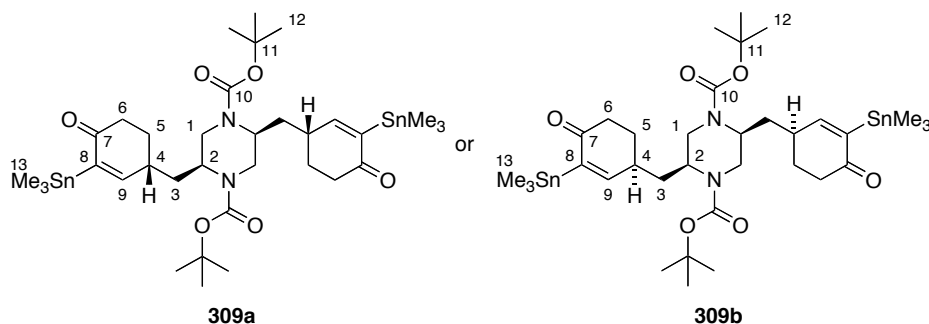
$^1\text{H}$  NMR ( $\text{CDCl}_3$ , 400 MHz)  $\delta$  7.74 (s, 1H,  $H$ -9), 4.36-4.20 (br m, 2H,  $H$ -2), 4.15-3.96 (br m, 2H,  $H_a$ -1), 2.78 (dt,  $J$  = 4.5 Hz,  $J$  = 16.6 Hz, 2H,  $H_a$ -6), 2.68-2.42 (m, 6H,  $H_b$ -1 and  $H$ -4 and  $H_b$ -6), 2.21-2.09 (m, 2H,  $H_a$ -5), 1.89-1.74 (m, 2H,  $H_b$ -5), 1.64-1.54 (m, 3H,  $H_a$ -3 and  $\text{H}_2\text{O}$ ), 1.51-1.39 (m, 20H,  $H_b$ -3 and  $H$ -12) ppm.

$^{13}\text{C}$  NMR ( $\text{CDCl}_3$ , 100 MHz)  $\delta$  192.0 (C-7), 162.2 (C-9), 155.7 (C-10), 104.1 (C-8), 81.33 (C-11), 50.7 (C-2), 41.8 (C-1), 37.2 (C-4), 36.4 (C-3), 35.9 (C-6), 29.4 (C-5), 28.6 (C-12) ppm.

HRMS (ESI) Calc. for  $\text{C}_{28}\text{H}_{44}\text{I}_2\text{N}_3\text{O}_6^+$ : 772.1314  $[\text{M}+\text{NH}_4]^+$

Found: 772.1307  $[\text{M}+\text{NH}_4]^+$ .

**(2*S*,5*S*)-di-*tert*-butyl 2,5-bis(((*R*)-4-oxo-3-(trimethylstannyl)cyclohex-2-enyl)methyl)piperazine-1,4-dicarboxylate (309a) or (2*S*,5*S*)-di-*tert*-butyl 2,5-bis(((*S*)-4-oxo-3-(trimethylstannyl)cyclohex-2-enyl)methyl)piperazine-1,4-dicarboxylate (309b)**



To a solution of the fast eluting iodoenone **259** (15 mg, 19.9  $\mu\text{mol}$ ) in degassed MePh (2.5 mL) was added hexamethylditin (14.3 mg, 43.7  $\mu\text{mol}$ ) and  $\text{Pd}(\text{PPh}_3)_4$  (2.3 mg, 1.99  $\mu\text{mol}$ ) and the resulting yellow solution was stirred for 5 h at 80  $^\circ\text{C}$ . The resulting dark solution was concentrated and the residue purified by normal phase flash column chromatography ( $\text{SiO}_2$  + 10w%  $\text{K}_2\text{CO}_3$ ,<sup>[318]</sup> PE/EtOAc = 3:1) to yield 7 mg (43%) of distannane **309** as a colorless oil.

$R_f = 0.2$  (PE/EtOAc = 2:1).

$[\alpha]_D^{24} = -4.0$  ( $c = 0.2$ ,  $\text{CH}_2\text{Cl}_2$ ).

IR (ATR):  $\tilde{\nu} = 2973$  (w), 2913 (w), 1693 (s), 1656 (s), 1583 (w), 1416 9m), 1365 (m), 1267 (w), 1240 (w), 1153 (m)  $\text{cm}^{-1}$ .

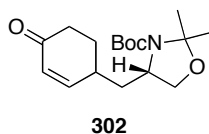
$^1\text{H}$  NMR ( $\text{CD}_2\text{Cl}_2$ , 600 MHz)  $\delta$  6.93 ( $m_c$ , 2H,  $H$ -9), 4.33-3.19 (br m, 2H, C-2), 4.08-4.93 (br m, 2H,  $H_a$ -2), 2.54 (dd,  $J = 10.7$  Hz,  $J = 14.1$  Hz, 2H,  $H_b$ -2), 2.39-2.25 (m, 4H,  $H$ -4 and  $H_a$ -6), 1.76-1.61 (m, 4H,  $H_a$ -3 and  $H_b$ -5), 1.44 (s, 18H,  $H$ -12), 1.36-1.27 (m, 2H,  $H_b$ -3), 0.14 ( $m_c$ , 18H,  $H$ -13) ppm.

$^{13}\text{C}$  NMR ( $\text{CD}_2\text{Cl}_2$ , 150 MHz)  $\delta$  202.3 (C-7), 163.6 (C-9), 155.9 (C-10), 144.9 (C-8), 80.5 (C-11), 51.6 (C-2), 42.5 (br, C-1), 37.2 (C-6), 37.1 (C-3), 35.3 (C-4), 29.6 (C-5), 28.6 (C-12), -7.6 (2x, C-13), -9.3 (C-13), -11.1 (2x, C-13) ppm.

HRMS (ESI) Calc. for  $\text{C}_{34}\text{H}_{62}\text{N}_3\text{O}_6$   $^{119}\text{Sn}_2^+$ : 846.2699  $[\text{M}+\text{NH}_4]^+$

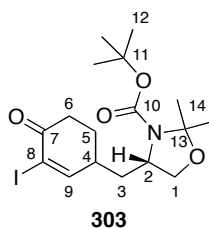
Found: 846.2680  $[\text{M}+\text{NH}_4]^+$ .

**(*S*)-*tert*-butyl 2,2-dimethyl-4-(((*R/S*)-4-oxocyclohex-2-enyl)methyl)oxazolidine-3-carboxylate (**302**)**



Cyclohexenone **302** was synthesized according to a procedure developed by G. Volpin.<sup>[275]</sup> The spectral data matched those reported earlier.

**(*S*)-*tert*-butyl 4-(((*R/S*)-3-iodo-4-oxocyclohex-2-enyl)methyl)-2,2-dimethyloxazolidine-3-carboxylate (**303**)**



To a solution of enone **302** (20.0 mg, 64.6  $\mu\text{mol}$ ) in  $\text{CH}_2\text{Cl}_2$ /pyridine (1.8 mL, 5:1) was added  $\text{I}_2$  (20.0 mg, 77.6  $\mu\text{mol}$ ) and the mixture was stirred overnight at RT. The mixture was diluted with EtOAc (50 mL) and washed with on a solution of saturated aqueous  $\text{Na}_2\text{S}_2\text{O}_3$ , brine and water (1:2:1, 1 x 40 mL), 1 N HCl (2 x 20 mL) and again brine. The organic extract was dried over  $\text{MgSO}_4$ , filtered and concentrated Normal phase flash column chromatography ( $\text{SiO}_2$ ; PE/EtOAc = 6:1) yielded 14 mg (50%) of vinyl iodide **303** (mixture of diastereomers) as a colorless, light- and temperature-sensitive oil. NMR indicated a ratio of 1:3 for the vinyl-protons.

$R_f$  = 0.6 (PE/EtOAc = 2:1).

$[\alpha]_D^{24} = -6.4$  ( $c$  = 0.86,  $\text{CH}_2\text{Cl}_2$ ).

IR (ATR):  $\tilde{\nu}$  = 2977 (m), 2935 (m), 2872 (m), 1683 (s), 1584 (w), 1386 (s), 1364 (s), 1256 (m), 1169 (m), 1087 (m), 1071 (m)  $\text{cm}^{-1}$ .

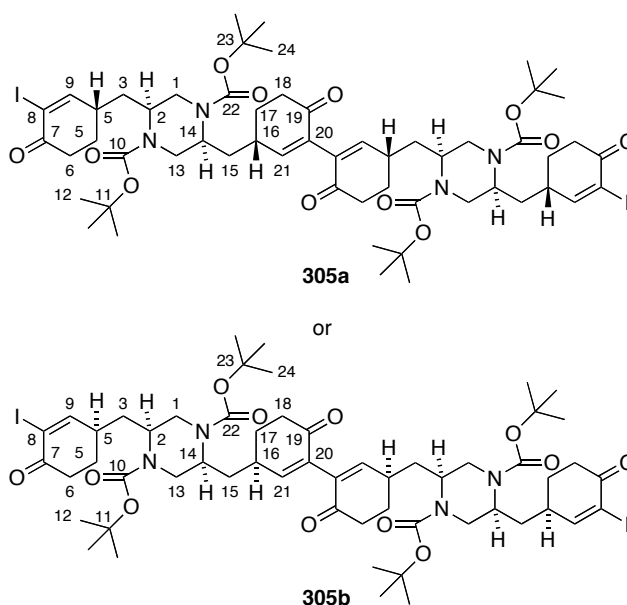
$^1\text{H}$  NMR ( $\text{CDCl}_3$ , 400 MHz; mixture of diastereomers and Boc rotamers)  $\delta$  7.76-7.57 (m, 1H, *H*-9), 4.16-3.86 (m, 2H, *H*<sub>a</sub>-1 and *H*-2), 3.79-3.67 (m, 1H, *H*<sub>b</sub>-1), 2.78 (ddd,  $J$  = 4.2 Hz,  $J$  = 5.9 Hz,  $J$  = 16.7 Hz, 1H, *H*<sub>a</sub>-6), 2.64-2.48 (m, 2H, *H*-4 and *H*<sub>b</sub>-6), 2.47-2.12 (m, 1H, *H*<sub>a</sub>-5), 2.04-1.72 (m, 3H, *H*-3 and *H*<sub>b</sub>-5), 1.62-1.54 (br m, 3H, *H*-14), 1.53-1.43 (m, 12H, *H*-12 and *H*-14) ppm.

$^{13}\text{C}$  NMR ( $\text{CDCl}_3$ , 100 MHz; mixture of diastereomers and Boc rotamers)  $\delta$  192.3 (*C*-7), 192.2 (*C*-7'), 192.0 (*C*-7\*), 191.9 (*C*-7\*''), 163.3 (*C*-9), 163.0 (*C*-9'), 162.9 (*C*-9\*), 161.4 (*C*-9''), 152.7 (*C*-10), 152.4 (*C*-10'), 151.6 (*C*-10\*), 151.5 (*C*-10\*''), 104.5 (*C*-8), 104.1 (*C*-8'), 103.9 (*C*-8\*), 103.8 (*C*-8\*''), 94.2 (2x, *C*-13), 93.7 (*C*-13\*), 93.6 (*C*-13\*''), 80.6 (*C*-11), 80.4 (*C*-11\*), 67.5 (*C*-1), 67.3 (*C*-1'), 67.2 (*C*-1\*), 67.1 (*C*-1\*''), 55.5 (*C*-2), 55.3 (*C*-2'), 55.1 (*C*-2\*), 54.9 (*C*-2\*''), 38.6 (*C*-3), 38.3 (*C*-3'), 38.1 (*C*-4), 38.0 (*C*-4'), 37.8 (*C*-3\*), 36.2 (*C*-6), 36.0 (*C*-6'), 35.7 (*C*-6\*), 35.5 (*C*-6\*''), 30.0 (*C*-5), 29.7 (*C*-5'), 28.8 (*C*-12), 28.7 (*C*-12'), 28.5 (*C*-12\* and *C*-5\*), 28.4 (*C*-12\*' and *C*-5\*''), 28.0 (2x, *C*-14), 27.3 (*C*-14'), 27.1 (*C*-14\*), 24.5 (*C*-14\*''), 23.2 (*C*-14'') ppm.

HRMS (EI)	Calc. for $\text{C}_{17}\text{H}_{26}^{127}\text{INO}_4^+$ :	435.0901 $[\text{M}]^+$
	Found:	435.0920 $[\text{M}]^+$ .

*Note: The following molecules have been isolated repeatedly from different experiments. Only exemplary procedures are given.*

**(*R/S,2S,2'S,5S,5'S*)-1,4-di-*tert*-butyl 5,5'-((3*R/S,3'R/S*)-6,6'-dioxo-1,1'-bi(cyclohex-1-ene)-3,3'-diyl)bis(methylene)bis(2-(((*R/S*)-3-iodo-4-oxocyclohex-2-enyl)methyl)piperazine-1,4-dicarboxylate) (**305**)**



To a suspension of  $\text{Ni(COD)}_2$  (6 mg, 21.9  $\mu\text{mol}$ ) in degassed THF (5 mL) was added  $\text{PBU}_3$  (10  $\mu\text{L}$ , 41.8  $\mu\text{mol}$ ) and solid, fast eluting iodoenone **259** (15 mg, 19.9  $\mu\text{mol}$ ) at  $-78^\circ\text{C}$ . The mixture was warmed to  $-20^\circ\text{C}$  and stirred for 1 h, then warmed to RT and stirred for additional 2 h. The reaction was poured on an aqueous  $\text{NH}_4\text{Cl}$  solution (20 mL) and extracted with EtOAc (3 x 20 mL). The combined extracts were dried over  $\text{Na}_2\text{SO}_4$ , filtered and concentrated. Preparative TLC ( $\text{SiO}_2$ ;  $\text{CH}_2\text{Cl}_2/\text{MeOH} = 95:5$ ) yielded 4 mg (16%) of dimer **305** as a colorless wax.

$R_f = 0.4$  ( $\text{CH}_2\text{Cl}_2/\text{MeOH} = 95:5$ ).

IR (ATR):  $\tilde{\nu} = 2927$  (w), 1689 (s), 1475 (w), 1416 (m), 1364 (m), 1267 (m), 1250 (m), 1164 (s)  $\text{cm}^{-1}$ .

$^1\text{H}$  NMR ( $\text{CDCl}_3$ , 600 MHz)  $\delta$  7.60 (d,  $J = 2.6$  Hz, 2H,  $H-9$ ), 6.62 (d,  $J = 2.0$  Hz, 2H,  $H-21$ ), 4.37-4.16 (br m, 4H,  $H-2$  and  $H-14$ ), 4.13-3.91 (br m, 4H,  $H_a-1$  and  $H_a-13$ ), 2.77 (dt,  $J = 4.5$  Hz,  $J = 9.5$  Hz, 2H,  $H_a-6$ ), 2.68-2.47 (m, 12H,  $H_b-1$  and  $H-4$  and  $H_b-6$  and  $H-16$  and  $H_a-$

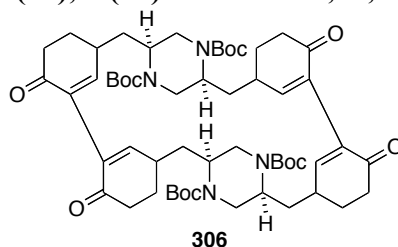
18), 2.47-2.30 (m, 6H,  $H_a$ -5 and  $H_a$ -17 and  $H_b$ -18), 1.82-1.67 (m, 8H,  $H_a$ -3 and  $H_b$ -5 and  $H_a$ -15 and  $H_b$ -17), 1.51-1.42 (m, 36H,  $H$ -12 and  $H$ -24), 1.39-1.32 (m, 4H,  $H_b$ -3 and  $H_b$ -15) ppm.

$^{13}\text{C}$  NMR ( $\text{CDCl}_3$ , 150 MHz)  $\delta$  197.2 (C-19), 192.0 (C-7), 162.1 (C-9), 155.8 (C-10 and C-22), 152.9 (C-21), 136.1 (C-20), 104.5 (C-8), 81.1 (C-11 or C-23), 81.0 (C-23 or C-11), 51.2 (C-2 and C-14), 37.9 (C-16), 37.1 (2x) (C-3 or C-15, and C-18), 36.5 (C-15 or C-3), 35.8 (C-6), 33.7 (C-4), 29.1 (C-5 or C-17), 28.9 (C-17 or C-5), 28.6 (C-12 and C-24) ppm.

*Note: Due to the low amount of material,  $^{13}\text{C}$ -signals were in part reconstructed from 2D-spectra (HSQC, HMBC). C-1 and C-13 could not be assigned owing to their low intensity due to ring inversion.*

HRMS (ESI) Calc. for  $\text{C}_{56}\text{H}_{84}\text{I}_2\text{N}_5\text{O}_{12}^+$ : 1272.4200  $[\text{M}+\text{NH}_4]^+$   
 Found: 1272.4201  $[\text{M}+\text{NH}_4]^+$ .

**[1,4-di-*tert*-butyl (2*S*,5*S*)-2,5-bis[(3-iodo-4-oxocyclohex-2-en-1-yl)methyl]piperazine-1,4-dicarboxylate; 15,17-di-*tert*-butyl (1*S*,14*S*)-6,9-dioxo-15,17-diazatetracyclo [12.2.2.1<sup>3,7</sup>.1<sup>8,12</sup>]icosa-7(20),8(19)-diene-15,17-dicarboxylate; 15,31,33,37-tetra-*tert*-butyl (1*S*,14*S*,17*S*,30*S*)-6,9,22,25-tetraoxo-15,31,33,37-tetraazaheptacyclo[28.2.2.2<sup>14,17</sup>.1<sup>3,7</sup>.1<sup>8,12</sup>.1<sup>19,23</sup>.1<sup>24,28</sup>]tetraconta-7(40),8(39),23(36),24(35)-tetraene-15,31,33,37-tetracarboxylate]] (306)**



#### Procedure A:

Solid bis(triphenylphosphine)nickel(II) chloride (28.6 mg, 43.7  $\mu\text{mol}$ ),  $\text{PPh}_3$  (22.9 mg, 87.5  $\mu\text{mol}$ ), KI (7.3 mg, 43.7  $\mu\text{mol}$ ) and Zn (2.9 mg, 43.7  $\mu\text{mol}$ ) were mixed in a flask. The vessel was flushed with argon three times, degassed DMF (1 mL) was added and the resulting mixture was heated to 55  $^\circ\text{C}$  for 30 min. The solution turned to a dark red. (*R,S*)-diiodide **259b** in degassed DMF (2 mL) was added drop-wise over 5 min and heating was continued for 3 h. The reaction was allowed to cool to RT and aqueous 10% NaCl solution (5 mL) was added. To the mixture was added EtOAc (30 mL) and the organic phase was extracted successively with aqueous 10% NaCl (2 x 5 mL), 2 M HCl (1 x 5 mL) and brine (1 x 5 mL). The organic extract was dried over  $\text{MgSO}_4$ , filtered and concentrated. Normal phase flash



column chromatography (SiO<sub>2</sub>; CH<sub>2</sub>Cl<sub>2</sub>/MeOH = 98:2 to 95:5) yielded 1 mg (5%) of macrocycle **306** as a colorless film.

*Procedure B:*

To a solution of CuCl (11.8 mg, 119 μmol) in degassed DMF (3 mL) was added distannane **309** (7 mg, 8.45 μmol) in degassed DMF (1.5 mL) over 15 min. at 70 °C. The mixture was stirred for further 30 min and then saturated aqueous NH<sub>4</sub>Cl (5 mL) and aqueous NH<sub>3</sub> (a few drops) and EtOAc (10 mL) were added and the open flask was stirred vigorously for 15 min. The phases were separated and the aqueous phase was extracted with EtOAc (2 x 10 mL). The combined organic extracts were washed with brine, dried over MgSO<sub>4</sub>, filtered and concentrated. Preparative TLC (SiO<sub>2</sub>; CH<sub>2</sub>Cl<sub>2</sub>/MeOH = 95:5) yielded 2 mg (24%) of macrocycle **306** as a colorless film.

R<sub>f</sub> = 0.2 (CH<sub>2</sub>Cl<sub>2</sub>/MeOH = 95:5).

IR (ATR):  $\tilde{\nu}$  = 2971 (w), 2927 (w), 1687 (s), 1477 (w), 1453 (w), 1417 (m), 1365 (m), 1249 (m), 1161 (s) cm<sup>-1</sup>.

<sup>1</sup>H NMR (CDCl<sub>3</sub>, 600 MHz)  $\delta$  6.71-6.32 (m, 4H), 3.37-4.16 (br m, 4H), 4.11-3.81 (br m, 4H), 2.90-2.73 (m, 2H), 2.70-2.10 (m, 17H), 1.91-1.65 (m, 7H), 1.55-1.31 (m, 42H) ppm.

*Note: Due to the low amount of material, neither a <sup>13</sup>C NMR nor suitable 2D-spectra could be obtained.*

HRMS (ESI) Calc. for C<sub>56</sub>H<sub>80</sub>N<sub>4</sub>NaO<sub>12</sub><sup>+</sup>: 1023.5665 [M+Na]<sup>+</sup>

Found: 1023.5660 [M+Na]<sup>+</sup>.

*Note: The [M+Na]<sup>+</sup> peak was confirmed by FAB-MS.*

### **III.2 Biology**

## 1) General Experimental Details and Instrumentation

### a) Cell Culture and Transfection

HEK293T cells were plated on poly-L-lysine-coated glass coverslips (VWR, 12 mm, No. 1) and maintained in DMEM (Biochrom, 4.5 g/L D-glucose) with 10% FBS (Biochrom) at 37 °C and 10% CO<sub>2</sub> atmosphere. Cells were transiently transfected with plasmids (gracious gift from Ehud Isacoff) using the Optifect reagent (Invitrogen). The amount of total transfected cDNA per 0.5 mL well was fixed at 0.8 µg. Visualization was achieved by co-transfection with YFP (1:20) for GluA2- and GluK2-type channels or by a GFP-fusion construct (LiGluR-type). Recordings of GluA2- and GluK2-derived channels were carried out 24 h and 48 h respectively after transfection.

### b) Mouse Cortical Slice Preparation

After cervical dislocation, the brain of *wt* mice (BL/6; P10-P16) was removed and placed in ice-cold artificial cerebrospinal fluid (ACSF) containing (in mM): 87 NaCl, 75 Sucrose, 25 NaHCO<sub>3</sub>, 2.5 KCl, 1.25 NaH<sub>2</sub>PO<sub>4</sub>, 0.5 CaCl<sub>2</sub>, 7 MgCl<sub>2</sub>, 25 Glucose, bubbled with 95% O<sub>2</sub> and 5% CO<sub>2</sub>. 300 µm coronal slices were cut from the visual cortex using a custom made slicer and kept in ACSF for 1 h at 34 °C and then for up to 8 h at RT.

### c) Mouse Retina Preparation

Four to eight weeks old triple knock-out mice (*cng*<sup>-/-</sup>; *rho*<sup>-/-</sup>; *opn4*<sup>-/-</sup>) were euthanized and their retinæ dissected in normal ringer (NR; in mM: 125 NaCl, 2.5 KCl, 1 MgCl<sub>2</sub>, 2 CaCl<sub>2</sub>, 1.25 NaH<sub>2</sub>PO<sub>4</sub>, 26 NaHCO<sub>3</sub>, 20 glucose) at RT. The NR was bubbled with carbogen gas (95% oxygen, 5% carbon dioxide) to reach pH = 7.3.

### d) Patch Clamp

Patch clamp recordings were carried out using a HEKA Patch Clamp EPC10 USB amplifier in whole cell mode. HEK cells and cortical neurons were voltage-clamped at -70 mV. Pipettes (Science Products GB200-F-8P with filament) were pulled with a Narishige PC-10 pipette puller and had resistances of 6-7 MΩ. For the experiments patch-pipettes were filled with a solution containing (in mM): 140 K-gluconate, 4 NaCl, 12 KCl, 4 Mg-ATP and 10 HEPES at pH = 7.2 (adjusted with KOH). For HEK cells the extracellular solution contained (in mM): 138 NaCl, 1.5 KCl, 1.2 MgCl<sub>2</sub>, 2.5 CaCl<sub>2</sub>, 5 HEPES and 10 D-glucose at pH = 7.4 (adjusted with NaOH). For experiments in hippocampal neurons the extracellular solution

contained (in mM): 125 NaCl, 2.5 KCl, 1 MgCl<sub>2</sub>, 2 CaCl<sub>2</sub>, 1.25 NaH<sub>2</sub>PO<sub>4</sub>, 26 NaHCO<sub>3</sub>, 20 glucose at pH 7.3 (with carbogen). HEK293T cells expressing GluK2-type channels were preincubated for 10 min in external solution containing 300 mg/L concanavalin A<sup>[252]</sup> (Con-A, type VI, Sigma-Aldrich) and for GluA2-type a construct bearing the L504Y mutation was used in order to block desensitization. L-Glutamate and the other compounds were applied as reported in text and figures with complete exchange of the bath solution occurring in less than 30 s. Bath perfusion was stopped prior to switching illumination wavelengths. Illumination was applied using a TILL Photonics Polychrome 5000 monochromator through a Nikon Fluor 60x/1.00w objective. The power output of the system was determined with a Thor Labs PM100USB power and energy meter:

**Supporting Table 2.** Power output of the Polychrom 5000 monochromator.

Entry	Wavelength $\lambda$ [nm]	Power Output <sup>[a]</sup> [mW/mm <sup>2</sup> ]
1	360 nm	5.15
2	380 nm	9.07
3	400 nm	12.7
4	420 nm	15.4
5	440 nm	17.0
6	460 nm	20.5
7	480 nm	20.3
8	500 nm	18.1
9	520 nm	16.9
10	540 nm	15.7
11	560 nm	14.3

[a] Calculated for the field of view area =  $70.7 \cdot 10^{-3} \text{ mm}^2$  ( $\phi = 300 \text{ }\mu\text{m}$ ).

The supplied HEKA PatchMaster software (V2x60) was used to control the monochromator and to record the data. The results are representative data from multiple cells as indicated in the graphs.

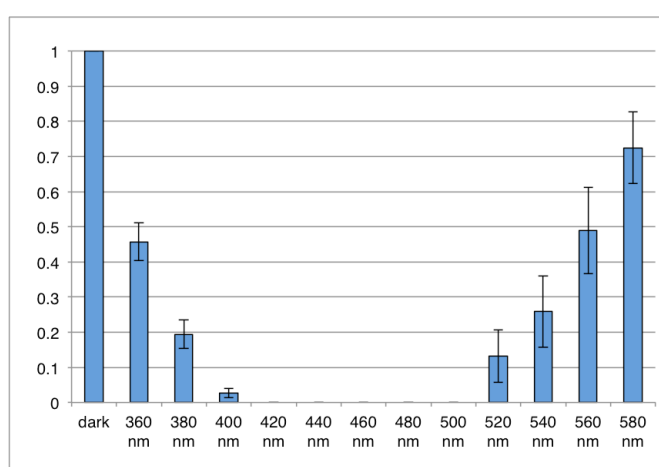
### e) MEA Recordings

After mounting the retinae on a 60-electrode multielectrode array (MEA; USB ME64 from Multichannel Systems), they were perfused with ringer's solution (NR + carbogen gas) at 34 °C with a flow rate of approx. 3-4 ml/min for 15-20 min, before the experiments were started. As a control experiment for ATA3 light switches between 480 nm and dark (each 20s) were applied to the retinae in the absence of the photoswitch. No light induced stimulation could be observed. Only retinae that had a viable spiking frequency right after mounting were taken for experiments and were analyzed. If retinae had no intrinsic activity, they were discarded. The light stimulation was done with a hand lamp (Ultrafire), which produces a

spectrum of illumination around 480 nm with high intensity ( $4.5 \text{ mW/cm}^2$ ). The analysis of the spiking frequency (rate, spikes) was done using a threshold of -4 STD of the noise level in each of the single channels and a high pass filter of 330 Hz to exclude population stimulations within the retina. Spike sorting was done with the MC-Rack software (Multichannel Systems).

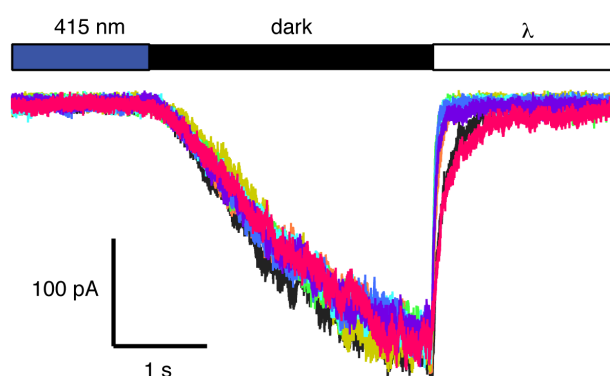
## 2) A Photochromic Agonist of AMPA Receptors – Supporting Information

### a) On Kinetics of ATA3 (89c) at GluA2 (L504Y)



**Supporting Figure 2.** Relative photocurrent evoked by  $50 \mu\text{M}$  ATA-3 (89c) acting on HEK293T cells expressing GluA2 (L504Y). The cells were exposed to darkness or illuminated with the respective wavelength for 5 s ( $n = 5$ ).

### b) Off Kinetics of ATA-3 (89c) at GluA2 (L504Y)



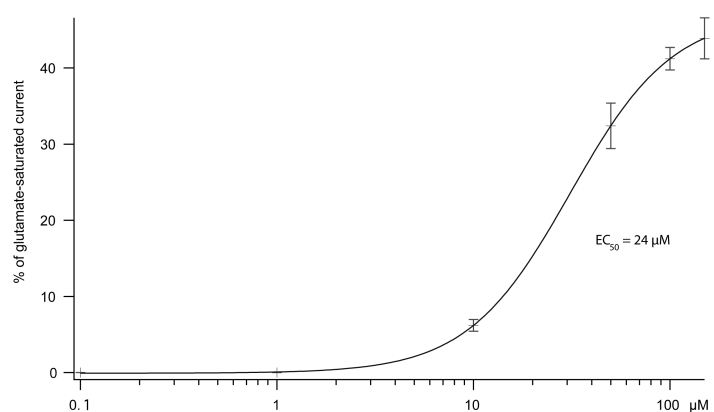
**Supporting Figure 3.** Voltage-clamp recording of ATA3 (89c) at  $50 \mu\text{M}$  concentration acting on a HEK293T cell expressing GluA2 (L504Y). The traces show distinctive off-kinetics when switching from darkness to different wavelengths of light.

**Supporting Table 3.** Time-constant  $\tau_{\text{off}}$  to reach a plateau current ( $n = 5$ ).[a]

Entry <sup>[b]</sup>	Wavelength l	$\tau_{\text{off}}$ <sup>[c]</sup>
1	360 nm	888 $\pm$ 54 ms
2	380 nm	440 $\pm$ 34 ms
3	400 nm	158 $\pm$ 19 ms
4	420 nm	72.1 $\pm$ 6.3 ms
5	440 nm	47.0 $\pm$ 11 ms
6	460 nm	48.0 $\pm$ 4.7 ms
7	480 nm	47.2 $\pm$ 7.7 ms
8	500 nm	49.5 $\pm$ 4.0 ms
9	520 nm	78.9 $\pm$ 6.3 ms
10	540 nm	197 $\pm$ 35 ms
11	560 nm	763 $\pm$ 80 ms

[a] reference: 415 nm [b] c = 50  $\mu$ M ATA-3 (**89c**) [c] mean  $\pm$  SEM

### c) EC<sub>50</sub> of *trans*-ATA-3 (**89c**) acting on GluA2 L504Y



**Supporting Figure 4.** Dose-response curve for ATA-3 (**89c**) in the dark recorded from HEK293T cells expressing GluA2 L504Y. Efficacy relative to saturating L-glutamate (300  $\mu$ M). Data ( $\pm$ SEM) were fitted to the Hill-equation ( $n = 5$  to 15 for each concentration). Due to insolubility, data points for concentrations higher than 120  $\mu$ M could not be obtained.

### 3) Mutagenesis and Cloning

Numbering of protein positions is assigned according to the direct translation of genes deposited at the NCBI. ATG = Met = position 1. Mutations were introduced into plasmids using the QuickChange method (Agilent) with custom primers:

**GluK2 D776K f:**

CCTATGGGCTCTCCATATCGAAAGAAAATCACCATAGCAATTCTT

**GluK2 D776K r:**

AAGAATTGCTATGGTGATTTTCTTTCGATATGGAGAGCCCATAGG

**GluK2 K531G f:**

TCGTGAGAAGGTCATCGACTTTTCAGGCCCGTTTATGACACTTGGA

**GluK2 K531G r:**

TCCAAGTGTCTATAAACGGGCCTGAAAAGTCGATGACCTTCTCACGA

**GluA2 Q607R f:**

GTGCCTTTATGCGGCGCGGATGCGATATTTTC

**GluA2 Q607R r:**

GAAATATCGCATCCGCGCCGCATAAAGGCAC

**GluA2 L671G f:**

CAGAAATTGCTTATGGAACAGGCGACTCTGGCTCCACTAAAG

**GluA2 L671G r:**

CTTTAGTGGAGCCAGAGTCGCCTGTTCCATAAGCAATTTCTG

**GluA2 L671A f:**

GAAATTGCTTATGGAACAGCCGACTCTGGCTCCACTAAAG

**GluA2 L671A r:**

CTTTAGTGGAGCCAGAGTCGGCTGTTCCATAAGCAATTTTC

**GluA2 L671S f:**

GAAATTGCTTATGGAACAAGCGACTCTGGCTCCACTAAAG

**GluA2 L671S r:**

CTTTAGTGGAGCCAGAGTCGCTTGTTCCATAAGCAATTTTC

**GluK2 V685G f:**

GATAGAGTATGGAGCAGGCGAGGACGGCGCAACCATG

**GluK2 V685G r:**

CATGGTTGCGCCGTCCTCGCCTGCTCCATACTCTATC

**GluA2 YeastKozak f:**

CATACTCTAGAACTAGTCCAAAAAAATGCAAAAGATTATGCATAT

**GluA2 YeastKozak r:**

ATATGCATAATCTTTTGCATTTTTTTGGACTAGTTCTAGAGTATG

**GluK2 YeastKozak f:**

ACTCTAGAACTAGTCCAAAAAAATGAAGATTATTTCCCCA

**GluK2 YeastKozak r:**

TGGGGAAATAATCTTCATTTTTTTGGACTAGTTCTAGAGT

For cloning of iGluRs DNA into yeast expression plasmids (pMet promoter), genes were amplified using PfuX polymerase (Jena Bioscience) and custom primers:

**GluA2 XbaI f:**

GAACTCTAGACCATGCAAAAGATTATGCATATTTCTGTCCTCC

**GluA2 XhoI r:**

GAACCTCGAGCTAAATTTTAACACTCTCGATGCCATATACGT

**GluK2 XbaI f:**

GAAC TCTAGA CC ATGAAGATTATTTCCCCAGTTTTAAGTAATCTAGT

**GluK2 XhoI r:**

GAAC CTCGAG TCATGCCATGGTTTCTTTACCTGGCAACCTTC

Vector and amplified genes were cut with XbaI and XhoI (NEB) restriction enzymes, purified and ligated in 1:1 to 1:3 molar ratios (vector:iGluR gene) using T4 ligase (NEB).

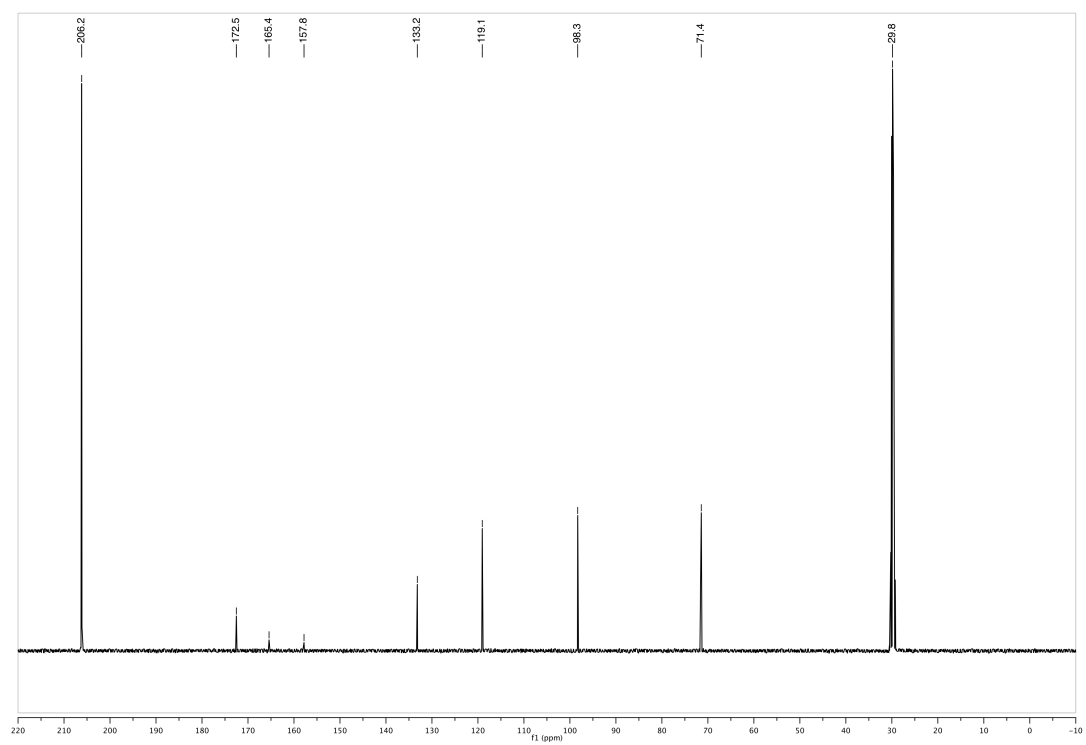
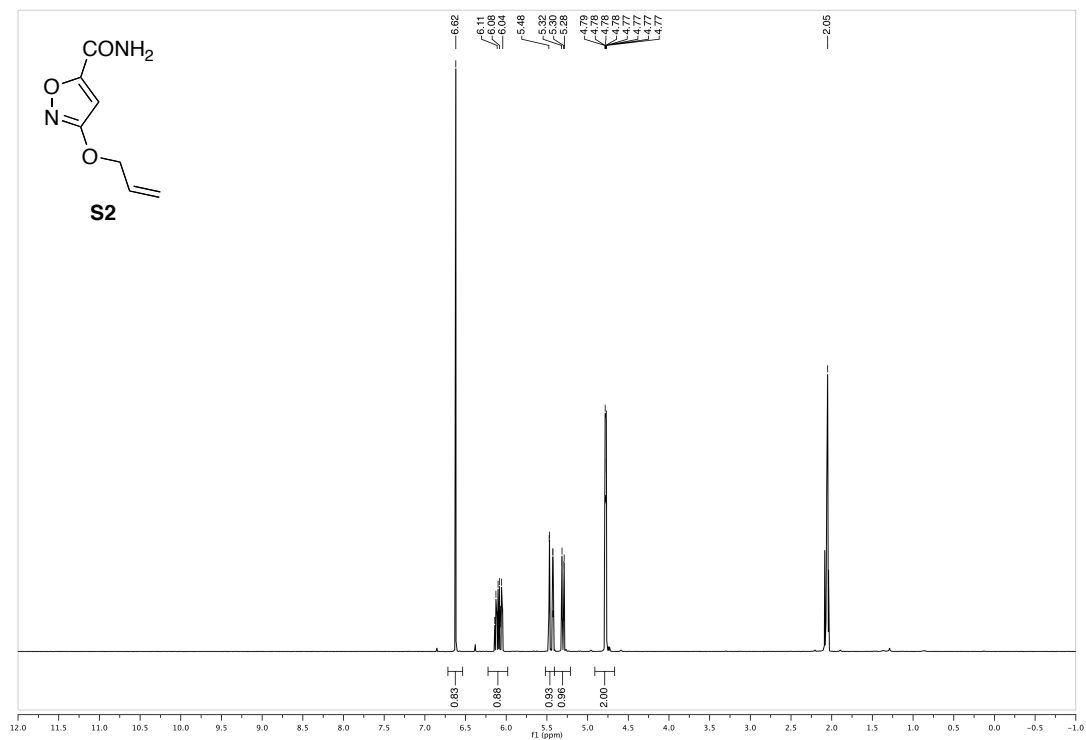
Clones were selected by ampicillin/kanamycin selection and verified by sequencing of both strands.

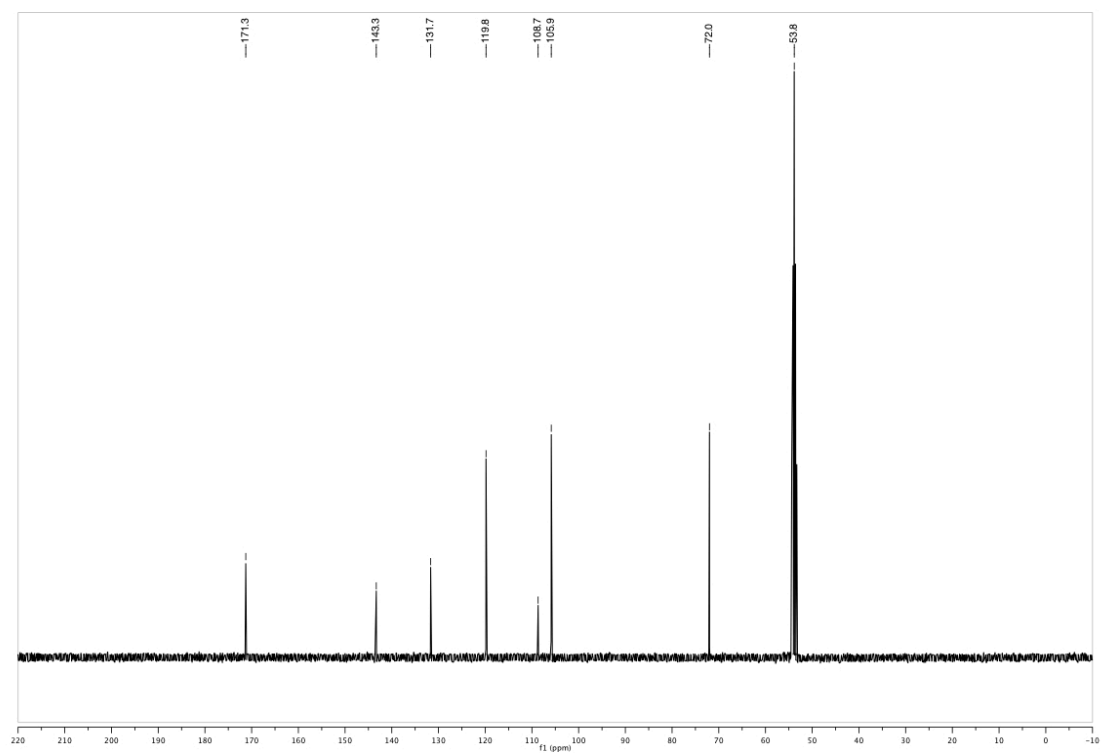
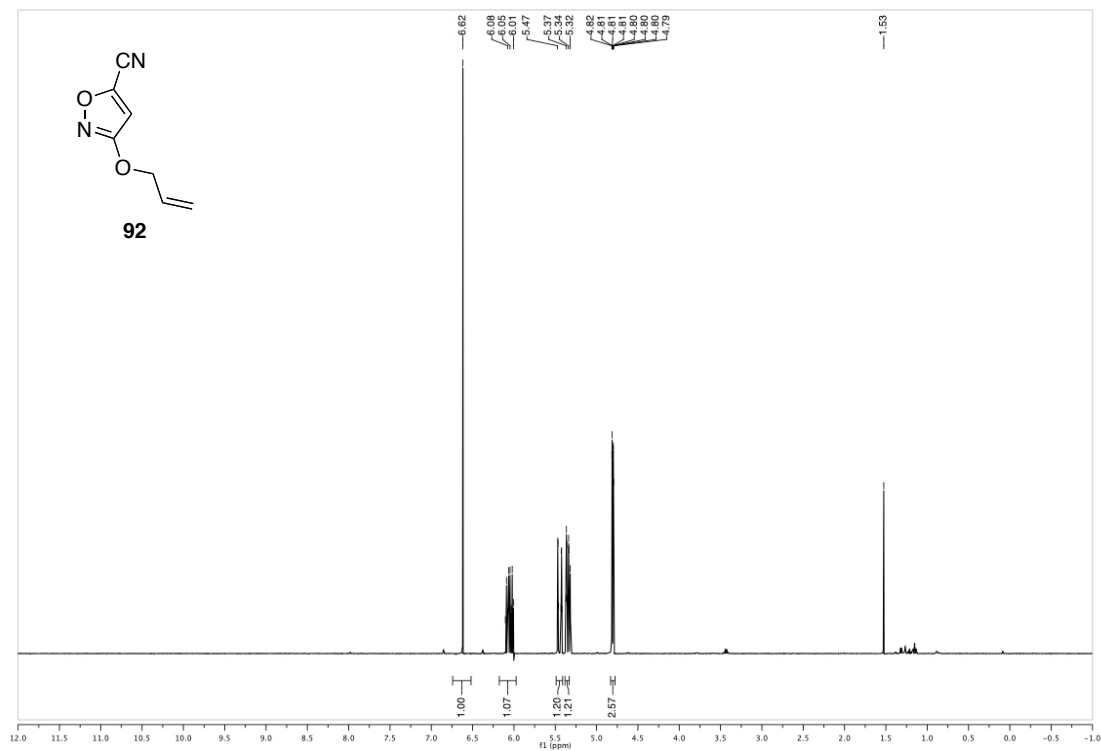


## **IV. Spectra**

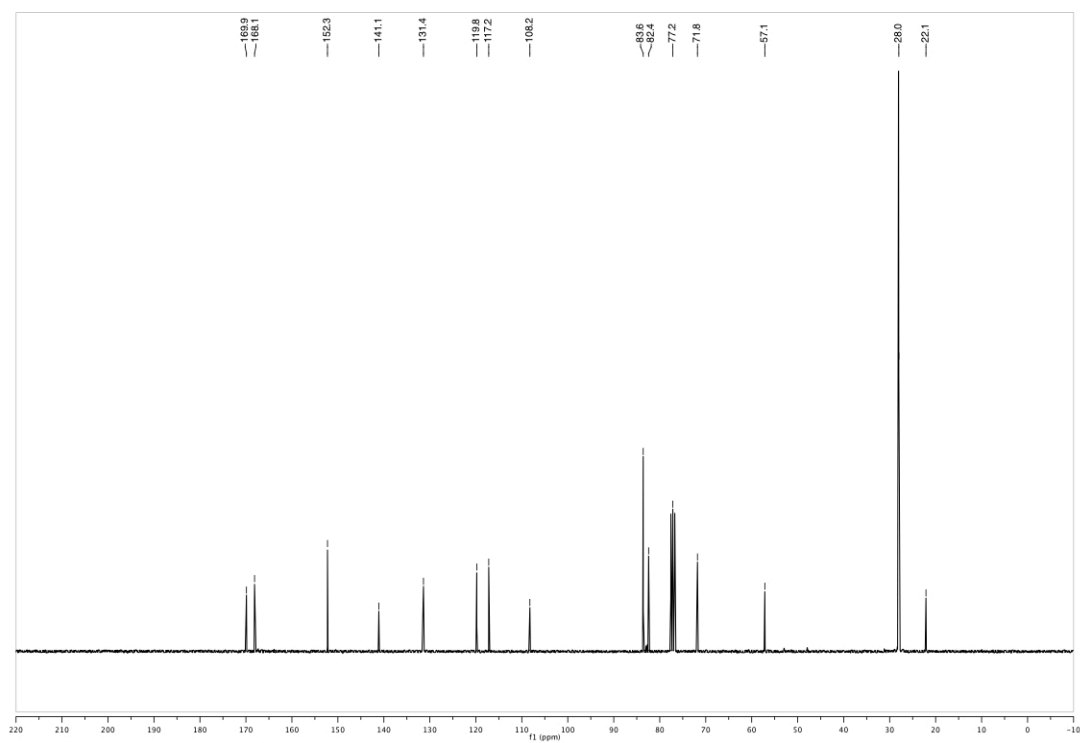
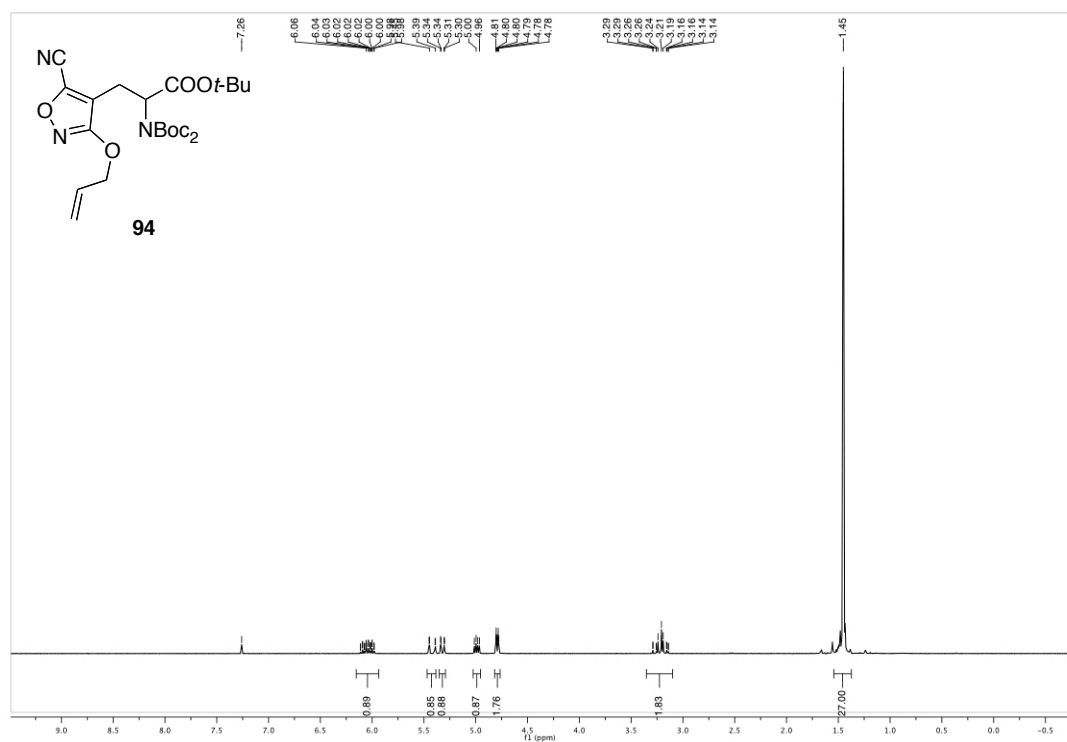
## 1) A Photochromic Agonist of AMPA Receptors

## 3-(allyloxy)isoxazole-5-carboxamide (S2)

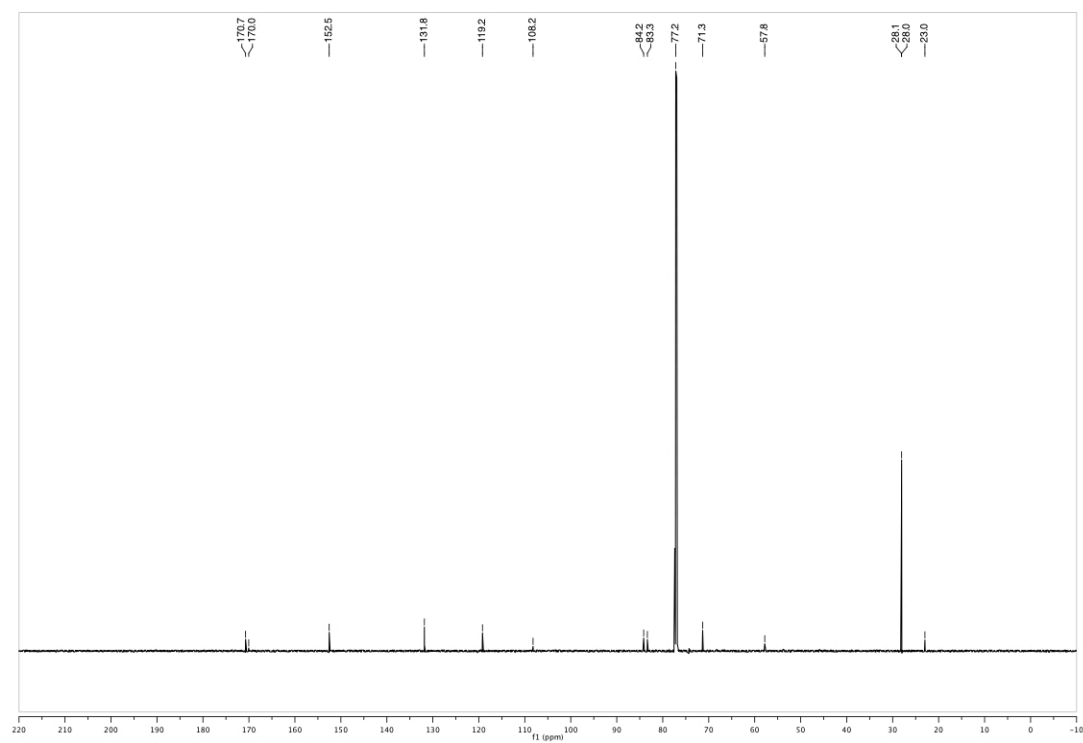
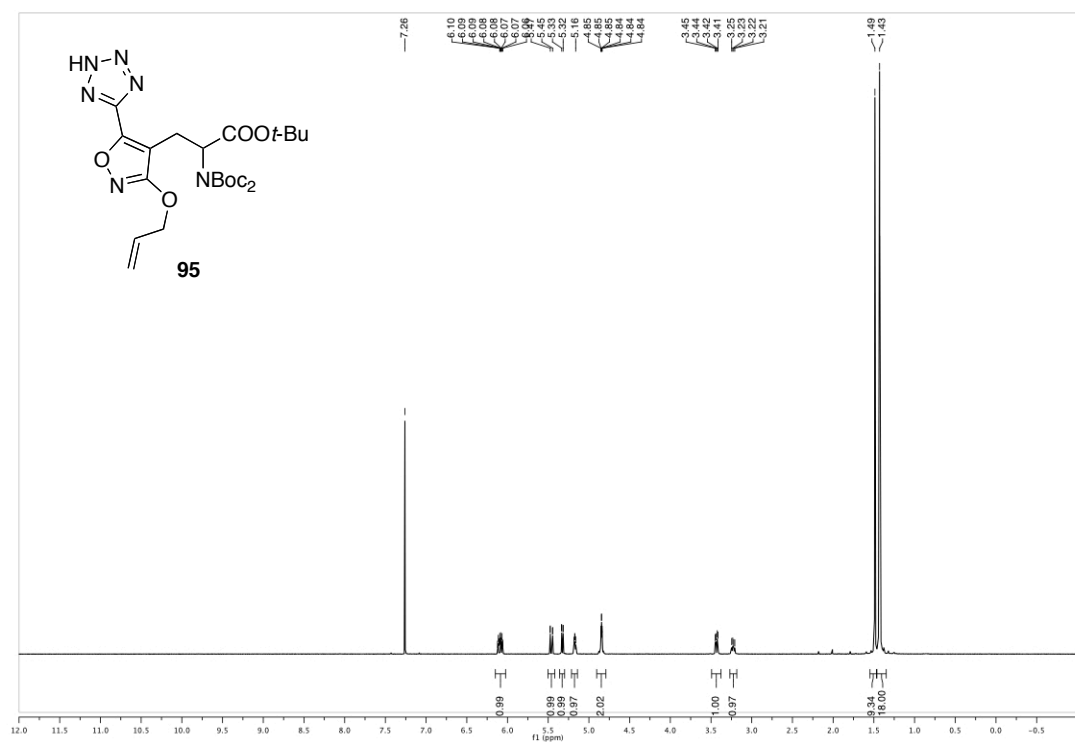


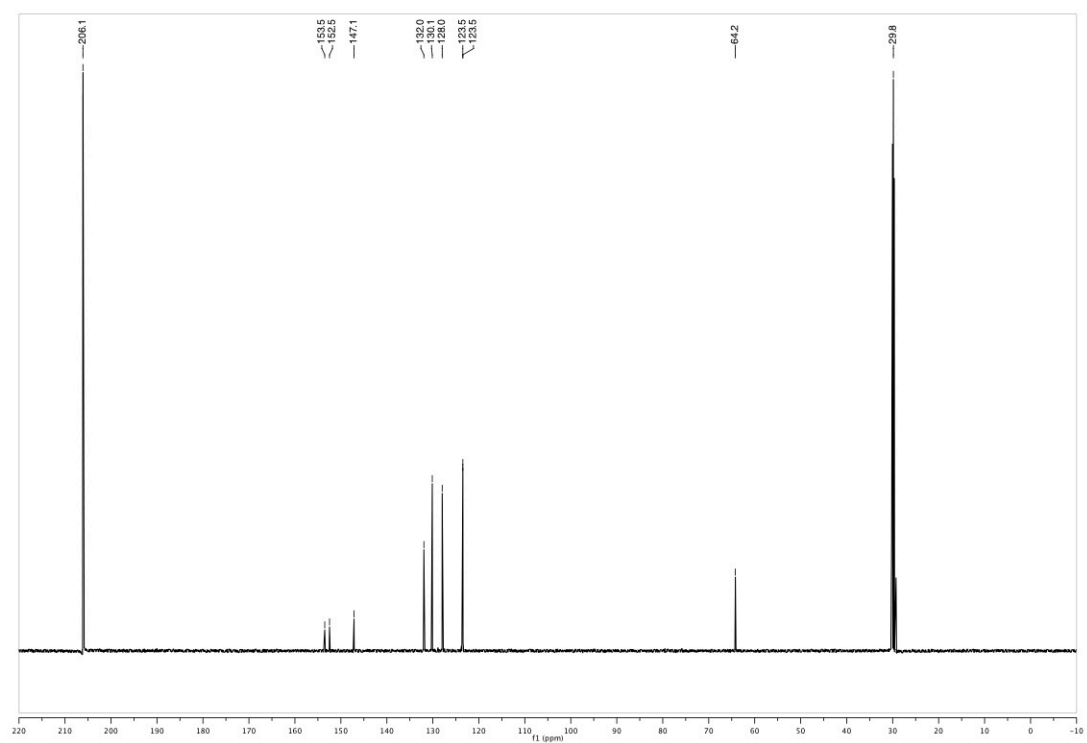
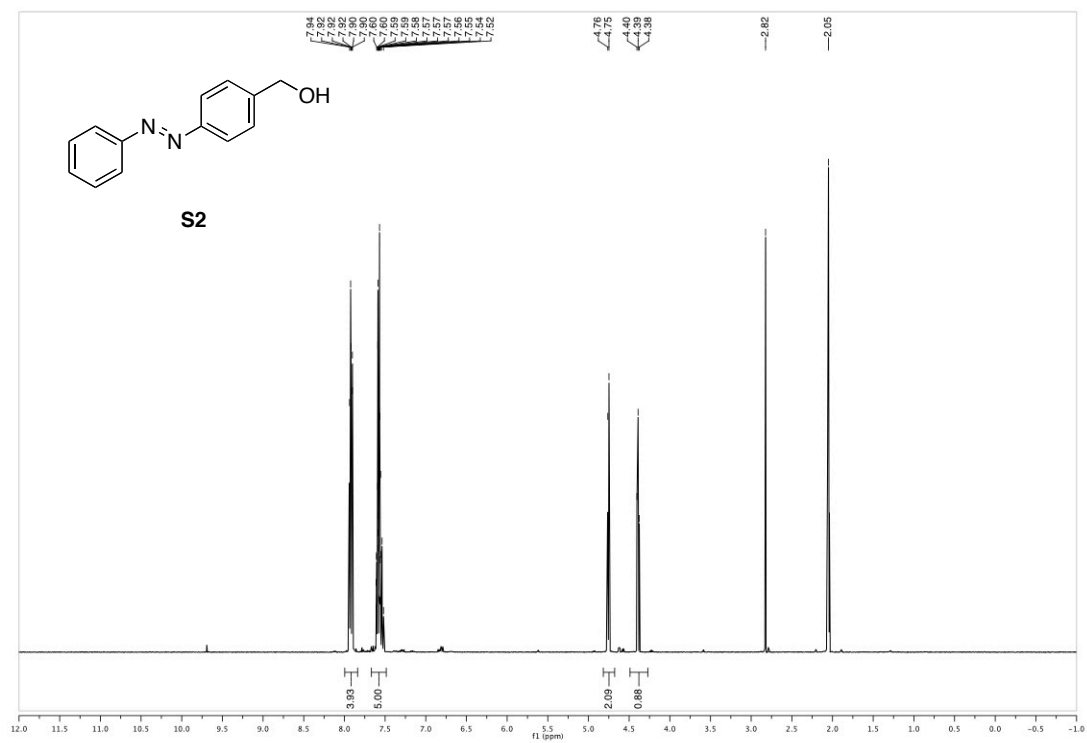
**3-(allyloxy)isoxazole-5-carbonitrile (92)**

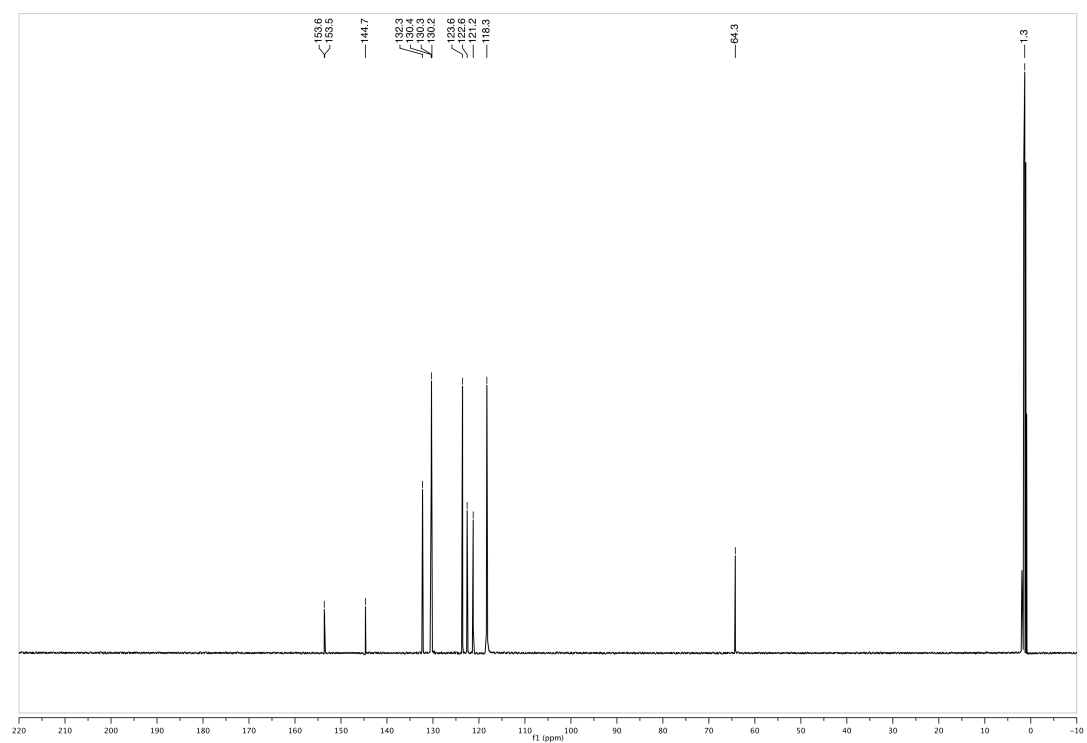
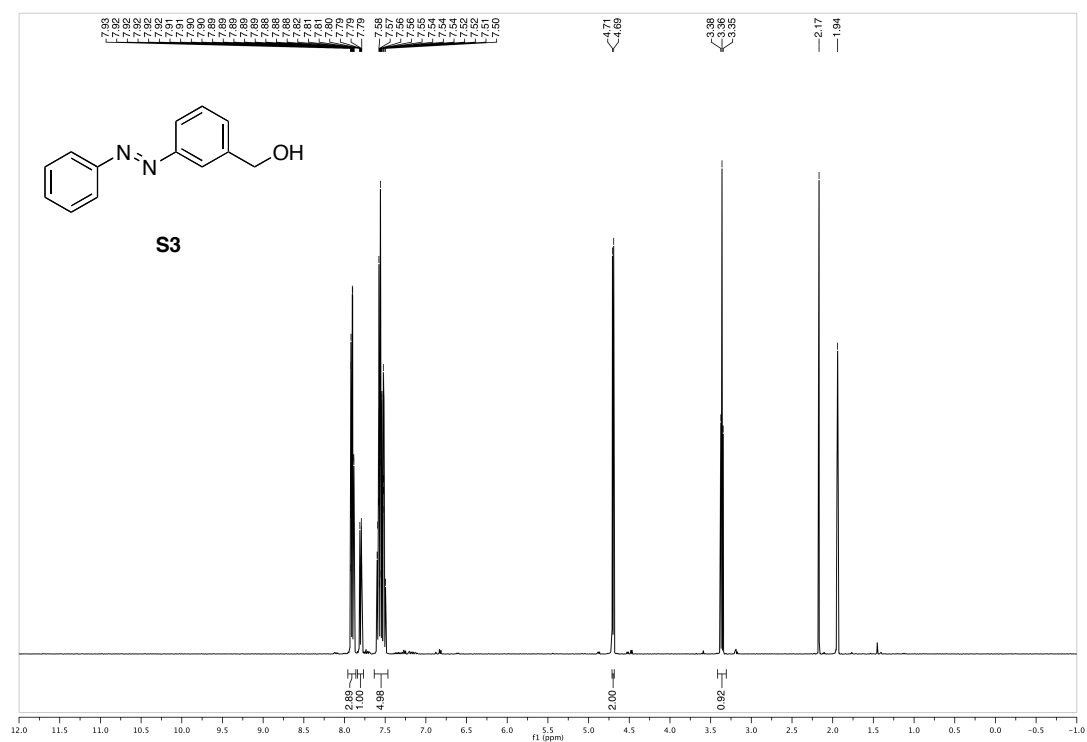
***tert*-butyl 3-(3-(allyloxy)-5-cyanoisoxazol-4-yl)-2-(bis(*tert*-butoxycarbonyl)amino)propionate (94)**



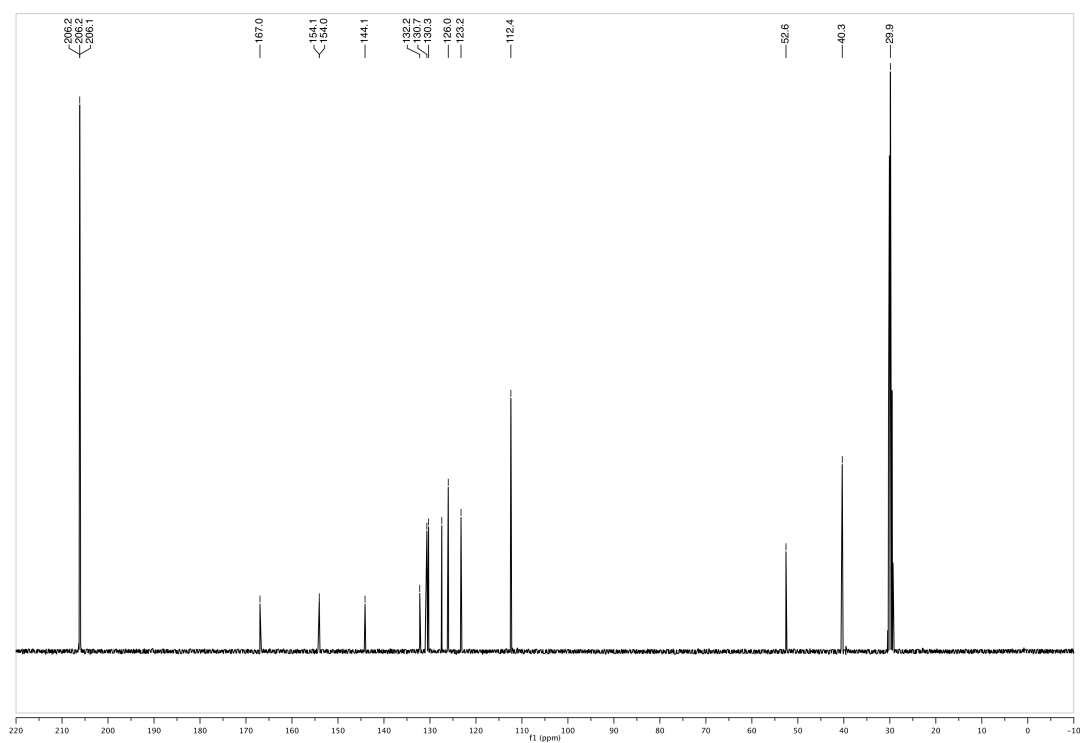
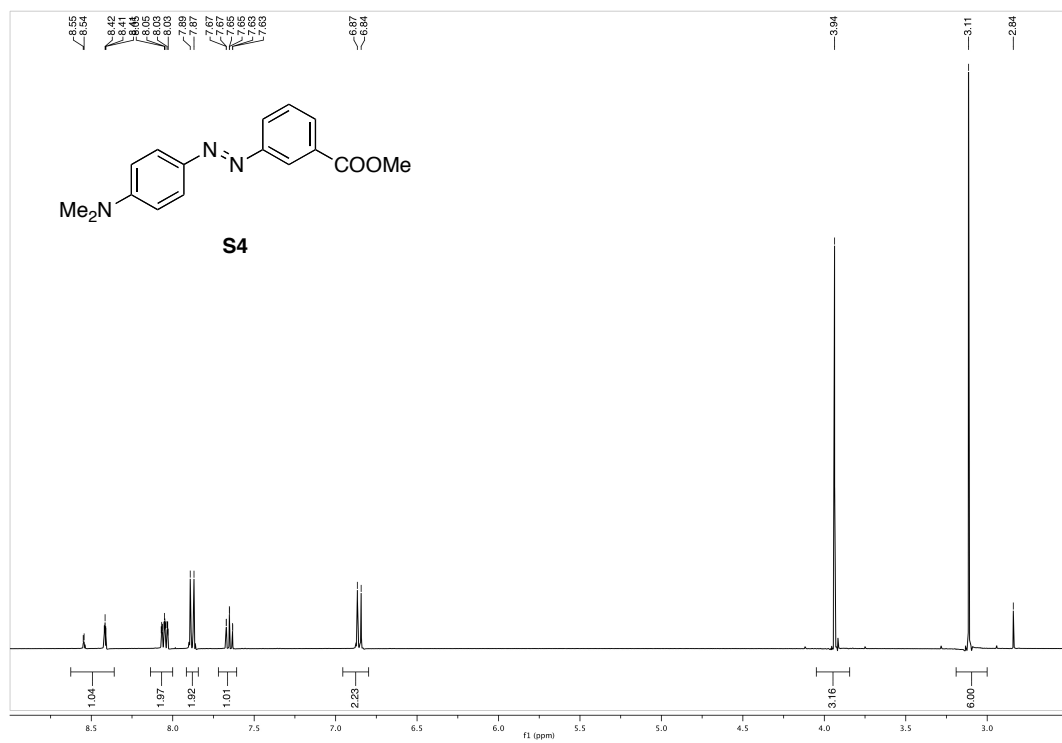
***tert*-butyl 3-(3-(allyloxy)-5-(2*H*-tetrazol-5-yl)isoxazol-4-yl)-2-(bis(*tert*-butoxycarbonyl)amino)propanoate (95)**



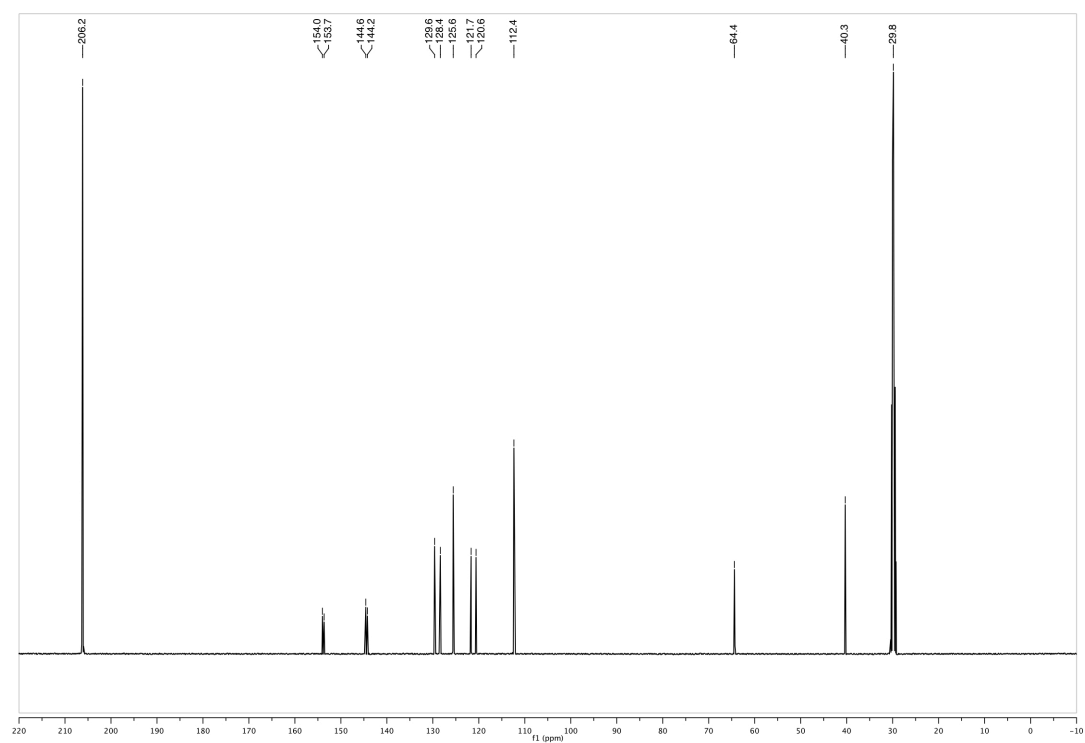
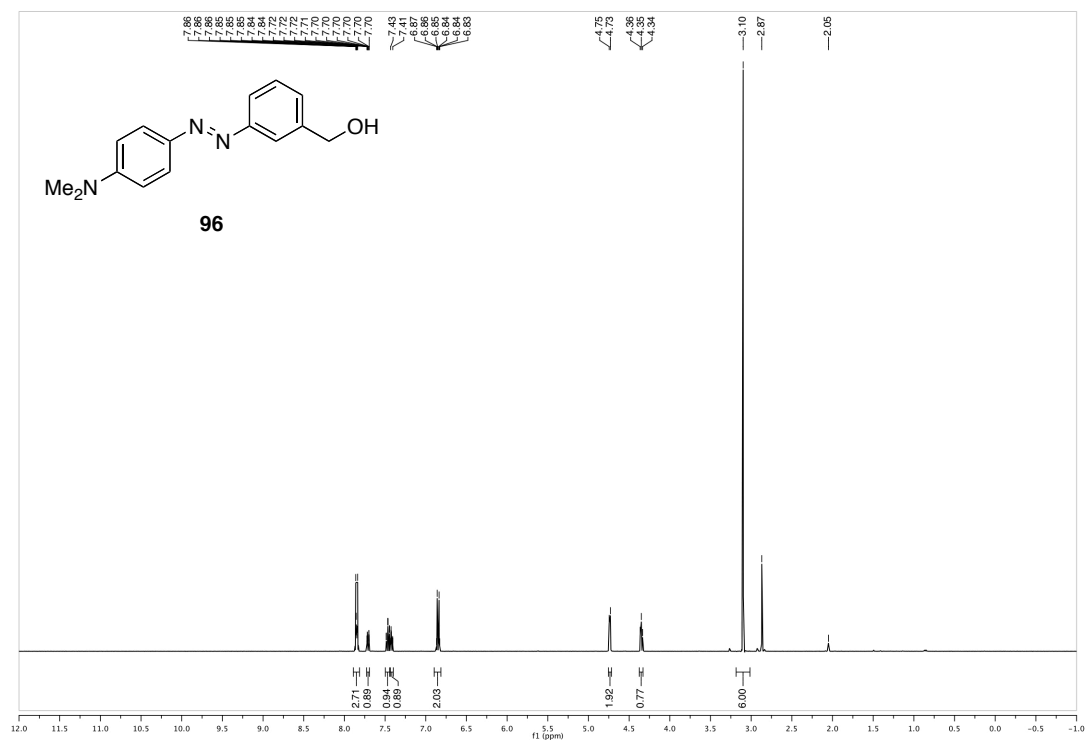
**(4-(phenyldiazenyl)phenyl)methanol (S2)**

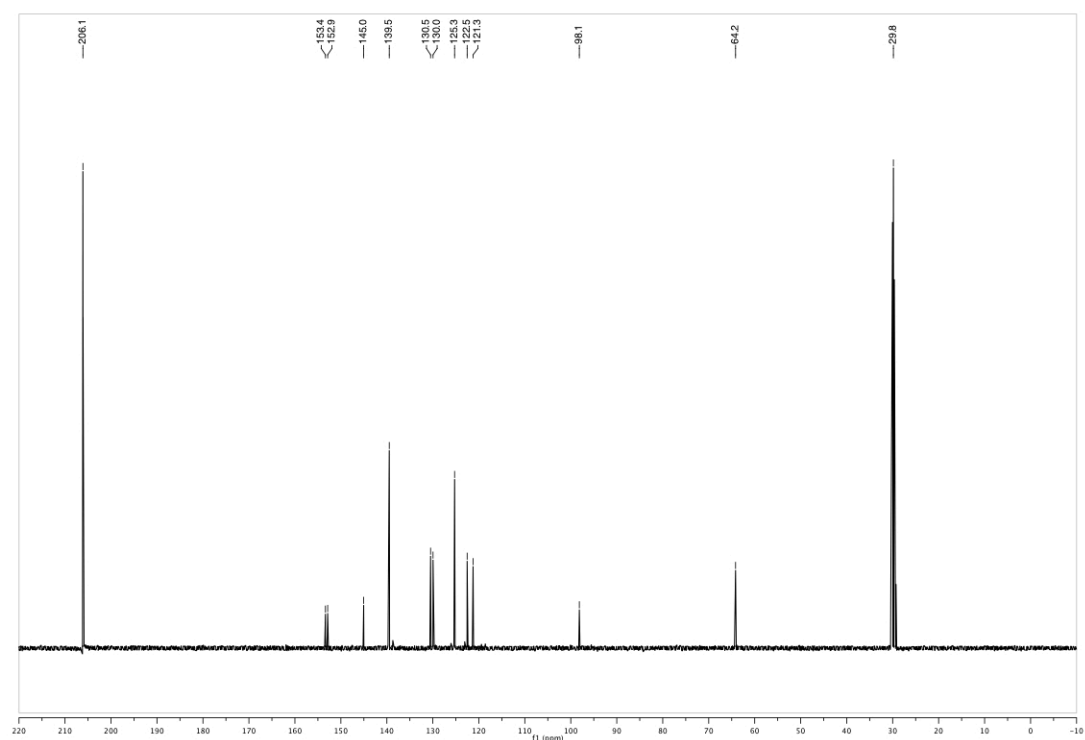
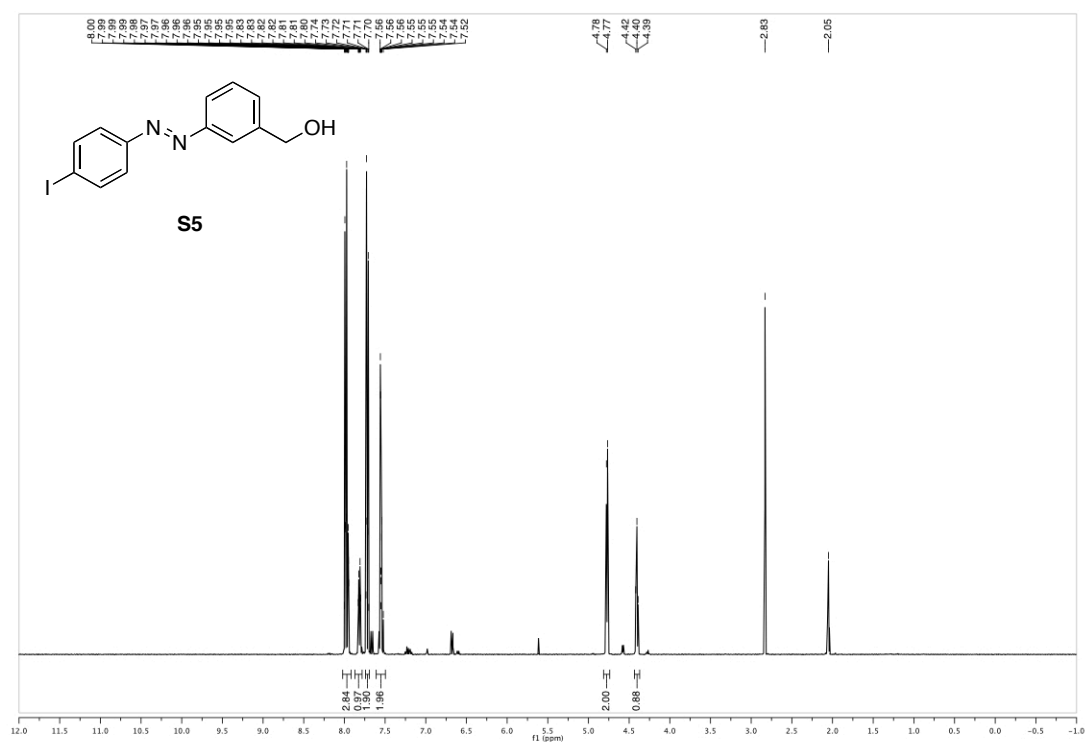
**(3-(phenyldiazenyl)phenyl)methanol (S3)**

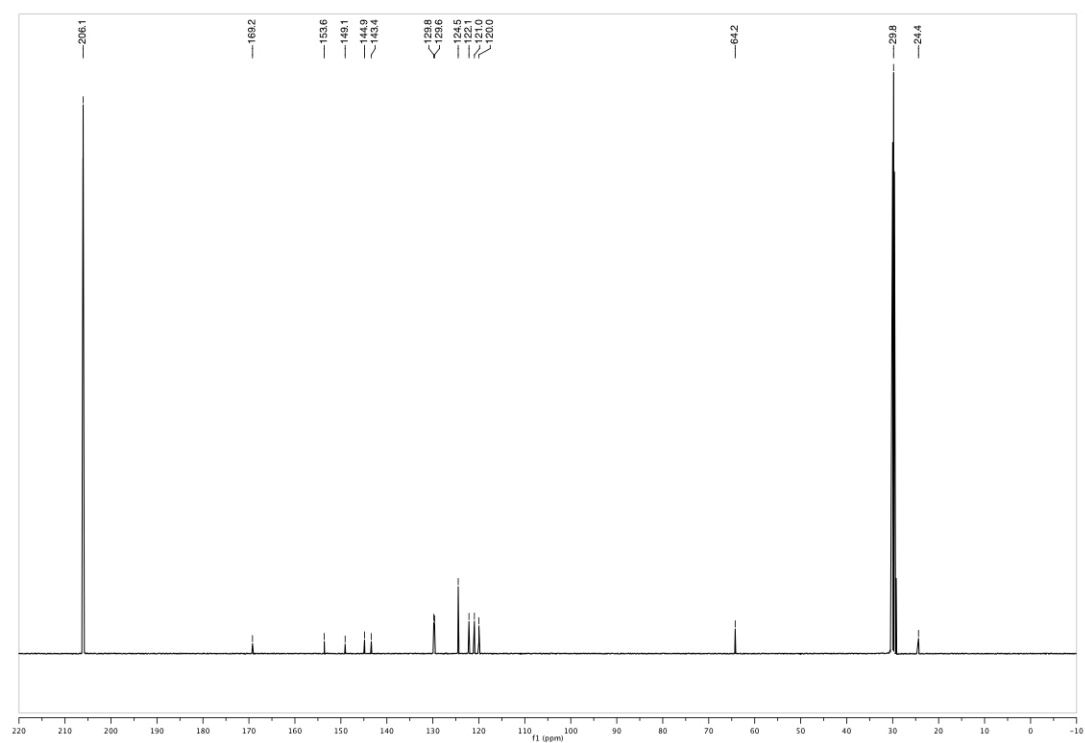
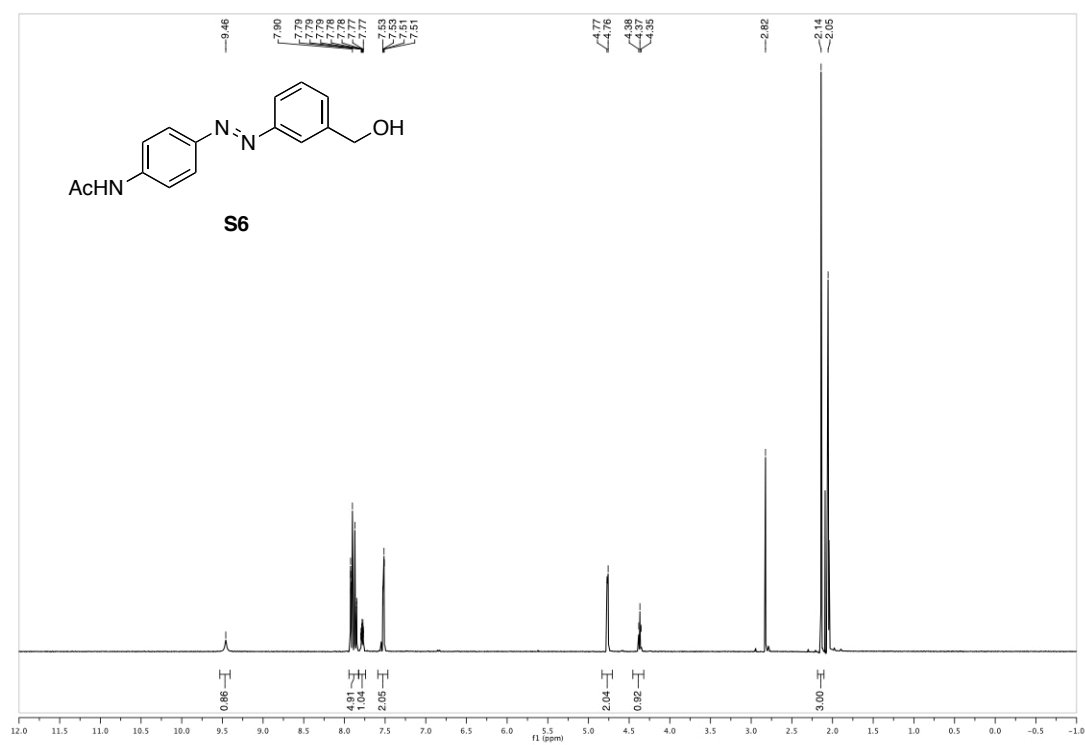
## methyl 3-((4-(dimethylamino)phenyl)diazenyl)benzoate (S4)

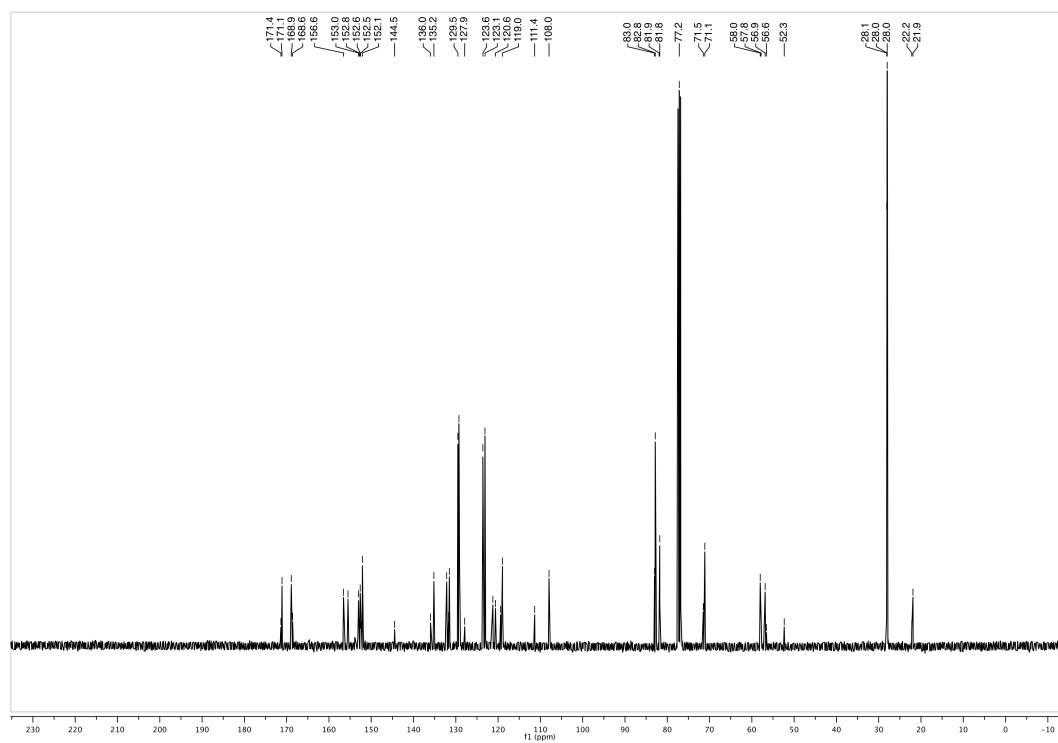




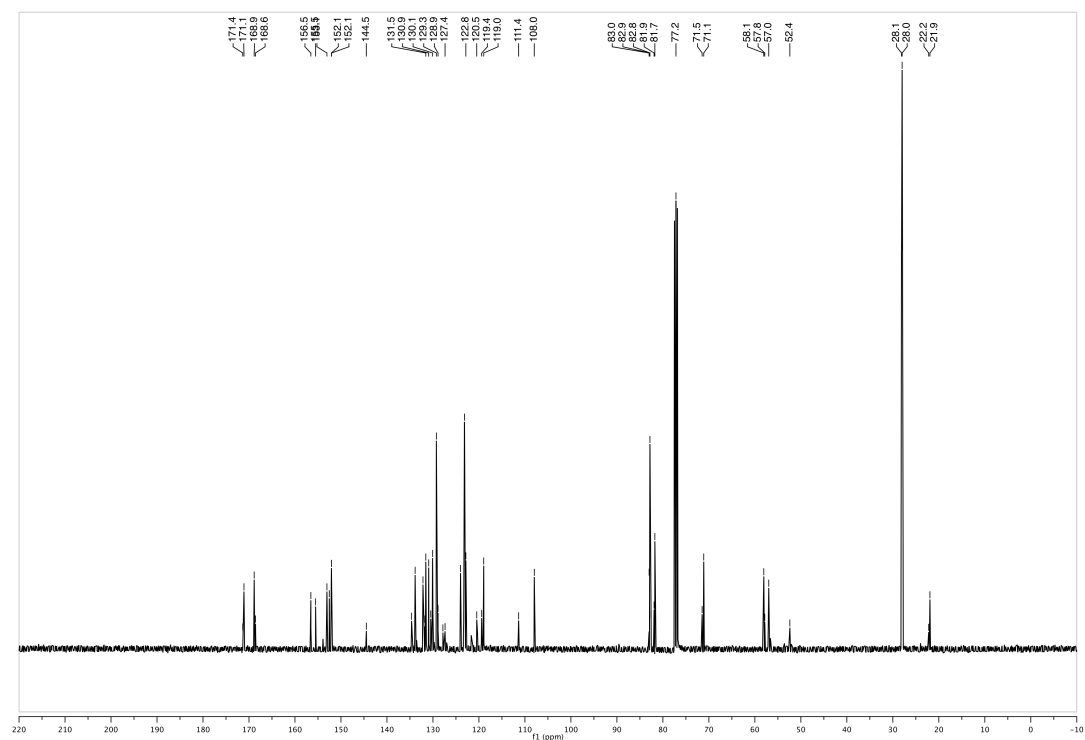
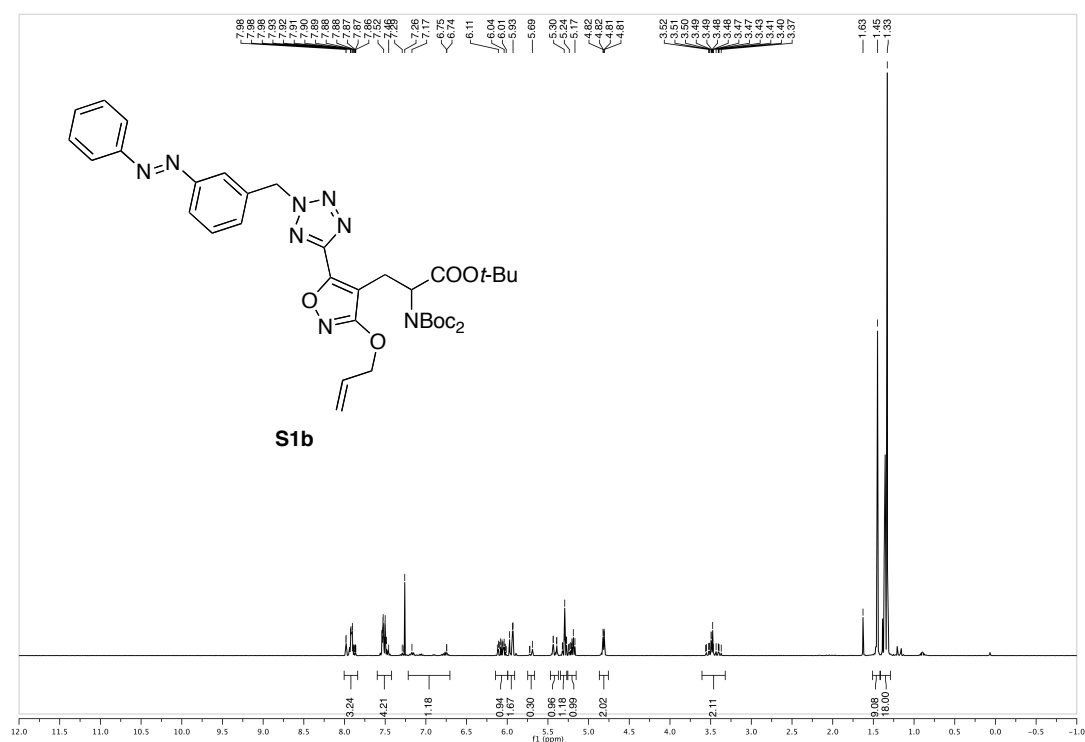
**3-((4-(dimethylamino)phenyl)diazenyl)phenyl)methanol (96)**

**(3-((4-iodophenyl)diazenyl)phenyl)methanol (S5)**

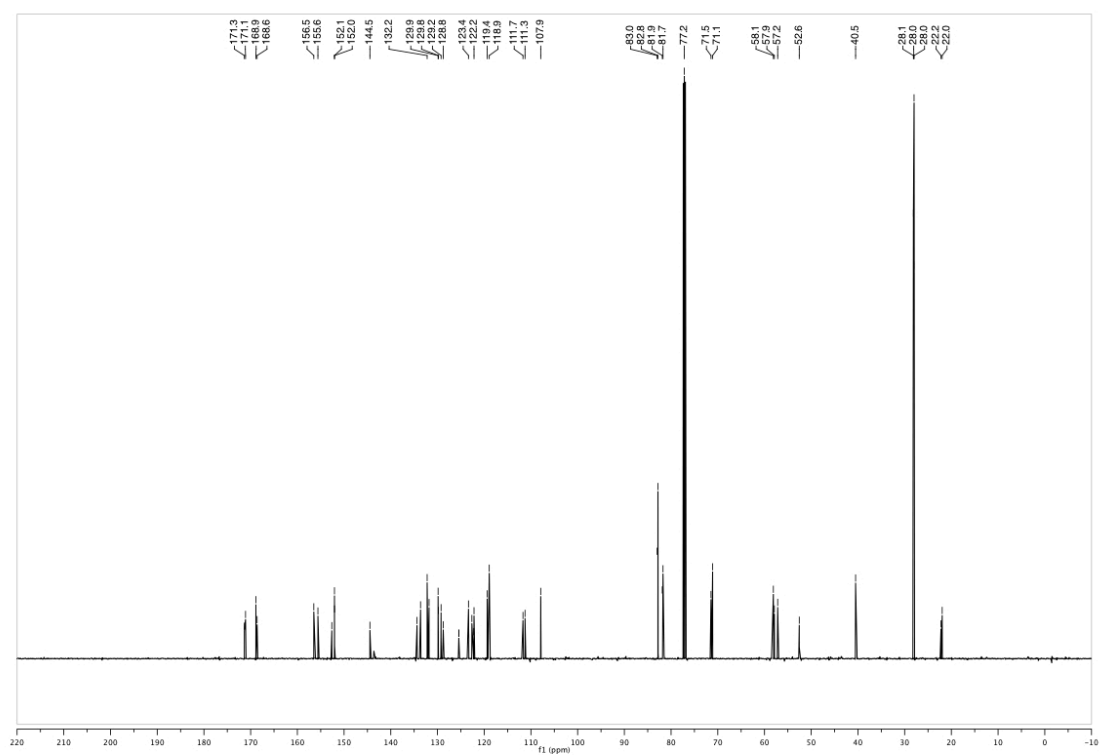
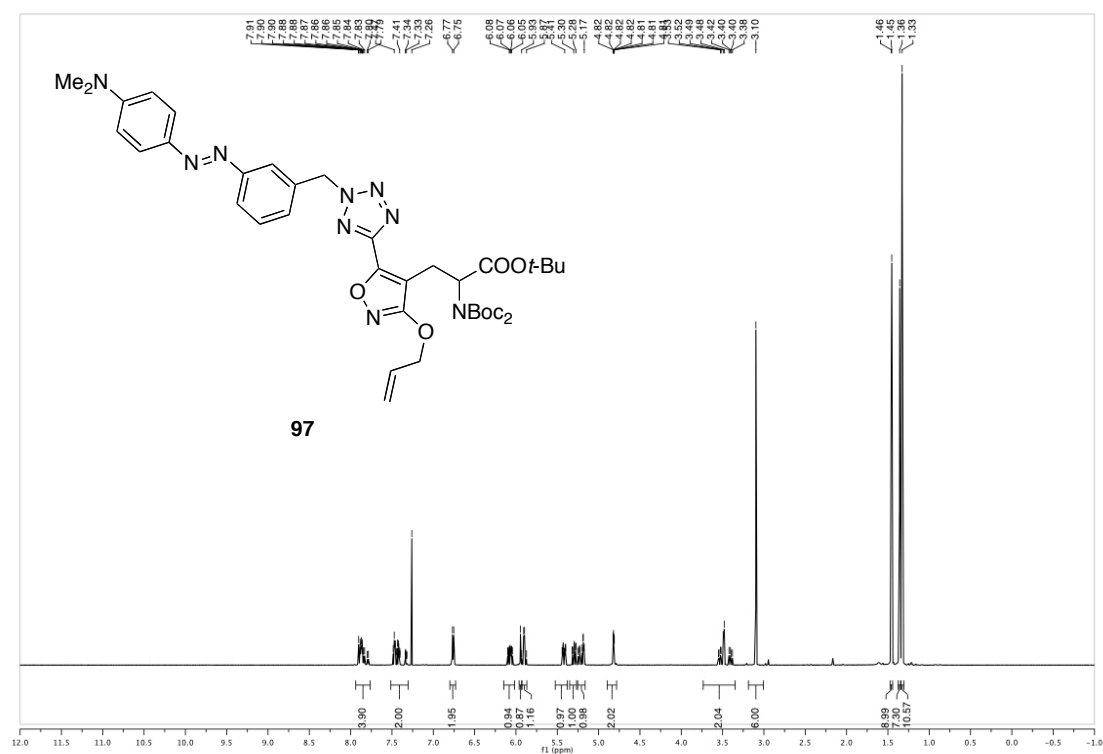
***N*-(4-((3-(hydroxymethyl)phenyl)diazenyl)phenyl)acetamide (S6)**



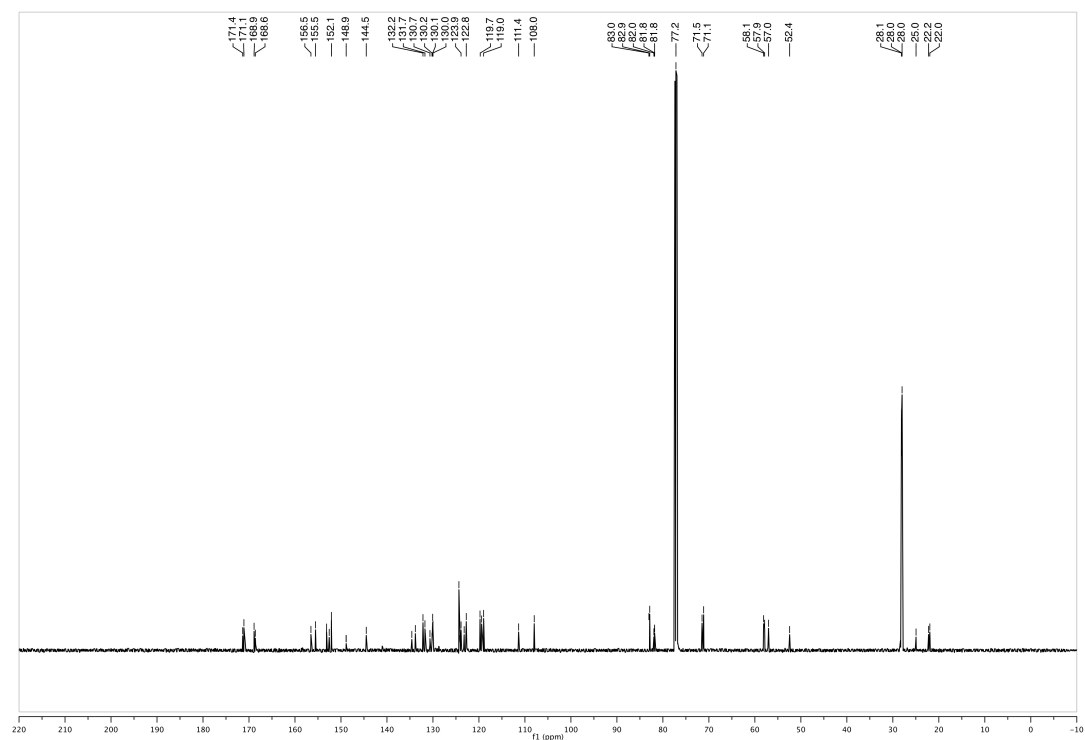
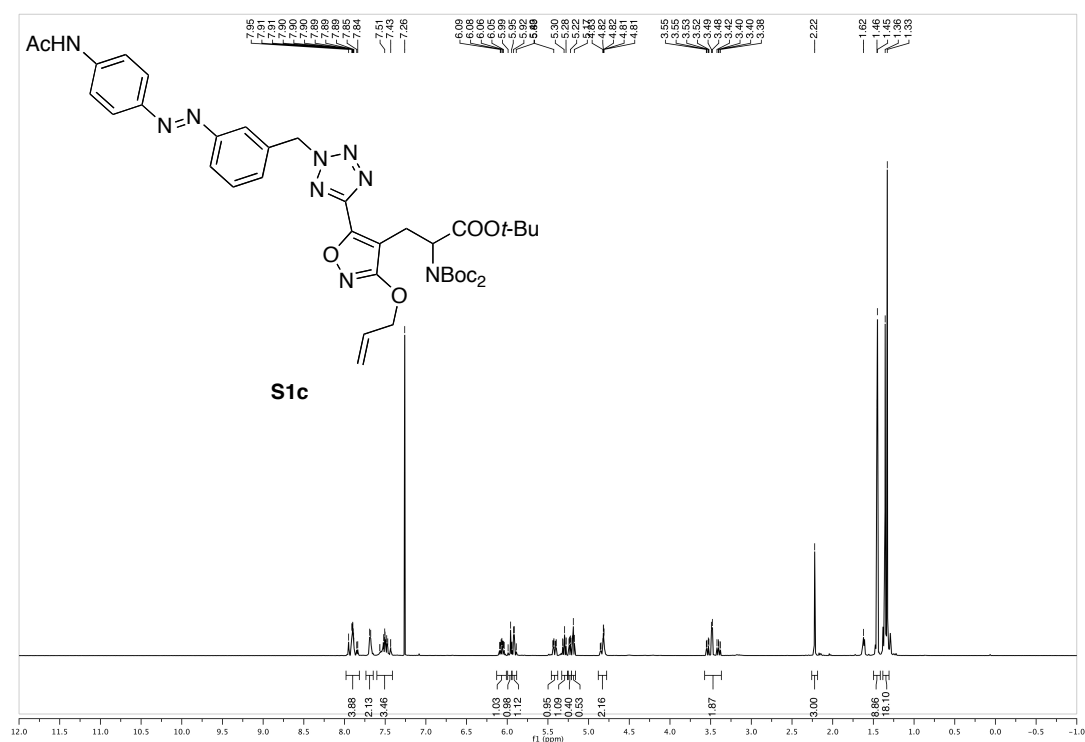
***tert*-butyl 3-(3-(allyloxy)-5-(2-(3-(phenyldiazenyl)benzyl)-2*H*-tetrazol-5-yl)isoxazol-4-yl)-2-(bis(*tert*-bu-toxycarbonyl)amino)propanoate (S1b)**



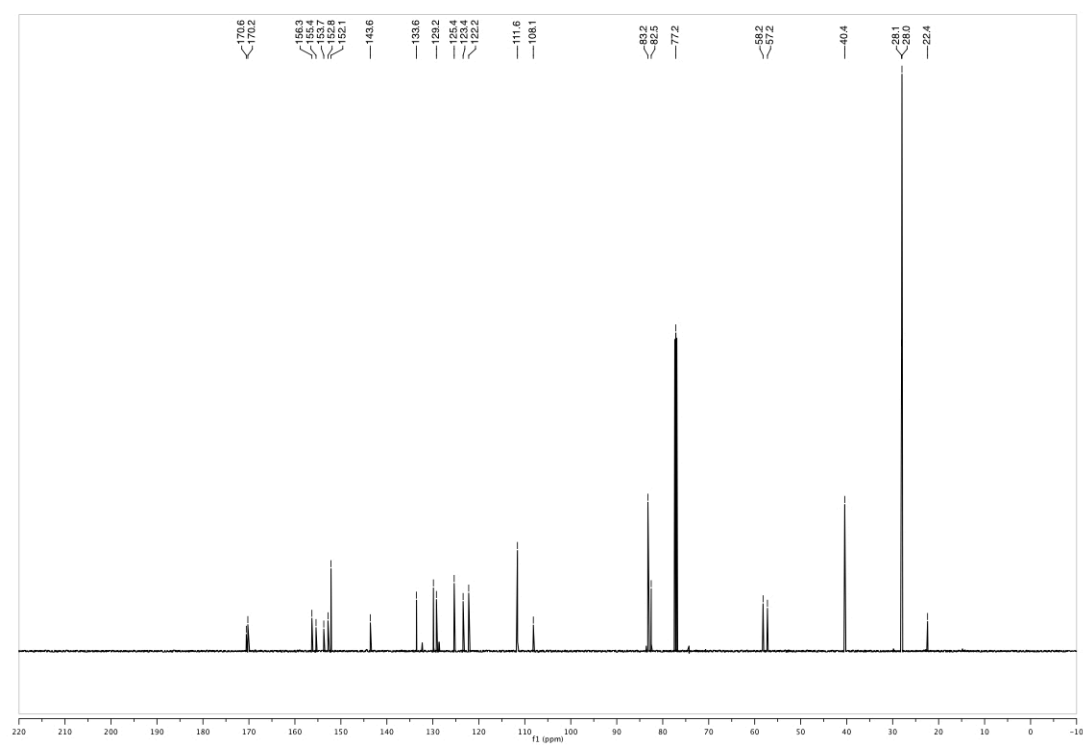
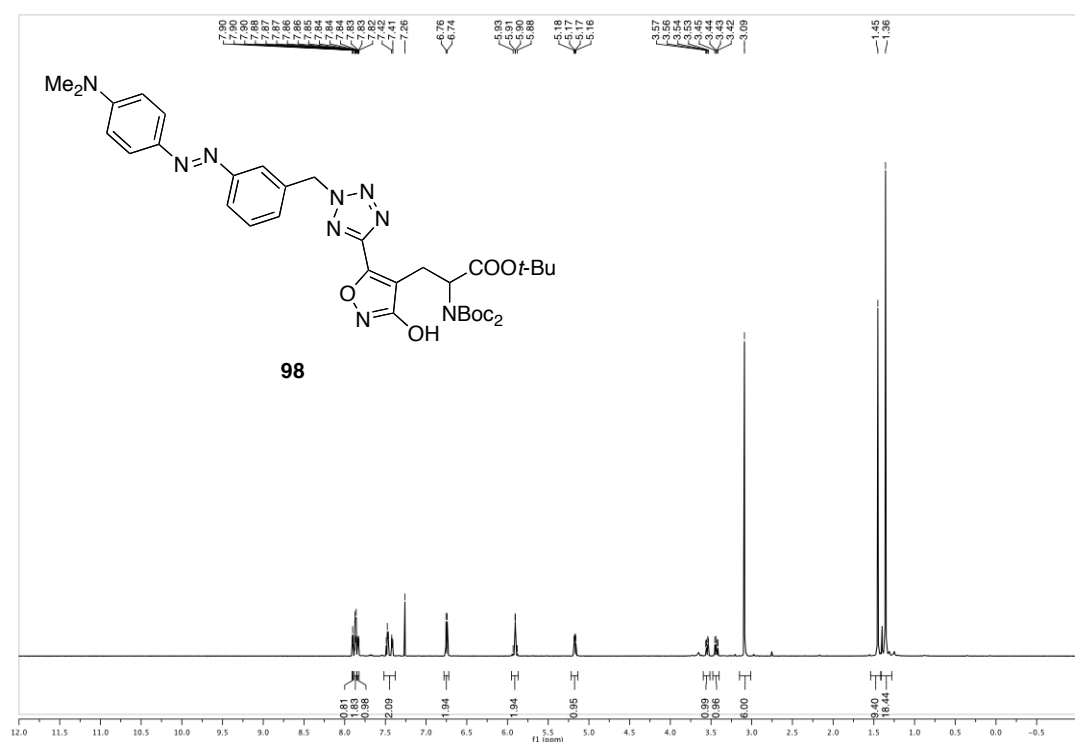
***tert*-butyl 3-(3-(allyloxy)-5-(2-(3-((4-(dimethylamino)phenyl)diazenyl)benzyl)-2*H*-tetrazol-5-yl)isoxa-zol-4-yl)-2-(bis(*tert*-butoxycarbonyl)amino)propanoate (97)**



***tert*-butyl 3-(5-(2-(3-((4-acetamidophenyl)diazenyl)benzyl)-2*H*-tetrazol-5-yl)-3-(allyloxy)isoxazol-4-yl)-2-(bis (*tert*-butoxycarbonyl)amino)propanoate (S1c)**

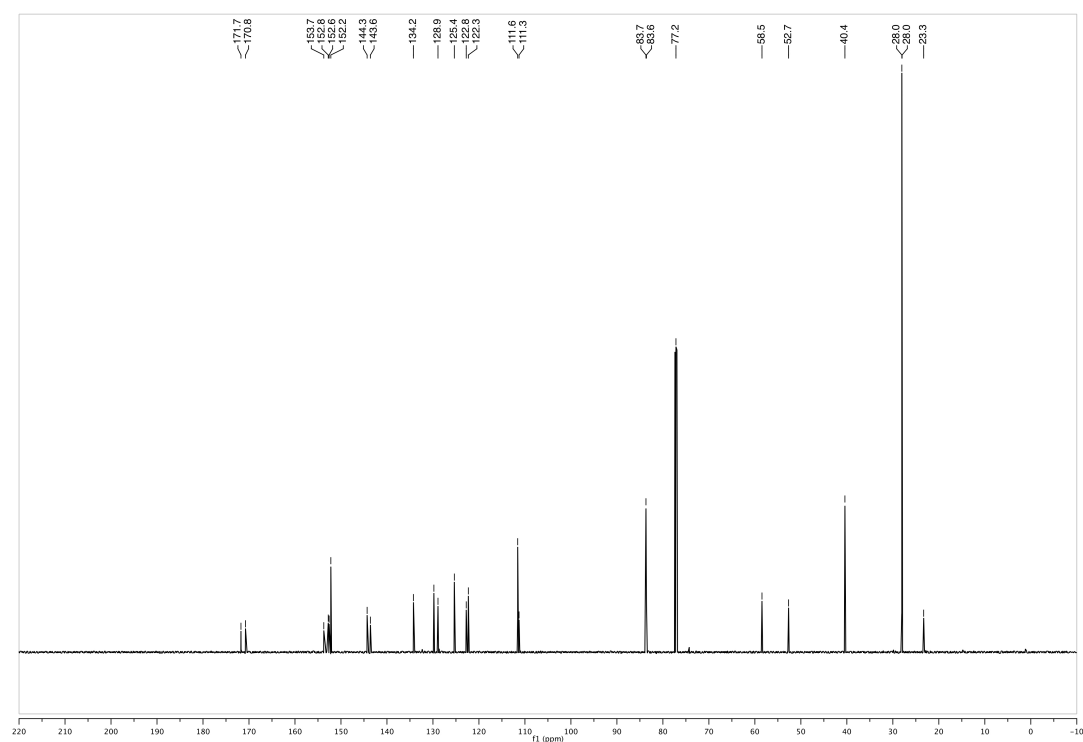
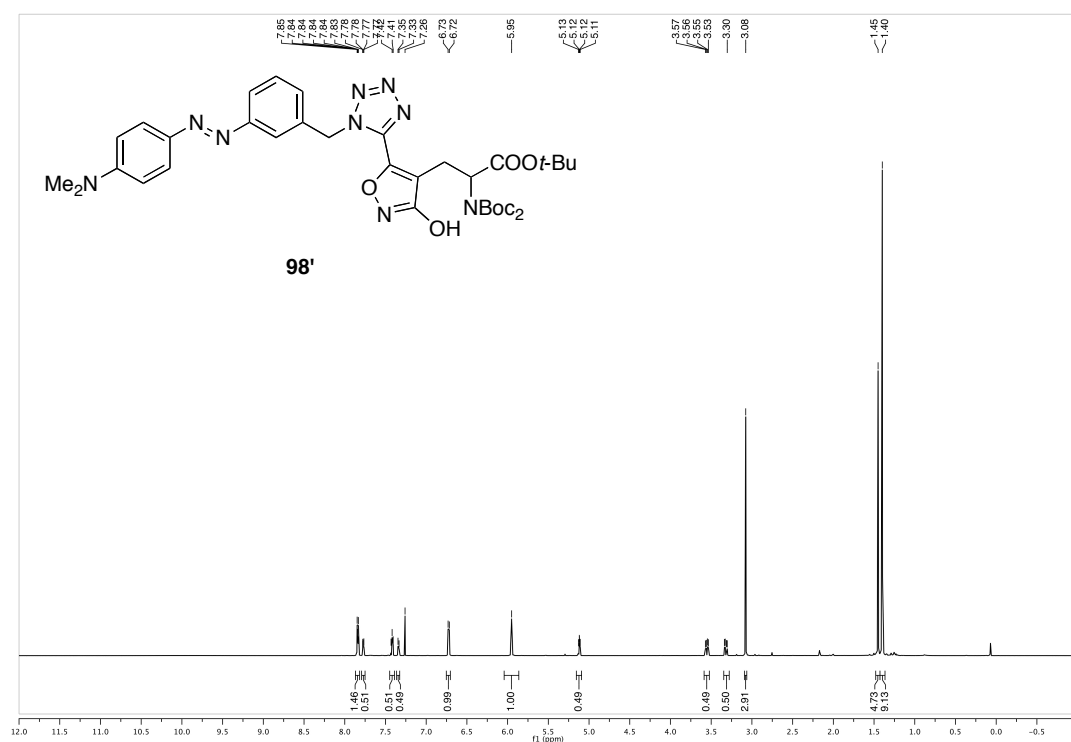


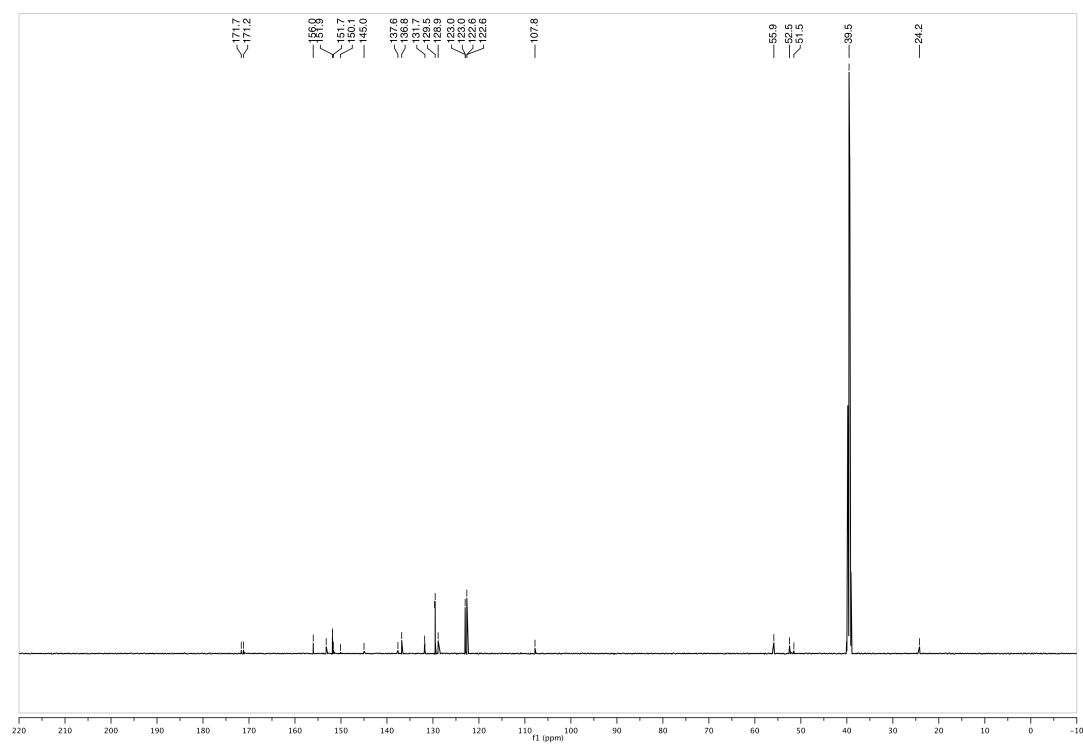
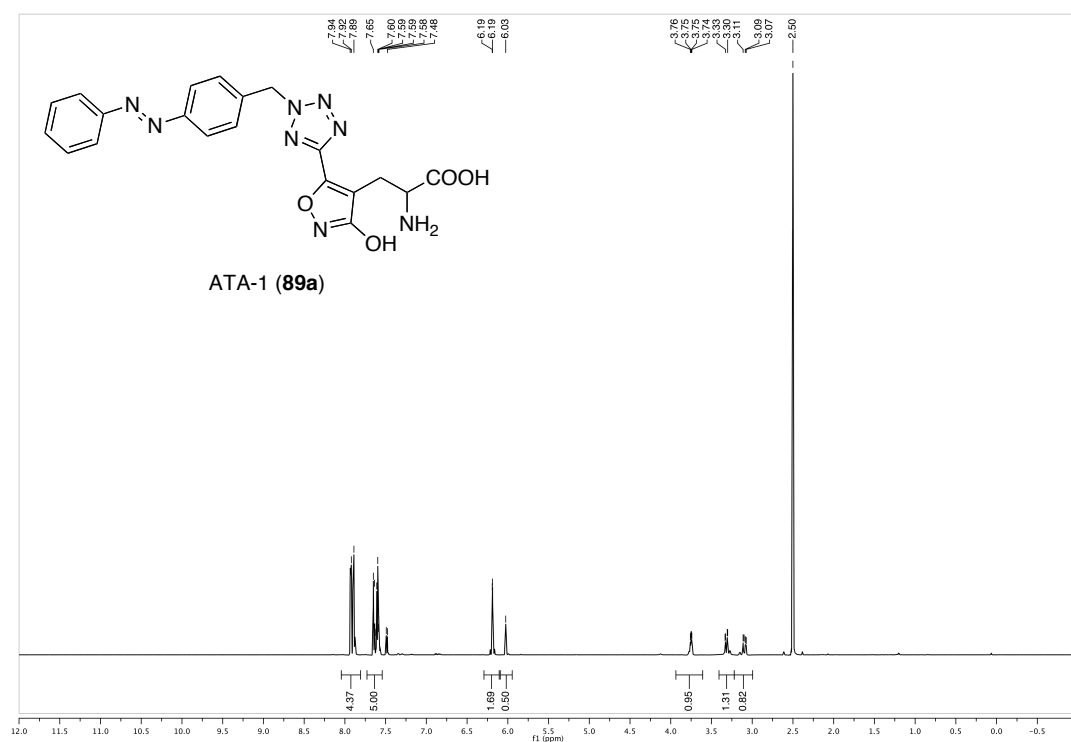
***tert*-butyl 2-(bis(*tert*-butoxycarbonyl)amino)-3-(5-(2-(3-((4-(dimethylamino)phenyl)diaz-enyl)benzyl)-2*H*-tetra-zol-5-yl)-3-hydroxyisoxazol-4-yl)propanoate (98)**



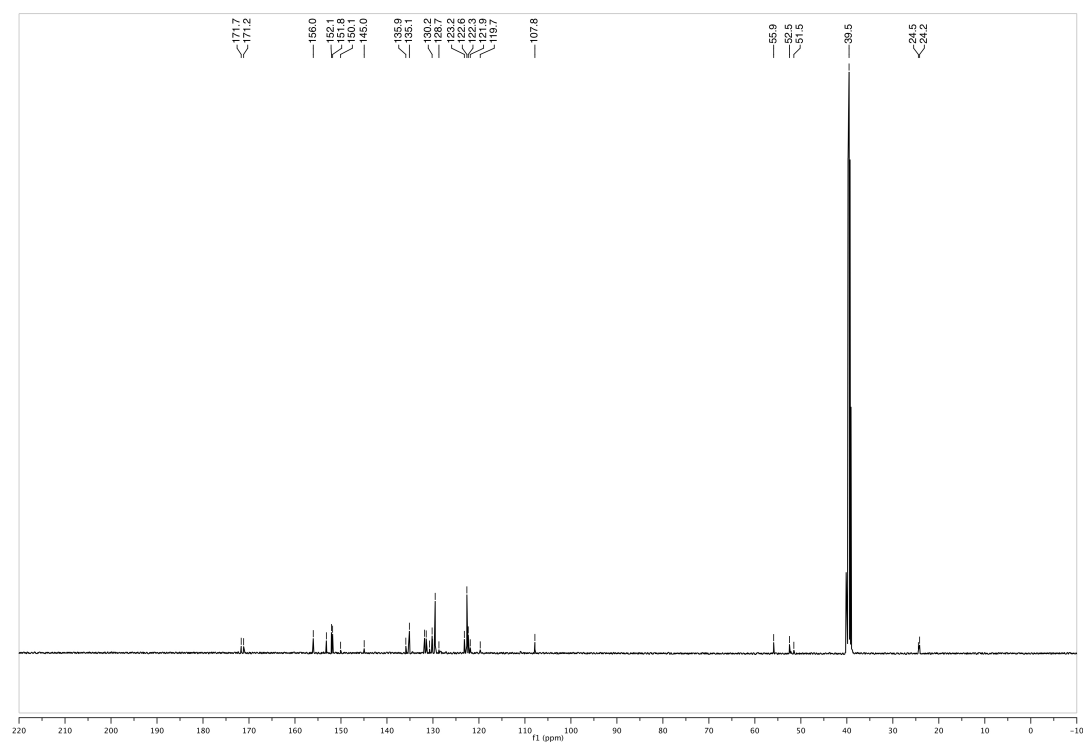
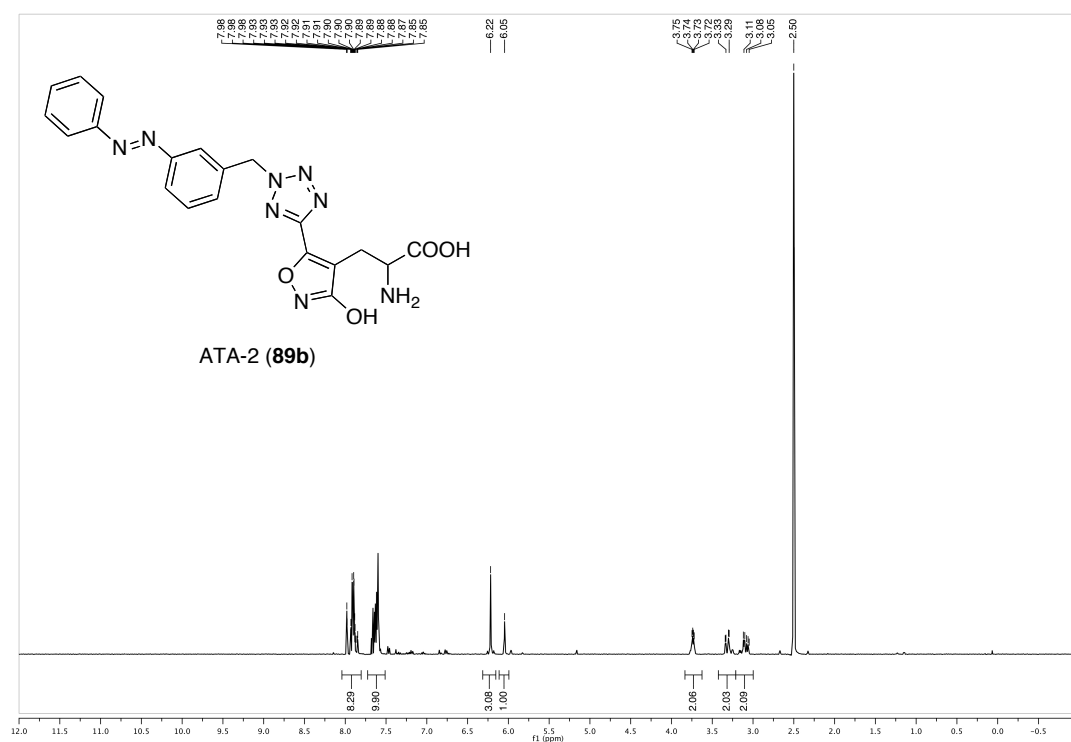


***tert*-butyl 2-(bis(*tert*-butoxycarbonyl)amino)-3-(5-(1-(3-((4-(dimethylamino)phenyl)diazenyl)benzyl)-1*H*-tetrazol-5-yl)-3-hydroxyisoxazol-4-yl)propanoate (98')**

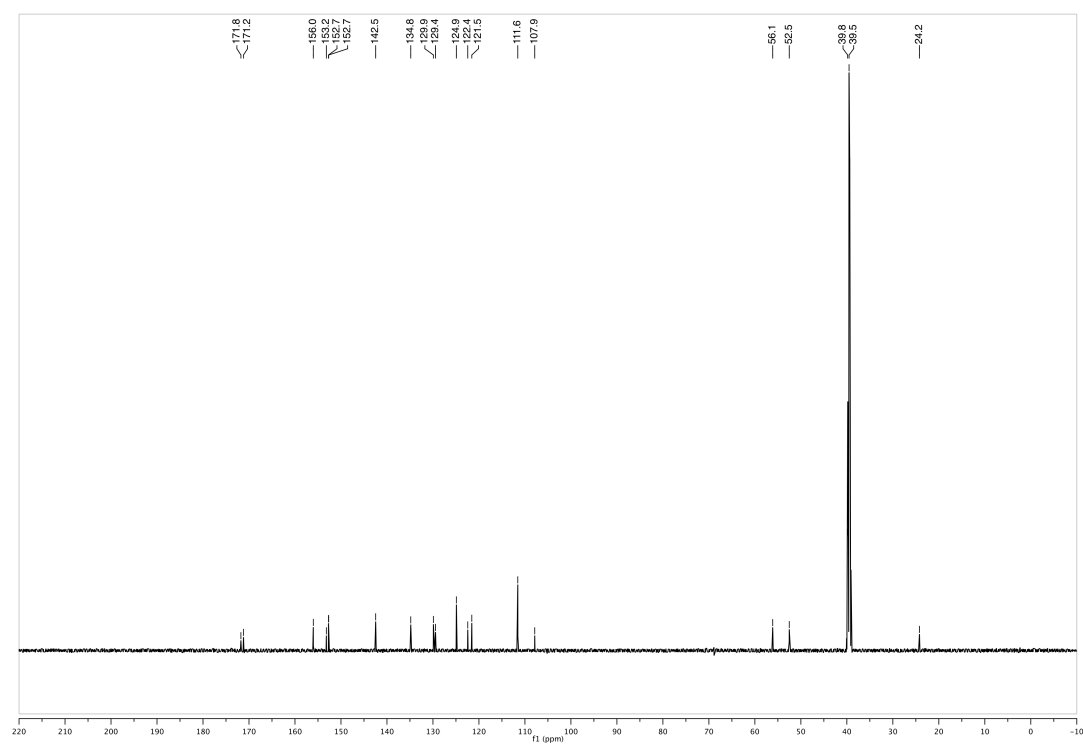
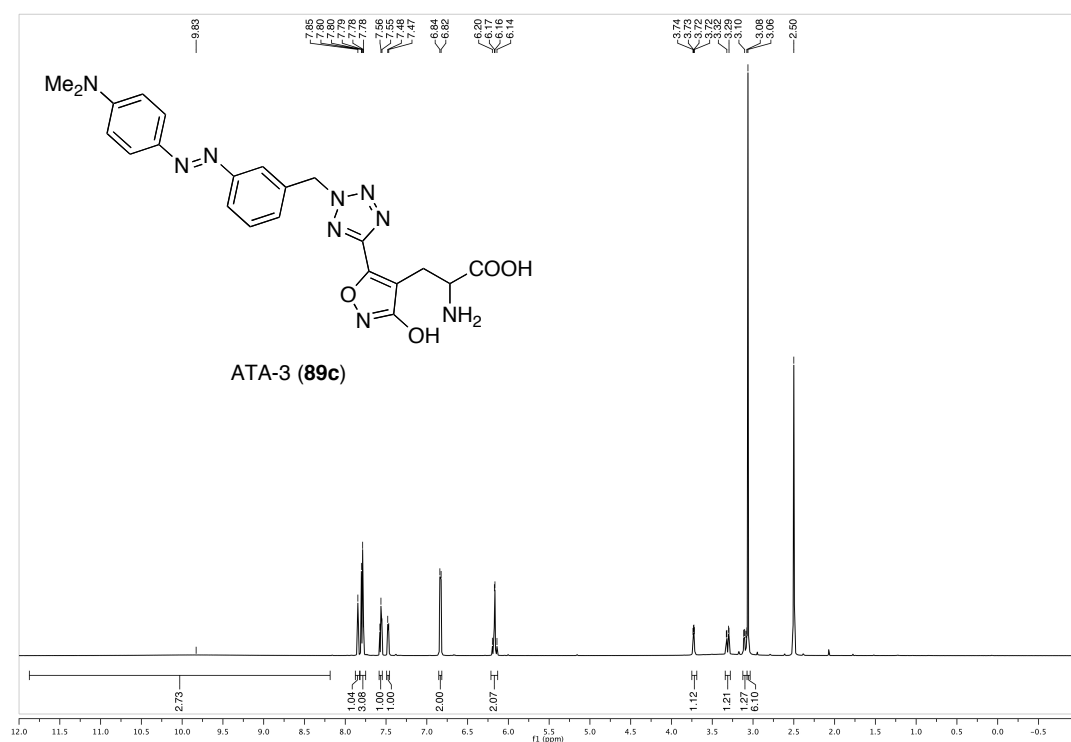


**2-amino-3-(3-hydroxy-5-(2-(4-(phenyldiazenyl)benzyl)-2H-tetrazol-5-yl)isoxazol-4-yl)propanoic acid (ATA-1, 89a)**

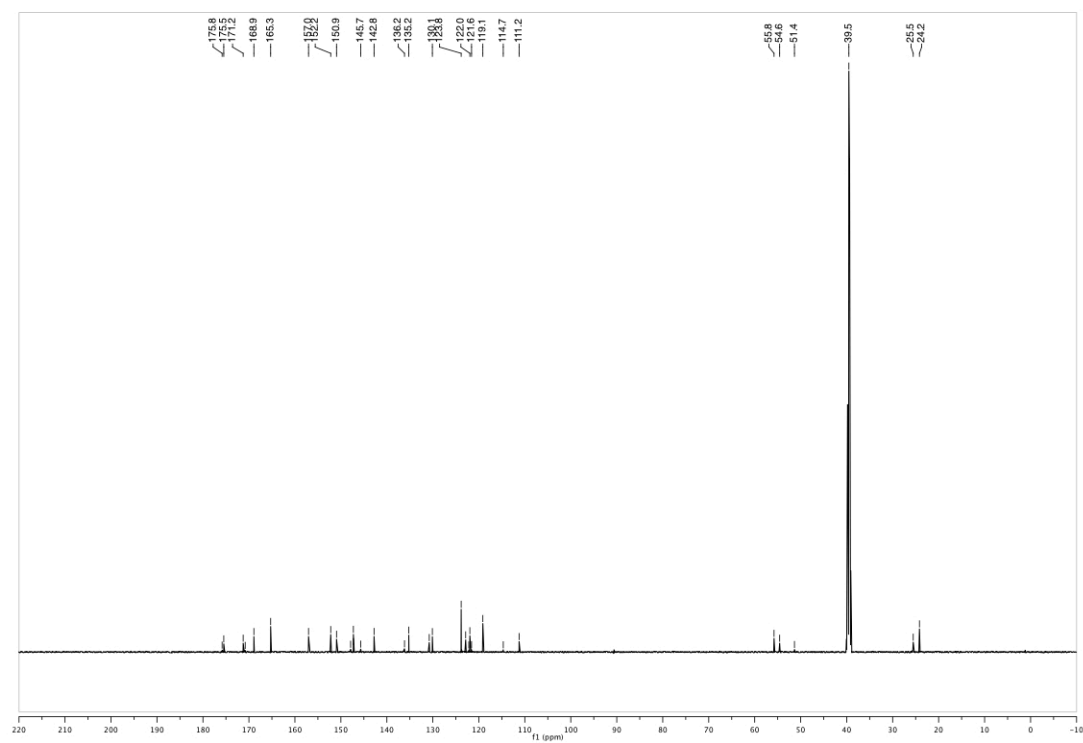
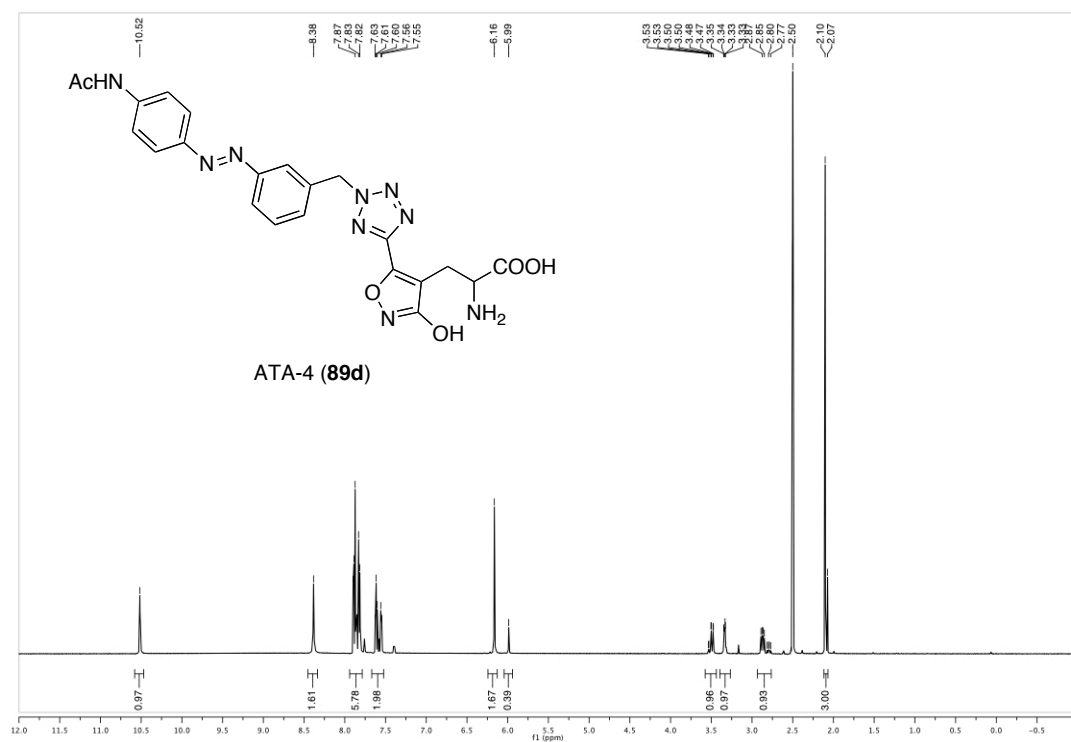
**2-amino-3-(3-hydroxy-5-(2-(3-(phenyldiazenyl)benzyl)-2H-tetrazol-5-yl)isoxazol-4-yl)propanoic acid (ATA-2, 89b)**



**2-amino-3-(5-(2-(3-((4-(dimethylamino)phenyl)diazenyl)benzyl)-2H-tetrazol-5-yl)-3-hydroxyisoxazol-4-yl)propanoic acid (ATA-3, 89c)**

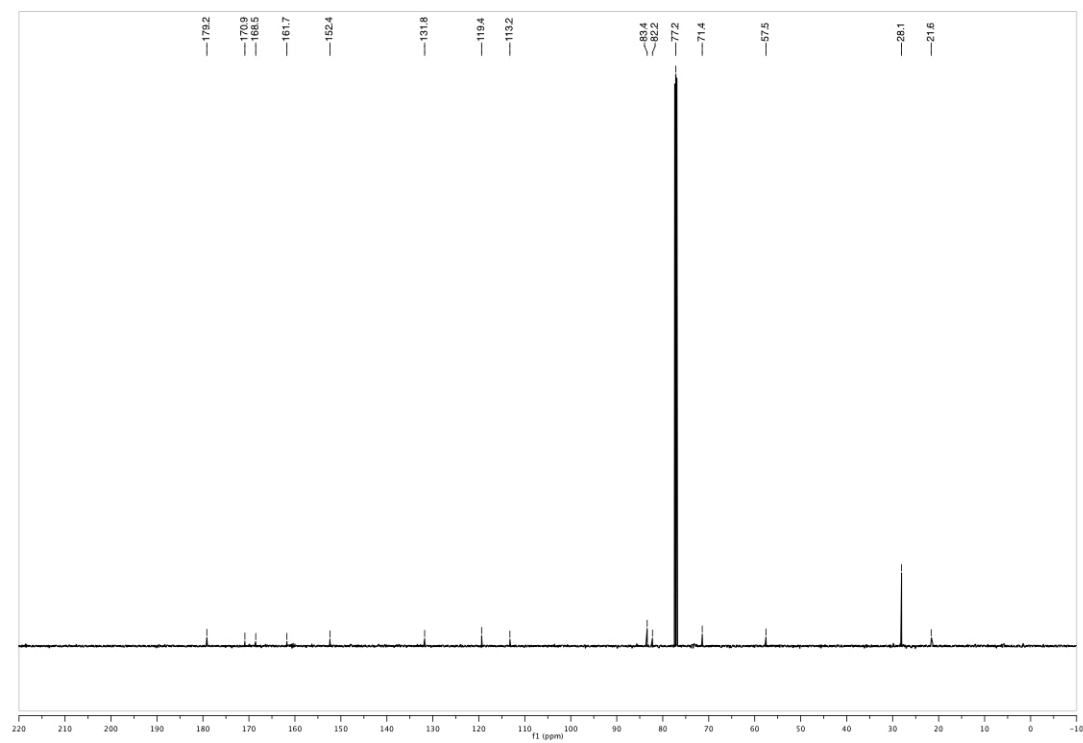
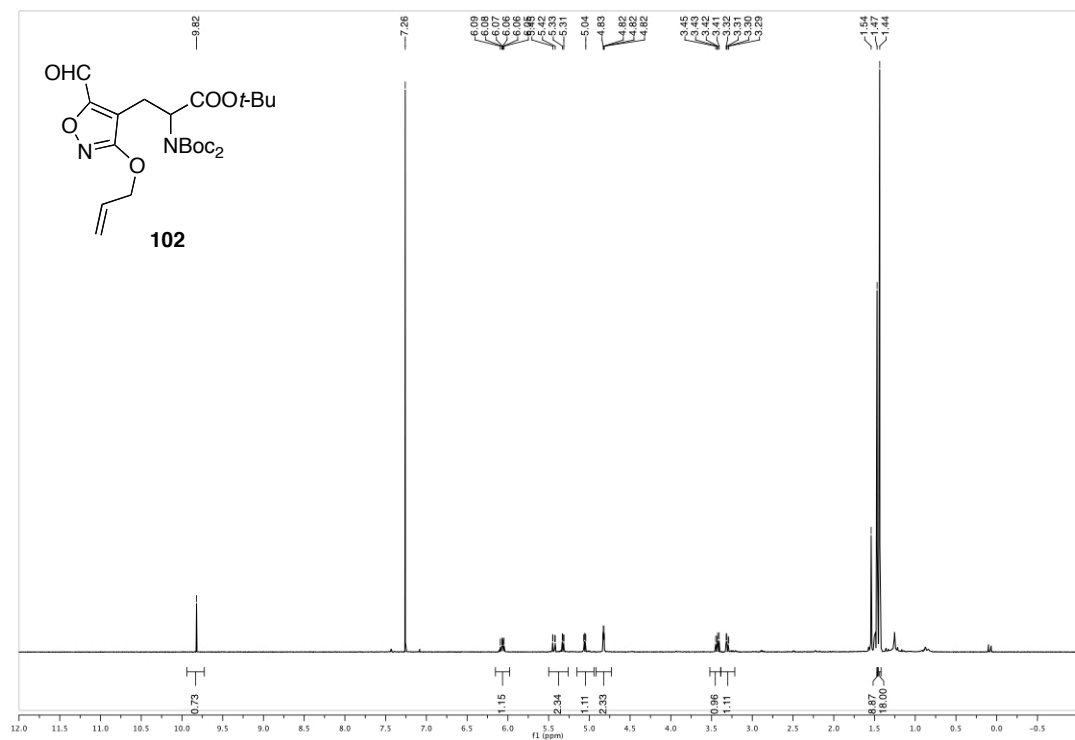


**3-(5-(2-(3-((4-acetamidophenyl)diazenyl)benzyl)-2H-tetrazol-5-yl)-3-hydroxyisoxazol-4-yl)-2-aminopropanoic acid (ATA-4, 89d)**

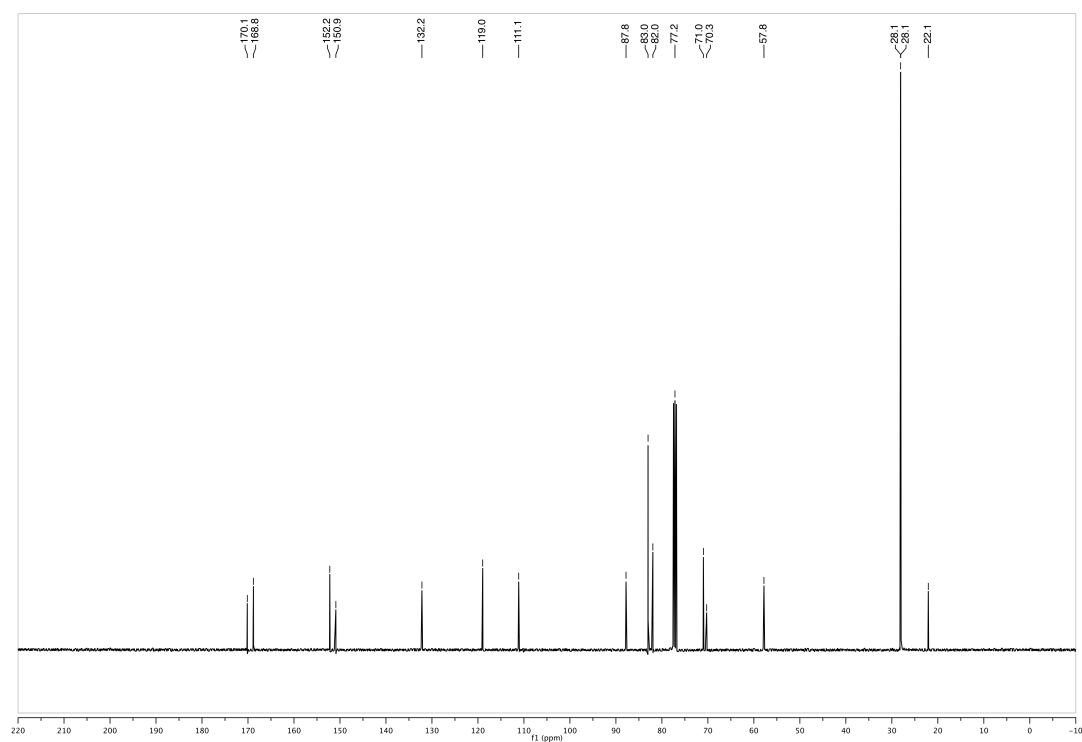
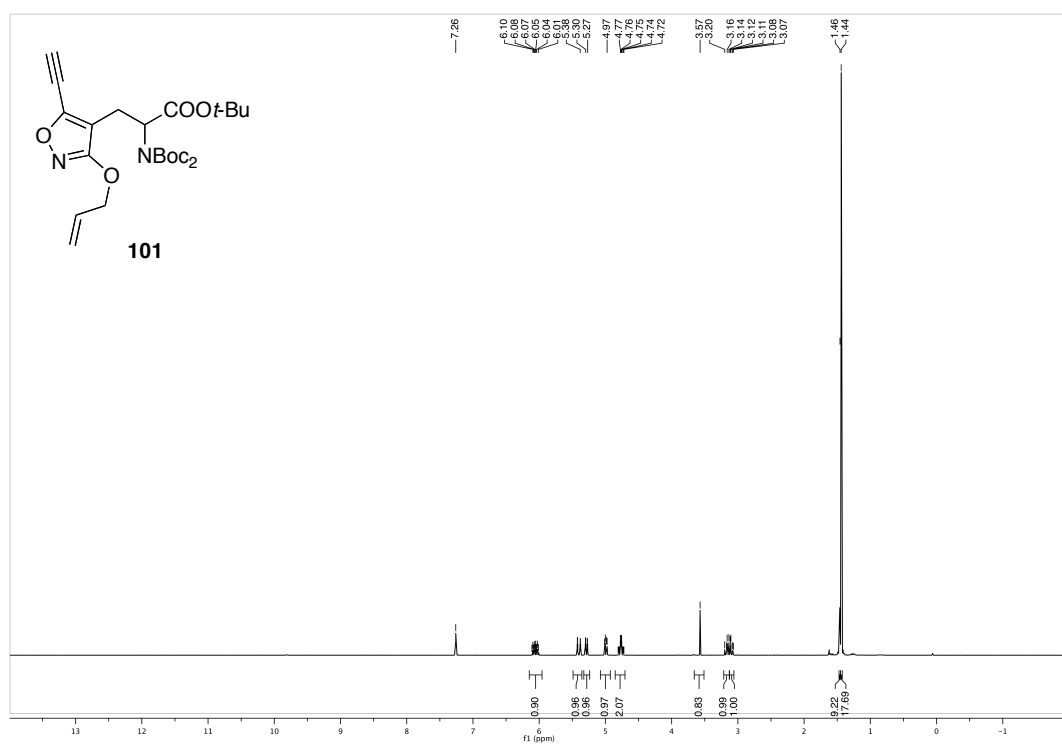


## 2) Triazolyl-Substituted AMPA derivatives

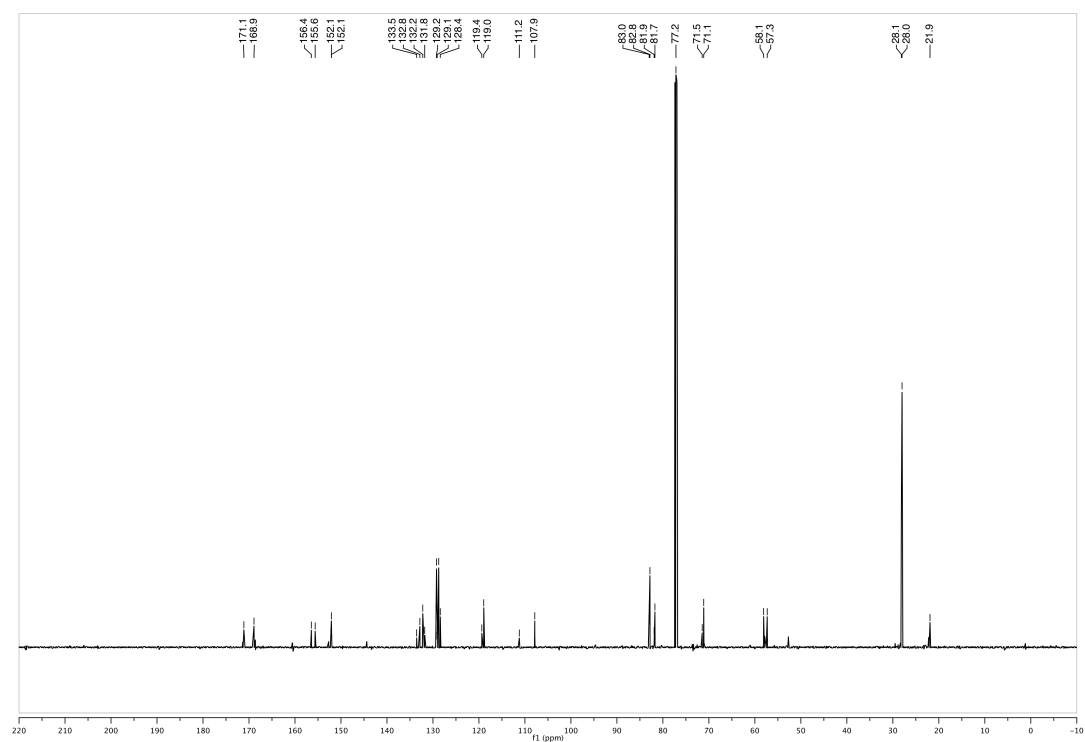
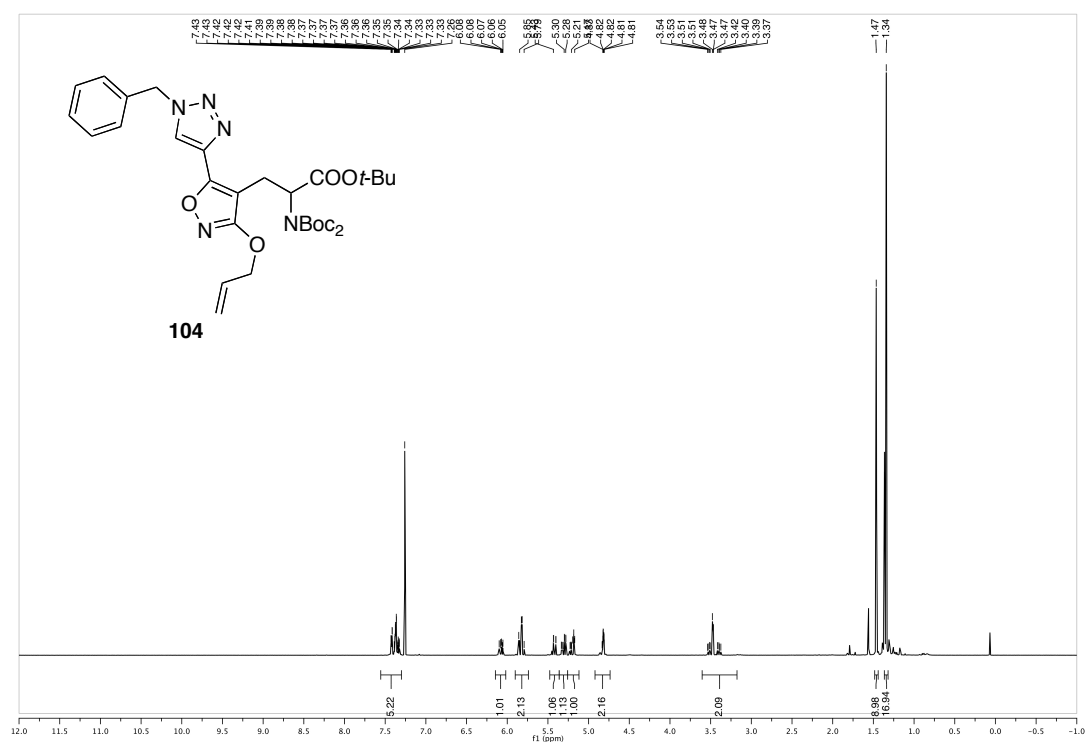
***tert*-butyl 3-(3-(allyloxy)-5-formylisoxazol-4-yl)-2-(bis(*tert*-butoxycarbonyl)amino)propionate (102)**



***tert*-butyl 3-(3-(allyloxy)-5-ethynylisoxazol-4-yl)-2-(bis(*tert*-butoxycarbonyl)amino)propanoate (101)**

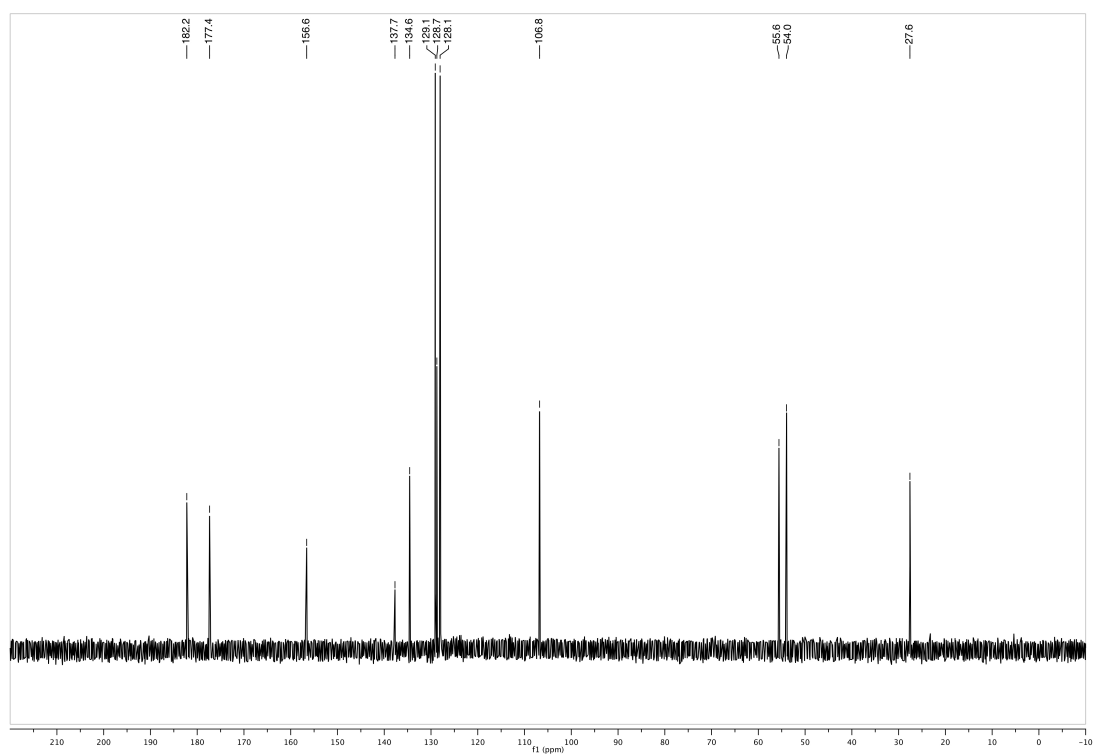
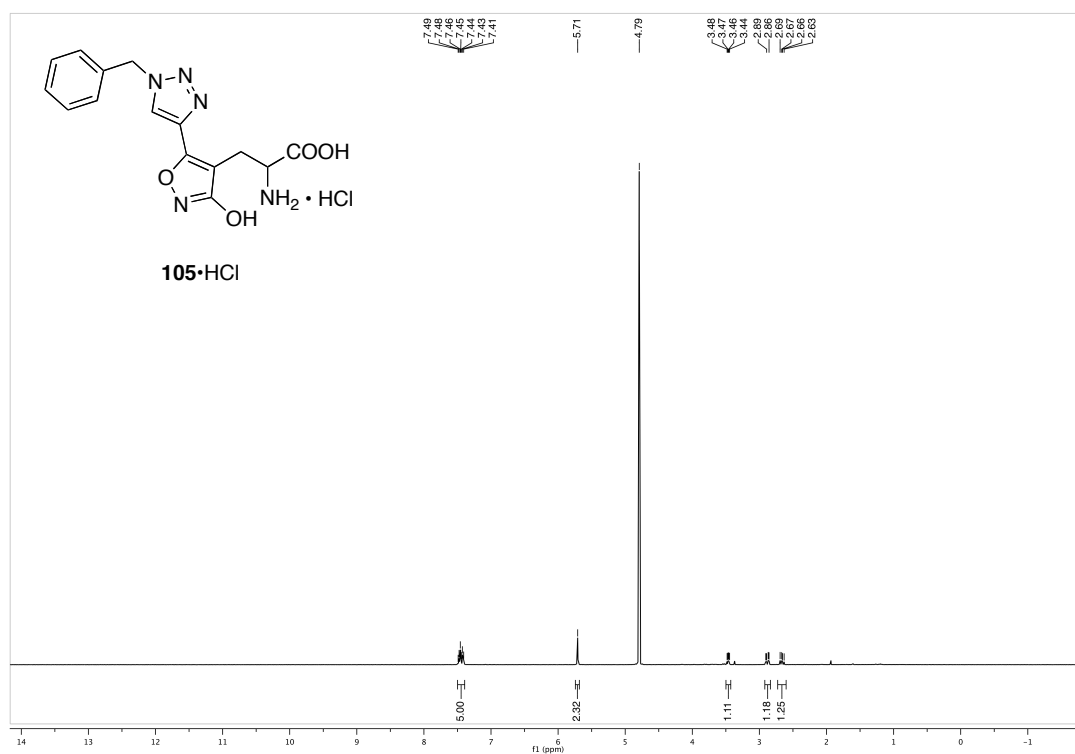


***tert*-butyl 3-(3-(allyloxy)-5-(1-benzyl-1*H*-1,2,3-triazol-4-yl)isoxazol-4-yl)-2-(bis(*tert*-butoxycarbonyl)amino)propanoate (104)**



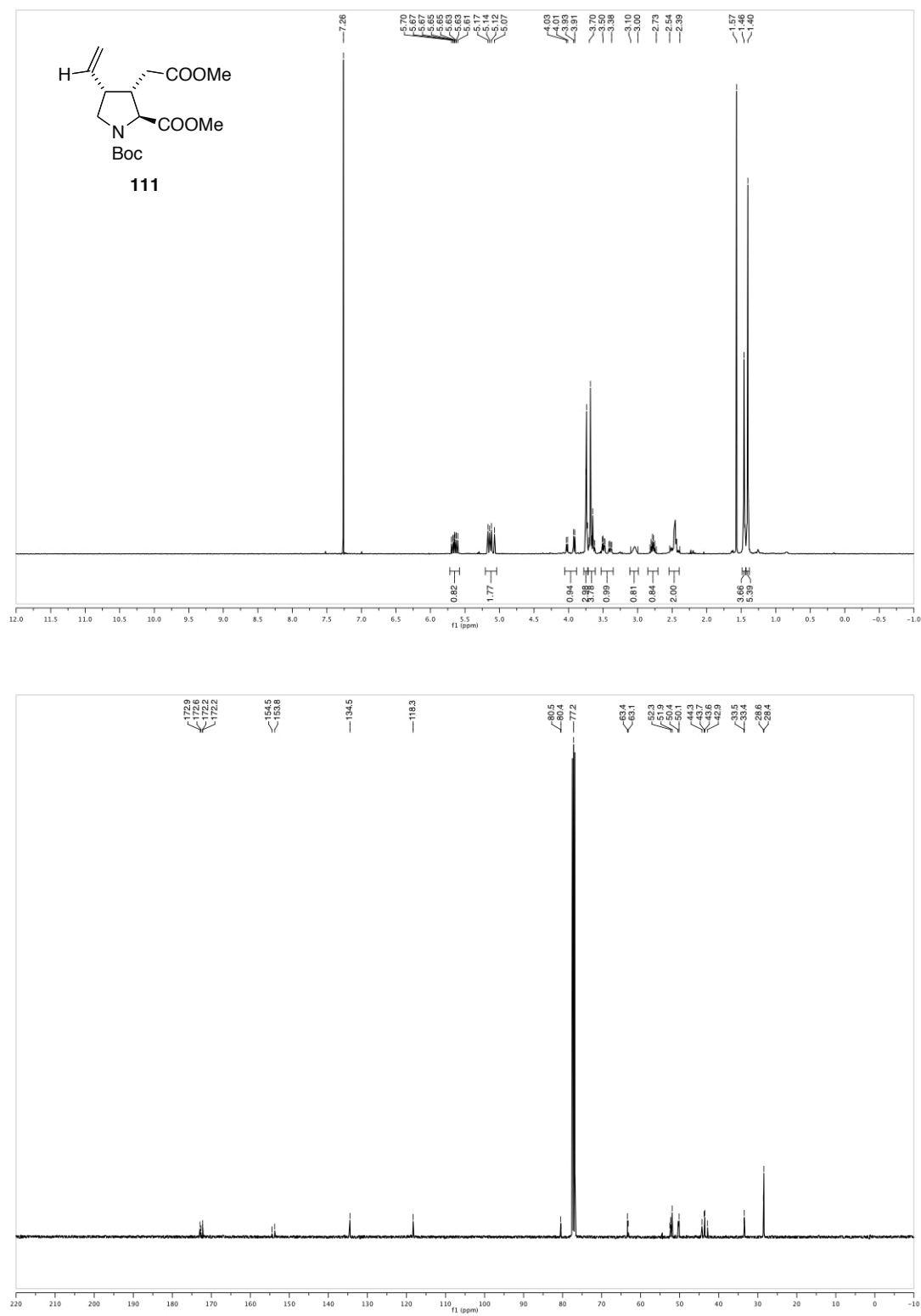


**2-amino-3-(5-(1-benzyl-1*H*-1,2,3-triazol-4-yl)-3-hydroxyisoxazol-4-yl)propanoic acid hydrochloride (105•HCl)**

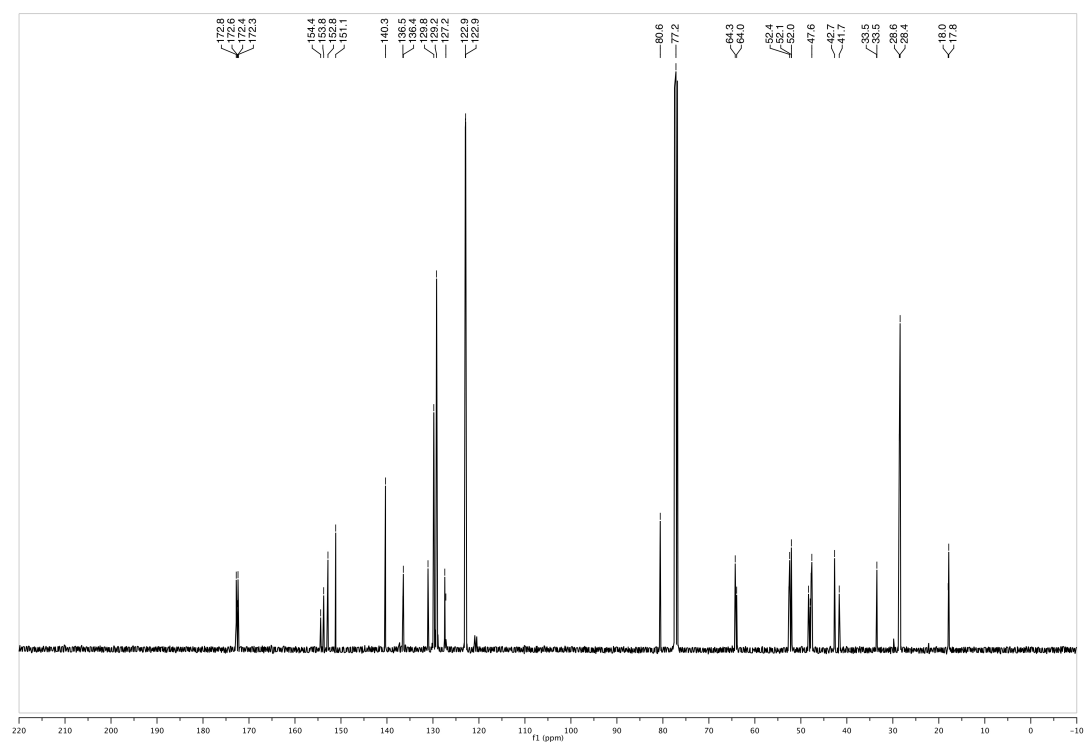
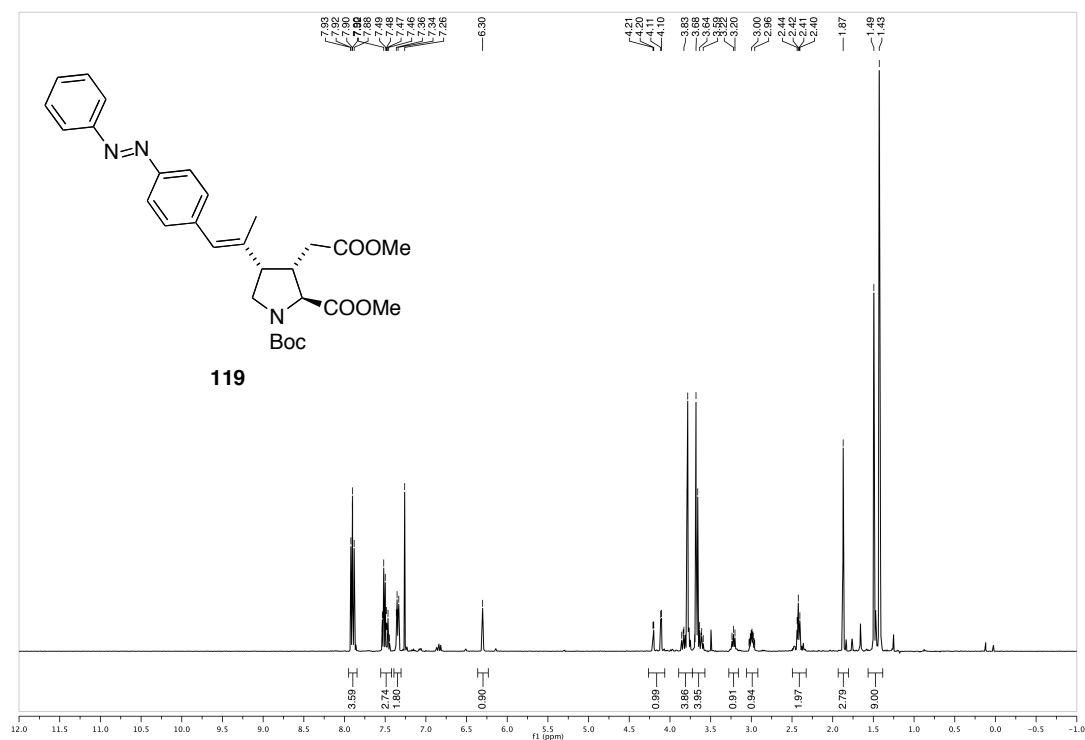


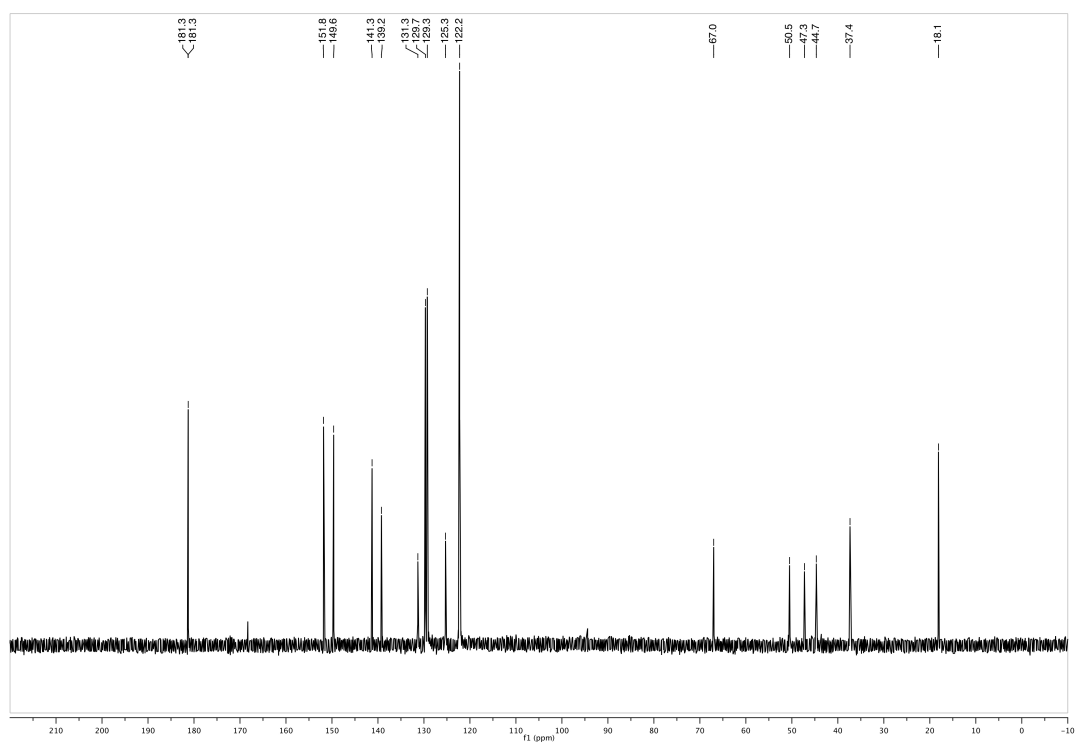
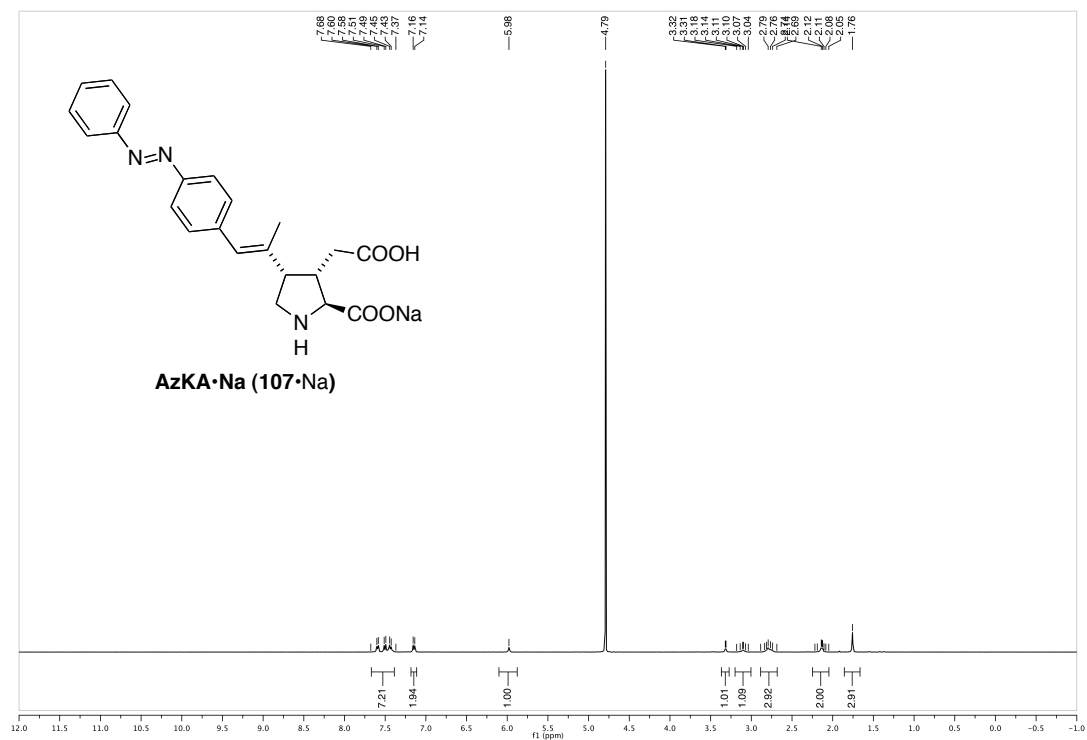
### 3) A Kainate-Derived Photoswitch

(2*S*,3*S*,4*R*)-1-*tert*-butyl 2-methyl 3-(2-methoxy-2-oxoethyl)-4-vinylpyrrolidine-1,2-dicarboxylate (**111**)



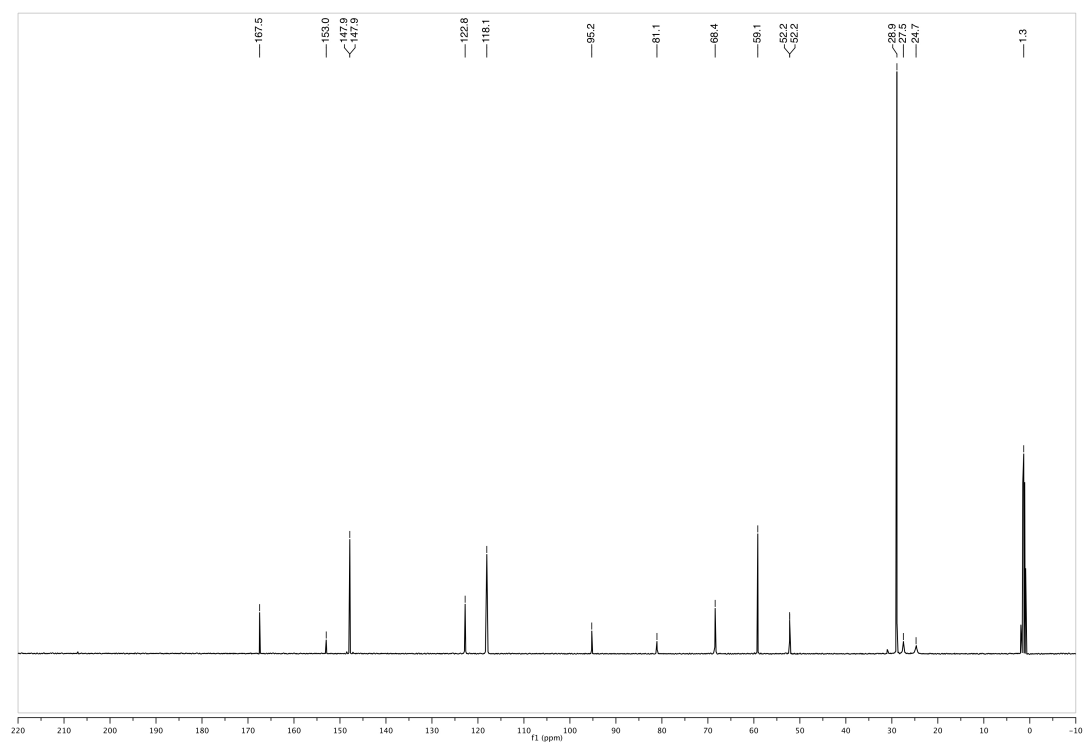
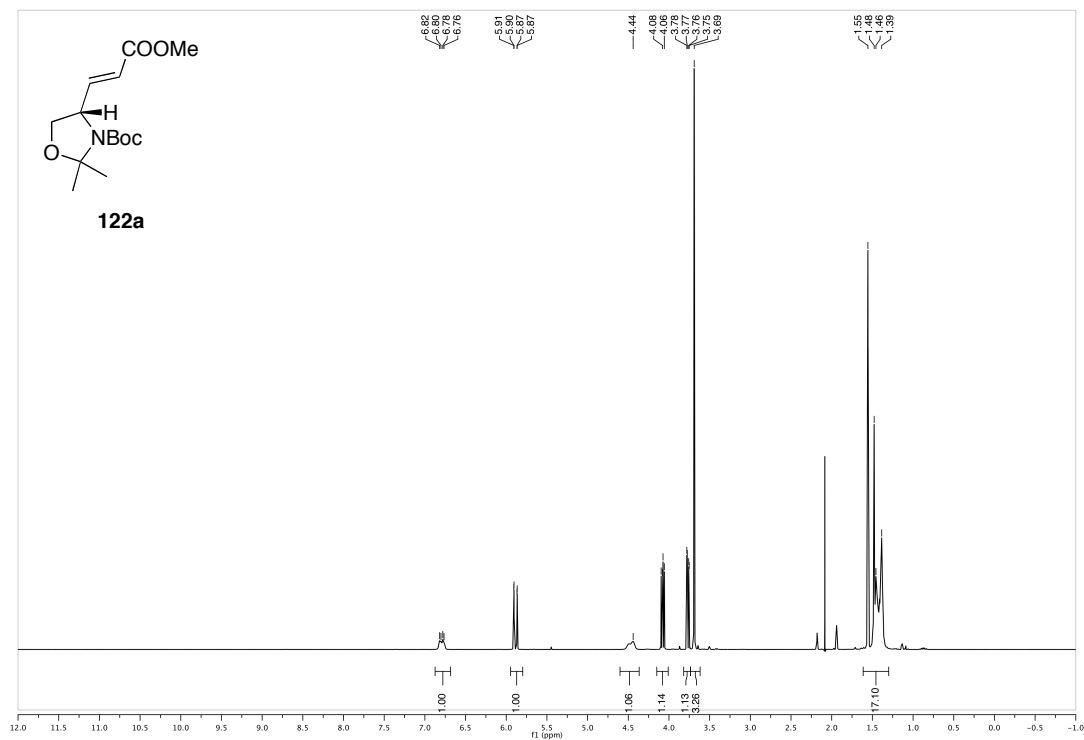
**(2*S*,3*S*,4*S*)-1-*tert*-butyl 2-methyl 3-(2-methoxy-2-oxoethyl)-4-((*E*)-1-(4-((*E*)-phenyldiazenyl)phenyl)prop-1-en-2-yl)pyrrolidine-1,2-dicarboxylate (119)**



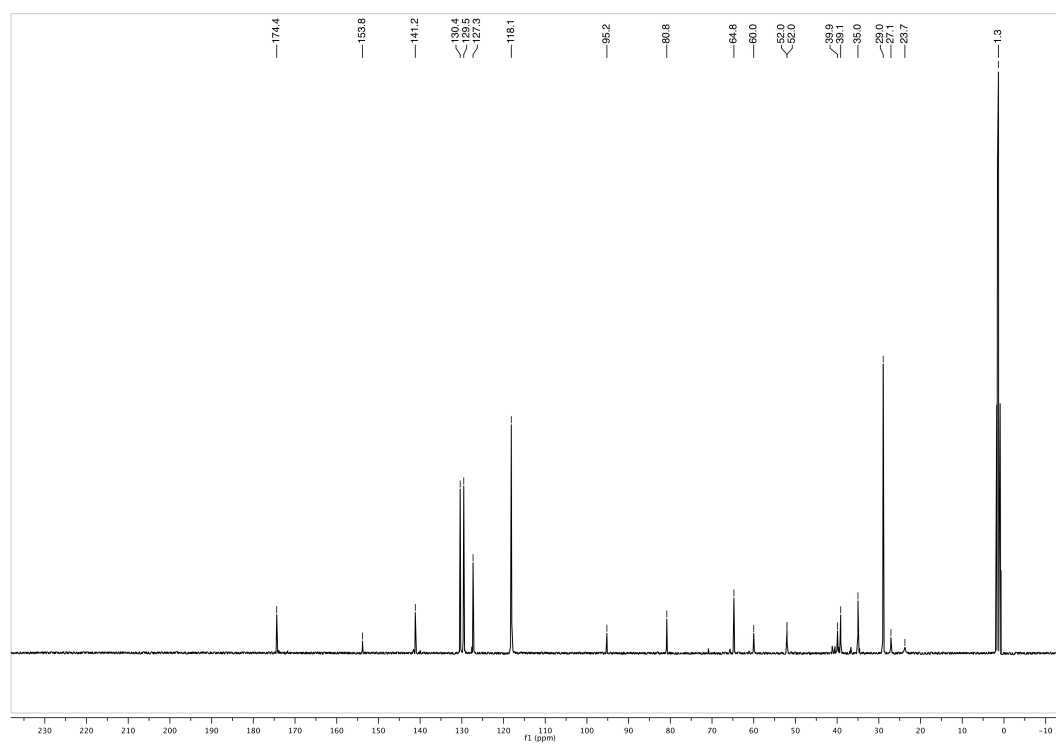
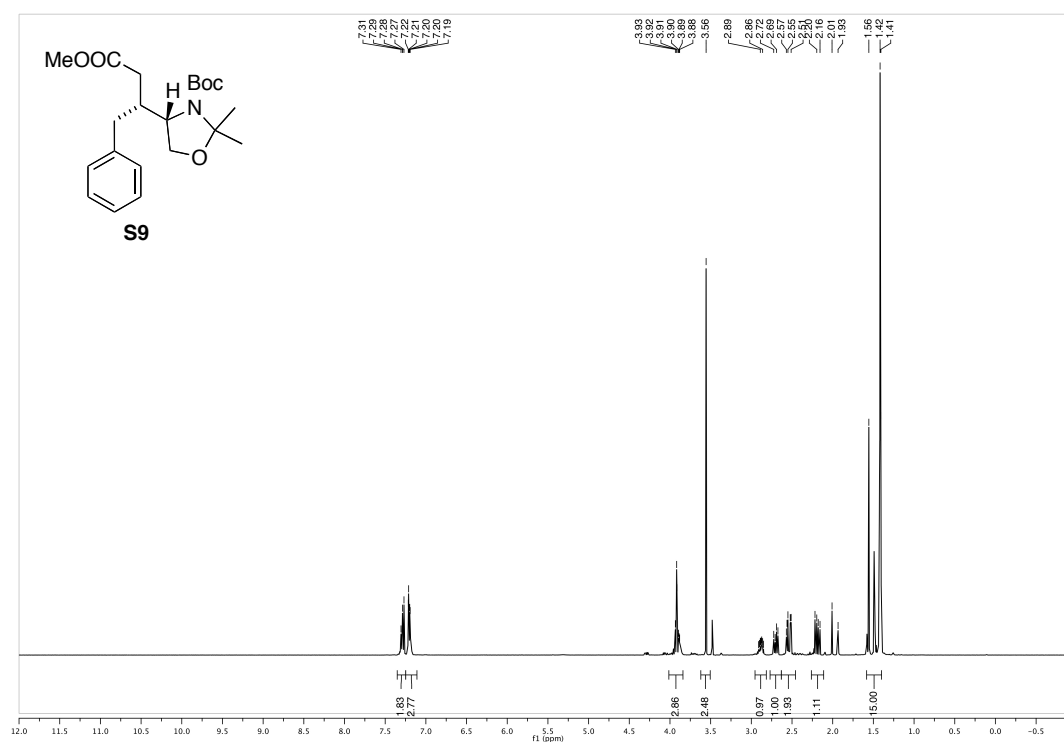
**AzKA•Na (107•Na)**

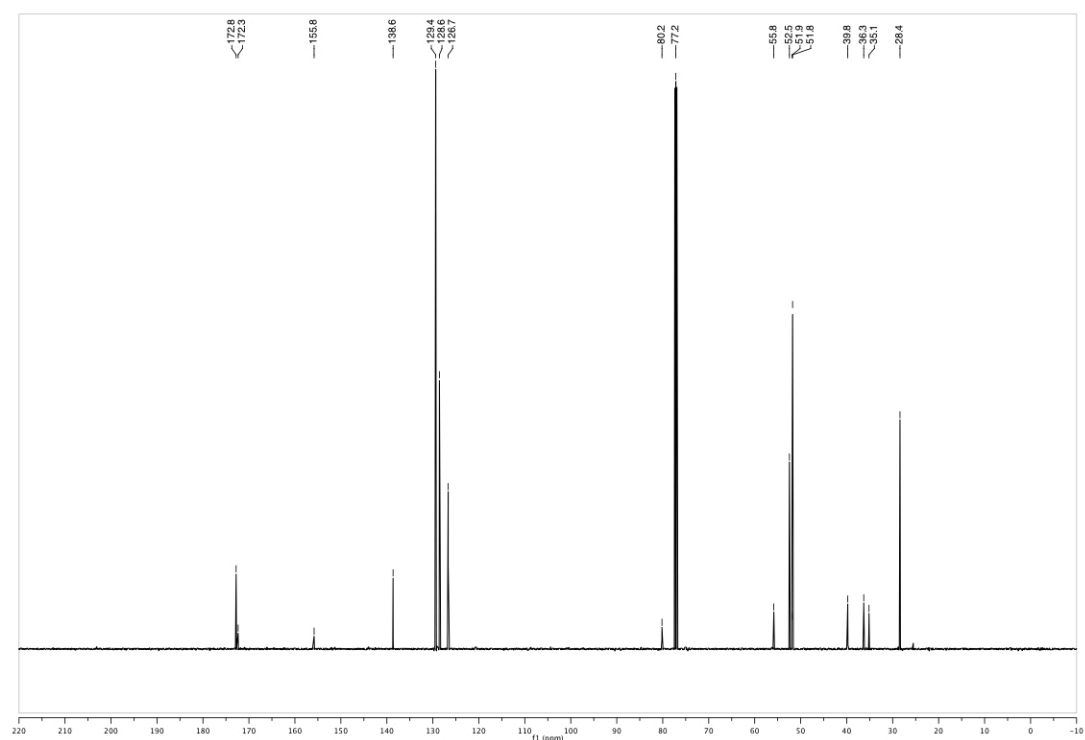
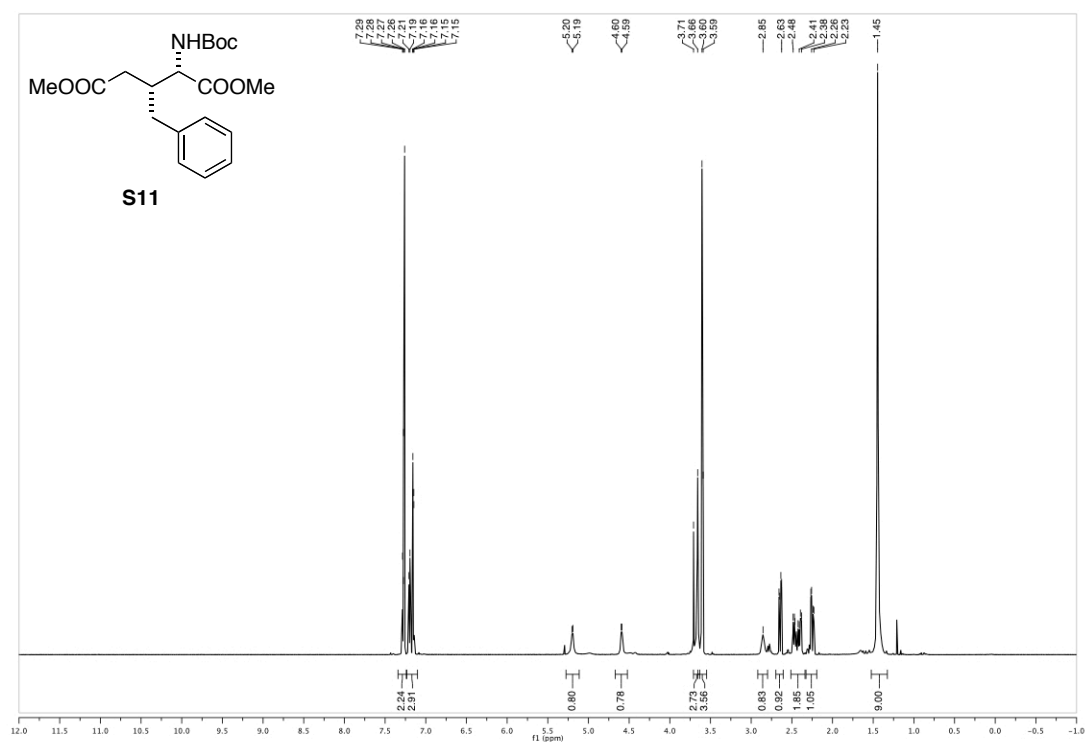
## 4) 3-D-Substituted Glutamate Analogues

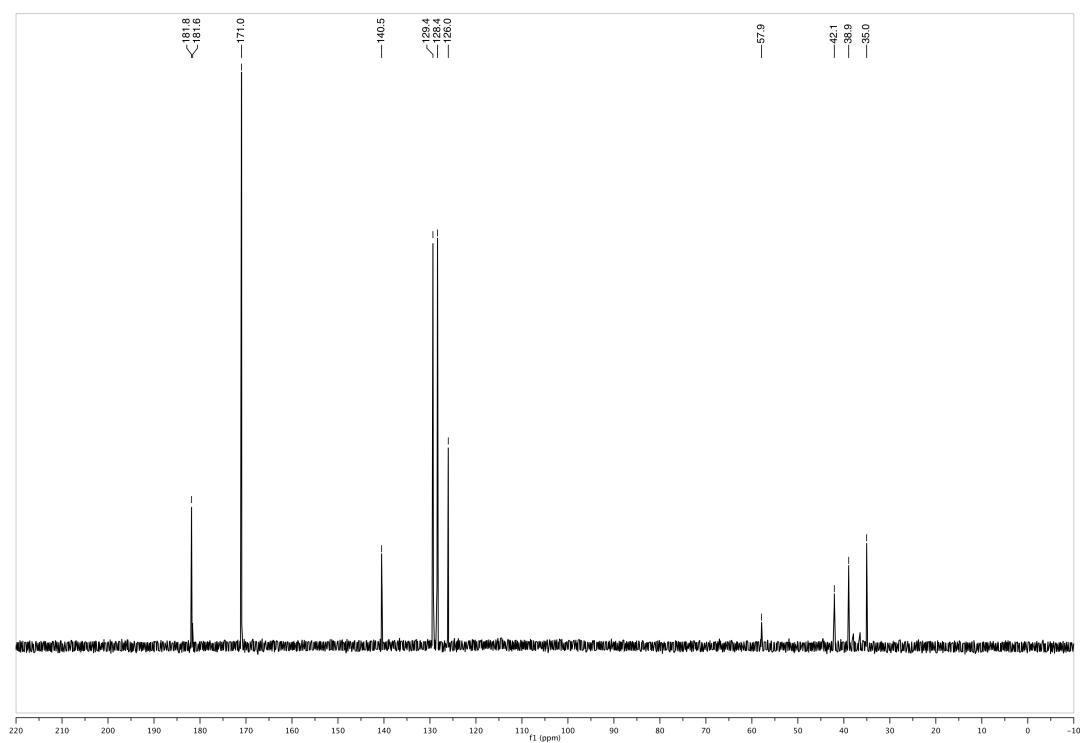
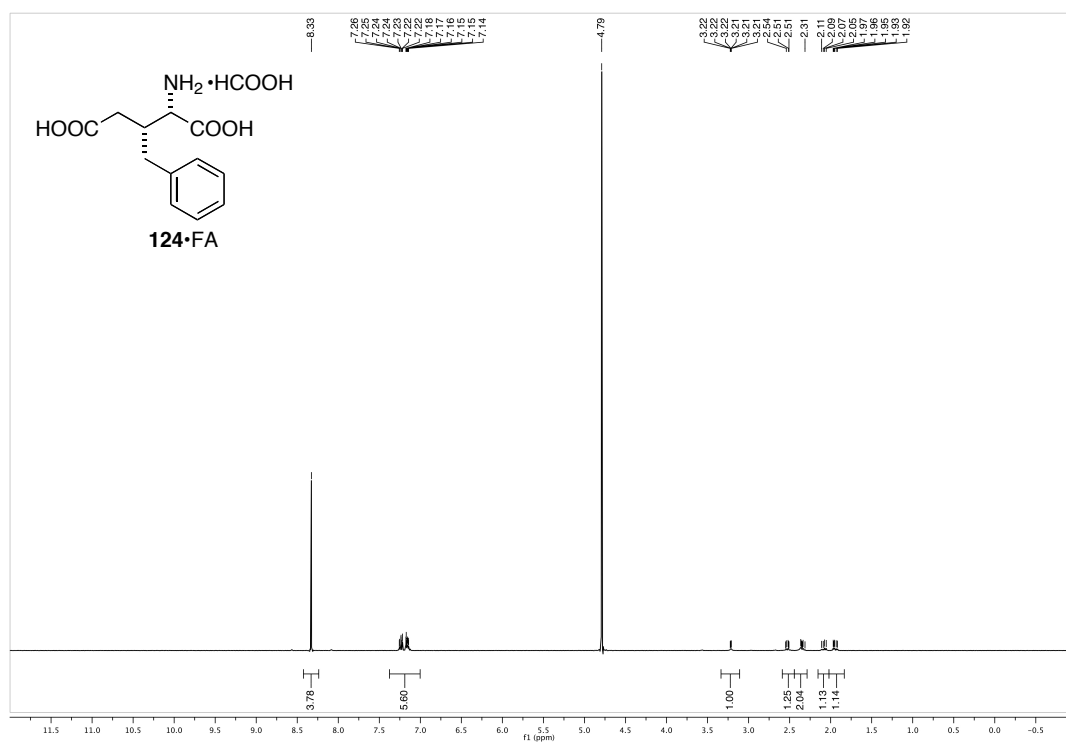
(*S,E*)-*tert*-butyl 4-(3-methoxy-3-oxoprop-1-enyl)-2,2-dimethyloxazolidine-3-carboxylate  
(122a)



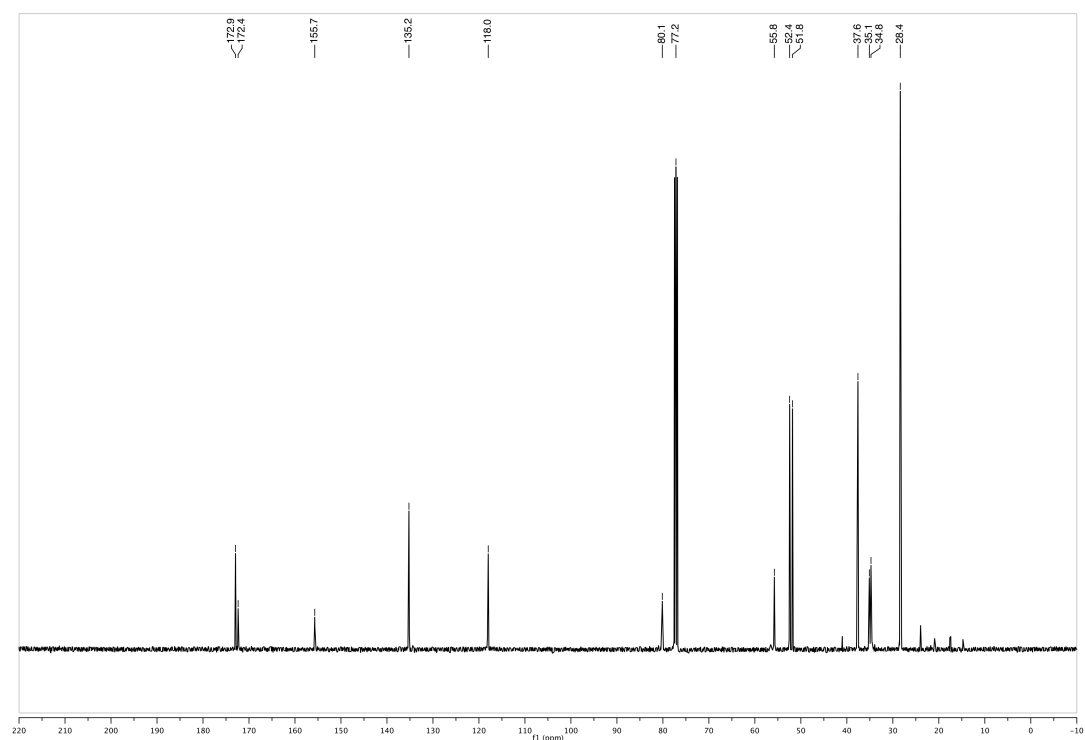
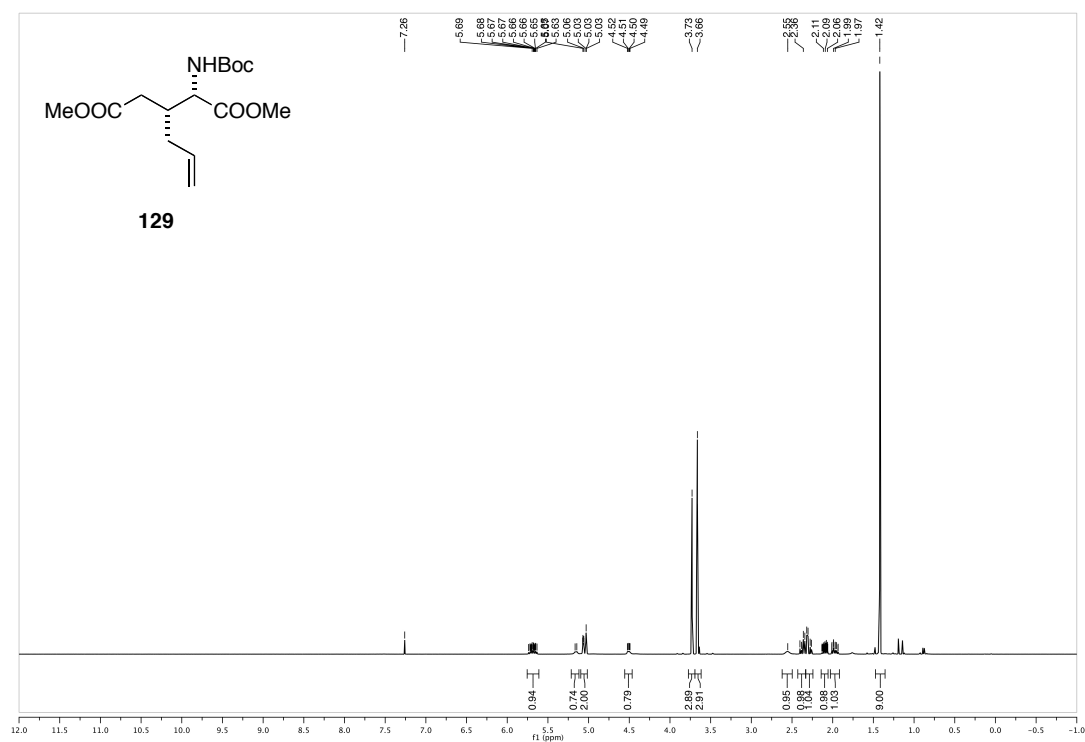
**(S)-tert-butyl 4-((R)-4-methoxy-4-oxo-1-phenylbutan-2-yl)-2,2-dimethyloxazolidine-3-carboxylate (S9)**

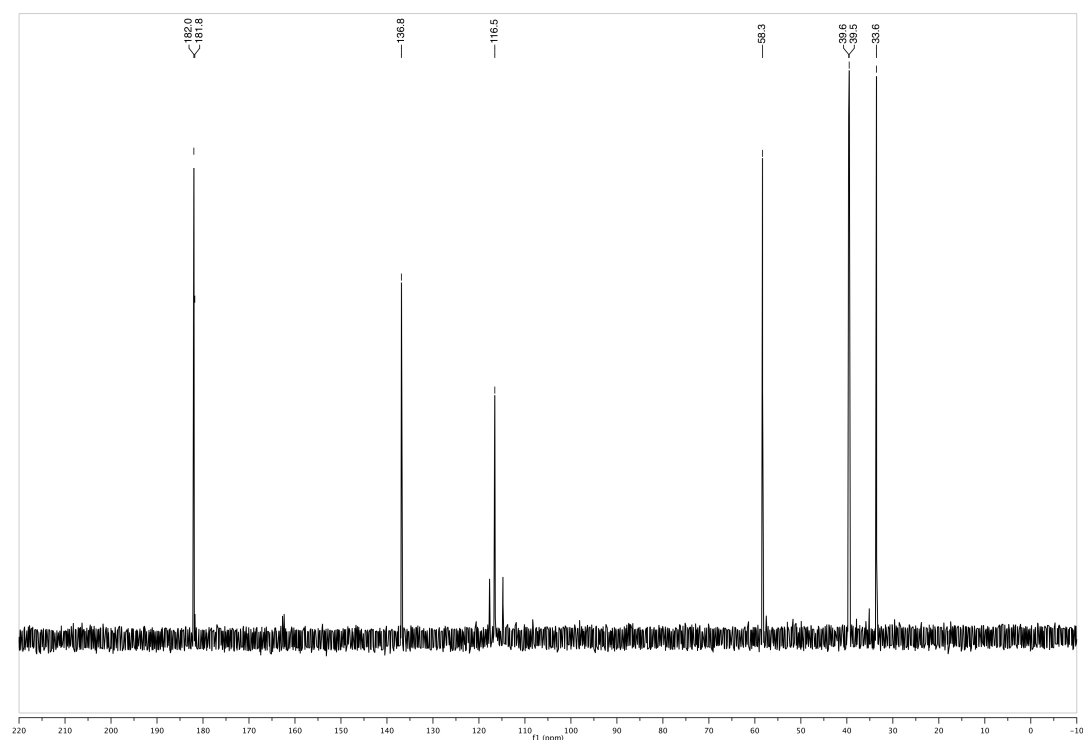
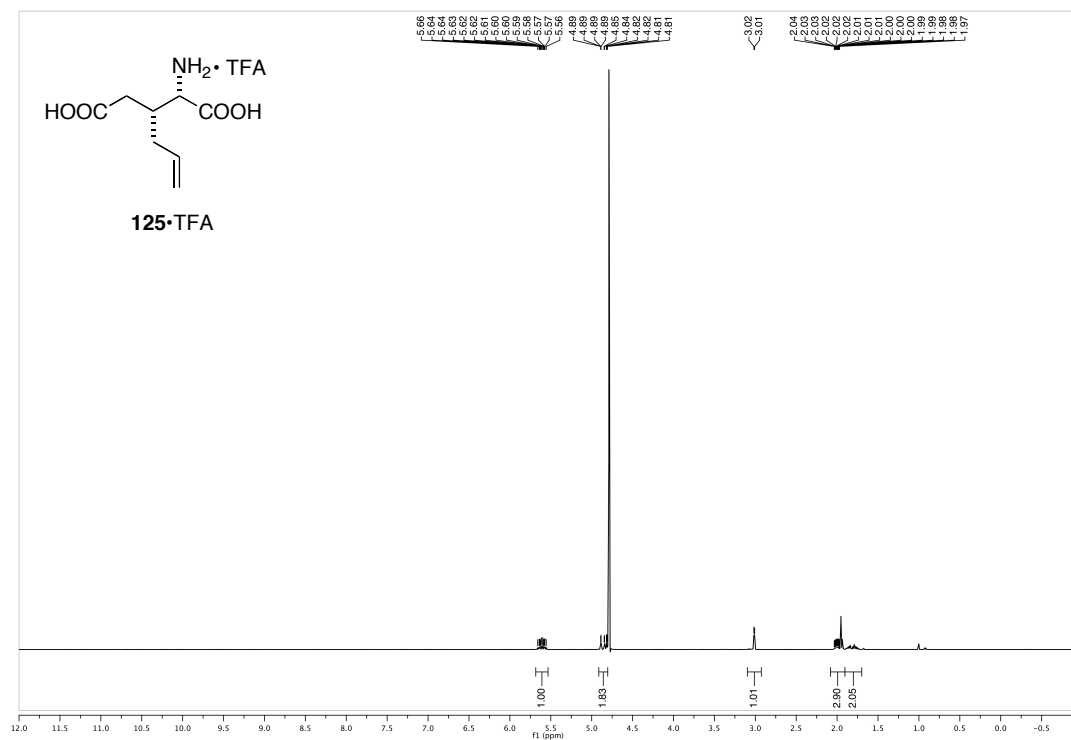


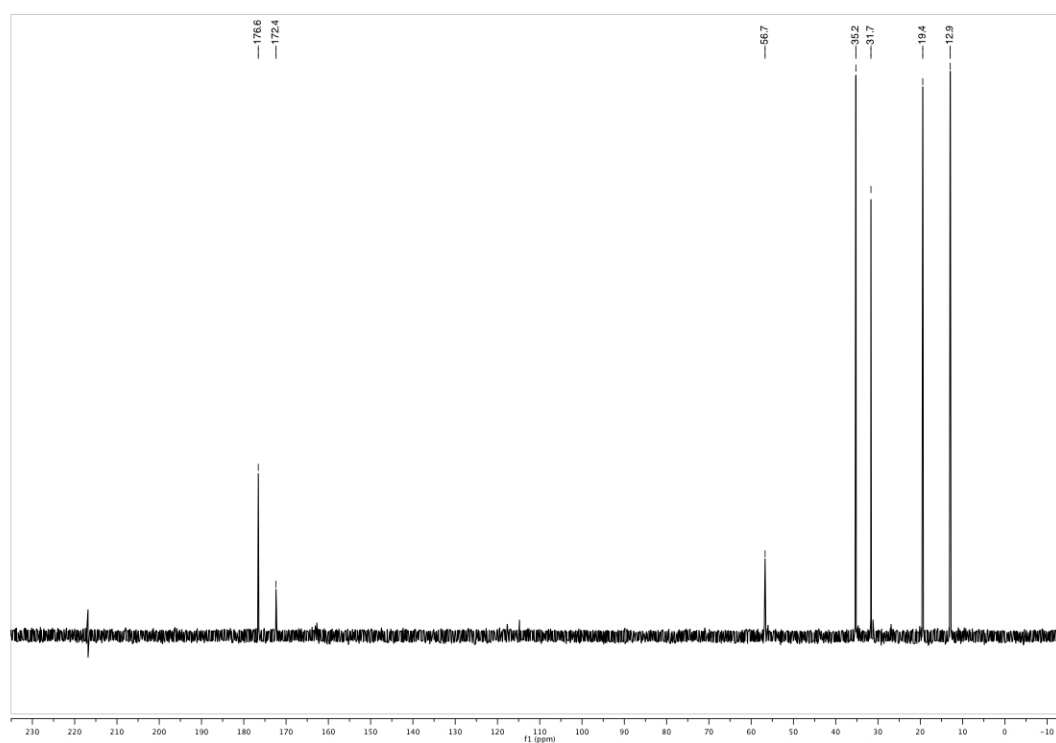
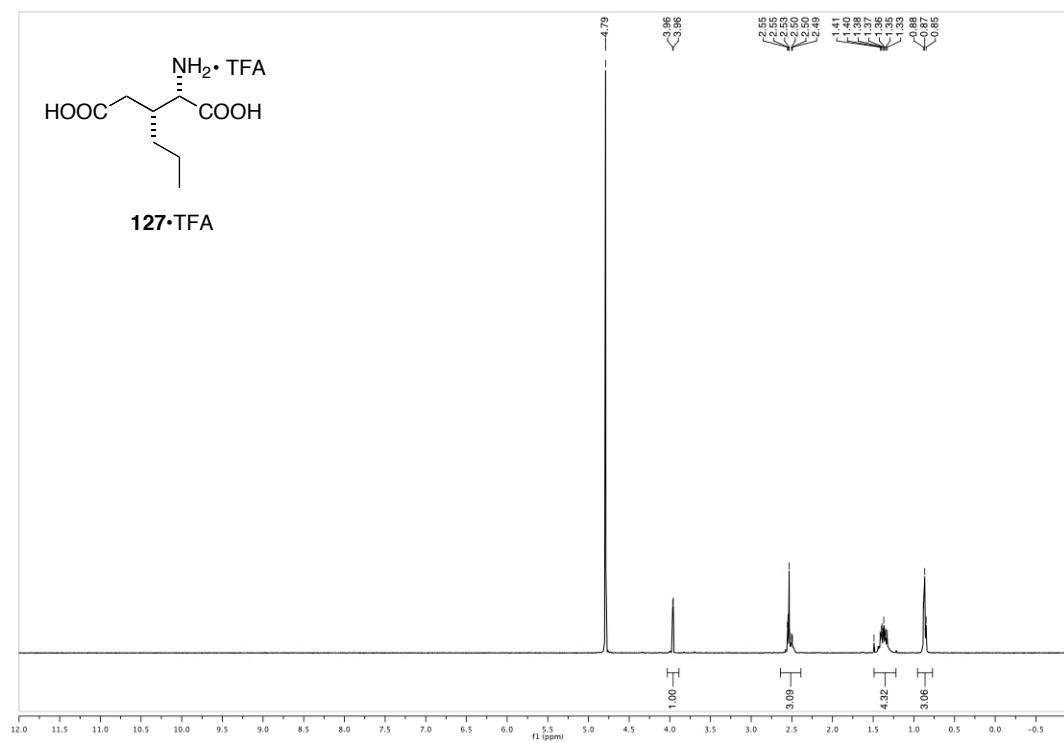
**(2*S*,3*R*)-dimethyl 3-benzyl-2-(*tert*-butoxycarbonylamino)pentanedioate (S11)**

**(2*S*,3*R*)-2-amino-3-benzylpentanedioic acid formate salt (124•FA)**

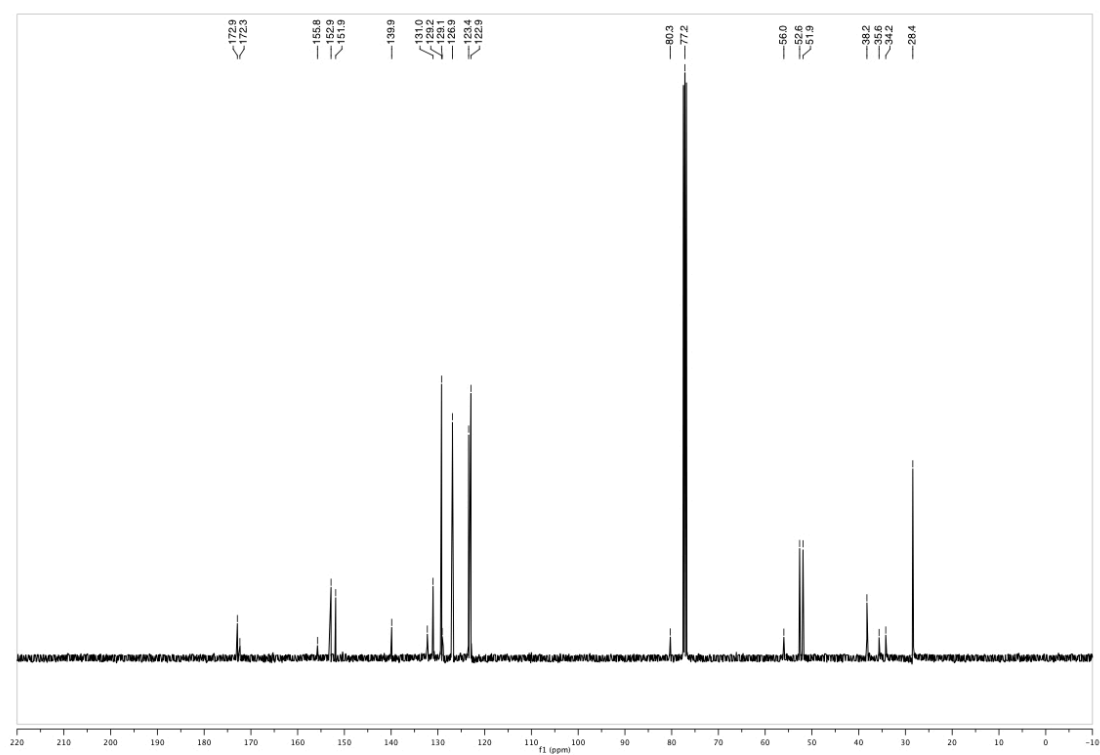
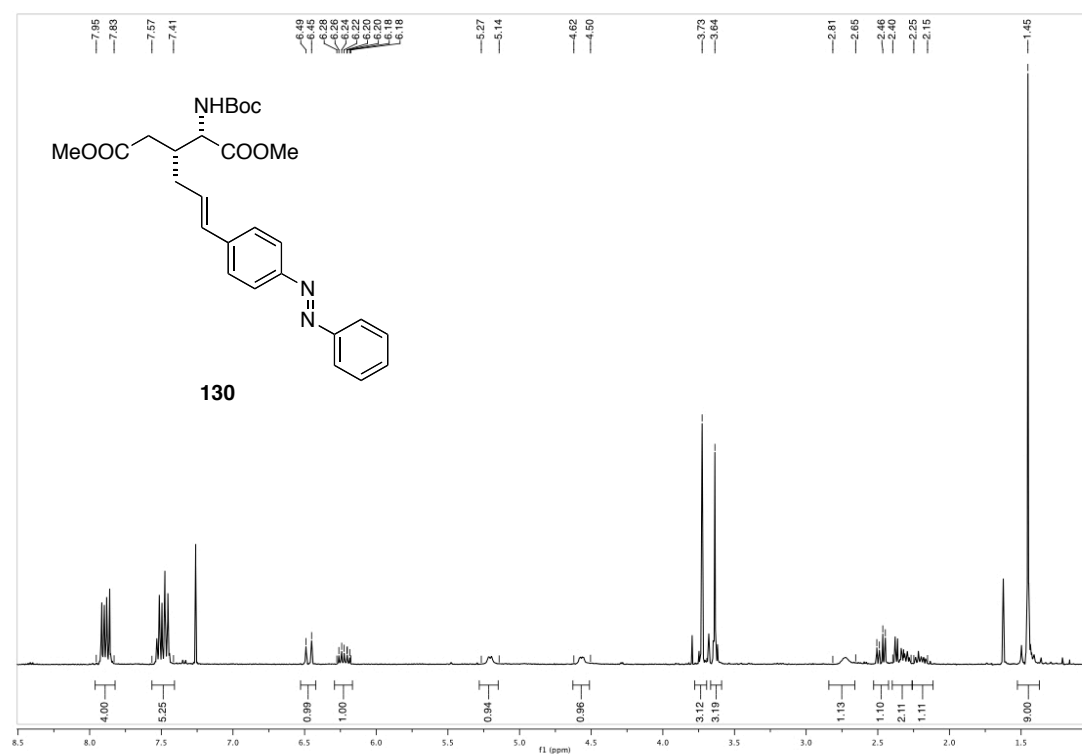


**(2*S*,3*R*)-dimethyl 3-allyl-2-(*tert*-butoxycarbonylamino)pentanedioate (129)**

**(2*S*,3*R*)-3-allyl-2-aminopentanedioic acid TFA salt (125•TFA)**

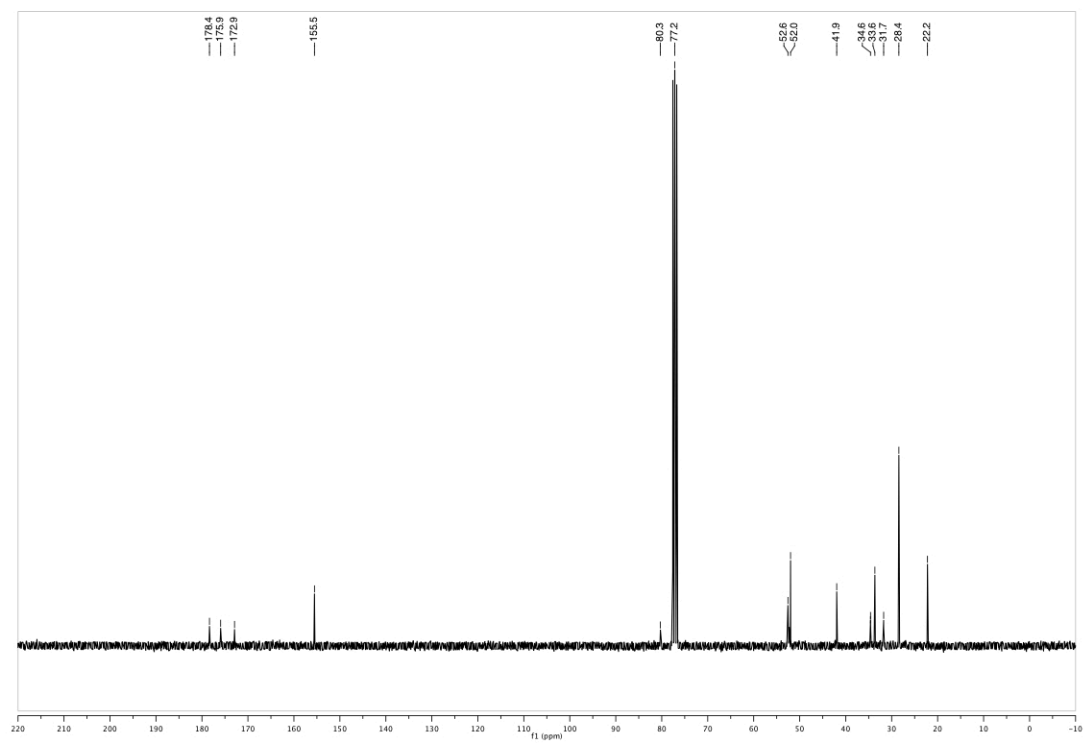
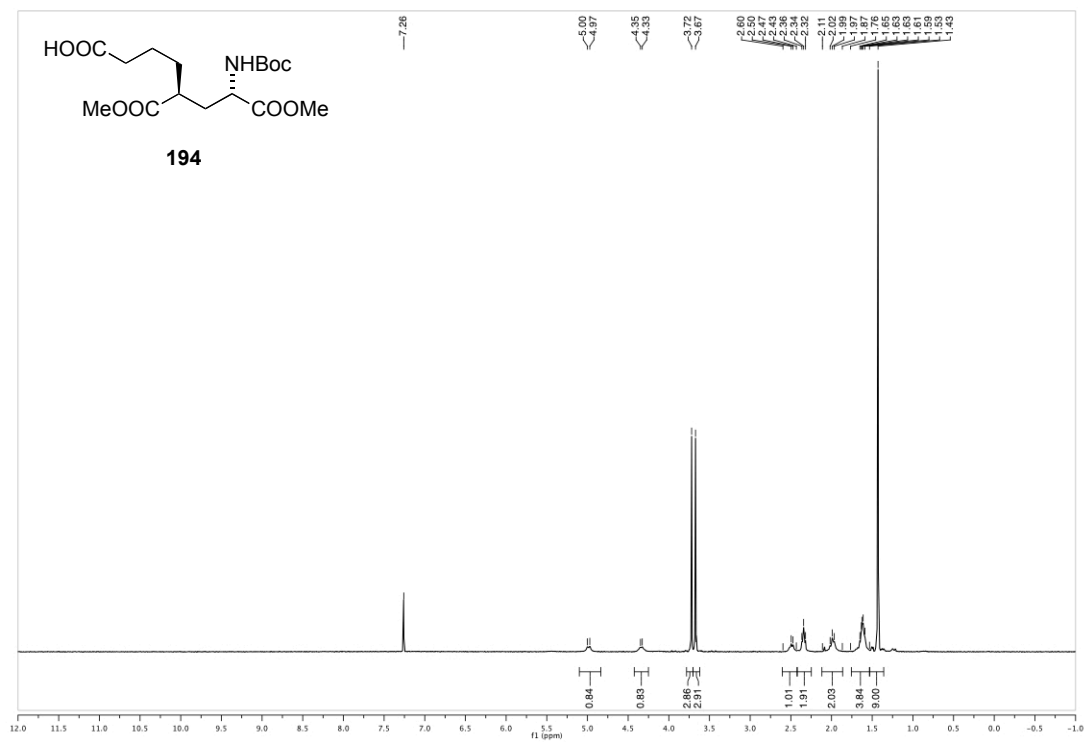
**(2*S*,3*R*)-2-amino-3-propylpentanedioic acid TFA salt (127•TFA)**

**(2*S*,3*R*)-dimethyl 2-(*tert*-butoxycarbonylamino)-3-((*E*)-3-(4-(phenyldiazenyl)phenyl)allyl)pentanedioate (130)**

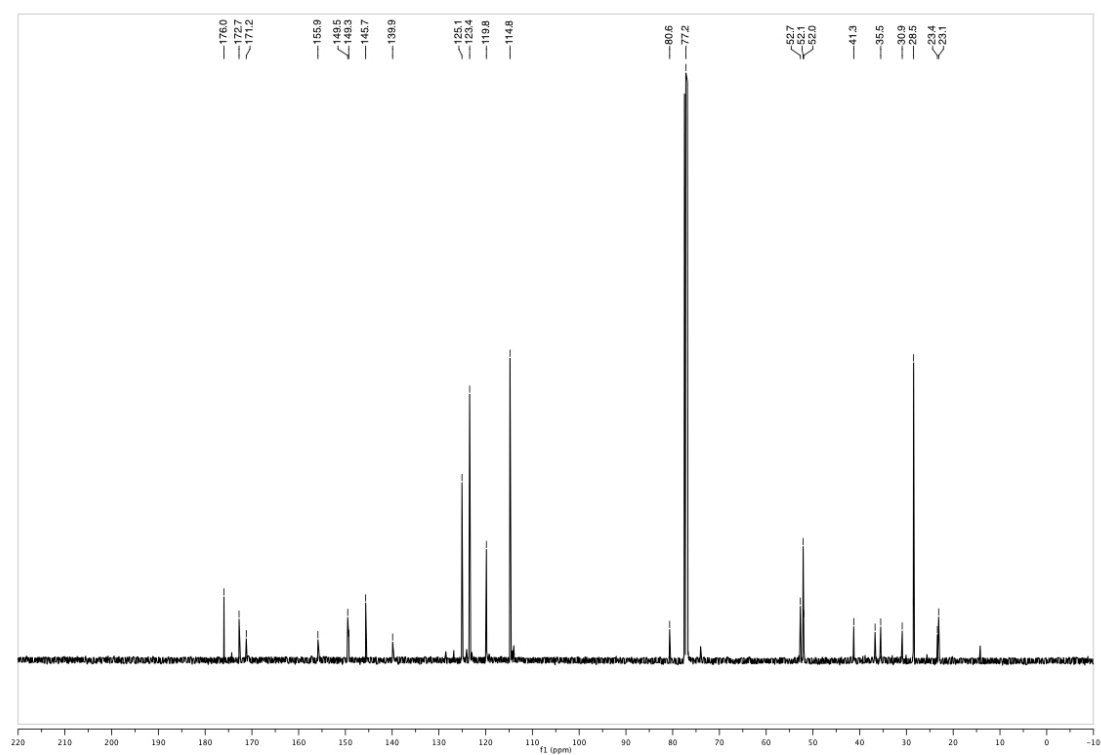
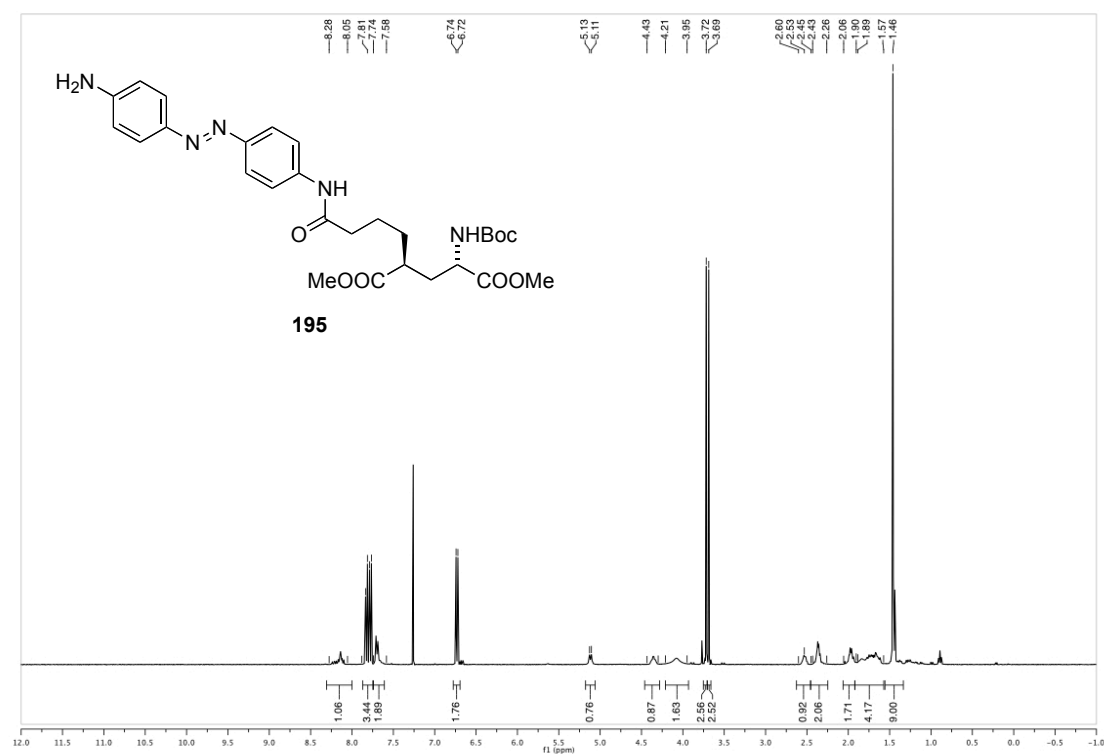


## 5) A Photoswitched Tethered Ligand of mGluRs

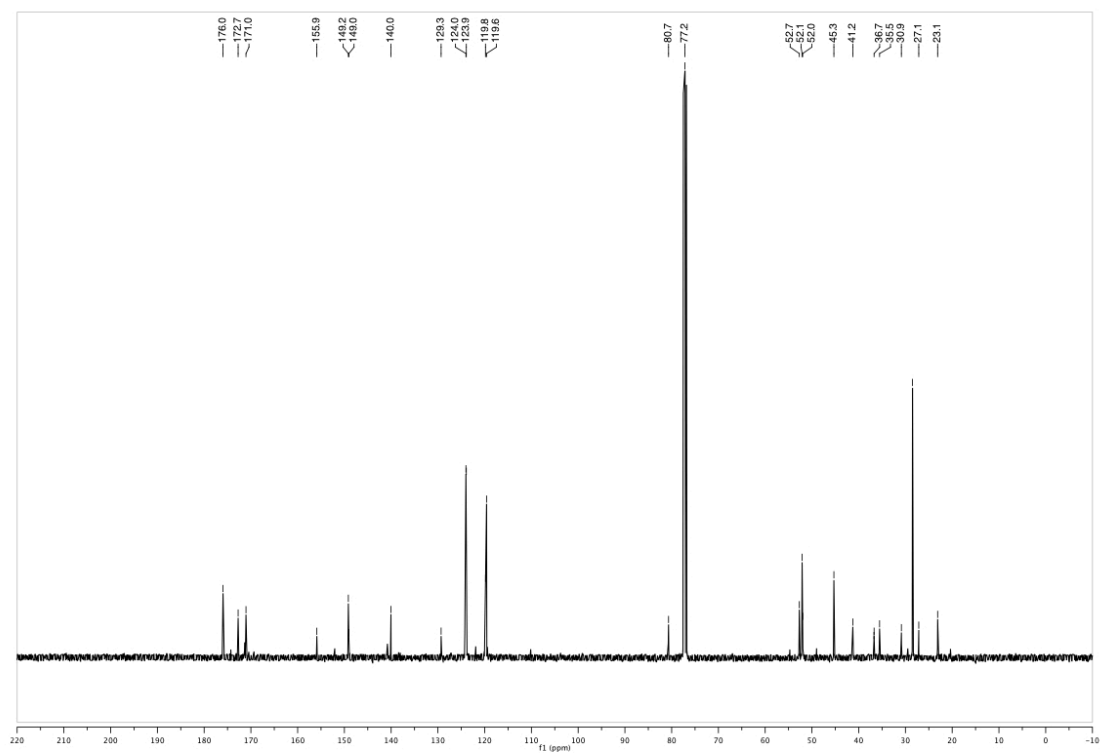
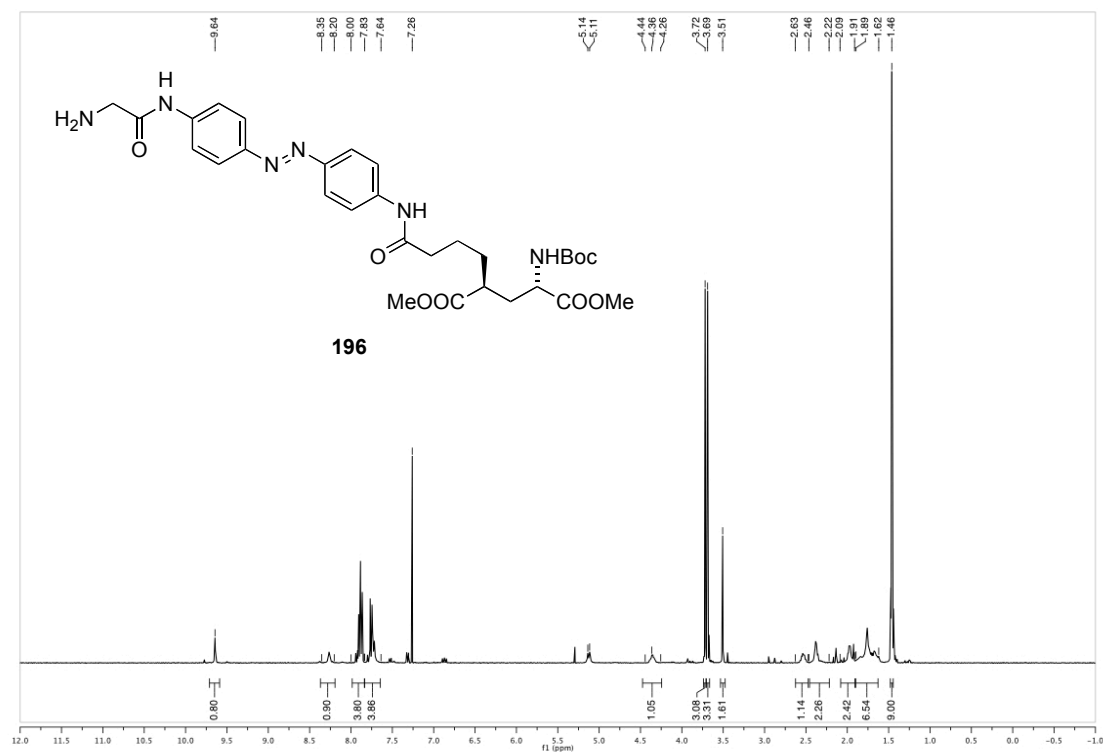
(5*S*,7*S*)-7-(*tert*-butoxycarbonylamino)-8-methoxy-5-(methoxycarbonyl)-8-oxo-octanoic acid (**194**)



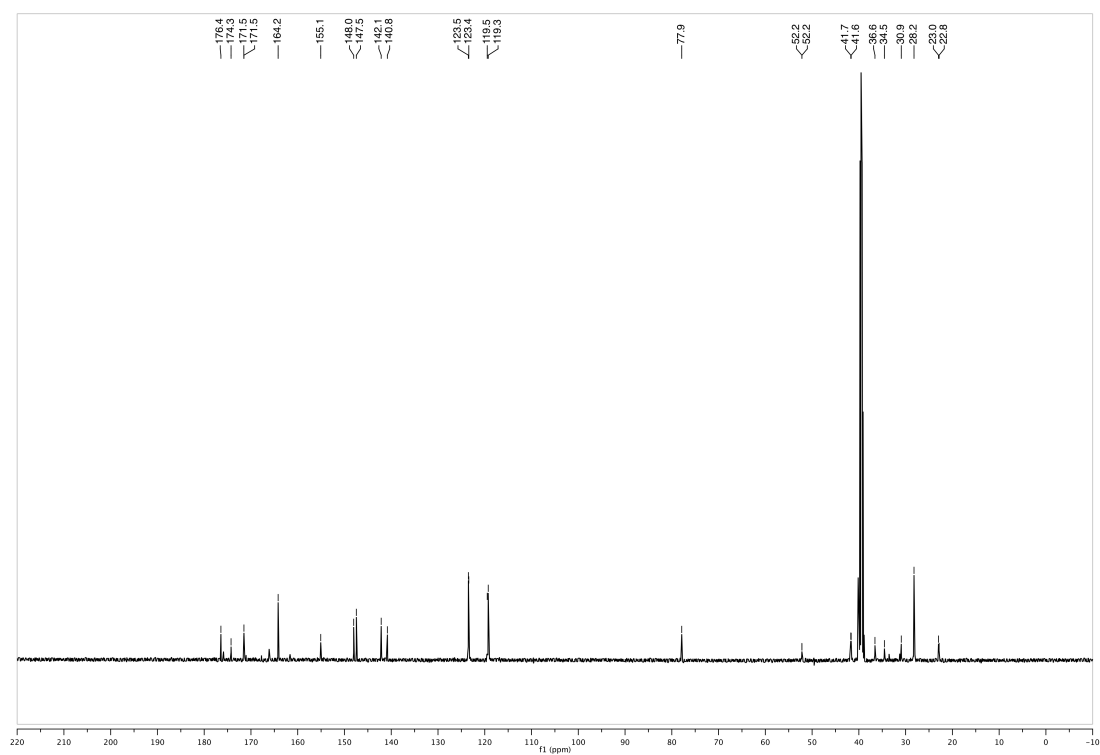
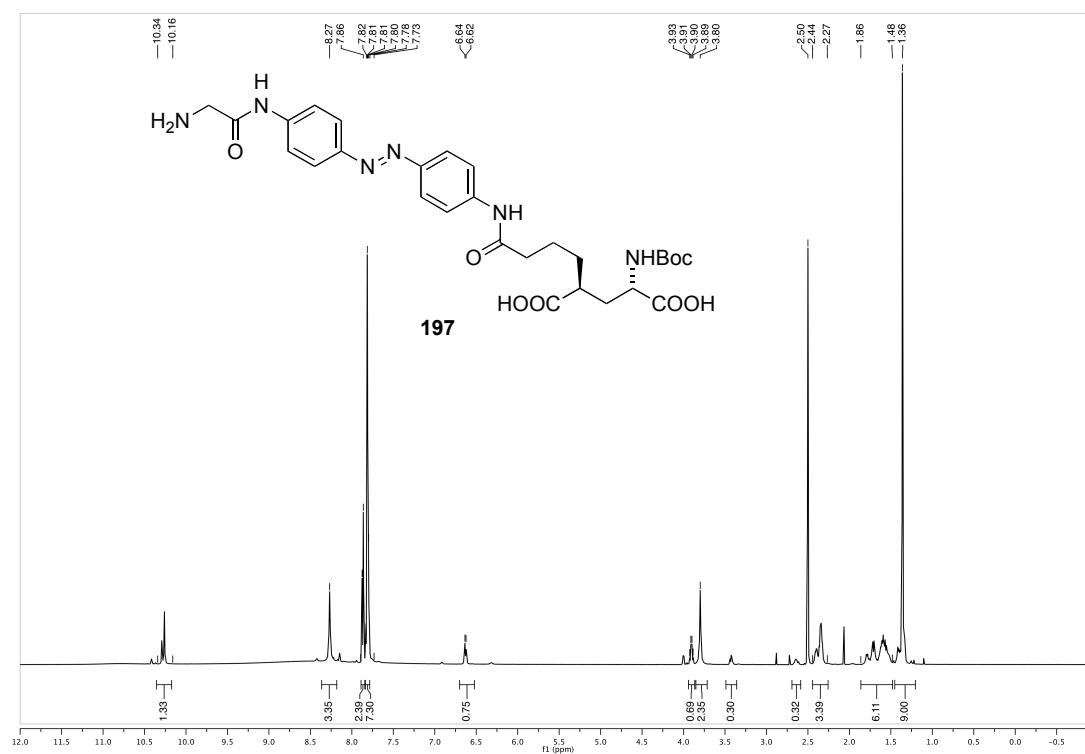
**(2*S*,4*S*)-dimethyl 2-(4-(4-((*E*)-(4-aminophenyl)diazenyl)phenylamino)-4-oxobutyl)-4-(*tert*-butoxycarbonylamino)pentanedioate (195)**



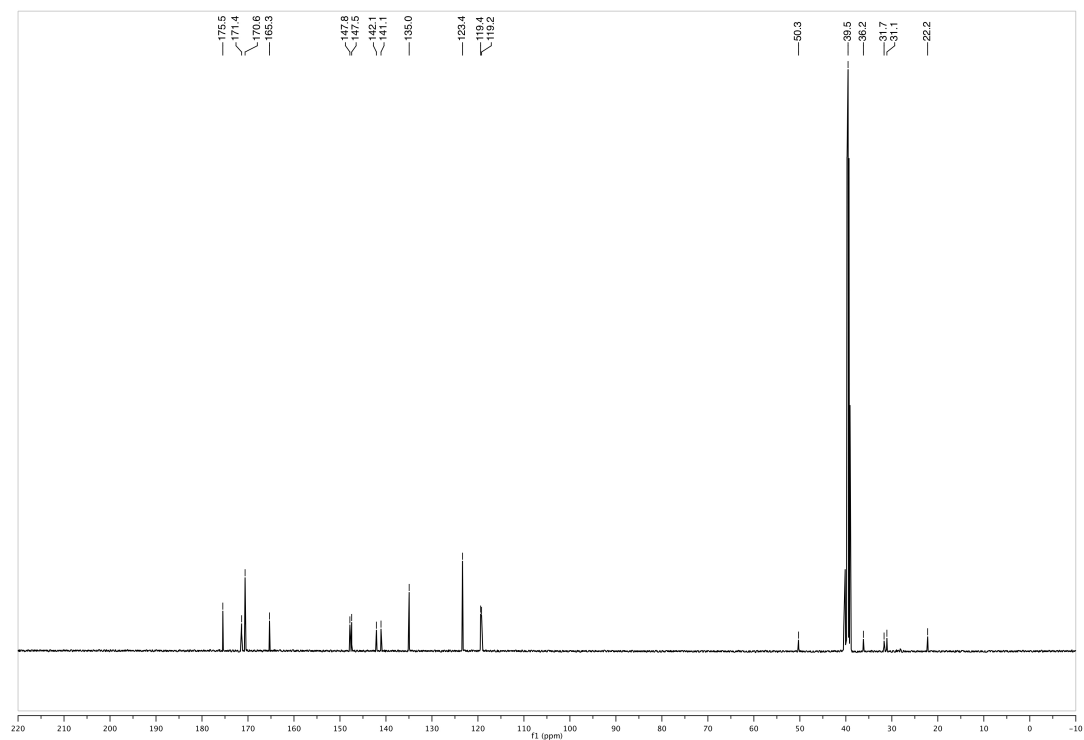
**(2*S*,4*S*)-dimethyl 2-(4-(4-((*E*)-(4-(2-aminoacetamido)phenyl)diazenyl)phenylamino)-4-oxobutyl)-4-(*tert*-butoxycarbonylamino)pentanedioate (196)**



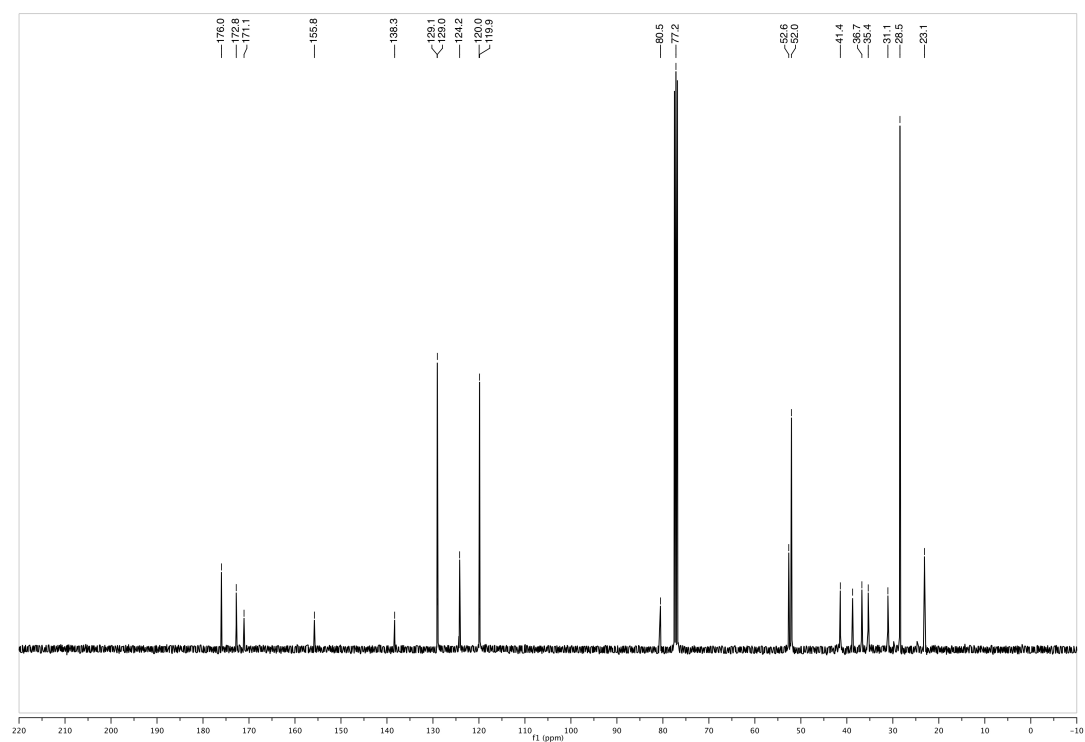
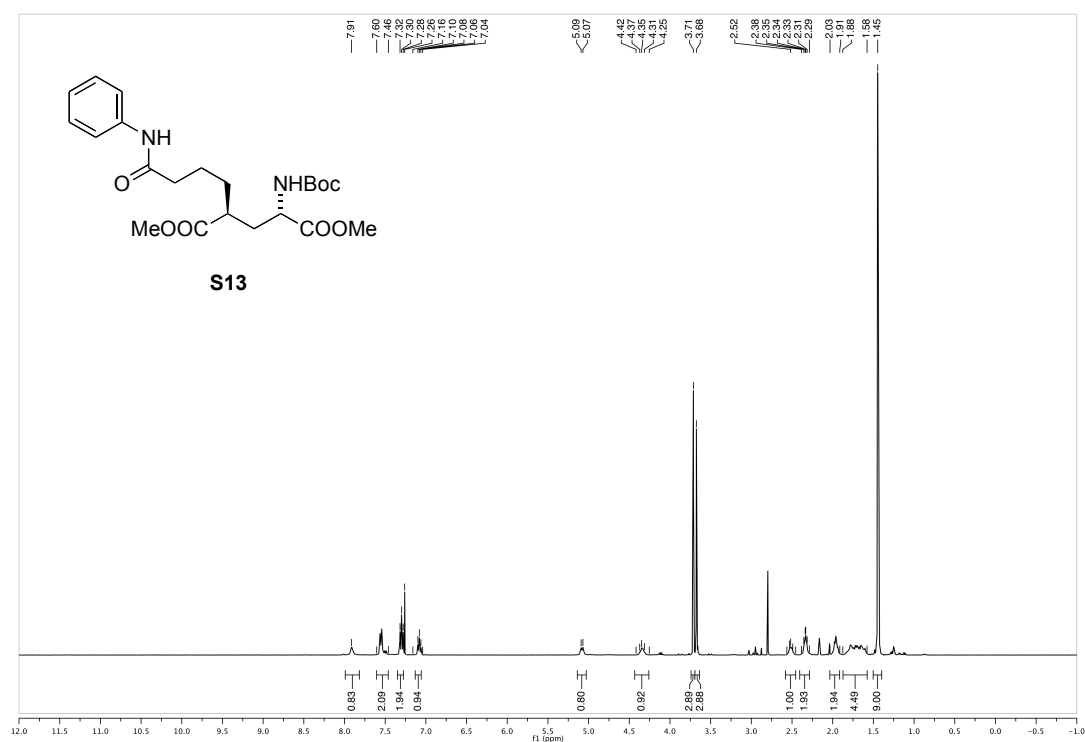
**(2*S*,4*S*)-2-(4-(4-((*E*)-(4-(2-aminoacetamido)phenyl)diazenyl)phenylamino)-4-oxo butyl)-4-(*tert*-butoxycarbonylamino)pentanedioic acid (197)**



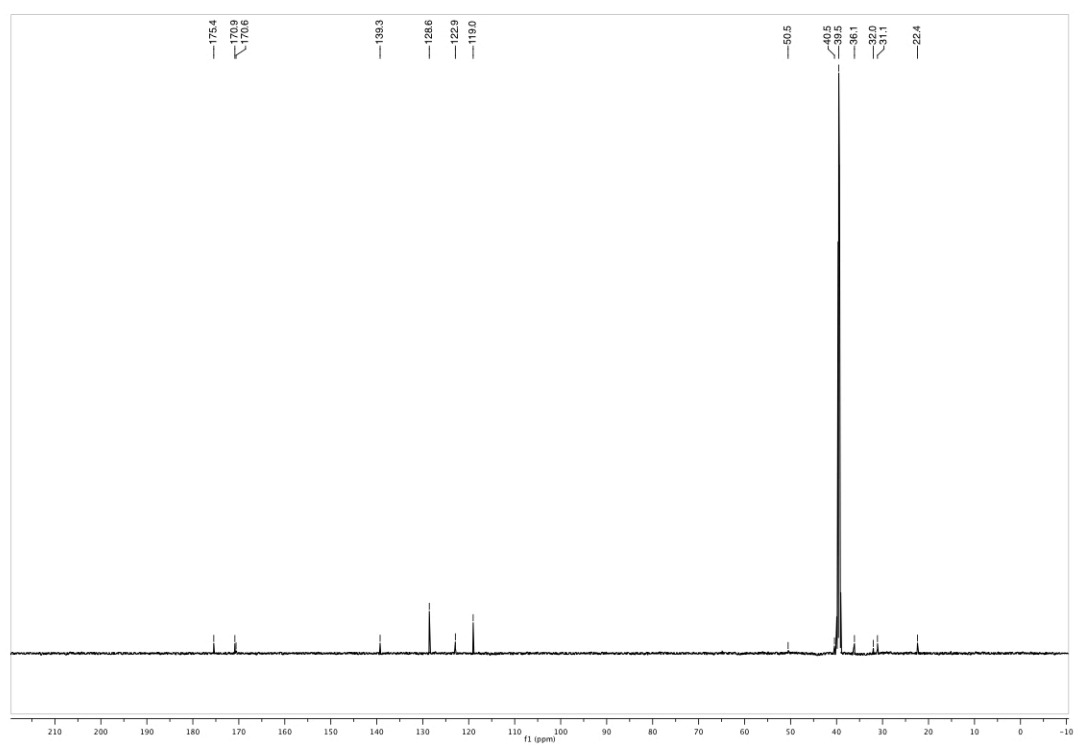
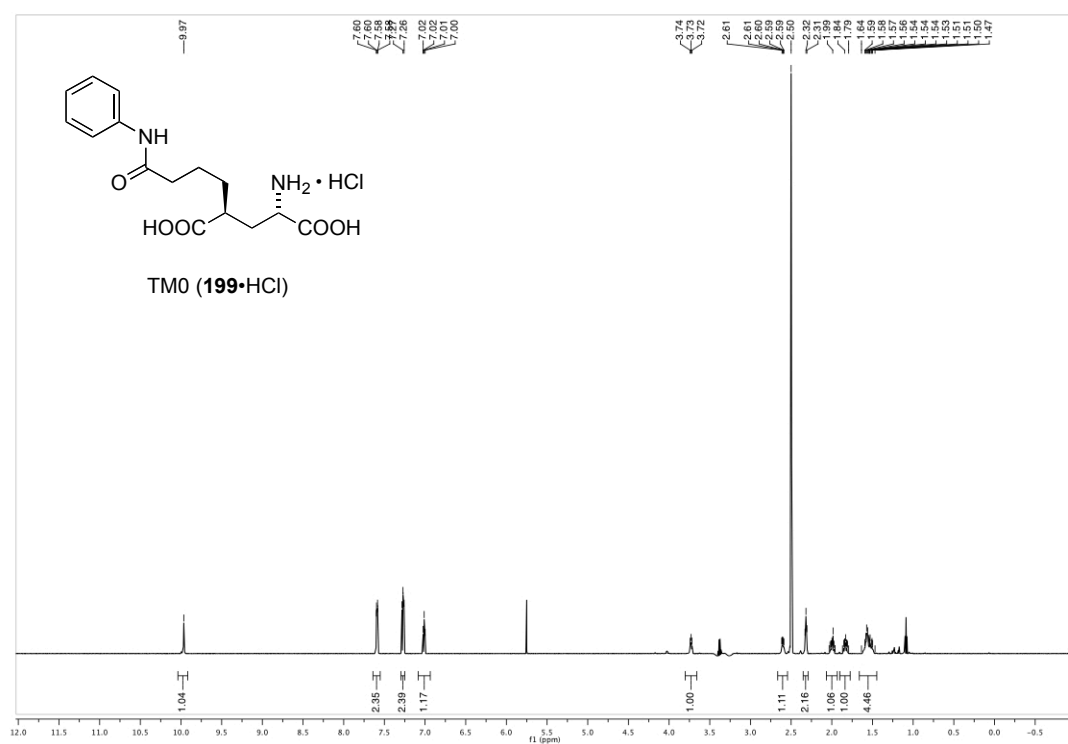




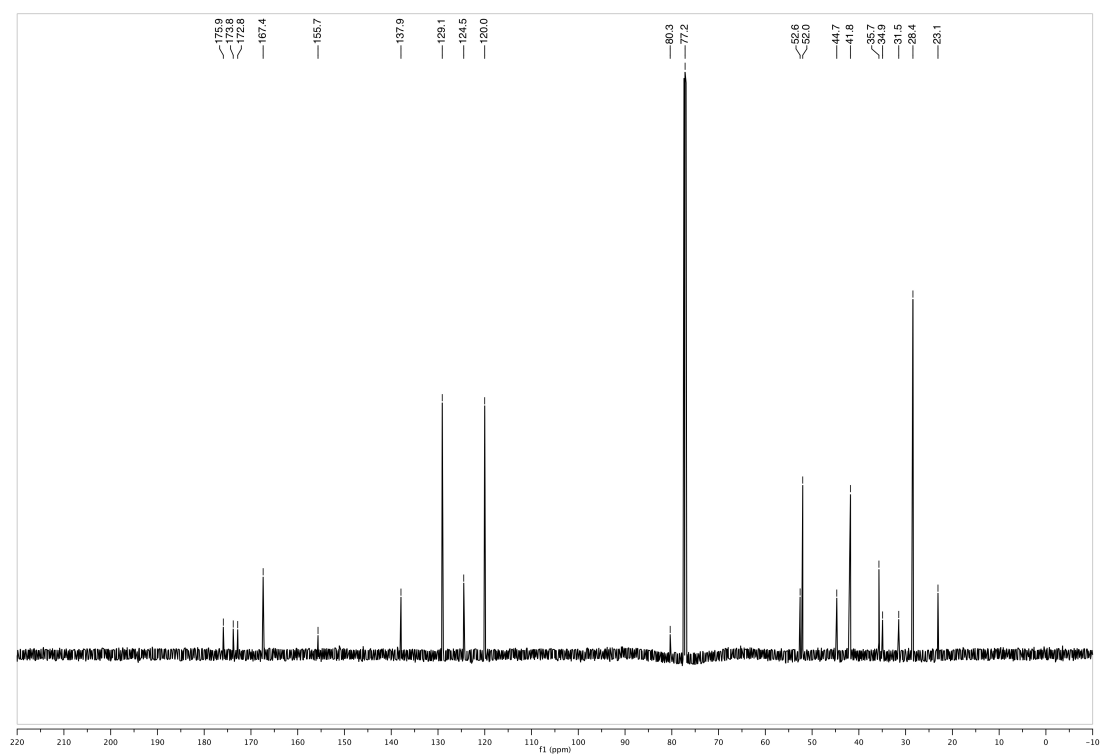
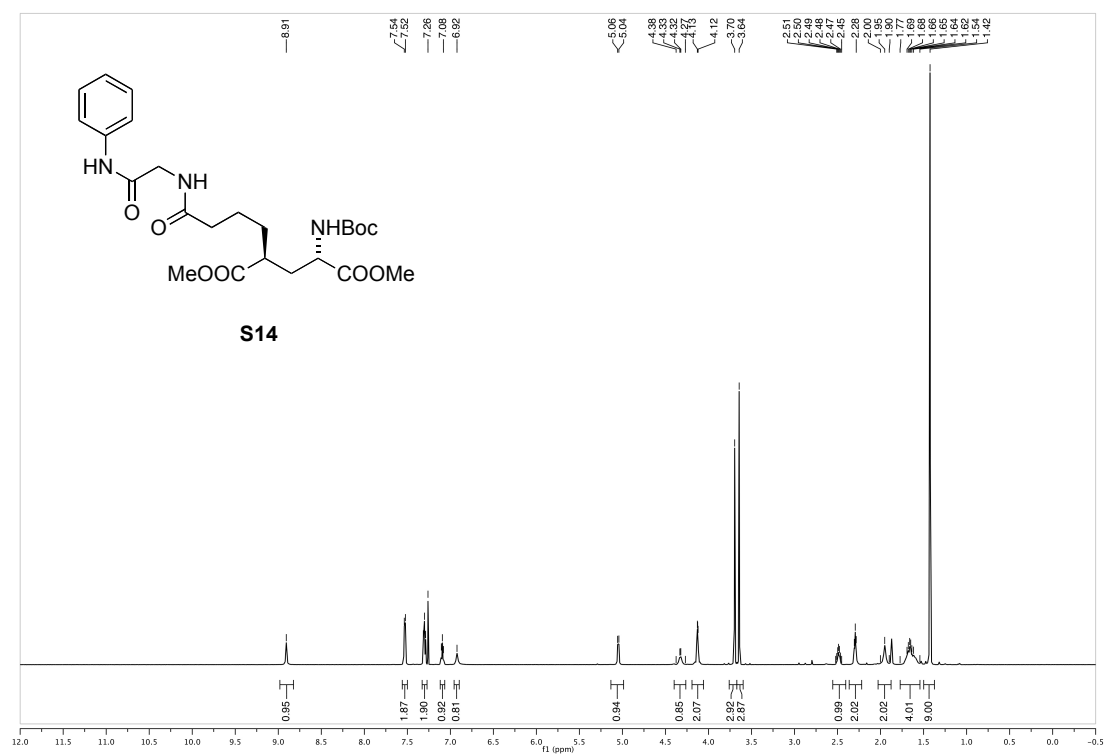
**(2*S*,4*S*)-dimethyl 2-(*tert*-butoxycarbonylamino)-4-(4-oxo-4-(phenylamino)butyl) pentane-dioate (S13)**



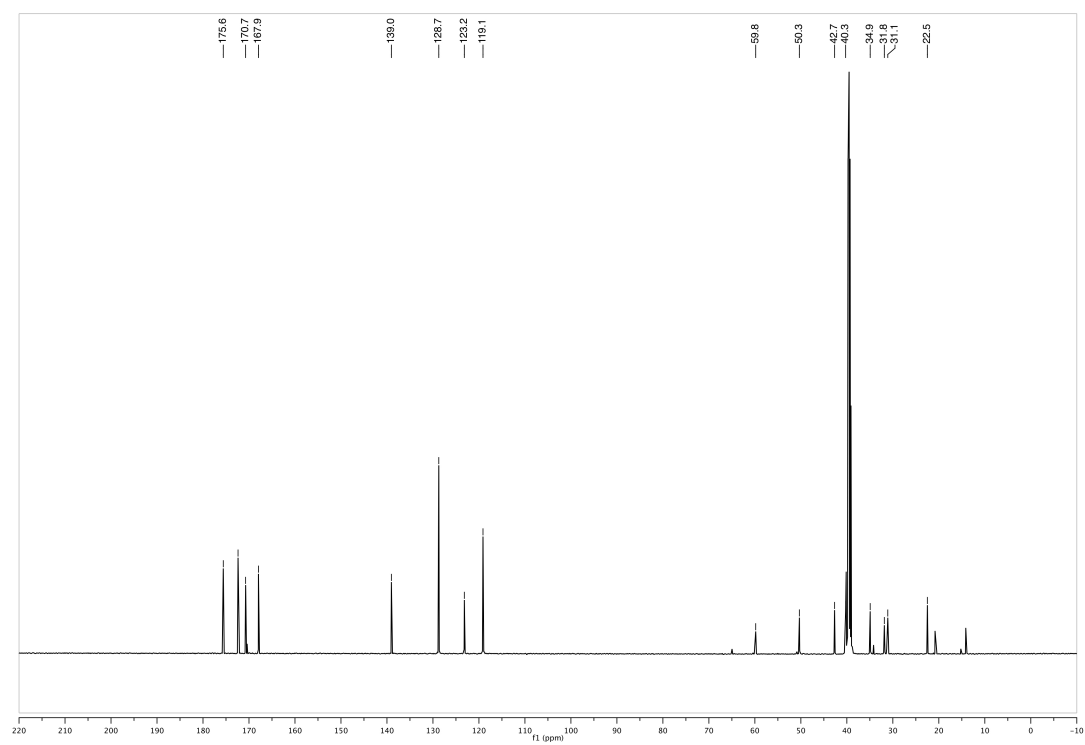
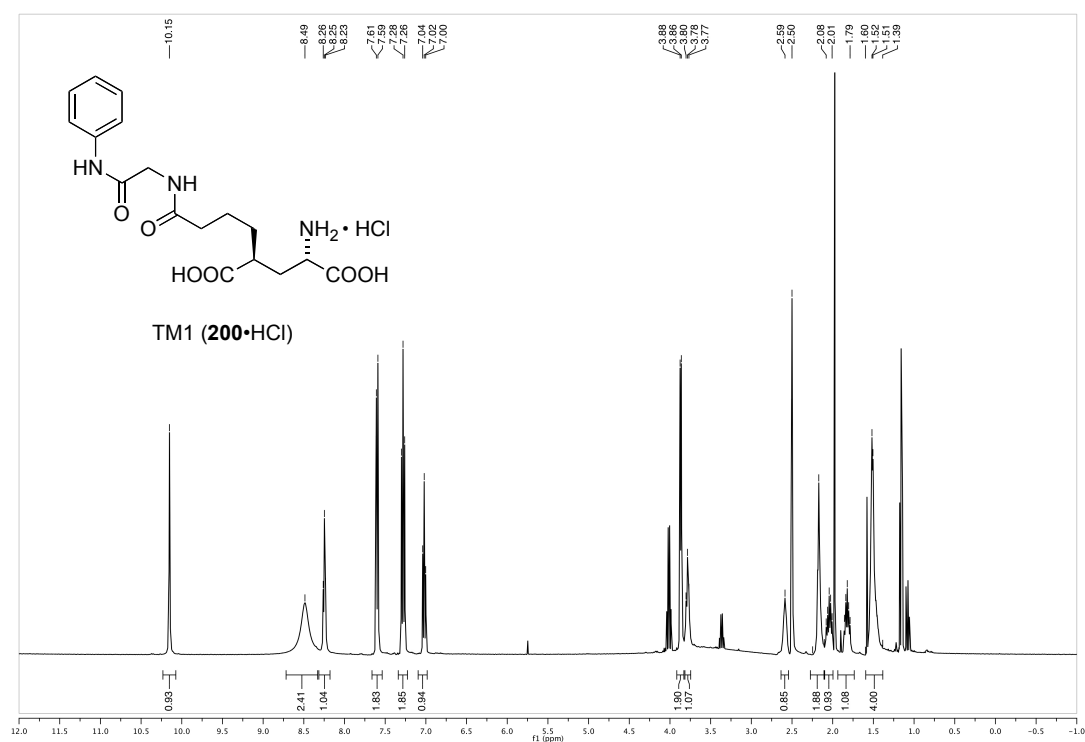
**(2*S*,4*S*)-2-amino-4-(4-oxo-4-(phenylamino)butyl)pentanedioic acid hydrochloride (TM-0, 199•HCl)**



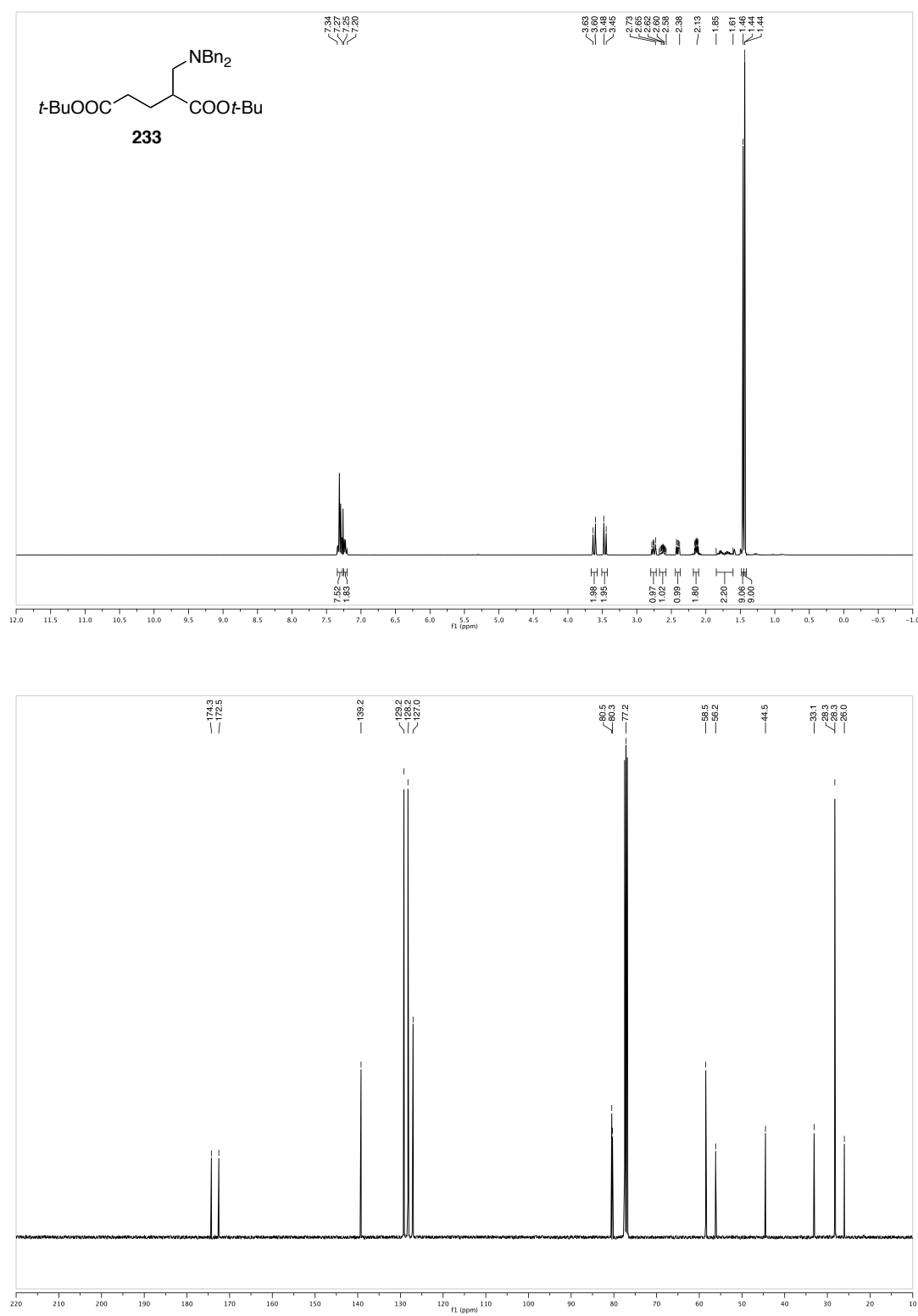
**(2*S*,4*S*)-dimethyl 2-(*tert*-butoxycarbonylamino)-4-(4-oxo-4-(2-oxo-2-(phenylamino)ethylamino)butyl)pentanedioate (S14)**

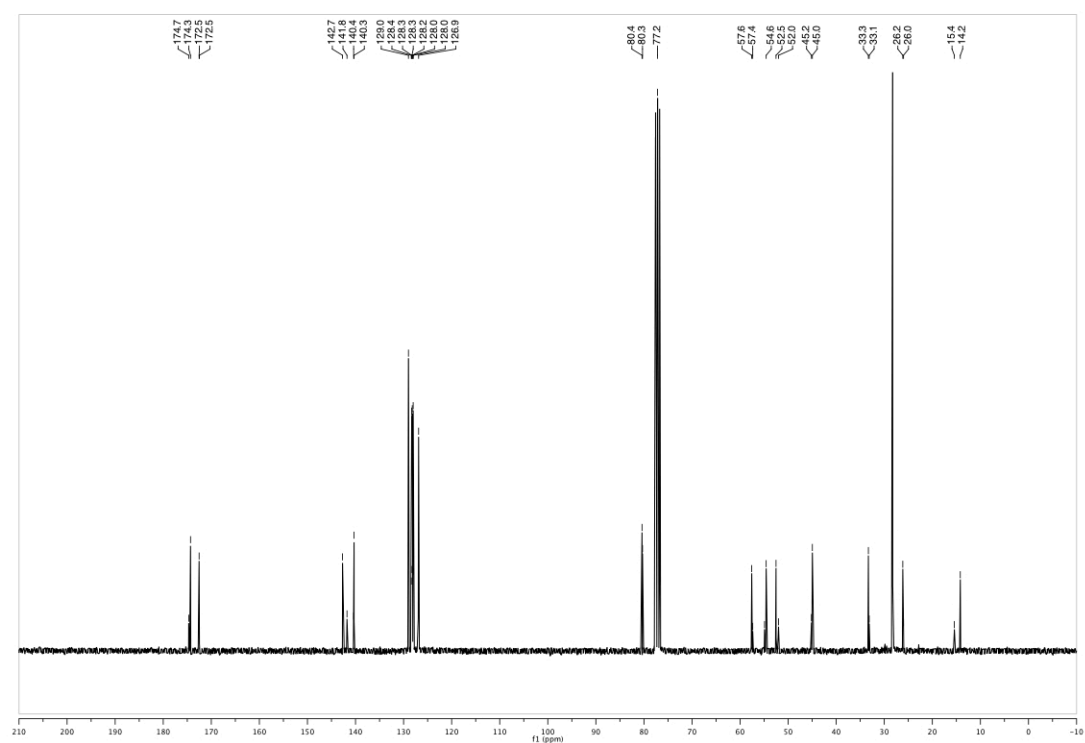
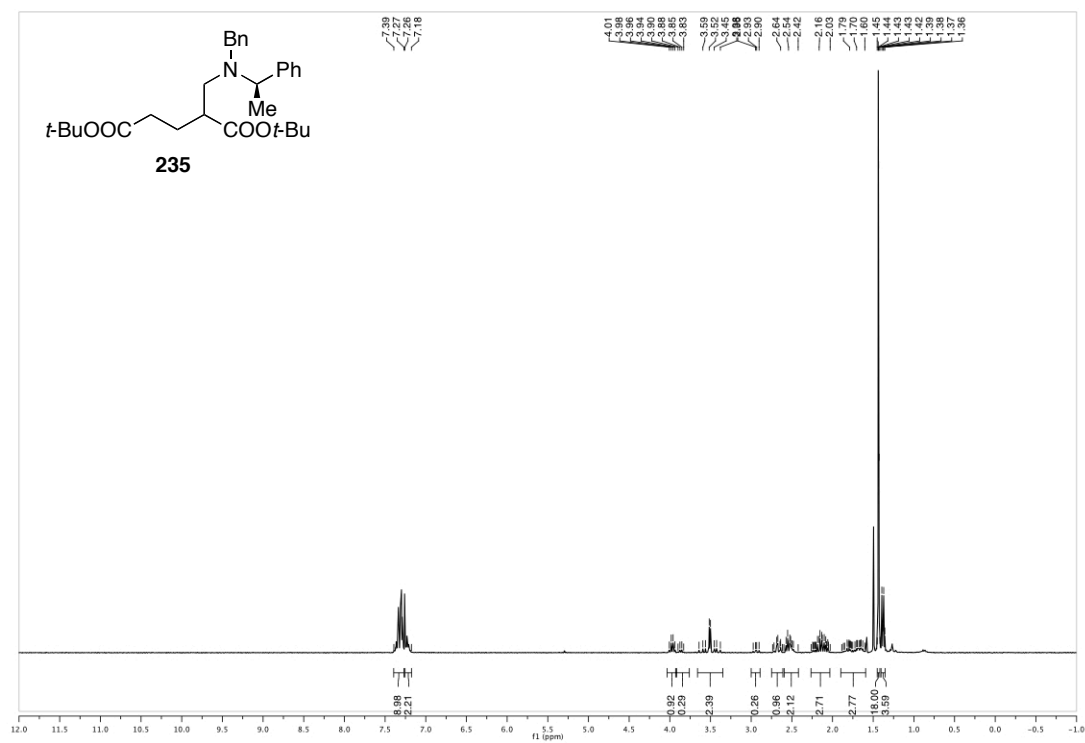


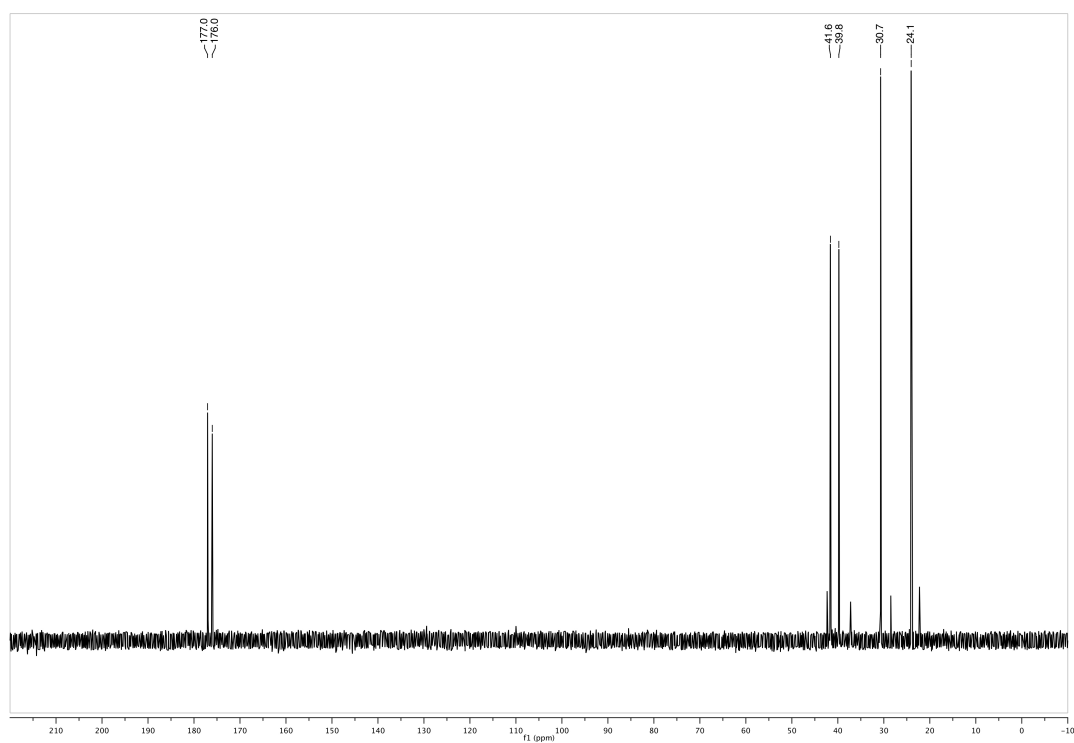
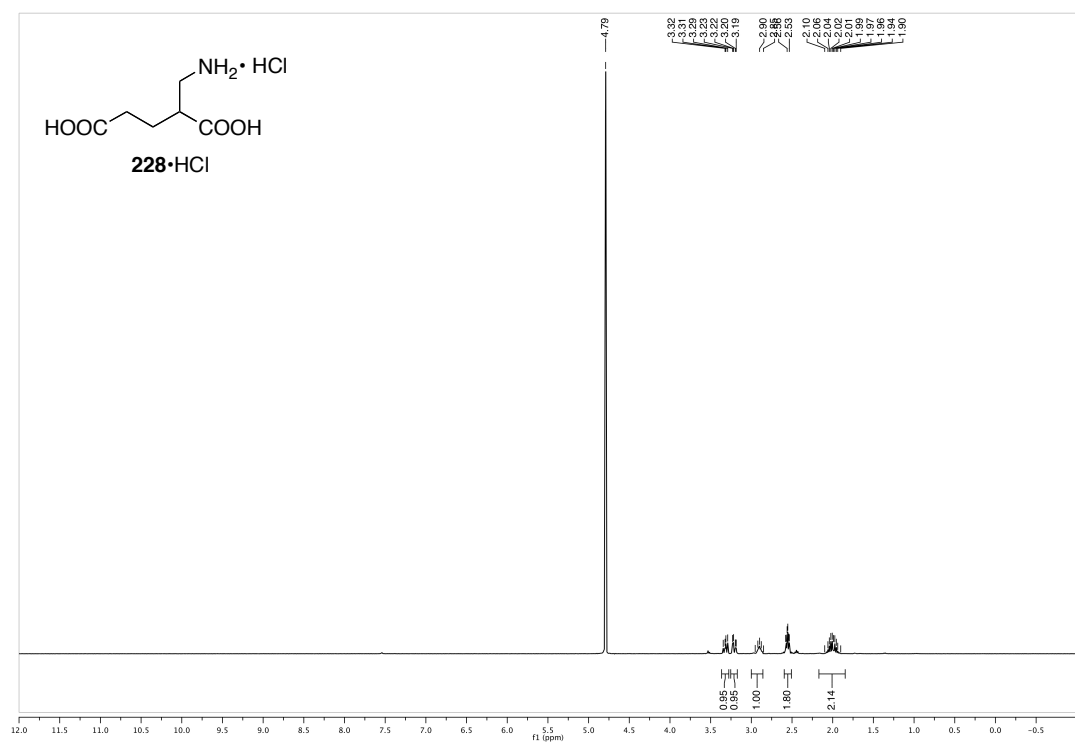
**(2*S*,4*S*)-2-amino-4-(4-oxo-4-(2-oxo-2-(phenylamino)ethylamino)butyl)pentane-dioic acid hydrochloride (TM-1, 200•HCl)**



## 6) Toward an Orthogonal Receptor-Ligand Pair based on iGluRs

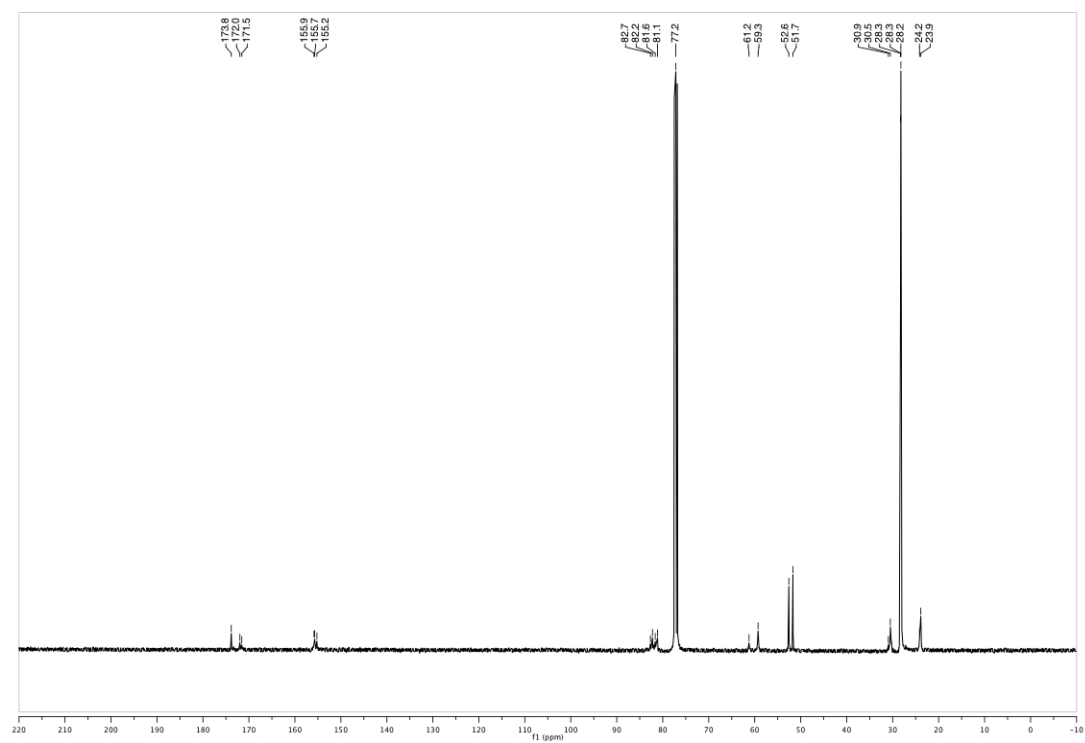
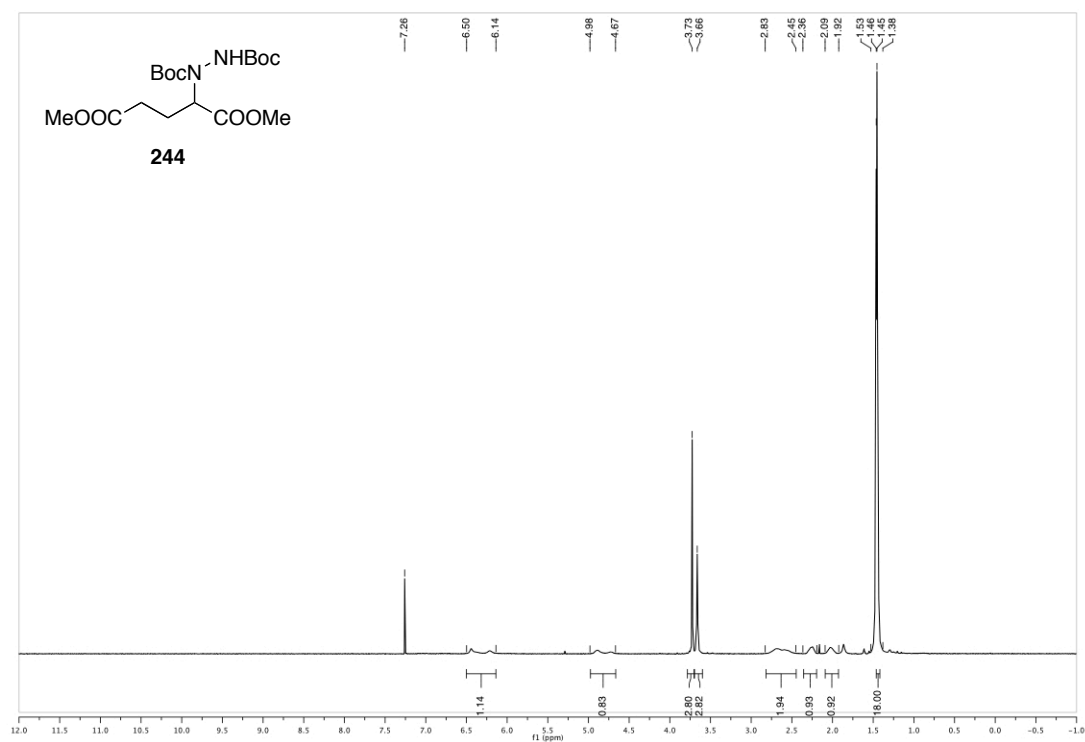
di-*tert*-butyl 2-((dibenzylamino)methyl)pentanedioate (233)

**(*R/S*)-di-*tert*-butyl 2-((benzyl(*R*)-1-phenylethyl)amino)methyl)pentanedioate (235)**

**(*R/S*)-2-(aminomethyl)pentanedioic acid hydrochloride (228•HCl)**

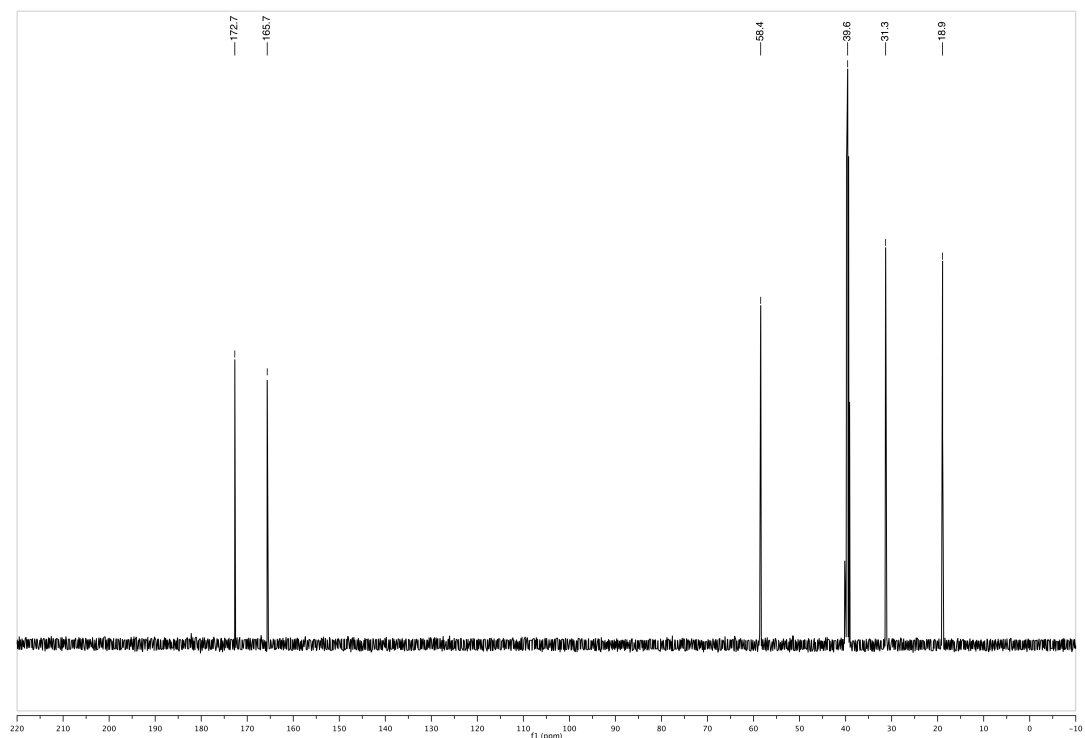
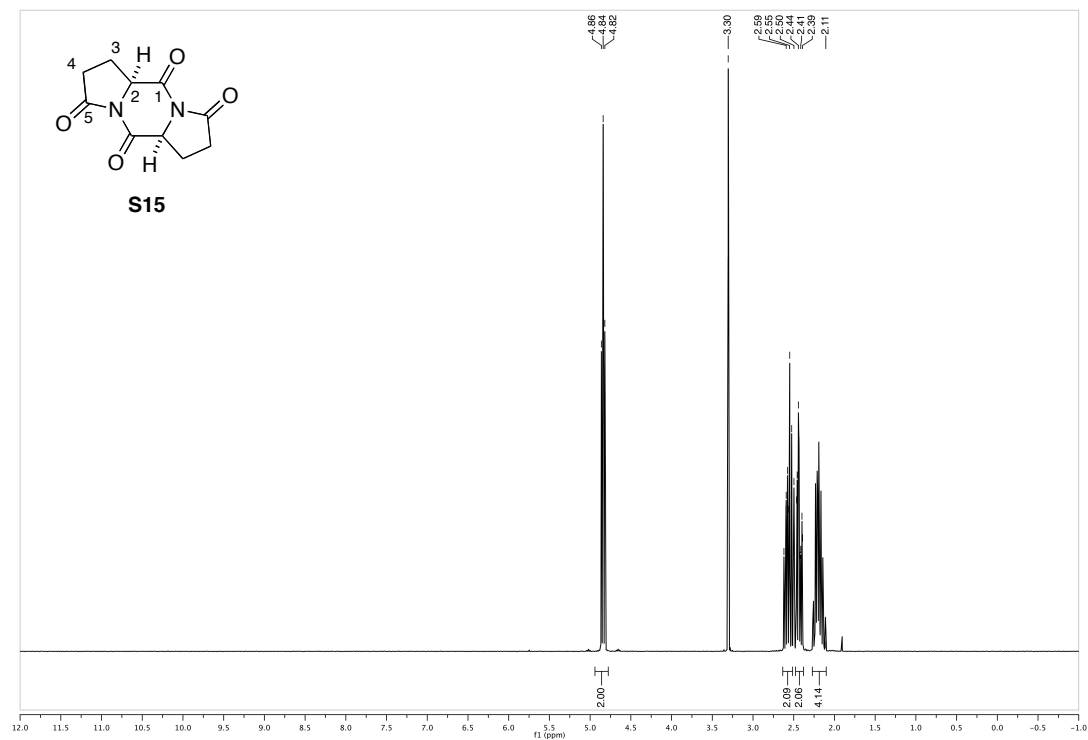


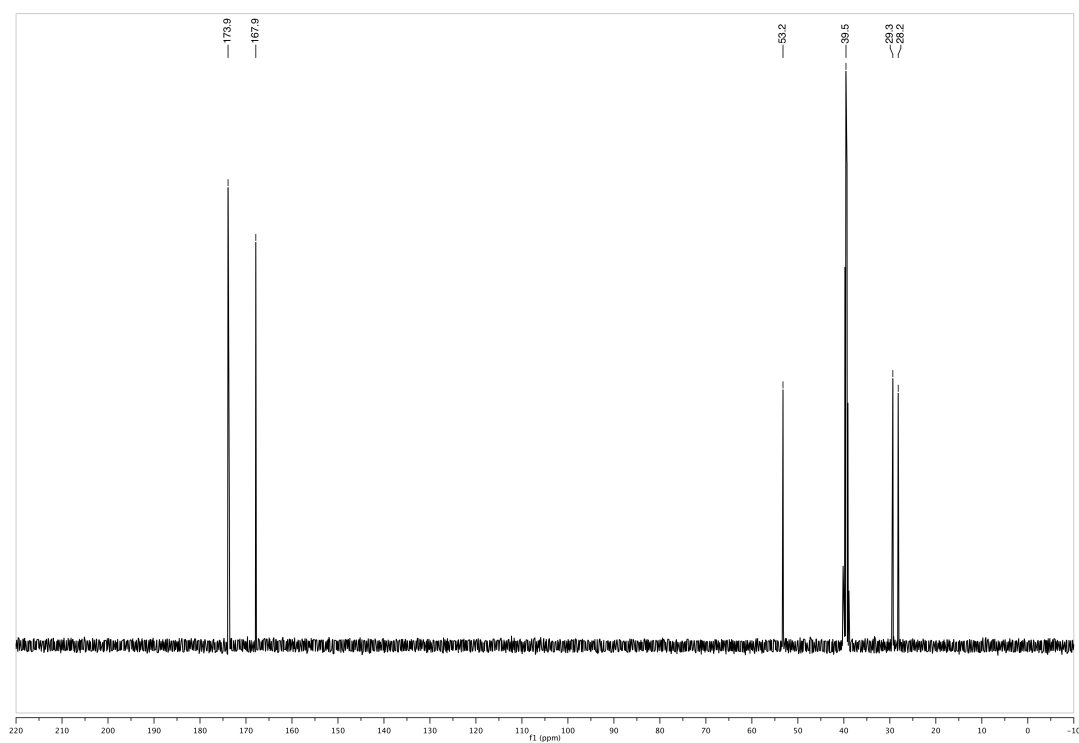
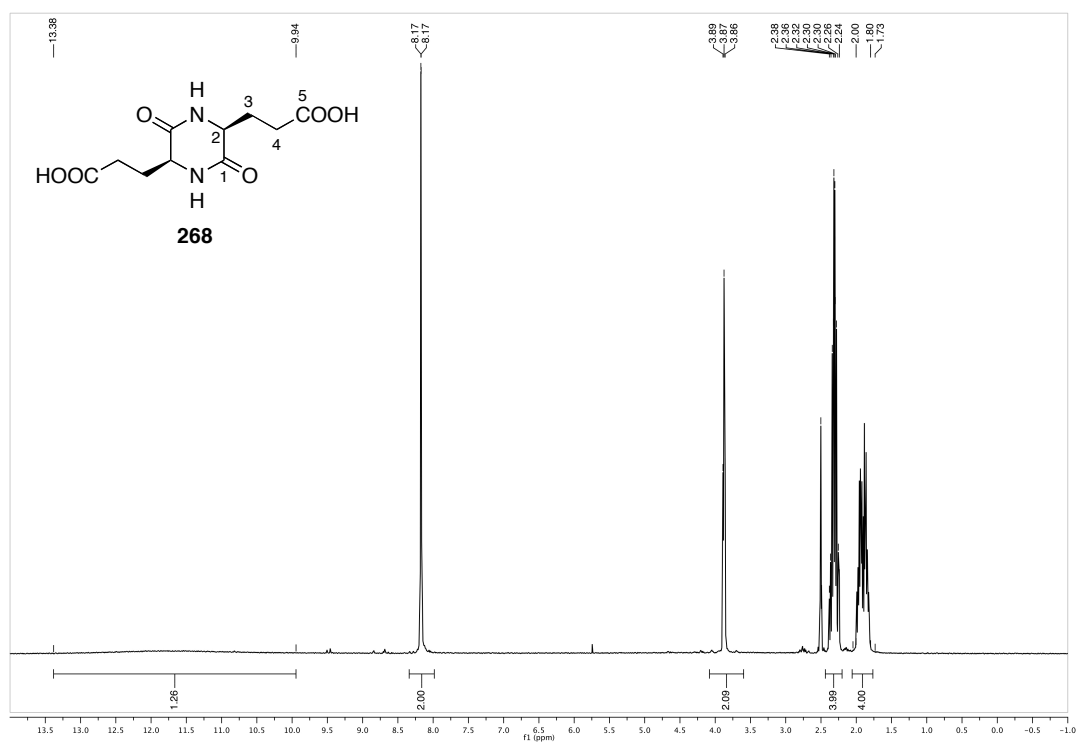
**(*R/S*)-di-*tert*-butyl 1-(1,5-dimethoxy-1,5-dioxopentan-2-yl)hydrazine-1,2-dicarboxylate**  
**(244)**

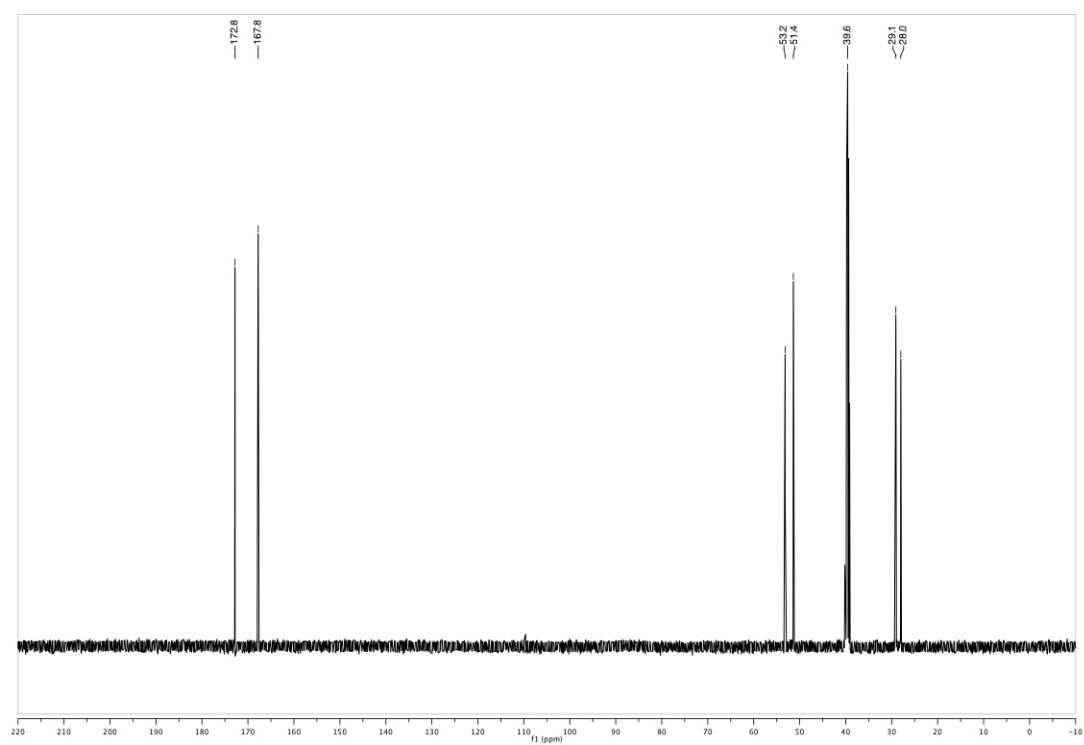
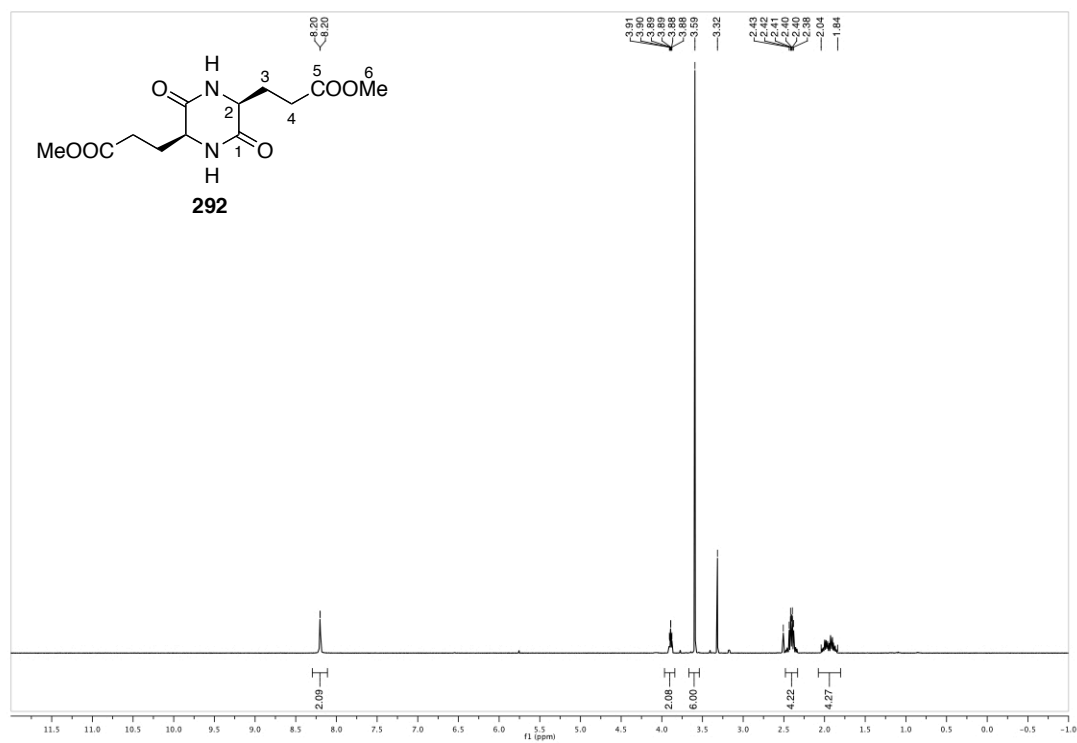


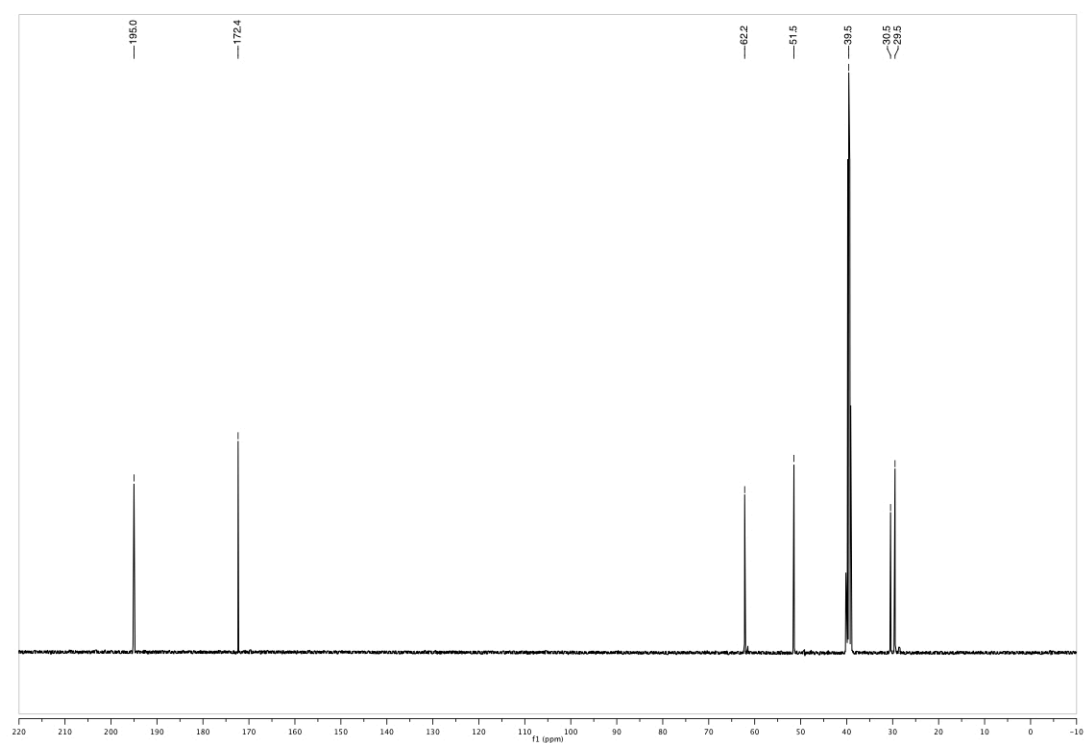
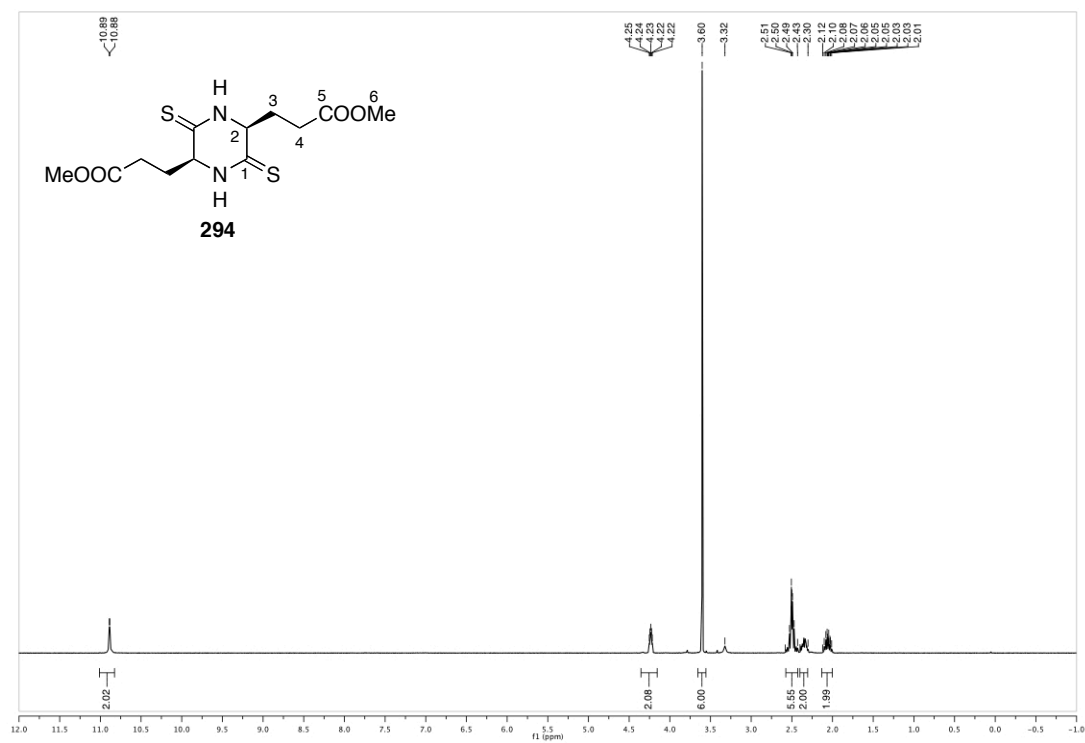
## 7) Toward the Total Synthesis of Herquiline A &amp; B

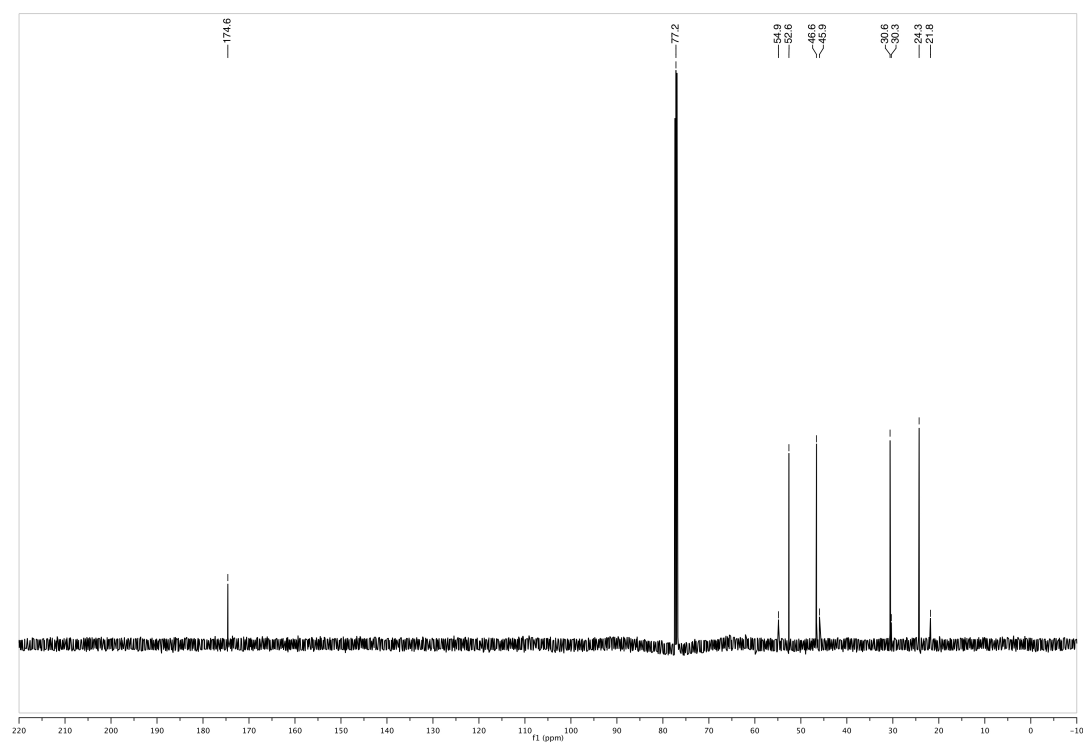
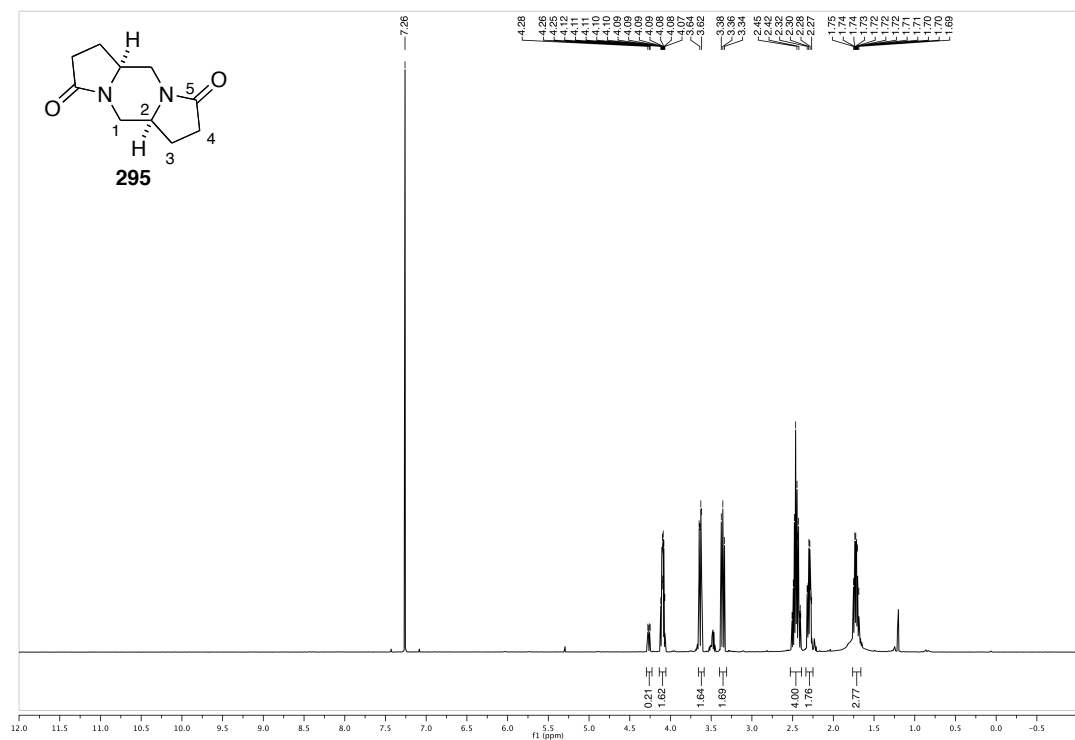
(5a*S*,10a*S*)-tetrahydrodipyrrolo[1,2-*a*:1',2'-*d*]pyrazine-3,5,8,10(5a*H*,10a*H*)-tetraone  
(S15)

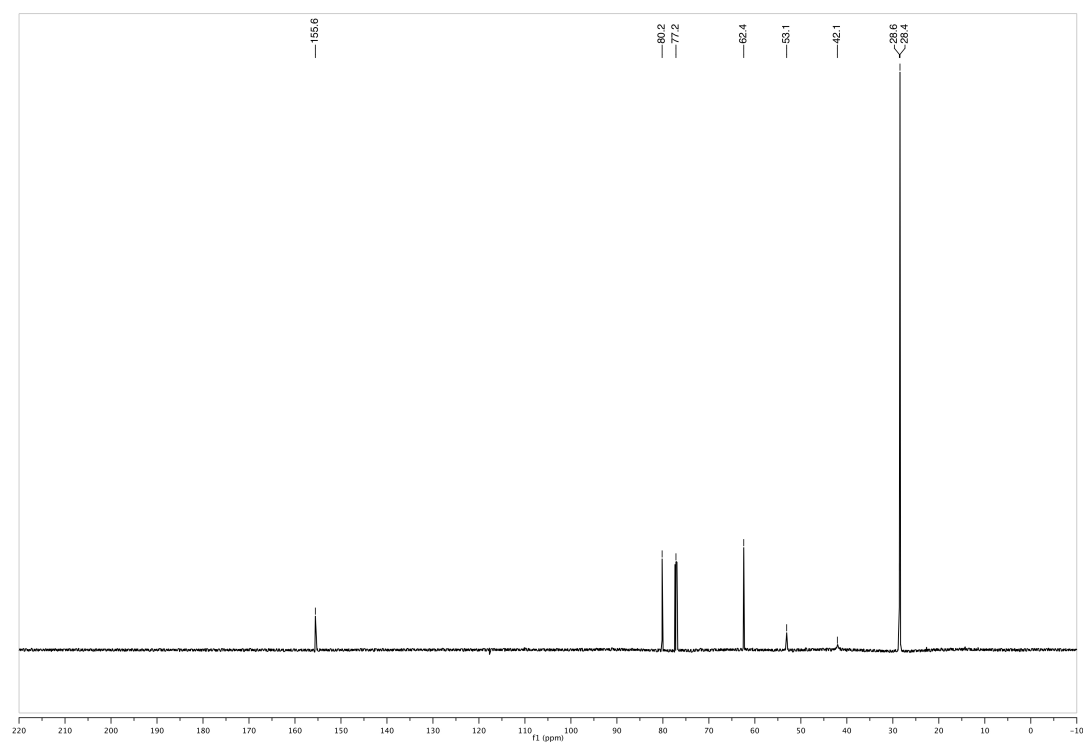
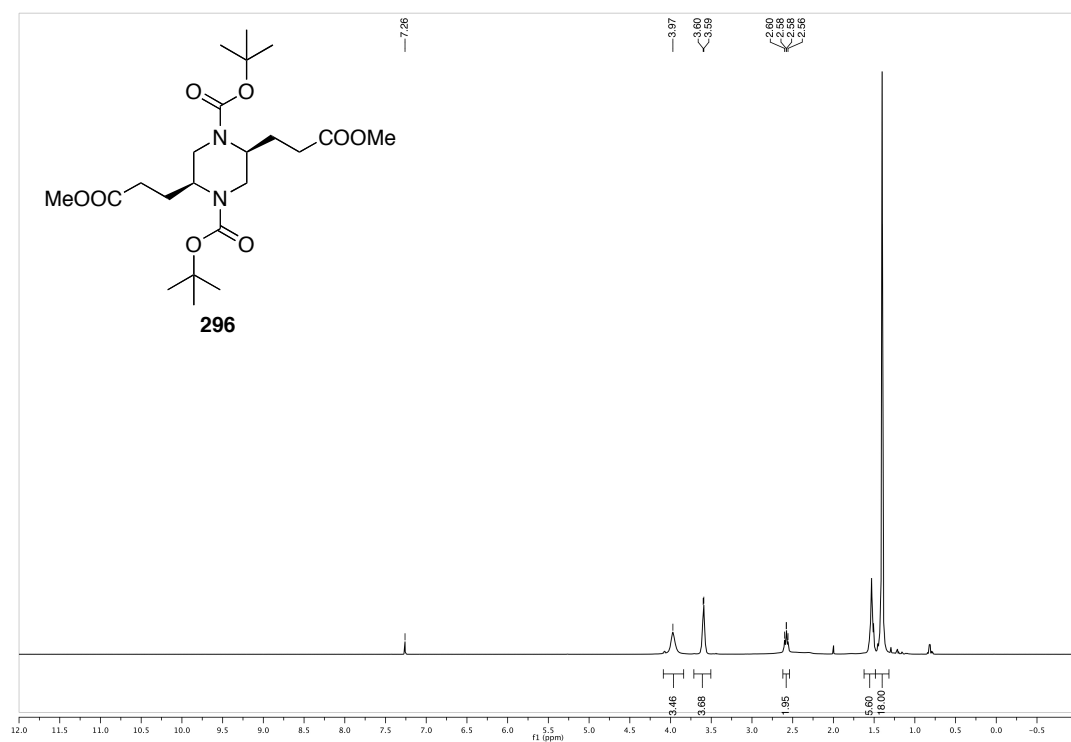


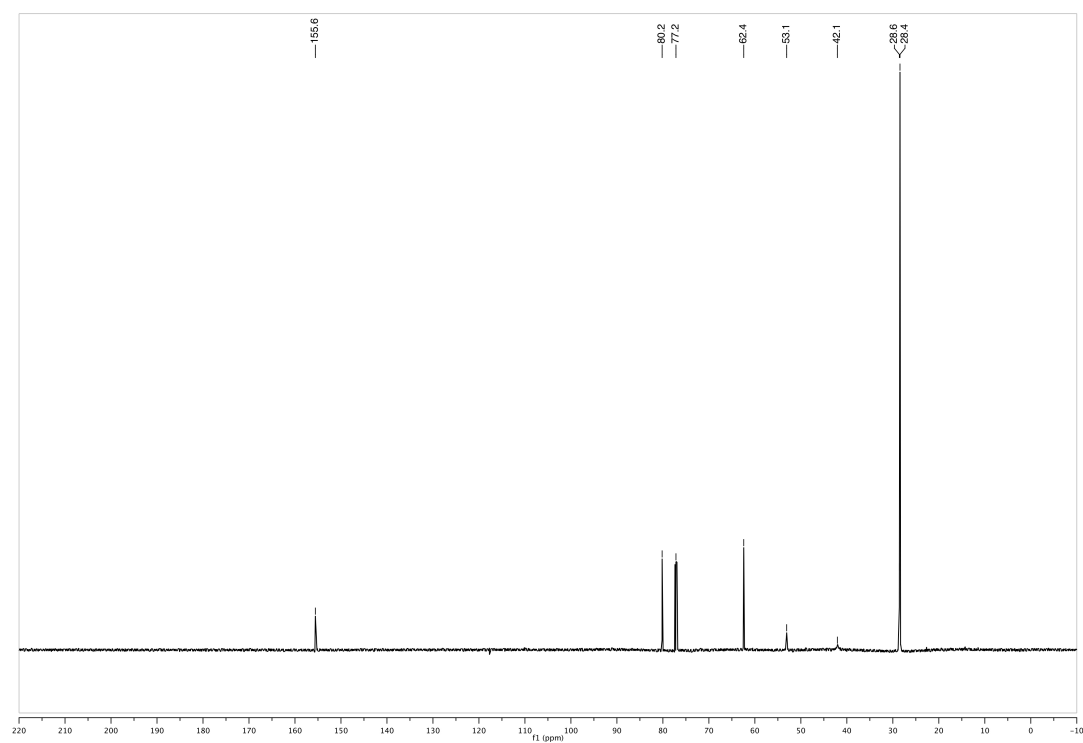
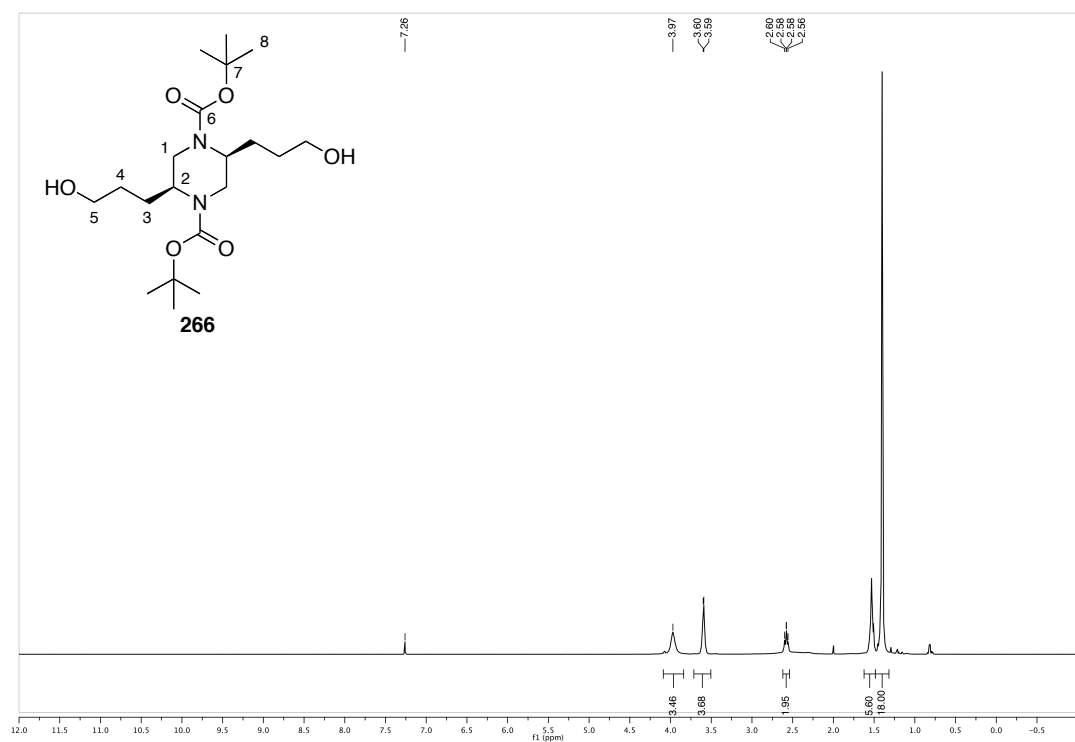
**3,3'-((2*S*,5*S*)-3,6-dioxopiperazine-2,5-diyl)dipropionic acid (268)**

dimethyl 3,3'-((2*S*,5*S*)-3,6-dioxopiperazine-2,5-diyl)dipropanoate (292)

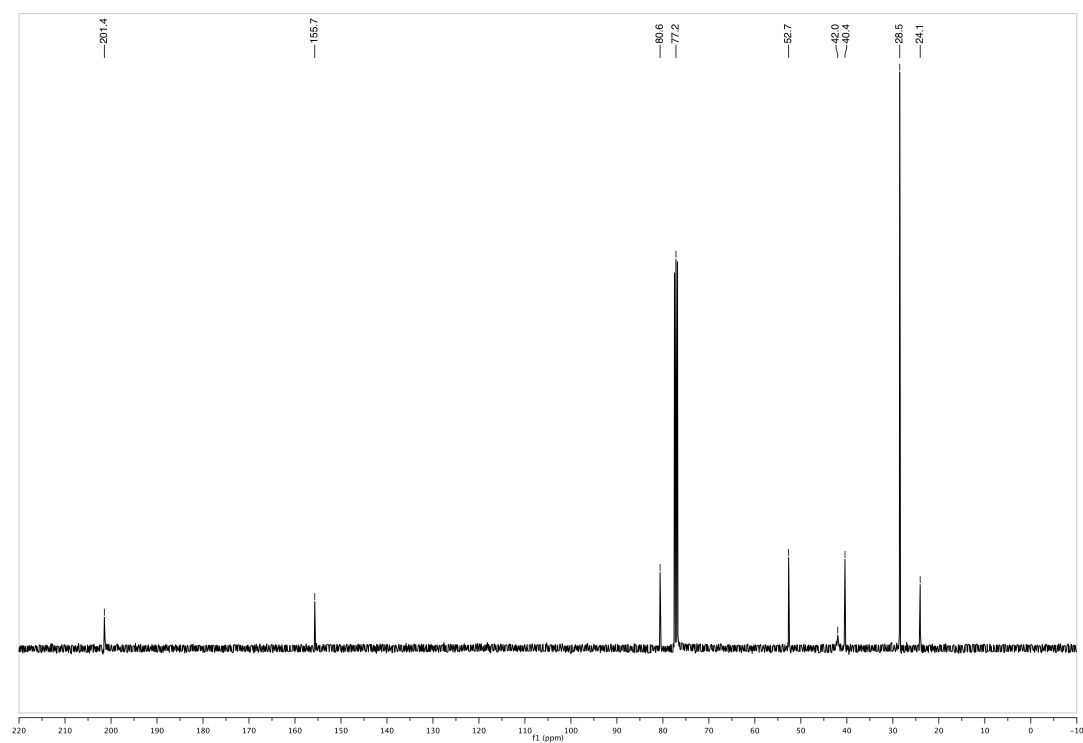
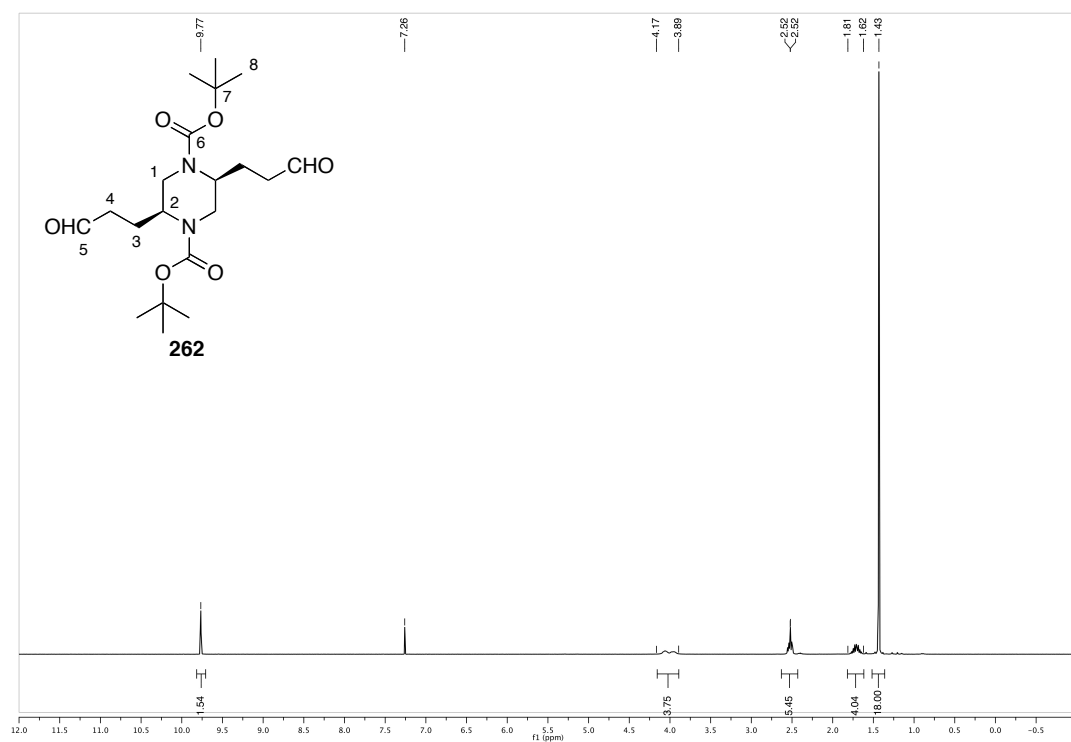
**dimethyl 3,3'-((2*S*,5*S*)-3,6-dithioxopiperazine-2,5-diyl)dipropanoate (294)**

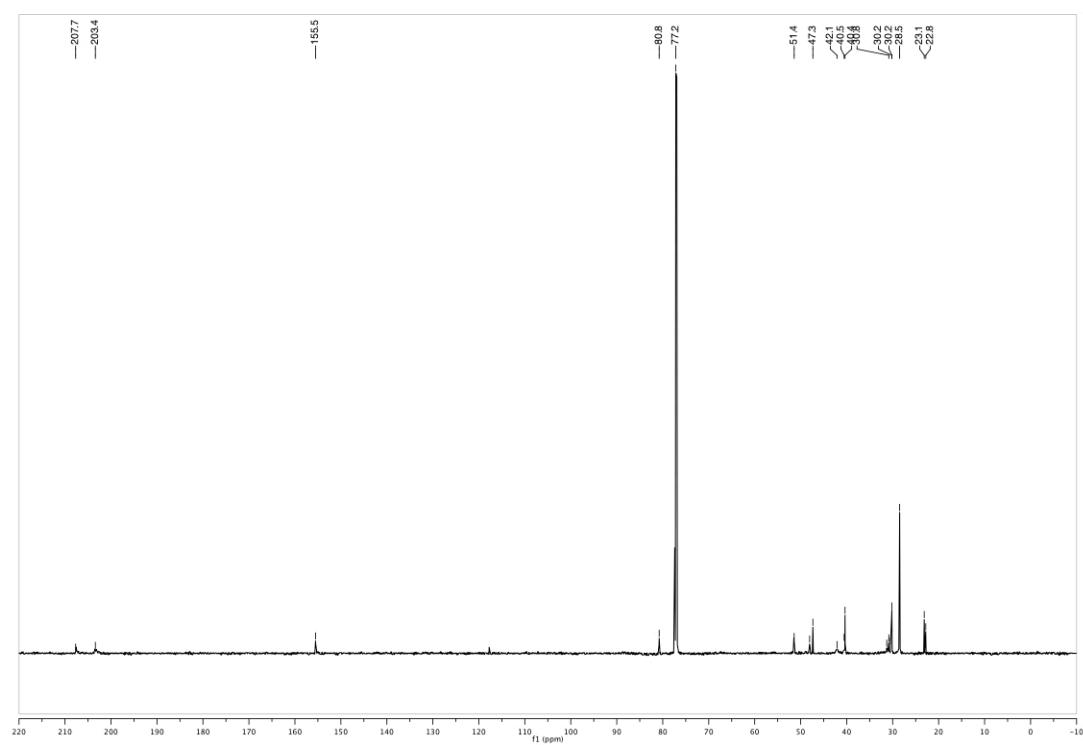
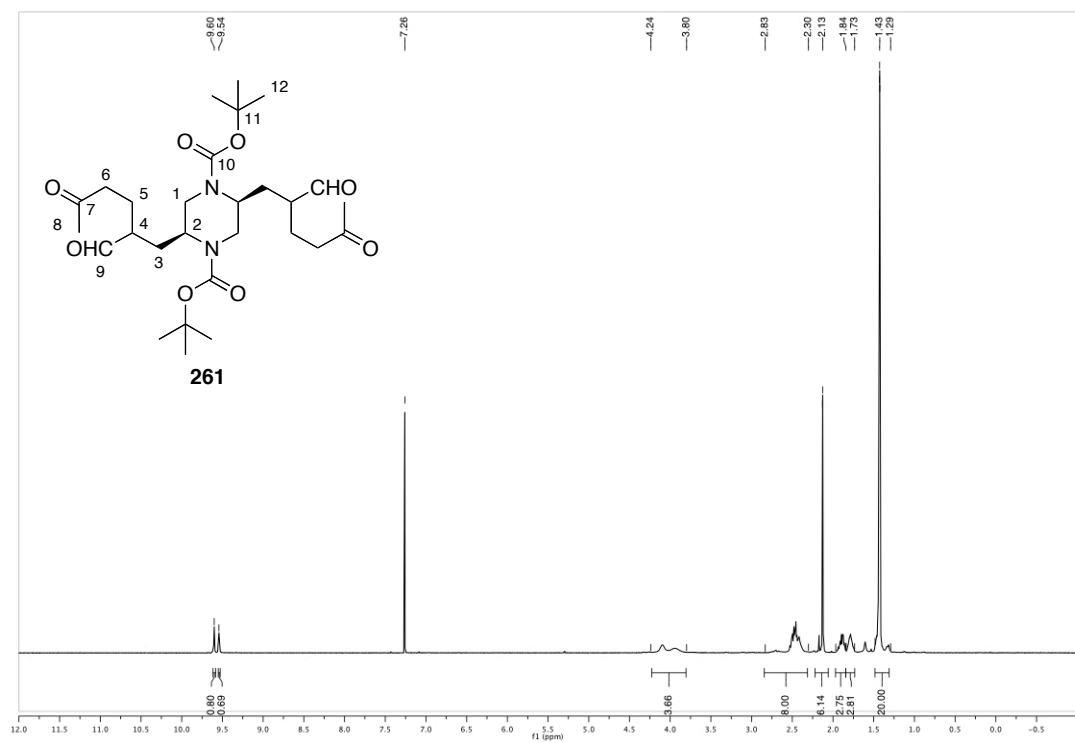
**(5a*S*,10a*S*)-octahydrodipyrrolo[1,2-*a*:1',2'-*d*]pyrazine-3,8-dione (295)**

**(2*S*,5*S*)-di-*tert*-butyl 2,5-bis(3-methoxy-3-oxopropyl)piperazine-1,4-dicarboxylate (296)**

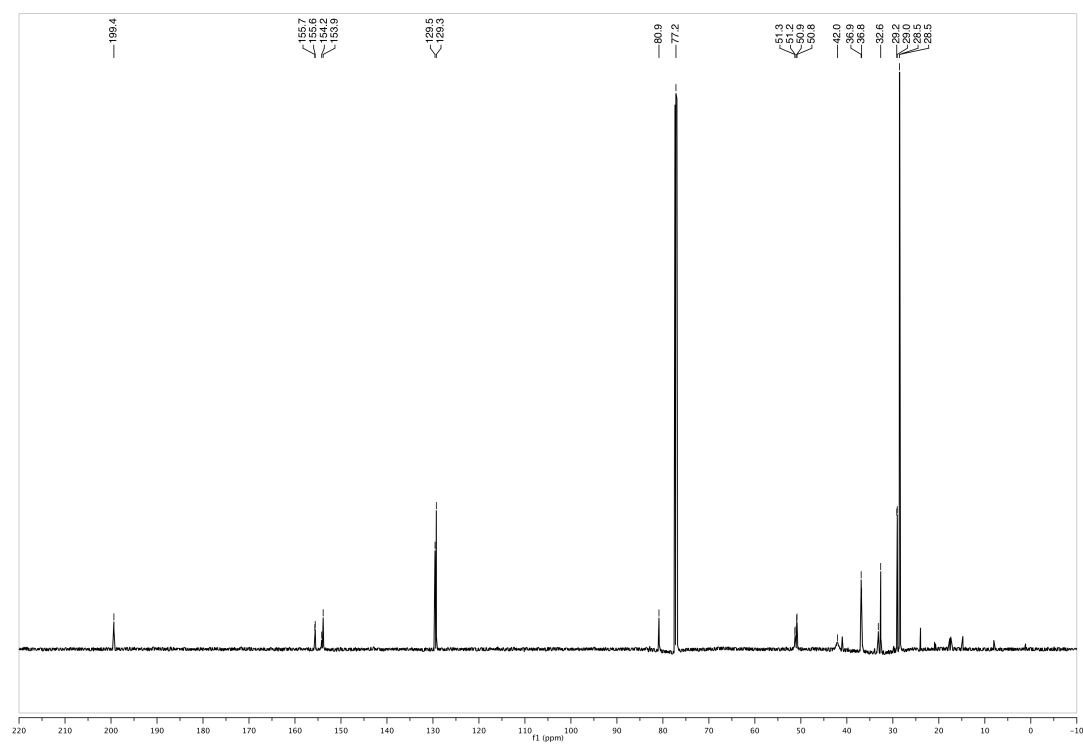
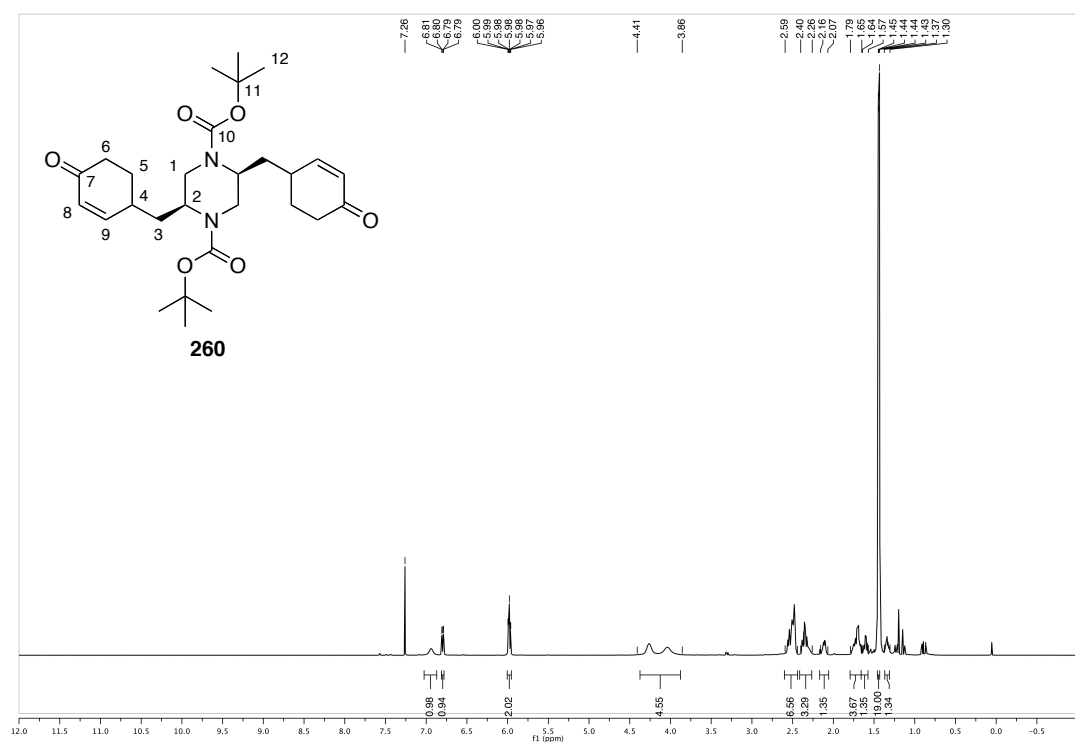
**(2*S*,5*S*)-di-*tert*-butyl 2,5-bis(3-hydroxypropyl)piperazine-1,4-dicarboxylate (266)**



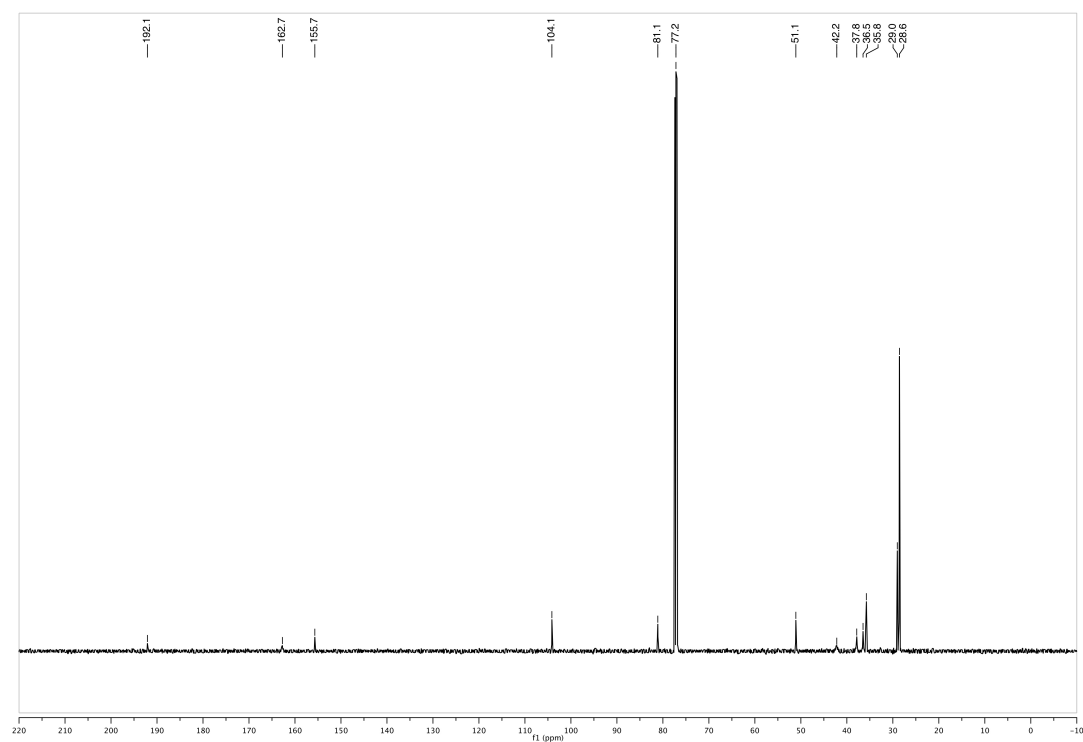
**(2*S*,5*S*)-di-*tert*-butyl 2,5-bis(3-oxopropyl)piperazine-1,4-dicarboxylate (262)**

**(2*S*,5*S*)-di-*tert*-butyl 2,5-bis(2-formyl-5-oxohexyl)piperazine-1,4-dicarboxylate (261)**

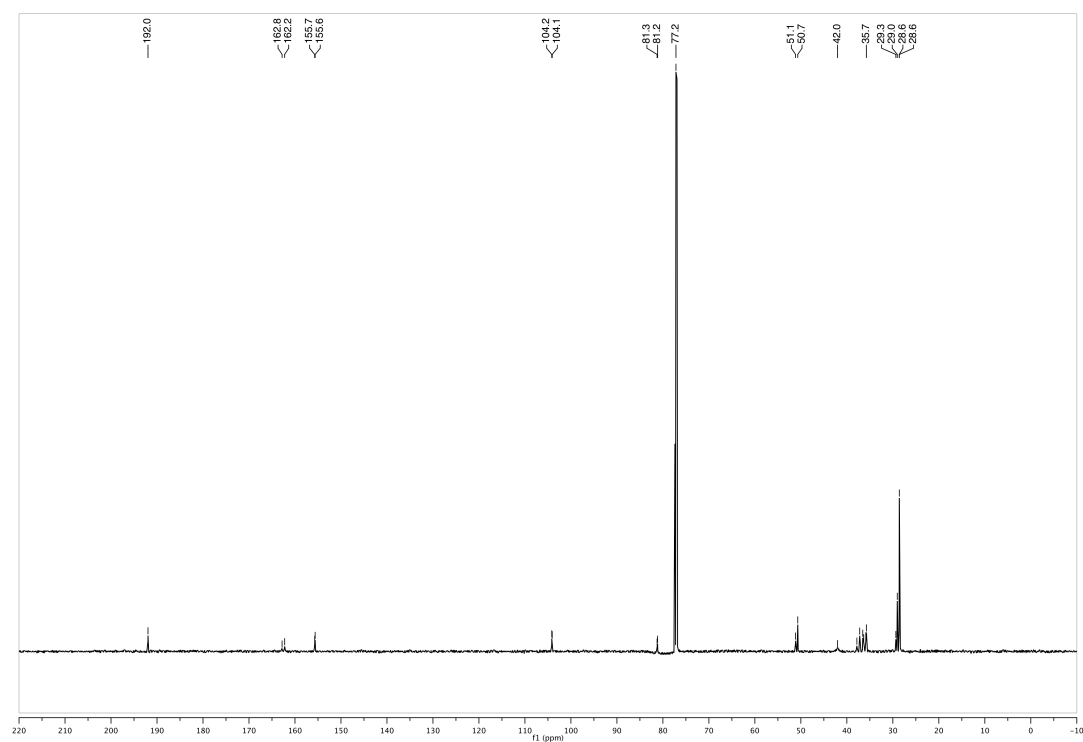
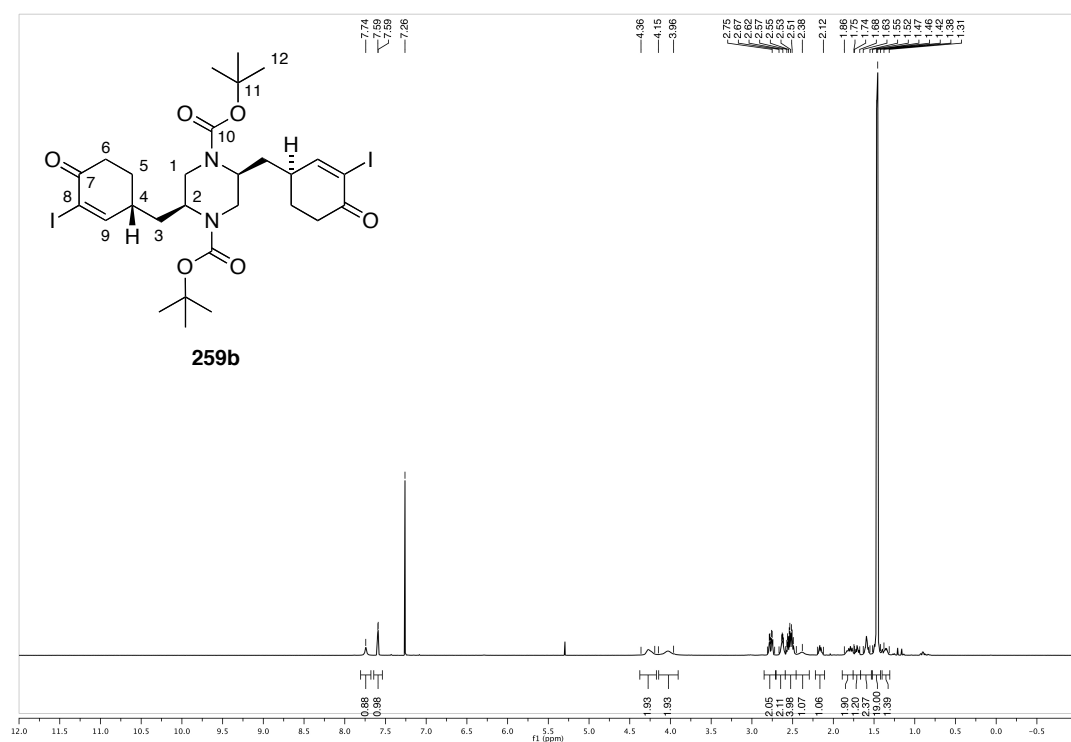
**(2*S*,5*S*)-di-*tert*-butyl 2,5-bis((4-oxocyclohex-2-enyl)methyl)piperazine-1,4-dicarboxylate (260)**



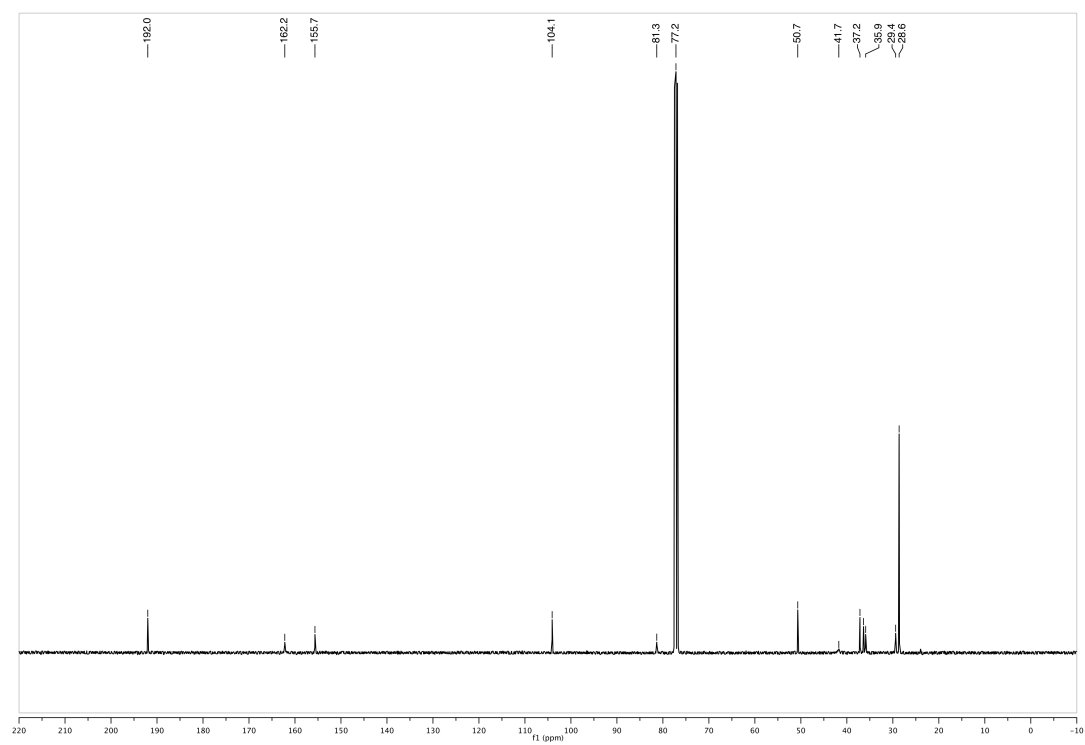
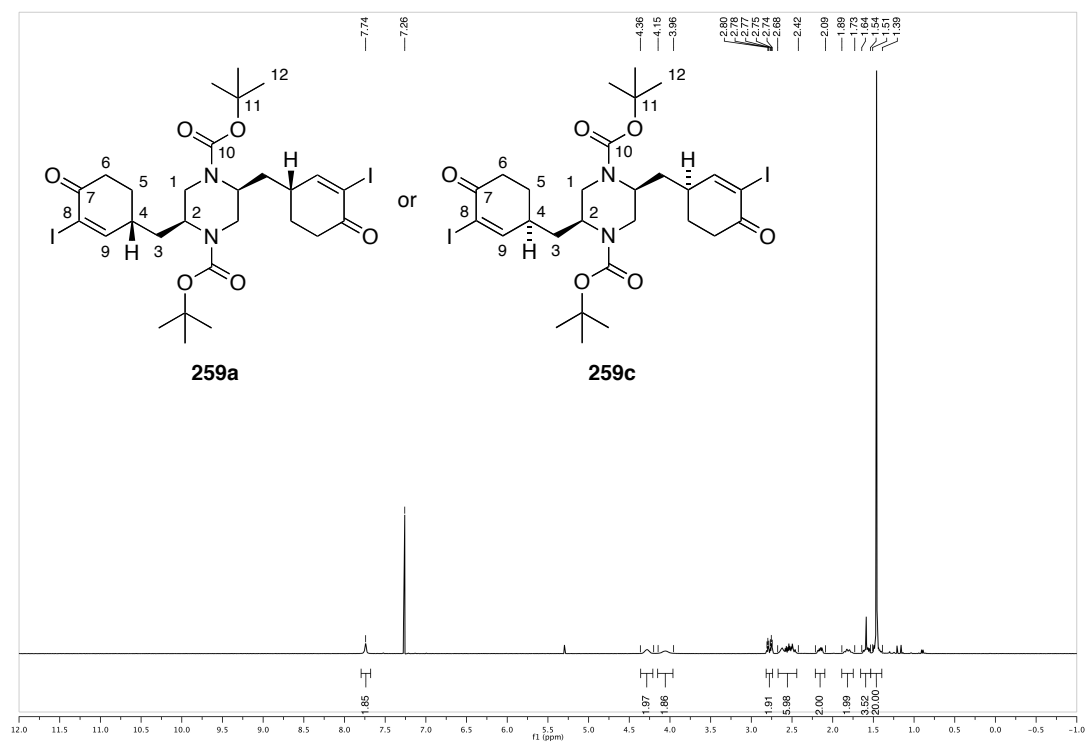
**(2*S*,5*S*)-di-*tert*-butyl 2,5-bis(((*R*)-3-iodo-4-oxocyclohex-2-enyl)methyl)piperazine-1,4-dicarboxylate or (2*S*,5*S*)-di-*tert*-butyl 2,5-bis(((*S*)-3-iodo-4-oxocyclohex-2-enyl)methyl)piperazine-1,4-dicarboxylate (259a or 259c)**



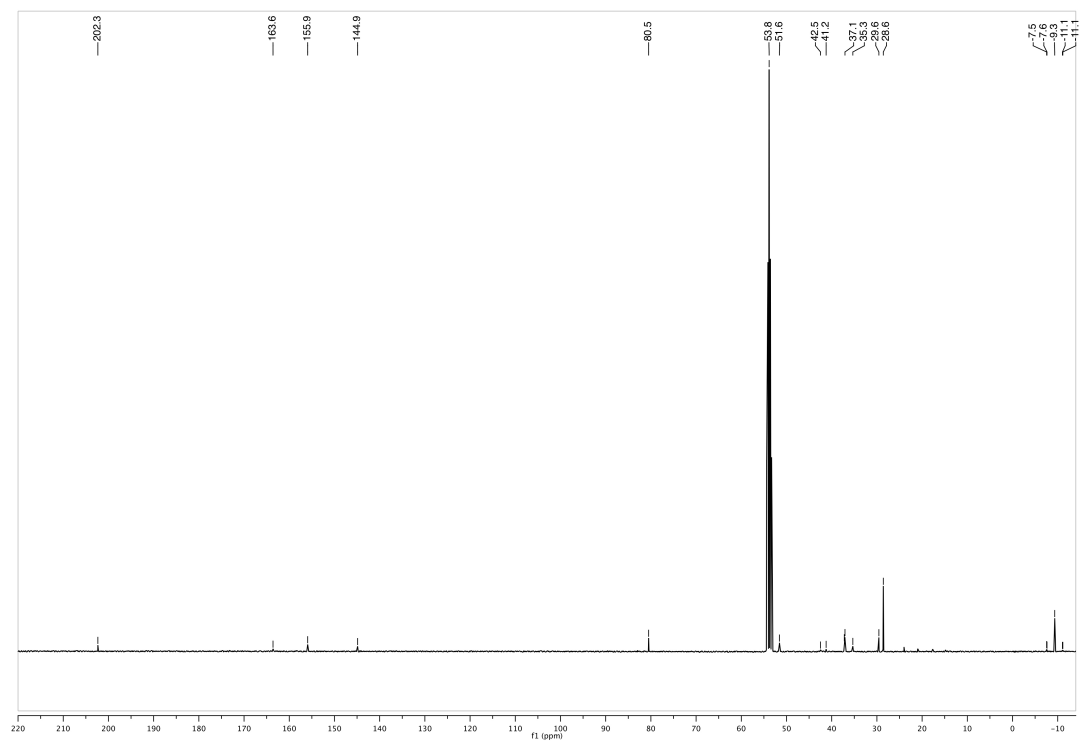
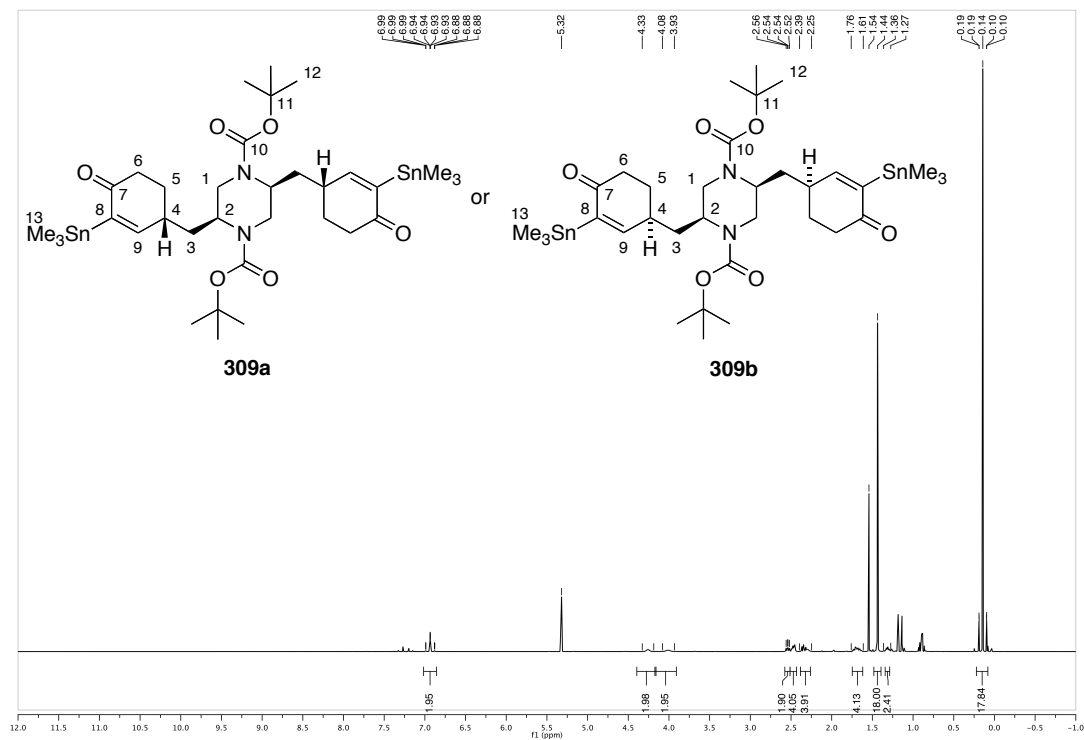
**(2*S*,5*S*)-di-*tert*-butyl 2-(((*R*)-3-iodo-4-oxocyclohex-2-enyl)methyl)-5-(((*S*)-3-iodo-4-oxocyclohex-2-enyl)methyl)piperazine-1,4-dicarboxylate (259b)**



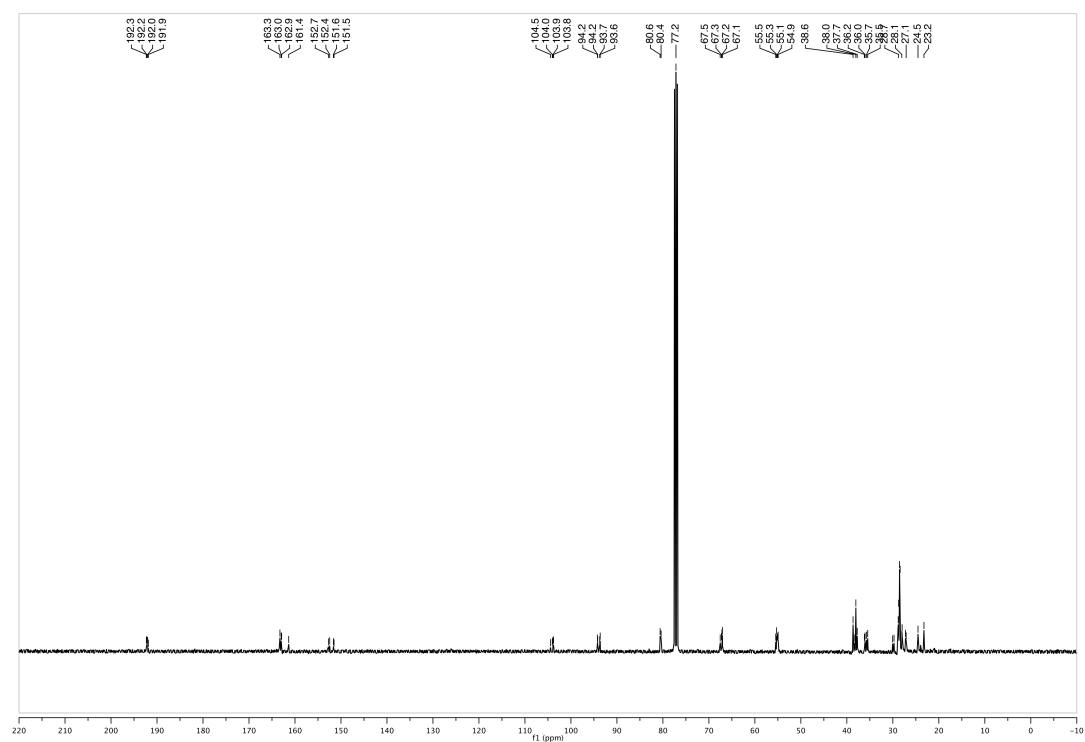
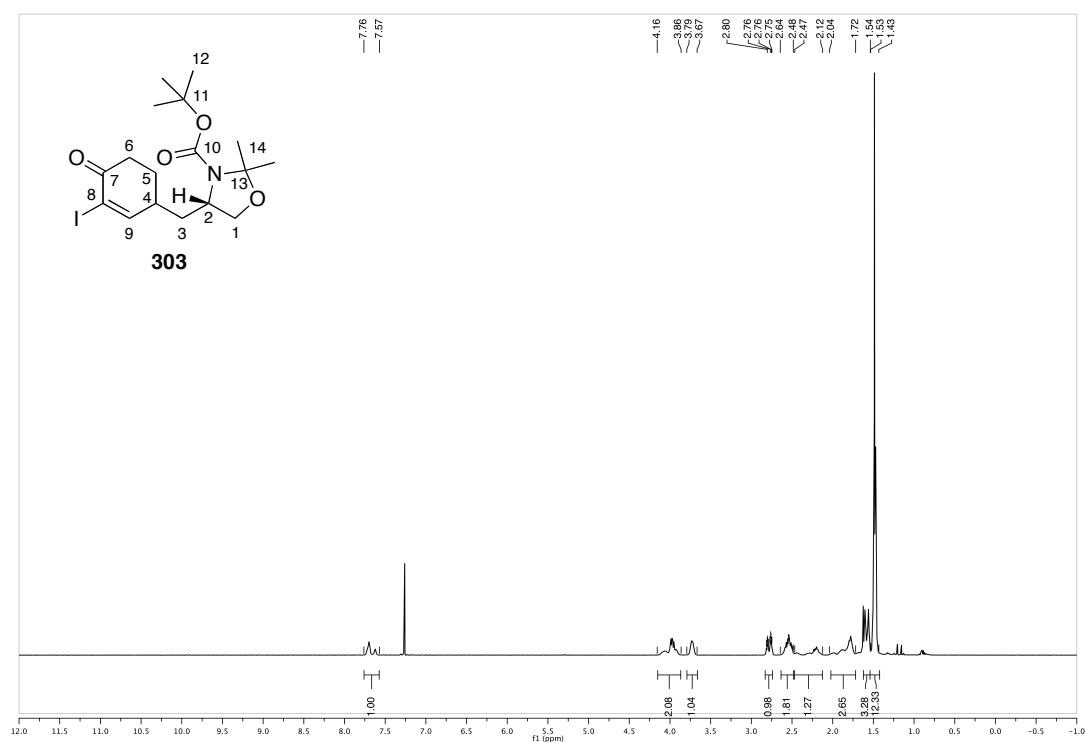
**(2*S*,5*S*)-di-*tert*-butyl 2,5-bis(((*S*)-3-iodo-4-oxocyclohex-2-enyl)methyl) piperazine-1,4-dicarboxylate or (2*S*,5*S*)-di-*tert*-butyl 2,5-bis(((*R*)-3-iodo-4-oxocyclohex-2-enyl)methyl) piperazine-1,4-di-carboxylate (259c or 259a)**



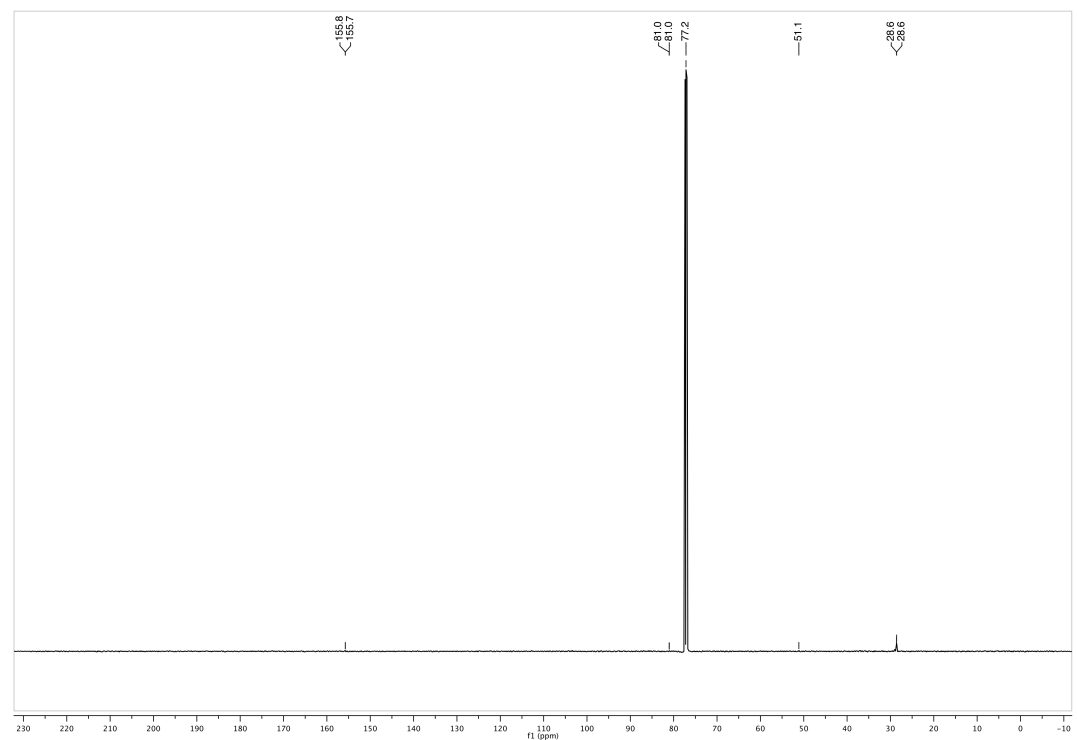
**(2*S*,5*S*)-di-*tert*-butyl 2,5-bis(((*R*)-4-oxo-3-(trimethylstannyl)cyclohex-2-enyl)methyl)piperazine-1,4-dicarboxylate (309a) or (2*S*,5*S*)-di-*tert*-butyl 2,5-bis(((*S*)-4-oxo-3-(trimethylstannyl)cyclohex-2-enyl)methyl)piperazine-1,4-dicarboxylate (309b)**

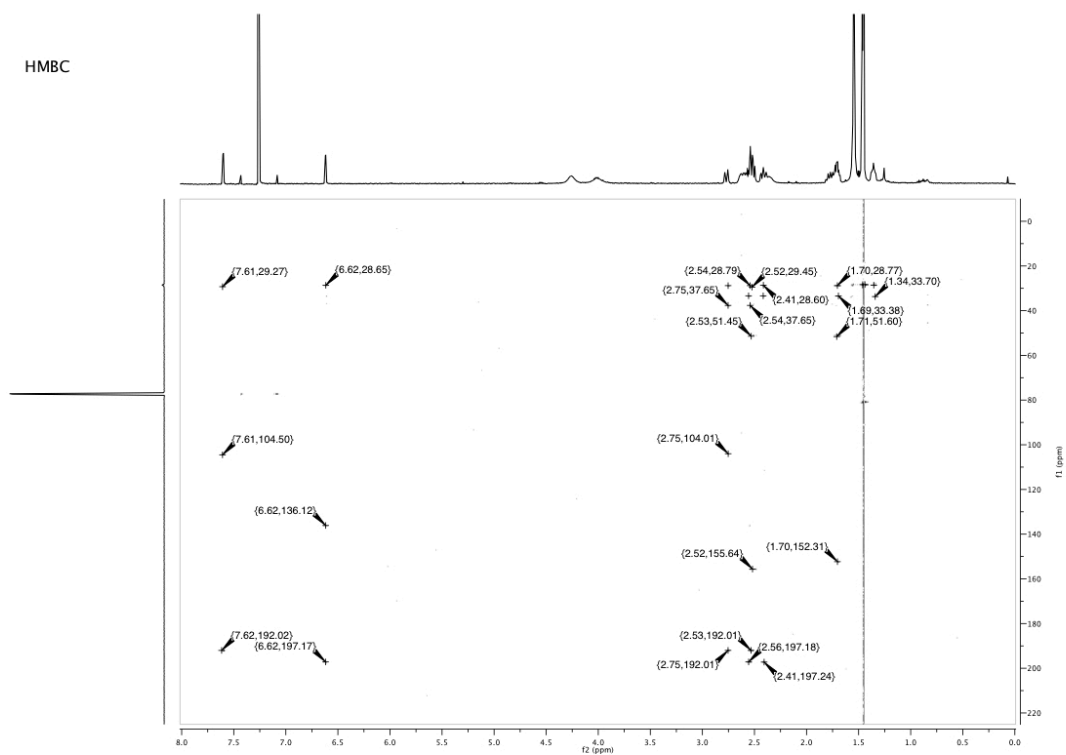
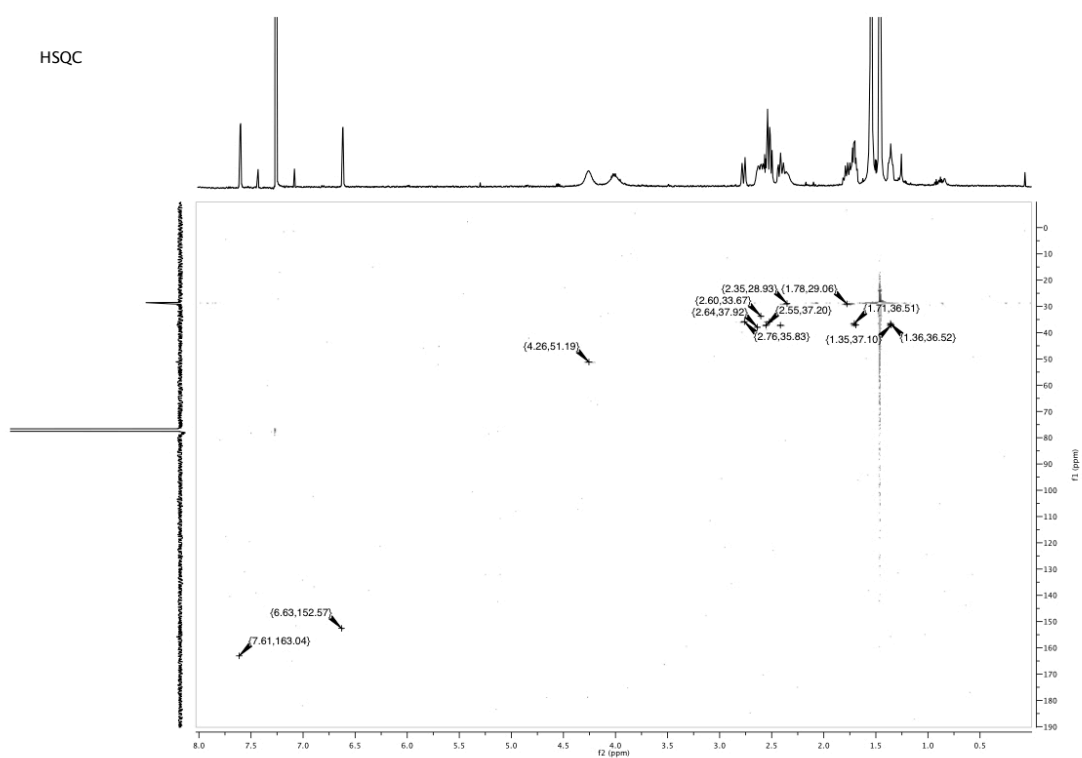


**(S)-tert-butyl 4-(((R/S)-3-iodo-4-oxocyclohex-2-enyl)methyl)-2,2-dimethyloxazolidine-3-carboxylate (303)**

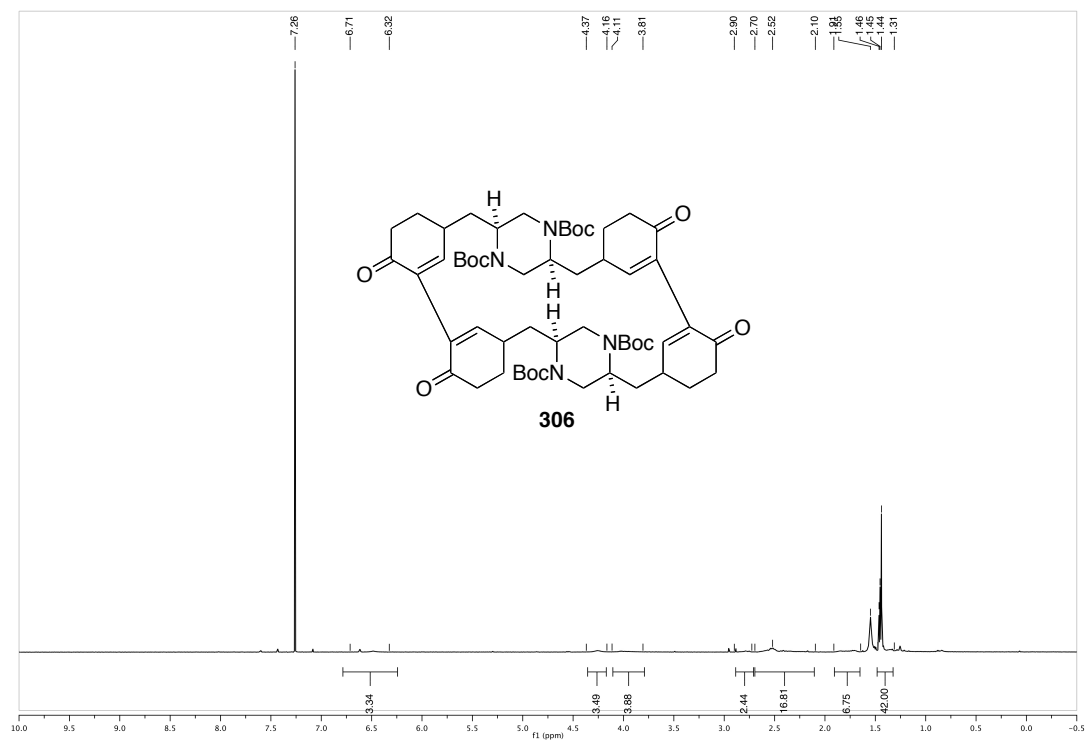








[1,4-di-*tert*-butyl (2*S*,5*S*)-2,5-bis[(3-iodo-4-oxocyclohex-2-en-1-yl)methyl]piperazine-1,4-dicarboxylate; 15,17-di-*tert*-butyl (1*S*,14*S*)-6,9-dioxo-15,17-diazatetracyclo [12.2.2.1<sup>3,7</sup>.1<sup>8,12</sup>]icosa-7(20),8(19)-diene-15,17-dicarboxylate; 15,31,33,37-tetra-*tert*-butyl (1*S*,14*S*,17*S*,30*S*)-6,9,22,25-tetraoxo-15,31,33,37-tetraazaheptacyclo[28.2.2.2<sup>14,17</sup>.1<sup>3,7</sup>.1<sup>8,12</sup>.1<sup>19,23</sup>.1<sup>24,28</sup>]tetraconta-7(40),8(39),23(36),24(35)-tetraene-15,31,33,37-tetracarboxylate]] (306)



## **V. Literature and Notes**

## V. Literature and Notes

- [1] F. A. C. Azevedo, L. R. B. Carvalho, L. T. Grinberg, J. M. Farfel, R. E. L. Ferretti, R. E. P. Leite, W. Jacob, R. Lent, S. Herculano-Houzel, *J. Comp. Neurol.* **2009**, *513*, 532-541.
- [2] S. G. Hormuzdi, M. A. Filippov, G. Mitropoulou, H. Monyer, R. Bruzzone, *Bba-Biomembranes* **2004**, *1662*, 113-137.
- [3] C. Hammond, *Cellular and Molecular Neurophysiology*, Academic Press, **2008**.
- [4] R. P. Seal, S. G. Amara, *Annu. Rev. Pharmacool. Toxicol.* **1999**, *39*, 431-456.
- [5] R. W. Gereau, G. Swanson, *The glutamate receptors*, Humana Press, Totowa, NJ, **2008**.
- [6] a) O. Yizhar, L. E. Fenno, T. J. Davidson, M. Mogri, K. Deisseroth, *Neuron* **2011**, *71*, 9-34; b) R. D. Airan, K. R. Thompson, L. E. Fenno, H. Bernstein, K. Deisseroth, *Nature* **2009**, *458*, 1025-1029.
- [7] T. Fehrentz, M. Schönberger, D. Trauner, *Angew. Chem. Int. Ed.* **2011**, *50*, 12156-12182.
- [8] P. Stawski, H. Janovjak, D. Trauner, *Biorg. Med. Chem.* **2010**, *18*, 7759-7772.
- [9] S. F. Traynelis, L. P. Wollmuth, C. J. McBain, F. S. Menniti, K. M. Vance, K. K. Ogden, K. B. Hansen, H. Yuan, S. J. Myers, R. Dingledine, D. Sibley, *Pharmacol. Rev.* **2010**, *62*, 405-496.
- [10] a) D. R. Madden, *Nat. Rev. Neurosci.* **2002**, *3*, 91-101; b) E. Gouaux, *J Physiol* **2004**, *554*, 249-253; c) G. T. Swanson, R. Sakai, *Prog. Mol. Subcell. Biol.* **2009**, *46*, 123-157.
- [11] M. L. Mayer, N. Armstrong, *Annu. Rev. Physiol.* **2004**, *66*, 161-181.
- [12] A. I. Sobolevsky, M. P. Rosconi, E. Gouaux, *Nature* **2009**, *462*, 745-756.
- [13] P. E. Chen, D. J. Wyllie, *Br. J. Pharmacol.* **2006**, *147*, 839-853.
- [14] H. M. Berman, J. Westbrook, Z. Feng, G. Gilliland, T. N. Bhat, H. Weissig, I. N. Shindyalov, P. E. Bourne, *Nucleic. Acids. Res.* **2000**, *28*, 235-242.
- [15] M. L. Mayer, R. Olson, E. Gouaux, *J. Mol. Biol.* **2001**, *311*, 815-836.
- [16] J. H. Lee, G. B. Kang, H. H. Lim, K. S. Jin, S. H. Kim, M. Ree, C. S. Park, S. J. Kim, S. H. Eom, *J. Mol. Biol.* **2008**, *376*, 308-316.
- [17] N. Armstrong, E. Gouaux, *Neuron* **2000**, *28*, 165-181.
- [18] R. Jin, E. Gouaux, *Biochemistry* **2003**, *42*, 5201-5213.
- [19] Y. Sun, R. Olson, M. Horning, N. Armstrong, M. Mayer, E. Gouaux, *Nature* **2002**, *417*, 245-253.

- [20] A. Hogner, J. S. Kastrup, R. Jin, T. Liljefors, M. L. Mayer, J. Egebjerg, I. K. Larsen, E. Gouaux, *J. Mol. Biol.* **2002**, 322, 93-109.
- [21] R. Jin, M. Horning, M. L. Mayer, E. Gouaux, *Biochemistry* **2002**, 41, 15635-15643.
- [22] C. Kasper, M. L. Lunn, T. Liljefors, E. Gouaux, J. Egebjerg, J. S. Kastrup, *FEBS Lett.* **2002**, 531, 173-178.
- [23] R. Jin, T. G. Banke, M. L. Mayer, S. F. Traynelis, E. Gouaux, *Nat. Neurosci.* **2003**, 6, 803-810.
- [24] A. Hogner, J. R. Greenwood, T. Liljefors, M. L. Lunn, J. Egebjerg, I. K. Larsen, E. Gouaux, J. S. Kastrup, *J. Med. Chem.* **2003**, 46, 214-221.
- [25] M. L. Lunn, A. Hogner, T. B. Stensbol, E. Gouaux, J. Egebjerg, J. S. Kastrup, *J. Med. Chem.* **2003**, 46, 872-875.
- [26] N. Armstrong, M. Mayer, E. Gouaux, *Proc. Natl. Acad. Sci. U.S.A.* **2003**, 100, 5736-5741.
- [27] A. Frandsen, D. S. Pickering, B. Vestergaard, C. Kasper, B. B. Nielsen, J. R. Greenwood, G. Campiani, C. Fattorusso, M. Gajhede, A. Schousboe, J. S. Kastrup, *Mol. Pharmacol.* **2005**, 67, 703-713.
- [28] B. B. Nielsen, D. S. Pickering, J. R. Greenwood, L. Brehm, M. Gajhede, A. Schousboe, J. S. Kastrup, *FEBS J.* **2005**, 272, 1639-1648.
- [29] R. Jin, S. Clark, A. M. Weeks, J. T. Dudman, E. Gouaux, K. M. Partin, *J. Neurosci.* **2005**, 25, 9027-9036.
- [30] M. M. Holm, P. Naur, B. Vestergaard, M. T. Geballe, M. Gajhede, J. S. Kastrup, S. F. Traynelis, J. Egebjerg, *J. Biol. Chem.* **2005**, 280, 35469-35476.
- [31] M. C. Weston, C. Gertler, M. L. Mayer, C. Rosenmund, *J. Neurosci.* **2006**, 26, 7650-7658.
- [32] N. Armstrong, J. Jasti, M. Beich-Frandsen, E. Gouaux, *Cell* **2006**, 127, 85-97.
- [33] S. B. Vogensen, K. Frydenvang, J. R. Greenwood, G. Postorino, B. Nielsen, D. S. Pickering, B. Ebert, U. Bolcho, J. Egebjerg, M. Gajhede, J. S. Kastrup, T. N. Johansen, R. P. Clausen, P. Krosgaard-Larsen, *J. Med. Chem.* **2007**, 50, 2408-2414.
- [34] I. H. Greger, P. Akamine, L. Khatri, E. B. Ziff, *Neuron* **2006**, 51, 85-97.
- [35] W. Zhang, Y. Cho, E. Lolis, J. R. Howe, *J. Neurosci.* **2008**, 28, 932-943.
- [36] M. Beich-Frandsen, D. S. Pickering, O. Mirza, T. N. Johansen, J. Greenwood, B. Vestergaard, A. Schousboe, M. Gajhede, T. Liljefors, J. S. Kastrup, *J. Med. Chem.* **2008**, 51, 1459-1463.

- [37] A. H. Ahmed, M. D. Thompson, M. K. Fenwick, B. Romero, A. P. Loh, D. E. Jane, H. Sonderrmann, R. E. Oswald, *Biochemistry* **2009**, *48*, 3894-3903.
- [38] A. H. Ahmed, R. E. Oswald, *J. Med. Chem.* **2010**, *53*, 2197-2203.
- [39] C. Kasper, D. S. Pickering, O. Mirza, L. Olsen, A. S. Kristensen, J. R. Greenwood, T. Liljefors, A. Schousboe, F. Watjen, M. Gajhede, B. W. Sigurskjold, J. S. Kastrup, *J. Mol. Biol.* **2006**, *357*, 1184-1201.
- [40] S. E. Ward, M. Harries, L. Aldegheri, D. Andreotti, S. Ballantine, B. D. Bax, A. J. Harris, A. J. Harker, J. Lund, R. Melarange, A. Mingardi, C. Mookherjee, J. Mosley, M. Neve, B. Oliosi, R. Profeta, K. J. Smith, P. W. Smith, S. Spada, K. M. Thewlis, S. P. Yusaf, *J. Med. Chem.* **2010**, *53*, 5801-5812.
- [41] B. H. Kaae, K. Harpsøe, J. S. Kastrup, A. C. Sanz, D. S. Pickering, B. Metzler, R. P. Clausen, M. Gajhede, P. Sauerberg, T. Liljefors, U. Madsen, *Chem. Biol.* **2007**, *14*, 1294-1303.
- [42] H. Hald, P. K. Ahring, D. B. Timmermann, T. Liljefors, M. Gajhede, J. S. Kastrup, *J. Mol. Biol.* **2009**, *391*, 906-917.
- [43] C. P. Ptak, A. H. Ahmed, R. E. Oswald, *Biochemistry* **2009**, *48*, 8594-8602.
- [44] K. Menuz, R. M. Stroud, R. A. Nicoll, F. A. Hays, *Science* **2007**, *318*, 815-817.
- [45] L. A. Cruz, E. Estebanez-Perpina, S. Pfaff, S. Borngraeber, N. Bao, J. Blethrow, R. J. Fletterick, P. M. England, *J. Med. Chem.* **2008**, *51*, 5856-5860.
- [46] A. H. Ahmed, Q. Wang, H. Sonderrmann, R. E. Oswald, *Proteins* **2009**, *75*, 628-637.
- [47] A. H. Ahmed, C. P. Ptak, R. E. Oswald, *Biochemistry* **2010**, *49*, 2843-2850.
- [48] A. Gill, A. Birdsey-Benson, B. L. Jones, L. P. Henderson, D. R. Madden, *Biochemistry* **2008**, *47*, 13831-13841.
- [49] C. Kasper, K. Frydenvang, P. Naur, M. Gajhede, D. S. Pickering, J. S. Kastrup, *FEBS Lett.* **2008**, *582*, 4089-4094.
- [50] A. Birdsey-Benson, A. Gill, L. P. Henderson, D. R. Madden, *J. Neurosci.* **2010**, *30*, 1463-1470.
- [51] A. J. Plested, R. Vijayan, P. C. Biggin, M. L. Mayer, *Neuron* **2008**, *58*, 720-735.
- [52] M. L. Mayer, A. Ghosal, N. P. Dolman, D. E. Jane, *J. Neurosci.* **2006**, *26*, 2852-2861.
- [53] P. Naur, B. Vestergaard, L. K. Skov, J. Egebjerg, M. Gajhede, J. S. Kastrup, *FEBS Lett.* **2005**, *579*, 1154-1160.
- [54] H. Hald, P. Naur, D. S. Pickering, D. Sprogø, U. Madsen, D. B. Timmermann, P. K. Ahring, T. Liljefors, A. Schousboe, J. Egebjerg, M. Gajhede, J. S. Kastrup, *J. Biol. Chem.* **2007**, *282*, 25726-25736.

- [55] R. P. Clausen, P. Naur, A. S. Kristensen, J. R. Greenwood, M. Strange, H. Brauner-Osborne, A. A. Jensen, A. S. Nielsen, U. Geneser, L. M. Ringgaard, B. Nielsen, D. S. Pickering, L. Brehm, M. Gajhede, P. Krosgaard-Larsen, J. S. Kastrup, *J. Med. Chem.* **2009**, 52, 4911-4922.
- [56] K. Frydenvang, L. L. Lash, P. Naur, P. A. Postila, D. S. Pickering, C. M. Smith, M. Gajhede, M. Sasaki, R. Sakai, O. T. Pentikainen, G. T. Swanson, J. S. Kastrup, *J. Biol. Chem.* **2009**, 284, 14219-14229.
- [57] A. J. Plested, M. L. Mayer, *Neuron* **2007**, 53, 829-841.
- [58] M. H. Nanao, T. Green, Y. Stern-Bach, S. F. Heinemann, S. Choe, *Proc. Natl. Acad. Sci. U S A* **2005**, 102, 1708-1713.
- [59] M. C. Weston, P. Schuck, A. Ghosal, C. Rosenmund, M. L. Mayer, *Nat. Struct. Mol. Biol.* **2006**, 13, 1120-1127.
- [60] C. Chaudhry, M. C. Weston, P. Schuck, C. Rosenmund, M. L. Mayer, *Embo J.* **2009**, 28, 1518-1530.
- [61] P. Naur, K. B. Hansen, A. S. Kristensen, S. M. Dravid, D. S. Pickering, L. Olsen, B. Vestergaard, J. Egebjerg, M. Gajhede, S. F. Traynelis, J. S. Kastrup, *Proc. Natl. Acad. Sci. U S A* **2007**, 104, 14116-14121.
- [62] H. Furukawa, E. Gouaux, *Embo J.* **2003**, 22, 2873-2885.
- [63] A. Inanobe, H. Furukawa, E. Gouaux, *Neuron* **2005**, 47, 71-84.
- [64] H. Furukawa, S. K. Singh, R. Mancusso, E. Gouaux, *Nature* **2005**, 438, 185-192.
- [65] R. Jin, S. K. Singh, S. Gu, H. Furukawa, A. I. Sobolevsky, J. Zhou, Y. Jin, E. Gouaux, *Embo J.* **2009**, 28, 1812-1823.
- [66] J. Kumar, P. Schuck, R. Jin, M. L. Mayer, *Nat. Struct. Mol. Biol.* **2009**, 16, 631-638.
- [67] G. L. Collingridge, R. W. Olsen, J. Peters, M. Spedding, *Neuropharmacology* **2009**, 56, 2-5.
- [68] G. Q. Chen, C. Cui, M. L. Mayer, E. Gouaux, *Nature* **1999**, 402, 817-821.
- [69] V. A. Derkach, M. C. Oh, E. S. Guire, T. R. Soderling, *Nat. Rev. Neurosci.* **2007**, 8, 101-113.
- [70] J. Lerma, *Curr. Opin. Pharmacol.* **2006**, 6, 89-97.
- [71] M. J. Berridge, M. D. Bootman, H. L. Roderick, *Nat. Rev. Mol. Cell. Biol.* **2003**, 4, 517-529.
- [72] a) S. J. Liu, R. S. Zukin, *Trends Neurosci.* **2007**, 30, 126-134; b) P. J. Grabowski, D. L. Black, *Prog. Neurobiol.* **2001**, 65, 289-308.
- [73] R. S. Petralia, Y. X. Wang, R. J. Wenthold, *J. Comp. Neurol.* **1994**, 349, 85-110.



- [74] R. S. Petralia, Y. X. Wang, R. J. Wenthold, *J. Neurosci.* **1994**, *14*, 6102-6120.
- [75] R. C. Edgar, *BMC Bioinformatics* **2004**, *5*, 113.
- [76] M. N. Price, P. S. Dehal, A. P. Arkin, *Mol. Biol. Evol.* **2009**, *26*, 1641-1650.
- [77] S. Kawamoto, S. Uchino, K. Q. Xin, S. Hattori, K. Hamajima, J. Fukushima, M. Mishina, K. Okuda, *Brain Res Mol Brain Res* **1997**, *47*, 339-344.
- [78] M. W. Fleck, E. Cornell, S. J. Mah, *J. Neurosci.* **2003**, *23*, 1219-1227.
- [79] S. J. Mah, E. Cornell, N. A. Mitchell, M. W. Fleck, *J. Neurosci.* **2005**, *25*, 2215-2225.
- [80] M. W. Fleck, *Neuroscientist* **2006**, *12*, 232-244.
- [81] a) J. P. Mothet, A. T. Parent, H. Wolosker, R. O. Brady, Jr., D. J. Linden, C. D. Ferris, M. A. Rogawski, S. H. Snyder, *Proc. Natl. Acad. Sci. U S A* **2000**, *97*, 4926-4931; b) H. Wolosker, E. Dumin, L. Balan, V. N. Foltyn, *FEBS J.* **2008**, *275*, 3514-3526; c) T. Fellin, *J. Neurochem.* **2009**, *108*, 533-544.
- [82] a) T. B. Stensbol, L. Borre, T. N. Johansen, J. Egebjerg, U. Madsen, B. Ebert, P. Krogsgaard-Larsen, *Eur. J. Pharmacol.* **1999**, *380*, 153-162; b) M. M. Nielsen, T. Liljefors, P. Krogsgaard-Larsen, J. Egebjerg, *Mol. Pharmacol.* **2003**, *63*, 19-25.
- [83] a) J. E. Baldwin, A. M. Fryer, G. J. Pritchard, *J. Org. Chem.* **2001**, *66*, 2588-2596; b) L. Bunch, P. Krogsgaard-Larsen, *Med Res Rev* **2009**, *29*, 3-28; c) A. F. Parsons, *Tetrahedron* **1996**, *52*, 4149-4174.
- [84] C. Pedregal, I. Collado, A. Escribano, J. Ezquerra, C. Dominguez, A. I. Mateo, A. Rubio, S. R. Baker, J. Goldsworthy, R. K. Kamboj, B. A. Ballyk, K. Hoo, D. Bleakman, *J. Med. Chem.* **2000**, *43*, 1958-1968.
- [85] a) V. A. James, R. J. Walker, *Br. J. Pharmacol.* **1978**, *62*, 432P-433P; b) T. W. Stone, *Br. J. Pharmacol.* **1984**, *81*, 175-181.
- [86] a) M. Volgraf, P. Gorostiza, R. Numano, R. H. Kramer, E. Y. Isacoff, D. Trauner, *Nat. Chem. Biol.* **2006**, *2*, 47-52; b) M. Volgraf, P. Gorostiza, S. Szobota, M. R. Helix, E. Y. Isacoff, D. Trauner, *J. Am. Chem. Soc.* **2007**, *129*, 260-261.
- [87] J. J. Chambers, H. Gouda, D. M. Young, I. D. Kuntz, P. M. England, *J. Am. Chem. Soc.* **2004**, *126*, 13886-13887.
- [88] H. Adesnik, R. A. Nicoll, P. M. England, *Neuron* **2005**, *48*, 977-985.
- [89] K. ShinYa, J. S. Kim, K. Furihata, Y. Hayakawa, H. Seto, *Tetrahedron Lett.* **1997**, *38*, 7079-7082.
- [90] A. Limon, J. M. Reyes-Ruiz, R. G. Vaswani, A. R. Chamberlin, R. Miledi, *Acs. Chem. Neurosci.* **2010**, *1*, 175-181.
- [91] J. v. Liebig, *Justus Liebigs Ann. Chem.* **1853**, *86*, 125-126.

- [92] Y. Yao, M. L. Mayer, *J. Neurosci.* **2006**, *26*, 4559-4566.
- [93] H. Gross, D. E. Goeger, P. Hills, S. L. Mooberry, D. L. Ballantine, T. F. Murray, F. A. Valeriote, W. H. Gerwick, *J. Nat. Prod.* **2006**, *69*, 640-644.
- [94] J. D. Faraldo-Gomez, E. Kutluay, V. Jogini, Y. Zhao, L. Heginbotham, B. Roux, *J. Mol. Biol.* **2007**, *365*, 649-662.
- [95] I. J. Reynolds, R. J. Miller, *Mol. Pharmacol.* **1989**, *36*, 758-765.
- [96] L. Bunch, T. Liljefors, J. R. Greenwood, K. Frydenvang, H. Brauner-Osborne, P. Krogsgaard-Larsen, U. Madsen, *J. Org. Chem.* **2003**, *68*, 1489-1495.
- [97] a) I. Tochitsky, M. R. Banghart, A. Mourot, J. Z. Yao, B. Gaub, R. H. Kramer, D. Trauner, *Nat. Chem.* **2012**, *4*, 105-111; b) A. Mourot, M. A. Kienzler, M. R. Banghart, T. Fehrentz, F. M. E. Huber, M. Stein, R. H. Kramer, D. Trauner, *Acs. Chem. Neurosci.* **2011**, *2*, 536-543; c) D. L. Fortin, T. W. Dunn, A. Fedorchak, D. Allen, R. Montpetit, M. R. Banghart, D. Trauner, J. P. Adelman, R. H. Kramer, *J. Neurophysiol.* **2011**, *106*, 488-496; d) H. Janovjak, S. Szobota, C. Wyart, D. Trauner, E. Y. Isacoff, *Nat. Neurosci.* **2010**, *13*, 1027-1032; e) Z. R. Abrams, A. Warriar, D. Trauner, X. A. Zhang, *Front. Neural. Circuit.* **2010**, *4*; f) M. R. Banghart, A. Mourot, D. L. Fortin, J. Z. Yao, R. H. Kramer, D. Trauner, *Angew. Chem. Int. Ed.* **2009**, *48*, 9097-9101; g) R. Numano, S. Szobota, A. Y. Lau, P. Gorostiza, M. Volgraf, B. Roux, D. Trauner, E. Y. Isacoff, *Proc. Natl. Acad. Sci. U.S.A.* **2009**, *106*, 6814-6819; h) C. Wyart, F. Del Bene, E. Warp, E. K. Scott, D. Trauner, H. Baier, E. Y. Isacoff, *Nature* **2009**, *461*, 407-410; i) S. Szobota, P. Gorostiza, F. Del Bene, C. Wyart, D. L. Fortin, K. D. Kolstad, O. Tulyathan, M. Volgraf, R. Numano, H. L. Aaron, E. K. Scott, R. H. Kramer, J. Flannery, H. Baier, D. Trauner, E. Y. Isacoff, *Neuron* **2007**, *54*, 535-545; j) M. Banghart, K. Borges, E. Isacoff, D. Trauner, R. H. Kramer, *Nat. Neurosci.* **2004**, *7*, 1381-1386.
- [98] G. Mayer, A. Heckel, *Angew. Chem. Int. Ed.* **2006**, *45*, 4900-4921.
- [99] G. Miesenbock, *Annu. Rev. Cell. Dev. Bi.* **2011**, *27*, 731-758.
- [100] C. Renner, L. Moroder, *Chembiochem* **2006**, *7*, 869-878.
- [101] C. Renner, U. Kusebauch, M. Lowenack, A. G. Milbradt, L. Moroder, *J. Pept. Res.* **2005**, *65*, 4-14.
- [102] G. T. Hermanson, *Bioconjugation Techniques*, Academic Press, San Diego, **1996**.
- [103] H. Kaufman, S. M. Vratsanos, B. F. Erlanger, *Science* **1968**, *162*, 1487-1489.
- [104] E. Bartels, N. H. Wassermann, B. F. Erlanger, *Proc. Natl. Acad. Sci. U.S.A.* **1971**, *68*, 1820-1823.

- [105] T. Cordes, C. Elsner, T. T. Herzog, C. Hoppmann, T. Schadendorf, W. Summerer, K. Rück-Braun, W. Zinth, *Chem. Phys.* **2009**, *358*, 103-110.
- [106] A. A. Beharry, G. A. Woolley, *Chem. Soc. Rev.* **2011**, *40*, 4422-4437.
- [107] T. Nägele, R. Hoche, Zinth, J. Wachtveitl, *Chem. Phys. Lett.* **1997**, *272*, 489-495.
- [108] H. M. D. Bandara, S. C. Burdette, *Chem. Soc. Rev.* **2012**, *41*, 1809-1825.
- [109] C. L. Forber, E. C. Kelusky, N. J. Bunce, M. C. Zerner, *J. Am. Chem. Soc.* **1985**, *107*, 5884-5890.
- [110] a) C. J. Brown, *Acta Crystallogr.* **1966**, *21*, 146-&; b) A. Mostad, C. Roemming, *Acta Chem. Scand.* **1971**, *25*, 3561-1568; c) A. Cembran, F. Bernardi, M. Garavelli, L. Gagliardi, G. Orlandi, *J. Am. Chem. Soc.* **2004**, *126*, 3234-3243; d) L. Gagliardi, G. Orlandi, F. Bernardi, A. Cembran, M. Garavelli, *Theor. Chem. Acc.* **2004**, *111*, 363-372; e) C. R. Crecca, A. E. Roitberg, *J. Phys. Chem. A* **2006**, *110*, 8188-8203.
- [111] W. M. Horspool, F. Lenci, *CRC handbook of organic photochemistry and photobiology*, 2nd ed., CRC Press, Boca Raton, **2004**.
- [112] H. Fliegl, A. Kohn, C. Hattig, R. Ahlrichs, *J. Am. Chem. Soc.* **2003**, *125*, 9821-9827.
- [113] P. Stawski, M. Sumser, D. Trauner, *Angew. Chem. Int. Ed.* **2012**, *51*, 5748-5751.
- [114] S. B. Vogensen, R. P. Clausen, J. R. Greenwood, T. N. Johansen, D. S. Pickering, B. Nielsen, B. Ebert, P. Krogsgaard-Larsen, *J. Med. Chem.* **2005**, *48*, 3438-3442.
- [115] M. Frey, V. Jäger, *Synthesis* **1985**, 1100-1104.
- [116] R. Riess, M. Schon, S. Laschat, O. Jäger, *Eur. J. Org. Chem.* **1998**, 473-479.
- [117] O. Satoru, I. Koji, T. Koj, O. Masaki, B. Yoshihiro, T. Hiroyuki, Y. Taihei, in *US Patent 20040082607* (Ed.: U. S. T. P. Office), USA, **2004**.
- [118] P. G. M. Wuts, T. W. Greene, *Greene's Protective Groups in Organic Synthesis*, 4th ed., John Wiley & Sons, Hoboken, NJ, **2006**.
- [119] S. S. Information.
- [120] S. B. Vogensen, H. S. Jensen, T. B. Stensbøl, K. Frydenvang, B. Bang - Andersen, T. N. Johansen, J. Egebjerg, P. Krogsgaard - Larsen, *Chirality* **2000**, *12*, 705-713.
- [121] S. Donevan, M. Rogawski, *Neuron* **1993**, *10*, 51-59.
- [122] R. H. Evans, A. A. Francis, A. W. Jones, D. A. S. Smith, J. C. Watkins, *Br. J. Pharmacol.* **1982**, *75*, 65-75.
- [123] Matthew Volgraf Dissertation, Berkeley 2008.
- [124] M. Fauré-Tromeur, S. Z. Zard, *Tetrahedron Lett.* **1998**, *39*, 7301-7304.
- [125] Y. S. Gyoung, J.-G. Shim, Y. Yamamoto, *Tetrahedron Lett.* **2000**, *41*, 4193-4196.
- [126] H. C. Kolb, M. G. Finn, K. B. Sharpless, *Angew. Chem. Int. Ed.* **2001**, *40*, 2004-+.

- [127] M. Meldal, C. W. Tornøe, *Chem. Rev.* **2008**, *108*, 2952-3015.
- [128] L. A. Paquette, *Encyclopedia of Reagents for Organic Synthesis*, 2 ed., Wiley, Chichester.
- [129] R. C. Larock, *Comprehensive Organic Transformations*, Wiley-VCH, New York, **1999**.
- [130] S. Muller, B. Liepold, G. J. Roth, H. J. Bestmann, *Synlett.* **1996**, 521-&.
- [131] J. M. Aizpurua, I. Azcune, R. M. Fratila, E. Balentova, M. Sagartzazu-Aizpurua, J. I. Miranda, *Org. Lett.* **2010**, *12*, 1584-1587.
- [132] J. A. Cardin, M. Carlen, K. Meletis, U. Knoblich, F. Zhang, K. Deisseroth, L. H. Tsai, C. I. Moore, *Nat. Protoc.* **2010**, *5*, 247-254.
- [133] S. A. Stanley, J. E. Gagner, S. Damanpour, M. Yoshida, J. S. Dordick, J. M. Friedman, *Science* **2012**, *336*, 604-608.
- [134] C. Brieke, F. Rohrbach, A. Gottschalk, G. Mayer, A. Heckel, *Angew. Chem. Int. Ed.* **2012**.
- [135] M. R. Hamblin, *Vol. 2012*, Boston.
- [136] D. Purves, *Neuroscience*, 4th ed., Sinauer, Sunderland, Mass., **2008**.
- [137] S. P. Daiger, S. J. Bowne, L. S. Sullivan, *Arch. Ophthalmol-Chic.* **2007**, *125*, 151-158.
- [138] H. Jayaram, S. M. Downes, *J. Med. Case. Rep.* **2008**, *2*, 80.
- [139] N. Caporale, K. D. Kolstad, T. Lee, I. Tochitsky, D. Dalkara, D. Trauner, R. Kramer, Y. Dan, E. Y. Isacoff, J. G. Flannery, *Mol. Ther.* **2011**, *19*, 1212-1219.
- [140] R. E. Marc, B. W. Jones, J. R. Anderson, K. Kinard, D. W. Marshak, J. H. Wilson, T. Wensel, R. J. Lucas, *Invest. Ophth. Vis. Sci.* **2007**, *48*, 3364-3371.
- [141] L. Laprell, PhD Thesis, LMU Munich (Munich), **2012-2015**.
- [142] G. J. Chader, J. Weiland, M. S. Humayun, *Prog. Brain. Res.* **2009**, *175*, 317-332.
- [143] a) L. Bunch, T. Gefflaut, S. Alaux, E. Sagot, B. Nielsen, D. S. Pickering, *Eur. J. Pharmacol.* **2009**, *609*, 1-4; b) S. R. Baker, D. Bleakman, J. Ezquerra, B. A. Ballyk, M. Deverill, K. Ho, R. K. Kamboj, I. Collado, C. Dominguez, A. Escribano, A. I. Mateo, C. Pedregal, A. Rubio, *Bioorg. Med. Chem. Lett.* **2000**, *10*, 1807-1810.
- [144] a) M. Yanagida, K. Hashimoto, M. Ishida, H. Shinozaki, H. Shirahama, *Tetrahedron Lett.* **1989**, *30*, 3799-3802; b) I. Jako, P. Uiber, A. Mann, C. G. Wermuth, T. Boulanger, B. Norberg, G. Evrard, F. Durant, *J. Org. Chem.* **1991**, *56*, 5729-5733.
- [145] S. Murakami, T. Takemoto, Z. Shimizu, *J. Pharm. Soc. Jpn.* **1953**, *73*, 1026.
- [146] a) S. Cacchi, G. Fabrizi, C. Gallina, *Synlett* **1996**, 54-56; b) M. Rodriquez, C. Bassarello, G. Bifulco, L. Gomez-Paloma, A. Mann, M. Marchetti, A. Schoenfelder,

- M. Taddei, *Synlett* **2005**, 1581-1585; c) J. E. Baldwin, A. M. Fryer, G. J. Pritchard, *Bioorg. Med. Chem. Lett.* **2000**, *10*, 309-311; d) E. Sivvas, G. Voukelatou, E. D. Kouvelas, G. W. Francis, D. W. Aksnes, D. Papaioannou, *Acta Chem. Scand.* **1994**, *48*, 76-79; e) G. A. Conway, J. S. Park, L. Maggiora, M. P. Mertes, N. Galton, E. K. Michaelis, *J. Med. Chem.* **1984**, *27*, 52-56; f) O. Goldberg, A. Luini, V. I. Teichberg, *J. Med. Chem.* **1983**, *26*, 39-42; g) O. Goldberg, A. Luini, V. I. Teichberg, *Tetrahedron Lett.* **1980**, *21*, 2355-2358.
- [147] C. I. Stathakis, E. G. Yioti, J. K. Gallos., *Eur. J. Org. Chem.* **2012**, *Early View*.
- [148] W. Oppolzer, K. Thirring, *J. Am. Ceram. Soc.* **1982**, *104*, 4978-4979.
- [149] S. Takita, S. Yokoshima, T. Fukuyama, *Org. Lett.* **2011**, *13*, 2068-2070.
- [150] a) B. R. Conklin, E. C. Hsiao, S. Claeysen, A. Dumuis, S. Srinivasan, J. R. Forsayeth, J. M. Guettier, W. C. Chang, Y. Pei, K. D. McCarthy, R. A. Nissenson, J. Wess, J. Bockaert, B. L. Roth, *Nat. Methods* **2008**, *5*, 673-678; b) A. I. Meyers, J. L. Romine, S. A. Fleming, *J. Am. Chem. Soc.* **1988**, *110*, 7245-7247.
- [151] a) D. Romo, J. L. Romine, W. Midura, A. I. Meyers, *Tetrahedron* **1990**, *46*, 4951-4994; b) W. Zhang, J. Bah, A. Wohlfarth, J. Franzen, *Chem-Eur. J.* **2011**, *17*, 13814-13824; c) R. H. Peters, D. F. Crowe, M. A. Avery, W. K. M. Chong, M. Tanabe, *J. Med. Chem.* **1989**, *32*, 1642-1652.
- [152] a) Y. G. Choi, J. D. White, *J. Org. Chem.* **2004**, *69*, 3758-3764; b) M. Oikawa, T. Ueno, H. Oikawa, A. Ichihara, *J. Org. Chem.* **1995**, *60*, 5048-5068.
- [153] D. L. Comins, A. Dehghani, *Tetrahedron Lett.* **1992**, *33*, 6299-6302.
- [154] T. Jeffery, J. C. Galland, *Tetrahedron Lett.* **1994**, *35*, 4103-4106.
- [155] W. F. Little, A. K. Clark, *J. Org. Chem.* **1960**, *25*, 1979-1982.
- [156] M. Hashimoto, K. Hashimoto, H. Shirahama, *Tetrahedron* **1996**, *52*, 1931-1942.
- [157] A. Dondoni, D. Perrone, M. M. Gleason, W. R. Roush, in *Organic Syntheses, Vol. 77*, Wiley, Weinheim, **2000**.
- [158] G. Majetich, A. Casares, D. Chapman, M. Behnke, *J. Org. Chem.* **1985**, *51*, 1745-1753.
- [159] C. Flamant-Robin, Q. Wang, A. Chiaroni, N. A. Sasaki, *Tetrahedron* **2002**, *58*, 10475-10484.
- [160] M. Brewer, C. A. James, D. H. Rich, *Org. Lett.* **2004**, *6*, 4779-4782.
- [161] C. M. Niswender, P. J. Conn, *Annu. Rev. Pharmacool. Toxicol.* **2010**, *50*, 295-322.
- [162] D. Tsuchiya, N. Kunishima, N. Kamiya, H. Jingami, K. Morikawa, *Proc. Natl. Acad. Sci. U.S.A.* **2002**, *99*, 2660-2665.

- [163] N. Kunishima, Y. Shimada, Y. Tsuji, T. Sato, M. Yamamoto, T. Kumasaka, S. Nakanishi, H. Jingami, K. Morikawa, *Nature* **2000**, *407*, 971-977.
- [164] T. Muto, D. Tsuchiya, K. Morikawa, H. Jingami, *Acta. Crystallogr. Sect. F Struct. Biol. Cryst. Commun.* **2007**, *63*, 627-630.
- [165] P. Rondard, J. Liu, S. Huang, F. Malhaire, C. Vol, A. Pinault, G. Labesse, J. P. Pin, *J. Biol. Chem.* **2006**, *281*, 24653-24661.
- [166] J. P. Pin, J. Kniazeff, C. Goudet, A. S. Bessis, J. Liu, T. Galvez, F. Acher, P. Rondard, L. Prezeau, *Biol. Cell.* **2004**, *96*, 335-342.
- [167] J. Kniazeff, A. S. Bessis, D. Maurel, H. Ansanay, L. Prezeau, J. P. Pin, *Nat. Struct. Mol. Biol.* **2004**, *11*, 706-713.
- [168] N. Wettschureck, S. Offermanns, *Physiol. Rev.* **2005**, *85*, 1159-1204.
- [169] T. Tanaka, D. Iwawaki, M. Sakamoto, Y. Takai, J. Morishige, K. Murakami, K. Satouchi, *Eur. J. Biochem.* **2003**, *270*, 1466-1473.
- [170] C. Goudet, F. Gaven, J. Kniazeff, C. Vol, J. Liu, M. Cohen-Gonsaud, F. Acher, L. Prezeau, J. P. Pin, *Proc. Natl. Acad. Sci. U.S.A.* **2004**, *101*, 378-383.
- [171] K. Stierand, P. C. Maass, M. Rarey, *Bioinformatics* **2006**, *22*, 1710-1716.
- [172] D. D. Schoepp, D. E. Jane, J. A. Monn, *Neuropharmacology* **1999**, *38*, 1431-1476.
- [173] T. Muto, D. Tsuchiya, K. Morikawa, H. Jingami, *Proc. Natl. Acad. Sci. U.S.A.* **2007**, *104*, 3759-3764.
- [174] E. Dobrovetsky, G. Khutoreskaya, A. Seitova, H. He, A. M. Edwards, C. H. Arrowsmith, C. Bountra, J. Weigelt, D. Cossar, A. Bochkarev, *To Be Published*.
- [175] R. Pellicciari, G. Costantino, E. Giovagnoni, L. Mattoli, I. Brabet, J. P. Pin, *Bioorg. Med. Chem. Lett.* **1998**, *8*, 1569-1574.
- [176] M. A. Varney, N. D. Cosford, C. Jachec, S. P. Rao, A. Sacaan, F. F. Lin, L. Bleicher, E. M. Santori, P. J. Flor, H. Allgeier, F. Gasparini, R. Kuhn, S. D. Hess, G. Velicelebi, E. C. Johnson, *J. Pharmacol. Exp. Ther.* **1999**, *290*, 170-181.
- [177] a) J. Cartmell, J. A. Monn, D. D. Schoepp, *J. Pharmacol. Exp. Ther.* **1999**, *291*, 161-170; b) T. Saitoh, M. Ishida, H. Shinozaki, *Br. J. Pharmacol.* **1998**, *123*, 771-779.
- [178] a) C. M. Niswender, K. A. Johnson, C. D. Weaver, C. K. Jones, Z. Xiang, Q. Luo, A. L. Rodriguez, J. E. Marlo, T. de Paulis, A. D. Thompson, E. L. Days, T. Nalywajko, C. A. Austin, M. B. Williams, J. E. Ayala, R. Williams, C. W. Lindsley, P. J. Conn, *Mol. Pharmacol.* **2008**, *74*, 1345-1358; b) M. J. Fell, K. A. Svensson, B. G. Johnson, D. D. Schoepp, *J. Pharmacol. Exp. Ther.* **2008**, *326*, 209-217.

- [179] a) D. D. Schoepp, B. G. Johnson, *J. Neurochem.* **1988**, *50*, 1605-1613; b) O. Manzoni, L. Fagni, J. P. Pin, F. Rassendren, F. Poulat, F. Sladeczek, J. Bockaert, *Mol. Pharmacol.* **1990**, *38*, 1-6.
- [180] H. Brauner-Osborne, F. A. Slok, N. Skjaerbaek, B. Ebert, N. Sekiyama, S. Nakanishi, P. Krogsgaard-Larsen, *J. Med. Chem.* **1996**, *39*, 3188-3194.
- [181] X. Li, E. L. Gardner, Z. X. Xi, *Neuropharmacology* **2008**, *54*, 542-551.
- [182] a) K. Palczewski, T. Kumasaka, T. Hori, C. A. Behnke, H. Motoshima, B. A. Fox, I. Le Trong, D. C. Teller, T. Okada, R. E. Stenkamp, M. Yamamoto, M. Miyano, *Science* **2000**, *289*, 739-745; b) Y. Geng, D. Xiong, L. Mosyak, D. L. Malito, J. Kniazeff, Y. Chen, S. Burmakina, M. Quick, M. Bush, J. A. Javitch, J. P. Pin, Q. R. Fan, *Nat. Neurosci.* **2012**, *15*, 970-978.
- [183] D. Trauner, B. Kane, Unpublished Work, Berkeley, **2006**.
- [184] E. Sagot, A. A. Jensen, D. S. Pickering, X. Pu, M. Umberti, T. B. Stensbol, B. Nielsen, Z. Assaf, B. Aboab, J. Bolte, T. Gefflaut, L. Bunch, *J. Med. Chem.* **2008**, *51*, 4085-4092.
- [185] E. Sagot, D. S. Pickering, X. Pu, M. Umberti, T. B. Stensbol, B. Nielsen, M. Chapelet, J. Bolte, T. Gefflaut, L. Bunch, *J. Med. Chem.* **2008**, *51*, 4093-4103.
- [186] a) J. Ezquerra, C. Pedregal, B. Yruretagoyena, A. Rubio, M. C. Carreno, A. Escribano, J. L. G. Ruano, *J. Org. Chem.* **1995**, *60*, 2925-2930; b) C. Moody, W. Douglas, *Journal of the Chemical Society, Perkin Transactions I* **1997**, 3519-3530; c) T. Kondo, I. Sugimoto, T. Nekado, K. Ochi, T. Ohtani, Y. Tajima, S. Yamamoto, K. Kawabata, H. Nakai, M. Toda, *Biorg. Med. Chem.* **2007**, *15*, 2715-2735.
- [187] a) H. H. Ibrahim, W. D. Lubell, *J. Org. Chem.* **1993**, *58*, 6438-6441; b) Z.-Q. Gu, D. P. Hesson, *Tetrahedron: Asymmetry* **1995**, *6*, 2101-2104; c) E. Beausoleil, B. L'Archeveque, L. Belec, M. Atfani, W. D. Lubell, *J. Org. Chem.* **1996**, *61*, 9447-9454; d) V. Bavetsias, A. L. Jackman, J. H. Marriott, R. Kimbell, W. Gibson, F. T. Boyle, G. M. F. Bisset, *J. Med. Chem.* **1997**, *40*, 1495-1510; e) Z.-Q. Gu, D. P. Hesson, J. C. Pelletier, M.-L. Maccacchini, L.-M. Zhou, P. Skolnick, *J. Med. Chem.* **1995**, *38*, 2518-2520; f) J. R. Medina, C. J. Becker, C. W. Blackledge, C. Duquenne, Y. Feng, S. W. Grant, D. Heerding, W. H. Li, W. H. Miller, S. P. Romeril, D. Scherzer, A. Shu, M. A. Bobko, A. R. Chadderton, M. Dumble, C. M. Gardiner, S. Gilbert, Q. Liu, S. K. Rabindran, V. Sudakin, H. Xiang, P. G. Brady, N. Campobasso, P. Ward, J. M. Axten, *J. Med. Chem.* **2011**, *54*, 1871-1895.
- [188] S. Hanessian, M. Roberto, *Tetrahedron Lett.* **1998**, *39*, 5887-5889.

- [189] J. M. Padrón, G. Kokotos, T. Martín, T. Markidis, W. A. Gibbons, V. S. Martín, *Tetrahedron: Asymmetry* **1998**, *9*, 3381-3394.
- [190] J. Louie, C. W. Bielawski, R. H. Grubbs, *J. Am. Chem. Soc.* **2001**, *123*, 11312-11313.
- [191] L. Ghosez, *Angewandte Chemie International Edition in English* **1972**, *11*, 852-853.
- [192] a) K. Deisseroth, *Nat Methods* **2011**, *8*, 26-29; b) G. Miesenbock, *Science* **2009**, *326*, 395-399.
- [193] K. L. Pierce, R. T. Premont, R. J. Lefkowitz, *Nat. Rev. Mol. Cell. Biol.* **2002**, *3*, 639-650.
- [194] G. M. Alexander, S. C. Rogan, A. I. Abbas, B. N. Armbruster, Y. Pei, J. A. Allen, R. J. Nonneman, J. Hartmann, S. S. Moy, M. A. Nicolelis, J. O. McNamara, B. L. Roth, *Neuron* **2009**, *63*, 27-39.
- [195] a) X. Li, D. V. Gutierrez, M. G. Hanson, J. Han, M. D. Mark, H. Chiel, P. Hegemann, L. T. Landmesser, S. Herlitze, *Proc. Natl. Acad. Sci. U.S.A.* **2005**, *102*, 17816-17821; b) B. V. Zemelman, G. A. Lee, M. Ng, G. Miesenbock, *Neuron* **2002**, *33*, 15-22.
- [196] a) B. Lin, A. Koizumi, N. Tanaka, S. Panda, R. H. Masland, *Proc. Natl. Acad. Sci. U.S.A.* **2008**, *105*, 16009-16014; b) Z. Melyan, E. E. Tarttelin, J. Bellingham, R. J. Lucas, M. W. Hankins, *Nature* **2005**, *433*, 741-745; c) X. Qiu, T. Kumbalasiri, S. M. Carlson, K. Y. Wong, V. Krishna, I. Provencio, D. M. Berson, *Nature* **2005**, *433*, 745-749.
- [197] a) J. M. Kim, J. Hwa, P. Garriga, P. J. Reeves, U. L. RajBhandary, H. G. Khorana, *Biochemistry* **2005**, *44*, 2284-2292; b) E. Oh, T. Maejima, C. Liu, E. Deneris, S. Herlitze, *J. Biol. Chem.* **2010**, *285*, 30825-30836.
- [198] D. V. Gutierrez, M. D. Mark, O. Masseck, T. Maejima, D. Kuckelsberg, R. A. Hyde, M. Krause, W. Kruse, S. Herlitze, *J. Biol. Chem.* **2011**, *286*, 25848-25858.
- [199] G. Wald, *Nature* **1968**, *219*, 800-807.
- [200] a) S. O. Smith, *Annu. Rev. Biophys.* **2010**, *39*, 309-328; b) C. H. Sung, J. Z. Chuang, *J Cell Biol* **2010**, *190*, 953-963.
- [201] M. R. Banghart, M. Volgraf, D. Trauner, *Biochemistry* **2006**, *45*, 15129-15141.
- [202] P. Gorostiza, E. Y. Isacoff, *Science* **2008**, *322*, 395-399.
- [203] C. Brock, N. Oueslati, S. Soler, L. Boudier, P. Rondard, J. P. Pin, *J. Biol. Chem.* **2007**, *282*, 33000-33008.
- [204] Y. Tanabe, M. Masu, T. Ishii, R. Shigemoto, S. Nakanishi, *Neuron* **1992**, *8*, 169-179.



- [205] a) S. R. Ikeda, D. M. Lovinger, B. A. McCool, D. L. Lewis, *Neuron* **1995**, *14*, 1029-1038; b) J. A. Saugstad, T. P. Segerson, G. L. Westbrook, *J. Neurosci.* **1996**, *16*, 5979-5985.
- [206] M. Yokoi, K. Kobayashi, T. Manabe, T. Takahashi, I. Sakaguchi, G. Katsuura, R. Shigemoto, H. Ohishi, S. Nomura, K. Nakamura, K. Nakao, M. Katsuki, S. Nakanishi, *Science* **1996**, *273*, 645-647.
- [207] D. Robbe, G. Alonso, S. Chaumont, J. Bockaert, O. J. Manzoni, *J. Neurosci.* **2002**, *22*, 4346-4356.
- [208] L. Kahn, G. Alonso, D. Robbe, J. Bockaert, O. J. Manzoni, *Neurosci. Lett.* **2001**, *316*, 178-182.
- [209] H. C. Lin, S. J. Wang, M. Z. Luo, P. W. Gean, *J. Neurosci.* **2000**, *20*, 9017-9024.
- [210] a) L. Lyon, P. W. Burnet, J. N. Kew, C. Corti, J. N. Rawlins, T. Lane, B. De Filippis, P. J. Harrison, D. M. Bannerman, *Neuropsychopharmacology* **2011**, *36*, 2616-2628; b) B. Altinbilek, D. Manahan-Vaughan, *Neuroscience* **2009**, *158*, 149-158.
- [211] Y. Morishima, T. Miyakawa, T. Furuyashiki, Y. Tanaka, H. Mizuma, S. Nakanishi, *Proc. Natl. Acad. Sci. U.S.A.* **2005**, *102*, 4170-4175.
- [212] G. A. Higgins, T. M. Ballard, J. N. Kew, J. G. Richards, J. A. Kemp, G. Adam, T. Woltering, S. Nakanishi, V. Mutel, *Neuropharmacology* **2004**, *46*, 907-917.
- [213] G. J. Marek, *Curr. Opin. Pharmacol.* **2004**, *4*, 18-22.
- [214] E. Doumazane, P. Scholler, J. M. Zwier, E. Trinquet, P. Rondard, J. P. Pin, *Faseb. J.* **2011**, *25*, 66-77.
- [215] A. Escribano, J. Ezquerra, C. Pedregal, A. Rubio, B. Yruretagoyena, S. R. Baker, R. A. Wright, B. G. Johnson, D. D. Schoepp, *Bioorg. Med. Chem. Lett.* **1998**, *8*, 765-770.
- [216] T. Tsuji, H. Takeuchi, T. Egawa, S. Konaka, *J. Am. Chem. Soc.* **2001**, *123*, 6381-6387.
- [217] G. Chang, W. C. Guida, W. C. Still, *J. Am. Chem. Soc.* **1989**, *111*, 4379-4386.
- [218] P. Gorostiza, M. Volgraf, R. Numano, S. Szobota, D. Trauner, E. Y. Isacoff, *Proc. Natl. Acad. Sci. U.S.A.* **2007**, *104*, 10865-10870.
- [219] a) L. Iacovelli, G. Molinaro, G. Battaglia, M. Motolese, L. Di Menna, M. Alfiero, J. Blahos, F. Matrisciano, M. Corsi, C. Corti, V. Bruno, A. De Blasi, F. Nicoletti, *Mol. Pharmacol.* **2009**, *75*, 991-1003; b) A. Raveh, A. Cooper, L. Guy-David, E. Reuveny, *Cell* **2010**, *143*, 750-760.
- [220] M. U. Ehrenguber, C. A. Doupnik, Y. Xu, J. Garvey, M. C. Jasek, H. A. Lester, N. Davidson, *Proc. Natl. Acad. Sci. U.S.A.* **1997**, *94*, 7070-7075.

- [221] a) R. Shigemoto, A. Kinoshita, E. Wada, S. Nomura, H. Ohishi, M. Takada, P. J. Flor, A. Neki, T. Abe, S. Nakanishi, N. Mizuno, *J Neurosci* **1997**, *17*, 7503-7522; b) T. Takahashi, I. D. Forsythe, T. Tsujimoto, M. Barnes-Davies, K. Onodera, *Science* **1996**, *274*, 594-597.
- [222] J. L. Leaney, *Eur. J. Neurosci.* **2003**, *18*, 2110-2118.
- [223] J. M. Bekkers, C. F. Stevens, *Proc. Natl. Acad. Sci. U.S.A.* **1991**, *88*, 7834-7838.
- [224] J. Perroy, G. J. Gutierrez, V. Coulon, J. Bockaert, J. P. Pin, L. Fagni, *J. Biol. Chem.* **2001**, *276*, 45800-45805.
- [225] a) M. Koch, *Prog Neurobiol* **1999**, *59*, 107-128; b) R. C. Eaton, R. A. Bombardieri, D. L. Meyer, *J. Exp. Biol.* **1977**, *66*, 65-81.
- [226] S. C. Neuhauss, *J. Neurobiol.* **2003**, *54*, 148-160.
- [227] H. A. Burgess, M. Granato, *J. Neurosci.* **2007**, *27*, 4984-4994.
- [228] H. Korn, D. S. Faber, *Neuron* **2005**, *47*, 13-28.
- [229] R. B. Eaton, W. Campbell, F. Milgrom, *Immunol. Commun.* **1984**, *13*, 337-350.
- [230] A. Poli, R. Lucchi, M. Storto, P. De Paolis, S. Notari, F. Nicoletti, G. Casabona, *Brain Res.* **1999**, *834*, 142-145.
- [231] J. Gonzalez-Maeso, R. L. Ang, T. Yuen, P. Chan, N. V. Weisstaub, J. F. Lopez-Gimenez, M. Zhou, Y. Okawa, L. F. Callado, G. Milligan, J. A. Gingrich, M. Filizola, J. J. Meana, S. C. Sealton, *Nature* **2008**, *452*, 93-97.
- [232] R. R. Gainetdinov, R. T. Premont, L. M. Bohn, R. J. Lefkowitz, M. G. Caron, *Annual Review of Neuroscience* **2004**, *27*, 107-144.
- [233] A. L. Hopkins, C. R. Groom, *Nat. Rev. Drug Discov.* **2002**, *1*, 727-730.
- [234] B. N. Armbruster, X. Li, M. H. Pausch, S. Herlitze, B. L. Roth, *Proceedings of the National Academy of Sciences* **2007**, *104*, 5163-5168.
- [235] P. Coward, H. G. Wada, M. S. Falk, S. D. H. Chan, F. Meng, H. Akil, B. R. Conklin, *Proceedings of the National Academy of Sciences* **1998**, *95*, 352-357.
- [236] C. D. Strader, T. Gaffney, E. E. Sugg, M. R. Candelore, R. Keys, A. A. Patchett, R. A. Dixon, *J. Biol. Chem.* **1991**, *266*, 5-8.
- [237] B. R. Conklin, *Proc. Natl. Acad. Sci. U.S.A.* **2007**, *104*, 4777-4778.
- [238] B. Stay, S. S. Tobe, *Annual Review of Entomology* **2007**, *52*, 277-299.
- [239] E. M. Tan, Y. Yamaguchi, G. D. Horwitz, S. Gosgnach, E. S. Lein, M. Goulding, T. D. Albright, E. M. Callaway, *Neuron* **2006**, *51*, 157-170.
- [240] D. F. Cully, D. K. Vassilatis, K. K. Liu, P. S. Paress, L. H. Van der Ploeg, J. M. Schaeffer, J. P. Arena, *Nature* **1994**, *371*, 707-711.

- [241] E. M. Slimko, S. McKinney, D. J. Anderson, N. Davidson, H. A. Lester, *J. Neurosci.* **2002**, *22*, 7373-7379.
- [242] a) J. Krusek, H. Zemkova, *Eur. J. Pharmacol.* **1994**, *259*, 121-128; b) B. S. Khakh, W. R. Proctor, T. V. Dunwiddie, C. Labarca, H. A. Lester, *J. Neurosci.* **1999**, *19*, 7289-7299; c) R. M. Krause, B. Buisson, S. Bertrand, P. J. Corringer, J. L. Galzi, J. P. Changeux, D. Bertrand, *Mol. Pharmacol.* **1998**, *53*, 283-294.
- [243] P. Wulff, T. Goetz, E. Leppa, A. M. Linden, M. Renzi, J. D. Swinny, O. Y. Vekovischeva, W. Sieghart, P. Somogyi, E. R. Korpi, M. Farrant, W. Wisden, *Nat. Neurosci.* **2007**, *10*, 923-929.
- [244] C. J. Magnus, P. H. Lee, D. Atasoy, H. H. Su, L. L. Looger, S. M. Sternson, *Science* **2011**, *333*, 1292-1296.
- [245] K. Shah, Y. Liu, C. Deirmengian, K. M. Shokat, *Proc. Natl. Acad. Sci. U.S.A.* **1997**, *94*, 3565-3570.
- [246] A. C. Bishop, J. A. Ubersax, D. T. Petsch, D. P. Matheos, N. S. Gray, J. Blethrow, E. Shimizu, J. Z. Tsien, P. G. Schultz, M. D. Rose, J. L. Wood, D. O. Morgan, K. M. Shokat, *Nature* **2000**, *407*, 395-401.
- [247] M. L. Mayer, *Nature* **2006**, *440*, 456-462.
- [248] G. Ayalon, Y. Stern-Bach, *Neuron* **2001**, *31*, 103-113.
- [249] K. Stierand, M. Rarey, *ACS Medicinal Chemistry Letters* **2010**, *1*, 540-545.
- [250] K. B. Hansen, R. P. Clausen, E. J. Bjerrum, C. Bechmann, J. R. Greenwood, C. Christensen, J. L. Kristensen, J. Egebjerg, H. Brauner-Osborne, *Mol. Pharmacol.* **2005**, *68*, 1510-1523.
- [251] Y. B. Lee, C. P. Glover, A. S. Cosgrave, A. Bienemann, J. B. Uney, *Exp. Physiol.* **2005**, *90*, 33-37.
- [252] K. M. Partin, D. K. Patneau, C. A. Winters, M. L. Mayer, A. Buonanno, *Neuron* **1993**, *11*, 1069-1082.
- [253] M. Hollmann, S. Heinemann, *Annual Review of Neuroscience* **1994**, *17*, 31-108.
- [254] a) J. D. Clements, *Trends Neurosci.* **1996**, *19*, 163-171; b) J. S. Diamond, C. E. Jahr, *J. Neurosci.* **1997**, *17*, 4672-4687.
- [255] J. Levitz, private communication.
- [256] Y. Feng, J. K. Coward, *J. Med. Chem.* **2005**, *49*, 770-788.
- [257] G. Bartoli, M. Bosco, E. Marcantoni, M. Petrini, L. Sambri, E. Torregiani, *J. Org. Chem.* **2001**, *66*, 9052-9055.
- [258] A.-L. Grillot, D. J. Hart, *Tetrahedron* **1995**, *51*, 11377-11392.

- [259] a) J. Vidal, L. Guy, S. Sterin, A. Collet, *J. Org. Chem.* **1993**, *58*, 4791-4793; b) J. Vidal, J.-C. Hannachi, G. Hourdin, J.-C. Mulatier, A. Collet, *Tetrahedron Lett.* **1998**, *39*, 8845-8848.
- [260] K. Speranskiy, M. Kurnikova, *Biochemistry* **2005**, *44*, 11508-11517.
- [261] I. Erlenbach, E. Kostenis, C. Schmidt, F. F. Hamdan, M. H. Pausch, J. Wess, *J. Neurochem.* **2001**, *77*, 1327-1337.
- [262] R. Sadja, K. Smadja, N. Alagem, E. Reuveny, *Neuron* **2001**, *29*, 669-680.
- [263] W. Tang, A. Ruknudin, W. P. Yang, S. Y. Shaw, A. Knickerbocker, S. Kurtz, *Mol. Biol. Cell.* **1995**, *6*, 1231-1240.
- [264] D. A. Doyle, J. Morais Cabral, R. A. Pfuetzner, A. Kuo, J. M. Gulbis, S. L. Cohen, B. T. Chait, R. MacKinnon, *Science* **1998**, *280*, 69-77.
- [265] a) Z. G. Wo, R. E. Oswald, *Trends Neurosci.* **1995**, *18*, 161-168; b) T. Kuner, P. H. Seeburg, H. R. Guy, *Trends Neurosci.* **2003**, *26*, 27-32.
- [266] H. Janovjak, G. Sandoz, E. Y. Isacoff, *Nat. Commun.* **2011**, *2*, 232.
- [267] P. C. Cirino, K. M. Mayer, D. Umeno, *Methods. Mol. Biol.* **2003**, *231*, 3-9.
- [268] D. Mumberg, R. Muller, M. Funk, *Nucleic. Acids Res.* **1994**, *22*, 5767-5768.
- [269] N. Burnashev, A. Villarroel, B. Sakmann, *J. Physiol.* **1996**, *496 ( Pt 1)*, 165-173.
- [270] a) N. Nayeem, Y. Zhang, D. K. Schweppe, D. R. Madden, T. Green, *Mol. Pharmacol.* **2009**, *76*, 534-542; b) Y. Stern-Bach, S. Russo, M. Neuman, C. Rosenmund, *Neuron* **1998**, *21*, 907-918.
- [271] R. Hamilton, C. K. Watanabe, H. A. de Boer, *Nucleic. Acids. Res.* **1987**, *15*, 3581-3593.
- [272] F. Wöhler, *Ann. Chim. Phys.* **1828**, *37*, 330-333.
- [273] a) E. J. Corey, I. Vlattas, K. Harding, *J. Am. Chem. Soc.* **1969**, *91*, 535-536; b) R. B. Woodward, *Pure Appl. Chem.* **1973**, *33*, 145-177.
- [274] K. C. Nicolaou, R. J. Aversa, J. Jin, F. Rivas, *J. Am. Chem. Soc.* **2010**, *132*, 6855-6861.
- [275] G. Volpin, Master thesis, Università degli studi di Urbino "Carlo Bò" (Urbino), **2012**.
- [276] a) Y. Enomoto, K. Shiomi, M. Hayashi, R. Masuma, T. Kawakubo, K. Tomosawa, Y. Iwai, S. Omura, *J. Antibiot.* **1996**, *49*, 50-53; b) S. Omura, A. Hirano, Y. Iwai, R. Masuma, *J. Antibiot. (Tokyo)* **1979**, *32*, 786-790.
- [277] A. Furusaki, T. Matsumoto, H. Ogura, H. Takayanagi, A. Hirano, S. Omura, *J. Chem. Soc., Chem. Commun.* **1980**, 698a-698a.

- [278] a) M. Kaneda, S. Tamai, S. Nakamura, T. Hirata, Y. Kushi, T. Suga, *J. Antibiot. (Tokyo)* **1982**, *35*, 1137-1140; b) S. Tamai, M. Kaneda, S. Nakamura, *J. Antibiot. (Tokyo)* **1982**, *35*, 1130-1136; c) P. Belin, M. H. Le Du, A. Fielding, O. Lequin, M. Jacquet, J. B. Charbonnier, A. Lecoq, R. Thai, M. Courcon, C. Masson, C. Dugave, R. Genet, J. L. Pernodet, M. Gondry, *Proc. Natl. Acad. Sci. U.S.A.* **2009**, *106*, 7426-7431.
- [279] T. Atsumi, K. Noriyoshi, *Nippon Kagakkai Koen Yokoshu* **2003**, *83*, 777.
- [280] J. R. Cochrane, J. M. White, U. Wille, C. A. Hutton, *Org. Lett.* **2012**, *14*, 2402-2405.
- [281] D. L. Boger, J. Zhou, *J. Am. Chem. Soc.* **1993**, *115*, 11426-11433.
- [282] A. D. Borthwick, *Chem. Rev.* **2012**, *112*, 3641-3716.
- [283] E. V. Anslyn, D. A. Daugherty, *Modern Ohysical Organic Chemistry*, University Science Books, Sausalito, California, **2006**.
- [284] a) G.-q. Lin, R. Hong, *J. Org. Chem.* **2001**, *66*, 2877-2880; b) P. H. Lee, D. Seomoon, K. Lee, *Org. Lett.* **2004**, *7*, 343-345.
- [285] N. Z. Burns, I. N. Krylova, R. N. Hannoush, P. S. Baran, *J. Am. Chem. Soc.* **2009**, *131*, 9172-9173.
- [286] M. Matveenko, G. Liang, E. M. Lauterwasser, E. Zubia, D. Trauner, *J. Am. Chem. Soc.* **2012**, *134*, 9291-9295.
- [287] D. A. Parrish, L. J. Mathias, *J. Org. Chem.* **2002**, *67*, 1820-1826.
- [288] J. M. Berg, J. L. Tymoczko, L. Stryer, *Biochemistry*, W.H. Freeman, Basingstoke, **2002**.
- [289] J. s. Ezquerra, A. Rubio, J. Martin, J. L. Garcia Navio, *Tetrahedron: Asymmetry* **1997**, *8*, 669-671.
- [290] a) P. R. R. Meira, A. V. Moro, C. R. D. Correia, *Synthesis* **2007**, *2007*, 2279-2286; b) S. R. Angle, M. Kim, *J. Org. Chem.* **2007**, *72*, 8791-8796; c) M. Cheng, Q. Li, B. Lin, Y. Sha, J. Ren, Y. He, Q. Wang, H. Hua, K. Ruud, *Tetrahedron: Asymmetry* **2006**, *17*, 179-183; d) R. B. Silverman, M. W. Holladay, *J. Am. Chem. Soc.* **1981**, *103*, 7357-7358; e) K. C. Nicolaou, W. E. Brenzovich, P. G. Bulger, T. M. Francis, *Organic & Biomolecular Chemistry* **2006**, *4*, 2119-2157; f) B. Figadere, X. Franck, A. Cave, *Tetrahedron Lett.* **1995**, *36*, 1637-1640; g) W. Wu, Z. Li, G. Zhou, S. Jiang, *Tetrahedron Lett.* **2011**, *52*, 2488-2491; h) M. C. Elliott, M. S. Long, *Organic & Biomolecular Chemistry* **2004**, *2*, 2003-2011; i) M. C. Elliott, M. S. Long, *Tetrahedron Lett.* **2002**, *43*, 9191-9194; j) A. B. Smith, G. K. Friestad, J. Barbosa, E. Bertounesque, J. J. W. Duan, K. G. Hull, M. Iwashima, Y. Qiu, P. G. Spoors, B. A. Salvatore, *J. Am. Chem. Soc.* **1999**, *121*, 10478-10486; k) A. J. Oelke, F. Antonietti, L.

- Bertone, P. B. Cranwell, D. J. France, R. J. M. Goss, T. Hofmann, S. Knauer, S. J. Moss, P. C. Skelton, R. M. Turner, G. Wuitschik, S. V. Ley, *Chemistry – A European Journal* **2011**, *17*, 4183-4194; l) T.-L. Wang, X. E. Hu, J. M. Cassady, *Tetrahedron Lett.* **1995**, *36*, 9301-9304; m) Y. Ohfuné, M. Tomita, *J. Am. Chem. Soc.* **1982**, *104*, 3511-3513; n) S. Hanessian, R. Margarita, A. Hall, S. Johnstone, M. Tremblay, L. Parlanti, *J. Am. Chem. Soc.* **2002**, *124*, 13342-13343; o) A. Arda, R. G. Soengas, M. I. Nieto, C. Jimenez, J. Rodriguez, *Org. Lett.* **2008**, *10*, 2175-2178; p) J. P. Vigneron, R. Meric, M. Larcheveque, A. Debal, G. Kunesch, P. Zagatti, M. Gallois, *Tetrahedron Lett.* **1982**, *23*, 5051-5054; q) Z. Xu, F. Zhang, L. Zhang, Y. Jia, *Organic & Biomolecular Chemistry* **2011**, *9*, 2512-2517; r) L. L. Silva, A. C. Joussef, *J. Nat. Prod.* **2011**, *74*, 1531-1534; s) S. Ikeda, M. Shibuya, Y. Iwabuchi, *Chem. Commun.* **2007**, 504-506; t) T. Fukuyama, G. Liu, S. D. Linton, S.-C. Lin, H. Nishino, *Tetrahedron Lett.* **1993**, *34*, 2577-2580; u) A. G. M. Barrett, J. Head, M. L. Smith, N. S. Stock, A. J. P. White, D. J. Williams, *J. Org. Chem.* **1999**, *64*, 6005-6018; v) A. M. P. Koskinen, M. Ghiaci, *Tetrahedron Lett.* **1990**, *31*, 3209-3212; w) S. Takano, K. Chiba, M. Yonaga, K. Ogasawara, *J. Chem. Soc., Chem. Commun.* **1980**, 616-617; x) Y.-C. Wu, M. Liron, J. Zhu, *J. Am. Chem. Soc.* **2008**, *130*, 7148-7152; y) I. E. Wrona, A. Gozman, T. Taldone, G. Chiosis, J. S. Panek, *J. Org. Chem.* **2010**, *75*, 2820-2835; z) I. E. Wrona, A. E. Gabarda, G. Evano, J. S. Panek, *J. Am. Chem. Soc.* **2005**, *127*, 15026-15027; aa) X.-K. Liu, J.-L. Ye, Y.-P. Ruan, Y.-X. Li, P.-Q. Huang, *J. Org. Chem.* **2012**; ab) S. Chooprayoon, C. Kuhakarn, P. Tuchinda, V. Reutrakul, M. Pohmakotr, *Organic & Biomolecular Chemistry* **2011**, *9*, 531-537.
- [291] a) J. Ezquerra, C. Pedregal, A. Rubio, J. J. Vaquero, M. P. Matia, J. Martin, A. Diaz, J. L. G. Navio, J. B. Deeter, *J. Org. Chem.* **1994**, *59*, 4327-4331; b) D. Ma, J. Yang, *J. Am. Chem. Soc.* **2001**, *123*, 9706-9707; c) M. C. Elliott, S. V. Wordingham, *Synthesis* **2006**, *2006*, 1162-1170; d) M. Cheng, Q. Li, B. Lin, Y. Sha, J. Ren, Y. He, Q. Wang, H. Hua, K. Ruud, *Tetrahedron: Asymmetry* **2006**, *17*, 179-183.
- [292] A. Endo, S. J. Danishefsky, *J. Am. Chem. Soc.* **2005**, *127*, 8298-8299.
- [293] a) P. J. Dransfield, S. Wang, A. Dilley, D. Romo, *Org. Lett.* **2005**, *7*, 1679-1682; b) N. Langlois, N. Van Bac, N. Dahuron, J.-M. Delcroix, A. Deyine, D. Griffart-Brunet, A. I. Chiaroni, C. Riche, *Tetrahedron* **1995**, *51*, 3571-3586.
- [294] X.-L. Qiu, F.-L. Qing, *J. Org. Chem.* **2005**, *70*, 3826-3837.
- [295] M. Y. Chen, A. S. Y. Lee, *J. Chin. Chem. Soc.* **2003**, *50*, 103-108.
- [296] S. Soukara, B. Wünsch, *Tetrahedron* **2001**, *57*, 4359-4363.

- [297] S. G. Davies, O. Ichihara, P. M. Roberts, J. E. Thomson, *Tetrahedron* **2011**, *67*, 216-227.
- [298] a) H. Hagiwara, N. Komatsubara, H. Ono, T. Okabe, T. Hoshi, T. Suzuki, M. Ando, M. Kato, *Journal of the Chemical Society, Perkin Transactions I* **2001**, 316-322; b) H. Hagiwara, H. Ono, T. Hoshi, *Org. Synth.* **2003**, *80*, 195-197.
- [299] a) K. Chen, Y. Ishihara, M. a. M. n. Galan, P. S. Baran, *Tetrahedron* **2010**, *66*, 4738-4744; b) K. C. Nicolaou, D. Sarlah, D. M. Shaw, *Angew. Chem. Int. Ed.* **2007**, *46*, 4708-4711.
- [300] D. Enders, H. Kipphardt, P. Gerdes, L. J. Breña-Valle, V. Bhushan, *Bull. Soc. Chim. Belg.* **1988**, *97*, 691-704.
- [301] R. T. Larson, M. D. Clift, R. J. Thomson, *Angew. Chem. Int. Ed.* **2012**, *51*, 2481-2484.
- [302] S. Bhagat, R. Sharma, A. K. Chakraborti, *J. Mol. Catal. A: Chem.* **2006**, *260*, 235-240.
- [303] J. S. Yadav, B. Thirupathaiah, P. Srihari, *Tetrahedron* **2010**, *66*, 2005-2009.
- [304] T.-T. Li, Y.-L. Wu, *Tetrahedron Lett.* **1988**, *29*, 4039-4040.
- [305] M. F. Semmelhack, P. Helquist, L. D. Jones, L. Keller, L. Mendelson, L. S. Ryono, J. Gorzynski Smith, R. D. Stauffer, *J. Am. Chem. Soc.* **1981**, *103*, 6460-6471.
- [306] S. Zhang, D. Zhang, L. S. Liebeskind, *J. Org. Chem.* **1997**, *62*, 2312-2313.
- [307] Y. Fukuyama, H. Yaso, K. Nakamura, M. Kodama, *Tetrahedron Lett.* **1999**, *40*, 105-108.
- [308] A.-C. Carbonnelle, J. Zhu, *Org. Lett.* **2000**, *2*, 3477-3480.
- [309] E. Piers, J. G. K. Yee, P. L. Gladstone, *Org. Lett.* **2000**, *2*, 481-484.
- [310] D. A. Everson, B. A. Jones, D. J. Weix, *J. Am. Chem. Soc.* **2012**, *134*, 6146-6159.
- [311] J. Hassan, M. Sevignon, C. Gozzi, E. Schulz, M. Lemaire, *Chem. Rev.* **2002**, *102*, 1359-1470.
- [312] K. Soai, A. Oshio, H. Yoneyama, *Tetrahedron: Asymmetry* **1992**, *3*, 359-360.
- [313] D. Soorukram, P. Knochel, *Org. Lett.* **2004**, *6*, 2409-2411.
- [314] Y. Miura, N. Hayashi, S. Yokoshima, T. Fukuyama, *J. Am. Chem. Soc.* **2012**, *134*, 11995-11997.
- [315] W. C. Still, M. Kahn, A. Mitra, *J. Org. Chem.* **1978**, *43*, 2923-2925.
- [316] G. R. Fulmer, A. J. M. Miller, N. H. Sherden, H. E. Gottlieb, A. Nudelman, B. M. Stoltz, J. E. Bercaw, K. I. Goldberg, *Organometallics* **2010**, *29*, 2176-2179.
- [317] S. B. Park, R. F. Standaert, *Tetrahedron Lett.* **1999**, *40*, 6557-6560.
- [318] D. C. Harrowven, D. P. Curran, S. L. Kostiuik, I. L. Wallis-Guy, S. Whiting, K. J. Stenning, B. Tang, E. Packard, L. Nanson, *Chem. Commun.* **2010**, *46*, 6335-6337.

## **VI. Acknowledgements**



## VI. Acknowledgements

- My Family: my girlfriend, my parents my sister and my brother. Thank you for your ongoing support throughout my entire life.
- Prof. Dr. Dirk Trauner: for a fascinating and challenging PhD experience. For giving me the freedom to explore and to learn – whatever I wanted to.
- Prof. Dr. Thomas Carell: for helpful discussions and for being second corrector of this thesis.
- Prof. Dr. Paul Knochel, Prof. Dr. Klaus Wanner, Prof. Dr. Manfred Heuschmann, Prof. Dr. Konstantin Karaghiosoff: for their participation in my PhD committee and their helpful comments and discussions.
- Dr. Martin Sumser: for giving me a kick-start into the realm of electrophysiology and for teaching me patience and confidence.
- My labmates: Sebastian Strych and Daniel Hog. Without you my PhD would have been unbearable. I would have been lost without you. Thank you!
- The Green Lab: Sebastian Strych, Daniel Hog, Timm Fehrentz, Matthias Schoenberger, Julian Egger and Harald Janovjak. The best lab!
- The Trauner Group – past and present. For making me part of great a team.
- The Trauner Group permanent staff: Heike Traub, Carrie Louis, Tobias Kauer. For bringing the scientific mind back to earth and making sure that all the additional things, which are necessary in a PhD's life, are up and running.
- My collaborators: Josh Levitz and Prof. Dr. Ehud Isacoff. Dr. Harald Janovjak. Maximilian Reuter and Prof. Dr. Katja Sträßer. Prof. Dr. Gisbert Schneider and Tim Geppert.
- LMU Analytical Departments. For making sure I got that analytical data as clean and as fast as possible.
- Fonds der Chemischen Industrie. For a generous Kekulé stipend.
- LMU Munich. for an excellent scientific environment